R.B. Singh · Udo Schickhoff
Suraj Mal *Editors*

Climate Change, Glacier Response, and Vegetation Dynamics in the Himalaya

Contributions Toward Future Earth Initiatives

Springer

Climate Change, Glacier Response, and Vegetation Dynamics in the Himalaya

R.B. Singh • Udo Schickhoff • Suraj Mal
Editors

Climate Change, Glacier Response, and Vegetation Dynamics in the Himalaya

Contributions Toward Future Earth Initiatives

Springer

Editors
R.B. Singh
Department of Geography
Delhi School of Economics
University of Delhi
Delhi, India

Suraj Mal
Department of Geography
Shaheed Bhagat Singh College
University of Delhi
Delhi, India

Udo Schickhoff
CEN Center for Earth System Research and Sustainability, Institute of Geography
University of Hamburg
Hamburg, Germany

ISBN 978-3-319-28975-5 ISBN 978-3-319-28977-9 (eBook)
DOI 10.1007/978-3-319-28977-9

Library of Congress Control Number: 2016933872

Printed on acid-free paper

This Springer imprint is published by Springer Nature
The registered company is Springer International Publishing AG Switzerland

Foreword

I have been working on a report for the FAO recently that is about how the mountains of the world reached the level of the United Nations that initiated a mountain chapter in the so-called Agenda 21 and with 10 mountain resolutions in the UN General Assembly between 1998 and 2014. In this report the Himalaya is playing a very important role.

In the present book, I found in 3 sections and 20 chapters having a lot of highly promising and fascinating scientific problems or approaches, which are fundamental for the future of our planet and its still growing population. In 1960 the world population was about three billion, but in 2050 only two countries, China and India, will have together three billion inhabitants, following the UN Population Division. In "the International Year of Mountains 2002", the FAO as task manager of the mountain chapter in Agenda 21 published a report that 718 million people are living in the mountains of the world, of these 625 million in developing countries and of these 250–370 million are with food insecurity. The ICIMOD (International Mountain Centre for Integrated Mountain Development) in Kathmandu has calculated that around 1,3 billion people are living in the watersheds of the ten most important rivers from the Himalaya and the Tibet Plateau. What will be the situation at the end of century?

This question is an introduction to the first section about "Climate Change", but as long as some big and powerful countries are not cooperating, we are confronted with very serious problems. All the same the chapters of the first section are looking very promising, and they have a high value also for the other sections. The second section with the title "Climate Change Impact on Glaciers and Hydrology" is fundamental, not only for the mountain communities, but also for the surrounding lowlands with an irrigation-depending agricultural production. Looking at the second half of our century, when the glaciers of the "Third Pole" (Himalaya) are getting smaller and thinner and the run-off will be reduced, and then we must know that the Himalaya is the most sensitive indicator for climate change. We should never forget that water is often crossing national borders in a vast regional mountain system like the Himalaya. Lonergan said in a publication in 2005 in the UNEP Journal "Our Planet" about "Water and War": "If there is a political will for peace, water will not

be a hindrance. If you want reasons to fight, water will give you ample opportunities". The third section with "Climate Change and Vegetation Dynamics" is not only concerning the treeline, but it is an indicator for the whole biodiversity. Different altitudinal belts represent a compression of different climatic zones in a vertical structure on a shortest possible horizontal distance. This means that the higher mountains and especially the Himalaya are indeed the "sentinels" of climate change.

From this overview with the three sections, let's go down to the 20 chapters and their authors. Where are they coming from and where are they going to? Most impressive are the mixed chapters with authors from the north and from the south. These chapters and the whole book reminded me of a speech of Kofi Annan, the UN Former Secretary-General, during the UN Millennium Declaration, valid until 2015: "What is needed is a true partnership of developed and developing countries – a partnership that includes science and technology. No nation can afford to be without science and technology capacity". It is fascinating to see the different research fields and places around the Himalaya. We hope that exactly this Springer publication will help for a north-south dialogue, but also for a science-policy dialogue and for a transboundary cooperation, as it was recommended in 2012 in the Rio+20 conference and described in the final document "The Future We Want". We select some sentences: Paragraph 210: "Mountain glaciers are retreating and getting thinner with increasing impacts on the environment and human wellbeing". Paragraph 211: "We invite States to strengthen cooperative action with effective involvement and sharing of experience of relevant stakeholders by strengthening existing arrangements and regional centres of excellence for sustainable mountain development". Paragraph 212: "We call for greater efforts towards the conservation of mountain ecosystems, including their biodiversity. We encourage States to adopt a long-term vision and holistic approaches through mountain specific policies into national sustainable development strategies". You may see that your book is fulfilling these UN declarations from 2012.

By the way, I have been strongly involved in the foundation of the ICIMOD and I was generously invited to its 30th anniversary in Kathmandu 2013. ICIMOD is the centre for eight Himalayan countries. I hope that transboundary cooperation with this institution will be possible in the future. I thank once more the small group of the three editors for their wonderful composition of the book, but my acknowledgements go also to all the authors of the 20 chapters for their engagement and cooperation for the highest mountain system of the world!

Ex-President, International Geographical Union Bruno Messerli
Professor Emeritus, Institute of Geography
University of Bern, Switzerland

Foreword

There are numerous reasons why this book is important and its publication is timely. Firstly, the role of glaciers in relation to climate change is akin to the role of canaries in a coal mine. They provide one of the first signals that something is amiss. Glaciers worldwide are recessing not all of them but the vast majority – and the scientific consensus is that the reason for this is global warming. But the glaciers in the Himalaya play a special role that is not well appreciated by those outside of the Indian subcontinent. The Himalaya themselves form a vertical massif that protrudes into the lower atmosphere. The heating and cooling of the surface of the Himalaya and the Tibetan plateau plays a major role in the dynamics of the atmospheric circulation and thus a major role in the climate of the Asian region. If and when the Himalayan glaciers recede, they will change the nature of the albedo, the reflected sunlight, and are thus expected to induce major changes in circulation and climate.

If and when the Himalayan glaciers recede, a possibly even more serious change will be that of the lifestyle of the population on the Indian subcontinent that rely on the waters that flow from melting glaciers. A continent that is presently well supplied with water through its fluvial system could then endure water scarcity. The likelihood is that for a region as densely populated as the Indian subcontinent, any sudden diminution of the water supply will cause social disruption if not chaos and possible armed conflict. Thus, the more we can learn about the dynamics of glaciers and vegetation in the Himalaya, the better.

Issues such as this will be studied by the new international research programme called Future Earth, which is the major new initiative of the International Council of Science (ICSU) that brings together at least three of the existing ICSU international research programmes into this new one. It seeks to examine the effects of global change on all aspects of the biosphere and anthroposphere. Although ICSU initiated this process of merging its four environmental programmes to become Future Earth, it has become a multipurpose programme cosponsored by many organizations including ICSU.

The scientific community is presently engaged in a global dialogue to determine how it can participate in and assist Future Earth. The International Union of Geodesy and Geophysics (IUGG) established a new entity, the Commission for Climate and

Environmental Change, to be the vehicle by which IUGG could co-ordinate its science in a way that would assist Future Earth, and the Commission has so far concentrated on the hydrological issues involved in the initiative known as Panta Rhei and in a study of the implications of weather, climate and food security.

Climate Change and Dynamics of Glaciers and Vegetation in the Himalaya is a topic that is of obvious importance to both of these initiatives, of importance to global change science and of importance to the future of the societies that live in the Indian subcontinent. In short it is a topic of importance to Future Earth and to the Future of the Earth.

Chair IUGG Commission for Climate and Environmental Change Tom Beer
Member, ICSU Committee for Scientific Planning and Review
Paris, France

Contents

Contributors

Tirtha Raj Adhikari Central Department of Hydrology and Meteorology, Tribhuvan University, Kirtipur, Kathmandu, Nepal

Simon K. Allen Department of Geography, University of Zurich, Zurich, Switzerland

Institute for Environmental Sciences, University of Geneva, Geneva, Switzerland

Benjamin Bechtel CEN Center for Earth System Research and Sustainability, Institute of Geography, University of Hamburg, Hamburg, Germany

M.R. Bhutiyani Defense Terrain Research Laboratory, Defense Research & Development Organization, New Delhi, India

M.P.S. Bisht Department of Geology, HNB Garhwal University, Srinagar (Garhwal), Uttarakhand, India

Maria Bobrowski CEN Center for Earth System Research and Sustainability, Institute of Geography, University of Hamburg, Hamburg, Germany

Jürgen Böhner CEN Center for Earth System Research and Sustainability, Institute of Geography, University of Hamburg, Hamburg, Germany

Tobias Bolch Institut für Kartographie, Technische Universität Dresden, Dresden, Germany

Geographisches Institut, Universität Zürich, Zürich, Switzerland

Achim Bräuning Institute of Geography, Friedrich-Alexander-University Erlangen-Nürnberg, Erlangen, Germany

Manfred Buchroithner Institut für Kartographie, Technische Universität Dresden, Dresden, Germany

Birgit Bürzle CEN Center for Earth System Research and Sustainability, Institute of Geography, University of Hamburg, Hamburg, Germany

Alton C. Byers Institute of Arctic and Alpine Research, University of Colorado at Boulder, Boulder, CO, USA

Ram Prasad Chaudhary RECAST Research Centre for Applied Science and Technology, Tribhuvan University, Kathmandu, Nepal

Gargi Chaudhuri Department of Geography and Earth Science, University of Wisconsin-La Crosse, La Crosse, WI, USA

Pritam Chand Centre for the Study of Regional Development, Jawaharlal Nehru University, New Delhi, India

Lochan Prasad Devkota Central Department of Hydrology and Meteorology, Tribhuvan University, Kirtipur, Kathmandu, Nepal

D.P. Dobhal Centre for Glaciology, Wadia Institute of Himalayan Geology, Dehradun, Uttarakhand, India

Lars Gerlitz Section Hydrology, GFZ German Research Centre for Geosciences, Potsdam, Germany

Tim Golletz Institut für Kartographie, Technische Universität Dresden, Dresden, Germany

Jussi Grießinger Institute of Geography, Friedrich-Alexander-University Erlangen-Nürnberg, Erlangen, Germany

Anil K. Gupta Wadia Institute of Himalayan Geology, Dehradun, Uttarakhand, India

Shabeh ul Hasson CEN Center for Earth System Research and Sustainability, Institute of Geography, University of Hamburg, Hamburg, Germany

Philipp Hochreuther Institute of Geography, Friedrich-Alexander-University Erlangen-Nürnberg, Erlangen, Germany

Nicolai Holzer Institut für Kartographie, Technische Universität Dresden, Dresden, Germany

Christian Huggel Department of Geography, University of Zurich, Zurich, Switzerland

Ajay Kumar Department of Geography, Delhi School of Economics, University of Delhi, Delhi, India

Manish Kumar Department of Geography, Kalindi College, University of Delhi, Delhi, India

Pankaj Kumar Department of Geography, Delhi School of Economics, University of Delhi, Delhi, India

Santosh Kumar Department of Geography, Delhi School of Economics, University of Delhi, Delhi, India

Jelena Lange Institute of Botany and Landscape Ecology, University of Greifswald, Greifswald, Germany

Andreas Linsbauer Department of Geography, University of Zurich, Zurich, Switzerland

Department of Geosciences, University of Fribourg, Fribourg, Switzerland

Suraj Mal Department of Geography, Shaheed Bhagat Singh College, University of Delhi, Delhi, India

Daene C. McKinney Department of Civil, Architectural & Environmental Engineering, University of Texas at Austin, Austin, TX, USA

Manish Mehta Wadia Institute of Himalayan Geology, Dehradun, Uttarakhand, India

Niti B. Mishra Department of Geography and Earth Science, University of Wisconsin-La Crosse, La Crosse, WI, USA

Harekrishna Misra Institute of Rural Management Anand, Anand, Gujarat, India

Gourav Misra International Water Management Institute, Anand, Gujarat, India

Michael Müller Department of Geosciences, Chair of Soil Science and Geomorphology, University of Tübingen, Tübingen, Germany

Ram Nagesh Prasad Centre for the Study of Regional Development, Jawaharlal Nehru University, New Delhi, India

Virendra Rana Department of Geology, HNB Garhwal University, Srinagar (Garhwal), Uttarakhand, India

S.S. Randhawa State Centre on Climate Change, Himachal Pradesh, India

Shouraseni Sen Roy Department of Geography and Regional Studies, University of Florida, Miami, FL, USA

Yvonne Schaub Department of Geography, University of Zurich, Zurich, Switzerland

Udo Schickhoff CEN Center for Earth System Research and Sustainability, Institute of Geography, University of Hamburg, Hamburg, Germany

Thomas Scholten Department of Geosciences, Chair of Soil Science and Geomorphology, University of Tübingen, Tübingen, Germany

Niels Schwab CEN Center for Earth System Research and Sustainability, Institute of Geography, University of Hamburg, Hamburg, Germany

Christopher A. Scott Udall Center for Studies in Public Policy/School of Geography & Development, University of Arizona, Tucson, AZ, USA

Milap Chand Sharma Centre for the Study of Regional Development, Jawaharlal Nehru University, New Delhi, India

Tanuj Shukla Centre for Glaciology, Wadia Institute of Himalayan Geology, Dehradun, Uttarakhand, India

R.B. Singh Department of Geography, Delhi School of Economics, University of Delhi, Delhi, India

Suman Singh Department of Geology, HNB Garhwal University, Srinagar (Garhwal), Uttarakhand, India

Swarnima Singh Department of Geography, Delhi School of Economics, University of Delhi, Delhi, India

Marcelo A. Somos-Valenzuela Department of Civil, Architectural & Environmental Engineering, University of Texas at Austin, Austin, TX, USA

Markus Stoffel Institute for Environmental Sciences, University of Geneva, Geneva, Switzerland

Dendrolab.ch, Institute of Geological Sciences, University of Berne, Berne, Switzerland

Teiji Watanabe Faculty of Environmental Earth Science, Hokkaido University, Sapporo, Hokkaido, Japan

Johannes Weidinger CEN Center for Earth System Research and Sustainability, Institute of Geography, University of Hamburg, Hamburg, Germany

Jakob Wernicke Institute of Geography, Friedrich-Alexander-University Erlangen-Nürnberg, Erlangen, Germany

Chapter 1
Climate Change and Dynamics of Glaciers and Vegetation in the Himalaya: An Overview

Udo Schickhoff, R.B. Singh, and Suraj Mal

Abstract Mountains are globally significant as 'water towers' of the Earth, as core areas of biodiversity and as source regions for important natural resources and ecosystem services. The ecological integrity of mountain environments is increasingly threatened by global environmental changes including climate change to which physical and ecological systems in mountains are highly vulnerable. Global warming rates have been higher in mountain regions compared to the global mean and have strongly affected the cryosphere, mountain biota and ecosystem processes.

Temperature trends in most Himalayan regions substantially exceed the global mean trend of 0.85 °C between 1880 and 2012, with winter season temperature trends being generally higher than those of other seasons. Precipitation patterns are spatio-temporally differentiated, but show rather decreasing than increasing trends, in particular during summer. On average, glacier mass budgets have been negative for the past five decades, with glaciers in the Himalaya and in the Hindu Kush showing distinct mass losses, while those in the Karakoram are close to balance. Shrinking rates are regionally variable, but often accelerating, corresponding approximately to a W-E gradient of increasing glacier retreat. Biotic responses to current climate change include elevational range shifts of species, intense recruitment of tree species in treeline ecotones and shifts in phenology, resulting in modified structure, composition and functioning of Himalayan ecosystems.

Keywords Climate warming • Glacier retreat • Phenology • Range shift • Treeline • Vulnerability

U. Schickhoff (✉)
CEN Center for Earth System Research and Sustainability,
Institute of Geography, University of Hamburg, Hamburg, Germany
e-mail: udo.schickhoff@uni-hamburg.de

R.B. Singh
Department of Geography, Delhi School of Economics, University of Delhi, Delhi, India

S. Mal
Department of Geography, Shaheed Bhagat Singh College, University of Delhi, Delhi, India

R.B. Singh et al. (eds.), *Climate Change, Glacier Response, and Vegetation Dynamics in the Himalaya*, DOI 10.1007/978-3-319-28977-9_1

1.1 Introduction

Mountain regions in general and the Himalaya in particular provide increasing evidence of ongoing impacts of climate change on physical and biological systems. Mountain ecosystems already show a high sensitivity to changing climatic conditions and will be highly vulnerable to continued climate change in the future (IPCC 2014). Distinct vulnerability of mountain environments must be attributed to high altitude with cryospheric systems, local relief with steep slopes, complex topography and condensed vertical ecological gradients as well as to specific and spatially intensive variability of human-environmental subsystems (Schickhoff 2011; Borsdorf et al. 2015). Mountain plant and animal species are adapted to relatively narrow ranges of temperature and precipitation. Thus, minor climatic changes would already have significant impacts (Körner 2003; Thuiller 2004; Grabherr et al. 2010a). High elevation environments with glaciers, snow, permafrost, water and a complex altitudinal zonation of vegetation and fauna are without a doubt among the most sensitive terrestrial systems to reflect effects of climatic changes (e.g. Grabherr et al. 2001, 2010a, b; Huber et al. 2005; Körner et al. 2005; Walther et al. 2005; WGMS 2008; Kohler et al. 2010; Schickhoff 2011).

Almost the entire globe has experienced surface warming after the end of the Little Ice Age, with each of the last three decades having been successively warmer than any preceding decade since 1850. Based on globally averaged combined land and ocean temperature data, warming has been in the order of 0.85 (0.65–1.06)°C over the period 1880–2012 (IPCC 2013). In most mountain regions, analyses of temperature trends showed that total temperature increase was higher than the global mean during the twentieth century (e.g. Diaz and Bradley 1997; Beniston 2000; Diaz et al. 2003; Rangwala and Miller 2012). It will most likely continue to be higher than average during the twenty-first century (cf. Nogués-Bravo et al. 2007).

High sensitivity and vulnerability to climate change on the one hand and above-average warming rates on the other result in mountain environments being exceptionally fragile. At the same time, mountains are high-risk areas for multiple natural hazards, as we became painfully aware once again by the devastating April 2015 earthquake in Nepal (Goda et al. 2015). In view of the global significance of mountain ecosystems, the susceptibility to climate and other environmental changes is giving rise to great concern. As important sources of water, energy, forest and agricultural products, minerals and other natural resources, and as biodiversity hotspots, mountains provide goods and services to about half of humanity (Ives et al. 1997; Byers et al. 2013). Water supply is arguably the key function of mountains for humanity since all of the world's major rivers and many smaller ones originate in mountains, while over 40 % of the world's population lives in the watersheds of rivers that have their sources in mountains (Körner et al. 2005; Viviroli et al. 2007). Mountains store immense amounts of freshwater as snow and ice and in lakes and reservoirs, thus playing a crucial role for supplying water to adjoining lowlands. The global significance of mountain water resources will become increasingly

apparent in future decades when a growing proportion of the world's population will most likely experience water scarcity.

Meanwhile, mountain issues feature prominently in global change research and sustainable development agendas. The process of raising local and global awareness for the importance of mountain environments and their peoples has seen notable progress in the past two decades (Price and Kohler 2013), concomitant to reinforced scientific interest in the response of mountain ecosystems to global environmental change. Several ground-breaking efforts to establish mountains as a research priority (e.g. Chapter 13 of Agenda 21, Rio Earth Summit 1992; International Year of the Mountains 2002) have contributed to achieving a higher level of integrating mountain issues in national and international research initiatives (Messerli 2012). Global programmes specifically devoted to mountains, e.g. the Global Observation Research Initiative in Alpine Environments (GLORIA), the Global Mountain Biodiversity Assessment (GMBA) and the Mountain Research Initiative (MRI), vividly illustrate the considerable recent attention mountains receive when addressing scientific and societal challenges in understanding and preparing for global environmental change. However, in spite of many joint initiatives, there is still a long way to go to achieve a standing comparable to oceans or rainforests (cf. Byers et al. 2013).

Current global warming has indeed extensive impacts on mountain environments. With regard to physical systems, it has left distinct traces in the cryosphere and hydrosphere. Degrading permafrost, decreasing snow cover and glacier retreat have cascading effects on regional biophysical systems with serious implications for supraregional ecosystem services and socioeconomic development. At most of the study sites at high latitudes and in mountain regions, permafrost temperatures have increased during the past three decades in response to increased air temperature and changing snow cover (Vaughan et al. 2013). Permafrost warming and thawing adversely affect the stability and morphodynamic behaviour of rock and debris slopes and may increasingly initiate slope instability processes and trigger mass movements and related natural hazards (Haeberli 2013). Glaciers provide the most visible signature of climate change in mountain regions; their volume has decreased considerably over the last 150 years with many small glaciers having already disappeared. In particular since the 1980s, almost all glaciers worldwide have experienced a loss of length, area, volume and mass (Fig. 1.1) and will continue to shrink in the future even without further temperature increase (Mernild et al. 2013; Vaughan et al. 2013).

The accelerating trend of glacier recession has severe implications for downstream run-off characteristics. Mountain water resources are of extraordinary importance for agricultural, domestic, energy and industrial uses in both mountains and lowlands as well as for the integrity of ecosystems. Any change in the hydrological cycle will alter the availability and seasonality of water supply and involve higher levels of uncertainty and risk, in particular for populated lowland regions (Beniston 2006; Kohler et al. 2010; de Jong 2015). Moreover, glacier melt significantly contributes to global mean sea level rise (Marzeion et al. 2012). Changes in snowpack and snowmelt run-off add to complex impacts of climate change on

Fig. 1.1 Retreat of the Rolwaling glacier and expansion of the pro-glacial Tsho Rolpa Lake, 4550 m, Nepal Himalaya (Source: Udo Schickhoff 2013)

mountain hydrology. Both duration and total accumulation of snow have declined at lower elevations in many mountain regions; a concomitant decrease of snowfall-rainfall ratio, snow water equivalent and snow depth during the melt season is being observed (Serquet et al. 2011; Beniston 2012). Increasingly higher elevations are projected to experience declines in snowpack accumulation and melt with continued warming (Stewart 2009).

Impacts of global warming are considered a major threat to mountain biodiversity. Generally, species respond to climate change by shifting their distributions to track preferred conditions, by adjusting their phenotypes via plasticity and/or by adapting to novel stresses (Anderson et al. 2012). The potential to further adapt in situ to the effects of ongoing climate change is limited for high-altitude plant species due to genotypic adaptations to their current environments such as slow and low growth. As phenotypic plasticity might also be restricted under harsh climatic conditions at higher altitudes, populations of montane and alpine species are more likely to change their distributions in response to a warmer climate. However, some sort of clonal, rather slow mode of propagation is widespread among alpine species, implying the retainment of space occupancy irrespective of climatic variations (Körner 2003). Thus, it is highly questionable whether rates of migrations are sufficient to track rapid climate change. To migrate to a more suitable habitat or to persist and compete with invading species implies a potential loss of biodiversity. Species which migrate from lower to higher altitudes exert competitive pressure on already established species which in turn may be restricted from shifting upwards

due to reduced available habitats, unrealizable niche requirements or the lack of migration corridors (Grabherr et al. 1995). Shifting upwards in elevation involves the risk that equivalent surface areas with similar habitat conditions are no longer available. Thus, high alpine species are extremely vulnerable to global warming. A particular high risk of extinction has been confirmed for many endemic species in mountain ecosystems as their populations become easily fragmented (Pauli et al. 2003). A disintegration of current vegetation patterns, a drastic decrease of distribution areas, population declines and even extinction of cryophilous plants are among the anticipated consequences of migration processes towards higher altitudes (Pauli et al. 2014).

Observations on all continents and oceans provide evidence that climate change is a powerful stressor on terrestrial and marine ecosystems, inducing shifts in phenology, species distributions, community structure as well as other ecosystem changes (e.g. Walther et al. 2002; Parmesan 2006; Settele et al. 2014). In mountain regions, widespread pattern of upslope range expansion by plant and animal species to cooler elevations becomes apparent, including a wide range of taxonomic groups and geographical locations (Rosenzweig et al. 2007; Gonzalez et al. 2010; Chen et al. 2011). The ability of montane/alpine plants to track climate warming through upslope range shifts has been documented for an increasing number of mountain regions (Lenoir et al. 2008; Gottfried et al. 2012; Jump et al. 2012; Pauli et al. 2012; Telwala et al. 2013). The altitudinal position of alpine treelines is expected to advance to higher elevations in the long term (Holtmeier 2009; Körner 2012), with the majority of global treelines already showing a respective response (Harsch et al. 2009). However, range shifts that are downhill have also been reported, often associated with drought stress or interactions with land use (cf. Lenoir and Svenning 2015). Observed shifts in distributions also revealed that individual species vary greatly in their rates of change, suggesting that the range shift of each species depends on multiple internal species traits and external drivers of change (Le Roux and McGeoch 2008; Chen et al. 2011). Asynchronous responses to external forcing result in the formation of no-analogue communities with modified competitive relationships, thus deviating ecosystem structure and functioning (Schickhoff 2011).

1.2 Observed Changes in the Himalaya

1.2.1 Climate Change

Across most of Asia, warming trends and increasing temperature extremes have been observed over the past century, with decreasing numbers of cold days and nights and increasing numbers of warm days and nights since about 1950 (Hijioka et al. 2014). While the Indian subcontinent on the whole has experienced average upward temperature trends in the order of 0.56–0.68 °C over the past century (Lal 2003; Chaudhry et al. 2009; Attri and Tyagi 2010), the warming trend was

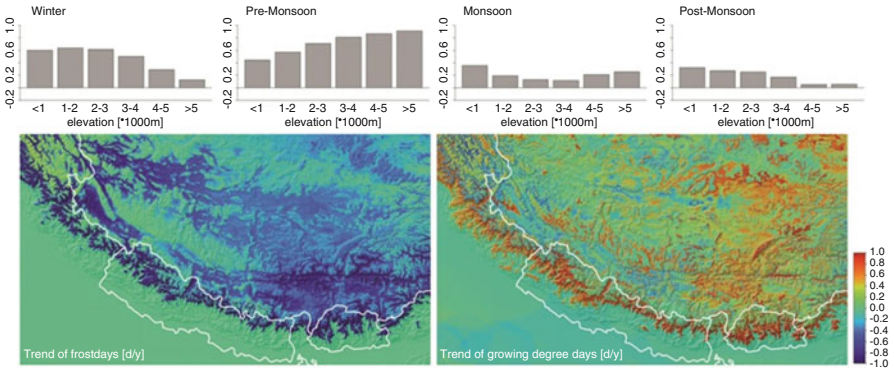

Fig. 1.2 Seasonal temperature trends [°C decade^{-1}] for different elevational belts (*top* panels) and spatial distribution of trends for frost and growing degree days over the Himalaya (*bottom* panels) (Source: Udo Schickhoff et al. 2015)

particularly strong in mountain regions of South and Central Asia, e.g. at higher altitudes in West, Central and East Himalaya (Bhutiyani et al. 2007; Dash et al. 2007; Singh et al. 2011; Gautam et al. 2013; Bhutiyani 2016b), over the adjacent Tibetan Plateau (Liu and Chen 2000; Wang et al. 2008; Yang et al. 2013; Hasson et al. 2016) and in surrounding mountain ranges (e.g. Giese et al. 2007; Dagvadorj et al. 2009). Temperature trends in most regions of the Himalayan mountain system substantially exceed the global mean trend of 0.85 °C between 1880 and 2012 (cf. IPCC 2013). At higher elevations, temperature has been increasing at a rate of up to 1.2 °C per decade since about 1980 (Shrestha et al. 1999; Liu et al. 2006, 2009; Bhutiyani et al. 2007, 2010; Shrestha and Aryal 2011; Yang et al. 2011), with an accelerating warming trend in the past two decades (Diodato et al. 2011; Kattel and Yao 2013; Gerlitz et al. 2014; Hasson et al. 2015).

While mean annual temperature increase in most of the Himalayan regions exceeds global average rates during recent decades, distinct patterns of spatial and seasonal differentiations emerge from recent observations. Examinations of vertical gradients show that the rate of warming is amplified with elevation. This phenomenon is prevalent over most of High Asia, subjecting high-mountain environments to more rapid changes in temperature than lower altitudes (Eriksson et al. 2009; Liu et al. 2009; Qin et al. 2009; Yang et al. 2013; Hasson et al. 2015; see also Pepin et al. 2015). High resolution temperature trends over the Himalaya for the period since 1989 (Gerlitz et al. 2014) showed a clear elevational gradient with maximum values of up to 1 °C per decade at higher altitudes (Fig. 1.2). A significant positive trend of growing degree days was detected along the Himalayan arc at elevations between 2000 and 3500 m, while a decrease of frost days (up to −17 days per decade) was found in the Nepal Himalaya at elevations between 3000 and 3500 m (cf. Fig. 1.2).

Observations of seasonal patterns show that winter season temperature trends are generally higher than those of other seasons or the annual mean. Rather high-temperature trends are also reported in pre-monsoon and post-monsoon seasons for most of the Himalayan regions. During monsoon season, temperature trends were found to be reduced throughout the mountain system, in particular in the NW Himalaya and Karakoram where even cooling of summer temperatures is registered at a series of climate stations. In the Upper Indus Basin of the Hindu Kush-Karakoram-Himalaya (N Pakistan), significant winter warming trends (roughly +0.6 °C) for the period 1961–1999 contrast with significant cooling of mean temperatures (roughly −1.0 °C) during summer (based on valley stations data; Fowler and Archer 2006; Williams and Ferrigno 2010). Bocchiola and Diolaiuti (2013) corroborated this pattern, but highlighted increasing autumn, winter and spring temperature trends since the 1990s as well as intra-regional climatic variability and dependence on altitude. Similar seasonal trends were also reported by Khattak et al. (2011), Hasson et al. (2015) and Raza et al. (2015) for mountain regions of N Pakistan. Farhan et al. (2015) observed a slight increase of annual and summer mean temperatures during the period 1996–2010 in the Astor Basin. In the Hindu Kush-Karakoram-Himalaya of N Pakistan, mean temperatures for the period 1980–2006 show an overall annual increase of c. 0.2 °C per decade and an accelerating trend (Steinbauer and Zeidler 2008). Rasul et al. (2012) estimated the warming trend in this region to be almost double the one of the remaining parts of Pakistan.

Higher warming rates in winter are consistently reported from the West and Central Himalaya in India. Over the northwestern subregion, winter temperature has shown an elevated rate of increase (1.4 °C/100 years) compared to the monsoon temperature (0.6 °C/100 years) during the period from 1866 to 2006 (Bhutiyani 2016a, b). Higher winter season mean temperature trends of up to +2.0 °C were detected for the period 1985–2008 (Bhutiyani et al. 2007, 2010; Shekhar et al. 2010; Dimri and Dash 2012). Seasonal maximum and minimum temperatures have increased by 2.8 and 1.0 °C, respectively, and show an increasing trend over the Pir Panjal, Shamshawari and Greater Himalayan ranges (Shekhar et al. 2010). In contrast to the conflictive winter and summer trends in the Karakoram, significantly increasing winter, monsoon and annual temperatures are reported from most stations (exceptions include monsoon temperature at Srinagar, Kashmir, 1901–1989) (Bhutiyani et al. 2010; Singh and Kumar 2014; see also Wani 2014). In Uttarakhand, temperature records of the past 100 years show a notable warming trend (Singh et al. 2016), particularly prominent during the last decade and at higher altitudes, with the last 5 years (2007–2012) being the warmest in all districts of Uttarakhand (Mishra 2014).

Large recent warming trends were observed in the Nepalese Himalaya, with warming rates reported to be higher in post-monsoon and winter seasons and at higher altitudes. The annual mean temperature of 49 stations in Nepal shows an average trend of 0.6 °C per decade for the period 1977–2000 (Shrestha and Aryal 2011), but may reach up to more than 0.8 °C per decade at some stations (Practical Action Nepal Office 2009; Nagy and Böhner 2015). A remarkably high increase in annual average maximum temperatures (up to 1.2 °C per decade in winter season)

was assessed for the period 1977–2000 (Shrestha et al. 1999; Shrestha and Aryal 2011). Mean maximum temperature trend in winter (Dec to Feb) is 0.9 °C per decade for the Himalayan region and 1.2 °C per decade for the trans-Himalayan region compared to the respective annual mean maximum temperature trends of 0.6 °C and 0.9 °C (Eriksson et al. 2009; Shrestha and Devkota 2010).

Warming trends are even stronger over the adjacent Tibetan Plateau, in particular in the Yarlung Zangbo River Basin, with current mean temperature trends of up to 0.73 °C per decade and much higher winter means (Liu and Chen 2000; Yang et al. 2006, 2011, 2013; You et al. 2007; Wang et al. 2008). Significant warming in the same magnitude or even higher is also reported for Bhutan and the eastern Himalaya in India and China. Tse-ring et al. (2010) state for the period 1985–2002 an increase of 0.5 °C in the non-monsoon season in Bhutan. Mean air temperature increase at high-elevation stations over the eastern Chinese Himalaya is in the order of 0.8–0.9 °C per decade between 1991 and 2007 (Yang et al. 2013; see also Yunling and Yiping 2005; Liu et al. 2006). Gerlitz et al. (2014) detected temperature trends of up to +0.8 °C per decade during winter season over the eastern Himalaya. Jhajharia and Singh (2011) observed large magnitudes of mean temperature increases in the months of October to December in NE India and, interestingly, higher trends in the monsoon season compared to winter and pre-monsoon months at several stations. Recent warming rates are significantly higher than the long-term warming trend of 0.6 °C for the Brahmaputra Basin in the twentieth century indicated by Immerzeel (2008).

To derive trends in annual precipitation for the Himalayan region over the past century proves to be difficult given the general lack of long-term observations and the strong variability ascertained in different subregions and seasons. It has been shown for South Asia in general that mean precipitation of the Indian summer monsoon shows inter-decadal variability, but a declining trend, with more frequent deficit monsoons under regional inhomogeneities (Kulkarni 2012; Lacombe and McCartney 2014). The observed recent weakening tendency of the summer monsoon is related to an increase in the number of monsoon break days and a decline in the number of monsoon depressions (Dash et al. 2009; Krishnamurthy and Ajayamohan 2010). Simultaneously, extreme rainfall events have become more frequent at the expense of weaker rainfall events (Christensen et al. 2013). In spite of recent decreases in monsoonal precipitation, all models and scenarios project an increase in total monsoon rainfall as well as increasing interannual variability and extremes for the coming decades. It is very likely that increased atmospheric moisture content will compensate for a weakening monsoon circulation (cf. Christensen et al. 2013; Hijioka et al. 2014).

Observations in the Greater Himalayan region show more decreasing than increasing precipitation trends. A notable exception is precipitation in the Upper Indus Basin (N Pakistan), for which upward trends were observed during the period 1961–1999 for both summer rainfall and winter precipitation (October to March), mainly originating from western disturbances (Archer and Fowler 2004; Khattak et al. 2011; Palazzi et al. 2013; see also Yao et al. 2012 for adjoining W Tibet). A slight recent (1996–2010) decrease in annual and summer precipitation was

observed in the Astore Basin (Farhan et al. 2015). However, no trend is observed in the long term (1895–1999), while wetter summer conditions as well as a reduction in the spatial average of snow depth are predicted for the coming decades (Terzago et al. 2014; Palazzi et al. 2015).

Negative trends of annual precipitation over the western Indian Himalaya were identified by Sontakke et al. (2008), Bhutiyani et al. (2010) and Bhutiyani (2016a, b), based on instrumental data. This trend mainly results from decreasing summer precipitation rates after the 1960s and is associated with a weakening of the Southern Oscillation and a decrease of temperature gradients over South Asia due to high warming rates over the Indian Ocean during recent decades (Basistha et al. 2009; Naidu et al. 2009). Contrary to monsoonal rains, winter precipitation shows an increasing but statistically insignificant trend; it has been above average during the period 1991–2006 (Bhutiyani 2016a, b). Guhathakurta and Rajeevan (2008) found regional inhomogeneities with increasing winter precipitation in Himachal Pradesh and decreasing winter rates in Jammu and Kashmir and in Uttarakhand during 1901–2003. Singh and Mal (2014) highlighted spatially varying trends of precipitation in Uttarakhand and confirmed negative trends of annual precipitation and monsoonal rainfall at higher altitudes, while winter precipitation shows mixed trends (see also Mishra 2014). Due to significant winter warming, the ratio of snowfall to rainfall is shifting towards an increasing rainfall component at mid- and lower elevations, resulting in decreased snowpack, earlier melt and respective hydrological consequences (cf. Stewart 2009).

Using ice cores from the Dasuopu glacier, Duan et al. (2006) detected a decline of monsoonal precipitation by c. 20 % over the twentieth century for the central Himalaya. However, an analysis of precipitation data (1959–1994) in Nepal did not reveal any significant long-term trends, but a downward trend after 1990 (Shrestha et al. 2000). Pronounced spatial variation within the Nepal Himalaya and a general slight positive trend in annual precipitation are indicated by station data for the period 1976–2005 (Practical Action Nepal Office 2009). Particularly for western Nepal, an enhanced frequency of winter and pre-monsoon drought events in recent decades has been reported by Wang et al. (2013). A decrease of precipitation potentially leads to enhanced drought stress for mountain biota, particularly in the pre-monsoon season, when high-temperature trends increase evapotranspiration rates. In Bhutan, the analysis of available observations showed largely random rainfall fluctuations with no detectable systematic change (Tse-ring et al. 2010). Likewise, no statistically significant trends of annual precipitation rates could be detected in the eastern Indian Himalaya (Jain et al. 2013). Mostly increasing trends, albeit not always statistically significant, were found in the eastern Chinese Himalaya and the central and eastern Tibetan Plateau (Wu et al. 2007; You et al. 2007; Xu et al. 2008), in particular for annual, winter and spring precipitation (Qin et al. 2010). A recent study in the Hengduan Mountains for the period 1960–2008 confirmed the pattern of non-significant increasing trends for annual, spring, autumn and winter precipitation and a decreasing trend of summer precipitation, but concurrently a high inter-decadal variability (Li et al. 2011).

1.2.2 Impact of Climate Change on Glaciers

The Hindu Kush-Himalayan mountain system accommodates the highest mountain glacier concentration outside of the polar regions, with a total of about 38,000 glaciers covering an area of more than 44,000 km^2 (Bajracharya and Shrestha 2011; Pfeffer et al. 2014; Mayer and Lambrecht 2015). The glacierized area includes several of the largest mountain glaciers of the world, some of them reaching more than 70 km in length. In general, glaciers are considered key indicators of recent climate change. Measured changes in glacier length, area, volume and mass provide evidence that almost all glaciers worldwide continue to shrink (Vaughan et al. 2013). The largely homogeneous global trend of glacier retreat and the increasing ice loss during the last two decades leave no doubt about the fact that the climate is changing at a global scale. Snow and ice disappearance has serious consequences at local to global scales, e.g. for the natural hazard situation, for societies dependent on glacier melt water, for continental-scale water supply and for global sea level fluctuations (WGMS 2008). Glaciers will continue to shrink in the future even without further climate warming since current glacier extents are out of balance with current climatic conditions (Vaughan et al. 2013).

Despite the robust evidence of global glacier shrinkage and a notable contribution of mass loss from glaciers in Asian mountains to global ice loss (Gardner et al. 2013), non-uniform regional patterns of changes in glacier length, area and mass were observed in the Hindu Kush-Himalayan mountain system. On average, the mass budgets of Himalayan glaciers (Bhutan, China, India, Nepal, Pakistan) have been negative for the past five decades (Fig. 1.3), with glaciers in the Himalaya and in the Hindu Kush showing distinct mass losses, while those in the Karakoram are close to balance (Bolch et al. 2012; Kääb et al. 2012; Jiménez Cisneros et al. 2014). However, most of the larger Karakoram glaciers had a net retreat between the 1920s and 1980s, contributing to the ice cover decline since the Little Ice Age (Hewitt 2014). Glacier mass changes in the Hindu Kush-Himalayan mountain system will inevitably continue. Predictions range between 2 % gain and 29 % loss by 2035 and show a model-mean loss of 45 % by 2100 under the RCP4.5 scenario (Radic et al. 2014). Although all models project mass loss in coming decades, a complete region-wide glacier disappearance can be ruled out with high certainty, even by 2100 (Bolch et al. 2012). Glaciers of the eastern Himalaya are projected to decline at a much faster rate over the twenty-first century compared to western glaciers of the Hindu Kush and Karakoram (Wiltshire 2014).

While most Himalayan glaciers are retreating at rates comparable to those in other mountain regions of the globe, some large glaciers in the NW Himalaya and Karakoram show inconsistent behaviour as evident from quasi-stability or even slightly positive mass balance in recent years (Hewitt 2005, 2011, 2014; Schmidt and Nüsser 2009; Cogley 2011; Copland et al. 2011; Iturrizaga 2011; Gardelle et al. 2012, 2013; Jacob et al. 2012; Kääb et al. 2012; Bahuguna et al. 2014; Bajracharya et al. 2015). Scherler et al. (2011) inferred from satellite imagery analysis that more than 50 % of Karakoram glaciers were advancing or stable between 2000 and 2008,

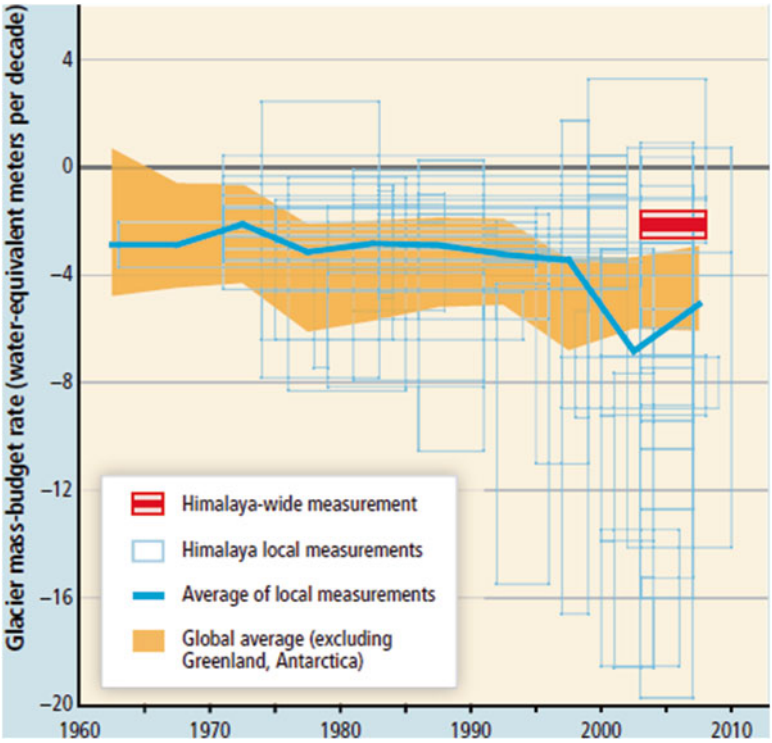

Fig. 1.3 Published glacier mass balance measurements from the Himalaya (Based on Bolch et al. 2012). Satellite laser altimetry was used for region-wide measurement (Kääb et al. 2012) (Source: Jimenez Cisneros et al. 2014)

in line with a descending trend of the equilibrium-line altitude modelled by Fujita and Nuimura (2011) for the period 1976–1995, an increase of snow cover between 2000 and 2009 over the Hunza Basin (Tahir et al. 2011), and statistically insignificant long-term trends of outflow from the Upper Indus Basin (Reggiani and Rientjes 2015). In a recent study of more than 1200 Karakoram glaciers, Rankl et al. (2014) confirmed the vast majority to have stable terminus positions and to show anomalous behaviour in comparison to glacier recession and thinning in adjacent mountain ranges. The so-called Karakoram anomaly is to be attributed to positive precipitation trends, decreasing summer temperatures and the topographical setting and high-altitude origin of glaciers, associated with different styles of nourishment, thermal regimes and a rather high percentage of surge-type glaciers (Hewitt 2014). The dominance of non-monsoonal winter precipitation exerts an additional influence on the glacier response to climate warming (cf. Kapnick et al. 2014). Another recent study on glacier thickness changes over the entire Pamir-Karakoram-Himalaya arc based on ICES at satellite altimetry (Kääb et al. 2015) revealed that the centre of the mass gain anomaly is located northeast of the Karakoram in the western Kunlun Shan, while the most negative rates of region-wide glacier elevation

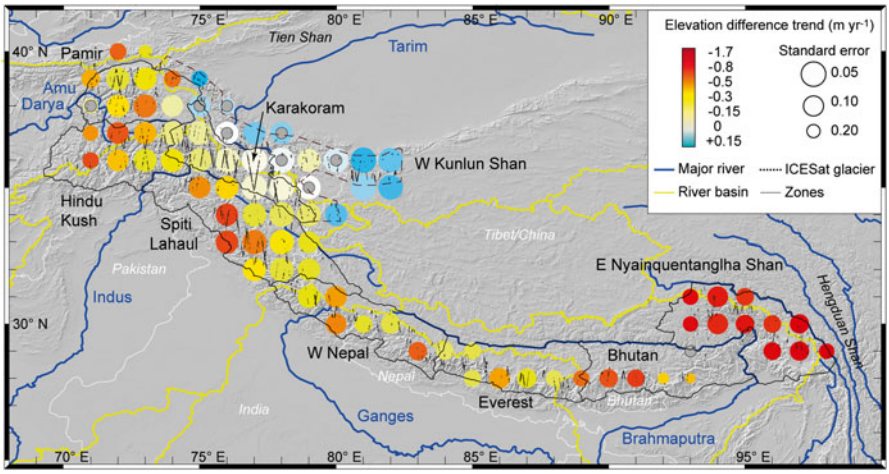

Fig. 1.4 Trends of glacier elevation differences over the Pamir-Karakoram-Himalaya arc during 2003–2008, based on ICESat satellite altimetry. Trends for all cells (*coloured data circles*) are statistically significant except for the cells that are marked with grey centres (Source: Kääb et al. 2015)

change are observed in SE Tibet and in the eastern Chinese Himalaya (Fig. 1.4). Current positive annual mass budgets for the western Kunlun Shan glaciers are also reported by Bao et al. (2015).

Proceeding from the centre of mass gain anomaly to the S and SE along the Himalayan arc, widespread glacial retreat is prevalent in the subsequent mountain regions (Bhambri and Bolch 2009; Bolch et al. 2012; Kulkarni and Karyakarte 2014; Racoviteanu et al. 2014). Shrinking rates are regionally variable, but accelerating, corresponding approximately to a W-E gradient of increasingly negative changes in length, area and mass budgets of glaciers. This spatial pattern supports the notion that monsoon-affected glaciers are more sensitive to climate warming than winter-accumulation-type glaciers (Fujita 2008). In the Indian trans-Himalaya of Ladakh, Schmidt and Nüsser (2012) assessed a shrinkage rate of the glaciated area of 0.3 % year^{-1} for small high-altitude glaciers over the last four decades. Average area loss rates of smaller Himalayan glaciers in Jammu and Kashmir, Himachal Pradesh and Uttarakhand reached up to 0.9 % year^{-1} over the same time period, with notable inter-decadal and regional variability (Kulkarni et al. 2007; Bhambri et al. 2011; Pandey et al. 2011). More recent area and mass loss rates (since 1990 and 2000) are usually higher compared to previous decades (Berthier et al. 2007; Bhambri et al. 2011; Vincent et al. 2013). The loss of glacierized areas is estimated to be more than 10 % during the last four to five decades (Kulkarni and Karyakarte 2014). Rates of glacier area decrease in the West and Central Himalaya in India translate into common front retreat rates of 20–30 m year^{-1}; in some cases, even more than 40 or 60 m year^{-1} were reported (Bhambri and Bolch 2009; Kamp et al. 2011; Mehta et al. 2011; Bhambri et al. 2012; Mal and Singh

2013; Kulkarni and Karyakarte 2014; Mal et al. 2016). Available glaciological mass balance data show consistently negative values (Vincent et al. 2013; Dobhal and Pratap 2015).

In the central and eastern Himalaya, area changes and mass budgets have been largely negative as well over the last decades. Glaciers in Nepal show a clear tendency to shrink which has resulted in an overall loss of glacierized areas of c. 20 % (Kulkarni et al. 2007; Bajracharya et al. 2011; Shrestha and Aryal 2011). Recession processes are reported from a variety of catchments (e.g. Fujita et al. 1997, 2001; Salerno et al. 2008; Fujita and Nuimura 2011; Baral et al. 2014; Shangguan et al. 2014; Thakuri et al. 2014). In Khumbu Himal (E Nepal), mass loss rates between 0.26 and 0.40 m water equivalent year^{-1} were detected for the last two decades (Bolch et al. 2011; Nuimura et al. 2012; Gardelle et al. 2013). Bolch et al. (2008) determined an average shrinkage rate of the glaciated area of 0.12 % year^{-1} between 1962 and 2005, with a higher rate of 0.24 % year^{-1} for clean ice glaciers. Racoviteanu et al. (2015) assessed an area loss of 0.43 % in eastern Nepal and Sikkim during the last decade, with retreat rates of clean glaciers (0.7 % year^{-1}) being almost double than those of debris-covered glaciers. The potential of debris cover to slow down retreat rates (also noted for the W Himalaya; Chand et al. 2016) is highlighted by Scherler et al. (2011; but see also Bolch et al. 2011; Kääb et al. 2012). A prominent example of rapid glacier retreat in Khumbu Himal is the Imja glacier, which has been shown to retreat by 74 m year^{-1} between 2000 and 2007 and to feed the growth of a hazardous glacial lake (Ren et al. 2006; Bajracharya and Mool 2010). A recent study identified the West Lhotse Glacier in Khumbu, which lost 55 % of its area between 1890 and 2010, as the fastest-retreating glacier of the Hindu Kush-Himalayan region (Bajracharya et al. 2015). Numerous lower elevation small glaciers have already completely disappeared in Khumbu since 1956 (Byers 2007).

Rapid shrinkage has been also assessed for the majority of glaciers in Sikkim (Raina 2009; Basnett et al. 2013) and Bhutan, with a recent area loss trend of 0.64 % year^{-1} (Ageta et al. 2003; Rupper et al. 2012; Bajracharya et al. 2014). The eastern Chinese Himalayan regions are as well characterized by rather high rates of glacier decline and extensive area and mass losses (Yao et al. 2007, 2012; Neckel et al. 2014; Kääb et al. 2015), with front retreat rates of up to more than 60 m year^{-1} (Nie et al. 2010). Thus, most of the West, Central and East Himalayan glaciers show a consistent pattern of recession processes over recent decades. A sustained mass loss is projected through the twenty-first century (e.g. Shea et al. 2015), further enhanced by the growing burden of deposited soot on glacier surfaces (cf. Yasunari et al. 2010; Qian et al. 2011), implying severe impacts on water availability during dry seasons. Peak-melt water dates have been projected between mid- and late centuries (Immerzeel et al. 2013), followed by a decrease in total annual melt water yield. Reduced seasonal water supply would adversely affect agriculture, hydropower generation and local water resources availability, threatening food security of millions of lowland people, in particular in the Indus and Brahmaputra basins (Immerzeel et al. 2010).

1.2.3 Climate Change and Vegetation Dynamics

Climate change is one of the major drivers of mountain ecosystem dynamics, most likely only exceeded in its impact by land use changes. However, compared to the wealth of literature pertaining to the state and fate of Himalayan glaciers, the number of available studies on climate change-induced vegetation dynamics, addressed in the third section of this book, is surprisingly low. From this it follows that accumulated knowledge of the alteration of Himalayan ecosystems in terms of plant cover, plant functional type dominance, species distributions, species composition, community structure, biomass or phenology is still profoundly deficient. In view of the high vulnerability of mountain ecosystems to climate change that will be an increasingly powerful stressor in the second half of the twenty-first century, we urgently need more information on vegetation and ecosystem responses to climatic change to be provided by field sampling (e.g. by the Himalayan GLORIA subnetwork; Salick et al. 2014), remote sensing, experimental studies and modelling approaches. Strongly reinforced research efforts and the dissemination of results are an indispensable condition for the development of appropriate management strategies directed towards the maintenance of mountain ecosystem integrity and the continuous provision of essential goods and services.

The Hindu Kush-Himalayan mountain system represents a major centre of global biodiversity. Four of the 34 global biodiversity hotspots and numerous ecoregions with significant conservation value are located in the Greater Himalayan region (Xu et al. 2009; Pandit et al. 2014). Sandwiched between the two mega-diverse countries India and China, the eastern Himalaya alone harbours more than 7000 plant species, 175 mammal species and more than 500 bird species, many of them endemic species with restricted distribution (Chettri et al. 2008). The total number of vascular plants in the Hindu Kush-Himalayan region is estimated to range between 8000 and 10,600, with a proportion of endemic plants increasing from 30 % in the W Himalaya to 40 % in the E Himalaya (Pandit and Kumar 2013; Pandit et al. 2014). Species with spatially restricted populations will be affected in particular by large magnitudes of climate change, fragmenting populations and reduced vigour and viability of species. However, negative impacts of climate change such as increasing temperature variability and declining precipitation during the dry season will affect the majority of species through range contractions as suggested by modelling studies (Li et al. 2013; Zhang et al. 2014).

Ongoing climatic changes will already have triggered shifts in species distributions and abundances in the Himalaya, widely without having been noticed or documented by science. Telwala et al. (2013) conducted the first detailed study of climate-induced species distribution changes, providing evidence of warming-driven elevational range shifts in 87 % of 124 studied endemic plant species in alpine Sikkim over the last 150 years. Species' upper elevation limits shifted between 23 and 998 m. The study suggests that present-day plant assemblages and community structures are definitely different from those of the nineteenth century. Upslope range expansion of woody species from dwarf-scrub communities into

Fig. 1.5 Colonization of recently deglaciated terrain by *Pinus wallichiana* in the foreland of Gangapurna glacier (3700 m), Manang, Nepal, Himalaya (Source: Udo Schickhoff 2013)

alpine meadows is attributed by Telwala et al. (2013) to climate warming. In NW Yunnan, shrub encroachment of alpine meadows was found to be influenced also by land use change (burning cessation, grazing effects) and shrub autocatalysis (Brandt et al. 2013). Land use change, in turn, plays a major role in hitherto documented tree line shifts (e.g. Baker and Moseley 2007). Anthropogenic treelines, i.e. treelines lowered from their natural altitudinal position by human impact, are predominant in the Himalaya (Schickhoff 2005). Upslope movement of these treelines is rather related to effects of land use change than to climatic changes. Near-natural Himalayan treelines are usually developed as krummholz treelines, which were found to be relatively unresponsive to a warming climate in the short term. However, a widespread treeline advance is most likely in the medium and long term considering the current intense recruitment of treeline trees within the treeline ecotone and beyond (Schickhoff et al. 2015; 2016 and references therein; Schwab et al. 2016, this volume). The current glacier retreat involves a large increase of recently deglaciated terrain which represents a highly dynamic alpine habitat. Receding glaciers have induced vegetation successions on glacier forelands (Fig. 1.5), which have been hardly addressed to date. Apart from a recent detailed summary of plant succession stages in glacial forelands in Langtang/Helambu (Nepal) (Miehe 2015), only preliminary studies are available analysing the colonization of glacier forelands by pioneer species such as *Pinus wallichiana* (Mong and Vetaas 2006; Vetaas 2007; Bisht et al. 2016).

Species-specific changes in phenological patterns belong to the inevitable consequences of climatic changes, potentially disrupting life cycles and interactions between species. Respective observations in the Himalaya are limited, but indicate

large-scale changes. Several species of rhododendrons are reported to currently flower a month earlier than in the past (Xu et al. 2009). Based on satellite-derived NDVI datasets, Shrestha et al. (2012) found an advancement of the start of the growing season by 4.7 days between 1982 and 2006, in line with an overall greening trend in NDVI magnitude and an earlier green-up in most parts of the Hindu Kush-Himalayan region (Panday and Ghimire 2012).

Changing species distributions, dynamics in treeline ecotones and glacier forelands and phenological changes represent responses to current climate change that will modify structure, composition and functioning of Himalayan ecosystems. It is not very likely that the capacity for natural adaptation will be sufficient to cope with the above-average rates and magnitudes of climate change projected for the twenty-first century without biodiversity decline, loss of species and impairment of ecosystem services. This will necessitate human-assisted adaptation, including large-scale habitat restoration, expansion of protected area networks and the reduction of non-climate stressors.

References

Ageta Y, Naito N, Iwata S, Yabuki H (2003) Glacier distribution in the Himalayas and glacier shrinkage from 1963 to 1993 in the Bhutan Himalayas. Bull Glaciol Res 20:29–40

Anderson JT, Panetta AM, Mitchell-Olds T (2012) Evolutionary and ecological responses to anthropogenic climate change. Plant Physiol 160:1728–1740

Archer DR, Fowler HJ (2004) Spatial and temporal variations in precipitation in the Upper Indus Basin, global teleconnections and hydrological implications. Hydrol Earth Syst Sci Discuss 8:47–61

Attri SD, Tyagi A (2010) Climate profile of India. Environment Monitoring and Research Center, India Meteorological Department, New Delhi

Bahuguna IM, Rathore BP, Brahmbhatt R, Sharma M, Dhar S, Randhawa SS, Kumar K, Romshoo S, Shah RS, Ganjoo K, Ganjoo RK, Ajai (2014) Are the Himalayan glaciers retreating? Curr Sci 106:1008–1013

Bajracharya SR, Mool P (2010) Glaciers, glacial lakes and glacial lake outburst floods in the Mount Everest region, Nepal. Ann Glaciol 50:81–86

Bajracharya SR, Shrestha B (2011) The status of glaciers in the Hindu Kush-Himalayan region. International Centre for Integrated Mountain Development (ICIMOD), Kathmandu

Bajracharya SR, Maharjan SB, Shrestha F (2011) Glaciers shrinking in Nepal Himalaya. In: Blanco J, Kheradmand H (eds) Climate change: geophysical foundations and ecological effects. InTech, Rijeka, pp 445–458

Bajracharya SR, Maharjan SB, Shrestha F (2014) The status and decadal change of glaciers in Bhutan from the 1980s to 2010 based on satellite data. Ann Glaciol 55:159–166

Bajracharya SR, Maharjan SB, Shrestha F, Guo W, Liu S, Immerzeel W, Shrestha B (2015) The glaciers of the Hindu Kush Himalayas: current status and observed changes from the 1980s to 2010. Int J Water Resour Dev 31:161–173

Baker BB, Moseley RK (2007) Advancing treeline and retreating glaciers: implications for conservation in Yunnan, P.R. China. Arct Antarct Alp Res 39:200–209

Bao WJ, Liu SY, Wei JF, Guo WQ (2015) Glacier changes during the past 40 years in the West Kunlun Shan. J Mt Sci 12:344–357

Baral P, Kayastha RB, Immerzeel WW, Pradhananga NS, Bhattarai BC, Shahi S, Galos S, Springer C, Joshi SP, Mool PK (2014) Preliminary results of mass-balance observations of Yala Glacier

and analysis of temperature and precipitation gradients in Langtang Valley, Nepal. Ann Glaciol 55:9–14
Basistha A, Arya DS, Goel NK (2009) Analysis of historical changes in rainfall in the Indian Himalayas. Int J Climatol 29:555–572
Basnett S, Kulkarni AV, Bolch T (2013) The influence of debris cover and glacial lakes on the recession of glaciers in Sikkim Himalaya, India. J Glaciol 59:1035–1046
Beniston M (2000) Environmental change in mountains and uplands. Arnold, London
Beniston M (2006) Mountain weather and climate: a general overview and a focus on climatic change in the Alps. Hydrobiologia 562:3–16
Beniston M (2012) Is snow in the Alps receding or disappearing? Wiley Interdiscipl Rev: Clim Change 3:349–358
Berthier E, Arnaud Y, Kumar R, Ahmad S, Wagnon P, Chevallier P (2007) Remote sensing estimates of glacier mass balances in the Himachal Pradesh (western Himalaya, India). Remote Sens Environ 108:327–338
Bhambri R, Bolch T (2009) Glacier mapping: a review with special reference to the Indian Himalayas. Progr Phys Geogr 33:672–704
Bhambri R, Bolch T, Chaujar RK, Kulshreshtha SC (2011) Glacier changes in the Garhwal Himalaya, India, from 1968 to 2006 based on remote sensing. J Glaciol 57:543–556
Bhambri R, Bolch T, Chaujar RK (2012) Frontal recession of Gangotri Glacier, Garhwal Himalayas, from 1965 to 2006, measured through high resolution remote sensing data. Curr Sci 102:489–494
Bhutiyani MR (2016a) Climate change in the northwestern Himalayas. In: Joshi R, Kumar K, Palni LMS (eds) Dynamics of climate change and water resources of northwestern Himalaya. Springer, Cham, pp 85–96
Bhutiyani MR (2016b) Spatial and temporal variability of climate change in high-altitude regions of NW Himalaya. In: Singh RB, Schickhoff U, Mal S (eds) Climate change, glacier response, and vegetation dynamics in the Himalaya. Springer, Cham
Bhutiyani MR, Kale VS, Pawar NJ (2007) Long-term trends in maximum, minimum and mean annual air temperatures across the northwestern Himalaya during the twentieth century. Clim Change 85:159–177
Bhutiyani MR, Kale VS, Pawar NJ (2010) Climate change and the precipitation variations in the northwestern Himalaya: 1866–2006. Int J Climatol 30:535–548
Bisht MPS, Rana V, Singh S (2016) Impact of glacial recession on the vegetational cover of Valley of Flowers National Park (a World Heritage Site), Central Himalaya, India. In: Singh RB, Schickhoff U, Mal S (eds) Climate change, glacier response, and vegetation dynamics in the Himalaya. Springer, Cham
Bocchiola D, Diolaiuti G (2013) Recent (1980–2009) evidence of climate change in the upper Karakoram, Pakistan. Theor Appl Climatol 113:611–641
Bolch T, Buchroithner M, Pieczonka T, Kunert A (2008) Planimetric and volumetric glacier changes in the Khumbu Himal, Nepal, since 1962 using Corona, Landsat TM and ASTER data. J Glaciol 54:592–600
Bolch T, Pieczonka T, Benn DI (2011) Multi-decadal mass loss of glaciers in the Everest area (Nepal Himalaya) derived from stereo imagery. Cryosphere 5:349–358
Bolch T, Kulkarni A, Kääb A, Huggel C, Paul F, Cogley JG, Frey H, Kargel JS, Fujita K, Scheel M, Bajracharya S, Stoffel M (2012) The state and fate of Himalayan glaciers. Science 336:310–314
Borsdorf A, Stötter J, Grabherr G, Bender O, Marchant C, Sanchez A (2015) Impacts and risks of climate change. In: Grover VI, Borsdorf A, Breuste JH, Tiwari PC, Frangetto FW (eds) Impact of global changes on mountains. Responses and adaptations. CRC Press, Boca Raton, pp 33–76
Brandt JS, Haynes MA, Kuemmerle T, Waller DM, Radeloff VC (2013) Regime shift on the roof of the world: alpine meadows converting to shrublands in the southern Himalayas. Biol Conserv 158:116–127

Byers AC (2007) An assessment of contemporary glacier fluctuations in Nepal's Khumbu Himal using repeat photography. Himal J Sci 4:21–26

Byers AC, Price LW, Price MF (2013) Introduction to mountains. In: Price MF, Byers AC, Friend DA, Kohler T, Price LW (eds) Mountain geography: physical and human dimensions. Univ California Press, Berkeley, pp 1–10

Chand P, Sharma MC, Prasad RN (2016) Heterogeneity in fluctuations of glacier with ice-cover, debris-cover and proglacial-lake in the Upper Ravi Basin, Himachal Himalaya (India) during the past four decades (1971–2013). In: Singh RB, Schickhoff U, Mal S (eds) Climate change, glacier response, and vegetation dynamics in the Himalaya. Springer, Cham

Chaudhry QUZ, Mahmood A, Rasul G, Afzaal M (2009) Climate change indicators of Pakistan. Technical report no. PMD-22/2009, Pakistan Meteorological Department, Islamabad

Chen IC, Hill JK, Ohlemüller R, Roy DB, Thomas CD (2011) Rapid range shifts of species associated with high levels of climate warming. Science 333:1024–1026

Chettri N, Shakya B, Thapa R, Sharma E (2008) Status of a protected area system in the Hindu Kush-Himalayas: an analysis of PA coverage. Int J Biodivers Sci Manag 4:164–178

Christensen JH, Kanikicharla KK, Aldrian E,An SI, Cavalcanti IFA, de Castro M, Dong W, Goswami P, Hall A, Kanyanga JK, Kitoh A, Kossin J, Lau NC, Renwick J, Stephenson DB, Xie SP, Zhou T (2013) Climate phenomena and their relevance for future regional climate change. In: IPCC, Climate change 2013: the physical science basis. Contribution of working group I to the fifth assessment report of the Intergovernmental Panel on Climate Change. Cambridge Univ Press, Cambridge, pp 1217–1308

Cogley JG (2011) Present and future states of Himalaya and Karakoram glaciers. Ann Glaciol 52:69–73

Copland L, Sylvestre T, Bishop MP, Shroder JF, Seong YB, Owen LA, Bush A, Kamp U (2011) Expanded and recently increased glacier surging in the Karakoram. Arct Antarct Alp Res 43:503–516

Dagvadorj D, Natsagdorj L, Dorjpurev J, Namkhainyam B (2009) Mongolian assessment report on climate change 2009. Ministry of Environment, Nature and Tourism, Mongolia

Dash SK, Jenamani RK, Kalsi SR, Panda SK (2007) Some evidence of climate change in twentieth-century India. Clim Change 85:299–321

Dash SK, Kulkarni MA, Mohanty UC, Prasad K (2009) Changes in the characteristics of rain events in India. J Geophys Res Atmos 114:D10109. doi:10.1029/2008JD010572

de Jong C (2015) Challenges for mountain hydrology in the third millennium. Front Environ Sci 3:38. doi:10.3389/fenvs.2015.00038

Diaz HF, Bradley RS (1997) Temperature variations during the last century at high elevation sites. Clim Change 36:253–279

Diaz HF, Grosjean M, Graumlich L (2003) Climate variability and change in high elevation regions: past, present and future. In: Diaz HF (ed) Climate variability and change in high elevation regions: past, present and future. Kluwer, Dordrecht, pp 1–4

Dimri AP, Dash SK (2012) Wintertime climatic trends in the western Himalayas. Clim Change 111:775–800

Diodato N, Bellocchi G, Tartari G (2011) How do Himalayan areas respond to global warming? Int J Climatol 32:975–982

Dobhal DP, Pratap B (2015) Variable response of glaciers to climate change in Uttarakhand Himalaya, India. In: Joshi R, Kumar K, Palni LMS (eds) Dynamics of climate change and water resources of northwestern Himalaya. Springer, Cham, pp 141–150

Duan K, Yao T, Thompson LG (2006) Response of monsoon precipitation in the Himalayas to global warming. J Geophys Res Atmos 111:D19110. doi:10.1029/2006JD007084

Eriksson M, Xu J, Shrestha AB, Vaidya RA, Nepal S, Sandström K (2009) The changing Himalayas. Impact of climate change on water resources and livelihoods in the greater Himalayas. ICIMOD, Kathmandu

Farhan SB, Zhang Y, Ma Y, Guo Y, Ma N (2015) Hydrological regimes under the conjunction of westerly and monsoon climates: a case investigation in the Astore Basin, northwestern Himalaya. Clim Dynam 44:3015–3032

Fowler HJ, Archer DR (2006) Conflicting signals of climatic change in the Upper Indus Basin. J Climate 19:4276–4293
Fujita K (2008) Effect of precipitation seasonality on climatic sensitivity of glacier mass balance. Earth Planet Sci Lett 276:14–19
Fujita K, Nuimura T (2011) Spatially heterogeneous wastage of Himalayan glaciers. Proc Natl Acad Sci 108:14011–14014
Fujita K, Nakawo M, Fujii Y, Paudyal P (1997) Changes in glaciers in Hidden Valley, Mukut Himal, Nepal Himalayas, from 1974 to 1994. J Glaciol 43:583–588
Fujita K, Kadota T, Rana B, Kayastha RB, Ageta Y (2001) Shrinkage of Glacier AX010 in Shorong region, Nepal Himalayas in the 1990s. Bull Glaciol Res 18:51–54
Gardelle J, Berthier E, Arnaud Y (2012) Slight mass gain of Karakoram glaciers in the early twenty-first century. Nat Geosci 5:322–325
Gardelle J, Berthier E, Arnaud Y, Kääb A (2013) Region-wide glacier mass balances over the Pamir-Karakoram-Himalaya during 1999–2011. Cryosphere 7:1885–1886
Gardner AS, Moholdt G, Cogley JG, Wouters B, Arendt AA, Wahr J, Berthier E, Hock R, Pfeffer WT, Kaser G, Ligtenberg SRM, Bolch T, Sharp MJ, Hagen JO, van den Broeke MR, Paul F (2013) A reconciled estimate of glacier contributions to sea level rise: 2003 to 2009. Science 340:852–857
Gautam MR, Timilsina GR, Acharya K (2013) Climate change in the Himalayas. Current state of knowledge, Policy research working paper 6516. The World Bank, Washington, DC
Gerlitz L, Conrad O, Thomas A, Böhner J (2014) Warming patterns over the Tibetan Plateau and adjacent lowlands derived from elevation- and bias- corrected ERA-Interim data. Clim Res 58:235–246
Giese E, Mossig I, Rybski D, Bunde A (2007) Long-term analysis of air temperature trends in Central Asia. Erdkunde 61:186–202
Goda K, Kiyota T, Pokhrel RM, Chiaro G, Katagiri T, Sharma K, Wilkinson S (2015) The 2015 Gorkha Nepal earthquake: insights from earthquake damage survey. Front Built Environ 1:8. doi:10.3389/fbuil.2015.00008
Gonzalez P, Neilson RP, Lenihan JM, Drapek RJ (2010) Global patterns in the vulnerability of ecosystems to vegetation shifts due to climate change. Global Ecol Biogeogr 19:755–768
Gottfried M, Pauli H, Futschik A, Akhalkatsi M, Barančok P, Benito Alonso JL, Coldea G, Dick J, Erschbamer B, Kazakis G, Krajči J, Larsson P, Mallaun M, Michelsen O, Moiseev D, Moiseev P, Molau U, Merzouki A, Nagy L, Nakhutsrishvili G, Pedersen B, Pelino G, Puscas M, Rossi G, Stanisci A, Theurillat JP, Tomaselli M, Villar L, Vittoz P, Vogiatzakis I, Grabherr G (2012) Continent-wide response of mountain vegetation to climate change. Nat Clim Change 2:111–115
Grabherr G, Gottfried M, Gruber A, Pauli H (1995) Patterns and current changes in alpine plant diversity. In: Chapin FS III, Körner C (eds) Arctic and alpine biodiversity: patterns, causes and ecosystem consequences. Springer, Berlin-Heidelberg, pp 167–181
Grabherr G, Gottfried M, Pauli H (2001) High mountain environment as indicator of global change. In: Visconti G, Beniston M, Iannorelli ED, Barba D (eds) Global change and protected areas. Kluwer, Dordrecht, pp 331–345
Grabherr G, Gottfried M, Pauli H (2010a) Climate change impacts in alpine environments. Geogr Compass 4:1133–1153
Grabherr G, Pauli H, Gottfried M (2010b) A worldwide observation of effects of climate change on mountain ecosystems. In: Borsdorf A, Grabherr G, Heinrich K, Scott B, Stötter J (eds) Challenges for mountain regions – tackling complexity. Böhlau, Wien, pp 49–57
Guhathakurta P, Rajeevan M (2008) Trends in the rainfall pattern over India. Int J Climatol 28:1453–1469
Haeberli W (2013) Mountain permafrost – research frontiers and a special long-term challenge. Cold Reg Sci Technol 96:71–76
Harsch MA, Hulme PE, McGlone MS, Duncan RP (2009) Are treelines advancing? A global meta-analysis of treeline response to climate warming. Ecol Lett 12:1040–1049

Hasson S, Böhner J, Lucarini V (2015) Prevailing climatic trends and runoff response from Hindukush–Karakoram–Himalaya, upper Indus basin. Earth Syst Dyn Discuss 6:579–653
Hewitt K (2005) The Karakoram anomaly? Glacier expansion and the 'elevation effect', Karakoram Himalaya. Mt Res Dev 25:332–340
Hewitt K (2011) Glacier change, concentration, and elevation effects in the Karakoram Himalaya, Upper Indus Basin. Mt Res Dev 31:188–200
Hewitt K (2014) Glaciers of the Karakoram Himalaya: glacial environments, processes, hazards and resources. Springer, Dordrecht
Hijioka Y, Lin E, Pereira JJ, Corlett RT, Cui X, Insarov GE, Lasco RD, Lindgren E, Surjan A (2014) Asia. In: IPCC, Climate change 2014: impacts, adaptation, and vulnerability. Part B: Regional aspects. contribution of working group II to the fifth assessment report of the Intergovernmental Panel on Climate Change. Cambridge University Press, Cambridge, pp 1327–1370
Holtmeier FK (2009) Mountain timberlines. Ecology, patchiness, and dynamics. Springer, Dordrecht
Huber UM, Bugmann HKM, Reasoner MA (eds) (2005) Global change and mountain regions. An overview of current knowledge. Springer, Dordrecht
Immerzeel W (2008) Historical trends and future predictions of climate variability in the Brahmaputra basin. Int J Climatol 28:243–254
Immerzeel WW, Van Beek LP, Bierkens MF (2010) Climate change will affect the Asian water towers. Science 328:1382–1385
Immerzeel WW, Pellicciotti F, Bierkens MFP (2013) Rising river flows throughout the twenty-first century in two Himalayan glacierized watersheds. Nat Geosci 6:742–745
IPCC (2013) Climate change 2013: the physical science basis. Contribution of the working group I to the fifth assessment report of the Intergovernmental Panel on Climate Change. Cambridge University Press, Cambridge
IPCC (2014) Climate change 2014: impacts, adaptation, and vulnerability. Part A: Global and sectoral aspects. Contribution of the working group II to the fifth assessment report of the Intergovernmental Panel on Climate Change. Cambridge University Press, Cambridge
Iturrizaga L (2011) Trends in 20th century and recent glacier fluctuations in the Karakoram mountains. Z Geomorphol Suppl Issues 55:205–231
Ives JD, Messerli B, Spiess E (1997) Mountains of the world – a global priority. In: Messerli B, Ives JD (eds) Mountains of the world – a global priority. Parthenon, New York, pp 1–15
Jacob T, Wahr J, Pfeffer WT, Swenson S (2012) Recent contributions of glaciers and ice caps to sea level rise. Nature 482:514–518
Jain SK, Kumar V, Saharia M (2013) Analysis of rainfall and temperature trends in northeast India. Int J Climatol 33:968–978
Jhajharia D, Singh VP (2011) Trends in temperature, diurnal temperature range and sunshine duration in Northeast India. Int J Climatol 31:1353–1367
Jiménez Cisneros BE, Oki T, Arnell NW, Benito G, Cogley JG, Döll P, Jiang T, Mwakalila SS (2014) Freshwater resources. In: IPCC, climate change 2014: impacts, adaptation and vulnerability. Part A: Global and sectoral aspects. Contribution of working group II to the fifth assessment report of the Intergovernmental Panel on Climate Change. Cambridge University Press, Cambridge, pp 229–269
Jump AS, Huang TJ, Chou CH (2012) Rapid altitudinal migration of mountain plants in Taiwan and its implications for high altitude biodiversity. Ecography 35:204–210
Kääb A, Berthier E, Nuth C, Gardelle J, Arnaud Y (2012) Contrasting patterns of early twenty-first-century glacier mass change in the Himalayas. Nature 488:495–498
Kääb A, Treichler D, Nuth C, Berthier E (2015) Brief communication: contending estimates of 2003–2008 glacier mass balance over the Pamir–Karakoram–Himalaya. Cryosphere 9:557–564
Kamp U, Byrne M, Bolch T (2011) Glacier fluctuations between 1975 and 2008 in the Greater Himalaya Range of Zanskar, southern Ladakh. J Mt Sci 8:374–389

Kapnick SB, Delworth TL, Ashfaq M, Malyshev S, Milly PCD (2014) Snowfall less sensitive to warming in Karakoram than in Himalayas due to a unique seasonal cycle. Nat Geosci 7:834–840

Kattel DB, Yao T (2013) Recent temperature trends at mountain stations on the southern slope of the central Himalayas. J Earth Syst Sci 122:215–227

Khattak MS, Babel MS, Sharif M (2011) Hydro-meteorological trends in the upper Indus River basin in Pakistan. Clim Res 46:103–119

Kohler T, Giger M, Hurni H, Ott C, Wiesmann U, Wymann von Dach S, Maselli D (2010) Mountains and climate change: a global concern. Mt Res Dev 30:53–55

Körner C (2003) Alpine plant life. Functional plant ecology of high mountain ecosystems, 2nd edn. Springer, Berlin

Körner C (2012) Alpine treelines. Functional ecology of the high elevation tree limits. Springer, Basel

Körner C, Ohsawa M, Spehn E, Berge E, Bugmann H, Groombridge B, Hamilton L, Hofer T, Ives J, Jodha N, Messerli B, Pratt J, Price M, Reasoner M, Rodgers A, ThonellJ YM (2005) Mountain systems. In: Hassan R, Scholes R, Ash N (eds) Ecosystems and human well-being: current state and trends, vol 1. Island Press, Washington, DC, pp 681–716

Krishnamurthy V, Ajayamohan RS (2010) Composite structure of monsoon low pressure systems and its relation to Indian rainfall. J Climate 23:4285–4305

Kulkarni A (2012) Weakening of Indian summer monsoon rainfall in warming environment. Theor Appl Climatol 109:447–459

Kulkarni AV, Karyakarte Y (2014) Observed changes in Himalayan glaciers. Curr Sci 106:237–244

Kulkarni AV, Bahuguna IM, Rathore BP, Singh SK, Randhawa SS, Sood RK, Dhar S (2007) Glacial retreat in Himalaya using Indian remote sensing satellite data. Curr Sci 92:69–74

Lacombe G, McCartney M (2014) Uncovering consistencies in Indian rainfall trends observed over the last half century. Clim Change 123:287–299

Lal M (2003) Global climate change: India's monsoon and its variability. J Environ Stud Policy 6:1–34

Le Roux PC, Mc Geoch MA (2008) Rapid range expansion and community reorganization in response to warming. Global Chang Biol 14:2950–2962

Lenoir J, Svenning JC (2015) Climate-related range shifts–a global multidimensional synthesis and new research directions. Ecography 38:15–28

Lenoir J, Gégout JC, Marquet PA, de Ruffray P, Brisse H (2008) A significant upward shift in plant species optimum elevation during the 20th century. Science 320:1768–1771

Li Z, He Y, Wang C, Wang X, Xin H, Zhang W, Cao W (2011) Spatial and temporal trends of temperature and precipitation during 1960–2008 at the Hengduan Mountains, China. Quat Int 236:127–142

Li X, Tian H, Wang Y, Li R, Song Z, Zhang F, Xu M, Li D (2013) Vulnerability of 208 endemic or endangered species in China to the effects of climate change. Reg Environ Chang 13:843–852

Liu X, Chen B (2000) Climatic warming in the Tibetan Plateau during recent decades. Int J Climatol 20:1729–1742

Liu X, Yin ZY, Shao X, Qin N (2006) Temporal trends and variability of daily maximum and minimum, extreme temperature events, and growing season length over the eastern and central Tibetan Plateau during 1961–2003. J Geophys Res Atmos 111:D19109. doi:10.1029/2005JD006915

Liu X, Cheng Z, Yan L, Yin ZY (2009) Elevation dependency of recent and future minimum surface air temperature trends in the Tibetan Plateau and its surroundings. Global Planet Change 68:164–174

Mal S, Singh RB (2013) Differential recession of glaciers in Nanda Devi Biosphere Reserve, Garhwal Himalaya, India. In: Cold and mountain region hydrological systems under climate change: towards improved projections. IAHS Publ 360: 71–76. IAHS Press, Wallingford

Mal S, Singh RB, Schickhoff U (2016) Estimating recent glacier changes in Central Himalaya, India, using remote sensing data. In: Singh RB, Schickhoff U, Mal S (eds) Climate change, glacier response, and vegetation dynamics in the Himalaya. Springer, Cham

Marzeion B, Jarosch AH, Hofer M (2012) Past and future sea-level change from the surface mass balance of glaciers. Cryosphere 6:1295–1322

Mayer C, Lambrecht A (2015) Die Gletscher der Hindukusch-Himalaya Region. In: Lozán JL, Grassl H, Kasang D, Notz D, Escher-Vetter H (eds) Warnsignal Klima. Das Eis der Erde. Wissenschaftliche Auswertungen, Hamburg, pp 130–137

Mehta M, Dobhal DP, Bisht MPS (2011) Change of Tipra glacier in the Garhwal Himalaya, India, between 1962 and 2008. Progr Phys Geogr 35:721–738

Mernild SH, Lipscomb WH, Bahr DB, Radić V, Zemp M (2013) Global glacier changes: a revised assessment of committed mass losses and sampling uncertainties. Cryosphere 7:1565–1577

Messerli B (2012) Global change and the world's mountains: where are we coming from, and where are we going to? Mt Res Dev 32(S1):S55–S63

Miehe G (2015) Glacial foreland successions. In: Miehe G, Pendry CA, Chaudhary R (eds) Nepal: an introduction to the natural history, ecology and human environment of the Himalayas. Royal Botanic Garden Edinburgh, pp 80–90

Mishra A (2014) Changing climate of Uttarakhand, India. J Geol Geosci 3:163. doi:10.4172/2329-6755.1000163

Mong CE, Vetaas OR (2006) Establishment of *Pinus wallichiana* on a Himalayan glacier foreland: stochastic distribution or safe sites? Arct Antarct Alp Res 38:584–592

Nagy L, Böhner J (2015) Climate change. In: Miehe G, Pendry CA, Chaudhary R (eds) Nepal: an introduction to the natural history, ecology and human environment of the Himalayas. Royal Botanic Garden Edinburgh, pp 74–80

Naidu CV, Durgalakshmi K, Muni Krishna K, Ramalingeswara Rao S, Satyanarayana GC, Lakshminarayana P, Malleswara Rao L (2009) Is summer monsoon rainfall decreasing over India in the global warming era? J Geophys Res 114:D24108. doi:10.1029/2008JD011288

Neckel N, Kropáček J, Bolch T, Hochschild V (2014) Glacier mass changes on the Tibetan Plateau 2003–2009 derived from ICESat laser altimetry measurements. Environ Res Lett 9, doi:10.1088/1748-9326/9/1/014009

Nie Y, Zhang Y, Liu L, Zhang J (2010) Glacial change in the vicinity of Mt. Qomolangma (Everest), Central High Himalayas since 1976. J Geogr Sci 20:667–686

Nogués-Bravo D, Araujo MB, Errea MP, Martinez-Rica JP (2007) Exposure of global mountain systems to climate warming during the 21st century. Global Environ Change 17:420–428

Nuimura T, Fujita K, Yamaguchi S, Sharma RR (2012) Elevation changes of glaciers revealed by multitemporal digital elevation models calibrated by GPS survey in the Khumbu region, Nepal Himalaya, 1992–2008. J Glaciol 58:648–656

Palazzi E, Hardenberg J, Provenzale A (2013) Precipitation in the Hindu-Kush Karakoram Himalaya: observations and future scenarios. J Geophys Res Atmos 118:85–100

Palazzi E, von Hardenberg J, Terzago S, Provenzale A (2015) Precipitation in the Karakoram-Himalaya: a CMIP5 view. Clim Dyn 45:21–45

Panday PK, Ghimire B (2012) Time-series analysis of NDVI from AVHRR data over the Hindu Kush–Himalayan region for the period 1982–2006. Int J Remote Sens 33:6710–6721

Pandey AC, Ghosh S, Nathawat MS (2011) Evaluating patterns of temporal glacier changes in Greater Himalayan Range, Jammu & Kashmir, India. Geocarto Int 26:321–338

Pandit MK, Kumar V (2013) Land use and conservation challenges in Himalaya: past, present and future. In: Sodhi NS, Gibson L, Raven PH (eds) Conservation biology: voices from the tropics. Wiley-Blackwell, Chichester, pp 153–163

Pandit MK, Manish K, Koh LP (2014) Dancing on the roof of the world: ecological transformation of the Himalayan landscape. Biol Sci 64:980–992

Parmesan C (2006) Ecological and evolutionary responses to recent climate change. Ann Rev Ecol Evol Syst 37:637–669

Pauli H, Gottfried M, Dirnböck T, Dullinger S, Grabherr G (2003) Assessing the long-term dynamics of endemic plants at summit habitats. In: Nagy L, Grabherr G, Körner C, Thompson DBA (eds) Alpine biodiversity in Europe. Springer, Berlin, pp 195–207

Pauli H, Gottfried M, Dullinger S, Abdaladze O, Akhalkatsi M, Alonso JLB, Coldea G, Dick J, Erschbamer B, Calzado RF, Ghosn D, Holten JI, Kanka R, Kazakis G, Kollar J, Larsson P, Moiseev P, Moiseev D, Molau U, Mesa JM, Nagy L, Pelino G, Puscas M, Rossi G, Stanisci A, Syverhuset AO, Theurillat JP, Tomaselli M, Unterluggauer P, Villar L, Vittoz P, Grabherr G (2012) Recent plant diversity changes on Europe's mountain summits. Science 336:353–355

Pauli H, Gottfried M, Grabherr G (2014) Effects of climate change on the alpine and nival vegetation of the Alps. J Mt Ecol 7(Suppl):9–12

Pepin N, Bradley RS, Diaz HF, Baraer M, Caceres EB, Forsythe N, Fowler H, Greenwood G, Hashmi MZ, Liu XD, Miller JR, Ning L, Ohmura A, Palazzi E, Rangwala I, Schöner W, Severskiy I, Shahgedanova M, Wang MB, Williamson SN, Yang DQ (2015) Elevation-dependent warming in mountain regions of the world. Nat Clim Change 5:424–430

Pfeffer WT, Arendt AA, Bliss A, Bolch T, Cogley JG, Gardner AS, Hagen JO, Hock R, Kaser G, Kienholz C, Miles ES, Moholdt G, Mölg N, Paul F, Sharp MJ (2014) The Randolph glacier inventory: a globally complete inventory of glaciers. J Glaciol 60:537–552

Practical Action Nepal Office (2009) Temporal and spatial variability of climate change over Nepal (1976–2005). Practical Action Nepal Office, Kathmandu

Price MF, Kohler T (2013) Sustainable mountain development. In: Price MF, Byers AC, Friend DA, Kohler T, Price LW (eds) Mountain geography: physical and human dimensions. University of California Press, Berkeley, pp 333–365

Qian Y, Flanner MG, Leung LR, Wang W (2011) Sensitivity studies on the impacts of Tibetan Plateau snowpack pollution on the Asian hydrological cycle and monsoon climate. Atmos Chem Phys 11:1929–1948

Qin J, Yang K, Liang S, Guo X (2009) The altitudinal dependence of recent rapid warming over the Tibetan Plateau. Clim Change 97:321–327

Qin N, Chen X, Fu G, Zhai J, Xue X (2010) Precipitation and temperature trends for the Southwest China: 1960–2007. Hydrol Process 24:3733–3744

Racoviteanu A, Bolch T, Bhambri R, Bajracharya S, Mool P, Chaujar RK, Kargel J, Leonard G, Furfaro R, Kääb A, Rauenfelder R, Sossna I, Kamp U, Byrne M, Kulkarni AV, Baghuna IM, Berthier E, Arnaud Y, Bishop MP, Shroder JF (2014) Himalayan glaciers (India, Bhutan, Nepal): satellite observations of thinning and retreat. In: Kargel JS, Leonard GJ, Bishop MP, Kääb A, Raup BH (eds) Global land ice measurements from space. Springer, Berlin, pp 549–582

Racoviteanu A, Arnaud Y, Williams M, Manley WF (2015) Spatial patterns in glacier area and elevation changes from 1962 to 2006 in the monsoon-influenced eastern Himalaya. Cryosphere 9:505–523

Radić V, Bliss A, Beedlow AC, Hock R, Miles E, Cogley JG (2014) Regional and global projections of twenty-first century glacier mass changes in response to climate scenarios from global climate models. Clim Dyn 42:37–58

Raina VK (2009) Himalayan glaciers: a state-of-art review of glacial studies, glacial retreat and climate change, MoEF discussion paper. Ministry of Environment and Forests, Delhi

Rangwala I, Miller JR (2012) Climate change in mountains: a review of elevation-dependent warming and its possible causes. Clim Change 114:527–547

Rankl M, Kienholz C, Braun M (2014) Glacier changes in the Karakoram region mapped by multimission satellite imagery. Cryosphere 8:977–989

Rasul G, Mahmood A, Sadiq A, Khan SI (2012) Vulnerability of the Indus delta to climate change in Pakistan. Pak J Meteorol 8:89–106

Raza M, Hussain D, Rasul G, Akbar M, Raza G (2015) Variations of surface temperature and precipitation in Gilgit-Baltistan (GB), Pakistan from 1955 to 2010. J Biodivers Environ Sci 6:67–73

Reggiani P, Rientjes THM (2015) A reflection on the long-term water balance of the Upper Indus Basin. Hydrol Res 46:446–462

Ren J, Jing Z, Pu J, Qin X (2006) Glacier variations and climate change in the central Himalaya over the past few decades. Ann Glaciol 43:218–222

Rosenzweig C, Casassa G, Karoly DJ, Imeson A, Menzel A, Rawlins S, Root TL, Seguin B, Tryjanowski P (2007) Assessment of observed changes and responses in natural and managed

systems. In: IPCC, climate change 2007: impacts, adaptation and vulnerability. Contribution of Working Group II to the fourth assessment report of the Intergovernmental Panel on Climate Change, Cambridge University Press, Cambridge, pp 79–131

Rupper S, Schaefer JM, Burgener LK, Koenig LS, Tsering K, Cook ER (2012) Sensitivity and response of Bhutanese glaciers to atmospheric warming. Geophys Res Lett 39:L19503. doi:10.1029/2012GL053010

Salerno F, Buraschi E, Bruccoleri G, Tartari G, Smiraglia C (2008) Glacier surface-area changes in Sagarmatha National Park, Nepal, in the second half of the 20th century, by comparison of historical maps. J Glaciol 54:738–752

Salick J, Ghimire SK, Fang Z, Dema S, Konchar KM (2014) Himalayan alpine vegetation, climate change and mitigation. J Ethnobiol 34:276–293

Scherler D, Bookhagen B, Strecker MR (2011) Spatially variable response of Himalayan glaciers to climate change affected by debris cover. Nat Geosci 4:156–159

Schickhoff U (2005) The upper timberline in the Himalayas, Hindu Kush and Karakorum: a review of geographical and ecological aspects. In: Broll G, Keplin B (eds) Mountain ecosystems. Studies in treeline ecology. Springer, Berlin, pp 275–354

Schickhoff U (2011) Dynamics of mountain ecosystems. In: Millington A, Blumler M, Schickhoff U (eds) Handbook of biogeography. Sage Publication, London, pp 313–337

Schickhoff U, Bobrowski M, Böhner J, Bürzle B, Chaudhary RP, Gerlitz L, Heyken H, Lange J, Müller M, Scholten T, Schwab N, Wedegärtner R (2015) Do Himalayan treelines respond to recent climate change? An evaluation of sensitivity indicators. Earth Syst Dyn 6:245–265

Schickhoff U, Bobrowski M, Böhner J, Bürzle B, Chaudhary RP, Gerlitz L, Lange J, Müller M, Scholten T, Schwab N (2016) Climate change and treeline dynamics in the Himalaya. In: Singh RB, Schickhoff U, Mal S (eds) Climate change, glacier response, and vegetation dynamics in the Himalaya. Springer, Cham

Schmidt S, Nüsser M (2009) Fluctuations of Raikot Glacier during the past 70 years: a case study from the Nanga Parbat massif, northern Pakistan. J Glaciol 55:949–959

Schmidt S, Nüsser M (2012) Changes of high altitude glaciers from 1969 to 2010 in the Trans-Himalayan Kang Yatze Massif, Ladakh, Northwest India. Arct Antarct Alp Res 44:107–121

Schwab N, Schickhoff U, Müller M, Gerlitz L, Bürzle B, Böhner J, Chaudhary RP, Scholten T (2016) Treeline responsiveness to climate warming: insights from a krummholz treeline in Rolwaling Himal, Nepal. In: Singh RB, Schickhoff U, Mal S (eds) Climate change, glacier response, and vegetation dynamics in the Himalaya. Springer, Cham

Serquet G, Marty C, Dulex JP, Rebetez M (2011) Seasonal trends and temperature dependence of the snowfall/precipitation-day ratio in Switzerland. Geophys Res Lett 38:L07703. doi:10.1029/2011GL046976

Settele J, Scholes R, Betts R, Bunn S, Leadley P, Nepstad D, Overpeck JT, Taboada MA (2014) Terrestrial and inland water systems. In: IPCC, climate change 2014: impacts, adaptation and vulnerability. Part A: Global and sectoral aspects. Contribution of working group II to the fifth assessment report of the Intergovernmental Panel on Climate Change. Cambridge University Press, Cambridge, pp 271–359

Shangguan D, Liu S, Ding Y, Wu L, Deng W, Guo W, Wang Y, Xu J, Yao X, Guo Z, Zhu W (2014) Glacier changes in the Koshi River basin, central Himalaya, from 1976 to 2009, derived from remote-sensing imagery. Ann Glaciol 55:61–68

Shea JM, Immerzeel WW, Wagnon P, Vincent C, Bajracharya S (2015) Modelling glacier change in the Everest region, Nepal Himalaya. Cryosphere 9:1105–1128

Shekhar MS, Chand H, Kumar S, Srinivasan K, Ganju A (2010) Climate-change studies in the western Himalaya. Ann Glaciol 51:105–112

Shrestha AB, Aryal R (2011) Climate change in Nepal and its impact on Himalayan glaciers. Reg Environ Chang 11(Suppl. 1):S65–S77

Shrestha AB, Devkota LP (2010) Climate change in the eastern Himalayas: observed trends and model projections. ICIMOD, Kathmandu

Shrestha AB, Wake CP, Mayewski PA, Dibb JE (1999) Maximum temperature trends in the Himalayas and its vicinity: an analysis based on temperature records from Nepal for the period 1971–1994. J Climate 12:2775–2786

Shrestha AB, Wake CP, Dibb JE, Mayewski PA (2000) Precipitation fluctuations in the Nepal Himalaya and its vicinity and relationship with some large scale climatological parameters. Int J Climatol 20:317–327

Shrestha UB, Gautam S, Bawa KS (2012) Widespread climate change in the Himalayas and associated changes in local ecosystems. PLoS One 7:e36741. doi:10.1371/journal.pone.0036741

Singh RB, Kumar P (2014) Climate change and glacial lake outburst floods in Himachal Himalaya, India. In: Singh M, Singh RB, Hassan MI (eds) Climate change and biodiversity. Springer, Tokyo, pp 3–14

Singh RB, Mal S (2014) Trends and variability of monsoon and other rainfall seasons in Western Himalaya, India. Atmos Sci Lett 15:218–226

Singh RB, Kumar S, Kumar A (2016) Climate change in Pindari region, Central Himalaya, India. In: Singh RB, Schickhoff U, Mal S (eds) Climate change, glacier response, and vegetation dynamics in the Himalaya. Springer, Cham

Singh SP, Bassignana-Khadka I, Karky BS, Sharma E (2011) Climate change in the Hindu Kush-Himalayas: the state of current knowledge. ICIMOD, Kathmandu

Sontakke NA, Singh N, Singh HN (2008) Instrumental period rainfall series of the Indian region (AD 1813–2005): revised reconstruction, update and analysis. Holocene 18:1055–1066

Steinbauer MJ, Zeidler J (2008) Climate change in the Northern Areas Pakistan. Impacts on glaciers, ecology and livelihoods. WWF Pakistan, Gilgit

Stewart IT (2009) Changes in snowpack and snowmelt runoff for key mountain regions. Hydrol Process 23:78–94

Tahir AA, Chevallier P, Arnaud Y, Neppel L, Ahmad B (2011) Modeling snowmelt-runoff under climate scenarios in the Hunza River Basin, Karakoram Range, northern Pakistan. J Hydrol 409:104–117

Telwala Y, Brook BW, Manish K, Pandit MK (2013) Climate-induced elevational range shifts and increase in plant species richness in a Himalayan biodiversity epicentre. PLoS One 8:e57103. doi:10.1371/journal.pone.0057103

Terzago S, von Hardenberg J, Palazzi E, Provenzale A (2014) Snowpack changes in the Hindu Kush–Karakoram–Himalaya from CMIP5 global climate models. J Hydrometeorol 15:2293–2313

Thakuri S, Salerno F, Smiraglia C, Bolch T, D'Agata C, Viviano G, Tartari G (2014) Tracing glacier changes since the 1960s on the south slope of Mt. Everest (central southern Himalaya) using optical satellite imagery. Cryosphere 8:1297–1315

Thuiller W (2004) Patterns and uncertainties of species' range shifts under climate change. Global Chang Biol 10:2020–2027

Tse-ring K, Sharma E, Chettri N, Shrestha A (2010) Climate change impact and vulnerability in the eastern Himalayas: synthesis report. ICIMOD, Kathmandu

Vaughan DG, Comiso JC, Allison I, Carrasco J, Kaser G, Kwok R, Mote P, Murray T, Paul F, Ren J, Rignot E, Solomina O, Steffen K, Zhang T (2013) Observations: cryosphere. In: IPCC, climate change 2013: the physical science basis. Contribution of working group I to the fifth assessment report of the Intergovernmental Panel on Climate Change. Cambridge University Press, Cambridge, pp 317–382

Vetaas OR (2007) Global changes and its effect on glaciers and cultural landscapes: historical and future considerations. In: Chaudhary RP, Aase TH, Vetaas OR, Subedi BP (eds) Local effects of global changes in the Himalayas: manang, Nepal. Tribhuvan University Nepal-University Bergen, Norway, pp 23–39

Vincent C, Ramanathan A, Wagnon P, Dobhal DP, Linda A, Berthier E, Sharma P, Arnaud Y, Azam MF, Jose PG, Gardelle J (2013) Balanced conditions or slight mass gain of glaciers in the Lahaul and Spiti region (northern India, Himalaya) during the nineties preceded recent mass loss. Cryosphere 7:569–582

Viviroli D, Dürr HH, Messerli B, Meybeck M, Weingartner R (2007) Mountains of the world, water towers for humanity: typology, mapping, and global significance. Water Resour Res 43:W07447. doi:10.1029/2006WR005653

Walther GR, Post E, Convey P, Menzel A, Parmesan C, Beebee TJC, Fromentin JM, Hoegh-Guldberg O, Bairlein F (2002) Ecological responses to recent climate change. Nature 416:389–395

Walther GR, Beißner S, Pott R (2005) Climate change and high mountain vegetation shifts. In: Broll G, Keplin B (eds) Mountain ecosystems. Studies in treeline ecology. Springer, Berlin, pp 77–96

Wang B, Bao Q, Hoskins B, Wu G, Liu Y (2008) Tibetan Plateau warming and precipitation changes in East Asia. Geophys Res Lett 35:L14702. doi:10.1029/2008GL034330

Wang SY, Yoon JH, Gillies RR, Cho C (2013) What caused the winter drought in western Nepal during recent years? J Climate 26:8241–8256

Wani RA (2014) Historical temporal trends of climatic variables over Kashmir Valley and discharge response to climate variability in upper Jhelum Catchment. In: Singh M, Singh RB, Hassan MI (eds) Climate change and biodiversity. Springer, Tokyo, pp 103–112

WGMS (World Glacier Monitoring Service) (2008) Global glacier changes: facts and figures. UNEP/WGMS, Zurich

Williams RJ, Ferrigno J (2010) Glaciers of Asia. U.S. Geological Survey Professional Paper 1386–F, US Govt Print Office, Washington, DC

Wiltshire AJ (2014) Climate change implications for the glaciers of the Hindu Kush, Karakoram and Himalayan region. Cryosphere 8:941–958

Wu S, Yin Y, Zheng D, Yang Q (2007) Climatic trends over the Tibetan Plateau during 1971–2000. J Geogr Sci 17:141–151

Xu ZX, Gong TL, Li JY (2008) Decadal trend of climate in the Tibetan Plateau – regional temperature and precipitation. Hydrol Process 22:3056–3065

Xu J, Grumbine RE, Shrestha A, Eriksson M, Yang X, Wang Y, Wilkes A (2009) The melting Himalayas: cascading effects of climate change on water, biodiversity, and livelihoods. Conserv Biol 23:520–530

Yang X, Zhang Y, Zhang W, Yan Y, Wang Z, Ding M, Chu D (2006) Climate change in Mt. Qomolangma region since 1971. J Geogr Sci 16:326–336

Yang X, Zhang T, Qin D, Kang S, Qin X (2011) Characteristics and changes in air temperature and glacier's response on the north slope of Mt. Qomolangma (Mt. Everest). Arct Antarct Alp Res 43:147–160

Yang J, Tan C, Zhang T (2013) Spatial and temporal variations in air temperature and precipitation in the Chinese Himalayas during the 1971–2007. Int J Climatol 33:2622–2632

Yao T, Pu J, Lu A, Wang Y, Yu W (2007) Recent glacial retreat and its impact on hydrological processes on the Tibetan Plateau, China, and surrounding regions. Arct Antarct Alp Res 39:642–650

Yao T, Thompson L, Yang W, Yu W, Gao Y, Guo X, Yang X, Duan K, Zhao H, Xu B, Pu J, Lu A, Xiang Y, Kattel DB, Joswiak D (2012) Different glacier status with atmospheric circulations in Tibetan Plateau and surroundings. Nat Clim Chang 2:663–667

Yasunari TJ, Bonasoni P, Laj P, Fujita K, Vuillermoz E, Marinoni A, Cristofanelli P, Duchi R, Tartari G, Lau KM (2010) Estimated impact of black carbon deposition during pre-monsoon season from Nepal Climate Observatory – Pyramid data and snow albedo changes over Himalayan glaciers. Atmos Chem Phys 10:6603–6615

You Q, Kang S, Wu Y, Yan Y (2007) Climate change over the Yarlung Zangbo river basin during 1961–2005. J Geogr Sci 17:409–420

Yunling H, Yiping Z (2005) Climate change from 1960 to 2000 in the Lancang River Valley, China. Mt Res Dev 25:341–348

Zhang MG, Zhou ZK, Chen WY, Cannon CH, Raes N, Slik JW (2014) Major declines of woody plant species ranges under climate change in Yunnan, China. Divers Distrib 20:405–415

Part I
Climate Change

Chapter 2
Recent Climate Change over High Asia

Shabeh ul Hasson, Lars Gerlitz, Udo Schickhoff, Thomas Scholten, and Jürgen Böhner

Abstract Though elevated regions have generally been spotted as climate change hotspots due to amplified signal of change observed over recent decades, such evidence for the Tibetan Plateau and its neighboring regions is supported only by a sparse observational network, less representative for the high-altitude regions. Using a larger database of widely used gridded observations (CRU and UDEL) and reanalysis datasets (NCEP-CFSR, ERA-Interim, and its downscaled variant ERA-WRF) along with high-quality homogeneous station observations, we report recent changes in mainly the mean monthly near-surface air temperature and its elevation dependence, as well as changes in precipitation over the Tibetan Plateau, its neighboring mountain ranges, and the basins of major rivers originating from them. Our station-based analysis suggests a well-agreed warming over and around the Tibetan Plateau, which is more pronounced mainly during winter and spring months and generally in agreement but higher in magnitude than that of previously reported. We found a varying skillset of considered gridded and reanalysis datasets in terms of suggesting robust spatial and elevation-dependent patterns of trends and their magnitudes. The UDEL, ERA-Interim, and CRU datasets, respectively, exhibit high- to medium-level agreement with the station observations in terms of their

S. Hasson • U. Schickhoff • J. Böhner (✉)
CEN Center for Earth System Research and Sustainability,
Institute of Geography, University of Hamburg, Hamburg, Germany
e-mail: juergen.boehner@uni-hamburg.de

L. Gerlitz
Section Hydrology, GFZ German Research Centre for Geosciences,
Potsdam, Germany

T. Scholten
Department of Geosciences, Chair of Soil Science and Geomorphology,
University of Tübingen, Potsdam, Germany

R.B. Singh et al. (eds.), *Climate Change, Glacier Response, and Vegetation Dynamics in the Himalaya*, DOI 10.1007/978-3-319-28977-9_2

trend magnitudes, which are generally underestimated. We found that all datasets agree with station observations as well as among each other for a strongest warming and drying in March over the northwestern region, for wet conditions in May over the southeastern Tibetan Plateau and Myanmar regions, as well as for the general warming pattern. Similarly, a strongest EDW rate per 1000 m elevation found in January is well agreed qualitatively among all datasets, except ERA-WRF. We also confirm high inter-dataset agreement for higher warming rates for highlands (above 2000 m asl) as compared to lowlands in December and January and with a mild agreement during the growing season (April–September). Except for winter months, NCEP-CFSR reanalysis largely contradicts the elevation-dependent warming signal. Our findings suggest that well-agreed likely changes in the prevailing climate will severely impact the geo-ecosystems of the High Asia and will have substantial influence on almost all dimensions of life in the region.

Keywords Climate change • High Asia • Elevation-dependent warming

2.1 Introduction

High-mountain ecosystems are widely recognized as among the most exposed environments to global warming (e.g., Grabherr et al. 2001, 2010a, b; Körner and Ohsawa 2005; Huber et al. 2005; Walther et al. 2005). This is evident by the fact that recently accelerated warming, being spatially heterogeneous and asynchronous among various regions (IPCC 2013), remained significantly higher within many mountain regions of the world than its twentieth-century global mean (e.g., Diaz and Bradley 1997; Shrestha et al. 1999; Beniston 2000; Bolch 2007; Bolch et al. 2012) and that it will most likely remain higher further during the twenty-first century (Nogués-Bravoet al. 2007; Liu et al. 2009; Pepin et al. 2015). The amplified warming in high-mountain areas, often referred to as elevation-dependent warming (EDW), is assumed to be generally due to a differentiated energy balance and its controlling processes (e.g., snow-albedo feedbacks, water vapor changes, latent heat release, surface water vapor, and radiative flux changes). A systematic review and assessment of mechanisms, contributing to an enhanced warming with elevation, is given in Pepin et al. (2015).

An essential prerequisite for the causal analysis of aberrant regional EDW pattern is before all a valid database, representative of the correct magnitude of temperature change signals observed over time in a spatially explicit manner. However, existing long-term meteorological station networks are sparse and further biased with respect to their locations, particularly within the mountainous regions, such as the Tibetan Plateau and its bordering high-mountain ranges of Hindu Kush–Karakoram–Himalaya (HKH). Within HKH and Tibetan Plateau, the available observatories are predominantly located within valley bottoms and thus are of limited representativeness of the actual high-mountain climates. Although the

extension of meteorological networks and the implementation of automated screens have improved the spatial coverage since 1990s, longer time series (i.e., 30 years or more) are still extremely rare. Owing to these limitations, Böhner's (1996) early analysis of temperature trends for 1951–1980 and 1961–1990 periods was based on mostly incomplete monthly time series from 160 almost undocumented meteorological stations, among which only three (19) were above an altitude of 4000 m asl (3000 m asl). Yan and Liu (2014) have considered a slightly better database for their investigation of warming trends over the Tibetan Plateau for 1961–2012 period; however, around 2 million km^2 area of Tibetan Plateau above 4000 m asl has been represented only by 11 (out of 139) meteorological stations, underlining the limited representativeness of the analyzed database for such a huge high-altitude region.

In view of these restrictions on the one hand and diverse needs on spatially explicit climatic information for case studies and climate impact assessments on the other, Qin et al. (2009) have used a validated moderate resolution imaging spectroradiometer (MODIS) mean monthly land surface temperature product, confirming warming magnitudes comparable to those derived from station observations that increase with elevation up to 5000 m asl over the Tibetan Plateau. Alternatively, Gerlitz et al. (2014) have proposed an integration of the observational database with the reanalysis datasets. Using SAGA-GIS-based approaches, Gerlitz et al. (2014) had integrated station observations with the elevation-corrected and bias-adjusted ERA-Interim reanalysis dataset for the overlapping period of record over the domain covering most of the Tibetan Plateau, its adjacent high-mountain ranges and its forelands. The resultant product of daily gridded temperature at 1 km^2 resolution had enabled an in-depth investigation of recent trends in various temperature indices. Differing from Pepin et al. (2015), who argued that reanalysis datasets are not homogenized for climatic trend analysis, Gerlitz et al. (2014) instead suggested a comparable dimension of temperature change between observations and the ERA-Interim reanalysis, though the magnitude of the latter tends to be slightly underestimated in some cases. Investigations of You et al. (2010) likewise confirm the principal suitability of ECMWF reanalysis products for trend analyses. For instance, time series from 71 homogenized meteorological stations and from their collocated 56 grid points from surface ERA-40 reanalysis for the eastern and central Tibetan Plateau region consistently showed a general warming trend, exhibiting also a good agreement for their seasonal and areal averages for 1961–2004 period. In contrast to ERA-Interim reanalysis, You et al. (2010) found that corresponding dataset from the NCEP largely failed to identify a general warming pattern, suggesting that their analysis datasets require a careful selection for the targeted analysis.

In general, differences in the temperature change signal from both the long-term meteorological stations and the reanalysis products illustrate that there is not one truth without uncertainties. For instance, properly homogenized in situ observations from the meteorological stations though undoubtedly are the most valuable and indispensable data source when analyzing climatic variations, their extrapolation for spatial scale investigations as well as for the subsequent findings requires a careful consideration of potential topoclimatic biases that can substantially limit the spatial representativeness (Böhner 1996). On the other hand, reanalysis products,

being increasingly utilized in diverse fields of climate-related research, provide largely consistent areal datasets (at least for time periods with a homogeneous data assimilation scheme), but require a critical assessment in comparison with observations, in view of the structural limitations and sub-grid scale parameterizations applied in the modeling schemes.

Against this background, we see a clear need to take into account a broader database for adequate investigation of climate variations over High Asia. Since temperature along with precipitation is the main driving force for moisture and vegetation distribution and also in perturbing the existing cryosphere of the region, our focus is on these two variables. Therefore, we present a systematic monthly analysis of temperature and precipitation trends, considering a suite of station observations and the widely used interpolated gridded products as well as model-driven reanalysis datasets. Apart from an updated overview of recent temperature and precipitation trends since 1981, our research design particularly attempts to investigate skill of the broader dataset considered here in identifying the EDW signals and its magnitude, meant as a contribution to the current debate about mechanisms and factors causing increased warming rates over high-mountain environments.

The study area covers the entire Tibetan Plateau and its bordering mountain ranges from the Tian Shan in the northwest, the Hindu Kush–Karakoram ranges in the west, and the Himalayas in the south. In order to embed our investigations in a broader spatial context, enabling a sufficient comparison of temperature change signals between the high- and lowlands, the study area also encompasses the major river basins, having their headwaters in High Asia.

2.2 Material and Methods

Observations of monthly mean temperatures are obtained from 55 stations from Gerlitz et al. (2014) and Hasson et al. (2015a) and from the Global Historical Climatology Network (GHCN) Monthly Summaries database up to an altitude above 4700 m asl. We have investigated the internal consistency and homogeneity of the observational datasets by using a penalized maximal F test in RH-TestV3 standardized toolkit (Wang 2008; Wang and Feng 2009), in absence of a reference time series and considering a most conservative threshold of 99 % significance level. Based on our results, 14 stations either with large missing data gaps or statistically identified in homogeneity, including topoclimatically affected valley bottom stations, were excluded from the analysis. Amidst 41 stations considered for our analysis, 25 stations lie above 2000; 18 stations lie above 3000; and 5 stations lie above 4000 m asl. Most of the considered stations are located in the eastern Tibetan Plateau, while five stations are located within central and eastern Himalayas and almost same numbers of stations are located in the Tian Shan.

Since observations used in many studies as well as those analyzed here generally constitute only a sample of unevenly and sparsely distributed stations from the

Tibetan Plateau, featuring severe limitations in further representation of the high-elevated regions, it is most likely that unmonitored regions may attribute to more prominent changes in the climatic pattern as compared to what have been shown by the station observations. Thus, there is an immense need for constructing a complete spatial picture of the climatic variables. In this regard, available datasets of spatially interpolated observations and reanalysis products from numerical models are the most appropriate choice. We have obtained the interpolated gridded monthly mean temperature and precipitation observations from the University of Delaware (UDEL – UDEL_AirT_Precip V3.01) and the Climate Research Unit (CRU – TS3.2) of East Anglia University available at 0.5° resolution. The regionalization procedure performed on these datasets is described in Harris et al. (2014) and Willmott and Matsuura (1998).

We have also obtained two widely used reanalysis datasets: the National Centers for Environmental Prediction (NCEP) Climate Forecast System Reanalysis (CFSR) (NCEP-CSFR) and the European Reanalysis (ERA-Interim) from the European Center for Medium-Range Weather Forecasts (ECMWF). These reanalysis datasets comprise of retrospective-modeled atmospheric fields for discrete troposphere levels and delineated surface climate variables with assimilated conventional observations (e.g., land surface, ship, radiosonde data) and satellite data. The NCEP-CFSR had been performed using a global, high-resolution, coupled atmosphere-ocean-land surface-sea ice system. The atmospheric, oceanic, and land surface output products from the CFSR are available at a horizontal resolution of 0.5° from the National Climatic Data Center (NCDC) and the National Center for Atmospheric Research (NCAR). The modeling procedure and data assimilation scheme used in NCEP-CFSR are described in Saha et al. (2010). The ERA-Interim reanalysis from ECMWF comprises of 6-hourly estimates of meteorological variables in a horizontal discretization of 0.7°, available from 1979 onward. The advanced 4D data assimilation system and the Integrated Forecast System (IFS) are described in Berrisford et al. (2009) and Dee et al. (2011).In view of the relatively coarse resolution of ERA-Interim, we additionally considered its 0.5° resolution derivative, dynamically downscaled by the Weather Research and Forecast (WRF) Model under the Coordinated Regional Downscaling Experiment (CORDEX) South Asia evaluation runs, available for the period 1989–2007.

Most of the station observations on the Tibetan Plateau typically start from the late 1950s (Liu and Chen 2000), while the chosen gridded observations are available since the start of the twentieth century. On the other hand, selected reanalysis datasets are available only since 1979 onward. In view of such data availability, we have selected a common period of 1981–2010 for our analysis in order to choose a consistent period of accelerated warming, which also encompasses the warmest period (1983–2012) in the Northern Hemisphere for the last 1400 years (IPCC 2013).

We have used a widely applied nonparametric Mann–Kendall (MK – Mann 1945; Kendall 1975) statistical trend test to assess the existence of a trend in a time series along with the Theil–Sen (TS – Theil 1950; Sen 1968) slope method to estimate true slope of the existing trend. The MK trend test is insensitive to the type of sample data distribution, missing data gaps, and outliers (Tabari and Talaee 2011;

Bocchiola and Diolaiuti 2013). In view of the sensitivity of MK statistic to sequential dependence properties of a time series, we have applied a pre-whitening procedure by following Zhang et al. (2000) prior to applying MK test. The adopted pre-whitening procedure first identifies optimal negative/positive significant correlations and the existing trend component from a time series in an iterative manner in order to avoid influence of one on the other during the pre-whitening procedure. Using optimal trend and autocorrelation magnitudes, our pre-whitening procedure yields a serially independent time series featuring a same trend as of the original time series. The details of the trend analysis methodology have been discussed in Hasson et al. (2015a).

In view of the large limitations due to regionalization techniques in highly difficult terrain of our study area for the gridded observations and systematic biases in the numerical weather models affecting reanalysis products, we assess the skill of these datasets in suggesting robust pattern of mainly the temperature change and its magnitude against the station observations by comparing their trends at those grid cells collocating with the station sites. Moreover, complementing the work of earlier studies (Diaz and Bradley 1997; Liu and Chen 2000; Liu et al. 2009; Qin et al. 2009), we have explored the elevation dependency of the observed warming signal but over the wider study domain using the updated period of record and from the breadth of analyzed datasets. For this, we have estimated an average rate of warming against 1000 m increase in elevation for each dataset. In order to explicitly show contributions from the low- and highlands to such EDW rate, we estimate it separately for the regions below and above 2000 m asl. A threshold of 2000 m asl to separate highlands from the lowlands has been considered by many studies (Aizen et al. 1997; Liu and Chen 2000; You et al. 2010). Given a huge extent of the investigated area, we assume that a typical latitudinal temperature change gradient and the longitudinal gradient – possibly present due to changes in east–west propagating monsoonal system and in the opposite direction, the westerly disturbances – have either overlaid or masked the EDW specific signal. Therefore, we have performed a multiple linear regression analyses using spatial coordinates and elevation as statistical predictors, in order to disentangle otherwise indiscernible EDW signal.

2.3 Results and Discussion

2.3.1 Warming and Cooling

Our trend analysis of mean monthly near-surface air temperature from the station dataset shows a well-agreed and statistically significant warming over the Tibetan Plateau and in the neighboring regions particularly during the winter and spring months (Table 2.1). Highest warming rates of 2.01–1.74 °C per decade are observed over the Tian Shan station (3639 m asl) in March and April, respectively. Following winter and spring months, monsoonal period experiences highest warming rates

Table 2.1 Warming rates in °C per decade. Stations are listed from highest to lowest elevation (Source: Authors)

Stations	Elev	Jan	Feb	Mar	Apr	May	Jun	Jul	Aug	Sep	Oct	Nov	Dec
Baingoin	4701	1.09	0.73	0.50	0.60	0.26	0.27	0.41	0.46	0.40	0.20	0.92	0.67
Tuotuohe	4535	1.40	1.14	0.72	0.87	0.55	0.38	0.76	0.74	0.72	0.64	0.69	0.85
Nagqu	4508	1.07	0.71	0.55	0.73	0.51	0.43	0.78	0.78	0.66	0.30	0.74	0.95
Madoi	4273	1.61	0.91	0.60	0.75	0.45	0.24	0.82	0.84	1.03	0.21	0.25	0.59
Qumarleb	4176	1.66	0.86	0.40	0.69	0.34	0.25	0.83	0.79	0.87	0.44	0.60	0.88
Darlag	3968	1.06	0.67	0.33	0.77	0.35	0.12	0.81	0.86	0.92	0.00	0.35	0.61
Litang	3950	1.17	0.75	0.44	0.44	0.29	0.00	0.53	0.85	0.63	0.41	0.63	0.63
Dengqen	3874	0.92	0.60	0.50	0.87	0.40	0.15	0.63	0.45	0.56	–0.08	0.50	0.65
Yushu	3717	1.22	0.75	0.59	0.75	0.40	0.31	0.93	1.01	1.03	0.22	0.83	0.95
Lhasa	3650	1.29	0.88	0.79	0.81	0.84	0.51	0.51	0.67	0.78	0.63	1.27	0.81
Tian_shan	3639	0.93	1.62	2.01	1.74	0.75	0.82	0.52	0.33	0.48	0.23	0.89	0.61
Garze	3394	0.87	0.50	0.43	0.40	0.18	0.11	0.64	0.74	0.68	–0.06	0.11	0.52
Deqen	3320	0.84	0.80	0.71	0.91	0.31	0.49	0.81	0.80	0.96	0.49	0.54	0.51
Qamdo	3307	0.85	0.55	0.38	0.50	0.18	0.00	0.63	0.36	0.38	–0.06	0.72	0.59
Gangca	3302	0.81	0.67	0.61	0.76	0.43	0.40	0.82	0.71	0.95	0.24	0.36	0.01
Dulan	3192	0.43	0.74	0.47	0.80	0.41	0.43	0.42	0.48	0.80	0.20	0.14	–0.30
Da qaidam	3174	0.88	1.00	0.79	0.90	0.61	0.82	1.07	0.98	1.22	0.46	0.67	0.13
Wushaoling	3044	0.33	1.17	0.89	0.81	0.33	0.74	0.79	0.48	0.59	0.40	0.46	–0.49
Jiulong	2994	0.68	0.45	0.46	0.63	0.18	0.01	0.40	0.44	0.57	0.37	0.27	0.55
Hezuo	2910	0.75	0.94	0.74	0.69	0.44	0.31	0.76	0.55	0.95	0.38	0.13	0.21
Songpan	2852	0.88	0.75	0.60	0.63	0.40	0.08	0.69	0.91	0.96	0.17	0.21	0.38
Lenghu	2771	0.81	0.94	0.38	0.50	0.05	0.50	0.79	0.50	0.70	0.40	0.49	0.22
Barkam	2666	0.67	0.40	0.38	0.46	0.17	–0.07	0.59	0.62	0.81	0.08	0.12	0.40
Lijing	2394	0.45	0.61	0.56	0.81	–0.13	0.05	0.18	0.31	0.23	0.08	0.35	0.17
Naryn	2041	0.19	0.91	1.21	0.30	0.33	0.47	–0.06	0.01	0.25	0.49	1.25	0.57
Yumenzhen	1527	0.10	1.27	0.91	0.79	0.31	0.83	0.81	0.34	0.34	0.54	1.04	–0.05
Bijie	1511	0.15	1.44	1.00	0.74	0.21	0.06	0.33	0.12	0.77	0.32	0.33	0.07
Jiuquan	1478	–0.21	0.92	0.76	0.69	0.35	0.93	0.65	0.27	0.24	0.52	0.90	–0.13
Otog qi	1381	0.43	1.39	1.12	0.56	0.17	0.72	0.57	0.56	0.47	0.38	0.85	0.37
Hotan	1375	0.71	0.70	1.77	0.89	0.82	1.04	0.56	0.59	0.73	1.03	1.25	0.83
Bayan mod	1329	–0.25	0.79	0.76	0.47	0.20	0.59	0.52	0.38	0.25	0.43	0.71	–0.19
Shache	1232	0.20	0.33	1.41	0.74	0.79	0.78	0.04	0.30	0.42	0.83	0.74	0.31
Bachu	1117	0.09	0.41	1.31	0.71	0.70	0.79	–0.11	0.20	0.22	0.67	0.95	0.16
Kuqa	1100	–0.84	0.11	0.67	0.04	–0.21	0.33	–0.33	–0.45	–0.18	0.14	0.64	–0.49
Ruoqiang	889	–0.09	0.82	1.27	0.75	0.17	1.04	0.47	0.15	0.53	0.65	0.80	0.18
Tikanlik	847	–0.12	0.93	1.03	0.53	0.04	0.85	0.58	0.31	0.61	0.53	0.72	0.02
Patiala	251	–0.16	0.86	1.08	1.31	0.36	–0.40	0.31	0.49	0.09	0.41	0.48	0.25
Hissar	221	0.01	1.15	1.08	1.56	0.88	0.12	0.60	0.45	0.09	0.77	0.27	0.29
New_Delhi	216	–0.15	0.71	0.86	1.09	0.14	–0.40	0.36	0.30	–0.08	0.15	0.12	–0.04
Patna	60	–0.31	0.55	0.61	0.45	0.06	0.14	0.42	0.40	0.49	0.44	0.37	0.13
Gauhati	54	0.24	0.77	0.55	0.47	0.54	0.15	0.52	0.44	0.65	0.43	0.56	0.56

as suggested by most of the stations. During such period, a highest warming rate of 1.22 °C per decade has been observed in September for Da Qaidam station (3174 m asl). Most of the temperature change signals shown in Table 2.1 are found to be statistically significant at 90 % level. We note that warming rates observed here are largely higher than the previously reported warming trends, suggesting a recent amplification of the signal of climate change. Agreed with our findings, Xie et al. (2010) further reported that warming signal in the mean temperature observed here is more pronounced for the minimum temperature rather than for the maximum temperature, resulting in narrowing down of the diurnal temperature range (DTR).

The warming signal over the Tibetan Plateau and over its neighboring regions has also been consistently shown in the past by the paleoclimate data reconstructed from ice cores (Yao et al. 1995).

In contrast to general warming, few stations feature anomalously cooling trends. For instance, around one fourth of the analyzed stations feature cooling tendencies in at least one or more months of the summer monsoonal period or in January and February months, where such an anomaly is mostly observed at lower elevation station, showing no clear relationship with the elevation. The cooling tendencies are likewise suggested by the long-term valley bottom stations within the western Himalayan and Karakoram regions since the second half of the last century as reported by Hasson et al. (2015a), most probably caused by the topographically altered local climate. However, using a suite of high-altitude automated weather stations (2200–4800 m asl) from the same region, Hasson et al. (2015a) suggested even a higher magnitude of cooling tendencies during the monsoon months, speculated to be caused by anthropogenically induced enhanced influence of the monsoonal system along its far northwest margins in addition to the effects of sophisticated local topoclimates.

In order to examine the suitability of gridded observations and the reanalysis datasets, we have compared their trends with the station observations for corresponding locations. Our comparison shows that all datasets generally underestimate the magnitude of station-based trends (Fig. 2.1). The UDEL dataset outperforms all datasets in suggesting comparable trend magnitudes with a relatively little underestimation. This is followed by ERA-Interim reanalysis and CRU, while the NCEP-CFSR performs simply worst in this regard. Such comparisons have suggested that UDEL, CRU, and ERA-Interim datasets have shown at least some skill in emulating the temperature trend over the study domain though a general underestimation of the trend magnitude prevails. In Fig. 2.2, we have summarized the spatially complete picture of trend magnitudes from all gridded and reanalysis dataset covering the whole study domain instead of trends at the select grid cell locations. We also show trends from the station observations for the sake of comparison. We generally found that CRU and ERA-Interim at least follow the monthly pattern of the observations. Their few higher magnitude of temperature trends as compared to station observations indicates areas of prominent change, not represented by the station dataset at all. Nevertheless, all datasets mostly underestimate the trends from the station observations at corresponding locations. The UDEL, NCEP-CFSR, and ERA-WRF datasets suggest relatively a large number of outliers, indicating inconsistent patterns at some locations (Fig. 2.3). Additionally, the UDEL dataset features a very narrow range of temperature change over the study domain.

All gridded and reanalysis datasets consistently exhibit strongest warming rate during the month of March. We note that such strongest warming signal features a positive gradient from east to west and south to north; thus the highest magnitude of warming observed during March is more obvious over the northwest region of the study domain. This signal was not apparent from the station observations since these stations are mostly located in the eastern Tibetan Plateau with almost no information from the northwestern region. The strongest warming signal in the

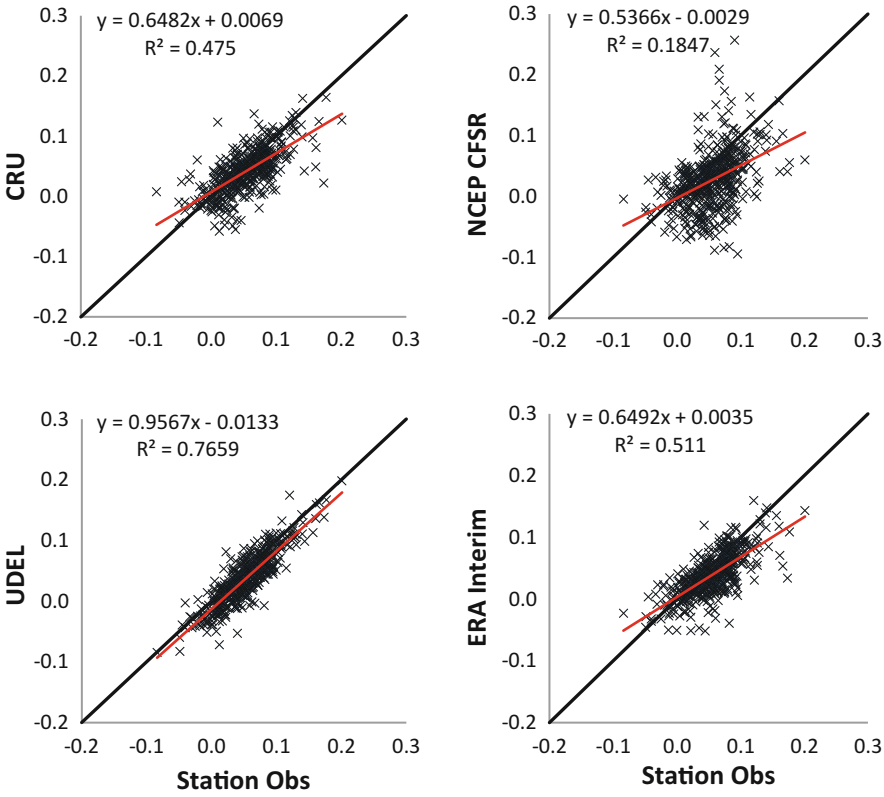

Fig. 2.1 Comparison of mean monthly temperature trend magnitudes between stations and regridded (*left column*) and reanalysis datasets (*right column*) (Source: Jürgen Böhner)

northwestern part during March has also been consistently shown by Hasson et al. (2015a) based on a suite of high-altitude automated weather stations within the western Himalayan and Karakoram regions. The strong warming signal in such regions may also indicate certain changes in mainly the solid moisture regime of the westerly disturbances prevailing therein, which based on the CMIP5 projections is expected to experience an increasing number of dry days during spring season (Hasson et al. 2015b). We note that the ERA-WRF downscaled data exhibits even more pronounced warming during the spring season but less consistent pattern of significant warming for the rest of year as compared to its forcing dataset.

A well-agreed warming signal over and around the Tibetan Plateau mostly during cold season is alarming for the elevated natural resources, as it can exacerbate already evident cryosphere loss, perturbation of subsequent melt runoff availability downstream, mountain ecosystems degradation, and extinction of indigenously dependent endangered species. As a counter effect, spring temperature increase

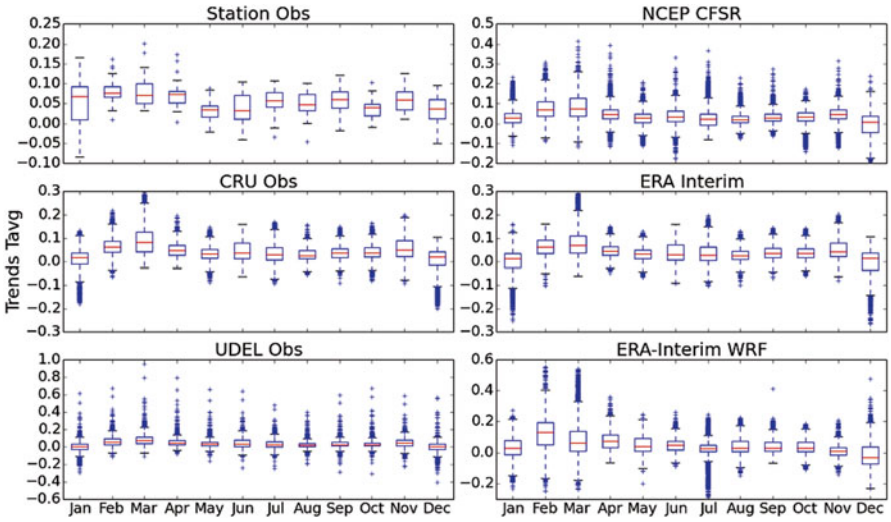

Fig. 2.2 Summary of trend magnitudes from station observations and from datasets covering the whole domain. *Red line* indicates the medians, *box* refers to first and third quartiles (interquartile range – IQR), whiskers are plotted at 1.5 IQR, and beyond this threshold trends are considered as outliers and are shown with *plus sign* (Source: Authors)

most likely promotes tree species recruitment at elevated regions (Camarero and Gutierrez 1999), may shorten the growing season length for mountainous crops, and even can bring more area under cultivation. Similar to the station trends, we also find cooling tendencies in the gridded datasets during the monsoonal period where such tendencies are relatively more pronounced in the reanalysis datasets. Cooling tendencies are almost vanished on an annual time scale.

2.3.2 *Elevation Dependent Warming*

For the station dataset, we have found that rate of warming above 2000 m asl is higher than the rate below this height on an annual time scale (Table 2.2), consistent with reports of EDW findings below and above 2000 m asl by Aizen et al. (1997). In particular, July–September period and December–January period have shown higher mean rates of warming above 2000 m asl than the rates below this height, where such difference was largest in January. We note that the strongest warming rate of 0.32 °C per decade per 1000 m elevation is found in January, while on an annual time scale, such rate is only 0.06 °C per decade. The strongest EDW in January can also be seen clearly from Table 2.1. Consistent to the EDW pattern identified for the mean temperatures here, Liu et al. (2009) have found an EDW

signal for the minimum temperature over and around the Tibetan Plateau, which is also more pronounced during the winter season.

Completing a spatial picture of the scattered station-based temperature change signal, CRU and UDEL gridded observations though quantitatively differ in the magnitude of warming rate against the station observations feature a well-agreed pattern of EDW on a qualitative scale. The CRU dataset suggests higher warming rate for highlands (above 2000 m asl) as compared to lowlands (below 2000 m asl) in the same months as suggested by the station observations but additionally in four months of February, April, June, and November where such warming rate differs only slightly among low- and highlands for the rest of months. The UDEL dataset distinctly showed a higher warming rate for the highlands relative to lowlands throughout the year. Moreover, both datasets suggest strongest rate of EDW for every 1000 m elevation increase during the month of January. On annual time scale, UDEL suggests a similar magnitude of EDW as of station observations, while CRU underestimates it.

Exploiting the reanalysis datasets, we have found that strongest January warming rate for every 1000 m elevation observed from stations and gridded datasets is consistently strongest among the reanalysis datasets (Table 2.2 and Figs. 2.3 and 2.4). On annual time scale, ERA-WRF underestimated the rate of station-based observed EDW; ERA-Interim suggested no trend at all and the NCEP-CFSR inconsistently suggested a cooling trend. Such inconsistent cooling rate by the NCEP-CFSR on an annual time scale has also been observed within a year except during the winter season.

You et al. (2010) have also reported that the NCEP-CFSR largely failed to show a general warming pattern. The ERA-Interim, however, suggested a higher warming rate for highlands than for the lowlands only in January, April, July, and December months. As compared to ERA-Interim, its dynamically downscaled derivative suggested higher warming rates for highlands throughout the year except for March and for the post-monsoon (October and November) months that show an opposite behavior. Analyzing statistically downscaled ERA-Interim reanalysis product, Gerlitz et al. (2014) have consistently found a distinct warming signals during winter and spring seasons with its highest magnitudes over the elevated altitudinal mountain regions. During the post-monsoon season, they also reported that warming signals were instead more pronounced at low elevations. Actually, our findings of an opposite EDW response during early spring and post-monsoon months are consistent among all datasets analyzed here, except for the UDEL and NCEP-CFSR. In contrast, recent findings of Yan and Liu (2014) suggested that EDW signal also exists for the autumn season during 1961–2012 period. Such conflicting findings may arise due to a direct comparison of studies that consider for their analysis either different time spans or a distinct sample size of the available station database with its uneven distribution across the study domain.

The ice core-based reconstructed record though also showed an elevation dependency of the temperature change signal (Thompson et al. 2003), You et al. (2010) cautioned to interpret such findings carefully as they have not found any simple

Table 2.2 Rate of temperature change per decade for above and below 2000 m asl and its elevation dependency for every 1000 m elevation increase (Source: Authors)

Obs	Jan	Feb	Mar	Apr	May	June	July	Aug	Sep	Oct	Nov	Dec	Year
<2000	−0.01	0.82	1.01	0.74	0.35	0.47	0.39	0.30	0.35	0.51	0.67	0.14	0.48
>2000	0.91	0.80	0.64	0.72	0.36	0.31	0.64	0.63	0.73	0.27	0.54	0.47	0.59
Delta 1000	**0.32**	–	–	–	–	–	–	–	–	*−0.07*	–	**0.17**	*0.06*
CRU													
<2000	0.01	0.62	0.87	0.44	0.34	0.43	0.32	0.27	0.35	0.41	0.55	0.01	0.38
>2000	0.48	0.70	0.86	0.62	0.33	0.45	0.44	0.36	0.37	0.38	0.57	0.23	0.48
Delta 1000	**0.15**	*−0.01*	**−0.01**	**0.05**	**0.03**	**0.03**	**0.07**	**0.06**	**0.04**	–	−0.01	**0.04**	**0.04**
UDEL													
<2000	−0.14	0.55	0.81	0.42	0.32	0.39	0.29	0.21	0.30	0.31	0.47	−0.09	0.32
>2000	0.47	0.72	0.87	0.74	0.42	0.45	0.46	0.33	0.38	0.33	0.52	0.24	0.49
Delta 1000	**0.21**	**0.03**	**0.03**	**0.09**	**0.07**	**0.04**	**0.08**	**0.06**	**0.06**	**0.01**	–	**0.09**	**0.06**
NCEP													
<2000	0.24	0.70	0.90	0.48	0.32	0.43	0.28	0.26	0.36	0.34	0.52	−0.06	0.40
>2000	0.63	0.94	0.73	0.48	0.08	0.09	0.14	0.05	0.25	0.17	0.38	0.03	0.33
Delta 1000	**0.14**	**0.05**	**−0.07**	**−0.03**	**−0.06**	**−0.08**	*−0.01*	**−0.04**	–	**−0.07**	**−0.08**	–	**−0.02**
ERA-Interim													
<2000	−0.08	0.63	0.85	0.45	0.33	0.40	0.31	0.28	0.38	0.41	0.56	−0.06	0.37
>2000	0.35	0.59	0.61	0.55	0.27	0.30	0.34	0.22	0.32	0.20	0.32	0.06	0.34
Delta 1000	**0.16**	**−0.02**	**−0.07**	**0.04**	**0.02**	*−0.01*	**0.04**	*0.01*	**0.02**	**−0.06**	**−0.09**	**0.02**	*0.00*
ERA-WRF													
<2000	0.21	1.25	0.88	0.76	0.50	0.47	0.20	0.36	0.39	0.37	0.14	−0.31	0.44
>2000	0.73	1.40	0.66	0.94	0.53	0.55	0.40	0.70	0.45	0.34	−0.05	0.58	0.60
Delta 1000	**0.13**	**−0.03**	**−0.09**	**0.04**	0.01	**0.02**	**0.10**	**0.10**	**0.03**	**0.02**	**−0.06**	**0.23**	0.04

Significant trends at 99 % level are shown in bold, while trends at 90 % level are shown in italic

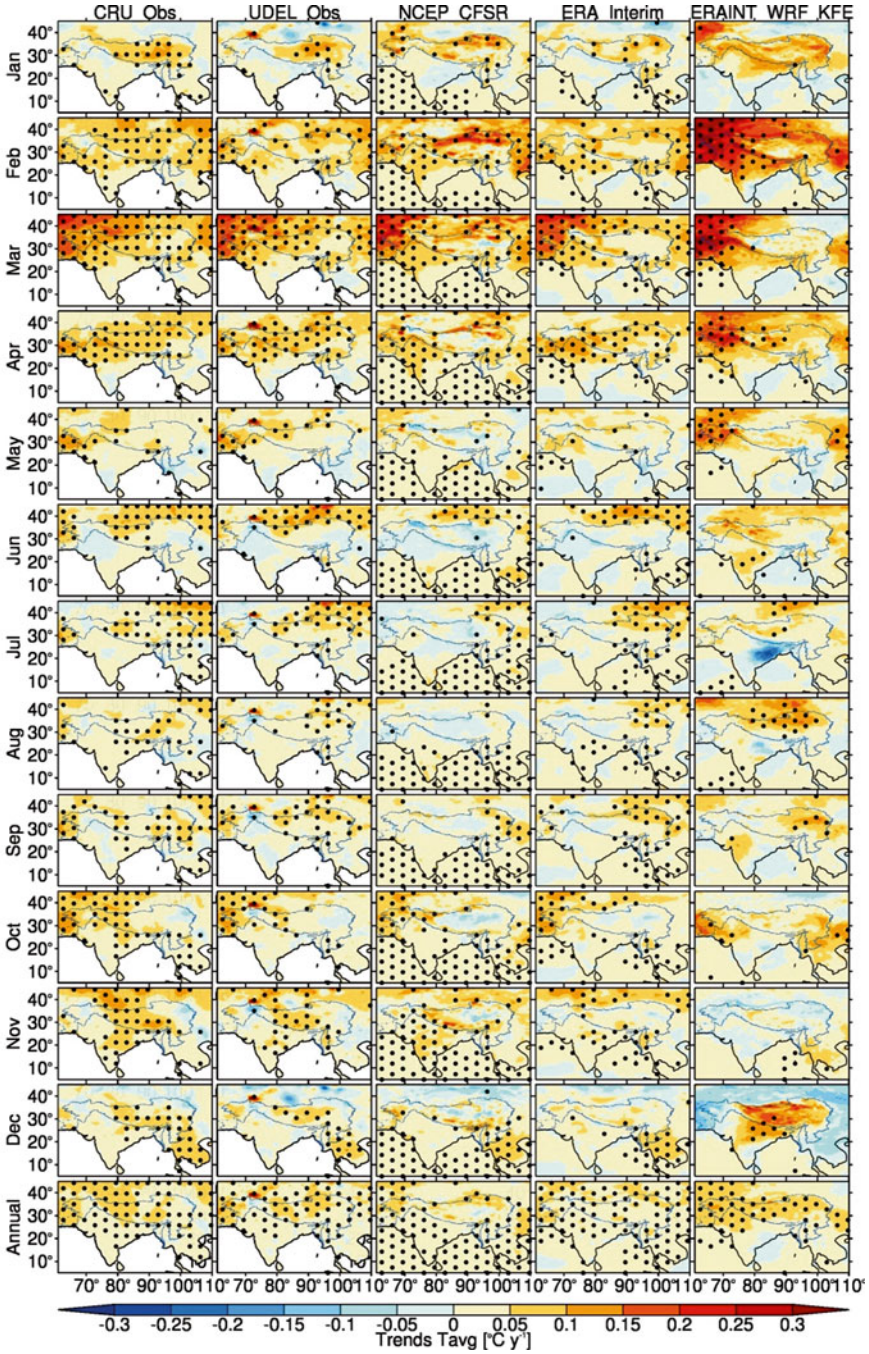

Fig. 2.3 Trend in mean monthly temperatures for all months of the year (*row-wise*) from all datasets considered (*column-wise*). Stipples indicate significant trends at 90 % level or above. *Black line* shows land–sea separation while *blue* polygon indicates the whole HKH and Tibetan Plateau region (Source: Authors)

relationship of seasonal or annual warming with the elevation for the station dataset, for the ERA-Interim, and for the NCEP reanalysis datasets. In contrast, our finding of strongest EDW signal observed in January, which is also well agreed among all datasets (Tables 2.1 and 2.2 and Figs. 2.3 and 2.4), suggested that the EDW signal in You et al. (2010) might have been lost while averaging out datasets into seasons and on annual time scale, underlying the need to perform such an analysis at high-temporal resolution. Nevertheless, our results confirmed that an EDW signal largely exists mainly for the winter months (December and January) among all datasets analyzed here and with a mild agreement during the growing season (April–September), which is also consistent with findings from most of the above mentioned studies.

2.3.3 Wetting and Drying

We have found the spatial patterns of precipitation change generally quite erratic (Fig. 2.5). However, widespread drying tendencies can be noted over most of the study area within the year. On annual time scale, a mild agreement among the datasets exists for the significant precipitation increase over eastern and central parts of the Tibetan Plateau. Consistently, Xu et al. (2008) have also suggested a positive change over most of the Tibetan Plateau. Although Xie et al. (2010) have also found a positive change in precipitation, their findings of a more pronounced increase in winter, followed by spring and summer, are not evident from the gridded and reanalysis datasets. Generally, the annual pattern of change in precipitation is consistent between the CRU and UDEL gridded observations and between all reanalysis datasets. The best agreement among all datasets exists for the precipitation increase over Myanmar region and the southeastern Tibetan Plateau for May.

Furthermore, dataset largely agrees for statistically significant precipitation decrease over the northwestern (HKH) region during March. We note that such region is mainly influenced by the extratropical westerlies, and we speculate that such a decrease in westerly precipitation regime over the northwest region during March may have triggered the strongest temperature increase therein during the same month as noted earlier. The NCEP-CFSR suggests the strongest increase/decrease over parts of the study area during the monsoon period and on annual scale, generally featuring a low agreement with the rest of datasets.

2.4 Conclusions and Outlook

Our station-based analysis suggests a well-agreed warming over and around the Tibetan Plateau, which is more pronounced mainly during winter and spring months and generally in agreement but higher in magnitude than that of previous findings. For the regridded and reanalysis datasets considered in the study, we have found

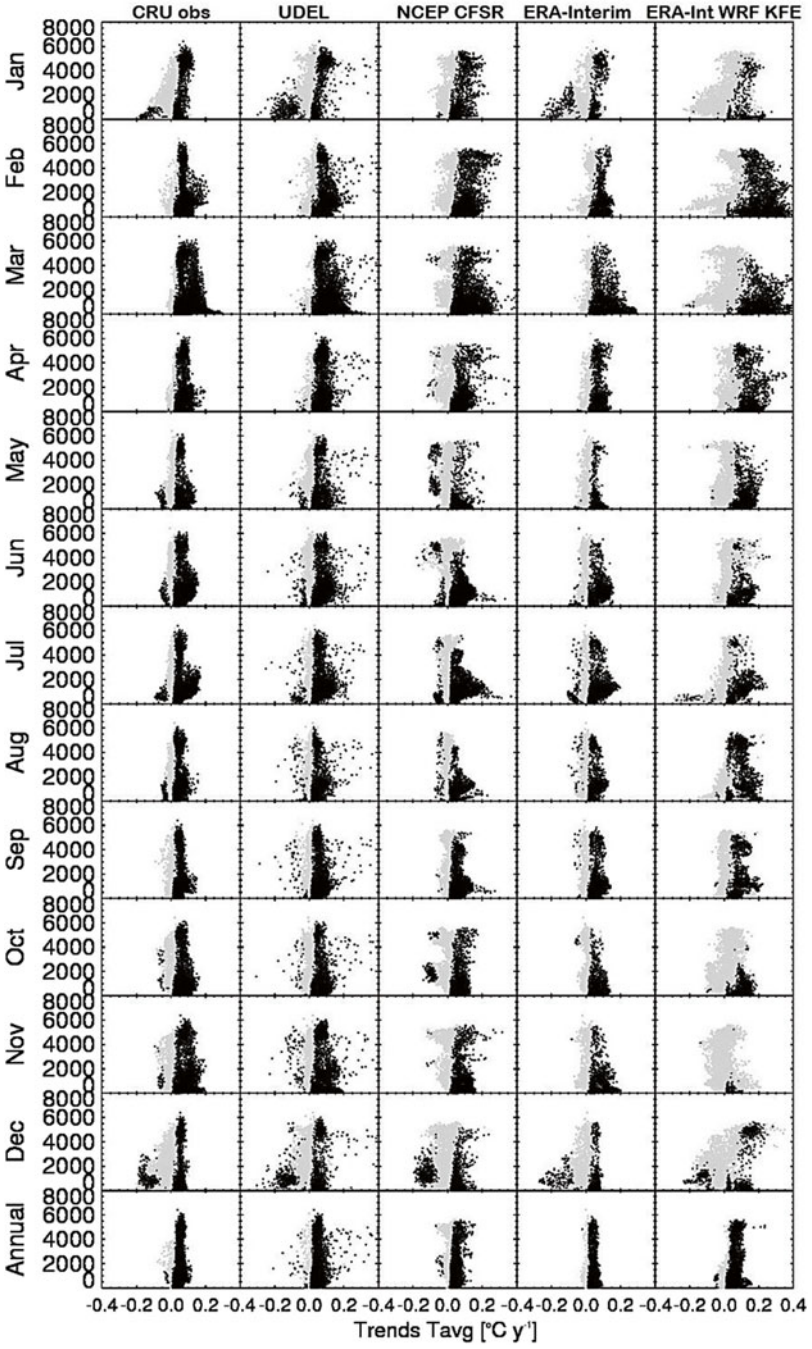

Fig. 2.4 Mean monthly temperature trend magnitudes versus elevation from all datasets. Significant trends at 90 % and above level are shown in *black*, while insignificant tendencies are shown in *gray* (Source: Authors)

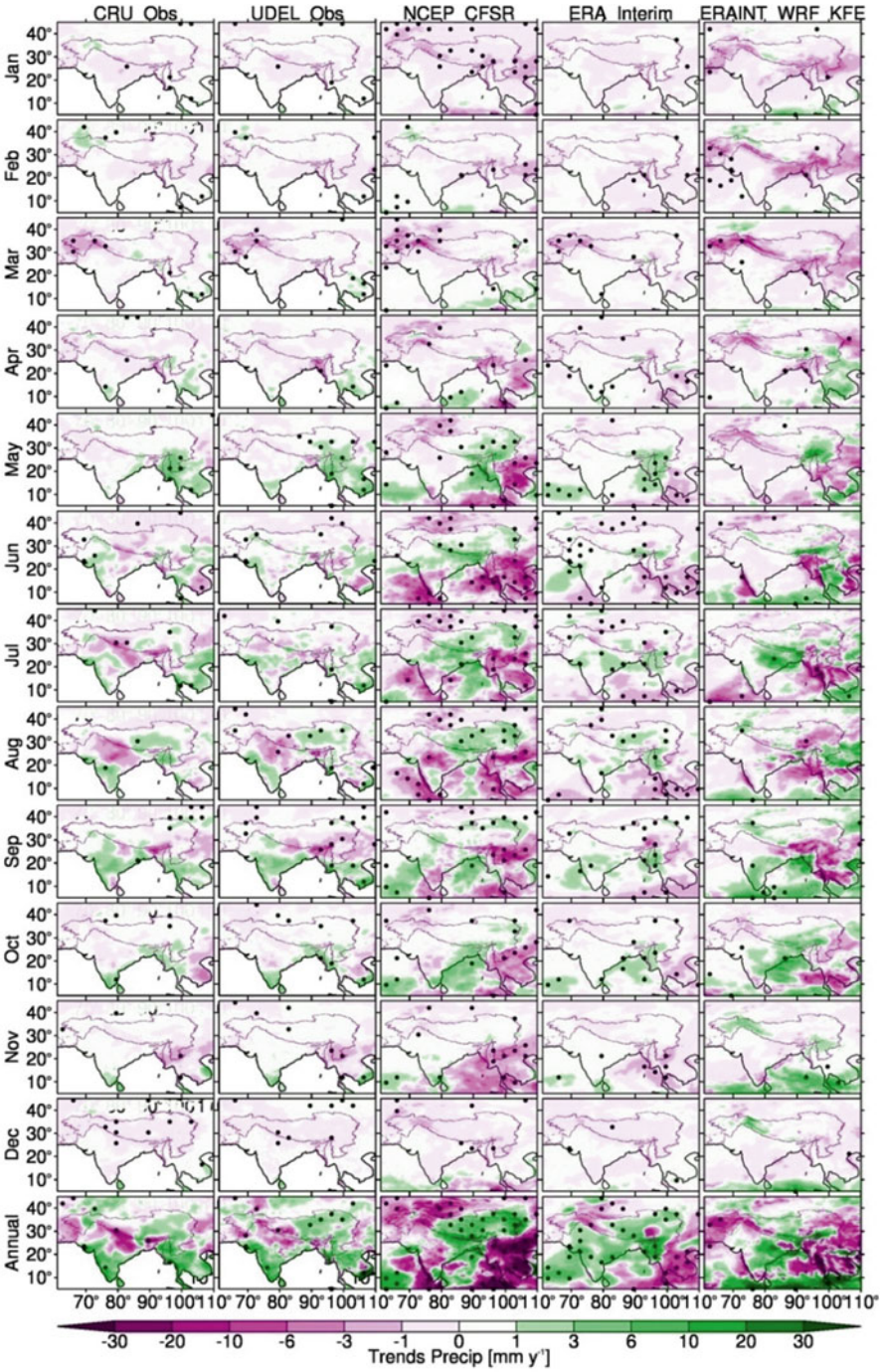

Fig. 2.5 Same as Fig. 2.3 but for monthly total precipitation. Here the whole HKH and Tibetan Plateau region is shown in *purple* (Source: Authors)

varying skills in terms of pattern and magnitude of trends and their elevation dependency. Though all datasets largely underestimate the trends from the station observations, UDEL outperforms all other datasets with little underestimation. However, UDEL suggests a very small variation of trends for most of the study domain with a large number of outliers. After UDEL, the ERA-Interim reanalysis followed by the CRU dataset exhibits a medium-level agreement with the magnitude of real trends. Nevertheless, UDEL, CRU, and ERA-Interim exhibit a quite good agreement with each other and with the station observations for the patterns of general warming, strongest warming and drying over the northwestern study domain in March, and wetting of southeastern Tibetan Plateau and Myanmar regions in May. Moreover, we have found a strongest EDW rate per 1000 m elevation increase in January, which is well agreed qualitatively among all the considered datasets, except ERA-WRF. Our results also confirm that higher warming rates for highlands (above 2000 m asl) as compared to lowlands exist mainly for the winter months (December and January), well agreed among all datasets analyzed here, and also during April–September with a mild agreement. Only NCEP-CFSR reanalysis largely contradicts the EDW signal, except during winter months. It is pertinent to mention that skillset of the gridded and reanalysis datasets considered in the study has been evaluated against a subset of available high-quality homogeneous observations mainly from the eastern Tibetan Plateau, which emphasizes a careful interpretation of their fidelity across the rest of study domain. In view of varying skillset of the considered datasets, we suggest to take into account even a broader database particularly exploiting the potential of the growing number of satellite observations in the recent past and reconstructed climate records from a variety of proxy datasets. Moreover, we eventually propose an integration of either outperforming regionalized, reanalysis, remotely sensed, or reconstructed datasets with the real observations, in order to develop spatially complete and locally refined climatic fields for an adequate climate change assessment over the region. In this regard, highly resolved climatic fields from the reanalysis products either achieved through dynamical or statistical downscaling can also be an excellent option that can provide a better insight into the ongoing climate change and its driving mechanisms. Nevertheless, a well-agreed amplified signal of climate change over the Tibetan Plateau and its surrounding highlands suggests its role as an early warning of the foreseeable severe impacts on the geo-ecosystems of High Asia and on every aspect of life associated with it.

Acknowledgments We acknowledge UDel_AirT_Precip data provided by the NOAA/OAR/ESRL PSD, Boulder, Colorado, USA, from their Web site at http://www.esrl.noaa.gov/psd/. We acknowledge the World Climate Research Programme's Working Group on Regional Climate, and the Working Group on Coupled Modelling, former coordinating body of CORDEX and responsible panel for CMIP5. We also thank the climate modeling groups for producing and making available the WRF-KFE evaluation run. We also acknowledge the Earth System Grid Federation infrastructure an international effort led by the US Department of Energy's Program for Climate Model Diagnosis and Intercomparison, the European Network for Earth System Modeling, and other partners in the Global Organization for Earth System Science Portals (GO-ESSP).

References

Aizen VB, Aizen M, Melack JM, Dozier J (1997) Climatic and hydrologic changes in the Tien Shan, Central Asia. J Clim 10:1393–1404

Beniston M (2000) Environmental change in mountains and uplands, vol 172. Arnold, London

Berrisford P, Dee D, Fielding K, Fuentes M, Kallberg P, Kobayashi S, Uppala S (2009) The ERA-interim archive, ERA report series [online] Available from: http://www.ecmwf.int/publications/library/do/references/list/782009. Accessed 15 Jan 2013

Bocchiola D, Diolaiuti G (2013) Recent (1980–2009) evidence of climate change in the upper Karakoram, Pakistan. Theor Appl Climatol 113:611–641

Böhner J (1996) Säkulare Klimaschwankungen und rezente Klimatrends Zentral- und Hochasiens. – Göttinger Geogr. Abh. 101, Göttingen, 180 S

Bolch T (2007) Climate change and glacier retreat in northern Tien Shan (Kazakhstan/Kyrgyzstan) using remote sensing data. Glob Planet Chang 56:1–12

Bolch T, Kulkarni A, Kääb A, Huggel C, Paul F, Cogley G, Frey H, Kargel JS, Fujita K, Scheel M, Bajracharya S, Stoffel M (2012) The state and fate of Himalayan glaciers. Science 336(6079):310–314

Camarero JJ, Gutierrez E (1999) Structure and recent recruitment at alpine forest-pasture ecotones in the Spanish Central Pyrenees. Ecoscience 6(3):451–464

Dee DP, Uppala SM, Simmons AJ, Berrisford P, Poli P, Kobayashi S, Andrae U, Balmaseda MA, Balsamo G, Bauer P, Bechtold P, Beljaars ACM, van de Berg L, Bidlot J, Bormann N, Delsol C, Dragani R, Fuentes M, Geer AJ, Haimberger L, Healy SB, Hersbach H, Hólm EV, Isaksen L, Kållberg P, Köhler M, Matricardi M, McNally AP, Monge-Sanz BM, Morcrette JJ, Park BK, Peubey C, de Rosnay P, Tavolato C, Thépaut JN, Vitart F (2011) The ERA-Interim reanalysis: configuration and performance of the data assimilation system. Q J R Meteorol Soc 137(553–597):2011. doi:10.1002/qj.828

Diaz HF, Bradley RS (1997) Temperature variations during the last century at high elevation sites. Clim Chang 36:253–279

Gerlitz L, Conrad O, Thomas A, Böhner J (2014) Warming patterns over the Tibetan Plateau and adjacent lowlands derived from elevation- and bias-corrected ERA-Interim data. Clim Res 58(3):235–246. doi:10.3354/cr01193

Grabherr G, Gottfried M, Pauli H (2001) High mountain environment as indicator of global change. In: Visconti G, Beniston M, Iannorelli ED, Barba D (eds) Global change and protected areas. Kluwer, Dordrecht, pp 331–345

Grabherr G, Gottfried M, Pauli H (2010a) Climate change impacts in alpine environments. Geogr Compass 4(8):1133–1153

Grabherr G, Pauli H, Gottfried M (2010b) A worldwide observation of effects of climate change on mountain ecosystems. In: Borsdorf A, Grabherr G, Heinrich K, Scott B, Stötter J (eds) Challenges for mountain regions – tackling complexity. Böhlau Verlag, Wien, pp 49–57

Harris I, Jones PD, Osborn TJ, Lister DH (2014) Updated high-resolution grids of monthly climatic observations – the CRU TS3.10 Dataset. Int J Climatol 34:623–642. doi:10.1002/joc.3711

Hasson S, Böhner J, Lucarini V (2015a) Prevailing climatic trends and runoff response from Hindukush–Karakoram–Himalaya, upper Indus basin. Earth Syst Dyn Discuss 6:579–653. doi:10.5194/esdd-6-579-2015.

Hasson S, Pascale S, Lucarini V, Böhner J (2015b) Seasonal cycle of precipitation over major river basins in South and Southeast Asia: a review of the CMIP5 climate models data for present climate and future climate projections. J Atmos Res (in review)

Huber UM, Bugmann HKM, Reasoner MA (2005) Global change and mountain regions. An overview of current knowledge. Kluwer, Dordrecht, p 650

IPCC 2013: Climate Change (2013) The physical science basis. In: Stocker TF, Qin D, Plattner GK, Tignor M, Allen SK, Boschung J, Nauels A, Xia Y, Bex V, Midgley PM (eds) Contribution of working group I to the fifth assessment report of the Intergovernmental Panel on Climate Change. Cambridge University Press, Cambridge, p 1535

Kendall MG (1975) Rank correlation methods. Griffin, London

Körner C, Ohsawa M (2005) Mountain systems. In: Hassan R, Scholes R, Ash N (eds) Ecosystems and human well-being: current state and trends, vol 1. Island Pre, Washington, DC/Covelo/London, pp 681–716

Liu X, Chen B (2000) Climatic warming in the Tibetan Plateau during recent decades. Int J Climatol 20:1729–1742

Liu X, Cheng Z, Yan L, Yin Z (2009) Elevation dependency of recent and future minimum surface air temperature trends in the Tibetan Plateau and its surroundings. Glob Planet Chang 68:164–174

Mann HB (1945) Nonparametric tests against trend. Econometrica 13:245–259

Nogués-Bravo D, Araújo MB, Errea MP, Martinez-Rica JP (2007) Exposure of global mountain systems to climate warming during the 21st century. Glob Environ Chang 17(3–4):420–428. doi:10.1016/j.gloenvcha.2006.11.007

Pepin N, Bradley RS, Diaz HF, Baraer M, Caceres EB, Forsythe N, Fowler H, Greenwood G, Hashmi MZ, Liu XD, Miller JR, Ning L, Ohmura A, Palazzi E, Rangwala I, Schöner W, Severskiy I, Shahgedanova M, Wang MB, Williamson SN, Yang DQ (2015) Elevation-dependent warming in mountain regions of the world. Nat Clim Chang 5:424–430. doi:10.1038/NCLIMATE2563

Qin J, Yang K, Liang S, Guo X (2009) The altitudinal dependence of recent rapid warming over the Tibetan Plateau. Clim Chang 97:321–327

Saha S, Moorthi S, Pan H-L, Wu X, Wang J, Nadiga S, Tripp P, Kistler R, Woollen J, Behringer D, Liu H, Stokes D, Grumbine R, Gayno G, Wang J, Hou Y-T, Chuang H-Y, Juang HMH, Sela J, Iredell M, Treadon R, Kleist D, Delst PV, Keyser D, Derber J, Ek M, Meng J, Wei H, Yang R, Lord S, Dool HVD, Kumar A, Wang W, Long C, Chelliah M, Xue Y, Huang B, Schemm JK, Ebisuzaki W, Lin R, Xie P, Chen M, Zhou S, Higgins W, Zou CZ, Liu Q, Chen Y, Han Y, Cucurull L, Reynolds RW, Rutledge G, Goldberg M (2010) The NCEP climate forecast system reanalysis. Bull Am Meteorol Soc 91:1015–1057

Sen PK (1968) Estimates of the regression coefficient based on Kendall's tau. J Am Stat Assoc 63:1379–1389

Shrestha AB, Wake CP, Mayewski PA, Dibb JE (1999) Maximum temperature trends in the Himalayas and its vicinity: an analysis based on temperature records from Nepal for the period 1971–1994. J Clim 12:2775–2786

Tabari H, Talaee PH (2011) Recent trends of mean maximum and minimum air temperatures in the western half of Iran. Meteorog Atmos Phys 111:121–131

Theil H (1950) A rank-invariant method of linear and polynomial regression analysis, I, II, III. Ned Akad Wetensch Proc 53:386–392, 512–525, 1397–1412

Thompson LG, Mosley-Thompson E, Davis ME, Lin PN, Henderson K, Mashiotta TA (2003) Tropical glacier and ice core evidence of climate change on annual to millennial time scales. Clim Chang 59:137–1553

Walther GR, Beißner S, Pott R (2005) Climate change and high mountain vegetation shifts. In: Broll G, Keplin B (eds) Mountain ecosystems, studies in treeline ecology. Springer, Heidelberg, pp 77–96

Wang XL (2008) Penalized maximal F-test for detecting undocumented mean shifts without trend-change. J Atmos Ocean Technol 25:368–384. doi:10.1175/2007JTECHA982.1

Wang XL, Feng Y (2009) RHtestsV3 user manual, report. Clim Res Div, Atmos Sci, and Technol Dir, Sci, and Technol Branch, Environ Canada, Gatineau, Quebec, Canada: 26 available at: http://etccdi.pacificclimate.org/software.shtml. Last accessed 15 Nov 2014

Willmott CJ, Matsuura K (1998) Global air temperature and precipitation: re-gridded monthly and annual climatologies (Version 3.01). Center for Climatic Research, Department of Geography, University of Delaware, Newark, data available at climate.geog.udel.edu/~climate

Xie H, Ye J, Liu X, Chongyi E (2010) Warming and drying trends on the Tibetan Plateau (1971–2005). Theor Appl Climatol 101:241–253

Xu ZX, Gong TL, Li JY (2008) Decadal trend of climate in the Tibetan Plateau – regional temperature and precipitation. Hydrol Process 22:3056–3065

Yan L, Liu X (2014) Has climatic warming over the Tibetan Plateau paused or continued in recent years? J Earth Ocean Atmos Sci 1:13–28

Yao T, Lonnie G, Thompson LG, Mosely-Thompson E, Yang Z (1995) Recent Warming as recorded in the Qinghai-Tibet cryosphere. Ann Glaciol 21:196–200

You Q, Kang S, Pepin N, Flügel WA, Yan Y, Behrawan H, Huang J (2010) Relationship between temperature trend magnitude, elevation and mean temperature in the Tibetan Plateau from homogenized surface stations and reanalysis data. Glob Planet Chang 71:124–133

Zhang X, Vincent LA, Hogg WD, Niitsoo A (2000) Temperature and precipitation trends in Canada during the 20th century. Atmos Ocean 38:395–429

Chapter 3
Analytic Comparison of Temperature Lapse Rates and Precipitation Gradients in a Himalayan Treeline Environment: Implications for Statistical Downscaling

Lars Gerlitz, Benjamin Bechtel, Jürgen Böhner, Maria Bobrowski, Birgit Bürzle, Michael Müller, Thomas Scholten, Udo Schickhoff, Niels Schwab, and Johannes Weidinger

Abstract High mountain regions have been identified as a major hotspot of climate change during recent decades, resulting in a rapid change of local geo- and ecosystems. The ecosystem response to changes of near-surface temperatures and precipitation is often analyzed and simulated by means of statistical or process-based modeling applications. However, these models require high-quality climate input data. Based on the assumption that freely available gridded climate data sets are often not suitable for climate change impact investigation due to their low spatial resolution and a lack of accuracy, this paper aims to suggest adequate statistical downscaling routines in order to facilitate the cooperation of climate and climate impact research. We firstly summarize the requirements of ecological climate impact studies and identify the deficiencies of freely available climate reanalysis and regionalization products. Based on a network of seven recently installed weather stations in the highly structured target area, the seasonal, diurnal, and spatial heterogeneity of near-surface temperatures and precipitation amounts is analyzed, and the major large-scale atmospheric and local-scale topographic forcing are specified.

L. Gerlitz (✉)
Section Hydrology, GFZ German Research Centre for Geosciences, Potsdam, Germany
e-mail: lars.gerlitz@gfz-potsdam.de

B. Bechtel • J. Böhner • M. Bobrowski • B. Bürzle • U. Schickhoff N. Schwab • J. Weidinger
CEN Center for Earth System Research and Sustainability, Institute of Geography, University of Hamburg, Hamburg, Germany

M. Müller • T. Scholten
Department of Geosciences, Chair of Soil Science and Geomorphology, University of Tübingen, Tübingen, Germany

R.B. Singh et al. (eds.), *Climate Change, Glacier Response, and Vegetation Dynamics in the Himalaya*, DOI 10.1007/978-3-319-28977-9_3

The analysis of observations highly suggests that local-scale climatic conditions are influenced by both large-scale atmospheric parameters and topographic characteristics. Based on related studies in similar environments, we eventually suggest a statistical downscaling approach integrating large-scale atmospheric fields (derived from reanalysis products or large-scale climate models) and GIS-based terrain parameterization in order to generate fully distributed fields of ecologically relevant climate parameters with high spatial resolution.

Keywords High mountain climates • Observations • Statistical downscaling • Lapse rates

3.1 Introduction

Accelerated rates of warming and changing precipitation patterns have been observed by various studies in high mountain regions all over the globe. Most likely this high sensitivity to changing greenhouse gas concentrations is caused by positive feedback effects arising from a decreasing albedo due to reduced snow cover rates or changing vegetation patterns as well as changes of moisture and downward longwave radiation (Pepin 2015; Rangwala and Miller 2012). Some studies indicate that the elevation-dependent warming in mountain environments alters the lapse rates of near-surface temperatures. It is consensus that the spatial pattern of warming has an explicit impact on the ecological balance of high mountain ecosystems; however, the interactions of local-scale climate change and ecological response are not yet fully understood. For many environmental investigations and modeling approaches, gridded temperature and precipitation estimates are essential input parameters (Araújo et al. 2005; Schoof 2013; Soria-Auza et al. 2010). Particularly in heterogeneous high mountain environments, such as the Himalayas, ecosystem patterns are largely influenced by local-scale variations of relevant climate parameters. Thus, the spatial resolution and quality of available near-surface climate data sets must be considered as a major source of uncertainty for climate and climate change impact assessments (Soria-Auza et al. 2010). Many state-of-the-art modeling applications, particularly in data sparse mountain environments, utilize freely available reanalysis products, such as ERA-Interim (Berrisford et al. 2009), to calibrate process-based or statistical climate impact models (Maignan et al. 2011; Rötter et al. 2013; Saino et al. 2011). However, due to their coarse spatial resolution, reanalysis products fail to adequately represent the local-scale variability of near-surface climates in complex terrain. Atmospheric boundary layer processes at the meteorological micro-β to meso-γ scale, such as topographically induced variations of solar insolation and surface heating, nocturnal cold air drainage, and pooling or orographic precipitation, are not explicitly resolved by large-scale climate models or reanalysis products (Gerlitz 2015; Gerlitz et al. 2015). Since most meteorological stations in mountain environments are located in valleys below the

elevation of the corresponding ERA-Interim grid cell, a strong cold bias of the ERA-Interim raw data has been detected, e.g., by Gao et al. (2014). The topographic variability of precipitation rates and its relationship to topographical features in complex terrain have been highlighted by many studies (Bookhagen and Burbank 2006; Wulf et al. 2010). Ménégoz et al. (2013) detected large discrepancies of ERA-Interim precipitation rates at the Himalayan foothills, where local-scale precipitation amounts are highly sensitive to specific topographic characteristics. Thus, the suitability of climate reanalyses for environmental studies on the local scale is fairly limited. Simple elevation adjustment techniques of precipitation (Lloyd 2005) and temperature (Gao et al. 2012; Gerlitz et al. 2014; Sheridan et al. 2010) can only rudimentary compensate for the deficiencies of reanalysis products. For example, observations from Langtang Himal by Immerzeel et al. (2014) show that temperature lapse rates and precipitation gradients are highly variable in space and time, indicating that the assumption of persistent values is rather imprecise.

Likewise, frequently applied interpolated climate data sets such as WorldClim (Hijmans et al. 2005) do not sufficiently capture the topographic variations of near-surface climates in mountain regions. The interpolation algorithm regionalizes monthly observations of precipitation and temperature based on a weighted linear regression approach, taking latitude, longitude, and elevation as statistical predictor variables. Despite the high spatial resolution of 1 km^2, the data set neglects local-scale atmospheric effects such as temperature inversions or orographic precipitation. Thus, WorldClim-forced ecological modeling applications lead to imprecise or even unrealistic results (Soria-Auza et al. 2010). It is therefore widely known that freely available gridded climate data sets often do not satisfy the requirements of ecological climate impact studies and impede the interdisciplinary investigation of climate change impacts on vulnerable ecosystems.

In the framework of the project TREELINE, the response of the undisturbed treeline ecotone in Rolwaling Himal/Nepal to global warming is analyzed based on an interdisciplinary ecosystemic approach integrating climate observations and modeling applications, field sampling and mapping, experimental treatments of various plant species, remote sensing, and ecological modeling. While on a global scale the low-temperature growth limitation determines the position of natural alpine treelines, the dynamics at local scales depend on multiple interactions of influencing factors and mechanisms (Körner and Paulsen 2004; Schickhoff 2005; Schickhoff et al. 2015). For an interdisciplinary cooperation of climate modelers and ecologists, precise climate data sets are essential (Soria-Auza et al. 2010; von Storch 1995). The presented preliminary study intends to identify the gap between freely available climatic data sets and the needs of ecological impact studies. Therefore, we firstly survey the various interactions of local-scale climate settings with ecological site conditions in order to identify the requirements of ecological investigations. Subsequently, we present first results of an observational campaign in the highly structured monsoonal influenced target area. The analysis of temperature lapse rates and precipitation gradients reflects the importance of meso- to microscale atmospheric processes for the formation of distinct topoclimates and

supports the unsuitability of freely available data sets. Based on previous studies in similar environments, we eventually suggest adequate climate downscaling and regionalization techniques in order to improve the interdisciplinary cooperation of climate and climate impact researchers.

3.2 Climate-Ecosystem Interactions in Treeline Environments

Vegetation patterns in natural alpine treeline environments are characterized by a large heterogeneity resulting from small-scale alterations of near-surface climates and soil conditions. On a global scale, the treeline position is mainly determined by a growing season temperature threshold value in the order of 5–6 °C (Körner and Paulsen 2004). In general treeline ecotones are distinguished by a sequence of changing vegetation types with increasing elevation, ranging from closed forests to alpine tundra communities, within a transition zone of often less than 100 m (Holtmeier and Broll 2005). In Rolwaling Himal, upper subalpine forests are primarily composed of *Betula utilis* and *Abies spectabilis*, with *Rhododendron campanulatum* and *Sorbus microphylla* forming a second tree layer. Closed forests give way to an extensive krummholz belt of *Rh. campanulatum* at 3900 m (NW-exp.)/4000 m (NE-exp.), which turn into alpine *Rhododendron* dwarf scrub heaths at c. 4000 m/4100 m (Schickhoff et al. 2015). Specific treeline investigations indicate that growth conditions and seedling performance of various plant species are highly influenced by local-scale climate conditions, including solar insolation and temperature variations, moisture availability, and wind patterns (Case and Duncan 2014; Miehe et al. 2007). Case and Duncan (2014) investigated several climate-related factors and their influence on treeline elevations. Particularly, thermal variables, such as solar insolation income and mean temperature during growing season, have been identified as important drivers of the vegetation distribution. Additionally, physiological stressors, e.g., cold air drainage and pooling, wind exposure, and moisture limitations, were found to determine the position and species composition of treeline ecotones. Lv and Zhang (2012) suppose that higher temperatures during growing season lead to better growth conditions and enhanced carbon storage, which might reduce the mortality of tree seedlings during harsh winter conditions. Likewise, investigations by Hofgaard et al. (2009) indicate that small-scale alterations of solar insolation and temperature, resulting in a variable growing season length, lead to specific constellations of ecological site conditions in high mountain environments. Camarero and Gutierrez (1999) illustrate that frost occurrence during spring results in enhanced mortality rates of tree seedlings. Thus increasing temperatures in spring season most likely promote the recruitment of tree species at higher elevations. Gaire et al. (2014) show that altering moisture conditions during premonsoon season are particularly important for the recruitment of *Betula utilis*, the principal treeline species in the western and central Himalayas.

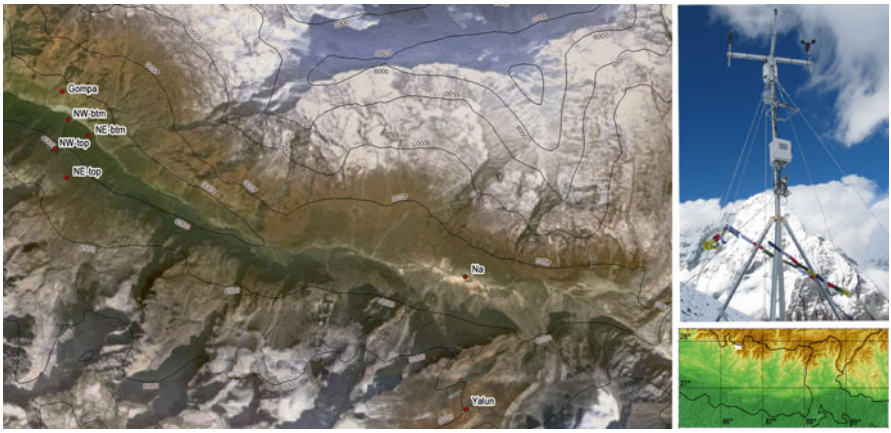

Fig. 3.1 The target area in Rolwaling Himal and the locations of seven automatic weather stations (Source: Google Earth). The *upper right* picture shows the station Yalun at 5032 m. The *lower right* map represents the location of the target area in Central Nepal (Source: Lars Gerlitz)

While *Betula utilis* was found to rapidly colonize moist sites, dry locations were found to be predominantly populated by dwarf shrub associations, which are better adapted to drought conditions. First observations from Rolwaling Himal likewise indicate that small-scale climatic conditions determine the distribution of particular tree species. The elevational positions of the treeline ecotone at northeast- and northwest-facing slopes (Fig. 3.1) differ considerably within a horizontal distance of approximately 100 m. The observed upward shift of vegetation belts at the northeasterly slope coincides with higher temperatures and solar insolation rates, particularly during spring season (Schickhoff et al. 2015) (see Sect. 3.3). Beside near-surface climate conditions, local-scale alterations of soil properties, in particular soil temperatures, highly influence tree growth and seedling performance in alpine ecosystems (Gehrig-Fasel et al. 2008; Hoch and Körner 2003, 2005; Körner and Paulsen 2004). The heat balance of soils is strongly affected by local-scale variations of near-surface temperature, solar insolation, vegetation cover, topography, and the local water regime. Elevational temperature gradients are highest in topsoils, which are affected by freeze-thaw cycles. Soil temperatures in particular are of great importance for complex physical, chemical, and biological processes, leading to specific physical and chemical soil characteristics. Many studies (Borgaonkar et al. 2011; Gaire et al. 2014; Liang et al. 2010; Singh and Yadav 2005) utilize climatic observations from only one or few nearby weather stations for the characterization of the treeline climate. However, ecological models require precise climate data sets, in order to simulate the potential range limits of alpine species under current and future climate conditions. Thus, the lack of spatially high-resolution climatic data must be considered as a major limitation of state-of-the-art ecological investigations and modeling applications (Soria-Auza et al. 2010).

3.3 Topoclimatic Observations from Rolwaling Himal, Nepal

With the objective of analyzing and quantifying the local-scale climatic variations in the target area, seven automatic meteorological stations were installed at elevations between 3700 and 5100 m a.s.l. These collect data for temperature, solar insolation, precipitation, relative humidity, wind speed, and wind direction with high accuracy and a temporal resolution of 15 min. All stations are equipped with HOBO data loggers and synotech sensors, suitable for high mountain environments. The locations were chosen as to represent the major meso- and microscale atmospheric processes leading to a formation of distinct topoclimates and consequential ecological site conditions (Fig. 3.1). Two transects were installed on a north-facing slope near the village of Beding, where the ecological sampling and mapping investigations of our project partners were performed. One of these transects is slightly northwest exposed; the other one faces toward northeast. Each transect contains one station in the valley bottom (NW-btm at 3739 m a.s.l. and NE-btm at 3750 m a.s.l.) and one station above the treeline (NW-top at 4055 m a.s.l. and NE-top at 4179 m a.s.l.). For a broader investigation of insolation and temperature variations in the target area, the station Gompa (3908 m a.s.l.) has been installed at the opposite south-facing slope. In order to better understand and quantify the valley internal circulation pattern, the station Na has been set up in the upper valley catchment (4219 m a.s.l.), and the station Yalun has been installed in a glacier-dominated environment on a north-facing slope at 5032 m a.s.l. Currently, more than 1 year of observations is available for most stations (April 2013 to June 2014); for the high-elevated station Yalun, the period of complete observations amounts to 9 months. Seasonal means for discrete time steps (0, 6, 12, 18 h Nepali time) were calculated for temperature, relative humidity, and incoming solar radiation for each station, respectively. Likewise, seasonal means of six-hourly precipitation sums (0–6, 6–12, 12–18, 18–0 h) were computed. Topographically induced six-hourly temperature lapse rates ($\Delta T/\Delta Z^{*}100$) and daily precipitation gradients ($\Delta P/\Delta Z^{*}100$) were derived for the two transects on the north-facing slope, for the south-facing slope (considering the time series of the stations Gompa and NW-btm), and for the upper valley catchment (under consideration of the stations Yalun and Na). Following the main Rolwaling valley, temperature lapse rates and precipitation gradients were computed by consideration of the stations Na and NE-btm. To account for large-scale weather variations, we processed the relative humidity at the 500 hPa level of the ERA-Interim reanalysis as well as the reanalysis internal free air temperature lapse rate between 500 and 700 hPa. In the following section, we summarize our main findings and give some interpretations for the observed heterogeneity of relevant climate parameters. In this regard, we focus on the identification of adequate topographic and large-scale atmospheric predictor variables for the explanation of observed temperature and precipitation variations.

Mean annual temperatures (for the period from April 2013 to March 2014) amount to 3.7 °C at the stations NW-btm and NE-btm and to 2.9 °C and 2.3 °C at NW-top and NE-top, respectively. As expected, the south-facing station Gompa is

significantly warmer (mean annual temperature of 4.0 °C), and the station Na shows a mean annual temperature of 0.7 °C. Due to several data gaps, no reliable assessment can be specified for the station Yalun; however, our observations suggest values in the order of −6 °C. The seasonal and diurnal temperature variations (shown in Table 3.1) give further insights into the topographic forcings of local-scale temperature variations. During clear nights, particularly in winter season (DJF), the mean nocturnal temperatures (0 h and 6 h) at the valley stations NE-btm and NW-btm are substantially lower compared with the upper slopes (represented by the stations Gompa, NW-top and NE-top). The occurrence of these positive temperature lapse rates of up to +3 °C/100 m at the southern slope (Fig. 3.2) is accompanied by low values of relative humidity at all stations. Likewise, the large-scale ERA-Interim reanalysis depicts values of relative humidity below 30 % during winter season. This clearly indicates the importance of radiative cooling at higher elevations and cold air drainage into the valleys for the nocturnal distribution of near-surface temperatures under dry conditions. During premonsoon (MAM) and postmonsoon season (SON), the relative humidity in the target area increases (values above 70 % are characteristic for all stations), and the radiative cooling at high elevations and nocturnal cold air drainage into the valley is clearly reduced (Table 3.1 and Fig. 3.2). The monsoon season (JJA) shows mainly negative lapse rates in the entire target area. However, these are shallower compared with the ERA-Interim internal lapse rate and the often suggested environmental lapse rate of 0.65 °C/100 m. The southern slope is characterized by the frequent occurrence of positive nocturnal lapse rates even during monsoon season. This highly suggests that cold air drainage and pooling continue during monsoon season, although the effect is distinctly less pronounced compared with dry season and the observed temperature lapse rates are in general better represented by the ERA-Interim reanalysis. Short dry periods in premonsoon and monsoon season (as observed in April and July 2013, Fig. 3.1) instantly release the formation of katabatic winds and cold air drainage into the valley and are accompanied by strong positive lapse rates at the south- and north-facing slopes. This leads to an enhanced frost risk in the valley bottom and might impede the survival of plant seedlings resulting in the formation of adapted vegetative associations (Lindkvist and Lindqvist 1997; Pypker et al. 2007). Periods with high relative humidity during winter (most likely due to the passage of westerly depressions) on the other hand show an obvious decline of nocturnal temperature lapse rates. The valley following lapse rate (under consideration of the stations Na and NE-btm) in general is better represented by the large-scale ERA-Interim reanalysis. During dry season, however, positive nocturnal lapse rates (of up to +1 °C/100 m) occur frequently. Under dry conditions during daytime (12 h an 18 h), the southern slope is likewise characterized by positive lapse rates in the order of +1 °C/100 m. This can be attributed to higher rates of solar insolation (mean 12 h insolation rates of 771 W/m^2 at the station Gompa have been observed in premonsoon season) and consequential surface heating. The shadowed north-facing slope shows distinct negative lapse rates at the same time. During monsoon season the observed mean temperature lapse rates at 12 h were between 0.45 and 0.73 °C/100 m and show a considerably reduced temporal variability.

Table 3.1 Seasonal mean values of temperature, solar insolation, and relative humidity for discrete time steps: 0 h, 6 h, 12 h, and 18 h Nepali time (from right toward left)

Tempeature[°C]	*Gompa*				*NW-top*				*NW-btm*				*NE-top*				*NE-btm*				*Na*				*Yalun*			
Winter	−1.9	−2.0	2.7	−1.7	−2.9	−3.0	−0.7	−2.9	−4.3	−4.5	2.3	−2.9	−4.0	−4.2	0.0	−3.8	−4.1	−4.4	2.1	−2.8	−6.2	−6.4	1.2	−5.1	−9.3	−9.5	−5.9	−8.6
Premonsoon	1.8	1.3	5.7	2.9	1.3	0.7	2.7	3.1	2.7	0.6	3.5	5.5	−0.7	−1.0	4.8	0.1	2.7	0.7	3.6	5.7	0.4	−1.1	1.9	3.4	−9.1	−9.3	−4.7	−8.0
Monsoon	8.2	8.0	9.8	8.9	7.6	7.1	8.0	8.6	9.0	8.0	9.2	10.3	6.8	6.7	10.1	7.9	8.7	7.7	9.1	10.2	2.2	6.3	2.5	3.9	–	–	–	–
Postmonsoon	3.9	3.8	7.6	4.5	3.7	3.5	5.1	4.3	3.9	3.2	7.3	5.1	2.2	2.3	6.0	2.8	3.9	3.1	7.2	5.2	1.0	0.5	4.8	2.4	−6.3	−6.4	−1.4	−5.5

Insolation [W/m²]	*Gompa*				*NW-top*				*NW-btm*				*NE-top*				*NE-btm*				*Na*				*Yalun*			
Winter	0.6	0.6	692.2	0.8	0.6	0.7	652.7	0.7	0.6	0.7	607.3	0.7	0.6	0.7	627.9	0.8	0.6	0.7	617.5	0.7	0.6	0.7	654.1	0.7	0.6	0.7	668.5	0.8
Premonsoon	0.6	9.7	771.4	13.9	4.7	7.1	432.5	374.5	4.4	5.3	423.7	392.9	0.6	16.5	762.7	11.5	4.0	5.2	431.1	385.9	5.2	7.3	485.1	405.4	0.6	19.2	904.5	5.8
Monsoon	0.6	25.6	317.9	15.8	6.2	17.9	228.5	237.5	5.7	14.3	243.6	288.2	0.6	42.2	448.9	17.3	5.4	14.3	236.4	277.2	3.7	16.8	277.3	322.8	–	–	–	–
Postmonsoon	0.6	5.5	655.1	1.8	0.7	5.8	431.5	79.1	0.7	4.6	463.3	92.1	0.6	9.1	535.2	1.3	0.7	4.5	455.8	85.6	0.8	1.3	442.1	234.4	0.6	2.3	764.7	0.6

Precipitation [mm]	*Gompa*				*NW-top*				*NW-btm*				*NE-top*				*NE-btm*				*Na*				*Yalun*			
Winter	0.0	0.0	0.2	0.0	0.0	0.0	0.2	0.0	0.0	0.0	0.2	0.0	0.0	0.0	0.4	0.0	0.0	0.0	0.2	0.0	0.0	0.0	0.2	0.0	0.0	0.0	0.1	0.0
Premonsoon	0.4	0.0	1.5	0.3	0.4	0.1	1.0	0.3	0.3	0.3	0.9	0.4	0.2	0.0	1.3	0.1	0.4	0.2	0.8	0.3	0.1	0.1	0.2	0.2	0.0	0.0	1.6	1.2
Monsoon	6.7	0.4	2.6	5.1	3.6	2.3	0.9	2.3	3.9	2.4	1.0	2.6	4.8	0.3	1.6	2.8	3.5	2.1	1.0	2.4	2.0	1.2	0.6	1.4	3.0	0.7	2.1	2.0
Postmonsoon	1.3	0.3	0.8	0.4	1.1	0.5	0.7	0.3	1.1	0.5	0.7	0.5	0.5	0.3	0.2	0.6	1.1	0.5	0.7	0.4	0.4	0.4	0.0	0.2	0.1	0.1	0.4	0.5

Rel. Humidity [%]	*Gompa*				*NW-top*				*NW-btm*				*NE-top*				*NE-btm*				*Na*				*Yalun*			
Winter	35.8	28.3	35.9	64.1	32.3	26.8	39.2	57.2	49.6	42.1	38.6	68.7	32.8	27.1	35.1	54.9	52.2	45.3	39.0	68.8	39.1	34.8	28.4	57.3	26.7	26.0	27.9	37.1
Premonsoon	78.1	64.3	75.7	92.1	83.1	67.2	69.2	84.6	85.6	80.1	74.4	80.3	69.1	54.6	66.2	88.8	86.0	82.0	75.2	80.0	83.2	72.4	66.7	77.0	50.1	35.6	46.5	73.5
Monsoon	98.9	96.7	98.2	99.6	99.6	97.8	96.8	98.9	99.7	99.7	98.0	97.5	98.6	96.2	95.9	99.7	99.7	99.7	98.1	97.5	93.6	98.6	91.6	89.9	–	–	–	–
Postmonsoon	71.9	63.5	71.2	83.7	77.3	70.6	80.6	85.7	84.9	81.5	78.8	90.1	65.2	57.2	67.2	76.7	85.9	82.9	78.9	90.4	68.2	64.1	60.7	76.2	29.3	20.5	25.8	38.6

For precipitation the seasonal means of 6-hourly precipitation sums are stated (0–6 h, 6–12 h, 12–18 h, and 18–0 h)

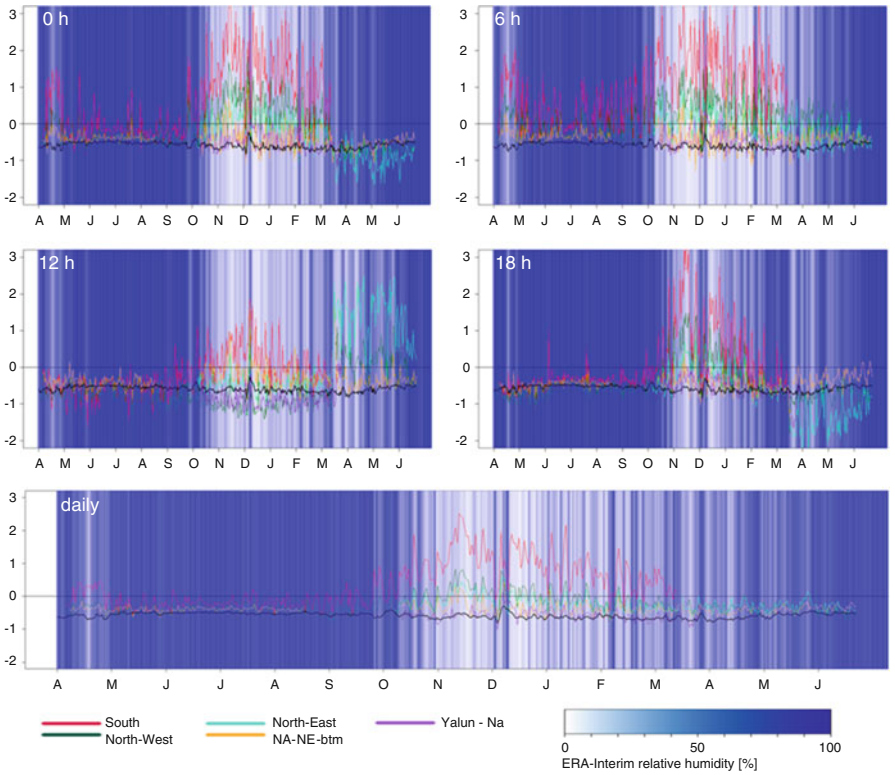

Fig. 3.2 Observed temperature lapse rates [°C/100 m] in different topographic settings for four discrete time steps (*upper panels*) and the daily mean (*lower panel*). The *background color* represents the large-scale relative humidity of the ERA-Interim reanalysis at the 500 hPa level (Source: Lars Gerlitz)

Temperature lapse rates in summer are in general well represented by the reanalysis internal lapse rate (0.51 °C/100 m). The particularly striking feature of highly positive premonsoon lapse rates at the northeast-facing slope at noon must be attributed to the diurnal variations of solar insolation. The east-facing slopes receive high insolation rates in the morning and thus are significantly warmer. Since the premonsoon season is characterized by diurnal convection and the development of convective clouds after midday, the opposite effect of enhanced warming of west-facing slopes in the afternoon cannot be observed. The ecological effect of these premonsoonal temperature variations on the local scale is obvious, as the treeline level and the major vegetation belts reach significantly higher elevations at the northeast-exposed slope.

The aggregated daily mean lapse rates (Fig. 3.1) still reflect large spatial and seasonal variations, indicating that a simple elevation adjustment of temperatures is not suitable for the regionalization of daily mean temperatures in the highly structured target area. Nevertheless, despite a slight underestimation, the lapse rates

during the monsoon season, which represents the growing season of the Himalayan treeline ecotone, are acceptably represented by the ERA-Interim internal temperature lapse rate.

The observations of precipitation are likewise highly characterized by seasonal, diurnal, and spatial variations. Annual precipitation sums amount to 1342 mm at NW-btm, 1226 mm at NW-top, 1187 mm at NE-btm, and 1231 mm at NE-top. The station Gompa receives significantly higher precipitation sums of 1802 mm annually. The upper valley catchment is considerably dryer with annual precipitation sums of 636 mm at Na. Between 70 % and 80 % of the annual precipitation amount falls during monsoon season. It must be noticed that the precipitation sums are most likely underestimated, particularly in winter season, due to the negligence of snow. However, the ecologically essential monsoonal precipitation rates are well represented by our observations. The depiction of seasonal means of six-hourly precipitation sums for four sections of the day (0–6 h, 6–12 h, 12–18 h and 18–0 h) in Table 3.1 impressively reflects the high precipitation intensities during monsoon season. Monsoonal precipitation rates are highest during the night at all stations. As mentioned above, katabatic winds and cold air drainage into the valley bottoms also occur during monsoon season. The convergence of moist air in the valley and cold air masses from higher elevations is likely to result in a destabilization of the atmospheric stratification and triggers the development of deep convective systems at night (Bollasina et al. 2002; Higuchi et al. 1982). For the high mountain station Yalun, a second diurnal precipitation maximum has been observed in the afternoon (12–18 h; see Table 3.1). This suggests the importance of upslope winds in the afternoon, which lead to high-intensity precipitation events in the very high elevations, while the valley remains dry. During winter and spring, the highest precipitation rates were observed in the afternoon. These precipitation events must be attributed to the diurnal valley circulation due to varying rates of solar insolation and surface heating and the consequential development of cumulus clouds, which occasionally result in intense precipitation events (Bhatt and Nakamura 2005). The spatial variations of precipitation in the Himalayan valley become particularly obvious by considering the valley following precipitation gradient computed based on the observations of NE-btm and Na. The annual precipitation sum decreases by almost 50 % within a horizontal distance of less than 5 km, resulting in an elevational precipitation gradient of up to −4 mm/100 m. We assume that the major moisture fluxes during monsoon season follow the valley shape. Due to the gradual increase of elevation, orographic precipitation occurs during monsoon season, and the moisture barren air masses release water before they reach the elevations above 4000 m. Additionally, the abovementioned mechanism of nocturnal atmospheric labilization requires the influence of cold air drainage and pooling, which is considerably more pronounced at lower elevations. The topographically induced precipitation gradients at lower elevations (see the gradients of the south- and northeast-exposed slopes in Fig. 3.3) are most likely due windward and leeward positions of the slopes. Particularly, the south-facing slope (represented by the station Gompa) is exposed to the moist air masses due to a slight right curve of the Rolwaling valley (Fig. 3.1). The dynamic increase of atmospheric pressure results

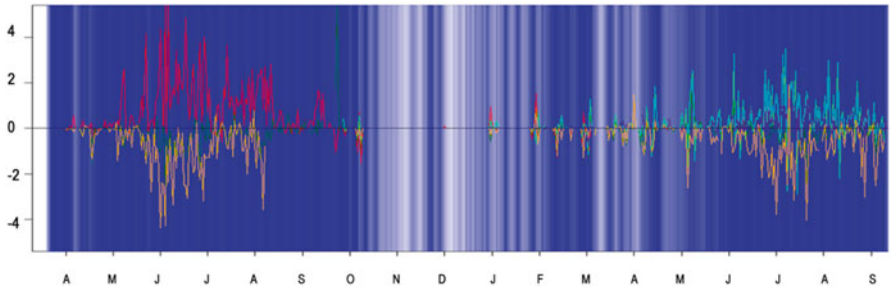

Fig. 3.3 Elevational precipitation gradients in mm/100 m. For legend see Fig. 3.2 (Source: Lars Gerlitz)

in an additional destabilization of the atmospheric stratification and leads to significantly increased precipitation amounts and to a considerably positive precipitation gradient of up to +4 mm/100 m at the south-facing slope. In contrast, over the northwest-facing slope, no distinct precipitation gradient could be detected. The northeast-exposed slope however shows a notable increase of precipitation with rising elevation in the order of +2 mm/100 m during monsoon season. This might be interpreted as a consequence of the frequently stressed diurnal valley circulation leading to higher precipitation amounts at the slopes and as far as arid conditions in the Himalayan valleys (Bhatt and Nakamura 2005).

Summarizing the distribution of both near-surface temperature and precipitation is highly influenced by large-scale atmospheric conditions (in particular by hydroclimatic variables) and the vast topography of this target area. The varying solar insolation rates could be identified as a major predictor variable for the spatial variations of temperatures during clear days. In clear nights, cold air drainage and pooling in the valley bottom lead to an inversion of the elevational temperature gradients. Precipitation considerably decreases with the horizontal distance from the valley edge. However, local-scale topographic distinctions (such as wind- and leeward slope positions and the relative elevation above the valley bottom) lead to an additional spatial heterogeneity of precipitation amounts.

3.4 Conclusions: Toward an Adequate Technique for Climate Downscaling and Regionalization

Although the physical processes which lead to spatial variations of temperature and precipitation in heterogeneous environments are evident, their physically based quantification remains complex and computationally intensive. Moreover, the demand of detailed input data increases with model complexity. Dynamically downscaled fields of relevant climatic parameters rarely achieve a spatial resolution below 10 km and thus still do not satisfy the requirements of case studies and climate impact analyses (Maussion et al. 2013). Many studies indicate that less

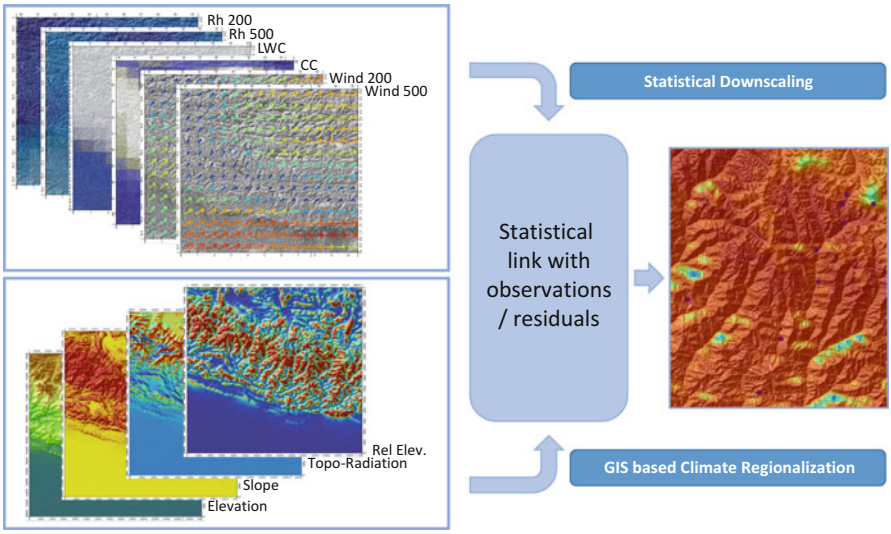

Fig. 3.4 Schematic structure of a statistically based high-resolution near-surface temperature parameterization under consideration of large-scale atmospheric and local-scale topographic predictor variables (Source: Lars Gerlitz)

complex statistical and GIS-based approaches often lead to comparable results (Schoof 2013; Wilby et al. 2004). However, traditional statistical downscaling approaches intend to link large-scale atmospheric fields to local-scale observations and thus generate point-scale estimates of relevant climate parameters. Based on the assumption that observed climatic conditions can be interpreted as combination of both, large-scale atmospheric processes and a topographically induced modification, we suggest estimating fully distributed temperature and precipitation fields with high spatial resolution as a statistical function of large-scale atmospheric conditions and local-scale terrain characteristics. While the former can be derived from freely available reanalysis products, such as ERA-Interim, the latter can be obtained from high-resolution digital elevation models by means of GIS-based terrain parameterization techniques. For the quantification of topographic characteristics, relevant for the formation of distinct topoclimatic conditions, we utilize the Free and Open Source Software SAGA-GIS (Conrad et al. 2015; saga-gis.org). SAGA offers enhanced options for the analysis of digital elevation models and provides several modules for the generation of derivational terrain parameters with respect to the diverse requirements at the climate modeling side (Böhner and Antonić 2009).

The integration of both large-scale atmospheric and local-scale topographic predictor variables can be interpreted as a combination of traditional (point-scale) statistical downscaling techniques and GIS-based climate regionalization methods (Fig. 3.4). After calibrating a robust statistical transfer function, the approach can be utilized for the parameterization of local-scale climatic conditions with high spatial resolution.

For the valley of Khumbu (located less than 20 km east of Rolwaling), a statistical approach has recently been applied in order to analyze the spatial heterogeneity of near-surface temperatures and its topographic driving forces (Gerlitz 2015). Therefore, six-hourly free atmospheric temperature fields at ground level with high spatial resolution of 1 km^2 have been generated by considering the ERA-Interim internal temperature lapse rate as suggested by Gerlitz et al. (2014). Subsequently, the free atmospheric temperatures were compared with in situ observations of six high mountain weather stations, installed in the framework of the EVK2CNR project (www.evk2cnr.org). The residuals were analyzed using a nonlinear and non-parametric regression tree approach with large-scale atmospheric and GIS-derived topographic parameters as potential predictor variables. As atmospheric predictors, we processed the relative humidity at different ERA-Interim pressure levels (rh 200 and rh 500), the liquid water column (LWC), the cloud cover rates, as well as the wind field. Elevation, slope, aspect, potential insolation, and the relative elevation above the valley bottom were utilized as potential topographic predictor variables (Fig. 3.4). The statistical model enables the identification of predominant influencing factors for the local-scale temperature distribution and quantifies typical temperature residuals as a function of synoptic variables and surface characteristics. For the high mountain region, the potential solar insolation was found to be the predominant predictor, but also hydroclimatic large-scale variables (such as relative humidity of cloud cover rates) were found to be crucial. During clear nights, the model showed a distinct elevational gradient of residuals which indicates the importance of nocturnal cold air drainage and accumulation for the local-scale temperature distribution in the highly structured target area.

For the refinement of monthly precipitation rates, a similar approach has been implemented for a model domain covering the entire Himalayan arc and the Tibetan Plateau (Gerlitz et al. 2015). Observed local-scale precipitation amounts from 157 meteorological stations were statistically linked with large-scale ERA-Interim pressure, humidity, and wind fields and local-scale terrain parameters by means of a nonlinear artificial neural network approach. For the assessment of the diurnal valley circulation and the consequential convective precipitation at the upper slopes, the elevation above the valley bottom was utilized as a topographic predictor variable. In order to parameterize orographic precipitation amounts, a wind effect parameter was introduced as an additional predictor variable, which identifies wind- and leeward slopes dependent on the large-scale ERA-Interim wind field and a high-resolution digital elevation model (Böhner and Antonić 2009). The statistical model sufficiently identified windward index as a major influencing factor for the distribution of monsoonal precipitation rates in the Himalayas, resulting in the formation of distinct bands of high precipitation at the windward Himalayan slopes. These have been found to be in accordance with remote sensing derived products such as the Tropical Rainfall Measuring Mission (TRMM) (Bhatt and Nakamura 2005; Bookhagen and Burbank 2006).

Summing up, GIS-based terrain parameterization techniques are powerful for the derivation of adequate predictor variables in order to statistically downscale fully distributed fields of climate parameters. However, robust statistical downscaling

applications in general require high-quality observational data. It must be noted that both of the abovementioned studies suffer from a rather insufficient number of meteorological stations and their spatially biased distribution. The estimation of local-scale temperature variations for the high mountain region of Khumbu was based on only six observational records. While the major topographic influencing factors for the local-scale temperature distribution could indeed be identified, their quantification remains unreliable so far. For the analysis of topographically induced precipitation amounts, a considerable data set of 157 time series was utilized, though most of the stations are located in valleys and thus do not thoroughly represent the topoclimatic variations in the vast target area. The newly introduced dense network of seven weather stations in Rolwaling Himal (only several kilometers away from the Khumbu valley) has been designed in order to identify and quantify topoclimatic variations in the highly structured mountain environment. In combination with the EVK2CNR-network, the observational data set will support the implementation and calibration of GIS-based statistical downscaling applications in the future. The uniquely dense network will enable the estimation of local-scale temperature and precipitation variations and thus improve the cooperation with climate impact researchers in order to investigate recent and future consequences of climate change in this highly climate-sensitive region.

References

Araújo MB, Pearson RG, Thuiller W, Erhard M (2005) Validation of species–climate impact models under climate change. Glob Chang Biol 11(9):1504–1513. doi:10.1111/j.1365-2486.2005.01000.x

Berrisford P, Dee D, Fielding K, Fuentes M., Kallberg P, Kobayashi S, Uppala S (2009) The ERA-Interim Archive, ERA report series [online]. Available from: http://www.ecmwf.int/publications/library/do/references/list/782009. Accessed 15 Jan 2013

Bhatt BC, Nakamura K (2005) Characteristics of monsoon rainfall around the Himalayas revealed by TRMM precipitation radar. Mon Weather Rev 133(1):149–165. doi:10.1175/MWR-2846.1

Böhner J, Antonić O (2009) Land-surface parameters specific to topo-climatology. In: Tomislav H, Hannes IR (eds) Developments in soil science, vol 33. Amsterdam, Elsevier, pp 195–226.

Bollasina M, Bertolani L, Tartari G (2002) Meteorological observations at high altitude in the Khumbu Valley, Nepal Himalayas, 1994–1999. Bull Glaciol Res 19:1–11

Bookhagen B, Burbank DW (2006) Topography, relief, and TRMM-derived rainfall variations along the Himalaya. Geophys Res Lett 33(8):L08405. doi:10.1029/2006GL026037

Borgaonkar HP, Sikder AB, Ram S (2011) High altitude forest sensitivity to the recent warming: a tree-ring analysis of conifers from western Himalaya, India. Quat Int Quat Int 236(1):158–166. doi:10.1016/j.quaint.2010.01.016

Camarero JJ, Gutierrez E (1999) Structure and recent recruitment at alpine forest-pasture ecotones in the Spanish Central Pyrenees. Ecoscience 6(3):451–464

Case BS, Duncan RP (2014) A novel framework for disentangling the scale-dependent influences of abiotic factors on alpine treeline position. Ecography 37(9):838–851. doi:10.1111/ecog.00280

Conrad O, Bechtel B, Bock M, Dietrich H, Fischer E, Gerlitz L, Wehberg J, Wichmann V, Böhner J (2015) System for automated geoscientific analyses (SAGA) v. 2.1.4. Geosci Model Dev 8:1991–2007. doi:10.5194/gmd-8-1991-2015

Gaire NP, Koirala M, Bhuju DR, Borgaonkar HP (2014) Treeline dynamics with climate change at the central Nepal Himalaya. Clim Past 10(4):1277–1290

Gao L, Bernhardt, Schulz K (2012) Downscaling ERA-interim temperature data in complex terrain. Hydrol Earth Syst Sci Discuss 9:5931–5953

Gao L, Hao L, Chen X (2014) Evaluation of ERA-interim monthly temperature data over the Tibetan Plateau. J Mt Sci 11(5):1154–1168. doi:10.1007/s11629-014-3013-5

Gehrig-Fasel J, Guisan A, Zimmermann NE (2008) Evaluating thermal treeline indicators based on air and soil temperature using an air-to-soil temperature transfer model. Ecol Model 213(3–4):345–355. doi:10.1016/j.ecolmodel.2008.01.003

Gerlitz L (2015) Using fuzzified regression trees for statistical downscaling and regionalization of near surface temperatures in complex terrain. Theor Appl Climatol 1–16. 122:337–352. doi:10.1007/s00704-014-1285-x

Gerlitz L, Conrad O, Böhner J (2015) Large-scale atmospheric forcing and topographic modification of precipitation rates over High Asia – a neural-network-based approach. Earth Syst Dyn 6:61–81. doi:10.5194/esd-6-61-2015

Gerlitz L, Conrad O, Thomas A, Böhner J (2014) Warming patterns over the Tibetan Plateau and adjacent lowlands derived from elevation- and bias-corrected ERA-Interim data. Clim Res 58(3):235–246. doi:10.3354/cr01193

Higuchi K, Ageta Y, Yasunari T, Inoue J (1982) Characteristics of precipitation during the monsoon season in high-mountain areas of the Nepal Himalaya. Hydrol Asp Alpine High Mt Areas 138:21–30

Hijmans RJ, Cameron SE, Parra JL, Jones PG, Jarvis A (2005) Very high resolution interpolated climate surfaces for global land areas. Int J Climatol 25(15):1965–1978. doi:10.1002/joc.1276

Hoch G, Körner C (2003) The carbon charging of pines at the climatic treeline: a global comparison. Oecologia 135(1):10–21. doi:10.1007/s00442-002-1154-7

Hoch G, Körner C (2005) Growth, demography and carbon relations of polylepis trees at the world's highest treeline. Funct Ecol 19(6):941–951

Hofgaard A, Dalen L, Hytteborn H (2009) Tree recruitment above the treeline and potential for climate-driven treeline change. J Veg Sci 20(6):1133–1144. doi:10.1111/j.1654-1103.2009.01114.x

Holtmeier FK, Broll G (2005) Sensitivity and response of northern hemisphere altitudinal and polar treelines to environmental change at landscape and local scales. Glob Ecol Biogeogr 14(5):395–410. doi:10.1111/j.1466-822X.2005.00168.x

Immerzeel WW, Petersen L, Ragettli S, Pellicciotti F (2014) The importance of observed gradients of air temperature and precipitation for modeling runoff from a glacierized watershed in the Nepalese Himalayas. Water Resour Res 50(3):2212–2226. doi:10.1002/2013WR014506

Körner C, Paulsen J (2004) A world-wide study of high altitude treeline temperatures. J Biogeogr 31(5):713–732. doi:10.1111/j.1365-2699.2003.01043.x

Liang E, Wang Y, Xu Y, Liu B, Shao X (2010) Growth variation in Abies georgei var. smithii along altitudinal gradients in the Sygera Mountains, southeastern Tibetan Plateau. Trees 24(2):363–373. doi:10.1007/s00468-009-0406-0

Lindkvist L, Lindqvist S (1997) Spatial and temporal variability of nocturnal summer frost in elevated complex terrain. Agric For Meteorol 87(2–3):139–153. doi:10.1016/S0168-1923(97)00021-X

Lloyd CD (2005) Assessing the effect of integrating elevation data into the estimation of monthly precipitation in Great Britain. J Hydrol 308(1–4):128–150. doi:10.1016/j.jhydrol.2004.10.026

Lv LX, Zhang QB (2012) Asynchronous recruitment history of Abies spectabilis along an altitudinal gradient in the Mt. Everest region. J Plant Ecol 5(2):147–156. doi:10.1093/jpe/rtr016

Maignan F, Bréon FM, Chevallier F, Viovy N, Ciais P, Garrec C, Trules J, Mancip M (2011) Evaluation of a global vegetation model using time series of satellite vegetation indices. Geosci Model Dev 4(4):1103–1114

Maussion F, Scherer D, Mölg T, Collier E, Curio J, Finkelnburg R (2013) Precipitation seasonality and variability over the Tibetan Plateau as resolved by the high Asia reanalysis. J Clim 27(5):1910–1927. doi:10.1175/JCLI-D-13-00282.1

Ménégoz M, Gallée H, Jacobi HW (2013) Precipitation and snow cover in the Himalaya: from reanalysis to regional climate simulations. Hydrol Earth Syst Sci 17(10):3921–3936. doi:10.5194/hess-17-3921-2013

Miehe G, Miehe S, Vogel J, Co S, La D (2007) Highest treeline in the northern hemisphere found in southern Tibet. Mt Res Dev 27(2):169–173. doi:10.1659/mrd.0792

Pepin N (2015) Elevation-dependent warming in mountain regions of the world. Nat Clim Chang 5(5):424–430. doi:10.1038/nclimate2563

Pypker TG, Unsworth MH, Mix AC, Rugh W, Ocheltree T, Alstad K, Bond BJ (2007) Using nocturnal cold air drainage flow to monitor ecosystem processes in complex terrain. Ecol Appl 17(3):702–714. doi:10.1890/05-1906

Rangwala I, Miller JR (2012) Climate change in mountains: a review of elevation-dependent warming and its possible causes. Clim Chang 114(3–4):527–547. doi:10.1007/s10584-012-0419-3

Rötter RP, Höhn J, Trnka M, Fronzek S, Carter TR, Kahiluoto H (2013) Modelling shifts in agroclimate and crop cultivar response under climate change. Ecol Evol 3(12):4197–4214. doi:10.1002/ece3.782

Saino N, Ambrosini R, Rubolini D, von Hardenberg J, Provenzale A, Hüppop K, Hüppop O, Lehikoinen A, Lehikoinen E, Rainio K, Romano M, Sokolov L (2011) Climate warming, ecological mismatch at arrival and population decline in migratory birds. Proc R Soc Lond B Biol Sci 278(1707):835–842. doi:10.1098/rspb.2010.1778

Schickhoff U (2005) The upper timberline in the Himalayas, Hindu Kush and Karakorum: a review of geographical and ecological aspects. In: Broll PDG, Keplin DB (eds) Mountain ecosystems. Springer, Berlin, pp 275–354 [online] Available from: http://link.springer.com/chapter/10.1007/3-540-27365-4_12 (Accessed 28 October 2014)

Schickhoff U, Bobrowski M, Böhner J, Bürzle B, Chaudhary RP, Gerlitz L, Heyken H, Lange J, Müller M, Scholten T et al (2015) Do Himalayan treelines respond to recent climate change? An evaluation of sensitivity indicators. Earth Syst Dyn 6:245–265

Schoof JT (2013) Statistical downscaling in climatology. Geogr Compass 7(4):249–265. doi:10.1111/gec3.12036

Sheridan P, Smith S, Brown A, Vosper S (2010) A simple height-based correction for temperature downscaling in complex terrain. Met Apps 17(3):329–339. doi:10.1002/met.177

Singh J, Yadav RR (2005) Spring precipitation variations over the western Himalaya, India, since A.D. 1731 as deduced from tree rings. J Geophys Res 110(D1):D01110. doi:10.1029/2004JD004855

Soria-Auza RW, Kessler M, Bach K, Barajas-Barbosa PM, Lehnert M, Herzog SK, Böhner J (2010) Impact of the quality of climate models for modelling species occurrences in countries with poor climatic documentation: a case study from Bolivia. Ecol Model 221(8):1221–1229

Von Storch H (1995) Inconsistencies at the interface of climate impact studies and global climate research. Meteorol Z 4(2):72–80

Wilby RL, Charles SP, Zorita E, Timbal B, Whetton P, Mearns LO (2004) Guidelines for use of climate scenarios developed from statistical downscaling methods. [online] Available from: http://www.narccap.ucar.edu/doc/tgica-guidance-2004.pdf. Accessed 28 Oct 2014

Wulf H, Bookhagen B, Scherler D (2010) Seasonal precipitation gradients and their impact on fluvial sediment flux in the Northwest Himalaya. Geomorphology 118(1–2):13–21. doi:10.1016/j.geomorph.2009.12.003

Chapter 4
Climate Change and Hydrological Responses in Himalayan Basins, Nepal

Tirtha Raj Adhikari and Lochan Prasad Devkota

Abstract Studies on water and related fields are vital for protecting the environment and climate. Lack of hydrometeorological data, particularly in a high-altitude region such as Nepal, hinders the process of understanding the systems of earth science dynamics. In this study, observed data were used for the period 1988–2010 from three high-altitude regions, viz., Annapurna, Langtang, and Khumbu, of Nepal. The Coupled Global Climate Model (CGCM3) for A1B SRES scenarios during the period 2001–2060 was used to determine projections. The statistical downscaling model (SDSM) was used to downscale precipitation and temperature data at the Modi, Langtang, and Dudh Koshi river basins. The simulated precipitation and temperature data were corrected for bias before implementation in the conceptual rainfall–runoff model Hydraologiska Byrans Vattenbalansavde (HBV) for hydrological response analysis. In the HVB-light 3.0, the Groups Algorithms Programming (GAP) optimization approach and calibration were used to obtain several parameter sets that were ultimately reproduced to observe the stream flow.

The CGCM3 model projects increasing trends in annual as well as seasonal precipitation, except in summer [June, July August, September (JJAS], during 2001–2060 for A1B SERS emission scenarios over the three sites under investigation. The model projects warmer days in every season of the entire period from 2001 to 2060. These warming trends are higher in maximum than in minimum temperatures throughout the year, which indicates an increasing trend of daily temperature range as the greenhouse effect increases. Further, trends for post-monsoon (ON) temperature are much cooler compared to the remaining three seasons (months) over all three sites. In addition, decreasing trends in summer discharge at Langtang Khola and increasing trends in Modi Khola and Dudh Koshi river basins are evident. Among all basins, the flow regime is more pronounced during the later parts of future decades as compared to the preceding decades.

Keywords Temperature • Precipitation and discharge trends • SDSM • HVB-light 3.0 • Bias correction

T.R. Adhikari (✉) • L.P. Devkota
Central Department of Hydrology and Meteorology, Tribhuvan University, Kirtipur, Kathmandu, Nepal
e-mail: tirtha43@yahoo.com

R.B. Singh et al. (eds.), *Climate Change, Glacier Response, and Vegetation Dynamics in the Himalaya*, DOI 10.1007/978-3-319-28977-9_4

4.1 Introduction

This research focuses on a comparative study of the impact of climate change on the flow regime in three perennial monsoon-dominated river basins of Nepal Himalaya. The Statistical Downscaling Model (SDSM), version 4.2.2, and HVB-light 3.0 software have been used for climate and river runoff simulation. The SDSM is a hybrid of a regression method and weather generator; mainly statistical downscaling methods have not been documented for the climate research in these river basins of Nepal (Rashid and Mukand 2012), so research based on SDSM and HVB-light 3.0 is at an early stage. The main objectives of this chapter are to evaluate the application of SDSM over these three basins in Nepal and to generate local-scale precipitation and temperature scenarios under future emission scenarios. The HVB-light 3.0 hydrological model, which is a conceptual hydrological model for continuous simulation of runoff, is used for discharge simulations in all three basins. This HVB model was originally developed at the Swedish Meteorological and Hydrological Institute (SMHI) in the early 1970s to assist hydropower operations (Bergstrom and Graham 1998) by providing hydrological forecasts. The HVB-light 3.0 model simulates daily discharge using daily rainfall and temperature data and monthly estimates of potential evaporation. In this study, basin-wise temperature and precipitation have been simulated on the basis of observed data for the climate change scenario, and these values have been used as input for the hydrological model HVB-light 3.0. In recent years, numerous studies have investigated the impact of climate change on hydrology and hydrological responses in many regions. Charlton et al. (2006) investigated the impact of climate change on water supplies and flood hazard in Ireland using a grid-based approach, the HYSIM model (Manley 1993), with statistically downscaled climate data from the Hadley Centre Climate Model, HadCM3 (Gordon et al. 2000). Murphy et al. (2006a) employed similar downscaled data to force the HYSIM model, modeling individual basins rather than a gridded domain. A regional climate model is used to produce the dynamically downscaled precipitation and temperature data that are required by the HVB-light 3.0 conceptual rainfall–runoff model.

The effects of global warming on the glaciers and ice reserves of Nepal has serious implications for freshwater reserves and consequently for low flows. Any significant change in glacier mass and groundwater storage will impact the water resource at a regional scale. Increases in temperature and precipitation in the Himalayas accelerate the melting of ice and snow as well as enhancing flooding events from direct runoff, whereas the dry season discharge (base flow) decreases. The projected changes in climatic parameters have an adverse effect on the water storage capacity of the Nepal Himalaya. The major concerns are the rapid reduction of glaciers in much of the Himalayan region and the upward shift of the snow line.

In the past, many attempts have been made to study climate change impact and hydrological responses. Most of these studies have focused on extreme events such as flood and drought, whereas climate change studies in Himalayan regions have

focused mainly on the melting and retreating of glaciers, glacial lake outburst floods (GLOF), and their trends. In this study, however, the temperature, precipitation, and discharge trends of three basins are presented.

4.2 Study Area

Nepal is situated in the middle of the Hindu Kush Himalayan region. The country extends between 26°22′ and 30°27′ N latitude and 80°40′ and 88°12′ E longitude; it is surrounded by India to the east, south, and west and China to the north. The country is about 885 km in length from east to west, and the north–south width varies from 145 to 241 km. Within this range, the altitudinal variations are from about 60 m above mean sea level (a.m.s.l.) in the southern plain (called Terai) to Mount Everest (8848 m) in the northeast. Of the total area of the country, 147,181 km^2, about 86 % of the area is composed of hilly and mountainous regions and the remaining 14 % of flatlands.

In general, the country is divided into five major physiographic zones: the Terai, Siwalik, Hill, middle mountain, and high mountain. The Terai is characterized by a long narrow belt of fertile agricultural flatland; it is part of the alluvial Gangetic Plains and ranges in altitude from 60 to 300 m. It lies between the Indian border in the south and the first outer foothills of Nepal in the north. The Siwalik range, 600–1500 m in elevation, lies in the north of the Terai region. To the north of Siwalik is a zone of discontinuous valleys (also called "Dun"). Intensive cultivation and decreasing forest cover have been causing serious problems of soil erosion in these valleys. Further north of these valleys is the Mahabharat Range (2700–3700 m), which, in terms of formation and elevation, is well developed in eastern and central Nepal and poorly developed in western Nepal. The northernmost part of Nepal is the snowy mountainous region (Himalaya), which is above 4000 m in elevation and stretches from the east to the west of the country.

This research focuses only on the impact of climate change on hydrological responses within three perennial monsoon-dominated river basins of Nepal's Himalayan region. The basins studied are the Modi Khola river basin in Annapurna region, the Langtang Khola river basin in Langtang region, and the Dudh Koshi river basin in Khumbu region.

Three watersheds—Modi Khola river basin (Annapurna), Langtang Khola river basin (Langtang), and Dudh Koshi river basin (Khumbu)—with areas of 640.79 km^2, 583.41 km^2, and 3710.30 km^2, respectively, were selected for this study. The Modi Khola river basin hydrological station is situated at latitude 28.12° N and longitude 83.42° E, and the meteorological station is situated at latitude 28.13°–28.31° N and longitude 83.42°–83.57° E. Its elevation ranges between 667 and 8024 m a.m.s.l. Similarly, the Syabrubesi hydrological station is located at latitude 28.16° N and

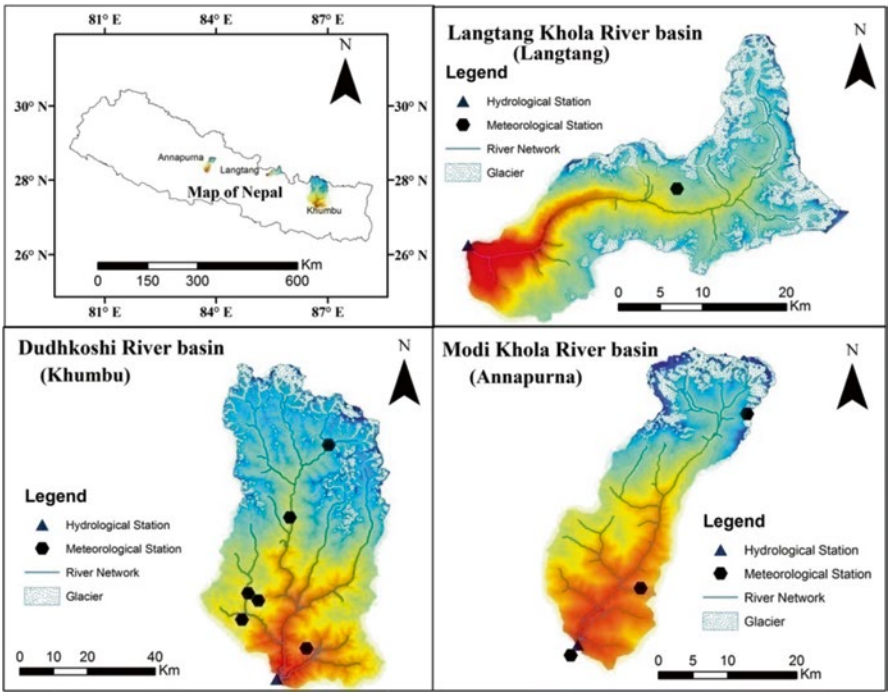

Fig. 4.1 Location of Langtang Khola, Dudh Koshi, and Modi Khola river basins in Nepal (Source: Author)

longitude 85.35° E and the Langtang Kyanging meteorological station at latitude 28.22° N and longitude 85.62° E. The elevation ranges from 1434 amsl up to the peak of Langtang Lirung at 7234 amsl. The Rabuwa Bazar hydrological station is found at latitude 27.16° N and longitude 86.65° E and the Khumbu region meteorological stations at latitude 27.21°–27.89° N and longitude 86.45°–86.83° E, where the elevation ranges from 439 to 8848 amsl. The location of each river basin in Nepal is presented in Fig. 4.1.

4.2.1 Watershed Characteristics of the Three Basins

Watershed characteristics depend upon peak discharge, time variation of runoff (hydrography), stage versus discharge, total volume of runoff, and frequency of runoff (statistics and return period). However, in this study, the flow regime of all three river basins is dependent on monsoon storms and the glacier area and its contribution to melting. In Nepal, the flow regime is divided into seven drainage basins:

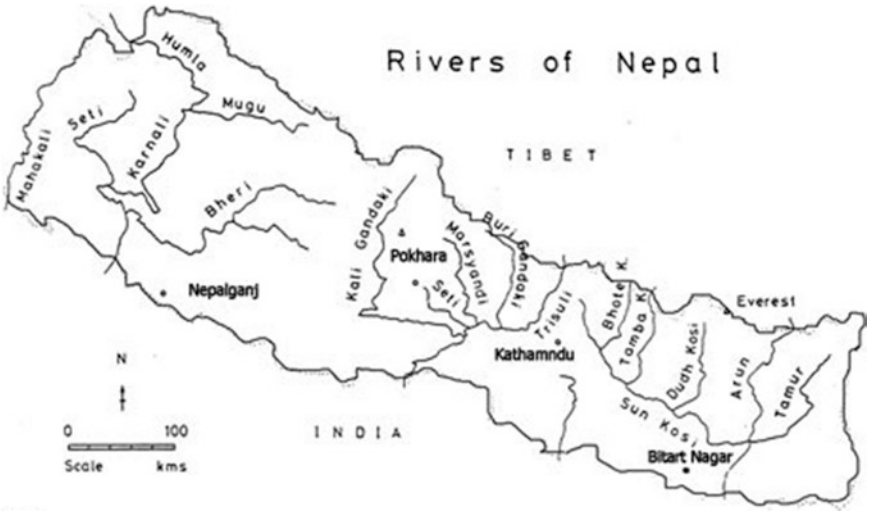

Fig. 4.2 The major river systems of Nepal (Source: Author)

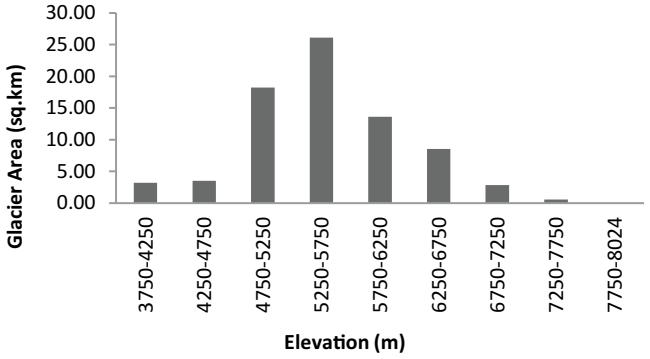

Fig. 4.3 Glacier area and elevation characteristics of Modi Khola river basin (Source: Author)

the Kankai Mai river basin, the Koshi river basin, the Bagmati river basin, the Narayani river basin, the West Rapti river basin, the Karnali river basin, and the Mahakali river basin (Fig. 4.2).

Among these, only three sub-river basins, that is, the Modi Khola, Langtang Khola, and Dudh Koshi river basins, were considered for this study. In the Modi Khola river basin, the highest glacier area was found between 2550 and 5750 m (Fig. 4.3) and in the Langtang Khola river basin between 5434 and 5934 m (Fig. 4.4). The Dudh Koshi river basin has the greatest glacier area, 413.2 km^2, between 4500 and 5000 m in elevation (Fig. 4.5).

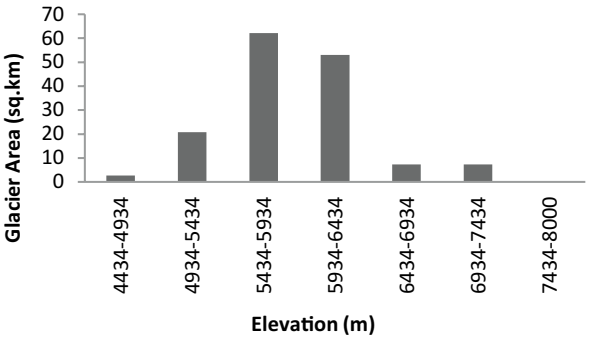

Fig. 4.4 Glacier area and elevation characteristics of Langtang Khola river basin (Source: Author)

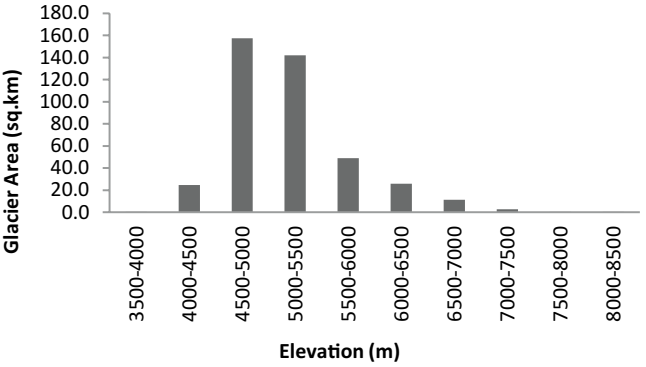

Fig. 4.5 Glacier area and elevation characteristics of Dudh Koshi river basin (Source: Author)

4.3 Data Collection and Quality Control

All necessary temperature, precipitation, and discharge data are collected for different periods from the Department of Hydrology and Meteorology (DHM), Government of Nepal (Table 4.1). The collected observed meteorological data from 1988 to 2010 and the observed discharge data from 1991 to 2010 were used for model calibration and validation purposes.

The time-series data are considered to be acceptable only if they satisfy the homogeneity and consistency of quality control (WMO 1988). Sen's slope method was used to check the quality of the available data. Annual meteorological data were shown as blank if there were missing values in the series for any period, because Sen's slope estimation method allows estimating trend with missing values. The double mass analysis (sometimes called double sum analysis) is a useful method for assessing homogeneity in a weather parameter (Allen et al. 1998; Raghunath 2006; Silveira 1997). It is a useful tool for checking the consistency of a climatic variable

Table 4.1 Characteristics of hydroclimatic data collected from Department of Hydrology and Meteorology (DMH), Government of Nepal

Station name	Type	Latitude (N)	Longitude (E)	Elevation (m)	Record period	Missing period
Machhapuchhre[a]	Climatic	28.31	83.57	3470	1987–2010	1996 and 1997
Lumle[a]	Climatic	28.18	83.48	1740	1969–2010	No
Parbat[a]	Precipitation	28.13	83.42	891	1969–2010	1969 (Jan–May)
Modi[b]	Hydrological	28.12	83.42	667	1991–2010	No
Langtang[a]	Climatic	28.22	85.62	3920	1987–2010	No
Sabrubasi[b]	Hydrological	28.16	85.35	1434	1991–2010	No
Dingboche Khumbu[a]	Climatic	27.89	86.83	4355	1987–2010	2000, 2001 and 2002
Chaurikhark[a]	Precipitation	27.42	86.43	2619	1949–2010	1952
Parkarns[a]	Precipitation	27.26	86.34	1982	1948–2010	No
Aiselukhark[a]	Precipitation	27.21	86.45	2143	1948–2010	No
Okhaldhunga[a]	Climatic	27.32	86.50	1720	1948–2010	1958
Mane Bhanjyang[a]	Precipitation	27.29	86.25	1576	1948–2010	No
Salleri[a]	Precipitation	27.3	86.35	2378	1948–2010	1962 – 1972
Dudh Koshi Rabuwa[b]	Hydrological	27.16	86.65	460	1964–2010	No

[a]Meteorological station
[b]Hydrological station

where the error results from such reasons as a change in the environment (or exposure) of a station, for example, planting trees or cutting nearby forest, which affects the catch of the gauge because of differences in wind pattern or exposure. Replacement of the recording instruments with a new system might also result in such deviations (Raghunath 2006).

4.4 Methodology

Analysis of the effects of climate change on hydrological responses in Modi Khola river basin (Annapurna region), Langtang Khola river basin (Langtang region), and Dudh Koshi river basin (Khumbu region) was selected for this study. Selections were made on the basis of the availability of relatively better hydrometeorological data compared to other regions of the Nepal Himalayas. The following methodology was applied in this study.

- Downloading SRTM DEM data (http://www.cgiar-csi.org/data/srtm-90m-digital-elevation-database-v4-1) and separation of the study basin were done by GIS software. The SRTM digital elevation data, produced by NASA originally, are a major breakthrough in digital mapping of the world and provide a major advance in accessibility of high-quality elevation data for large portions of the tropics and other areas of the developing world.
- Collection of daily hydrometeorological data and evaluation of data quality included classification into seasons: winter, December of the previous year to February (DJF); spring, March to May (MAM); summer, June to September (JJAS); and autumn, October to November (ON).
- Calibration of SDSM and validation of the SDSM model followed the generation of a temperature and rainfall scenario by SDSM. The generated rainfall and temperature data are compared with observed and modeled data for bias correction.
- The biased rainfall and temperature data have been corrected and were used later in the hydrological model for the generation of the discharge scenario. These generated scenario data were computed for generating the seasonal trends.
- Comparison of the seasonal trend of all three basins.

4.4.1 Bias Correction Methodology

Results from GCMs and regional climate models (RCMs) always show some degree of bias for both temperature and precipitation data. The reasons for such biases include systematic model errors caused by imperfect conceptualization, discretization, and spatial averaging within the grids. The bias correction approach is used to eliminate the biases from the daily time-series of downscaled data (Salzmann et al. 2007). In this study, Eqs. 4.1 and 4.2 are used to de-bias daily temperature and precipitation data (Mahmood and Mukand 2012):

$$T_{\text{deb}} = T_{\text{SCEN}} - \left(\overline{T}_{\text{CONT}} - \overline{T}_{\text{obs}}\right) \tag{4.1}$$

$$P_{\text{deb}} = P_{\text{SCEN}} \times \left(\frac{\overline{P}_{\text{obs}}}{\overline{P}_{\text{CONT}}}\right) \tag{4.2}$$

where $\boldsymbol{T}_{\text{deb}}$ and $\boldsymbol{P}_{\text{deb}}$ are bias-corrected daily temperature and precipitation, respectively; $\boldsymbol{T}_{\text{SCEN}}$ and $\boldsymbol{P}_{\text{SCEN}}$ are daily temperature and precipitation, respectively, obtained from downscale data (SDSM); $\bar{\boldsymbol{T}}_{\text{obs}}$ and $\bar{\boldsymbol{P}}_{\text{obs}}$ are long-term monthly mean of observed temperature and precipitation, respectively; and $\bar{\boldsymbol{T}}_{\text{CONT}}$ and $\bar{\boldsymbol{P}}_{\text{CONT}}$ are long-term monthly mean of temperature and precipitation, respectively, simulated using SDSM for the observed period.

In Sen's method, if a linear trend is present in a time-series, then the true slope (change per unit time) can be estimated by using a simple nonparametric procedure developed by Sen (1968); thus, in the linear model $f(t)$ can be described as

$$f(t) = Qt + B \tag{4.3}$$

where Q is the slope and B is a constant. To derive an estimate of the slope Q, the slopes of all data pairs are calculated:

$$Q_i = \frac{Z_j - Z_k}{(j-k)} \text{ where } j > k \tag{4.4}$$

If there are n values of Z_j in the time-series, we obtain as many as $N = n(n-1)/2$ slope estimates of Q_{i}. Sen's estimator of slope is the median of these N values of Q_{i}. The N values of Q_{i} are ranked from the smallest to the largest, and Sen's estimator is

$$Q = \begin{cases} Q_{\frac{N+1}{2}} & \text{if } N \text{ is odd} \\ \frac{1}{2}\left\{Q_{\frac{N}{2}} + Q_{\frac{N+2}{2}}\right\} & \text{if } N \text{ is even} \end{cases} \tag{4.5}$$

The foregoing equations were used for the Mann–Kendall test and Sen's slope estimation in this study. The normal variate statistics (Z) and Sen's slope were obtained from the calculation for each month and also for the annual time-series. The presence of a statistical significance of trend was evaluated using the Z value.

To test for either an upward or downward monotone trend (a one-tailed test) at the α-level of significance, H_0 (no trend) was rejected if the absolute value of Z is greater than $Z_{1-\alpha}$ where $Z_{1-\alpha}$ was obtained from the standard normal cumulative distribution tables. The significance level of 0.05 means that there is a 5 % probability that the values of Z_{i} are from a random distribution, and with that probability we are in error when rejecting H_0 of no trend. Sen's slope is available as average change per year; a negative value indicates a negative trend and a positive value indicates a positive trend.

4.4.2 HVB-Light 3.0 Methodology for Model Calibration and Validation

The present study builds on the work of Wang (2006) to develop a methodology that is used with an ensemble of dynamically downscaled climate data to investigate the impacts of climate change on the hydrology of Irish rivers. Wang (2006) used the HBV model (Bergstrom 1992) from the Swedish Meteorological and Hydrological Institute (SMHI), which is usually calibrated using a manual trial-and-error approach. Here, it has been replaced by the HVB-*light 3.0* model of Seibert (2005) because its interface allows Monte Carlo simulations. Calibration using the Monte Carlo method yields an ensemble of simulations that allows accounting for parameter uncertainty in analysis. A Monte Carlo approach to calibration was used in which the 99th percentile of an ensemble of 10,000 parameter sets was selected for use in the impact study. This approach allows the inclusion of an uncertainty parameter in the study, which provides a range of possible values, rather than a single value, that further allows an estimation of confidence in the research outcome. The HVB-*light 3.0* model was validated for a reference period (1961–2000) to ensure that stream flow was modeled correctly. A persistent positive bias in the downscaled precipitation was observed and removed to improve the agreement between modeled and observed stream flow. It was shown that the impact of parameter uncertainty on the validation of seasonal (winter and summer) flow was less significant than in the annual maximum daily mean flow. To investigate the hydrological and catchment characteristics, analysis of the affecting parameter was carried out, the missing dataset of temperature and precipitation was filled by the statistical downscaling model, and the conceptual model was run several times to generate three different results by varying the parameter affecting the hydrological characteristics. Three sets of methods including one without using a glacier component and another using the glacier component were derived, and finally simulation of river discharge by the HVB-*light 3.0* model was carried out by assuming the temperature increase. Konz and Merz (2010) applied the HBV model for the Tamor River to estimate runoff at Tapethok, Taplejung, in eastern Nepal. In general, the HBV model was able to correctly simulate low flow, except for some sharp peaks caused by isolated precipitation events (Konz and Merz 2010). In this study, a similar analysis was carried out, and similar results were obtained because the HBV model was able to simulate low flows very well, with the exception of sharp peaks. The model HVB-*light 3.0* was calibrated for the three river basins, and basin areas were divided into 15 elevation zones in the Modi Khola river basin, into 13 elevation zones in the Langtang river basin, and into 17 elevation zones in Dudh Koshi river basin. Two vegetation zone, namely, the glacier and the vegetated area for the calibration period, were used, and the HVB-*light 3.0* model was calibrated by trial-and-error technique in the study of the three basins.

4.5 Results

4.5.1 Observed Maximum Temperature

The observed seasonal maximum temperature is approximately 13.2 °C in spring at Annapurna, and similarly the observed seasonal minimum temperature is around −8.0 °C during winter at Khumbu, whereas the observed seasonal mean annual temperature is about 3.3 °C at Annapurna and Khumbu, for all seasons (Tables 4.2, 4.3, 4.4).

Table 4.2 Observed seasonal maximum temperature (°C) (1988–2010)

Season[a]	Annapurna	Langtang	Khumbu
DJF	4.4	3.6	3.5
MAM	11.6	7.8	11.0
JJAS	13.2	11.7	10.1
ON	6.3	5.0	5.2
Annual	13.2	11.7	11.0

[a]*DJF* December January February, *MAM* March April May, *JJAS* June July August September, *ON* October November

Table 4.3 Observed minimum temperature (°C) (1988–2010)

Season	Annapurna	Langtang	Khumbu
DJF	−4.3	−6.3	−8.0
MAM	1.4	−1.1	−1.2
JJAS	6.7	6.2	2.9
ON	0.4	−0.8	−1.6
Annual	−4.3	−6.3	−8.0

Table 4.4 Observed seasonal mean annual temperature (°C) (1988–2010)

Season	Annapurna	Langtang	Khumbu
DJF	−1.9	−1.3	−3.4
MAM	4.9	3.4	3.7
JJAS	8.1	8.9	6.2
ON	2.2	2.1	1.3
Annual	3.3	3.3	2.0

4.5.2 Observed Annual Temperature Trend

Observed seasonal maximum temperature trends for 1988–2010 are depicted in Table 4.5. All three regions show the highest maximum and mean temperature, with an increasing trend, in winter (DJF). The lowest minimum temperature trends are found to occur during spring (MAM) in Annapurna and summer (JJAS) in the Khumbu regions. Similarly, the highest annual maximum temperature trend, of 0.1414 °C/year, is found in the Langtang region among the three regions, and the lowest minimum temperature trend observed was −0.0024 °C/year in the Khumbu region.

4.5.3 Observed Precipitation Distribution

The month of July has the highest rainfall, followed by August, in the Modi Khola and the Dudh Koshi river basins. The monsoon precipitation is more pronounced in the Modi Khola and Dudh Koshi river basins. In the Langtang Khola river basin, the month of August yields the highest rainfall, followed by July. The total precipitation in the Modi Khola river basin during the summer (JJAS) is 2062 mm, of which 85 % of the rainfall occurs in the monsoon season, and rainfall of 44 mm occurs during winter (DJF). Similarly, the total precipitation of Langtang Khola river basin during the summer (JJAS) is 492 mm, of which 78 % of the precipitation occurs in the monsoon season, with precipitation of 20 mm during the autumn (ON) season. The total precipitation for the Dudh Koshi river basin during the summer (JJAS) is 345 mm, of which 80 % of precipitation occurs in the monsoon season, with precipitation of 9 mm in winter (DJF) (Table 4.6). The maximum coefficient of variation was exceeded in November at the Modi Khola river basin (Fig. 4.6) and the Dudh Koshi river basin (Fig. 4.7). Similarly, the coefficient of variation was exceeded in October at the Langtang Khola river basin (Fig. 4.8).

4.5.4 Observed Precipitation Trends

The observed highest precipitation trend of 2.2249 mm/year was found during winter (DJF) in the Langtang region (Table 4.7). The lowest precipitation trend, −0.3386 mm/year, occurs in the Khumbu region in summer (JJAS). Similarly, observed annual precipitation trends are found to increase at a rate of 2.7452 mm/year in the Annapurna region. The observed annual precipitation trend has been found to be decreasing at the rate of −0.8264 mm/year in the Khumbu region.

Table 4.5 Observed temperature trends of the three river basins (1988–2010)

	Maximum			Minimum			Mean		
Season	Annapurna	Langtang	Khumbu	Annapurna	Langtang	Khumbu	Annapurna	Langtang	Khumbu
DJF	0.1129	0.1852	0.0857	0.0242	0.1267	0.0108	0.0657	0.1529	0.0857
MAM	0.0956	0.1718	0.0628	−0.0438	0.1115	0.0101	0.031	0.1421	0.0628
JJAS	0.081	0.1182	0.0499	0.0135	0.049	−0.0024	0.047	0.0838	0.0499
ON	0.0878	0.0992	0.0495	0.0021	0.0857	0.0045	0.0421	0.0924	0.0495
Annual	0.0955	0.1414	0.0639	0.0002	0.0884	0.0036	0.0499	0.0098	0.0639

Table 4.6 Observed precipitation distribution of the three river basins (1988–2010)

Seasons	Annapurna		Langtang		Khumbu	
	Seasonal total (mm)	Seasonal %	Seasonal total (mm)	Seasonal %	Seasonal total (mm)	Seasonal %
DJF	44	2	28	4	9	2
MAM	220	9	94	15	57	13
JJAS	2062	85	492	78	345	80
ON	109	4	20	3	20	5
Annual	2436	100	634	100	431	100

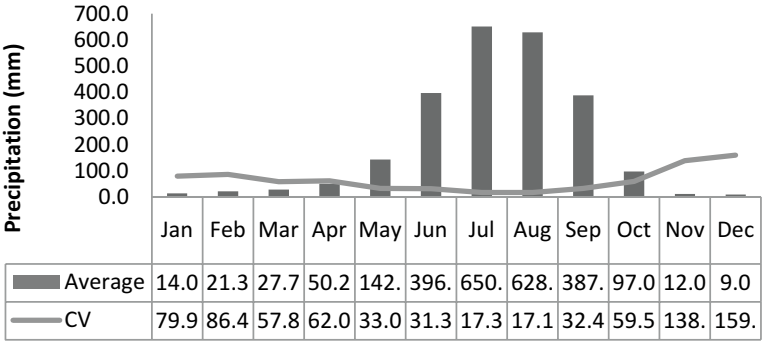

Fig. 4.6 Precipitation distribution of Modi Khola river basin (Source: Author)

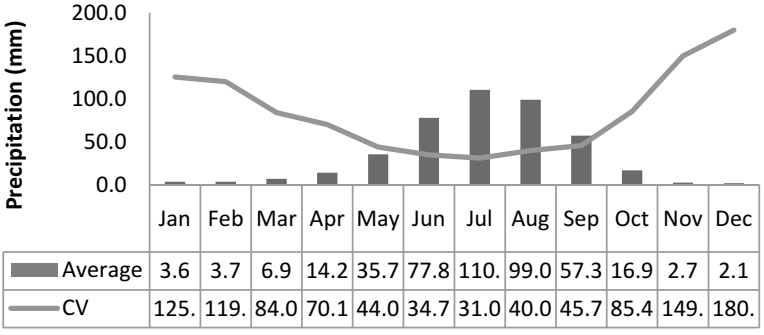

Fig. 4.7 Precipitation distribution of Dudh Koshi river basin (Source: Author)

4.5.5 Observed Discharge Distribution of the Three River Basins

The maximum discharge observed in the Annapurna region is 76 % in the Modi Khola basin, in the Langtang region, 57 % in the Langtang Khola basin, and in the Khumbu region, 77 % of the discharge, in the Dudh Koshi basin, is obtained in the summer season because of the monsoonal effect (Table 4.8).

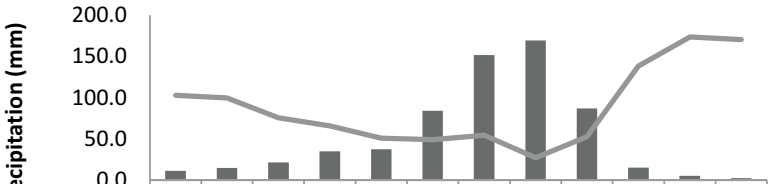

Fig. 4.8 Precipitation distribution of Langtang Khola river basin (Source: Author)

Table 4.7 Observed annual and seasonal precipitation trends of the three basins (1988–2010)

Season	Annapurna	Langtang	Khumbu
DJF	–0.6227	–0.2995	–0.0508
MAM	0.1094	0.2846	0.1320
JJAS	0.4398	2.2249	–0.3386
ON	1.3555	0.7979	0.1598
Annual	2.7452	10.608	–0.8264

Table 4.8 Seasonal observed discharge distribution (m^3/s) (1991–2010)

	Annapurna		Langtang		Khumbu	
Season	Seasonal total	Seasonal %	Seasonal total	Seasonal %	Seasonal total	Seasonal %
DJF	41	7	51	14	142	6
MAM	46	7	56	15	148	6
JJAS	468	76	212	57	1846	77
ON	62	10	51	14	276	11
Annual	617	100	369	100	2413	100

4.5.6 Observed Discharge and Trends of Three Basins

The annual trends of –0.2984 m^3/s and –0.3799 m^3/s are of decreasing order in Annapurna and Langtang regions, whereas the trend of 2.3072 m^3/s is of increasing order in the Khumbu region (Table 4.9).

Table 4.9 Observed discharge and trends of the three basins (1991–2010)

	Annapurna		Langtang		Khumbu	
Season	1991–2000	2001–2010	1991–2000	2001–2010	1991–2000	2001–2010
DJF (m^3/s)	11.1	15.8	17.5	16.5	43.1	47.9
MAM (m^3/s)	13.7	17.3	19.6	17.8	48.1	46.4
JJAS (m^3/s)	129.3	101.6	58.4	49.3	432	525.9
ON (m^3/s)	66	57.8	54.9	47.7	267.2	247.5
Annual (m^3/s)	54.9	47.1	33.4	28.9	189.2	219.8
Annual trend (1991–2010)	–0.2984		–0.3799		2.3072	

Table 4.10 Projected seasonal maximum temperature trend of A1B scenarios

	Maximum temperature (2001–2030)			Maximum temperature (2031–2060)		
Season	Annapurna	Langtang	Khumbu	Annapurna	Langtang	Khumbu
DJF	0.0183	0.0147	0.0216	0.0222	0.0071	0.0131
MAM	0.0285	0.0043	0.0294	0.0413	0.0037	0.0350
JJAS	0.0080	0.0160	0.0038	0.0159	0.0160	–0.0019
ON	0.0120	0.0085	–0.0102	–0.0059	–0.0012	–0.0032
Annual	0.0122	0.0144	0.0123	0.0203	0.0075	0.0116

Table 4.11 Projected seasonal minimum temperature trend of A1B scenarios

	Minimum temperature (2001–2030)			Minimum temperature (2031–2060)		
Season	Annapurna	Langtang	Khumbu	Annapurna	Langtang	Khumbu
DJF	0.0170	0.0366	–0.0039	0.0214	0.0249	–0.0013
MAM	0.0410	0.0414	0.0162	0.0517	0.0522	0.0043
JJAS	0.0102	0.0172	0.0241	0.0036	0.0139	0.0303
ON	–0.0650	0.0268	–0.0170	–0.0084	0.0278	0.0062
Annual	0.0151	0.0294	0.0085	0.0188	0.0300	0.0119

4.5.7 Projected Temperature Trends

The CGCM3-projected seasonal maximum temperature trend of A1B scenarios (Table 4.10) shows the highest maximum temperature with increasing trend in spring (MAM), except in Langtang (2001–2030), among all three regions. The lowest maximum temperature trend will occur in autumn (ON) among all three regions (2031–2060). Similarly, the highest annual maximum temperature trend, of 0.0203 °C/year, is found in the Annapurna region (2031–2060).

The CGCM3-projected seasonal minimum temperature trend of A1B scenarios is shown in Table 4.11. Lowest minimum temperature trends are found to occur in autumn (ON) in all regions except the Langtang region. The minimum temperature trends are found to increase during spring (MAM) in Annapurna and Langtang,

Table 4.12 Seasonal precipitation trend of A1B scenarios

	Precipitation trend of A1B (CGCM3: 2001–2030)			Precipitation trend of A1B (CGCM3: 2031–2060)		
Season	Annapurna	Langtang	Khumbu	Annapurna	Langtang	Khumbu
DJF	–0.0919	0.0174	0.0158	–0.1544	–0.00400	0.00070
MAM	–0.2728	0.0728	0.4109	0.55800	0.2220	0.2196
JJAS	–0.1327	0.0949	0.2420	0.02250	–0.1462	–0.2755
ON	–0.489	0.0072	–0.1277	2.7913	0.05850	–0.20770
Annual	2.9232	0.7621	1.9991	1.4753	0.20840	–0.8604

except in Khumbu (2031–2060). However, the lowest minimum temperature trends will occur in different seasons (2031–2060). Similarly, the highest annual minimum temperature trend, 0.0300 °C/year, is found to be increasing in Langtang compared to Khumbu and Annapurna regions during both projected periods.

4.5.8 Projected Precipitation Trends

The seasonal precipitation trends of the A1B scenarios is depicted in Table 4.12 (CGCM3: 2001–2060). In the Annapurna region, the precipitation trends are decreasing in all seasons, and the lowest precipitation occurs in autumn (ON), comparing all three regions (2001–2030), whereas the highest precipitation trends are found to occur in different seasons. Similarly, the highest precipitation trend, 2.7913 mm/year, is found to occur during autumn (ON) in Annapurna compared to Langtang and Khumbu (2031–2060). The lowest precipitation trend, –0.2755 mm/year, is found in the Khumbu region in summer (JJAS). Similarly, annual precipitation trends are increasing at the rate of 2.9232 mm/year and 1.4753 mm/year in Annapurna region (2001–2030 and 2031–2060, respectively), whereas in the Khumbu region, the annual precipitation trend has been found to be decreasing at –0.8604 mm/year (2001–2060). The annual precipitation trends of 0.7621 mm/year and 0.20840 mm/year are found in the Langtang region.

4.5.9 Projected Discharge Trends

The CGCM3-projected seasonal maximum discharge trend of A1B scenarios over the period of 2001–2060 is presented in Table 4.13. The maximum discharge in both Annapurna and Khumbu regions is found to be increasing in summer (JJAS), except in the Langtang region (2001–2030). Similarly, maximum discharge trends occur in different seasons (2031–2060). The lowest maximum discharge trend is found to occur during summer (JJAS) in the Langtang region (2001–2030) and during autumn (ON) in the Khumbu region (2031–2060). Similarly, annual maximum

Table 4.13 Projected seasonal maximum discharge trends of A1B scenarios

	Maximum (2001–2030)			Maximum (2031–2060)		
Season	Annapurna	Langtang	Khumbu	Annapurna	Langtang	Khumbu
DJF	0.0054	0.0479	0.2841	0.0135	0.0365	–0.0291
MAM	0.0788	0.0611	0.6692	0.0943	–0.0195	0.3399
JJAS	0.1315	–0.1010	1.7764	0.2535	0.0101	0.0984
ON	0.0693	0.1198	0.4291	0.0566	0.1408	–0.5431
Annual	0.0833	0.0277	0.7282	0.1208	0.0315	0.0193

Table 4.14 Projected seasonal minimum discharge trends of A1B scenarios

	Minimum (2001–2030)			Minimum (2031–2060)		
Season	Annapurna	Langtang	Khumbu	Annapurna	Langtang	Khumbu
DJF	0.0282	0.0279	0.0291	–0.0033	0.0038	0.0128
MAM	0.0235	0.0175	1.1798	0.0531	0.8885	0.9675
JJAS	0.1895	–0.0285	1.2070	0.2500	–0.1545	–0.7023
ON	–0.0051	0.0565	0.2222	–0.0196	–0.0408	–0.9862
Annual	0.0714	0.0234	0.6947	0.0925	–0.0552	–0.1522

discharge has an increasing trend in Khumbu, at rates of 0.7282 m^3/s/year (2001–2030) and 0.1208 m^3/s/year (2031–2060), compared to other regions.

The CGCM3-projected seasonal minimum discharge trend of A1B scenarios over the period 2001–2060 is shown in Table 4.14. The minimum discharge trends in Annapurna and Khumbu are found to be increased in summer, whereas in Langtang the trend is found to be increased during autumn (ON) and decreased in summer (JJAS) in the period 2001–2030. In Langtang and Khumbu, the minimum discharge trend is increasing during spring (MAM), but during summer (JJAS) in Annapurna, in the period 2031–2060. Similarly, the minimum discharge trends are found to occur in Annapurna and Khumbu, whereas these occur during summer in Langtang (JJAS) (2031–2060). The highest annual minimum discharge trend is found in the Khumbu region at the rate of 0.6947 m^3/s/year (2001–2030), whereas it is 0.0925 m^3/s/year in the Annapurna region (2031–2060), and the lowest value of –0.1522 m^3/s/year, is found in the Khumbu region.

4.6 Discussion

The observed highest annual maximum temperature trend of 0.1414 °C/year is found in the Langtang region, and the lowest minimum temperature trend (–0.0024 °C/year) is observed in the Khumbu region. The GCMS-simulated seasonal and annual range of mean of 20 ensembles for temperature scenarios with

A1B emission scenarios at Annapurna, Langtang, and Khumbu region, and the projected annual maximum and minimum temperature trends (0.0203 °C/year and 0.0300 °C/year), are found to be increasing in Langtang compared to Khumbu and Annapurna regions for the period 2031–2060. The observed annual precipitation trends are increasing at the rate of 2.7452 mm/year and 10.608 mm/year in Annapurna and Langtang regions, respectively. However, the observed annual precipitation trend has been found decreasing at −0.8264 mm/year in the Khumbu region.

The projected annual precipitation trends are found to be increasing at the rate of 2.9232 mm/year and 1.4753 mm/year in Annapurna region (2001–2030 and 2031–2060, respectively), although decreasing at 0.7621 mm/year and 0.2084 mm/year in Langtang region (2001–2030 and 2031–2060, respectively). Correspondingly, projected annual precipitation has an increasing trend of 1.9991 mm/year and a decreasing trend of −0.8264 mm/year in the Khumbu region for 2001–2030.

The annual observed discharge trends of −0.2984 $m^{3/}$s/year, −0.3799 m^3/s/year, and 2.3072 m^3/s/year are found in Annapurna, Langtang, and Khumbu regions, respectively, whereas annual observed discharge has an increasing trend in Khumbu. The projected annual maximum discharge at the rate of 0.0833 m^3/s/year and 0.1208 m^3/s/year is found in Annapurna region (2001–2030 and 2031–2060, respectively). The projected highest annual maximum discharge trend is found in Langtang region at the rate of 0.0277 m^3/s/year and 0.0315 m^3/s/year (2001–2030 and 2031–2060, respectively). The projected highest annual maximum discharge trend is found in Khumbu region at the rate of 0.7282 m^3/s/year and 0.0193 m^3/s/year (2001–2030 and 2031–2060, respectively). Similarly, the highest projected annual minimum discharge trend of 0.0714 m^3/s/year and 0.0925 m^3/s/year occurs in Annapurna, that of 0.0234 m^3/s/year and −0.0552 m^3/s/year in Langtang region, and that of 0.6947 m^3/s/year and −0.0552 m^3/s/year in Khumbu region (2001–2030 and 2031–2060, respectively). By using the A1B scenario from the CGCM3 data set and downscaling precipitation and temperature data for discharge projection, the results showed that the downscaled precipitation data are suitable for the study of climate change impact on flow regime in these three glacier-fed basins. The results of observed and simulated discharge obtained from the HVB-*light 3.0* model display a similar pattern when comparing the performance in simulation of historical stream flows in the three river basins.

The overall summary and results of analysis of the seasonal temperature obtained from the A1B scenario of climate projection show that a significant increase in maximum temperature during the spring season is projected, except in the Langtang region, whereas the discharge trend is increasing in summer in Annapurna and Langtang regions. Similarly, minimum temperature is found to have an increasing trend in the spring season in Annapurna and Langtang regions, whereas the minimum discharge is increasing in the subsequent season summer season during 2001–2030, except in Langtang and Khumbu regions, during 2031–2060; this difference could be caused by the melting of snow and the glacier combined with a decrease in rainfall in these regions. Similarly, the seasonal analysis of the precipitation data shows precipitation trends to increase significantly during the spring season in most

cases but the flow regime (discharge) is more pronounced in the subsequent season, that is, in summer; this finding results from the good response of the discharge scenario for temperature and precipitation.

4.7 Conclusion

The performance of SDSM downscaling, based on GCM predictors at three basins, was evaluated using the statistical properties of daily climate data. It is found that the application of SDSM for statistical downscaling is suitable for developing daily climate scenarios. To demonstrate the procedure of developing such scenarios, SDSM is applied based on the daily outputs of common climate variables from GCM simulations, which have been widely used in the development of daily climate scenarios; the results can be used in many areas of climate change impact studies. Based on the analysis of results, CGCM3 model has been found to be a useful model for the simulation of future temperature and precipitation scenario.

Both the annual (maximum and minimum) temperature trends of the A1B scenario in all three regions are found to have increasing trends for the periods of 2001–2030 and 2031–2060. The distribution of precipitation is controlled by the orientation of the mountain systems. This effect causes the middle mountain and windward side to receive relatively more precipitation than the high mountain, valley, and leeward side. Observed annual precipitation is increasing in Annapurna and Langtang regions, whereas no such trend is found in the Khumbu region. The annual precipitation of the A1B scenario of all three regions is increasing in both periods, 2001–2030 and 2031–2060, except in the Khumbu region for 2031–2060.

The annual maximum discharges of the A1B scenario of three basins are increasing during both periods, 2001–2030 and 2031–2060, as a consequence of monsoonal rainfall responses. The minimum discharge scenario is increasing only in the Annapurna region, but a decreasing trend is found in the Langtang and Khumbu regions for the period 2031–2060. The flow regime (discharge) trend is more pronounced after the subsequent summer (JJAS) season during both the 2001–2030 and 2031–2060 time periods.

Acknowledgments The authors thank Dr. Rishi Ram Sharma, the director general, and Mr. Suresh Chand Pradhan, hydrologist, of the Department of Hydrology and Meteorology (DHM), Government of Nepal, for providing the necessary data for this research. We heartily acknowledge Dr. Jan Seibert and the Uppsala University's Department of Earth Hydrology for supporting the software HBV-Light 3.0. We are grateful to the Data Access Integration (DAI, see http://quebec.ccsn.ca/DAI/) Team for providing the data and technical support. The DAI data download gateway is a collaboration among the Global Environmental and Climate Change Centre (GEC3), the Adaptation and Impacts Research Division (AIRD) of Environment Canada, and the Drought Research Initiative (DRI).

References

Allen RG, Pereira L, Raes D, Smith M (1998) Crop evapo-transpiration: guidelines for computing crop water requirements. FAO Irrigation and Drainage Paper 56. FAO, Rome, p 17

Bergstrom S (1992) The HBV model its structure and applications. SMHI Reports Hydrology, No. 4. Norkioping, Sweden: 32

Bergstrom S, Graham LP (1998) The Baltic basin – a focus for interdisciplinary research. Nordic Hydrological Conference, Aug 11–12, Helsinki

Charlton R, Fealy R, Moore S, Sweeney J, Murphy C (2006) Assessing the impact of climate change on water supply and flood hazard in Ireland using statistical downscaling and hydrological modeling techniques. Clim Change 74:475–491

Gordon C, Cooper C, Senior CA, Banks H, Gregory JM, Johns TC, Mitchell JFB, Wood RA (2000) The simulation of SST, sea ice extents and ocean heat transport in a version of the Hadley Centre coupled model without flux adjustments. Clim Dyn 16:147–168

Konz M, Merz J (2010) An application of the HBV model to the Tamor basin in Eastern Nepal. J Hydrol 7:49–58

Mahmood R, Mukand BS (2012) Evaluation of SDSM developed by annual and monthly submodels for downscaling temperature and precipitation in the Jhelum basin, Pakistan and India. Theor Appl Climatol 113:27–44

Manley RE (1993) HYSIM reference manual. RE Manley Consultancy, Cambridge

Murphy C, Charlton R, Sweeney J, Fealy R (2006a) Catering for uncertainty in a conceptual rainfall runoff model: model preparation for climate change impact assessment and the application of GLUE using Latin Hypercube Sampling. In: Proceedings of the National Hydrology Seminar, Tullamore, 2006

Raghunath HM (2006) Hydrology, principles, analysis and design. New Age International (P) Limited, New Delhi

Rashid M, Mukand BS (2012) Evaluation of SDSM developed by annual and monthly sub-models for downscaling temperature and precipitation in the Jhelum basin, Pakistan and India.

Salzmann N, Frei C, Vidale P, Hoelzle M (2007) The application of regional climate model output for the simulation of high-mountain permafrost scenarios. Global Planet Change 56:188–202

Seibert J (2005) HBV light version 2, user's manual. Institute of Earth Sciences, Department of Hydrology, Uppsala University, Uppsala

Sen PK (1968) Estimates of the regression coefficient based on Kendall's tau. J Am Stat Assoc 63:1379–1389

Silveira L (1997) Multivariate analysis in hydrology: the factor correspondence analysis method applied to annual rainfall data. Hydrol Sci 42(2):215–224

Wang H (2006) Inter-annual and seasonal variation of the Huang He (Yellow River) water discharge over the past 50 years: connection to impacts from ENSO events and dams. Global Planet Change 50:212–225

WMO (1988) Analyzing long time series of hydrological data with respect to climate variability. Project description. WCAP-3. Technical Report, World Meteorological Organization, Geneva

Chapter 5
Spatial and Temporal Variability of Climate Change in High-Altitude Regions of NW Himalaya

M.R. Bhutiyani

Abstract The high mountain areas such as the Alps, the Rockies, the Himalaya, etc. are considered as the "hotspots" over the surface of the earth where impacts of climate change are likely to be felt significantly. With regard to the Himalaya, their vulnerable ecosystem appears to have reacted to even the slightest possible changes in the temperature and precipitation conditions. The cascading effects of these changes on the vast expanse of water existing in the form of glacier ice and snow in the Himalaya, the forest cover, the health, and the socioeconomic conditions of the population inhabiting the Indo-Gangetic Plains have been the issues of serious concern.

The analyses of the temperature data collected manually at different observatories during the period from 1866 to 2012 show significant rate of warming during the winter season (1.4 °C/100 years) than the monsoon temperature (0.6 °C/100 years), due to rapid increase in both the maximum and minimum temperatures, with the maximum increasing much more rapidly. Annual rate of warming (1.1 °C/100 years) is abnormally higher than the global rate (about 0.7 °C/100 years) during this period. Not all regions of the north-western Himalaya (NWH) have reacted uniformly to the specter of climate change. Studies have confirmed significant spatial and temporal variations in magnitude of winter as well as summer warming in different ranges. While the windward side of the Pir Panjal and parts of the Greater Himalayan and Karakoram Ranges have shown statistically significant winter and summer warming, leeward sides of these ranges have not shown much change. The most remarkable finding of this study is the significant decreasing trend experienced at almost all stations above the equilibrium line (>5300 m in altitude) in winter warming as well as winter precipitation in higher reaches of the Karakoram Himalaya in the last three decades.

From the precipitation point of view, significant decreasing trends (at 95 % confidence level) in the monsoon and overall annual precipitation during the study period are indicated. In contrast, the winter precipitation has shown an increasing

M.R. Bhutiyani (✉)
Defence Terrain Research Laboratory, Defence Research & Development Organization, Metcalfe House, New Delhi 110054, India
e-mail: mahendra_bhutiyani@yahoo.co.in

R.B. Singh et al. (eds.), *Climate Change, Glacier Response, and Vegetation Dynamics in the Himalaya*, DOI 10.1007/978-3-319-28977-9_5

but statistically insignificant trend (at 95 % confidence level). Rising winter air temperatures have caused decreasing snowfall component and increasing rainfall component in total winter precipitation on the windward side of the Pir Panjal Range and parts of Greater Himalayan and the Karakoram Ranges. The analyses also show that although winter precipitation in the NWH has remained trendless in the last 140 years, there are significant increasing trends in the extreme snowfall events during winters and rainfall events during summers in Pir Panjal and Shamshawari Ranges in the last three decades and insignificant but increasing trends in the Great Himalayan and Karakoram Range. Decrease in winter snowfall amounts and increasing rainfall component at almost all stations have been affected to some extent by the increase in winter air temperature during this period.

The spatial and temporal variations in winter and summer warming and consequent precipitation changes in different ranges/regions of the NWH are attributed to varying scales of anthropogenic activities and growing urbanization of the areas. Decreasing temperatures in the last three decades in the Karakoram Himalaya with altitudes above the equilibrium line (>5300 m) are attributed to prevalence of permanent snow cover which appears to have influenced their microclimatology. These studies have significant bearing on the mass balance of the glaciers in the region and the hydrological behavior of various river systems in the Himalaya.

Keywords Climate change • High-altitude regions • Winter warming • NW Himalaya

5.1 Introduction

The climate in the Himalaya exercises a dominant control over the meteorological and hydrological conditions in the Indo-Gangetic Plains as majority of rivers derive significant portion of their discharge from seasonal snowmelt and/or melting of Himalayan glaciers. In view of their overall importance in the context of Indian subcontinent, the study of long-term and short-term climate changes in the Himalaya and their perilous impacts on its fragile ecosystem assumes importance. Because of the vast spread and large variations in hydrometeorological conditions in different parts and impracticability of carrying out such work for the entire Himalaya, this chapter covers the northwestern portion only, comprising of the states of Jammu and Kashmir and Himachal Pradesh (Fig. 5.1). This region, besides being influenced by, more or less, similar meteorological conditions, has a significant concentration of glaciers in its river basins and better network of meteorological stations as compared to the central and eastern Himalaya.

The climate in NWH is influenced by the western disturbances during the winter months from October to May and southwest monsoon from July to September. Precipitation during monsoon period is highest in Siwalik and Pir Panjal Ranges,

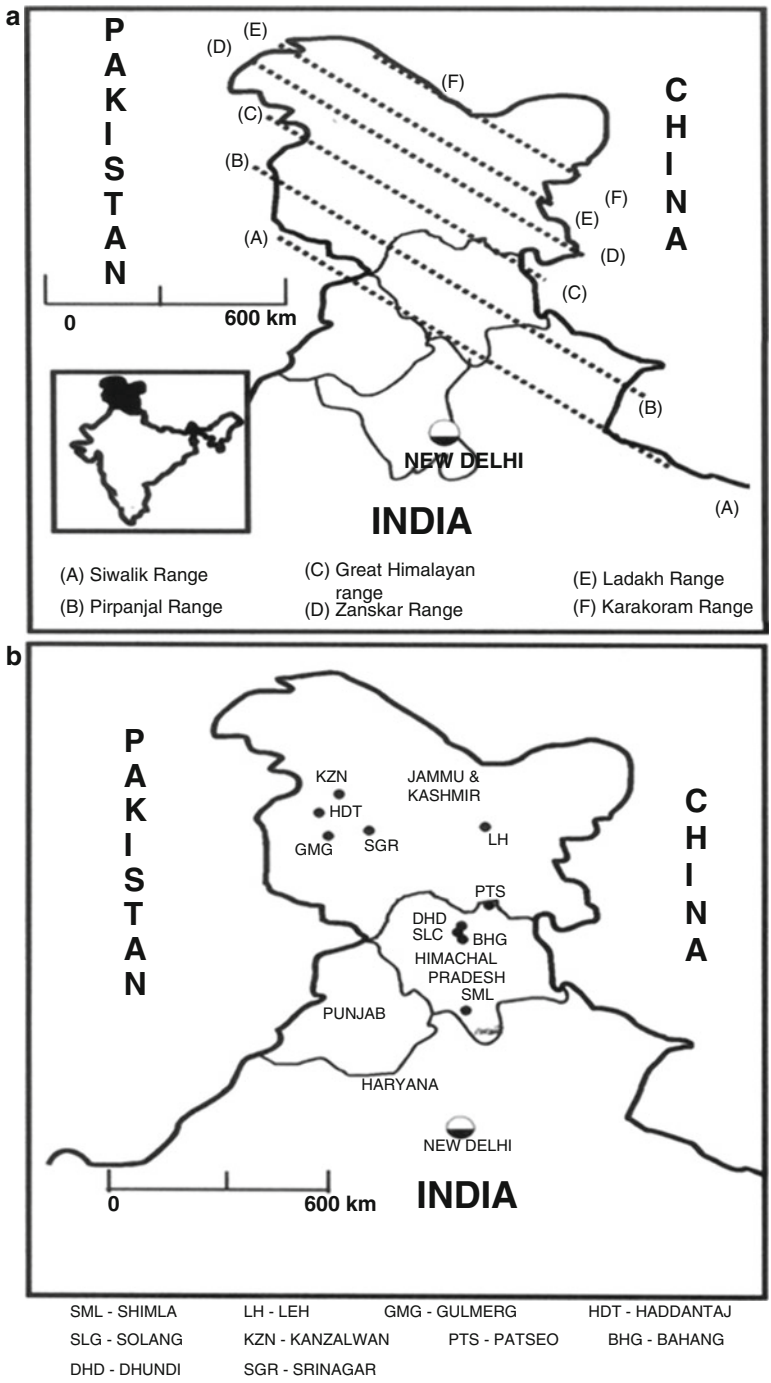

Fig. 5.1 Map of the northern western Himalaya showing approximate location of various ranges (**a**) and the meteorological stations (**b**) (Source: Bhutiyani et al. 2007)

and it reduces as one traverses northward into the Great Himalayan, Zanskar, Ladakh, and Karakoram Ranges (Rakhlecha et al. 1983). Significant variation is also observed in annual winter snowfall due to western disturbances in the NWH as various ranges in the NWH receive different amounts of snowfall ranging from about 100 to >1600 cm (snow depth). It is maximum in the Pir Panjal Range and decreases as one goes northward. Because of the variation in the mean air temperature, the changes occur in the percentage of solid precipitation (snowfall) to rainfall, duration of seasonal snow cover, snow settlement (densification) rates, and ablation rates in different ranges of the NWH (Mohan Rao et al. 1987; Bhutiyani 1992).

As compared to some studies on high-elevation regions round the globe such as by Diaz and Bradley (1997), Beniston et al. (1997), Beniston (2003), Diaz et al. (2003), and Rebetez (2004), very few studies have been carried out on the fluctuations in the climate in the Himalayan Mountains, primarily because of inaccessible terrain and inadequate database. Using the instrumental records, a few studies have examined the rainfall and temperature variations in the Nepal Himalaya and the Tibetan Plateau (Li and Tang 1986; Seko and Takahashi 1991; Borgaonkar et al. 1996) and Upper Indus Basin in Karakoram Himalaya (Fowler and Archer 2006). Temperature trends at Kathmandu in Nepal Himalaya and the Kosi Basin in Central Himalaya have been studied from the point of view of long-term trends (Sharma et al. 2000; Shreshtha et al. 2000). The precipitation and temperature trends in the western Himalaya and NWH have also been studied in the last century (Borgaonkar et al. 1996; Bhutiyani et al. 2000, 2004, 2007, 2008, 2010; Borgaonkar and Pant 2001; Yadav et al. 2004; Shekhar et al. 2010; Dimri and Dash 2012).

Based on proxy data of the ice cores from the Tibetan Plateau and tree-ring analyses from the hill regions of Uttaranchal, some authors have attempted to reconstruct the past climatic conditions during the last few centuries (Pant and Borgaonkar 1984; Liu and Chen 2000; Thompson et al. 2000).

A few studies have indicated that different regions of the NWH have not reacted uniformly to the specter of climate change and have confirmed significant spatial and temporal variations in magnitude of winter as well as summer warming in different ranges (Shekhar et al. 2010; Dimri et al. 2012). With a view to understand these aspects of climate change in NWH better, a systematic and detailed study was undertaken to analyze and evaluate temperature and precipitation trends in the NWH using instrumental data for the last 140 years. This chapter presents the results of this study.

5.2 Temperature Variations

The analyses of the temperature data show that significant increasing trends exist in annual temperature in almost all three main stations, namely, Shimla, Srinagar, and Leh in the NWH in the last century. The annual air temperature has shown an increase of about 1.1 °C during this period. Warming effect is particularly significant during the winter season. For NWH region as a whole, average winter

temperature has shown an elevated rate of increase (1.4 °C/100 years) than the monsoon temperature (0.6 °C/100 years) during the period from 1866 to 2006 (Fig. 5.2). Increase in winter air temperature during the three decades is unusually high (about 4.4 °C), as compared to an average rate of about 1.4 °C/100 years in the entire last century. The "warming" in the NWH has been primarily due to rapid increase in both the maximum and minimum temperatures, with the maximum increasing much more rapidly. Consequently, the diurnal temperature range (DTR) has also shown a significantly increasing trend in both winter and monsoon seasons in the last century (Bhutiyani et al. 2007, 2010). This is in contrast to the findings of studies in the Alps and Rockies (Beniston 1997; Brown et al. 1992) and similar observations on the global scale (Karl et al. 1995), where the minimum temperatures have increased at a higher rate.

Based on the analyses of the temperature data, three different epochs/periods were identified. An episode of comparatively higher (above-average) temperatures from 1876 to 1892 was followed by three more periods of temperature variation. Below-average mean air temperature persisted from 1893 to 1939 indicating a cooler episode, followed by a period of relatively stable/average temperatures till around 1969. The periods from 1969 to 1990 and from 1991 till 2006 are characterized by above-normal temperatures indicating warmer episodes. Temperature seems to have increased at markedly different rates during these two periods. The rate of increase appears to be highest since 1991 as compared to the period prior to 1991 (Bhutiyani et al. 2010), indicating unusual warming in the last two decades. This is also confirmed by the analysis of short-term data available for seven stations for the recent decades.

With regard to variation in monthly air temperatures during winter in the last three decades, the studies have indicated nonuniform rate of increase through the winter. Although the beginning of winter (November) has shown an increasing, but statistically insignificant trend, the onset of spring (March) has been marked by substantial warming (Table 5.1).

5.3 Precipitation Variations

Certain variations have occurred in precipitation patterns on the global scale in response to rising temperatures and resultant changes in evaporation from the oceans (Srivastava et al. 1992; Fallot et al. 1997; Zhai et al. 1999). Because of its high temporal and spatial variability and high sensitivity to circulation characteristics, precipitation has rarely been studied in as much details as temperature, as an index of climatic change (Thapliyal and Kulshrestha 1991; Srivastava et al. 1992).

Present study shows a statistically significant decreasing trend (at 95 % confidence level) in the monsoon and overall annual precipitation during the study period. In contrast, the winter precipitation has shown an increasing but statistically insignificant trend (at 95 % confidence level) (Fig. 5.2). This is generally in good

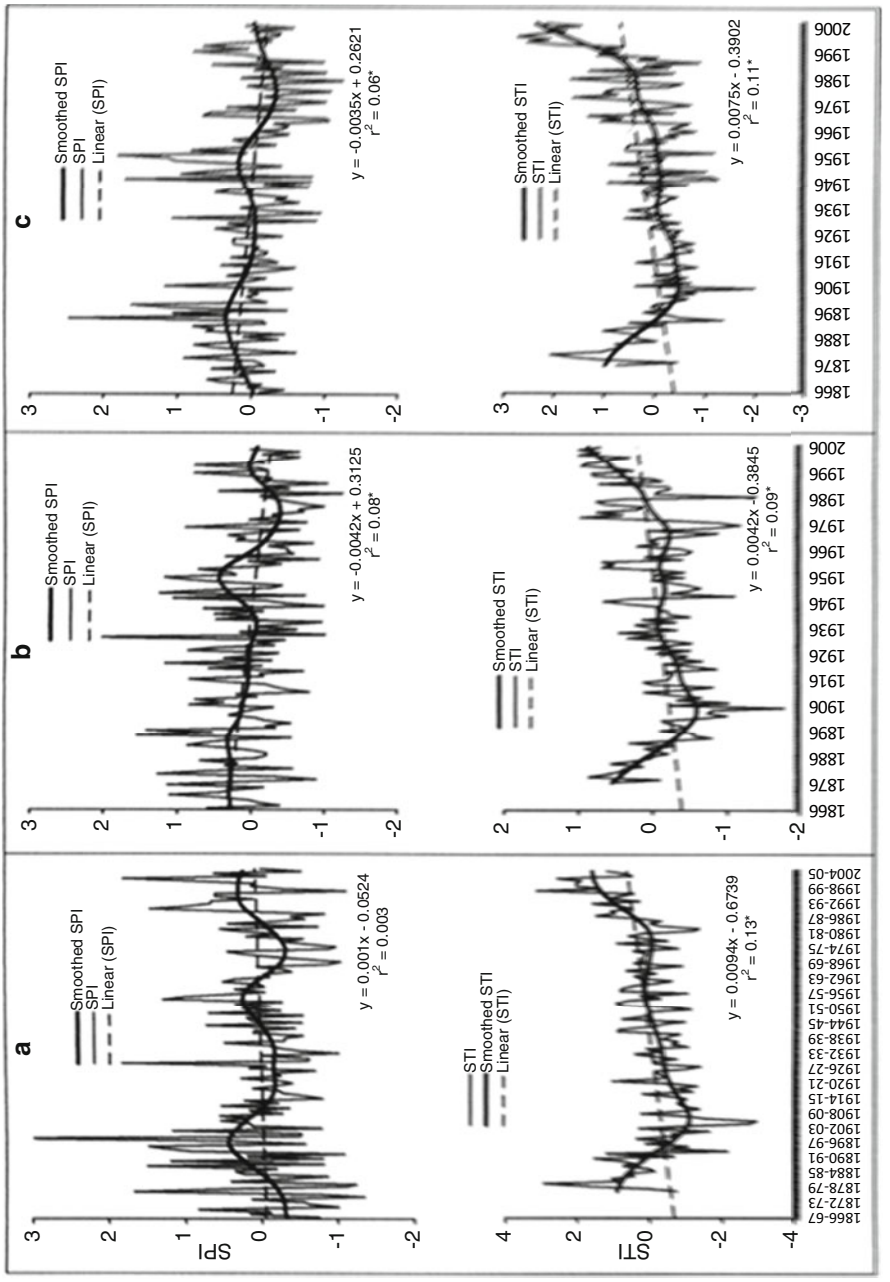

Fig. 5.2 Temporal variation of winter (**a**), monsoon (**b**), and annual (**c**) standardized precipitation index (*SPI*) and standardized temperature index (*STI*) in the northwestern Himalaya (*NWH*) during the period 1866–2006

Table 5.1 Linear trends in monthly air temperatures during winters in the NWH in the last three decades

Station	Altitude (in m)	Data span	Months					
			Nov	Dec	Jan	Feb	Mar	Apr
Bahang	2192	1977–1978 to 2009–2010	(+)	(+)	(+)[a]	(+)	(+)[a]	(+)
Kanzalwan	2440	1996–1997 to 2009–2010	(+)[a]	(+)[a]	(+)	(+)	(+)[a]	(+)[a]
Solang	2480	1996–1997 to 2009–2010	(+)	(−)	(−)[a]	(−)	(+)	(+)
Gulmarg	2800	1996–1997 to 2009–2010	(+)[a]	(−)	(−)	(+)	(+)	(−)
Dhundi	3050	1989–1990 to 2009–2010	(+)	(+)	(−)	(−)	(+)[a]	(+)
Haddan Taj	3080	1996–1997 to 2009–2010	(+)	(+)	(−)	(−)	(+)[a]	(−)
Patseo	3800	1996–1997 to 2009–2010	(+)	(+)	(−)	(+)	(−)	(−)

(+) increasing trend, (−) decreasing trend
[a]Significant at 95 % confidence level

agreement with the results of other studies carried out in western parts of Himalayan foothills (Borgaonkar et al. 1996), Nepal Himalaya (Shreshtha et al. 2000), and Upper Indus Basin in the Karakoram Himalaya (Archer and Fowler 2004). It can also be seen from the above data that during the period under study, episodes of above-average and below-average winter and monsoon precipitation almost alternated each other with a periodicity varying from 20 to 60 years. With regard to the last few decades, it is seen that whereas monsoon precipitation has remained below average from 1965 to 2006, winter precipitation has been above average during the period between 1991 and 2006.

5.4 Winter Warming and Its Relationship with Winter Snowfall

Although winter precipitation was above average during the period between 1991 and 2006, studies have shown that rising winter air temperatures have caused decreasing snowfall component in total winter precipitation. This effect is more prominent on the windward side of the Pir Panjal Range and, to a lesser extent, some portions on the leeward side. Increasing temperatures during the months of November and March during the last three decades probably point toward the late onset of winter and early advent of spring season in the NWH. The studies have also indicated that the onset of winter has been delayed by about 2 days per decade and onset of spring has been advanced by about 3 days per decade. This has effectively reduced the duration of winter and consequently the snowfall duration period by 5–6 days per decade and approximately by about 2 weeks in the last three decades (Bhutiyani et al. 2010). Identical results have also been reported from studies in Upper Indus Basin in Karakoram Himalaya (Archer and Fowler 2004), Nagaoka in Japan (Nakamura and Shimizu 1996), the Swiss Alps (Beniston 1997; Laternser and Schneebeli 2003), and Bulgarian mountainous region (Petkova et al. 2004; Brown and Petkova 2007).

Effects of winter warming in the last three decades are visible on the Eurasian landmass as a whole. Temporal variation of Eurasian snow cover area (ESCA) in March (Brown 1997, 2002) and winter mean air temperature in the NWH (Fig. 5.3) demonstrate insignificant trend in the variation of ESCA from 1922 till the late 1960s. Consequent decrease in ESCA thereafter is marked by a period of rapidly increasing winter air temperatures in the NWH, indicating a direct inverse relationship between these two parameters. Depleting snow cover area as a result of rising winter temperatures in the last three decades may have further amplified the magnitude of winter warming in the Himalaya.

Snow, being a highly reflective material, looses back a large portion of incoming radiation to the atmosphere, thus making a very small portion of energy available for transfer to the ground below. It also acts as a thermal insulator between the ground and the atmosphere, inhibiting the heat transfer between them by conduction and convection.

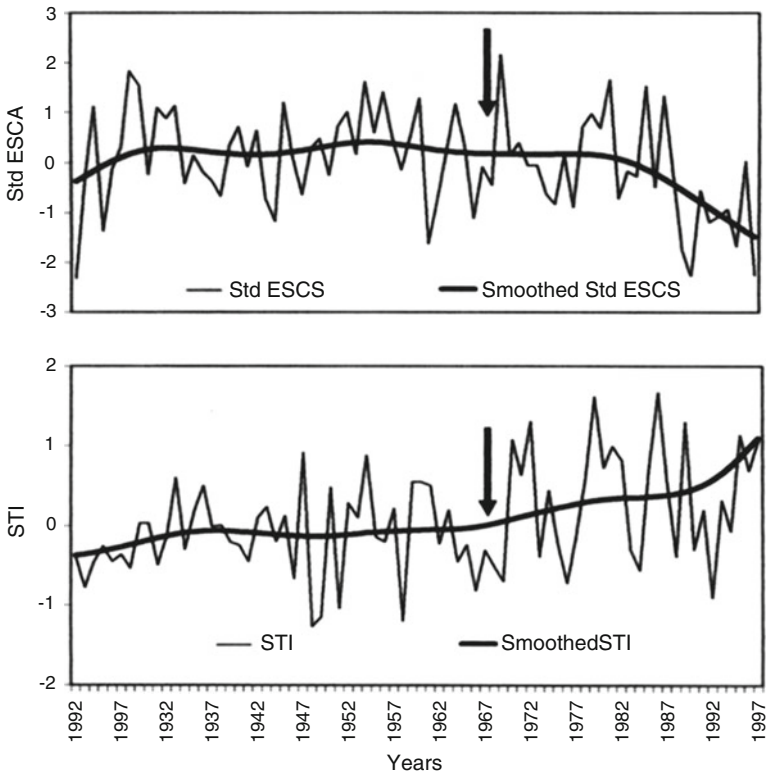

Fig. 5.3 Temporal variation of standardized Eurasian snow cover area (*ESCA*) (March) (Data Source – Brown 2002) and winter standardized temperature index (*STI*) in the northwestern Himalaya (*NWH*) during the period of 1922–1992. An onset of period of rapidly increasing winter air temperature and decreasing Eurasian snow cover is indicated by *black arrow*

As more and more land area gets exposed because of decreasing snow cover, larger amount of energy is now available for heating the ground. Consequent higher terrestrial radiation because of elevated ground surface temperatures and higher energy from incoming shortwave radiation increase the net energy balance of the area, which further raises the air temperature of the contiguous areas giving rise to a positive "feedback mechanism." This effect, which is similar to the "urban heat island" phenomenon generally associated with highly polluted cities, could be termed as "mountain heat island" effect.

Spatial study of the response of various ranges of the NWH Mountains reveals some interesting variations in warming rates in different parts of this region. While windward side of the Pir Panjal and parts of Greater Himalayan and Karakoram Ranges have shown statistically significant winter and summer warming, leeward sides of these ranges have not shown much change. This has led to significant reduction in winter snowfall amounts and rise in contribution of rain in total precipitation in this part of the Himalaya (Fig. 5.4). The most remarkable finding of this study is the significant decreasing trend experienced at almost all stations above the equilibrium line (>5300 m in altitude) in winter warming as well as winter precipitation in higher reaches of the Karakoram Himalaya in the last three decades (Fig. 5.5).

From the precipitation point of view, significant decreasing trends (at 95 % confidence level) in the monsoon and overall annual precipitation during the study period are indicated. In contrast, the winter precipitation has shown an increasing but statistically insignificant trend (at 95 % confidence level). Rising winter air temperatures have caused decreasing snowfall component and increasing rainfall component in total winter precipitation on the windward side of the Pir Panjal Range and parts of Greater Himalayan and the Karakoram Ranges. The analyses also show that although winter precipitation in the NWH has remained trendless in the last 140 years, there are significant increasing trends in the extreme snowfall events during winters and rainfall events during summers in Pir Panjal and Shamshawari Ranges in the last three decades and insignificant but increasing trends in the Great Himalayan and Karakoram Range. Decrease in winter snowfall amounts and increasing rainfall component at almost all stations has been affected to some extent, by the increase in winter air temperature during this period.

The spatial and temporal variations in winter and summer warming and consequent precipitation changes in different ranges/regions of the NWH are attributed to varying scales of anthropogenic activities and growing urbanization of the areas. Decreasing temperatures in the last three decades in the Karakoram Himalaya with altitudes above the equilibrium line (>5300 m) are attributed to prevalence of permanent snow cover which appears to have influenced their microclimatology. These studies have significant bearing on the mass balance of the glaciers in the region and the hydrological behavior of various river systems in the Himalaya.

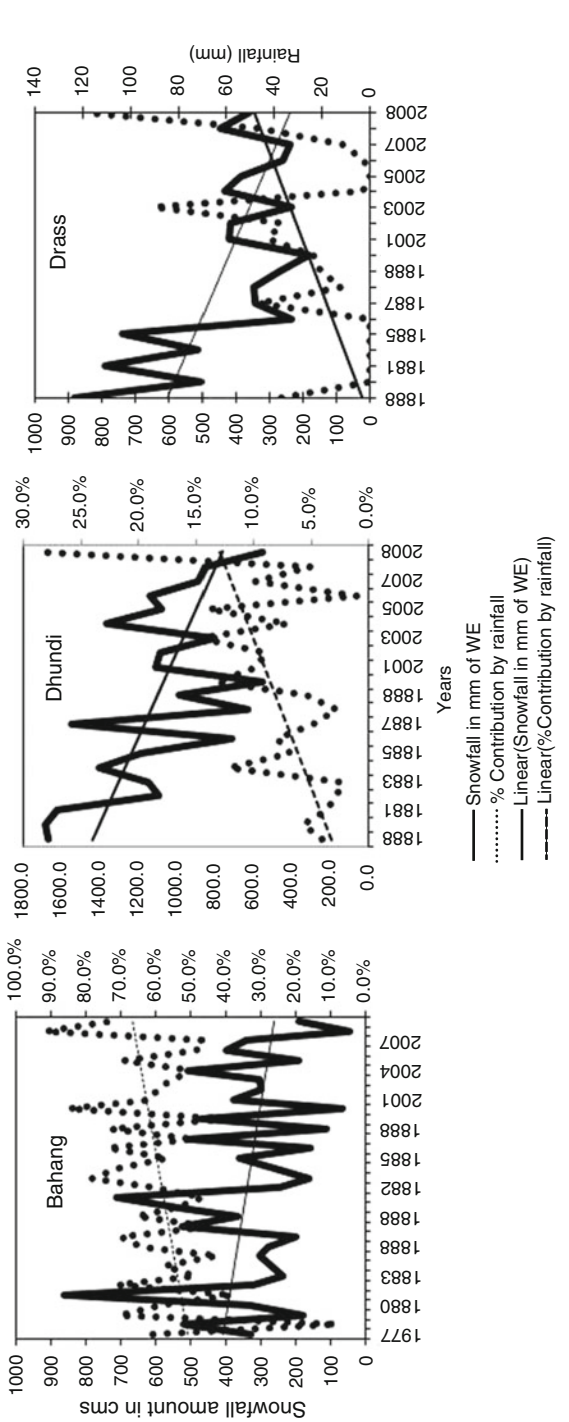

Fig. 5.4 Temporal and spatial variations of winter snowfall amounts and rainfall amounts at Behang and Dhundi in Pir Panjal Himalaya and Drass in the Greater Himalaya

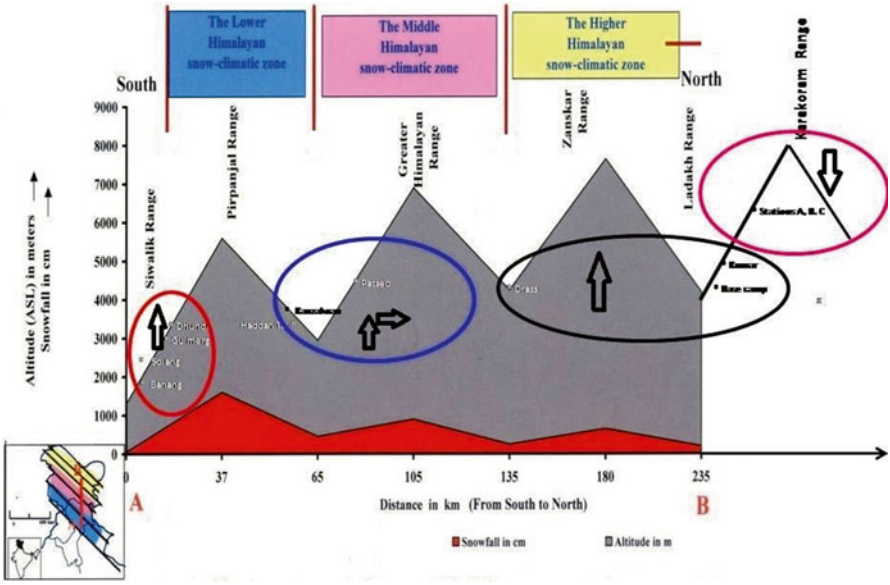

Fig. 5.5 Warming trends (winter season) in different ranges of the NW Himalayan Mountains. *Upward arrow* indicates significant rising trend, *downward arrow* indicates a significant decreasing trend, and both *arrows* together indicate a mixed response

5.5 Possible Role of Anthropogenic Activities

The studies have demonstrated that although the temperatures continued to increase from the beginning of the last century, the epochal behavior of the precipitation ensured presence of comparatively cooler and warmer periods till the early 1970s. The analysis of the diurnal temperature range (DTR) data shows regular periodicity. This periodicity, however, breaks after the mid-1970s (Bhutiyani et al. 2007).

It is evident from the foregoing discussion that some natural extra-regional factors such as the quasi-biennial oscillation (QBO) on higher frequency scale of few years and the sunspot activity on the comparatively smaller frequency scale of multi-decades appear to be largely responsible for the precipitation variation in the NWH till the early 1970s. The equatorial eastern and central Pacific sea surface temperature (SST) and the ENSO-related events had a very limited role to play in these fluctuations. Although, the temperatures continued to increase from the beginning of the last century, the epochal behavior of the precipitation ensured presence of comparatively cooler and warmer periods (Krishna Kumar et al. 1999). The periods of excess (deficient) annual precipitation, with overall increase (decrease) in cloud cover, were associated with lower (higher) temperatures, because of the decrease (increase) in net radiation balance. A remarkable feature from the standpoint of the climate change in the NWH is that these tele-connections appear to have weakened considerably in the last three decades, i.e., after the early 1970s

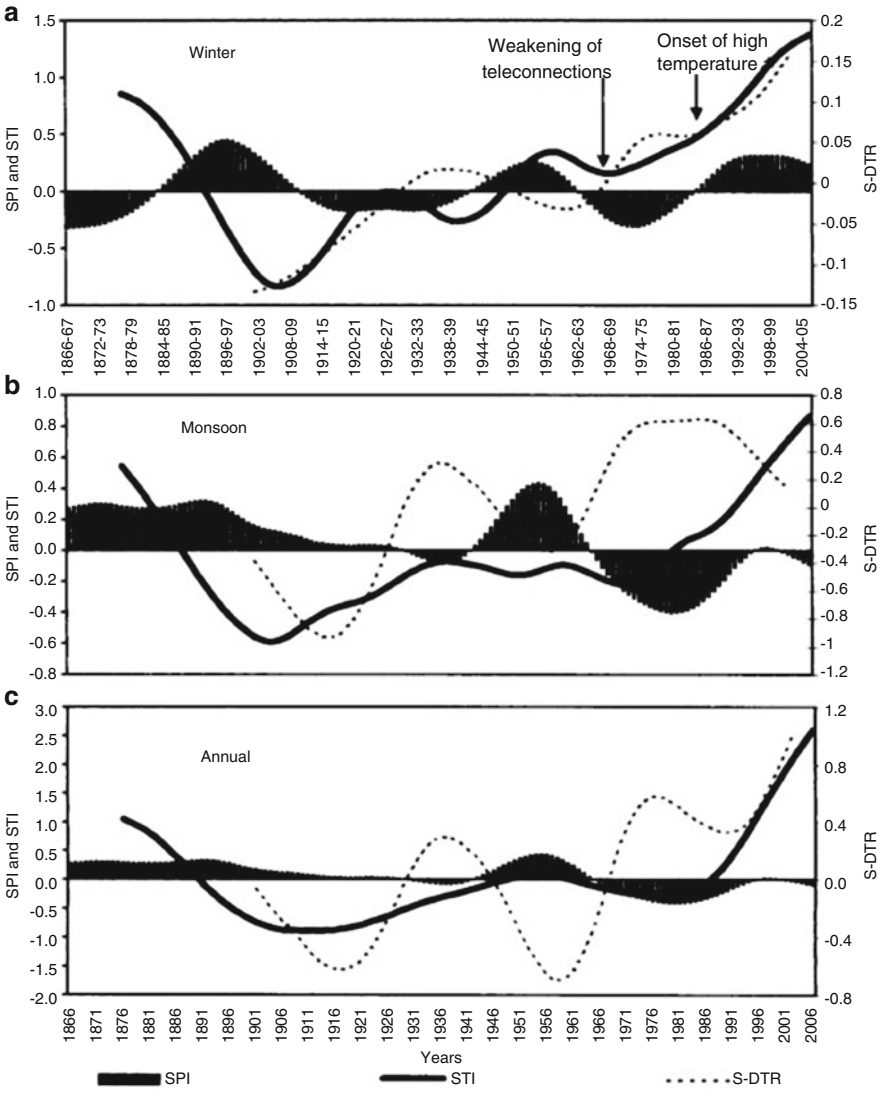

Fig. 5.6 Relationship between (**a**) winter, (**b**) monsoon, and (**c**) annual SPI, STI, and standardized diurnal temperature range (*S-DTR*) in the NWH (Source: Bhutiyani et al. 2010)

(Fig. 5.6) (Krishna Kumar et al. 1999; Baines and Folland 2007; Bhutiyani et al. 2007, 2010).

This convincingly indicates the waning effect of the natural factors in this period. The rise in air temperature has continued unabatedly in this period with both maximum and minimum temperature increasing at an alarming rate. This "warming" is unusually high, and it is difficult to be fully accounted for by the natural forcings alone, as discussed above, and there appear to be some additional factors, which

may have played a significant role (Easterling et al. 1997; Crowley 2000). One of the external factors could be the increasing concentration of greenhouse gases in the atmosphere. The largest sources of the production of these greenhouse gases are the anthropogenic activities related to rapid industrialization and urbanization. Therefore, monitoring of changes in population and land use patterns and the greenhouse gases emissions may provide an insight into the probable causes of the climatic change in the NWH.

5.6 Conclusion

The study has confirmed conclusively that the climate change in the NWH is an inevitable reality today and not a myth anymore. The region has "warmed" significantly during the last century at a rate which is disturbingly higher than the global average. Unlike other high mountainous regions such as the Alps and Rockies, where the minimum temperatures have increased at a higher rate, the rise in air temperature in the NWH has been primarily due to rapid increases in both the maximum and minimum temperatures, with the maximum temperature increasing more rapidly. With regard to precipitation, statistically significant decreasing trends in the monsoon and overall annual precipitation are observed during the study period. In contrast, the winter precipitation has shown an increasing but statistically insignificant trend. Rising winter air temperatures have caused decreasing snowfall component in total winter precipitation, particularly on the windward side of the Pir Panjal Range. The studies have indicated reduction in effective duration of winter by about 2 weeks in the last three decades.

The present study has demonstrated the existence of possible tele-connections between the extra-regional factors such as the quasi-biennial oscillation (QBO), the sunspot activity, etc. and the precipitation variation in the NWH till the early 1970s in the last century. However, in the post 1970s, these links appear to have grown weaker considerably, signifying the diminishing effect of the natural forcings during this period and indicating a vital role played by other factors, such as increasing concentration of greenhouse gases in the atmosphere.

Acknowledgments The author is thankful to Defence R&D Organization HQ, New Delhi, for providing funds for the research project. Help rendered by the Director of India Meteorological Department (IMD) and Director of Snow and Avalanche Study Establishment (SASE) for this work is duly acknowledged.

References

Archer DR, Fowler HJ (2004) Spatial and temporal variations in precipitation in the Upper Indus Basin, global teleconnections and hydrological implications. Hydrol Earth Syst Sci 8(1):47–61

Baines PG, Folland CK (2007) Evidence for rapid global climate shift across the late 1960s. J Climate 20:2721–2744

Beniston M (1997) Variation of snow depth and duration in the Swiss Alps over the last 50 years: links to changes in large-scale climatic forcings. Clim Change 36:281–300
Beniston M (2003) Climatic change in mountainous regions: a review of possible impacts. Clim Change 59:5–31
Beniston M, Diaz FD, Bradley RS (1997) Climatic change at high elevation sites: an overview. Clim Change 36:233–251
Bhutiyani MR (1992) Avalanche problems in Nubra and Shyok valleys in Karakoram Himalaya, India. J Inst Mil Eng India 3:3–5
Bhutiyani MR, Kale VS, Pawar NJ (2000) Variations in Glacio-hydrological characteristics of some northwestern Himalayan river basins in this century. Proceedings of national seminar on geodynamics and environment management of Himalaya, pp 130–138
Bhutiyani MR, Kale VS, Thakur DS, Gupta NK (2004) Variations in winter snowfall precipitation and snow depth patterns in the northwestern Himalaya in the last century: a fallout of global warming? Proceedings of international symposium on snow and its manifestations, Manali (India), 2004
Bhutiyani MR, Kale VS, Pawar NJ (2007) Long-term trends in maximum, minimum and mean annual air temperatures across the northwestern Himalaya during the 20th century. Clim Change 85:159–177
Bhutiyani MR, Kale VS, Pawar NJ (2008) Changing streamflow patterns in the rivers of northwestern Himalaya: implications of global warming in the 20th century. Curr Sci 95(5):618–626
Bhutiyani MR, Kale VS, Pawar NJ (2010) Climate change and the precipitation variations in the northwestern Himalaya: 1866–2006. Int J Climatol 30:535–548
Borgaonkar HP, Pant GB (2001) Long-term climate variability over monsoon Asia as revealed by some proxy sources. Mausam 52:9–22
Borgaonkar HP, Pant GB, Rupa Kumar K (1996) Ring-width variations in Cedrus deodara and its climatic response over the western Himalaya. Int J Climatol 16:1409–1422
Brown RD (1997) Historical variability in North Hemisphere spring snow covered area. Ann Glaciol 25:340–346
Brown RD (2002) Reconstructed North American, Eurasian, and Northern Hemisphere snow cover extent, 1915–1997. National Snow and Ice Data Center. Digital Media, Boulder
Brown RD, Petkova N (2007) Snowcover variability in Bulgarian mountainous regions. Int J Climatol 27:1215–1229
Brown TB, Barry RG, Doesken NJ (1992) An exploratory study of temperature trends for Colorado Paired Mountain-High plains Stations. American Meteorological Society sixth conference on mountain meteorology, Portland, OR, pp 181–184
Crowley TJ (2000) Causes of climate change over the past 1000 years. Science 289:270–276
Diaz HF, Bradley RS (1997) Temperature variations during the last century at high elevation sites. Clim Change 36:253–279
Diaz HF, Grosjean M, Graumlich L (2003) Climate variability and change in high elevation regions: past, present and future. Clim Change 59:1–4
Dimri AP, Dash SK (2012) Wintertime climatic trends in the western Himalayas. Clim Change 111(3–4):775–800
Easterling DR, Horton B, Jones PD, Peterson TC, Karl TR, Parker DE, Salinger JM, Razuvzyev V, Plummer N, Jamason P, Folland CK (1997) Maximum and minimum temperature trends for the globe. Science 227:364–365
Fallot JM, Barry RG, Hoogstrate D (1997) Variation of mean cold season temperature, precipitation and Snow depths during the last 100 years in the former depths during the last 100 years in the former Soviet Union (FSU). Hydrol Sci J 42:301–327
Fowler HJ, Archer DR (2006) Conflicting signals of climatic change in the Upper Indus Basin. J Climate 19:4276–4293
Karl TR, Knight RW, Plummer N (1995) Trends in high frequency climate variability in the twentieth century. Nature 377:217–220

Krishna Kumar K, Rajgopalan B, Cane MK (1999) On the weakening relationship between the Indian Monsoon and ENSO. Science 284:2156–2159

Laternser M, Schneebeli M (2003) Long-term snow climate trends of the Swiss Alps (1931–99). Int J Climatol 23:733–750

Li C, Tang M (1986) Changes of air temperature of Qinghai–Xizang plateau and its neighbourhood in the past 30 years. Plateau Meteorol 5:322–341

Liu X, Chen H (2000) Climatic warming in the Tibetan Plateau during recent decades. Int J Climatol 20:1729–1742

Mohan Rao N, Rangachary N, Kumar V, Verdhan A (1987) Some aspects of snow cover development and avalanche formation in Indian Himalaya. Proceedings of Davos symposium on avalanche formation, movement and effects. IAHS Publication No. 162, pp 453–462

Nakamura T, Shimizu M (1996) Variation of snow, winter precipitation and winter air temperature during the last century at Nagaoka, Japan. J Glaciol 42:136–140

Pant GB, Borgaonkar HP (1984) Climate of the hill regions of Uttar Pradesh. Himal Res Dev 3:13–20

Petkova N, Koleva E, Alexandrov V (2004) Snowcover variability and change in mountainous regions of Bulgaria, 1931–2000. Meteorol Z 13:19–23

Rakhlecha PR, Kulkarni AK, Mandal BN, Dhar ON (1983) Winter and spring precipitation over the northwestern Himalaya. Proceedings of the first national symposium on seasonal snow cover, New Delhi, vol 2, pp 175–181

Rebetez M (2004) Summer 2003 maximum and minimum daily temperature over a 3300 m altitudinal range in the Alps. Climate Res 27:45–50

Seko K, Takahashi S (1991) Characteristics of winter precipitation and its effects on glaciers in Nepal Himalaya. Bull Glacier Res 9:9–16

Sharma KP, Moore B III, Vorosmarty CJ (2000) Anthropogenic, climatic and hydrologic trends in the Kosi Basin, Himalaya. Clim Chang 47:141–165

Shekhar MS, Chand H, Kumar S, Srinivasan K, Ganju A (2010) Climate-change studies in the western Himalaya. Ann Glaciol 51(54):105–112(8)

Shreshtha AB, Wake CP, Dibb JE, Mayewski PA (2000) Precipitation fluctuations in the Nepal Himalaya and its vicinity and relationship with some large-scale climatological parameters. Int J Climatol 20:317–327

Srivastava HN, Dewan BN, Dikshit SK, PrakashaRao GS, Singh SS, Rao KR (1992) Decadal trends in climate over India. Mausam 43:7–20

Thapliyal V, Kulshrestha SM (1991) Decadal changes and trends over India. Mausam 42:333–338

Thompson LG, Yao T, Mosley-Thompson E, Davis ME, Henderson KA, Lin PN (2000) A high-resolution millennial record of the South Asian monsoon from Himalayan ice cores. Science 289:16–19

Yadav RR, Park W-K, Singh J, Dubey B (2004) Do the western Himalaya defy global warming? Geophys Res Lett 31:L17201

Zhai P, Sun A, Ren F, Xiaonin L, Gao B, Zhang Q (1999) Changes in climate extreme in China. Clim Chang 42:203–218

Chapter 6
Assessing Climate Change Signals in Western Himalayan District Using PRECIS Data Model

R.B. Singh, Swarnima Singh, and Shouraseni Sen Roy

Abstract The meteorological measurements across Kangra, a western Himalayan district, are examined and analyzed for the past 43 years since 1970 and have been analyzed. Noticeable increase in temperature trends with a considerable variation during different seasons over the past quartile period has been noted. Much perceptible and significant variation among the mean minimum and mean maximum temperature in the northeastern and southwestern part of the district has been brought out. The exchanges between airflow and temperature across the hills, plains, and monsoon may significantly lead to variations in the microclimate. This is essential in predicting global and regional climate variations, because it determines the extent of human influence on the climate and makes sound projections about natural rhythm of changing climate as well as anthropogenic stimulus. The mean monthly maximum and minimum temperature and precipitation together with annual minima and maxima for the period 1970–2013 have been calculated for three stations across Kangra. The differential decadal and annual trend exhibits inconsistent signals of cooling in the high-altitude northeastern block in the district as compared to other parts in the region. Atmospheric Infrared Sounder (AIRS) satellite, Tropical Rainfall Monitoring Mission (TRMM), and Providing Regional Climates for Impacts Studies (PRECIS) data have been considered to analyze the gap.

Keywords Climate change • PRECIS • AIRS • TRMM • Downscaling • Mann-Kendall nonparametric test

R.B. Singh (✉) • S. Singh
Department of Geography, Delhi School of Economics, University of Delhi, Delhi, India
e-mail: rbsgeo@gmail.com

S.S. Roy
Department of Geography and Regional Studies,
University of Florida, Miami, FL, USA

R.B. Singh et al. (eds.), *Climate Change, Glacier Response, and Vegetation Dynamics in the Himalaya*, DOI 10.1007/978-3-319-28977-9_6

6.1 Introduction

The significant changes in statistical distribution of long-term weather conditions are known as climate change. These climatic processes take place over periods ranging from few decades to millions of years to unveil some pattern. It is caused by factorial variations in its processes such as altering wind, precipitation, insolation, temperature, Outgoing Longwave Radiation (OLR), albedo, air pressure, radiative forcing, etc. These dynamic factors are hybrid in nature, thereby it incorporates both natural and anthropogenic elements that significantly cause variation in recent pattern. One can observe daily weather changes, but subtle climate changes are not readily detectable, although the weather and climate take similar elements into account. Any variation in even one weather element may produce visible changes in regional climate (Chettri et al. 2007; Deressa et al. 2008). The internal and external forces together induce climate variability. External forces refer to processes external to the climate system (though not necessarily external to the earth) that influence climate. There are various systems that can amplify or diminish the initial forcing both internally and externally like the oceans and ice caps that respond slowly in reaction to the climate forcing, while land uses, flora, and fauna respond instantly. Attribution of recent climate change focuses on the first three types of forcing. First is an orbital cycle that varies slowly over tens of thousands of years and thus is too gradual to cause temperature changes observed in the past century. Secondly, the naturally occurring greenhouse gases (GHGs) have a mean warming effect of about 33° Celsius (°C) or 59 °F (IPCC 2013). The major greenhouse gases are water vapor, which causes about 36–70 % of the greenhouse effect, carbon dioxide (CO_2) that causes 9–26 %, methane (CH_4) that causes 4–9 %, and ozone (O_3) that causes 3–7 % of the GHG effect (IPCC 2013; Shrestha et al. 1999). Clouds also affect the radiation balance, but they are composed of liquid water or ice and so have different effects on radiation from water vapor. Thirdly, the Industrial Revolution in 1750 has induced high amount of GHGs into the atmosphere due to escalating human activity afterward. It has led to an increase in the radiative forcing through high concentration of carbon dioxide (CO_2), methane (CH_4), tropospheric ozone (O_3), chlorofluorocarbons (CFCs), and nitrous oxide (NOx). The concentrations of CH_4 and CO_2 have increased by 147 % and 38 %, respectively, after the Industrial Revolution. The anthropogenic activity together with fossil fuel burning has generated about three-quarters of the augmentation in CO_2 over the past 15 years, while land use/land cover change particularly deforestation can be held responsible for the rest (GCOS 2003, 2011; Government of India 2004; IMD 2010, 2013; Singh and Singh 2011, 2014).

If these variations occur over a longer period, it influences the climate and the impacts are expansive across livelihoods, lives, and sectors. The variability of the climatic parameters from its long-term mean is quite unique for an area, as no two places can have the same amount of climatic variability; therefore, it is a prerequisite to analyze region-specific long-term deviation in average weather condition while investigating impact of climate change. The knowledge of climate variability

over the period of instrumental records and beyond on different temporal and spatial scales is important to understand the nature of different climate systems. This is essential in predicting global and regional climate variations, because it determines the extent of human influence on the climate and makes sound projections about natural rhythm of changing climate as well as anthropogenic stimulus. Thus, in order to understand the present and prospective climatic pattern, the past or historical instrumental records have been used for investigation in this study through theoretical simulated models.

6.2 Data Base and Methodology

6.2.1 Baseline Data Requirement

The mean monthly maximum and minimum temperature and precipitation together with annual minima and maxima from networks of seven stations, for the period 1970–2013, have been compiled because these are fundamental instrumental statistics for the analysis of climate dynamics in the micro-study area (Fig. 6.1). Primarily,

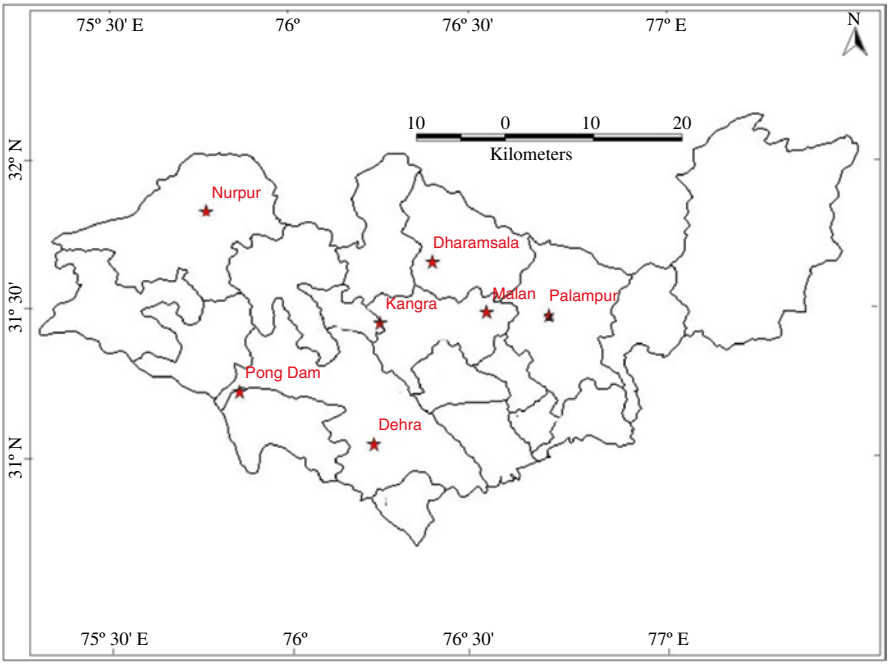

Fig. 6.1 Locations of meteorological stations in Kangra district, 2011 (Source: Author)

the India Meteorological Department (IMD) has been considered with its monthly weather records that have been updated for the period 1970–2013 with the help of downscaling Atmospheric Infrared Sounder (AIRS) satellite, TRMM, and PRECIS data to analyze the gap in IMD data set. Consequently, several checks have been made for missing values in the previous data set to distinguish the regular pattern of regional precipitation and temperature variation in the district. The annual as well as seasonal temperature and precipitation progression for the winter months (November to January), pre-monsoon (March to May), monsoon (June to August), and post-monsoon (October to November) months has been calibrated. These variations have been recorded for the entire district from all the three regions, the *Shivalik* hill, the mid hill, and the high-hill region. To calibrate the past and current climatic trends, two different data sources have been taken into consideration, the ground rain gauge station IMD data and the satellite data. The ground station data has been acquired from the CSK University, Palampur, in Kangra district, and the satellite data have been acquired from AIRS, TRMM from the National Aeronautics and Space Administration (NASA), and PRECIS from the Climate Research Unit (CRU), United Kingdom.

6.2.2 Satellite Data Mechanism

The AIRS data is having high spectral resolution spectrometer on board Aqua satellite with 2,378 bands in the thermal infrared (3.7–15.3 μm) and four bands in the visible (0.4–7.8 μm). These ranges have been precisely elected to allow atmospheric temperature and humidity in troposphere with a precision of 0.5 °C in 1 km thick layer and 80 % accuracy in the case of humidity in 2 km thick layers. The nadir is scanned in every 2 s afterward a prompt scan in two-thirds of the second by appropriating standardization-related data of four independent strip/band.

Cold space views (CSVs). These CSVs are onboard, namely, the blackbody calibrator, spectral reference source, two views combining a photometric calibrator for the visible spectrum (VS), and near-infrared (NIR) photometer where each scan line includes 90 IR paths for detailed information. The VS/NIR spatial resolution is around 2.31 km at nadir and provides 15-channel microwave temperature sounder at two independent operated modules of advanced microwave sounding units (AMSU). These modules are Module-1 (AMSU-A1) in the 50–58 GHz oxygen absorption and 89 GHz surface moisture band information and Module 2 (AMSU-A2) that has two channels for surface temperature and moisture (total precipitable water and cloud liquid water) information separately. With the help of these AMSU, the daily temperature and precipitation data for longer period has been generated with a great accuracy through merged data of TRMM and AIRS. That is essential for climate and climate change study in any region through monitored gridded temperature and rainfall data (Fig. 6.2).

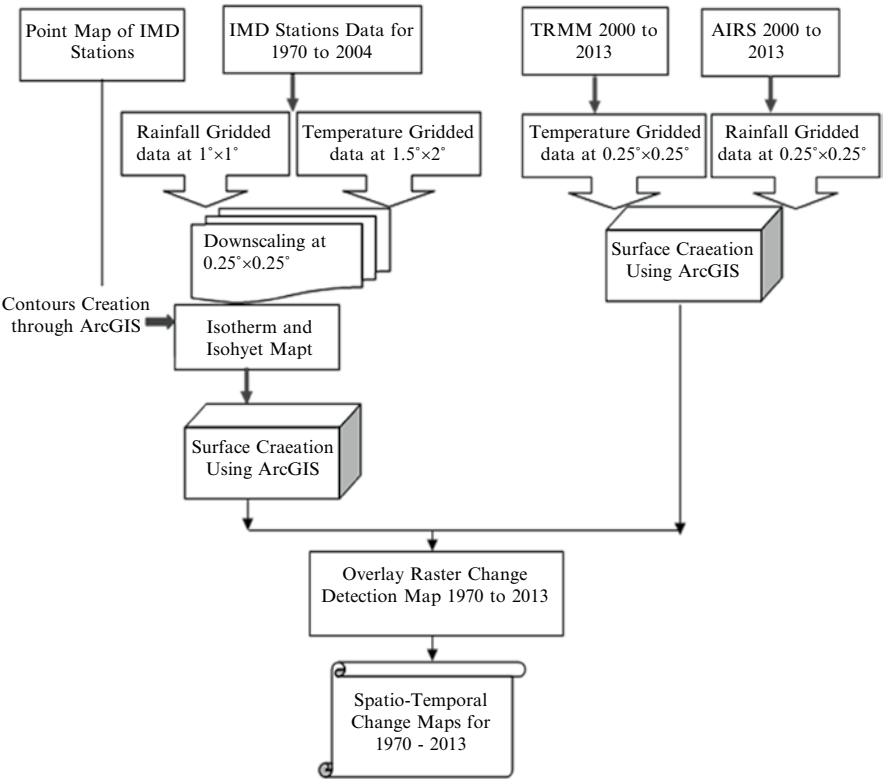

Fig. 6.2 Methodological framework for preparing spatiotemporal maps (Source: Author)

6.2.3 Data Base and Methodology for Climate Change Modeling

The climate change modeling has been done based on 1970–2013 baselines to find out a definite consciousness from infinite number of equally credible changes. Basically, it should be consistent with current understanding of real calibrations without assuming that the future will resemble the past and the present. PRECIS based on Hadley Regional Climate Model (HadRM) downscaling methodology (shepherd method) data has been used on IMD, AIRS, and TRMM combined with gridded data to generate climate change with a resolution of 25×25 km approximately (1 = 102.3 km on tropics).

The regional monthly temperature trends are calculated by simple average of the fundamental grid point data of the respective block region. The temperature trend is computed through the slope of a simple linear regression fitted line against time to each of the series. The statistical significance of trend is assessed by means of the F-ratio subsequently, by annexing into account the autocorrelation. Therefore, both the ground and satellite data have been taken into consideration for the last one

decade to minimize the gap/error in climate change simulations for the baseline study. The Mann-Kendall nonparametric test has been calculated for the 43-year (1970–2013) baseline temperature and rainfall data from

$$T = \sum_{i=2}^{n} \sum_{j=2}^{i-2} \left(xi - xj \right)$$

$$R = \sum_{i=2}^{n} \sum_{j=2}^{i-2} \left(xi - xj \right)$$

where n = data set length, while xi and $x\,j$ = standard chronological data values.

The independent and randomly distributed variables from T_{max}, T_{min}, and T_{mean} provide data set length $n \geq 3$ similarly for R_{total} and R_{days} where $n \geq 2$. The nonparametric temperature statistic T and R is distributed normally with variance and neutral or zero mean. With the time-series length, the standardized test statistic is calibrated from Zt score for temperature and Zr for rainfall value to test the null hypothesis as

$$Zt = \left[T - \frac{1}{\sqrt{V}} \right]$$

$$Zr = \left[R - \frac{1}{\sqrt{V}} \right]$$

if variance $V > 0$, or $V = 0$, or V is < 0

The increasing temperature T_{max} and T_{min} trend indicates $a + Z$ value, and a decreasing T_{max} and T_{min} temperature trend indicates $-Z$ value. The significant T_{max} and T_{min} levels of 0.05, 0.01, and 0.001 have been converted into percent later.

The temperature and rainfall are shaped by GHG emissions. This is based on computing average, z-score, standard deviation, and moving average for temperature variability and identification of dry/wet years for rainfall. A regional climate model (RCM) for the Kangra district has been downscaled at grid resolution of about $0.25 \times 0.25°$ (Fig. 6.3). The input and output in the RCM climatological parameters cannot be generated without a parent global circulation model (GCM), whereas it also provides opportunities to superimpose the microscale regional detail for modeling, which might offer present climate pattern and extreme events and simulate climate pattern realistically at high resolution (~25 km and below). For downscaling, the regional adaptive responses for climate change have been computed as

$$\boldsymbol{Cs_c = f\,(C_L,\, Ps)}$$

where Cs_c is the microscale climate, which is downscaled through the functional relationship of C_L which is the large scale climate, and Ps is the microlevel

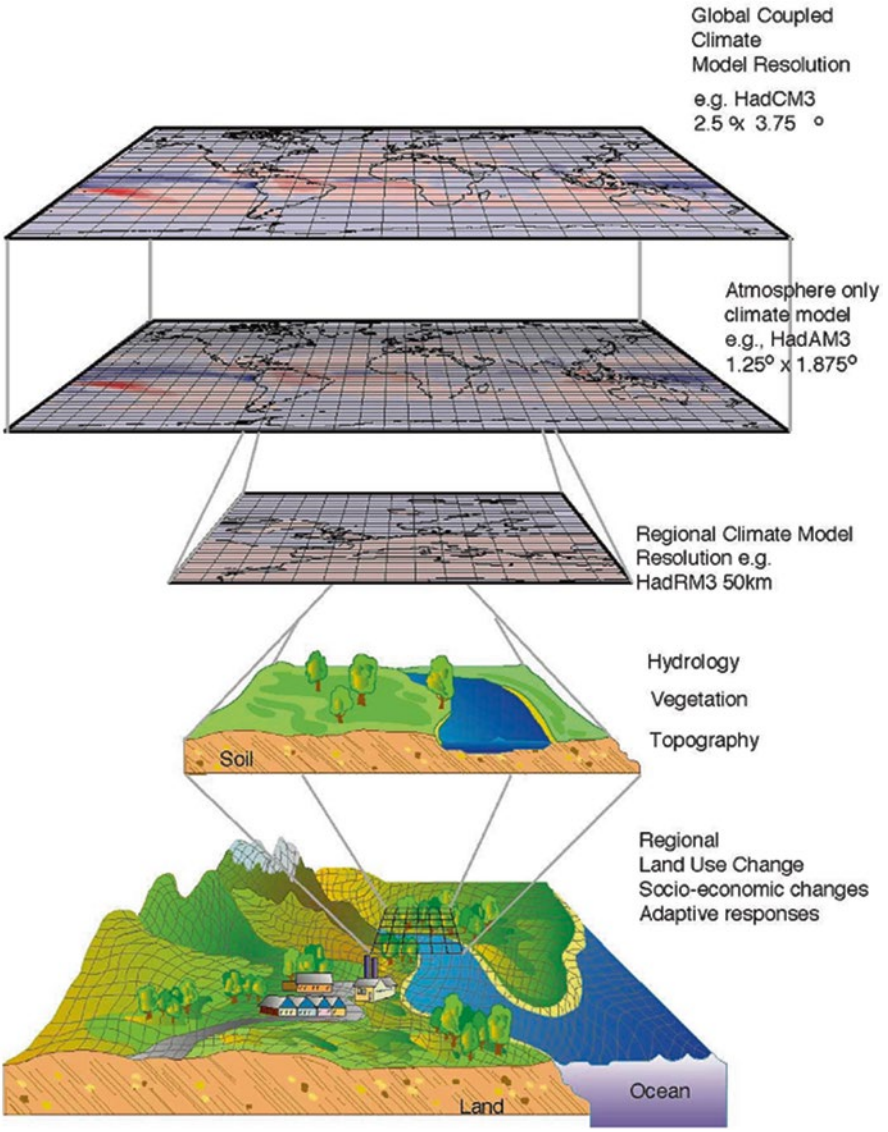

Fig. 6.3 Climate change modeling mechanism GCM downscaling to regional adaptive responses of RCMs (Source: Author – based on http://consulclima.co.uk/climate-modelling/downscaling-gcm-outputs/#downscaling

physiographic details. These steps of downscaling from GCM to RCM have been adopted to fill the gap in IMD databases for the given missing years (1975–1981, 1987–1992, and 1998–2000).

6.3 Result and Discussion

6.3.1 The Observed Spatiotemporal Change in Temperature

The temporal change in temperature and rainfall has been plotted based on monthly decadal average for the region for four decades, namely, 1970–1990 and 1990–2010. The summer (June) and winter (January) temperature in 1990–2010 has witnessed variable change. The maximum and minimum temperature increase ranges between 0 and 0.8 °C. While a noticed decline of almost 10 cm of rainfall during 3-month summer monsoon (June, July, and August) averaging from 49.3 cm (1970–1990) to 39.3 cm (1990–2010) has been perceived, the winter rainfall months, November, December, and January, have been seen with a decline of 4.5 cm from 7.6 cm during 1970–1990 to 3.1 cm during 1990–2010. Comparably, IPCC Vth Assessment Report observed global amplification in the average surface temperature of around 1.74 ± 0.18 °C (2.33 ± 0.32 °F) during the twentieth century steered by the increasing emission of GHGs ever since the last century (IPCC 2013). During the last 40 years, the temperature has shown a great variability with an average rise of about 0.5 °C for the month of June. The average temperature during the 1970s–1990s rose from 22.9 to 23.7 °C during 1990–2010 though the temperature graph shows a decline in the later part. The mean annual temperature of Kangra district shows that a significant warming trend of 0.8 °C per 10 years through the period 1970–2010 represents a considerable increase of rate of the warming in the last four decades (Fig. 6.4). Therefore, the aggregated data from seven meteorological stations, Nurpur, Dharamsala, Pong Dam, Palampur, Kangra, Malan, and Dehra, have been computed on spatial scale in this Cwa type of climate.

The longitudinal temporal trend has also been analyzed separately from TRMM data at 0.5 × 0.5° on the graph to provide valid reasoning on latitudinal climate change over the time beside temporal and spatial isothermal shifts. This trend has been calibrated at grid level of 180 × 360 row and columns that has been downscaled to 3 × 4 row and columns (latitude x longitude). There are three latitudes (30°5′N, 31°5′N, and 32°5′ N) together with four longitudes (74°5′E, 75°5′E, 76°5′E, and 77°5′E) on which the temperature variations have been calibrated for around a decade from 2003 to 2011 for three months (June, July, and August). This has been plotted through MATLAB R2009a.

The average annual temperature ranges between 10 and 26 °C in the month of January, while in the summer month of June, the temperature ranges between 14 and 36 °C. The district climate changes from subtropical in low hills and valleys to subhumid to temperate in the mid and the high hills, respectively. Southward and eastward latitudinal shifts in isotherms have been observed, and it is markedly visible in central and southern section of the district over 1970 and 2010. Meanwhile, a marginal shift in the northern and extreme eastern section of the region is also witnessed. The January isotherm of 12 °C, 14 °C, and 20 °C has noticed strong shift similarly in the case of June isotherms. The major shift in June isotherms can be noticed in 20 °C, 22 °C, 30 °C, and 31 °C isotherms, which are passing through central and western tracts where the general direction of shift is southwestward.

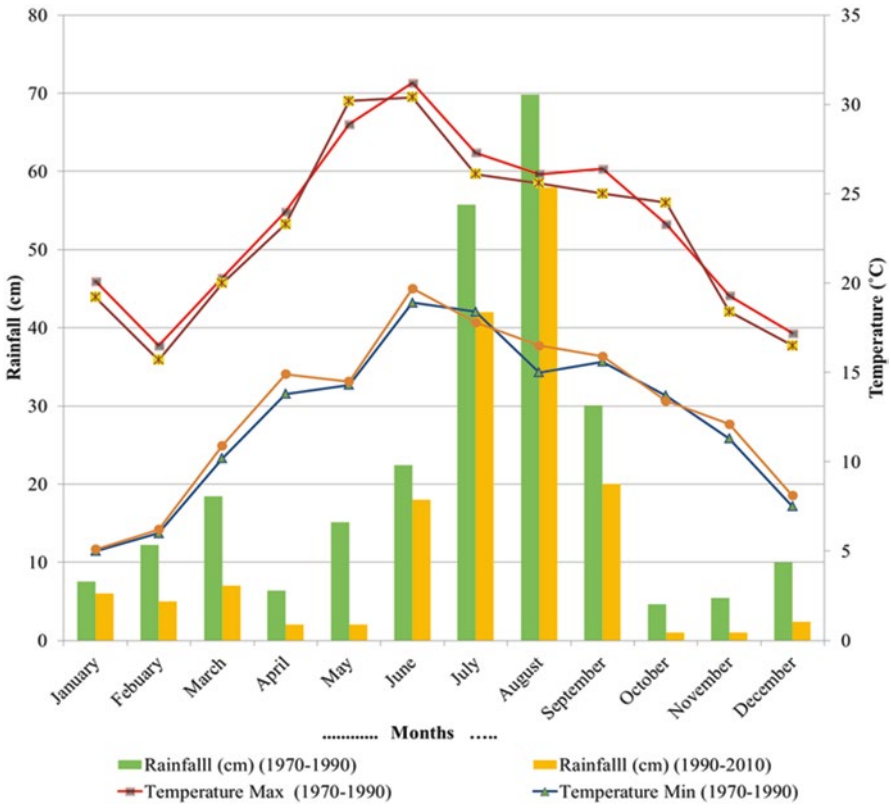

Fig. 6.4 Comparative status of average monthly decadal rainfall (cm), maximum and minimum temperature (°C) of Kangra district for 1970–1990 and 1990–2010 (Source: Author)

The winter isotherms show maximum deviation where 10 °C and 12 °C isotherms are shifting much northward and 20 °C isotherm intruding in central and eastern blocks of the district. Over the last 30 years, Palampur and Baijnath have witnessed 16 °C and 18 °C isotherm shift toward more northward during June, and Dehra Gopipur, Kangra, and Pong Dam have been witnessing the average northward and central shift in 30 °C, 32 °C, and 36 °C isotherm which pass through western and southern parts in the district. The mean annual temperature displays substantial trend of warming of 0.06 °C/10 years all through the period till 1970 and 0.22 °C/10 years during recent decade of 2000–2010. During the last three to four decades, it shows a significant increase in the rate of the warming; therefore, it portrays a major turnaround in the asymmetry of the diurnal trends of temperature. From spatiotemporal analysis, it is quite evident that the temperature change ranges between 0 and 0.5 °C during summer months with western and central section in Nurpur, Fatehpur, Dehra, and Kangra that are experiencing highest change between 0.6 and 0.8 °C in the month of June over the years. The least change in temperature of about 0 and 0.2 °C has been seen in eastern part of Bada Bhangal, Tarmehr, and

Baijnath region. For winter season, the maximum change noticed is of 1.0–1.2 °C and a minimum of 0.2–0.4 °C, respectively, in western and eastern region. The trends of temperature that rise in October to January months are just reverse of what one can observe during June to July months (Fig. 6.5a, b).

The T_{max} and T_{min} trends are determined for entire Kangra region with the help of Mann-Kendall nonparametric test to evaluate the probability of temperature test on how it is statistically different from zero. In this test, the parameters are always in sequential order and depending upon the number of occurrences or chances with greater than mean is counted. This method has been used to find out the increase as well as decrease in the slope of trends in the temperature time series during the same time period of 1970–2010. The Mann-Kendall nonparametric test for the independent and randomly distributed temperature and rainfall variables for T_{max}, T_{min}, T_{mean}, R_{total}, and R_{days} provides data set length $n \geq 5$, whereas the temperature and rainfall statistics are distributed normally with the variance and neutral or zero mean. The increasing temperature T_{max} and T_{min} trend indicates a + Zt value and a decreasing temperature trend indicates -Zt value. The significant T_{max} and T_{min} levels of 0.05, 0.01, and 0.001 have been converted in 2 % to plot the monthly deviation in the data graph.

On a regional level, the variation in mean maximum and minimum temperatures over the period of 1970–2010 has observed a net escalation in temperature ranges from 0.86 °C ± 0.04 °C. The five color categories of seasonal temperature change ranging from less than 0.0 °C to more than 0.75 °C of Kangra district with a general rise in mean seasonal temperature in all its blocks from 1970 to 2010 explain that the temperature variability has increased over time (Fig. 6.6). The northeastern Multhan, Baijnath, and small adjoining parts of Bhawarna are the only area to experience a decrease in seasonal temperature. A very significant increase in the north region (between 0.45 and 0.75 °C), including Talnu, Satobari, Naddi, Bhagsunag, Dal Lake, and Baradar, has been observed. The temperature trend is not uniform over the northeastern region, and annual temperature has risen by 1.5 °C in the last century with winter warming (Bhutiyani et al. 2007, 2009). Increasing trend of temperature in post-monsoon and winter while decreasing trend in monsoon has been observed for Nurpur, Panchrukhi, Baijnath, and Dehra Gopipur, whereas Multhan has experienced warming during the last 100 years (based on data analysis). Increase in temperature of 0.0–0.25 °C has been observed across Lambagaon, Rait, and the very northern portions of Kothi Kohar of Baijnath block, while increase between 0.25 and 0. 5 °C has been found along Palampur, Sulah, Pragpur, and southernmost part of Kundalia and Jwalamukhi. Lastly, a small noticeable increase of less than 0.25 °C has been observed in much of southern Multhan, north and western parts of Rait and Nagrota Surian, and southwestern part of Jaisinghpur Tehsil including Thural Sub Tehsil. During 1970 to 2010, approximately 51 % of the total area and almost 52 % of the total population of the district have experienced 0.25–0.5 °C increase. Some 14.5 % of the population acknowledged a more significant increase of 0.75 °C and more, signifying almost 30.1 % of the total district's geographical area.

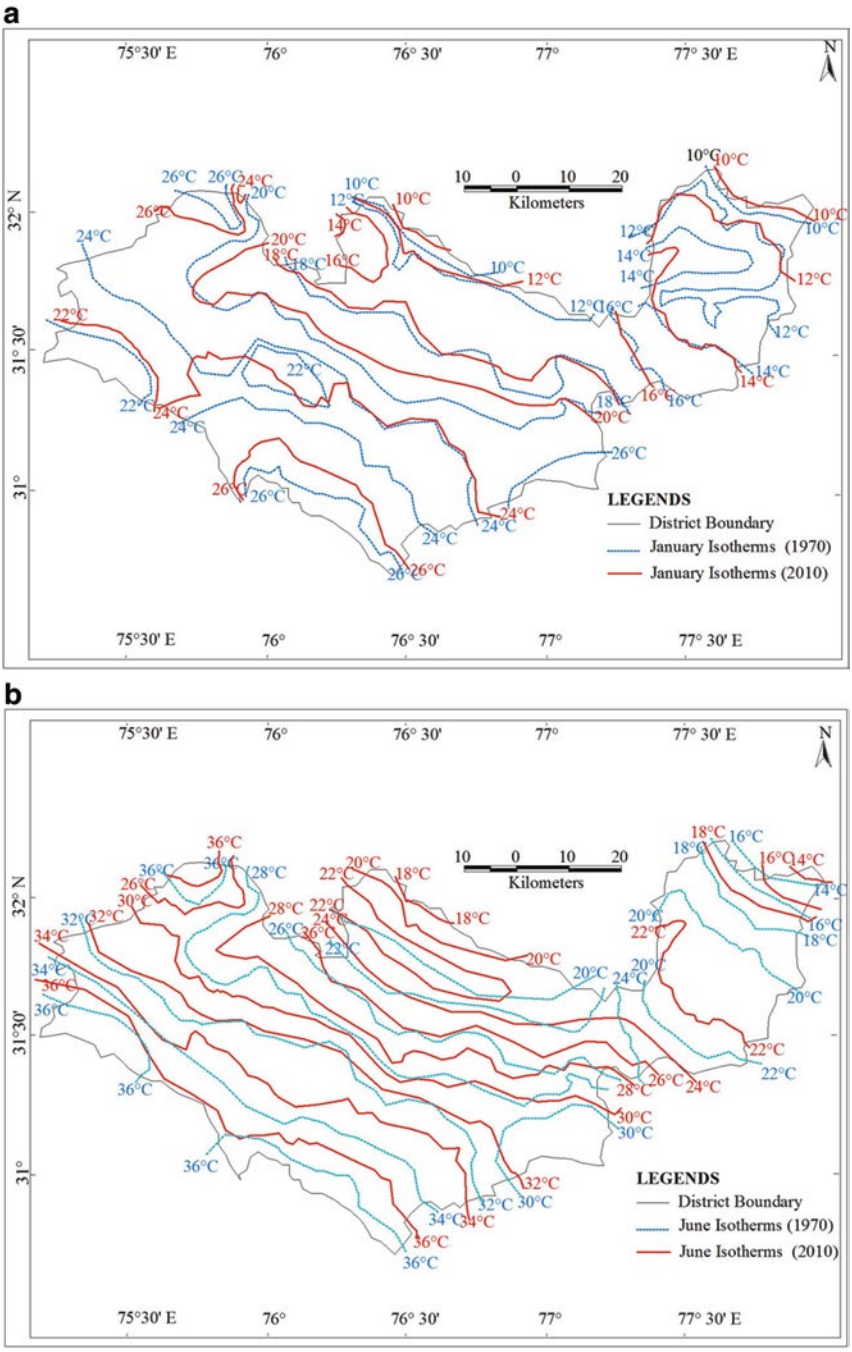

Fig. 6.5 (**a**) Spatiotemporal change in January isotherm and 1.5 (Source: Author), (**b**) change in June isotherm for the years 1970 and 2010 (Source: Author)

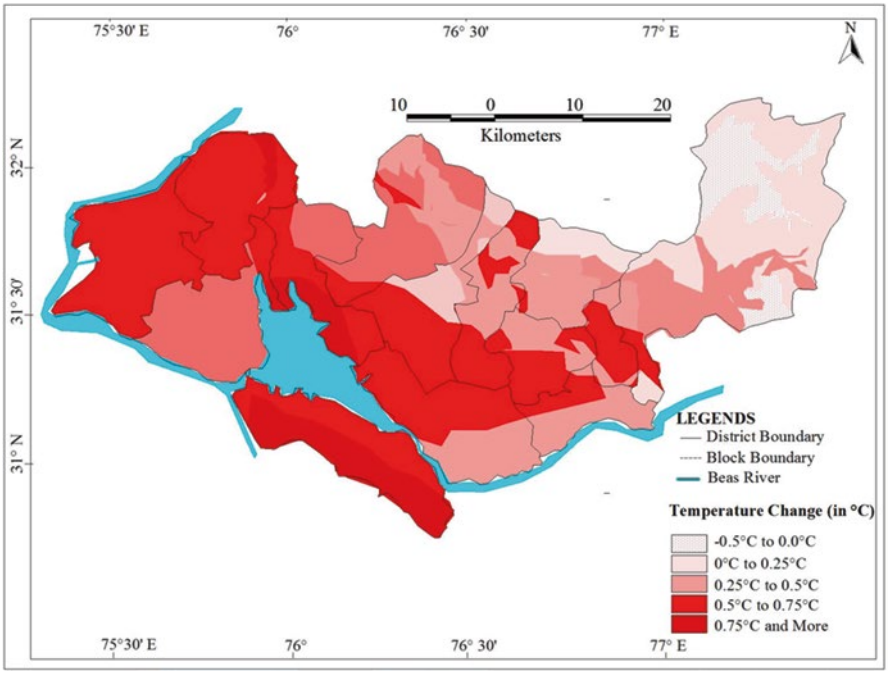

Fig. 6.6 Mean seasonal temperature pattern in Kangra district over the period of 1970–2010 and T_{max} and T_{min} graph of mean monthly change in climatological records (percent) during 40 years (Source: Author)

6.4 Conclusion

Kangra occupies one of the largest percentages of Himachal Pradesh in terms of population as well as agricultural output. The important perennial river Beas provides water for drinking, irrigation, and hydropower to nearly 80 % of its total population directly or indirectly. The climate of the district has shown changes. There is an average rise of 0.5 °C in temperature over the region. The rise in winter temperature is almost the double of rise in summer temperature. Spatially, the western part of the region has experienced greater change in temperature than the eastern part during summer months, whereas this trend is reversed during winter months. The rise in temperature experienced over the years in winter season is greater in eastern parts than in western. The rainfall pattern shows dual characteristics. The annual average rainfall has increased in western part, but at the same time, it has decreased in eastern part of the region. The precipitation trend over the past 40 years has been very variable, but an average decrease has been noticed in the annual precipitation. The underlying mechanism behind these changes is blamed on the rising GHG concentration through its fragile forests and global circulation of rising GHG concentration. The local factors affecting the rise in temperature, increased cloud cover, and decreasing rainfall over the region can be studied in more integrated and

elaborative manner. The effects of changing climate are likely to be exacerbated, which may adversely impact the ecosystem through increased temperature, altered precipitation patterns, episodes of drought, and anthropogenic land use/land cover change and influences. It would not only impact the very sustenance of the indigenous communities in uplands but also alter the life of downstream dwellers across the region, country, and beyond. Therefore, there is an urgent need for giving special attention to sustain this fragile ecosystem.

References

Bhutiyani MR, Kale VS, Pawar NJ (2007) Long-term trends in maximum, minimum and mean annual air temperatures across the northwestern Himalaya during the twentieth century. Clim Change 85:9185–9196

Bhutiyani MR, Kale VS, Pawar NJ (2009) Climate in the northwestern Himalaya: 1866–2006. Int J Climatol. doi:10.1002/joc.1920. Published online in Wiley Inter Science (www.interscience.wiley.com)

Chettri N, Sharma E, Shakya B, Bajracharya B (2007) Developing forested conservation corridors in the Kangchenjunga landscape, eastern Himalaya. Mt Res Dev 27(3):211–214

Deressa M, Alexander A, Xie SP, Phillips AS (2008) Sea surface temperature variability: patterns and mechanisms. Ann Rev Mar Sci 2:115–143

GCOS (2003) The second report on the adequacy of the Global Observing Systems for Climate in support of the UNFCCC. GCOS-82, WMO/TD 1143: 74 [Available online at http://www.wmo.int/pages/prog/gcos/Publications/gcos-82_2AR.pdf]

GCOS (2011) Systematic observation requirements for satellite based data products for climate. GCOS 154:1–127

Government of India (2004) India's Initial National Communication to the UNFCCC, chapter 3: vulnerability and adaptation, ministry of environment and forests. GOI, pp 59–71

India Meteorological Department (2010) Climatological tables for (1931–2010). Indian Meteorological Department, Pune

India Meteorological Department (2013) Climatological tables for (1970–2013). Indian Meteorological Department, Pune

IPCC (2013) Summary for policy makers. In: Stocker TF, Qin D, Plattner GK, Tignor M, Allen SK, Boschung J, Nauels A, Xia Y, Bex V, Midgley PM (eds) Climate change 2013: the physical science basis. Contribution of Working Group I to the fifth assessment report of the Intergovernmental Panel on Climate Change. Cambridge University Press, Cambridge, pp 1–30. doi:10.1017/CBO9781107415324.004

Shrestha AB, Wake CP, Mayewski PA, Dibb JE (1999) Maximum temperature trends in the Himalaya and its vicinity: an analysis based on temperature records from Nepal for the period 1971–94. J Clim 12(9):2775–2786

Singh RB, Singh S (2011) Anthro-biome: integrated global climate change modeling. In: proceeding 3rd International Indian Geography Congress on sustainable natural resource management under changing climatic scenarios, Kozhikode, Kerala 6–8 May, 2011, 1. pp 95–101

Singh RB, Singh S (2014) Human induced biome and livelihood security. In: Singh RB, Hietala R (eds) Livelihood security of Northwestern Himalaya: case studies from changing socio-economic environments in Himachal Pradesh, Springer publication 4. pp 53–66

Chapter 7
Climate Change in Pindari Region, Central Himalaya, India

R.B. Singh, Santosh Kumar, and Ajay Kumar

Abstract The impending threat due to changing climate has accentuated the vulnerability of all ecosystems. The fragile ecosystems like that of high Himalaya are most susceptible to the climate change which not only disrupts the physical processes but also has its impact on the livelihood of local people. The changes in glaciers have far-reaching impacts on the downstream ecosystems also. In order to prevent the future disastrous events, it becomes necessary to analyze the climatic variability in the region and access the associated vulnerability. The Pindari region is one such example from Himalaya which is under threat due to climate change and represents clusters of glaciers comprising the main Pindari Glacier as trunk part. Pindari Glacier is a small valley-type glacier of Kumaon Himalaya, situated at an elevation 5200 m. The study is based on the medium-resolution monthly average temperature and rainfall data obtained from the India Meteorological Department for the Pindari region from year 1901 to 2010. The results show that the annual temperature has substantially increased by around 1 °C from 1901 to 2010. All seasons in the Pindari region indicate no significant increase in rainfall. A study of data illustrates that the main trunk of the Pindari Glacier has been in a continuous state of recession during the past century.

Keywords Climate variability • Mountain ecosystem • Glacier retreat • Water resources • Pindari region

7.1 Introduction

Climate change is considered as a significant anthropogenic global environmental challenge currently facing the humankind today, evident in the form of increase in global mean temperatures and perceptible changes in precipitation patterns

R.B. Singh (✉) • S. Kumar • A. Kumar
Department of Geography, Delhi School of Economics, University of Delhi, Delhi, India
e-mail: rbsgeo@hotmail.com

R.B. Singh et al. (eds.), *Climate Change, Glacier Response, and Vegetation Dynamics in the Himalaya*, DOI 10.1007/978-3-319-28977-9_7

(Goswami and Ramesh 2006). Climate change induced by anthropogenic activities has resulted in the average surface temperature increase by 0.74 °C in the last 150 years (IPCC 2007). The warming has a direct impact on the temperature-sensitive snow and ice cover, resulting in rapid glacial melt and causing variations in discharge of the rivers downstream (Bates et al. 2008). The rising temperature and loss of ice and snow have an increasing stress on water availability, biodiversity, tree-line movements, high-elevation ecosystem changes and monsoonal shifts (Xu et al. 2009). The Himalaya has the largest concentration of glaciers apart from the polar region. The Indian Himalayan region covers vast areas, with about 17 % of the region being under permanent snow cover and glaciers and about 30–40 % under seasonal snow cover, forming a unique water reservoir, giving rise to nine major rivers in Asia and providing water to almost one-third of humanity. Recent evidence suggests that most glaciers in the Himalaya have been retreating with greater pace in terms of climate change. This variation in climate has led to changes in freshwater regimes and is likely to have a dramatic impact on drinking water supplies, biodiversity, hydropower, industry, agriculture and others, with far-reaching adverse implications for the people of the region and the earth's environment. According to the Fourth Assessment Report of the IPCC, smaller glaciers are more vulnerable to a warmer world and climate change (Rosenzweig et al. 2008). The Pindari Glacier region is among the most vulnerable cryosphere regions due to geological reasons, stress caused by increased pressure of population, exploitation of natural resources and other related challenges. These effects are likely to be exacerbated due to the impact of climate change, which may adversely affect the Himalayan ecosystem through increased temperature, altered precipitation patterns, episodes of drought and biotic influences. Therefore, the present paper attempts to assess the climate variability in the Pindari region in order to reduce the future vulnerability of the region to climate change.

7.2 Mountain Ecosystem and Climate Change

Mountain ecosystems are very sensitive to the habitat and climate change due to the interaction of tectonic, geomorphic, environmental and climate agents. Mountain ecosystems provide many goods and services which are critical to individuals and societies, and they are also fundamental to environmental functioning and sustainability (Singh et al. 2013; Singh 1998). Beyond their common characteristics of high relative relief and steep slopes, mountains are remarkably diverse and globally important as centres of biological diversity (Ives et al. 2004). The complexity of mountain systems presents major problems for assessing the potential impacts of climate change. This applies to assessments of changes in biophysical systems (Rizzo and Wiken 1992; Halpin 1994) and societal systems (Price 1990). Climate provides ecosystem and services to human society, but climate change also has potential to alter these ecosystem services; hence, climate is an integral part of mountain ecosystems, and arresting climate change is critical for survival of

mankind at large. The retreat of glaciers and the thawing permafrost is an indication of the increase in the average temperature in the mountain region during the past three decades. On an average, surface air temperatures in the Himalayan region have gone up by 1° in the last decade (Srinivasan et al. 2006). Recent studies over the Himalayan glaciers using ground-based and space-based observations and computer models indicate a long-term trend of climate variability, and change may accelerate melting of the Himalayan glaciers (Lau et al. 2008). Other studies also suggest a decreasing trend in snowfall, which has historically served as a main source of precipitation for maintaining the glaciers and freshwater resources in this region. In the Himalaya, nature-determined environmental fragility scores high. As glacial recession is taking place at a faster pace, a new equilibrium at the cost of loss of entire habitats is possible. For this reason, Himalaya, along with other continental ice masses like Alaska, Patagonia and the Karakoram, has been identified as critical regions in the world (Sen Roy and Singh 2002). Communities inhabiting mountain ecosystems are particularly vulnerable to extreme weather conditions such as high temperatures, altering rainfall patterns, receding glaciers and permafrost thawing. Recent instances include the disastrous cloud bursts near Kedarnath and Kapkot in Uttarakhand and Leh in Ladakh in Kashmir the shifting of apple orchards to higher altitudes. This vulnerability is critical for the local communities as they are highly dependent on natural resources for their livelihood. Vulnerability and adaptation to climate change as also other causes would therefore need to address this issue by enhancing people's livelihood in an economy which nurtures rather than destroys their habitat.

7.3 Climate Change Studies in India

Recognizing the critical concern of global warming in India, various studies have been conducted in the region to analyze trends in hydrometeorological variables at regional and basin level (Hingane et al. 1985; Sinha et al. 1997; Arora et al. 2005). Hingane et al. (1985) analyzed long-term mean annual temperature records from 1901 to 1982 over India and detected an increasing trend in mean surface air temperatures. It was observed that about 0.4 °C warming has taken place over India during the last eight decades mainly due to rise in maximum temperatures. Sinha et al. (1997), however, showed that the changes in mean annual temperatures are partly due to the rise in the minimum temperature caused by rapid urbanization. Pant and Kumar (1997) have reported an increase in mean annual temperatures in India at the rate of 0.57 °C per 100 years. Arora et al. (2005) investigated temperature trend all over India using Mann-Kendall non-parametric technique and linear regression method. The results showed that mean temperature has increased by 0.94 °C per 100 years for the post-monsoon season and 1.1 °C per 100 years for the winter season. Ramesh and Goswami (2007) reported the shrinking of the Indian summer monsoon in terms of total rain days as well as in terms of total area of rainfall. Goswami and Ramesh (2006) conducted a study using high-resolution gridded

rainfall data for a period from 1951 to 2003 wherein it was found that the frequency and magnitude of extreme rainfall events during summer monsoon over central India are increasing, while moderate events are decreasing.

7.4 Study Area

Pindari region is geographically located in the southern side of Greater Himalaya in Uttarakhand. It is part of Kumaon Himalayan region. The Pindari glacial region extends from 29°50′4″ N to 30°19′4″ N and 79°42′ E to 80°8′4″ E (Fig. 7.1). It represents the part of the Kumaon Himalaya with height ranging from 800 to 6800 m. The Pindari region is bounded by Chamoli district in the north and north-west, Pithoragarh district in the east and Garud, Bageshwar and Kanda block of Bageshwar district in the south. The geographical area of the Pindari region is 593.5 km^2. The Pindari region represents clusters of glaciers comprising the main Pindari Glacier as trunk part. Pindari Glacier is a small valley-type glacier of Kumaon Himalaya, situated at an elevation 5200 m. The glacier lies between the Nanda Devi and Nanda Kot peaks and its snout is an elevation 3627 m. The glacier is 5 km long and 300–400 m wide. The permanent snow cover is reported to be above elevation 4600 m. High-elevation zone in catchment area rises up to about 6600 m. Pindar River originates from the 'Pindari Glacier' in Bageshwar district (32 km) and, flowing an approximate 124 km with its numerous tributaries, confluences into the Alaknanda river at Karnaprayag in Chamoli district. The watersheds of the Ramganga in the south, the Saryu in the east, the Nandakini in the north and the Alaknanda in the northwest delimit it and give it a distinct socio-geographical identity.

7.5 Database and Methodology

Present study is based on the medium-resolution monthly average temperature and rainfall data prepared by the India Meteorological Department for the Pindari region from year 1901 to 2010. This data has been collected for one observation station of IMD in Bageshwar. The data is available for January to December for each year. Only two climatic parameters such as temperature and rainfall have been taken to find out climate change in the region. Mean annual highest temperature, mean annual minimum temperature, average annual temperature and rainfall data of Bageshwar station have been taken due to their close proximity to glaciated region and also for regular data recording. The study based on only one weather station because no other weather station is near about the area. The upper part of Pindari region did not have any regular data-recording stations of IMD from the past 30 and more years and even recent establishment of certain stations in this remote and hilly

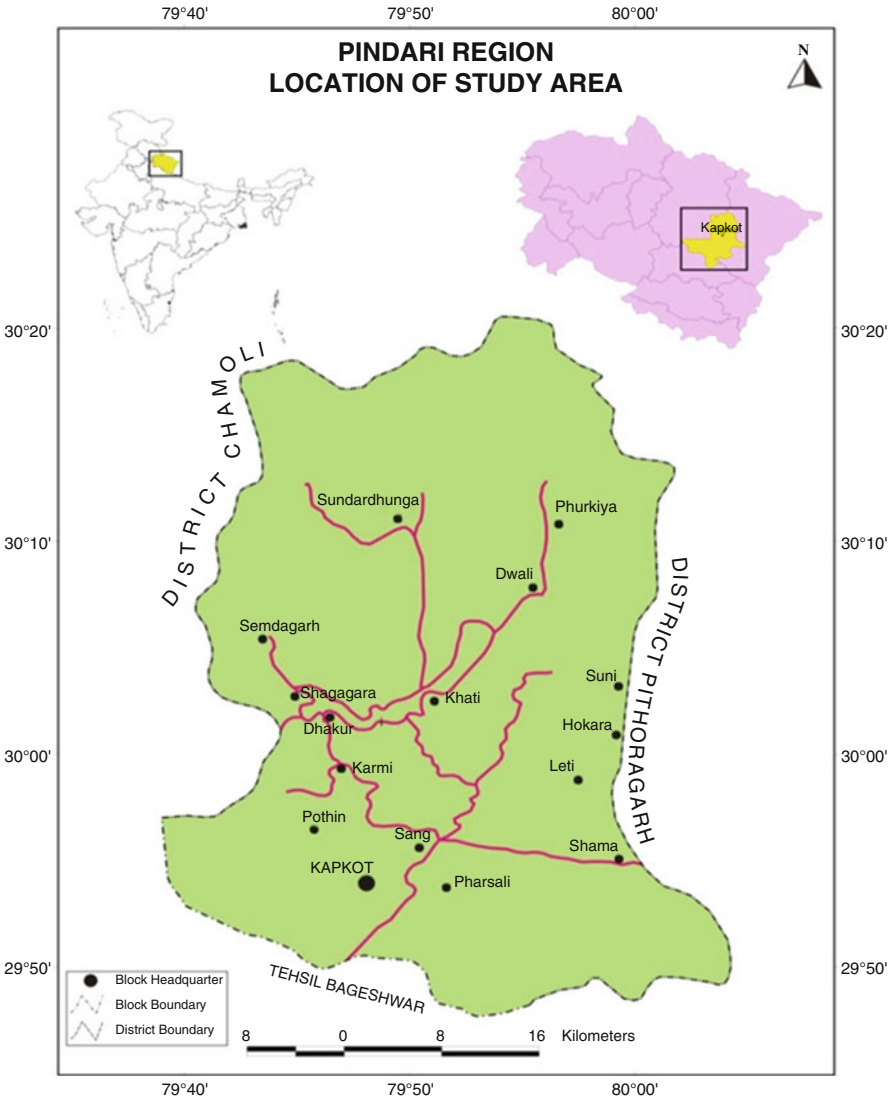

Fig. 7.1 Location of the study the area

area not having proper mechanism to record data due to adverse climatic conditions of harsh winter.

In order to analyze climate change and variation in study area, temperature and rainfall data of the last 30 years has been tabulated in MS word excel sheet. Statistical diagrams and techniques like line diagram, histogram, regression method and trend line have been used in order to show seasonal variability in temperature and rainfall. One whole year has been divided into three seasons, i.e. winter (October, November,

December, January, February), summer (March, April and May) and monsoon (June, July, August, September); temperature and rainfall data has been clubbed and classified on the basis of season. Then seasonal trend analysis has been done through regression method. Apart from seasonal climatic variation, yearly rainfall and temperature variation have been calculated using slope value of linear regression method.

The study also focuses on the delimitation of the spatial extent of glacier fluctuation in light of climate change in Pindari region. The results are deduced from the published data such as topographical maps and satellite images in consonance with GPS-aided intensive glaciological field survey. The topographical maps of 1955 (1:250,000) were collected from website add which is primarily derived from map (1927) of Survey of India (SOI), Dehradun, for earlier record of glaciers. The toposheet of 1955 was compiled by US Army from half-inch series, 1:126,720, Survey of India, 1938; Garhwal Himalaya-Ost, 1:150,000, Schweizerischen Stiffing fur Alpine Forschungen, 1938; and quarter-inch series, 1:253,440, AMS, 1946, Survey of India, 1927. The ASTER (Advanced Spaceborne Thermal Emission and Reflection Radiometer) orthorectified satellite imageries for different time periods (1976, 1998 and 2013) have been downloaded from Land Processes Distributed Active Archive Center-US Geological Services (LPDAAC-USGS), Glovis and Bhuvan website. Himalayan Glaciology Programme coordinated by the Department of Science and Technology, Government of India, the International Centre for Integrated Mountain Development (ICIMOD), Wadia Institute of Himalayan Geology and Glaciological Study of India under the Geological Survey of India comprise other sources of secondary database. In order to record the present snout positions and altitude information of deferent places over the glacier, two intensive field visits were conducted with GPS-aided survey of glaciers in the Pindari region. During the field visit, various other features such as moraine, nature of slope, rock type, vegetation cover, drainage pattern, etc. were also investigated in the study area.

The GIS study related to glacial analysis heavily depends on co-registration of the spatial data of selected area. The selected ASTER satellite images were already orthorectified and geo-registered to Universal Transverse Mercator (UTM) projection with Ellipsoid and Datum-WGS 84. The SOI topographical sheets (published by US Army) were co-registered using image to image co-registration function in ERDAS Imagine 10. The registration accuracy was within 1 pixel in most regions. The mapping of glacial extent in 1976, 1998 and 2013 was done on ASTER images using ArcGIS 10 and ERDAS Imagine 10 software and autocalculating the area using GIS methodology.

The application of manual digitization in GIS environment helped in delineating glaciers boundary on SOI topographical map. The glacial boundary on satellite imagery was mapped using standard combination of bands, i.e. false colour composite (FCC). Image enhancement technique was used to enhance difference between glacial and non-glacial areas. The glacier boundary was digitized and georeferred as well. Position of snout of the glaciers was cross-checked and verified by the field investigations using Global Positioning System (GPS-Etrex vista HCX)

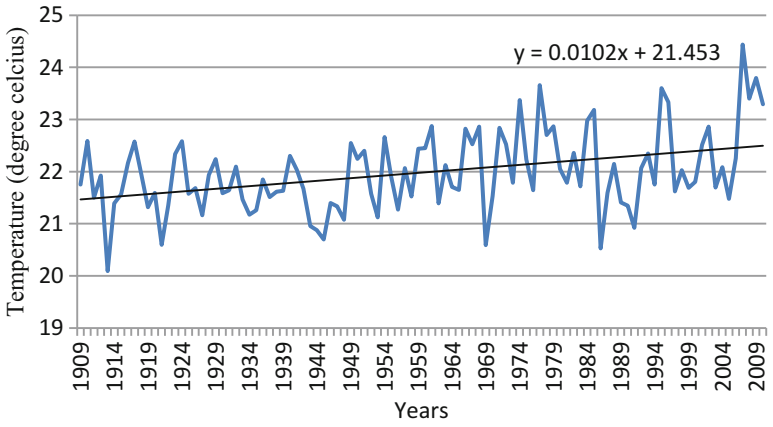

Fig. 7.2 Seasonwise (winter) annual mean maximum temperature trend of Bageshwar station of Pindari region (1901–2010) (Source: Based on IMD data)

and by comparing relative position of snout with geomorphological features such as moraines, origin of stream from snout. The area vacated by the glacier due to recession is estimated by union-geo-processing method (standard GIS function) using the glacier boundary of 1976, 1998 and 2013. Findings related to glacial measurement done by other scientists also incorporated and supported the study. It is obvious that some ambiguity might have occurred during these processes. But it was attempted to accomplish the job as carefully as possible.

7.6 Results and Discussion

7.6.1 Seasonwise Annual Trend in Maximum Temperature

Annual temperature trend of Bageshwar meteorological station is showing substantial increase of around 1 °C from 1901 to 2010 (Fig. 7.2). In the year 1977, the mean maximum temperature was 25.31 °C, while it was 26.65 °C in 2007. The range of maximum temperature for the same period is 2.46 °C. The highest maximum temperature for the station has been recorded 31.36 °C in the year 2007. The increase in the temperature over a period of 110 years for which the data has been procured from IMD is alarming. At about 1 °C increase in the mean maximum temperature has been calculated.

The trend line plotted shows that in the year 1901, the initial point of trend line was around 23.1 °C, while in the year 2007, it is at around 24.2 °C. The range of the minimum and maximum recorded temperature comes out to be 2.85 °C. The annual maximum temperature has shown rapid increase from 1990 onward. For Pindari region as a whole, seasonwise annual maximum temperature shows a gradual increasing trend during all the three: winter, summer and monsoon season over the

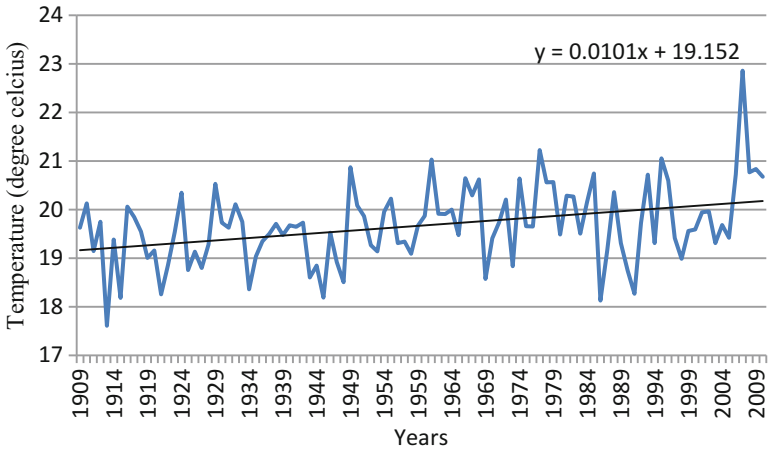

Fig. 7.3 Seasonwise (summer) annual mean maximum temperature trend of Bageshwar station of Pindari region (1901–2010) (Source: Based on IMD data)

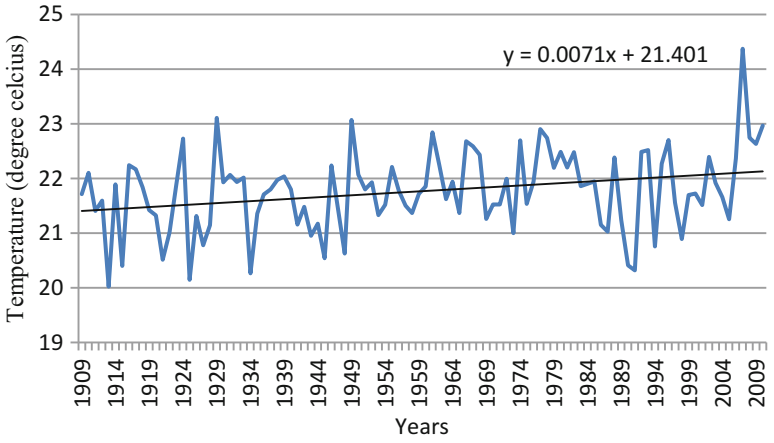

Fig. 7.4 Seasonwise (monsoon) annual mean maximum temperature trend of Bageshwar station of Pindari region (1901–2010) (Source: Based on IMD data)

period 1901–2010 (Figs. 7.3 and 7.4, Table 7.1). On the seasonal level, the trends in the frequency of occurrence of temperature extremes are slightly different. The homogeneous trend shows in monsoon season, but winter and summer seasons show a significant fluctuating trend in frequency of hot days. The winter season shows comparatively highest increasing trend in the annual maximum temperature.

Mean maximum annual temperature for all seasons is showing decrease in temperature from the year 1973 to 1990.

Table 7.1 Seasonwise change in mean maximum temperature (1901–2010)

Season	Winter	Summer	Monsoon
Rate of change (°C/year)	0.0102	0.0101	0.0071
Change 1901–2008 (°C)	1.1016	1.0908	0.7668
Coefficient of variation (%)	3.4681	4.0556	3.3612

Source: Based on IMD data

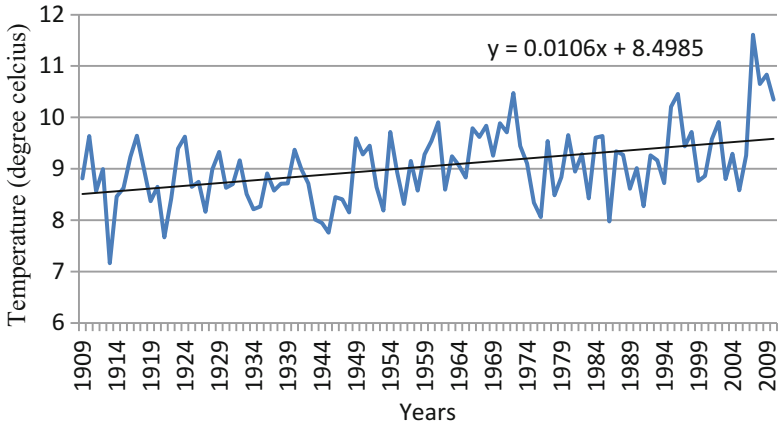

Fig. 7.5 Mean minimum temperature trend (winter) of Bageshwar station of Pindari region (year 1901–2010) (Source: Based on IMD data)

7.6.2 Annual Trend in Minimum Temperature

Mean annual minimum temperature of Pindari region showed a very significant increasing trend and increased by 1.026 °C per 110 years during the period 1901–2010 (Figs. 7.5, 7.6, 7.7 and Table 7.2). There are some conspicuous changes noted in different subperiods in the minimum temperature. During the period 1901–1977, the Pindari region mean annual minimum temperature shows a warming tendency, but after 1977, it decreases slowly up to 1997 and later it gradually increases. In the recent two and a half decades, the region mean annual minimum temperature shows a significant warming trend. The warming during the recent period (2004–2010) may have played a vital role in making the trend statistically significant in glacier fluctuation analysis. On the seasonal scale, all the seasons show significant warming trends with significant temporal variations in summer season.

7.6.3 Annual Mean Temperature Trend

Indian annual mean temperature showed significant warming trend of 0.51 °C per 100 years, during the period 1901–2007 (Kothawale et al. 2010). Accelerated warming has been observed in the recent period 1971–2007, mainly due to intense

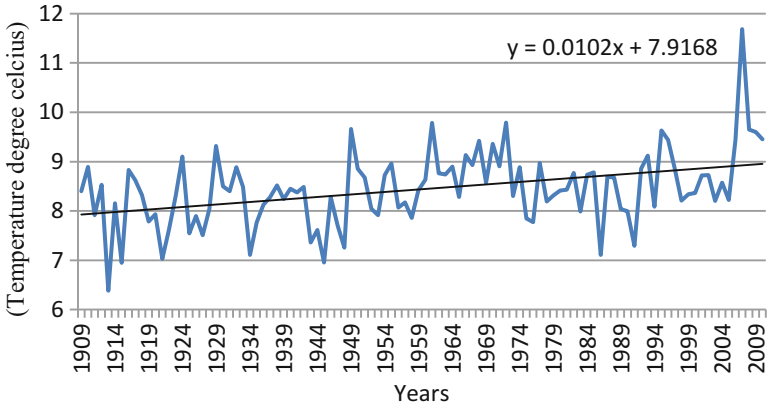

Fig. 7.6 Mean minimum temperature trend (summer) of Bageshwar station of Pindari region (year 1901–2010) (Source: Based on IMD data)

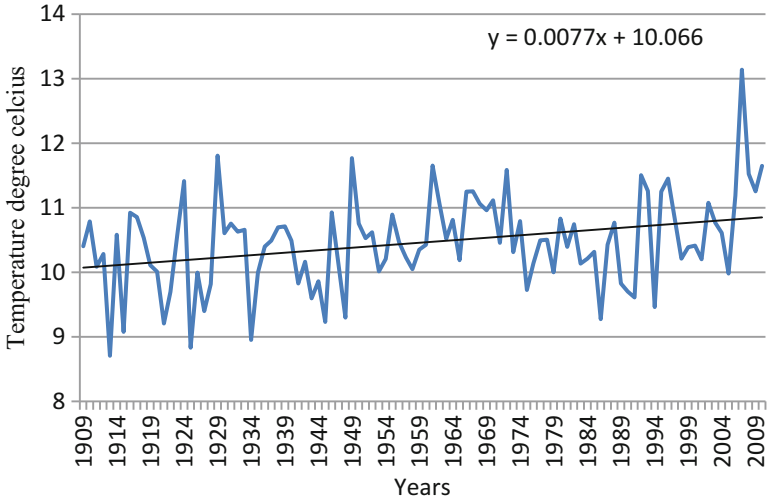

Fig. 7.7 Mean minimum temperature trend (monsoon) of Bageshwar station of Pindari region (year 1901–2010) (Source: Based on IMD data)

warming in the recent decade 1998–2007. Ground observations of air temperature measurements show strong spatial and seasonal gradients across the Himalayan-Tibetan Plateau. For example, the atmosphere over the Western Himalaya, which contains major glaciers and makes headwater to major rivers including the Indus and the Ganga, was found to be associated with enhanced warming trends in the past three decades from the longest record of microwave satellite observations. The two crucial seasons, i.e. the winter season (snow accumulation period) and pre-monsoon season (snowmelt period and important to the onset of the monsoon), are associated with increasing temperatures most discernible in the past two to three decade period (UNEP 2009).

Table 7.2 Seasonwise change in minimum temperature (1901–2010)

Season	Winter	Summer	Monsoon
Rate of change (°C/year)	0.0106	0.0102	0.0077
Change 1901–2008 (°C)	1.1448	1.1016	0.8316
Coefficient of variation (%)	7.8805	8.8505	6.8046

Source: Based on IMD data

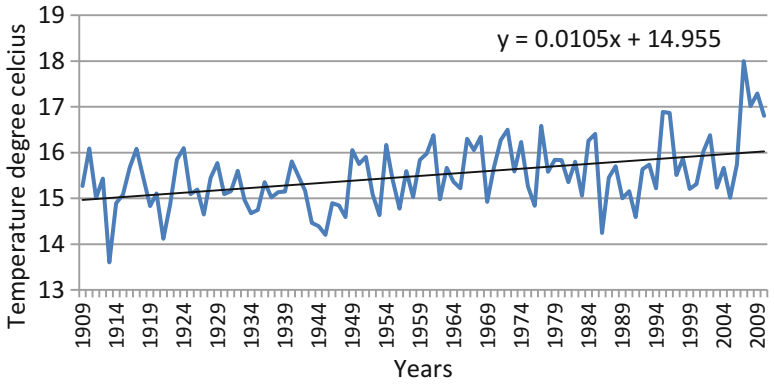

Fig. 7.8 Annual mean temperature trend (winter) of Bageshwar station of Pindari region (1901–2010) (Source: Based on IMD data)

Present study of seasonwise annual mean temperature for a meteorological station of Pindari region is showing an increase in the mean temperature in all seasons (Figs. 7.8, 7.9, 7.10 and Table 7.3). Annual mean temperature increased by about 1.02 °C for the period 1901–2010 with a much steeper increase in minimum temperature than maximum temperature. In the most recent decade, maximum temperature was significantly higher compared to the long-term (1901–1971) mean, with a stagnated trend during this period, whereas minimum temperature showed an increasing trend, almost equal to that observed during 1971–2010. On a seasonal scale, pronounced warming trends in mean temperature were observed in winter and monsoon seasons. Accelerated warming has been observed in the recent period 1977–2010, mainly due to intense warming in the recent decade 1997–2010. This warming is mainly contributed by the winter and post-monsoon seasons, which have increased by 0.80 °C and 0.82 °C, respectively, in the last hundred years. The summer and monsoon temperatures also indicate a warming trend. Kothawale and Rupa Kumar (2005) reported earlier that over these two regions (WH and WC), pre-monsoon maximum temperatures have increased significantly. The significant decreasing trend in cold days over these two regions may be a manifestation of the increasing trend in seasonal maximum temperatures. Further, Kripalani et al. (2003) have reported that the spring snow cover of Western Himalaya has been declining and that the snow was melting faster from winter to spring after 1993, which is consistent with the trends observed in the present study.

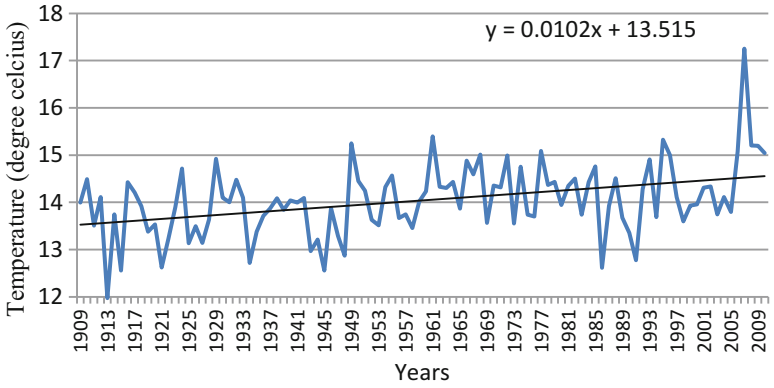

Fig. 7.9 Annual mean temperature trend (summer) of Bageshwar station of Pindari region (1901–2010) (Source: Based on IMD data)

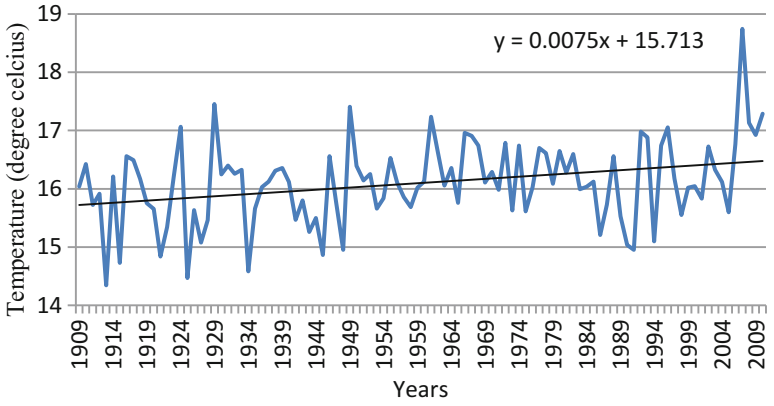

Fig. 7.10 Annual mean temperature trend (monsoon) of Bageshwar station of Pindari region (1901–2010) (Source: Based on IMD data)

Table 7.3 Seasonwise change in average temperature (1901–2010)

Change	Winter	Summer	Monsoon
Rate of change (°C/year)	0.0105	0.0102	0.0075
Change 1901–2008 (°C)	1.134	1.1016	0.81
Coefficient of variation (%)	4.5888	5.3118	4.3776

Source: Based on IMD data

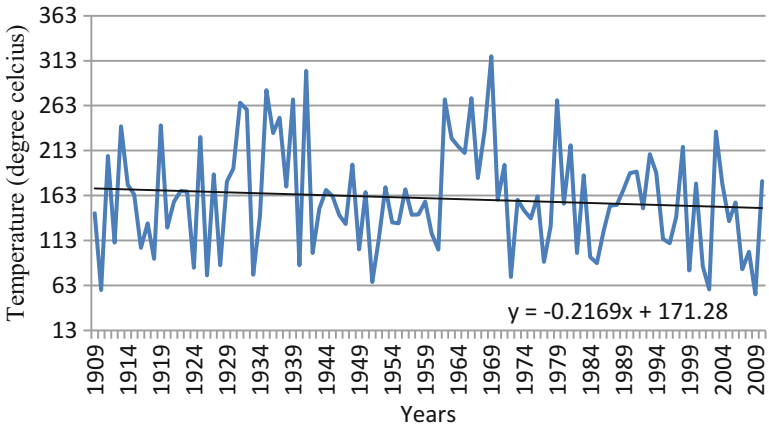

Fig. 7.11 Annual mean rainfall trend (winter) of Bageshwar station of Pindari region (1901–2010) (Source: Based on IMD data)

7.6.4 Seasonwise Annual Trend in Rainfall

The total annual rainfall in the state is maximum over the Pindari region of Bageshwar district. The total annual rainfall for the region is 149 cm and the total annual number of rainy days is 65. The rainfall over the region increases towards southern region during winter and monsoon.

The southwest monsoon season is the principal rainy season over the region. Of the total annual rainfall, about 73 % is received in the southwest monsoon season (June to September), about 9 % is received in the winter season (January and February), about 11 % is received in the pre-monsoon season (March to May) and about 6 % is received in the post-monsoon season (October to December). The percentage of the seasonal number of rainy days with respect to the annual number of rainy days is 63 % for the southwest monsoon season, 16 % for the pre-monsoon season, 7 % for the post-monsoon season and 13 % for the winter season (Figs. 7.11, 7.12, 7.13 and Table 7.4).

Annual mean rainfall trend plotted for winter, summer and monsoon is not showing any clear picture of either decreasing or increasing trend. In winter season, mean rainfall trend is showing decreasing trend with high fluctuation but summer and monsoon seasons showing constant trend in precipitation but also showing high degree of variability from the mean rainfall. All seasons in the Pindari region indicate anno significant increase in rainfall. Annual mean of heaviest rainfall in 24 h is showing a decreasing trend over the period. Bageshwar meteorological station data is showing a decreasing trend but with varying degree.

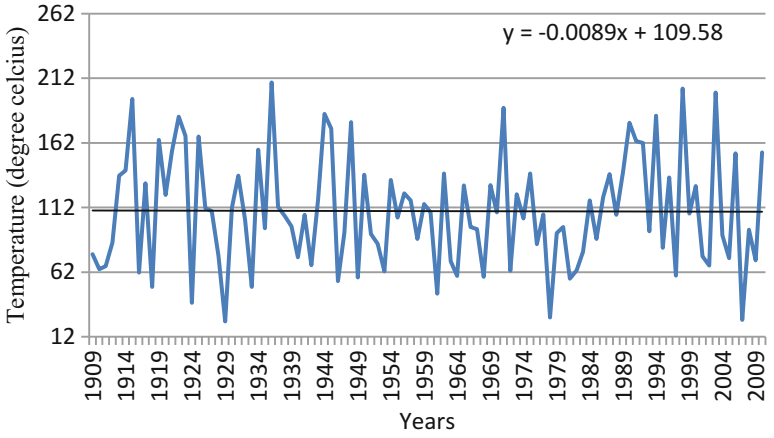

Fig. 7.12 Annual mean rainfall trend (summer) of Bageshwar station of Pindari region (1901–2010) (Source: Based on IMD data)

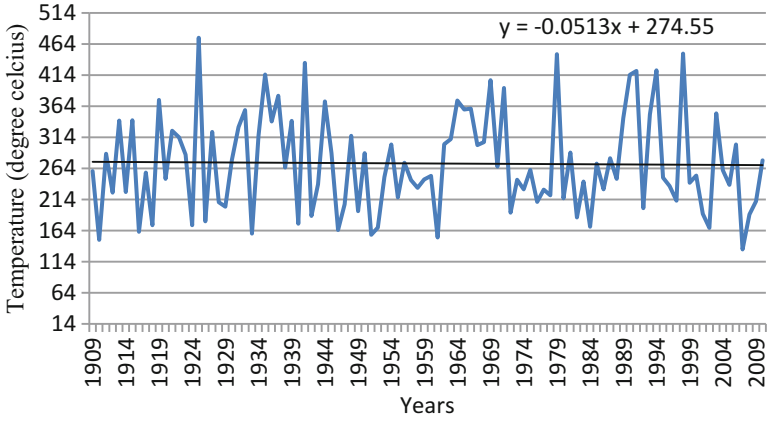

Fig. 7.13 Annual mean rainfall trend (monsoon) of Bageshwar station of Pindari region (1901–2010) (Source: Based on IMD data)

Table 7.4 Seasonwise change in average precipitation (1901–2010)

Season	Winter	Summer	Monsoon
Rate of change (mm/year)	0.2169	0.0089	0.0513
Change 1901–2008 (mm)	23.4252	0.9612	5.5404
Coefficient of variation (%)	37.1909	39.6412	29.0851

Source: Based on IMD data

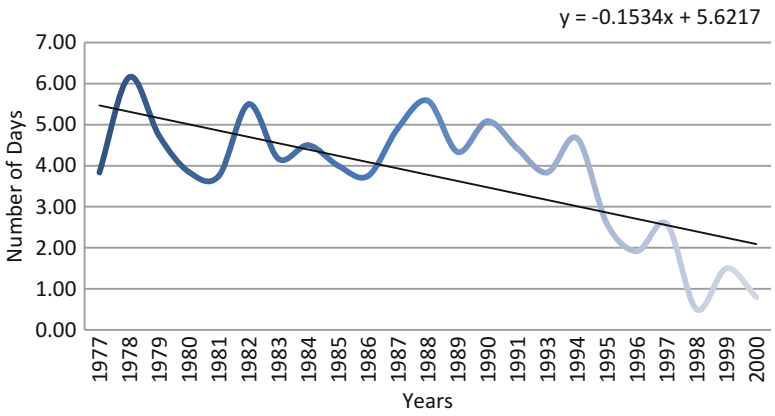

Fig. 7.14 Annual average snow days at Bageshwar station (1977–2000) (Source: Based on IMD data)

7.6.5 Annual Average Snow Days

Annual average number of snow day's data is available only for Bageshwar meteorological stations. Analysis of the data reveals the fact that average days with snow in a year is also showing decreasing trend. The decrease is of around 3.4 days in a period of 23 years (Fig. 7.14). Less number of snow days in the region is going to give less amount of snowfall. The decreasing snow will affect the volume and thickness of a snow area; thus, glaciers will become more vulnerable as the mean minimum temperature is showing an overall increase. This will result in gradual decline of total snow area in the region in coming decades. The decrease in the number of days with snow is alarming after the year 1995.

Evidence from a recent snowfall study shows reduced snowfall over Western Himalaya (Dimri and Kumar 2008). Yet another study concluded decreasing trend of snowfall over all the mountain ranges with different magnitudes. The study noted a decrease in total seasonal snowfall of 280 cm over the entire Western Himalaya between 1988/1989 and 2007/2008 (Shekhar et al. 2010).

7.6.6 Climate Change and Glacier Recession in Pindari Region

Pindari Glacier has been receding regularly with varying rate since the last 'little ice age'. The tributary glaciers (Chhanguch) have also shrunk and some of them have even got separated from the main trunk of the glacier. This fact is evident by systematic studies going on since 1906 on the movement of the glacier snout and by the presence of recessional features such as terminal and lateral moraines (GSI 2001). A comparative analysis of the glacier's snout position was carried out using data

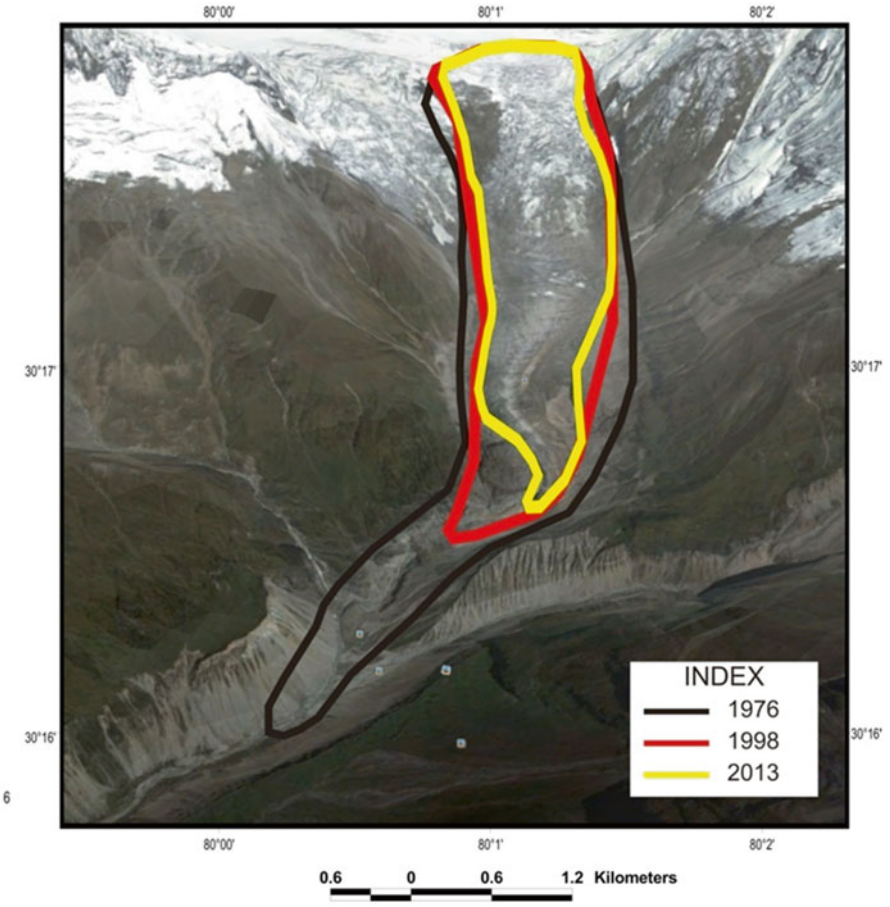

Fig. 7.15 Recession of Pindari Glacier (1976, 1998 and 2013) (Source: Based on LANDSAT image, Overlaid on the Google Earth Image)

from secondary sources and interpretations from various satellite imageries over the past three decades.

A study of data from all available sources illustrates that the main trunk of the Pindari Glacier has been in a continuous state of recession during the past century. The length of the glacier has been computed for different years based on available data. The trend shows that the length of the glacier has reduced by about 0.535 km in 37 years, from 1976 to 2013, with an average retreat rate of 14.459 m/year. Based on the comparison of satellite imageries of the Pindari Glacier for the years 1976, 1998 and 2013, our analysis shows that the glacier is not only receding in length but also in terms of glaciated area from all the sides. The possible reasons behind this retreat may be linked with two main factors: (a) reduction in snowfall and (b) an increase in the temperature of the region. Analysis shows that between 1976 and 2013, Pindari Glacier area has reduced by 0.998 km^2, with an average loss of

26.97 m^2 per year. This reduction in glacier area is 14.9 % over 1976. With a reduction in the area and length of the Pindari Glacier, there has also been a retreat in the snout position (Fig. 7.15). The shift of tongue or snout position of the glacier is as response to environmental changes in the region (Fig. 7.16).

7.6.7 Climate Prediction over Pindari Region

Model prepared by the Indian Institute of Tropical Meteorology (IITM) in collaboration with the Hadley Centre for Climate Prediction and Research, UK, generated high-resolution climate scenarios for different states of India. For Himalayan region including Pindari region, the indicative predictions were that for the period 2030 with reference to the baseline of 1970, the annual temperature is projected to increase from 0.9 ± 0.6 to 2.6 ± 0.7 °C in 2030s. The net increase in temperature is ranging from 1.7 to 2.2 °C with respect to the 1970. Seasonal air temperatures also show rise in all seasons. However, winter temperatures during October, November and December in the Q1 simulations show a decrease by 2.6 °C in 2030 with respect to 1970 (INCCC 2010). The précis run for 2030s indicates that the annual rainfall in the Himalayan region may vary between 1268 ± 225.2 and 1604 ± 175.2 mm, respectively. The projected precipitation shows a net increase in 2030s with respect to the simulated rainfall of 1970s in the Himalayan region by 60–206 mm. The increase in annual rainfall in 2030s with respect to 1970s ranges from 5 to 13 %. All seasons in the Himalayan region indicate an increase in rainfall, with the monsoon months of June, July, August and September showing the maximum increase in rainfall by 12 mm.

Fig. 7.16 Moraines in valley: indicator of glacial retreat

7.7 Conclusion

Analysis of data for the period 1901–2010 suggests that annual mean temperature for the country as a whole has risen by 0.56 °C. The country as a whole, all India annual and monsoon rainfall for the period 1901–2010 does not show any significant trend. More or less the same trend has been noticed in the Pindari region where mean annual temperature is showing an increase. Rainfall is not showing any clear picture. Increase in temperature has resulted into retreat in snow area. Overall climate change is the result of seasonwise changes in temperature, cloud cover and the timing, intensity, duration and form of precipitation (i.e. snow versus rain), all of which are equally important determinants of glacial retreat in the area. Analysis of recent climatic trends reveals a significant warming trend in the recent decades which has been even more pronounced at Himalayan region. The recent formation of glacier lakes and changes in position of glacier snouts suggest that it is due to rise in temperature which indicates a corresponding change in climate. Changing climate may be harsher in Himalayan region because of its effects on glacio-hydrological regimes and the resulting impact on water resources.

References

Arora M, Goel NK, Singh R (2005) Evaluation of temperature trends over India. Hydrol Sci J 50(1):81–93

Bates BC, Kundzewicz ZW, Wu S, Palutikof JP (2008) Climate change and water (ed), Technical paper, Intergovernmental Panel on Climate Change, Geneva

Dimri AP, Kumar A (2008) Climatic variability of weather parameters over the western Himalaya: a case study. In: Satyawali PK, Ganju A (eds) Proceedings of the national snow science workshop, Chandigarh: Snow and Avalanche Study Establishment, pp 167–173

Goswami P, Ramesh KV (2006) A comparison of interpolated NCEP (I-NCEP) rainfall with high-resolution satellite observations. Geophys Res Lett 33(19):L19821

Halpin PN (1994) Latitudinal variation in montane ecosystem response to potential climatic change. In: Beniston M (ed) Mountain ecosystems in changing climates. Routledge Publishing Company, London, pp 180–203

Hingane LS, Rup Kumar K, Ramanamurthy BV (1985) Long term needs of surface air temperature in India. Int J Climatol 5:521–528

GSI (2001) Glaciology of Indian Himalaya: a bilingual contribution in 150 year of Geological Survey of India: Special Publication No. 63. Geological Survey of India, p 216

IPCC (2007) The physical science basis. Contribution of Working Group I to the fourth assessment report of the Intergovernmental Panel on Climate Change, pp 235–337

INCCC (2010) Climate change and India: A 4 × 4 Assessment (A sectoral and regional analysis for 2030s). Ministry of Environment and Forest, Government of India, p 41

Ives JD, Messerli B, Spiess E (2004) Mountains of the world: Global priorities. In: Messerli B, Ives JD (eds) Mountains of the world: a global priority. Parthenon Publishing Group, New York/London, pp 1–15

Kothawale DR, Rupa Kumar K (2005) On the recent changes in surface temperature trends over India. Geophys Res Lett 32:L18714. doi:10.1029/2005GL023528

Kothawale DR, Munot AA, Krishna KK (2010) Surface air temperature variability over India during 1901–2007, and its association with ENSO. Climate Res 42:89–104

Kripalani RH, Kulkarni A, Sabade SS (2003) Western Himalayan snow cover and Indian monsoon rainfall: a re-examination with INSAT and NCEP/NCAR data. Theor Appl Climatol 74(1-2):1–18

Lau KM, Ramanathan V, Wu GX, Li Z, Tsay SC, Hsu C, Siika R, Holben B, Lu D, Tartari G, Chin M, Koudelova P, Chen H, Ma Y, Huang J, Taniguchi K, Zhang R (2008) The joint aerosol-monsoon experiment: a new challenge in monsoon climate research. Bull Am Meteorol Soc 89:369–383

Pant GB, Kumar R (1997) Climate of South Asia. Wiley, Chichester

Price MF (1990) Temperate mountain forests: common-pool resources with changing, multiple outputs for changing communities. Nat Resour J 30:685–707

Ramesh KV, Goswami P (2007) The shrinking of Indian summer monsoon, research report, geophysical research letters (in press). CSIR Centre for Mathematical Modelling and Computation Simulation, Bangalore

Rizzo B, Wiken E (1992) Assessing the sensitivity of Canada's ecosystems to climatic change. Clim Change 2:37–54

Rosenzweig C, Karoly D, Vicarelli M, Neofotis P, Wu Q, Casassa G, Imeson A (2008) Attributing physical and biological impacts to anthropogenic climate change. Nature 453(7193):353–357

Sen Roy S, Singh RB (2002) Climate variability, extreme events and agricultural productivity in Mountain Regions. Oxford and IBH Publications co. Pvt. Ltd., New Delhi

Shekhar SK, Chand H, Kumar S, Srinivasan K, Ganju A (2010) Climate change studies in the western Himalaya. Ann Glaciol 51(54):105–112

Singh RB (1998) Land use/cover changes, extreme events and eco-hydrological responses in the Himalayan region. In: Singh RB (ed) Sustainable development of mountain environment in India and Canada-CIDA-SICI project experience. Oxford and IBH Publishing Co, New Delhi, pp 53–67

Singh RB, Kumar R, Kumar A (2013) Climate change and ecosystem services in Kullu Himalaya, Himachal Himalaya. In: Singh RB, Heitala R (eds) Livelihood security in Northwestern Himalaya. Springer, Tokyo

Sinha Ray KC, Mukhopadhya RK, Chowdhary SK (1997) Trend in maximum and minimum temperature and sea level pressure over India. INTROMET 1997 IIT Delhi. HauzKhas, New Delhi

Srinivasan J, Chakraborty A, Nanjundiah RS (2006) Theoretical aspects of the onset of Indian summer monsoon from perturbed orography simulations in a GCM. Ann Geophys 24(8):2075–2089

UNEP (2009) Recent trends in melting glaciers, tropospheric temperatures over the Himalaya and summer monsoon rainfall over India. Division of Early Warning and Assessment (DEWA), United Nations Environment Programme (UNEP), Nairobi

Xu J, Eriksson M, Shrestha AB, Vaidya RA, Nepal S, Sandström K (2009) The changing Himalaya – impact of climate change on water resources and livelihoods in the greater Himalaya. ICIMOD, Kathmandu

Part II
Climate Change Impacts on Glaciers and Hydrology

Chapter 8
Glacier Variations in the Trans Alai Massif and the Lake Karakul Catchment (Northeastern Pamir) Measured from Space

Nicolai Holzer, Tim Golletz, Manfred Buchroithner, and Tobias Bolch

Abstract Glacier area and length changes were measured in the central Trans Alai of the northeastern Pamir, including the entire catchment of Lake Karakul. Annual shrinkage determined from Landsat 7 ETM+ imagery accounted for -0.8 ± 0.4 % a^{-1}, corresponding to -8.8 ± 4.8 % from 1455 ± 51 km^2 in 2000 to 1327 ± 48 km^2 in 2011. Several glaciers could be mapped back to 1973 based on a KH-9 Hexagon reconnaissance image. Measured glacier extents of 550 ± 10 km^2 in 1973, 540 ± 9 km^2 in 2000, and 521 ± 9 km^2 in 2011 indicate accelerated shrinkage for the last decade in the Trans Alai. Glaciers retreated on average by -4.3 ± 0.5 m a^{-1} before 2000 and subsequently advanced by $+6.1 \pm 1.0$ m a^{-1} until 2011. Geodetic mass balances of four selected glaciers were determined from a Digital Elevation Model extracted from a 2010 ALOS-PRISM tri-stereo image and the February 2000 SRTM-3 elevation dataset (1999). Its difference image reveals highly variable glacier elevation changes. While three glaciers showed probably a minor loss (-0.16 ± 0.68 m w.e. a^{-1} to -0.06 ± 0.68 m w.e. a^{-1}), a more pronounced mass loss was observed for Uisuu Glacier (-0.50 ± 0.68 m w.e. a^{-1}). This study reveals significant glacier variations and numerous indications of surges in the Trans Alai, a well-known phenomenon in the Pamir.

Keywords Glacier variations • Geodetic mass balance • ALOS-PRISM • KH-9 Hexagon • Trans Alai • Northeastern Pamir

N. Holzer (✉) • T. Golletz • M. Buchroithner
Institut für Kartographie, Technische Universität Dresden,
Helmholtzstraße 10, 01069 Dresden, Germany
e-mail: nicolai.holzer@gmx.de

T. Bolch (✉)
Institut für Kartographie, Technische Universität Dresden,
Helmholtzstraße 10, 01069 Dresden, Germany

Geographisches Institut, Universität Zürich,
Winterthurerstrasse 190, 8057 Zürich, Switzerland
e-mail: tobias.bolch@geo.uzh.ch

R.B. Singh et al. (eds.), *Climate Change, Glacier Response, and Vegetation Dynamics in the Himalaya*, DOI 10.1007/978-3-319-28977-9_8

8.1 Introduction

Glaciers are of high importance for freshwater supply and act as valuable key indicator of climate change. Spatially and temporally heterogeneous glacier variations coming along with an increasing number of floods and droughts suggest that the glaciers of High Mountain Asia are affected by a changing climate (IPCC 2013). Heterogeneous glacier variations on the so-called Third Pole might be induced by changing atmospheric circulation patterns, with a weakening monsoon and strengthening westerlies (Yao et al. 2012).

Little is known about recent glacier changes in the remote and high mountain regions of the Pamir. In this study, we determined areal and length changes of glaciers in the Lake Karakul catchment and the Trans Alai mountain range of the Pamir (Tajikistan). The highly continental and arid study site (39°N, 73°E) with Pik Lenin (7134 m a.s.l.) as the highest elevation is strongly influenced by the westerlies. The majority of these mostly winter accumulation-type glaciers drain in the endorheic Lake Karakul basin at 3915 m a.s.l. (Peel et al. 2007; Komatsu et al. 2010; Maussion et al. 2014).

Multitemporal remote-sensing data as used in this study offers an efficient alternative to expensive and complicated field measurements. We hereby present the first detailed investigation of glacier variations within the Lake Karakul catchment and the Trans Alai.

8.2 Database

Glacier area and length changes were mapped from 2000 to 2011 based on orthorectified imagery of Landsat 7 ETM+ (level L1t). Several glaciers of the Trans Alai are also covered by a KH-9 Hexagon spy photograph (cf. Burnett 2012) of the year 1973. A Digital Elevation Model (DEM) was extracted from ALOS-PRISM tri-stereoscopic imagery (cf. Takaku et al. 2007) of the year 2010. This DEM was used to compare changes in glacier elevation with the Shuttle Radar Topography Mission (SRTM-3) elevation model (cf. Jarvis et al. 2008) and to calculate mass budgets of four selected glaciers. Terrain-corrected L1t imagery of Landsat-7 ETM+ served as horizontal reference and elevations of the hole-filled SRTM-3 version 4.1 (2000) as vertical reference. All data were projected to WGS84 and the EGM96 geoid at UTM zone 43N. Table 8.1 summarizes all satellite data used in this study.

Table 8.1 Properties and purpose of remote-sensing datasets used in this study

Sensor	Date	ID	Resolution	Usage
Landsat-7 ETM+	24 Aug 2000	LE71510332000237SGS00	30 m (pan: 15 m)	Area change, horizontal reference
	20 Aug 2010	LE71510332010232EDC00		
	23 Aug 2011	LE71510332011235PFS00		
	8 Sep 2011	LE71510332011251PFS00		
ALOS-PRISM	20 Aug 2010	ALPSMF243482755	2.5 m	Elevation change, mass balance
		ALPSMN243482810		
		ALPSMB243482865		
SRTM-3[a]	11–22 Feb 2000	Hole-filled SRTM-3 v4.1 of CGIAR-CSI	90 m (X-band: 25 m)	Elevation change, mass balance, vertical reference
KH-9 Hexagon	30 Jul 1973	DZB1206-500068L013001_b	6–9 m	Area change

[a]SRTM-3 roughly represents the glacier surface at the end of the ablation period of 1999, due to C-band radar penetration into ice and snow

8.3 Data Processing

8.3.1 Glacier Area and Length Changes

Orthorectification of the KH-9 Hexagon photograph by means of the PCI Geomatica 2013 software package is based on the SRTM-3 elevation model. We measured 53 ground control points (GCPs) from Landsat 7 (x, y coordinates) and SRTM-3 (z coordinates). Residuals in terms of RMSE at 11.6 m in x and 18.7 m in y direction were acceptable considering the spatial resolution and accuracy of the reference datasets.

Automatic delineation of clean-ice glaciers is based on established band-ratio techniques (e.g., Racoviteanu et al. 2009; Bolch et al. 2010; Paul et al. 2013). We tested different band combinations and thresholds with the multispectral Landsat 7 dataset of the year 2000. A ratio of Landsat 7 band 4 divided by band 5 with a threshold of 3.0 proved to produce the best results for accurate ice delineation. Isolated pixels were eliminated by 3×3 median filtering, followed by smoothing of the converted outline polygons. We only considered glacierized areas larger than 0.01 km^2, which also displayed slope angles below 60°.

Reflection of supra-glacial debris is similar to that one of the surrounding moraines, and the glaciers had, hence, to be delineated manually. Mapping of debris-covered glaciers as well as ice divides was based on the panchromatic channel of the Landsat 7 dataset and derived morphometric parameters from SRTM-3. Outlines were finally cross-checked in Google Earth and the panchromatic band of the imagery as well. The final outlines of 2000 were subsequently adjusted to the glacier extent of 2011 from the corresponding Landsat 7 image. Outline adaption for the year 1973 was restricted by the KH-9 Hexagon photograph which does not cover the entire site. Changes in glacier length were measured along the central flow line for 41 glaciers, with an extent of at least 10 km^2 from 2000 to 2011. Most of these glaciers (38 in total) were also covered by the KH-9 Hexagon scene and could be investigated back to the year 1973.

8.3.2 Elevation Changes and Geodetic Mass Balances

Geodetic glacier mass balances were determined for the period 1999–2010 by subtracting SRTM-3 elevations from a more recent DEM derived from ALOS-PRISM tri-stereo imagery. DEM differencing and subsequent mass balance measurements were restricted to glaciers covered by the ALOS-PRISM scene. We chose the Great Saukdara Glacier (size: 74 km^2), the October Glacier (77 km^2), the Uisuu Glacier (56 km^2), and the Western October Glacier (19 km^2) to calculate their volume change relative to the SRTM-3 elevation model (1999).

8.3.2.1 ALOS-PRISM DEM Extraction

Terrain extraction from ALOS-PRISM tri-stereoscopic imagery was carried out with the PCI 2013 Geomatica OrthoEngine software and its rational functions model. The accuracy reached using ephemeris information (RPC data) was improved by measured GCPs in plain relief portions. Two DEMs with 30 m spatial resolution were extracted from the backward- and nadir- as well as the nadir- and forward-looking views. Elevations with the best obtained matching score were used for the final DEM. We up-sampled the SRTM-3 elevations to a resolution of 30 m using cubic convolution, followed by re-sampling of the ALOS-PRISM DEM to the raster grid extent of the up-sampled SRTM-3. This allowed a common resolution and exact raster alignment of both elevation datasets.

8.3.2.2 Outlier Detection and Gap Filling

ALOS-PRISM elevations with stereo matching scores below 0.75 were ignored due to their insufficient accuracy. Remaining outliers were subsequently determined by quantile analysis. For each investigated glacier, we calculated 1.5 times

interquartile range of elevation differences relative to the up-sampled SRTM-3 (cf. Pieczonka et al. 2013). Elevation differences beyond these bounds were set to no data.

The equilibrium line altitude (ELA) separates glacier ablation from accumulation zone and was estimated from snowline mapping in satellite imagery. For Western October Glacier, it was determined to be at 5200 m and for the other three investigated glaciers at 5000 m. Data gaps in glacier ablation zones proved to be marginal in the ALOS-PRISM DEM and were not filled. Glacier accumulation zones, however, were affected by high noise and large areas of poor or no elevation estimates. This is a result from oversaturation and low-contrast alterations due to extensive snow coverage. Data voids were filled with zero since in these areas we only assume minor elevation changes over time.

8.3.2.3 DEM Co-registration and Post-processing

Co-registration of the ALOS-PRISM DEM to the SRTM-3 reference is based on an analytical approach by Nuth and Kääb (2011). Remaining inaccuracies after horizontal co-registration were 1.81 m in x and 0.93 m in y direction. We observed a spatially varying elevation offset in the form of a slight tilt relative to the SRTM-3 surface. A two-dimensional linear trend surface was subtracted from the DEM of ALOS-PRISM which reduced the mean height offset on stable terrain relative to SRTM-3 to zero (Bolch et al. 2008; Holzer et al. 2015).

Elevation differences between SRTM C- and X-band surfaces were compared in order to estimate the impact of C-band radar wave penetration into glacier ice (Gardelle et al. 2012). It was hereby assumed that the end-of-summer surface of 1999 is detected. The average elevation difference was 1.5 m for glacierized areas which is close to the 1.6 m penetration estimate of Gardelle et al. (2013) for the Pamir. This correction value for ice-covered areas of the SRTM C-band DEM might, however, be underestimated, since the X-band beam penetrates into glacier ice as well (Kääb et al. 2015).

The glacier volume to ice mass conversion is based on a presumed ice density of 850 ± 60 kg/m^3 (Huss 2013).

8.3.3 Uncertainty Assessment

To estimate the uncertainty of glacier mapping from Landsat 7 imagery, we buffered the glacier area with ±7.5 m, which is half of the resolution of the panchromatic band. A buffer of ±10 m was used for mapping from the KH-9 Hexagon photograph to take difficult image geometry and film distortions into account (Bolch et al. 2010). The precision of DEM differencing was estimated as the standard deviation on stable and ice-free terrain. Hereby we only considered terrain below a slope of

30° and eliminated outliers outside of the 1.5 times interquartile range. The standard deviation of valid elevation differences was measured to be 7.3 m and is close to the 68.3 % quantile at 7.5 m. Uncertainties of glacier changes are defined by the root sum squares of each error term.

8.4 Results

8.4.1 Glacier Area Changes

The investigated glacierized area shrank from 1455 ± 51 km² in 2000 to 1327 ± 48 km² in 2011. The total area loss of −128 ± 70 km² (−8.8 ± 4.8 %) corresponds to −11.6 ± 6.4 km² per year or to an annual rate of −0.8 ± 0.4 %. In 2000, we counted 1582 glaciers, 1502 of which were shrinking. Moreover, a total number of 142 shrinking glaciers disappeared by 2011. We observed that larger glaciers were less vulnerable than smaller glaciers that showed a greater areal loss. Glacier shrinkage was particularly pronounced in the northern and northeastern parts of the study area. The shrinkage of 19 glaciers larger than 10 km² was −3.5 % from 2000 to 2011. Area reduction in the range of −22.7 % was much higher for 1347 glaciers which were smaller than 1 km². Twenty-two glaciers between 5 and 10 km² in size shrank −4.8 %, and 194 glaciers with extents in the range of 1–5 km² shrank −9.0 % (Fig. 8.1).

We subdivided the glacierized area in altitude zones of 100 m to investigate their hypsometric distribution. Glaciation was observed to be maximal at ~5100 m a.s.l., with a gradual decrease to lower and higher altitudes. This distribution did not significantly change from 2000 to 2011. The maximal absolute shrinkage was observed at 5100 m a.s.l. as well, while relative area loss with −17.0 % was highest at altitudes of ~4500 m. Supra-glacial debris coverage increased by +23.0 ± 9.0 % and accounted for 6.2 ± 0.4 % (90.2 ± 5.1 km²) of the total glacierized area of the year 2000 and to 8.3 ± 0.5 % (110.7 ± 6.6 km²) in 2011.

Moreover, we identified area changes of 11 glaciers larger than 20 km², based on terrain-corrected KH-9 Hexagon photography from 1973 (Fig. 8.2). The investigated glaciers had an extent of 550 ± 10 km² in 1973 and shrank by −0.1 ± 0.1 % a^{-1} (−1.8 ± 2.4 %) to 540 ± 9 km² in 2000. A further areal reduction to 521 ± 9 km² in 2011 corresponds to an approximately three times higher rate at −0.3 ± 0.2 % a^{-1} (−3.5 ± 2.4 %). The total glacier shrinkage of −29.0 ± 13.5 km² from 1973 to 2011 corresponds to a rate of −0.2 ± 0.1 % a^{-1} (−5.3 ± 2.5 %). This is less than the value measured for the entire study area, presumably because only larger glaciers were investigated. However, glacier shrinkage was already occurring before the year 2000 and is apparently increasing till today.

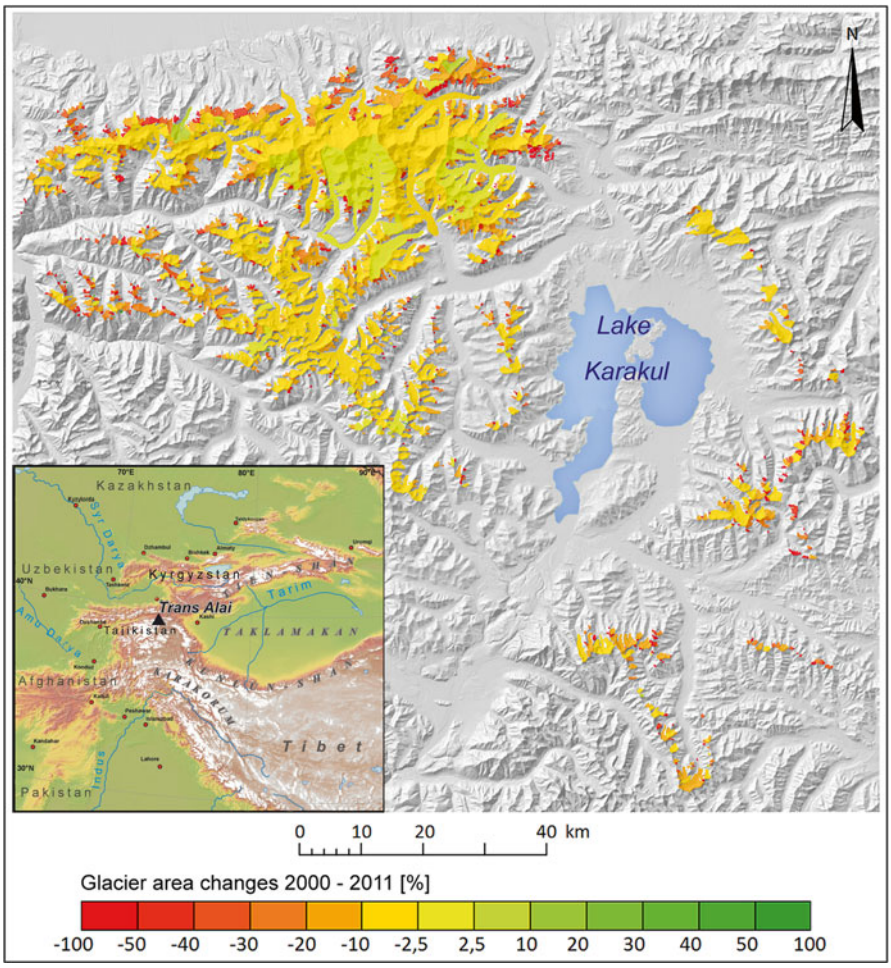

Fig. 8.1 Relative area loss per glacier from 2000 to 2011 in the Lake Karakul catchment with overview map of the Trans Alai study site (Source: Author)

8.4.2 Glacier Length Changes

The investigated glaciers retreated on average by -4.3 ± 0.5 m a^{-1} (-115 ± 13 m) during the period of 1973–2000, while glaciers subsequently advanced in a mean of $+6.1 \pm 1.0$ m a^{-1} ($+68 \pm 11$ m) until 2011. Several glaciers showed evidence of surges and advanced considerably, in some cases, by several hundred meters. Small Saukdara Glacier showed the most pronounced advance of all glaciers, $+2350 \pm 13$ m from 1973 to 2000. No significant changes, however, could be determined in the following period until 2011. Dzerzhinsky Glacier retreated -90 ± 13 m from 1973 to 2000 and subsequently advanced $+570 \pm 11$ m until 2011 (Fig. 8.3). Overall, most

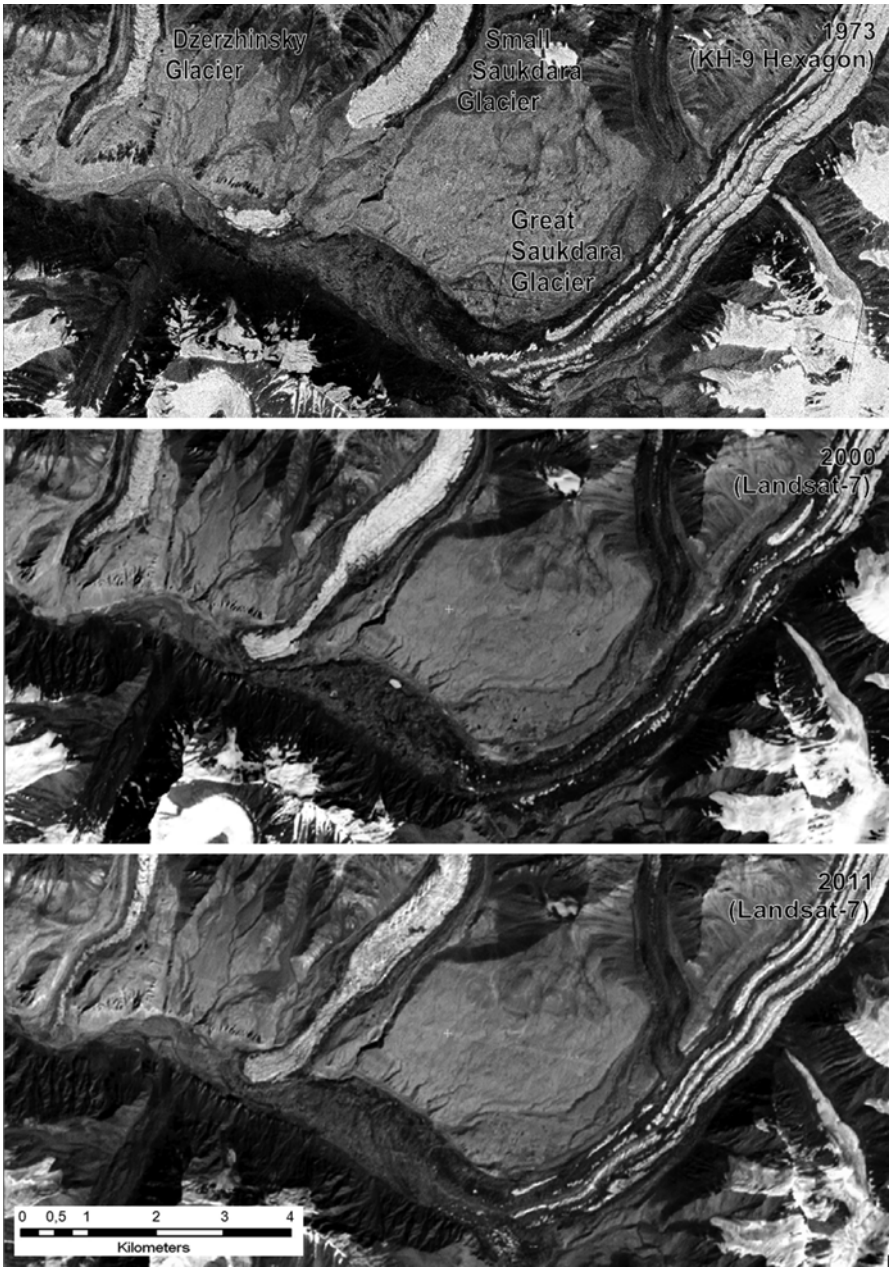

Fig. 8.2 Terrain-corrected imagery of KH-9 Hexagon (1973) and Landsat 7 ETM+ of the years 2000 and 2011, showing area changes of Dzerzhinsky, Small Saukdara, and Great Saukdara Glacier in the Trans Alai (Source: Author)

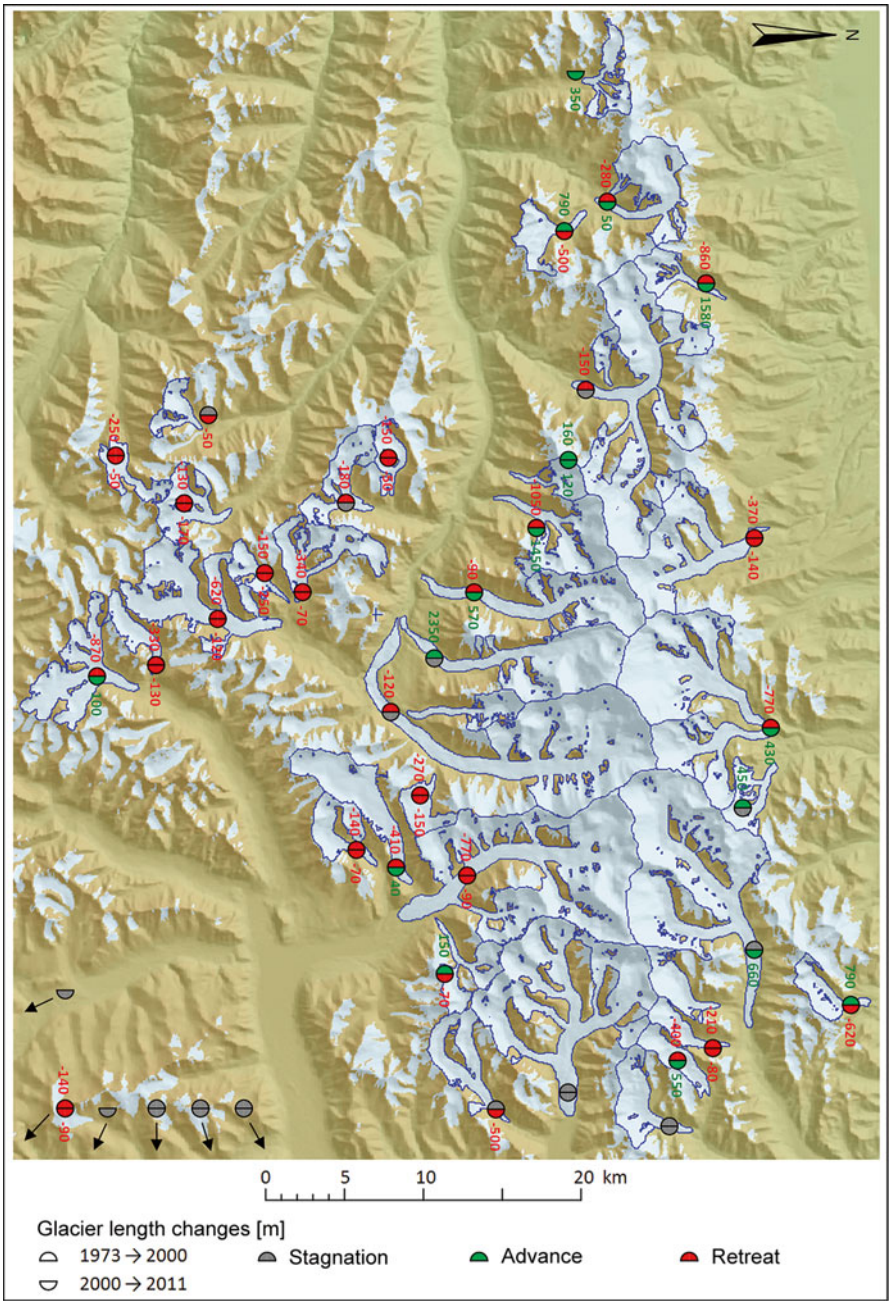

Fig. 8.3 Distribution and magnitude of investigated glacier length changes in the Trans Alai from 1973 to 2000 and from 2000 to 2011 (Source: Author)

Table 8.2 Number and type of observed glacier length changes in the Trans Alai

Glacier tongue	1973 → 2000	2000 → 2011	1973 → 2011
Retreating	24	18	22
Stagnant	8	12	5
Advancing/surging	6	11	11
Evidence of surge			14

glaciers retreated, but a considerable amount, i.e., 14 glaciers, showed signs of surges during the study time period. Advancing glaciers almost doubled within the recent period (Table 8.2).

8.4.3 Glacier Thickness Change and Mass Balances

Strong glacier elevation changes were observed by differencing SRTM-3 elevations (representing 1999) from the more recent DEM of ALOS-PRISM (2010) (Fig. 8.4). The surface elevation increase at the tongue of Lenin Glacier (1) is in accordance with an observed advance of +430 ± 11 m during the same period. Its eastern tributary, however, lost mass. The DEM differencing does not cover the tongue of Korschenewski Glacier (2), but volume gain at its tongue could also be assumed due to its advance of +660 ± 11 m. The assumption of glacier surge is supported by the observed lowering at its middle part. Small Saukdara Glacier (3) gained volume at its tongue, despite a stable terminus position. Sulumart Glacier (4) shows no significant elevation change, despite a retreat of −120 ± 11 m. At Great Saukdara Glacier (5), we measured highly positive as well as negative elevation differences of more than ±100 ± 11 m. Strong lowering at its middle part and surface elevation increase at its tongue suggest that this glacier is about to surge. However, we were not able to identify significant changes at its debris-covered tongue after 2000. Surface elevation increase was highest where the tongue bends into western direction. The average elevation change is almost zero, and the estimated mass change of −0.06 ± 0.68 m w.e. a^{-1} is consequently low. With regard to elevation change, the October Glacier (6) presents the opposite behavior as compared to Great Saukdara Glacier. Down-wasting at its tongue and surface elevation increase at its middle part may indicate a previous surge. Its mass balance at −0.16 ± 0.68 m w.e. a^{-1} is slightly negative. The Western October Glacier (7) shows little surface lowering with a slightly negative mass budget of −0.10 ± 0.68 m w.e. a^{-1}. Uisuu Glacier (8) indicates surface lowering of the entire glacierized area, including the accumulation zone. This is the only investigated glacier with a more negative mass balance, which is in the range of −0.50 ± 0.68 m w.e. a^{-1}.

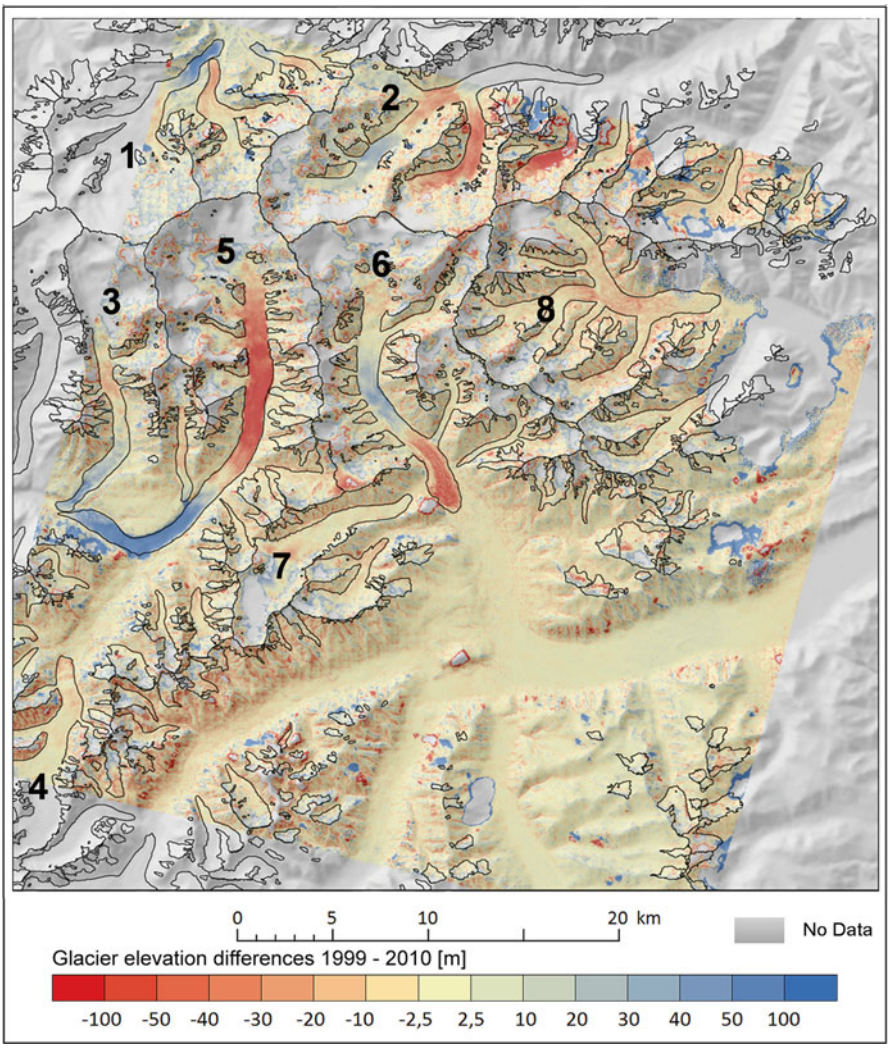

Fig. 8.4 Elevation differences in glacierized areas of the Trans Alai. Results from DEM differencing of ALOS-PRISM (2010) minus SRTM-3 (1999) after outlier post-processing (Source: Author)

8.5 Discussion

The obtained results show a heterogeneous behavior with many advancing and surging glaciers. Numerous surges in the Pamir were also confirmed by Kotlyakov et al. (2008) and Gardelle et al. (2013), including October Glacier the surge of which ended in 1990. An increase of surge activities as found for our study region was also reported for the Karakoram (Copland et al. 2011). However, in contrast to the Karakoram, where on average no significant glacier area changes were found during the last decades (e.g., Bhambri et al. 2013), our studies reveal clear glacier shrinkage which is dominated by smaller glaciers. Equally, Aizen and Aizen (2014) found for the entire Pamir an area loss of ~5 % from ~1970 to 2009 with the highest shrinkage at smaller glaciers, while the largest glaciers remained almost stable. Since 1928, Fedchenko Glacier, by far the largest glacier of the Pamir, shrank only −1.4 % at its debris-covered tongue, but lost more than −5 km^3 (−6.0 %) of its volume during the last eight decades (Lambrecht et al. 2014). Relative stability of the Fedchenko Glacier system was also confirmed by Zhang et al. (2014). Increasing glacier shrinkage was observed by Khromova et al. (2006) in the Zulumart Ranges, close to our study area. In the subsequent decade, areal reduction of glaciers there increased from −0.65 % a^{-1} (1978–1990) to −1.05 % a^{-1} (1990–2001), which is close to our results of -0.8 ± 0.4 % a^{-1}. Glaciers in eastern Pamir experienced both shrinkage and retreat, but at a lower rate (−0.07 % a^{-1} and −0.9 m a^{-1}, respectively; Yao et al. 2012).

The mass budgets of the investigated glaciers are slightly negative or almost balanced. This is in accordance to Gardner et al. (2013) who determined mass balances in the range of -0.13 ± 0.22 m w.e.a^{-1} for the entire Hissar Alai and Pamir based on ICES at laser altimetry data. Gardelle et al. (2013), however, found positive budgets after 1999 with $+0.14 \pm 0.13$ m w.e. a^{-1}. A clear mass loss for the Pamir is reported by Kääb et al. (2015), which can likely be attributed to different estimates of the SRTM C-band radar beam penetration into snow and ice. Available Landsat scenes of the study region from January to March 2000 show relatively low snow coverage. Our estimate of the penetration is in line with Gardelle et al. (2013), but the more recent studies of Kääb et al. (2015) indicate that SRTM C-band penetrations could be more pronounced.

The average mass budget for a west-orientated glacier at Muztagh Ata (~200 km east of Trans Alai) was observed to be positive (+0.25 m w.e. a^{-1}) from 2005/2006 to 2009/2010 by Yao et al. (2012). Holzer et al. (2015) measured a similar rate of $+0.21 \pm 0.27$ m w.e. a^{-1} for this glacier by geodetic means. The study of Holzer et al. (2015) revealed – similar to the results of this study – strong spatial and temporal glacier variations for most of the eastern Pamir. Elevation changes, however, are less pronounced at Muztagh Ata as compared to the Trans Alai. Average mass budgets at both study areas are slightly negative or almost balanced. In contrast to the increasing area loss in the Trans Alai, the observed shrinkage at Muztagh Ata is, however, insignificant.

8.6 Conclusion

We observed highly variable and heterogeneous glacier variations in the Trans Alai in the northeastern Pamir. For the period of 1999–2010, differencing elevations of SRTM-3 from an ALOS-PRISM-derived DEM revealed strong and heterogeneous elevation changes for several glacierized areas. Three of the four calculated mass budgets are slightly negative or almost balanced. Great Saukdara and other glaciers show surging activities, while October Glacier seems to be in a post-surging phase. The average glacier area changes in the study area indicate continuous and increasing shrinkage from 1973 to 2011. Glacier length changes were on average negative before the year 2000 and positive afterwards. More precise data of mass changes and total glacier ice volume would be of high interest, particularly with regard to glacier meltwater discharge within this arid region.

Acknowledgments This study was supported by the German Federal Ministry of Education and Research (BMBF) program "Central Asia – Monsoon Dynamics and Geo-Ecosystems" (CAME) within the WET project ("Variability and Trends in Water Balance Components of Benchmark Drainage Basins on the Tibetan Plateau") under code 03G0804F. T. Bolch acknowledges funding by the German Research Foundation (DFG, BO 3199/2-1) and the European Space Agency, Project Glaciers_cci (4000101778/10/I-AM). KH-9 Hexagon imagery and Landsat 7 ETM+ satellite imagery were provided by the US Geological Survey (USGS). ALOS-PRISM imagery was purchased by the GAF AG and provided by JAXA (Japan Aerospace Exploration Agency). Hole-filled SRTM-3 v4.1 data was obtained from the Consortium for Spatial Information of the Consultative Group for International Agricultural Research (CGIAR-CSI). We acknowledge the support of Tino Pieczonka in data co-registration and thank Juliane Peters, Jan Kropácek, and Benjamin Schröter for fruitful discussions.

References

Aizen VB, Aizen EM (2014) The Central Asia climate and cryosphere/water resources changes. In: Materials of the international conference "Remote- and Ground-based Earth Observations in Central Asia". 8–9 Sept 2014. Bishkek

Bhambri R, Bolch T, Kawishwar P, Dobhal D, Srivastava D, Pratap B (2013) Heterogeneity in glacier response in the Shyok valley, northeast Karakoram. The Cryosphere 7(5):1384–1398. doi:10.5194/tc-7-1385-2013

Bolch T, Buchroithner MF, Pieczonka T, Kunert A (2008) Planimetric and volumetric glacier changes in Khumbu Himalaya since 1962 using Corona, Landsat TM and ASTER data. J Glaciol 54(187):592–600. doi:10.3189/002214308786570782

Bolch T, Yao T, Kang S, Buchroithner MF, Scherer D, Maussion F, Huintjes E, Schneider C (2010) A glacier inventory for the western Nyainqentanglha Range and the Nam Co Basin, Tibet, and glacier changes 1976–2009. The Cryosphere 4(3):419–433. doi:10.5194/tc-4-419-2010

Burnett MG (2012) Hexagon (KH-9) – mapping camera program and evolution. National Reconnaissance Office (NRO), Center for the Study of National Reconnaissance (CSNR), Chantilly

Copland L, Sylvestre T, Bishop MP, Shroder JF, Seong YB, Owen LA, Bush A, Kamp U (2011) Expanded and recently increased glacier surging in the Karakoram. Arct Antarct Alp Res 43(4):503–516. doi:10.1657/1938-4246-43.4.503

Gardelle J, Berthier E, Arnaud Y (2012) Impact on resolution and radar penetration on glacier elevation changes computed from DEM differencing. J Glaciol 58(208):419–422. doi:10.3189/2012JoG11J175

Gardelle J, Berthier E, Arnaud Y, Kääb A (2013) Region-wide glacier mass balances over the Pamir-Karakoram-Himalaya during 1999–2011. The Cryosphere 7(4):1263–1286. doi:10.5194/tc-7-1263-2013

Gardner AS, Moholdt G, Cogley JG, Wouters B, Arendt AA, Wahr J, Berthier E, Hock R, Pfeffer WT, Kaser G, Ligtenberg SRM, Bolch T, Sharp MJ, Hagen JO, van den Broeke MR, Paul F (2013) A reconciled estimate of glacier contributions to sea level rise: 2003 to 2009. Science 340(6134):852–857. doi:10.1126/science.1234532

Holzer N, Vijay S, Yao T, Xu B, Buchroithner MF, Bolch T (2015) Four decades of glacier variations at Muztagh Ata (eastern Pamir): a multi-sensor study including Hexagon KH-9 and Pléiades data. The Cryosphere 9(6):2071–2088. doi:10.5194/tc-9-2071-2015

Huss M (2013) Density assumptions for converting geodetic glacier volume change to mass change. The Cryosphere 7(3):877–887. doi:10.5194/tc-7-877-2013

IPCC (2013) Climate change 2013: the physical science basis. Contribution of working group I to the 5th assessment report of the intergovernmental panel on climate change. Cambridge University Press, Cambridge

Jarvis A, Reuter HI, Nelson A, Guevara E (2008) Hole–filled seamless SRTM data v4.1, International Centre for Tropical Agriculture (CIAT), http://srtm.csi.cgiar.org

Kääb A, Treichler D, Nuth C, Berthier E (2015) Brief communication: contending estimates of 2003–2008 glacier mass balance over the Pamir–Karakoram–Himalaya. The Cryosphere 9(2):557–564. doi:10.5194/tc-9-557-2015

Khromova T, Osipova GB, Tsvetkov D, Dyurgerov MB, Barry RG (2006) Changes in glacier extent in the eastern Pamir, Central Asia, determined from historical data and ASTER imagery. Remote Sens Environ 102(1–2):24–32. doi:10.1016/j.rse.2006.01.019

Komatsu T, Watanabe T, Hirakawa K (2010) A framework for late quaternary lake-level fluctuations in Lake Karakul, eastern Pamir, focusing on lake–glacier landform interaction. Geomorphology 119(3–4):198–211. doi:10.1016/j.geomorph.2010.03.025

Kotlyakov V, Osipova G, Tsvetkov D (2008) Monitoring surging glaciers of the Pamir, central Asia, from space. Ann Glaciol 48(1):125–134. doi:10.3189/172756408784700608

Lambrecht A, Mayer C, Aizen V, Floricioiu D, Surazakov A (2014) The evolution of Fedchenko glacier in the Pamir, Tajikistan, during the past eight decades. J Glaciol 60(220):233–244. doi:10.3189/2014JoG13J110

Maussion F, Scherer D, Mölg T, Collier E, Curio J, Finkelnburg R (2014) Precipitation seasonality and variability over the Tibetan Plateau as resolved by the High Asia Reanalysis. J Clim 27(5):1910–1927. doi:10.1175/JCLI-D-13-00282.1

Nuth C, Kääb A (2011) Co-registration and bias corrections of satellite elevation data sets for quantifying glacier thickness change. The Cryosphere 5(1):271–290. doi:10.5194/tc-5-271-2011

Paul F, Barrand N, Baumann S, Berthier E, Bolch T, Casey K, Frey H, Joshi S, Konovalov V, Le Bris R, Mölg N, Nosenko G, Nuth C, Pope A, Racoviteanu A, Rastner P, Raup B, Scharrer K, Steffen S, Winsvold S (2013) On the accuracy of glacier outlines derived from remote-sensing data. Ann Glaciol 54(63):171–182. doi:10.3189/2013AoG63A296

Peel MC, Finlayson BL, McMahon TA (2007) Updated world map of the Köppen-Geiger climate classification. Hydrol Earth Syst Sci 11(5):1633–1644. doi:10.5194/hess-11-1633-2007

Pieczonka T, Bolch T, Wei J, Liu S (2013) Heterogeneous mass loss of glaciers in the Aksu-Tarim Catchment (Central Tien Shan) revealed by 1976 KH-9 Hexagon and 2009 SPOT-5 stereo imagery. Remote Sens Environ 130:233–244. doi:10.1016/j.rse.2012.11.020

Racoviteanu AE, Paul F, Raup B, Khalsa SJS, Armstrong R (2009) Challenges and recommendations in mapping of glacier parameters from space: results of the 2008 Global Land Ice Measurements from Space (GLIMS) workshop, Boulder, Colorado, USA. Ann Glaciol 50(53):53–69. doi:10.3189/172756410790595804

Takaku J, Futamura N, Iijima T, Tadono T, Shimada M (2007) High resolution DSM generation from ALOS PRISM. In: Geoscience and remote sensing symposium, IGARSS 2007. IEEE International, pp 1974–1977, IGARSS, Barcelona. doi:10.1109/IGARSS.2007.4423215

Yao T, Thompson L, Yang W, Yu W, Gao Y, Guo X, Yang X, Duan K, Zhao H, Xu B, Pu J, Lu A, Xiang Y, Kattel DB, Joswiak D (2012) Different glacier status with atmospheric circulations in Tibetan Plateau and surroundings. Nat Clim Chang 2(9):663–667. doi:10.1038/nclimate1580

Zhang Q, Kang S, Chen F (2014) Glacier variations in the Fedchenko Basin, Tajikistan, 1992–2006: insights from remote-sensing images. Mt Res Dev 34(1):56–65. doi:10.1659/MRD-JOURNAL-D-12-00074.1

Chapter 9
Heterogeneity in Fluctuations of Glacier with Clean Ice-Covered, Debris-Covered and Proglacial Lake in the Upper Ravi Basin, Himachal Himalaya (India), During the Past Four Decades (1971–2013)

Pritam Chand, Milap Chand Sharma, and Ram Nagesh Prasad

Abstract Comprehensive multi-temporal observations of Himalayan glaciers during the past half century indicate the continuous shrinkage of most of the glaciers. In addition to this, the present study analyses the fluctuations of glacier with clean ice-covered, debris-covered and proglacial lake in the upper Ravi basin, Himachal Himalaya (India), from 1971 to 2013 using high-resolution satellite datasets with supplement of field observations for selected glaciers. The study reveals the heterogeneity in fluctuations of glacier as higher terminus and frontal area change for the clean ice-covered glaciers compared to debris-covered glaciers. Field measurements for selected glaciers also suggest a retreating trend and validate the measured glacier changes using remotely sensed temporal data. Glacier retreat rates especially for debris-covered glaciers in the Ravi basin were lower than previously reported for selected glaciers in the similar basin and other basins of the Himachal Himalaya.

Keywords Himachal Himalaya • Clean ice-covered glacier • Debris-covered glacier • Terminus change • High-resolution satellite datasets

9.1 Introduction

The Himalayan region encompasses permanent snowfields, which form the largest bodies of ice outside of polar ice caps (Raina and Srivastava 2008). As a major regional water resource, the Himalayan glaciers and seasonal snow melts make an important contribution to the drinking water, agriculture and hydropower supply of

P. Chand (✉) • M.C. Sharma • R.N. Prasad
Centre for the Study of Regional Development, Jawaharlal Nehru University, New Delhi 110067, India
e-mail: pritamiirs@gmail.com

R.B. Singh et al. (eds.), *Climate Change, Glacier Response, and Vegetation Dynamics in the Himalaya*, DOI 10.1007/978-3-319-28977-9_9

densely populated regions in downstream river basin of Himalayas (Immerzeel et al. 2010). Thus, in context to reported climate warming during the last century, detailed and reliable data on present-day glacier and snow fluctuations and its impact on regional water balance are essential for predicting future water supplies for this region (Bolch et al. 2012; Immerzeel et al. 2013). Since the end of the Little Ice Age (LIA) (~1850s), Himalayan glaciers have been in a general state of recession (Mayewski and Jeschke 1979; Bhambri and Bolch 2009). Himalayan glacier studies indicate that many glaciers show an increased, receding trend over the past few decades (Kulkarni et al. 2007; Bolch et al. 2008a; Kulkarni 2012), although recent studies indicate that many H-K glaciers have stable fronts since 2000 (Bhambri et al. 2013; Bahuguna et al. 2014). However, some glaciers have advanced during recent decades (tributaries of Panmah and Liligo glaciers in the Karakoram region of Pakistan) (Hewitt 2007; Schmidt and Nüsser 2009). Therefore, the regional irregularities of Himalayan glacier fluctuations suggest the direct comparisons and extrapolations of result from well-studied glaciers in one region to the poorly observed glaciers in the other regions of the Himalaya cannot make directly. Thus, regular monitoring of the glaciers from the poorly observed region of Himalayan is important for improving our knowledge of glacier response to climate change. Moreover, the characteristic of glacier surface cover (e.g. supraglacial debris cover) is one of the critical factors to influence the glacier dynamics especially the fluctuations of glacier terminus (Scherler et al. 2011; Benn et al. 2012). Recent studies reported the heterogeneity in glacier terminus change as higher for the clean ice-covered as compared to debris-covered glaciers across the Himalayan region (Scherler et al. 2011). Besides, studies found several debris-covered glaciers with stagnant terminus position in different regions of Himalaya (Bahuguna et al. 2014). Although growing melt water ponds and surface lowering indicate that such glaciers are currently shrinking, their fronts remain remarkably stable as has also been observed in other regions (Banerjee and Shankar 2013; Basnett et al. 2013).

Although field investigations are highly recommended for glacier studies, however only a limited number of glaciers can be investigated owing to time and logistical constraints in remote mountain regions (Chand and Sharma 2015a, b). Thus, multi-temporal and multispectral remotely sensed data enable mapping and monitoring of glaciers with large spatial scales at regular temporal intervals (Racoviteanu et al. 2009; Bhambri and Bolch 2009; Bolch et al. 2010a; Paul et al. 2013). Additionally, most of the present glacier fluctuation study involved monitoring of the terminus of glaciers selected on the basis of their physiography, approach, distribution and orientation. In particular changes in glacier length and its snout are easy-to-follow witnesses of past and ongoing climatic variations and their shifting trends (Paul and Svoboda 2009). Most of the glacier studies are based on glacier terminus monitoring and mostly used the Survey of India (SoI) toposheets and coarser satellite resolution datasets (e.g. Landsat MSS) with few exceptions (Kulkarni and Rathore 2005; Kulkarni et al. 2007; Mehta et al. 2011, 2014; Pandey et al. 2011; Mir et al. 2013; Pandey and Venkataraman 2013). However, recent studies have shown inaccuracies in SoI topographical maps and difficulties with coarser resolution images in terms of identifying the accurate terminus positions and mostly in case of debris-covered glacier (Bhambri and Bolch 2009; Chand and Sharma

2015a, b). Thus, the declassified high-spatial-resolution imagery of Corona and Hexagon acquired during the period of 1960s and 1970s provides great potential to derive the past/historic glacier outlines in comparison with contemporary glacier outlines derived from high-resolution satellite images or field observations (Bhambri and Bolch 2009; Bolch et al. 2010b; Chand and Sharma 2015b).

Taking all these into consideration, the present study has a broader objective to fill a gap for the poorly observed glaciers in the upper Ravi basin, Himachal Himalaya, and provides the comprehensive multi-temporal fluctuation records of the glaciers with different surface characteristics. The sub-objectives of the present study are (i) to analyse the frontal area and length changes for the glaciers with clean ice-covered, debris-covered and proglacial lakes during the past four decades (1971–2013), (ii) to elucidate the possible impact of climate parameters on the glacier fluctuation (iii) and to assess the suitability of SoI toposheets for the mapping of the historical glacier outlines and their change.

9.2 Regional Settings of the Study Area

The upper Ravi basin is located within southeastern part of Chamba district and northeastern part of Kangra district in Himachal Pradesh. The geographical extent of Ravi basin lies between 32°39′59.94″ and 32°10′42.99″ north latitude and 76°15′45.72″ and 77°04′29.95″ east longitude, covered by SoI toposheet number 52-D and 52-H (Fig. 9.1). Physiographically, it lies between the lesser and the greater Himalayas. The Ravi flows in a northwest direction for most of its course. It follows the strike between two parallel mountain ranges, namely, Dhaula-Dhar to the south, which separates the Beas basin from Ravi basin, and Pir-Panjal to the north, which divides the watershed between the Ravi and Chenab (Marh 1986). The total upper basin area is ~2500 km^2 with altitude varying from 1200 to 6000 m a.s.l. The geomorphic history of the Ravi basin can be associated with the Pleistocene to Holocene climatic changes (Marh 1986). The thick sequence of glacial and glaciofluvial, e.g. boulder deposits and moraine deposits, can be recognized in different parts of the basin and laid during the Pleistocene glacial and interglacial periods (Marh 1986).

The climate of the study area is transitional between the winter-dry climate of the Indo-Gangetic plains (CWg by Koppen's classification) and the highland climates (H) of the western Himalaya (Spate and Learmonth 1967). The basin lies between the transition zone of the maximum (Dharamshala) and minimum (Lahaul) precipitation areas of Himachal Pradesh. The northern aspect of the Dhaula-Dhar range is in a rain shadow and, therefore, experiences minimum precipitation as compared to southern aspect of the Pir-Panjal range. However, the rainfall decreases from south (e.g. Dhaula-Dhar range) to north (e.g., Pir-Panjal range) direction and minimum in the interior areas of Pir-Panjal range (Fig. 9.2). A range of small to large valley glaciers are identified in the basin, ranging in area from 0.02 to 10.3 km^2 with a mean size of 0.6 km^2 (Chand and Sharma 2015b). The mean size of glaciers

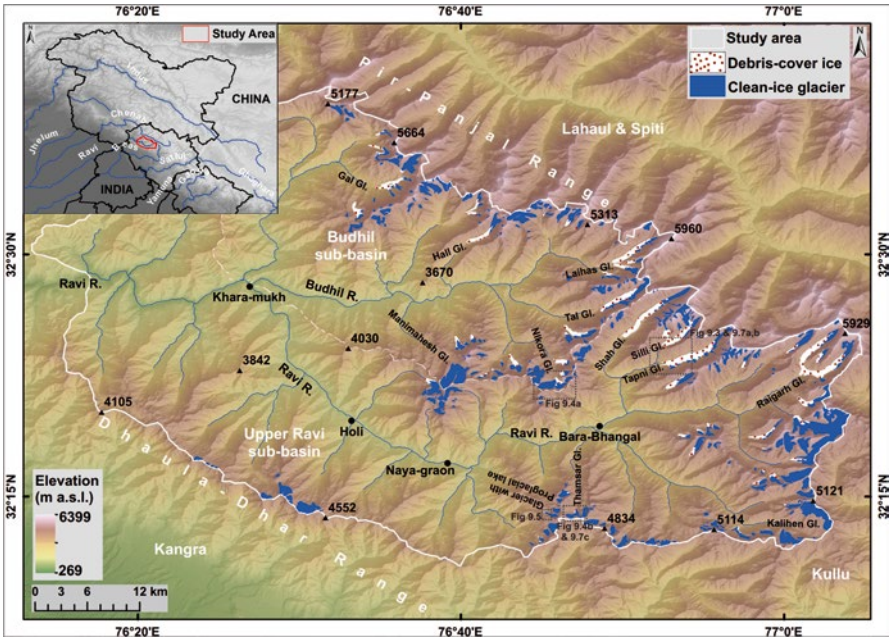

Fig. 9.1 Location of study area; *inset picture* shows the location of study area in the Himalaya with major river systems of the Indian subcontinent (Satellite data from USGS)

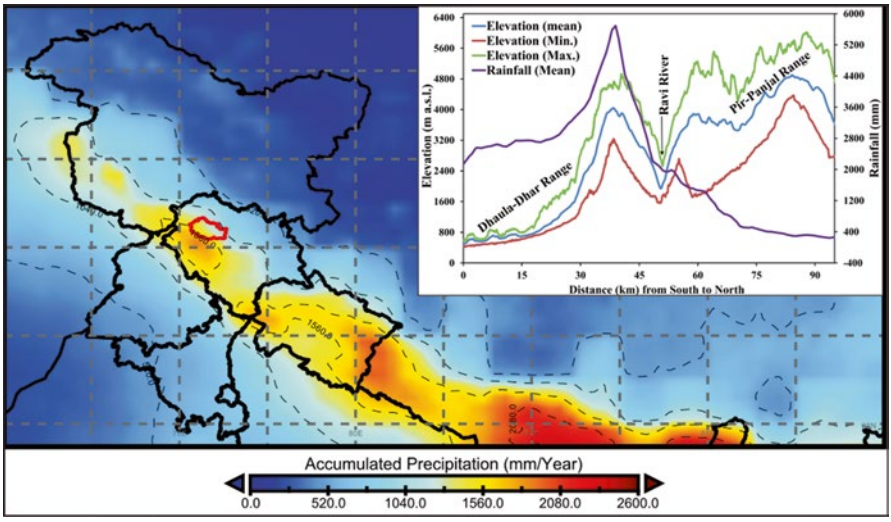

Fig. 9.2 Accumulated precipitation (1998–2013) for northwestern Himalaya using TRMM 3B4 V7 Data; *inset* picture shows topography–rainfall relationship from south to north (Satellite data from USGS)

in the study area is comparatively lower than other glaciated basins of the H-K region (Chand and Sharma 2015b). However, in the Ravi basin most of the small to medium glaciers are clean ice covered, whereas the large valley glaciers with high-relief catchment area have extensive debris cover on their ablation area (Fig. 9.1).

9.3 Data and Methodology

9.3.1 Datasets and Its Selection

The present study used multi-temporal, multispectral and medium to high-resolution images to derive the glacier changes with supplement of field observations for selected glaciers. The early US military reconnaissance Corona KH-4B (1971) satellite high-spatial-resolution images were used to widen the time span for monitoring the historic extent of the glacier back to the 1960s–1970s and conceivably provide more consistent results than SoI topographic maps and coarse-resolution satellite datasets (Bhambri et al. 2011; Chand and Sharma 2015b). Landsat satellite data of multi-spatial, spectral and temporal sensor of TM (1990s ±2), ETM+ (2000s ±2) and OLI (2014) were used since 1990s for mapping glacier terminus in the respective years (Table 9.1). ASTER (2002) image with an overlaid areal coverage was also used to assist and identify the glacier terminus from Landsat ETM+ (2002) images. All the selected Landsat TM/ETM+ imageries are available as ortho-rectified in the processing level L1T, but the Landsat TM image of 1989 was only processed to L1G. This latter image shows a slight horizontal shift of a pixel (~30 m) as compared to 2002 Landsat ETM+ reference image; hence, it was co-registered to the reference image using the projective transformation algorithm available in Erdas Imagine 10 (Bhambri et al. 2011; Chand and Sharma 2015b). Additionally, the spline method of ESRI ArcGIS 10 was used for rectification of Corona images (Chand and Sharma 2015b). The study focused on the adjustment of the area around the glacier on Corona images in respect of Landsat ETM+ PAN (2002) merged image for consistency of results. To assess positional accuracy, 24 common ground location points (GCPs) such as river and road junctions, peaks and rocky outcrops were identified in the rectified image of Corona (1971) and simultaneously in reference image of Landsat ETM+ PAN (2002). The horizontal shift between the both images was 5.27 m (1.76 pixels). In addition, the SoI toposheets 1:50,000 scale (52 D 11 and 15) with 40 m contour interval (planimetric accuracy ±12.5 m and elevation accuracy ±6.5 m) (Raju and Ghosh 2003) were used for comparison and extraction of glacier outlines from SoI toposheets and high-resolution Corona image. The ASTER GDEM V2 (~30 m spatial resolution) from Japan Space Systems (http://gdem.ersdac.jspacesystems.or.jp/) was used as reference DEM for extraction of glacier topographic parameters. For climate trends, the present study used freely available reanalysis climatic data of MERRA (~1979–2014) and NCEP/NCAR (~1950–2010). Reanalysis data has been extensively used for the climate change studies throughout the Himalayan region including glaciated area on

Table 9.1 Satellite database used for the present study

Satellite/sensor	Date of acquisition	Spatial resolution (m)	Scene/product/path and row ID/details
Corona KH-4B	28 Sep 1971	3	70 MM × DS1115-2282DF062
Landsat 5 TM	9 Oct 1989	30, 60	ETP147R37_5T19891009/ETP147R38_5T19891009
Landsat 7 ETM+	2 Aug 2002	15, 30, 60	LE71470372002214SGS00
Landsat 8 OLI/TRIS	25 Sep 2013	15, 30, 100	LC81470382013268LGN00
ASTER	28 Oct 2002	15, 30, 90	AST_L1A_003_10282002054845_11112002172853
Reanalysis Data			
MERRA-2D	1979–2014	2/3° × 1/2°	Temperature at 250 hPa, temperature at 850 hPa, temperature at 500 hPa
NCEP/NCAR	1950–2014	0.5° × 0.5°	Temperature at 600 hPa, temperature at 700 hPa, temperature at 850 hPa
NCEP/NCAR	1950–2014	0.5° × 0.5°	Precipitation and perceptible water

multi-temporal scale (Agrawal et al. 2014; Kumar et al. 2014). The data has been downloaded by selecting an area of interest, a rectangular block of 32.25° N–32.5° N and 76.5° E–76.75°E with a grid size of 0.25° × 0.25° in the world's map. MERRA is the reprocessing of atmospheric observations (Badarinath et al. 2010) collected over the satellite era (1979–2014). This study has utilized MERRA (Modern-Era Retrospective Analysis for Research and Applications) Monthly History Data Collections (2D), version 5.2.0 of the GEOS-5-ADAS with a 1/2° latitude × 2/3° longitude × 72 layer model configuration. It is a NASA reanalysis for the satellite era using a major new version (V5) of the Goddard Earth Observing System (GEOS) Data Assimilation System (DAS) (NASA Giovanni 2013). The products are distributed through GES-DISC (http://disc.sci.gsfc.nasa.gov/MDISC/dataprods/merra_products.shtml). In the present study, MERRA-2D temperature at pressure levels 250, 500 and 850 hectopascals (hPa) has been used to quantify changes in the physical parameters of the regional climate. In addition, the long-term (~1950–2014) NCEP/NCAR reanalysis temperature (at 600, 700 and 850 hPa) and precipitation data has been used for analysing long-term trends (http://www.esrl.noaa.gov/psd/data/gridded/data.ncep.reanalysis.html). Monthly data were used to obtain average indices for annual and seasonal (December, January, February (DJF); June, July, August (JJA)) values of temperature and precipitation. A nonparametric Mann–Kendall (MK) test was used to determine statistical significance trend (Kendall 1970; Bhambri et al. 2011). The Mann–Kendall trend test should be applied on data series that does not show serial dependency (Hamed and Ramachandra Rao 1998). In the presence of Lag-1 autocorrelation coefficient, the trend-free pre-whitening (TFPW)-MK method has been used (Duhan et al. 2013). However, Yue and Hashino (2003) had reported that the application of pre-whitening to serially correlated data series reduces the detection rate. Therefore, the modified Mann–Kendall test (Hamed and Ramachandra Rao 1998; Rao et al. 2003) has been used for trend estimation of autocorrelated data series. Additionally, the sequential values u(t) (forward) and u'(t) (backward) from progressive analysis of Mann–Kendall trend test have been used to estimate the variation in trend over the time period, whereas Sen's nonparametric test has been used to calculate the true slope of an existing trend (Sen 1968; Sneyers 1990).

9.3.2 Glacier Mapping, Change and Uncertainty

The classification of the Global Land Ice Measurements from Space (GLIMS) initiatives (http://www.glims.org/MapsAndDocs/guides.html) was adopted to map the glacier boundaries from satellite images (Chand and Sharma 2015b). Manual digitization was preferred to map the debris-covered glacier areas as spectral signature on satellite images doesn't differentiate debris-covered ice with surrounding bare moraines (Paul et al. 2009; Bhambri et al. 2011). High-resolution datasets of Bhuvan 2D/3D and Google Earth (GE) were used as additional sources to improve the glacier outlines of debris-covered glaciers (e.g. Paul et al. 2013). Determination of the

most likely position of the glacier termini was based on signs of movement (identified with overlays of multi-temporal images), emerging melt water streams at the end of the terminus, breaks in surface slope, spectral colour deference and the presence of small melt water ponds (Bhambri et al. 2013; Chand and Sharma 2015b). The historic glacier extents from 1971 Corona images were manually delineated. Field investigations of selected glaciers (e.g. Tapni) using GPS, field photographs and field mapping of recessional moraine further facilitated in determining recent glacier termini. The change in glacier length was calculated by drawing parallel line stripes at 25 m distance interval. The length change was calculated as the average length from the intersection of the stripes with the glacier outlines and further along the central flow line in comparison with average change (Bhambri et al. 2012; Chand and Sharma 2015a). The mapping uncertainty for the glacier has been calculated on the basis of a buffer around the glacier margins as suggested by Granshaw and Fountain (2006). The buffer size was chosen to be half of the estimated shift caused by misregistration as only one side can be affected by the shift (Bolch et al. 2010a). Thus, the buffer size was set to 2.5 m, 7.5 m and 15 m for the Corona, Landsat 7 ETM+/Landsat 8 OLI and Landsat TM, respectively, by taking the positional accuracy and half of pixel size into account. This study used glacier length change uncertainty (e) as suggested by Hall et al. (2003):

$$e = \sqrt{(a1)^2 + (a2)^2} + E_{\text{reg}}, \tag{9.1}$$

where $a1$ and $a2$ are the pixel resolution of imagery 1 and imagery 2, respectively, and E_{reg} is the registration error. Accordingly, the uncertainty calculated for Corona (1971), Landsat TM (1989) and Landsat 8 OLI (2013) was 20.6 m, 41.3 m and 26.6 m, respectively. The uncertainty for glacial area change was estimated by multiplication of the uncertainty of length with glacier width (Bhambri et al. 2012; Chand and Sharma 2015a).

9.4 Results

9.4.1 Frontal Area and Terminus Change for the Debris-Covered Glaciers

There are 71 debris-covered glaciers mapped in the basin for 2002 inventory with varying debris-covered area percentage (Chand and Sharma 2015b). However, some of the valley glaciers, e.g. Tapni and Silli, have extensive debris cover in their ablation zone. Thus, these two glaciers are considered as representative glacier to elucidate the change in debris-covered glacier terminus and area during the last four decades. Silli Glacier is a small valley having ~47 % of debris covers in its ablation zone. It has a total area and length of ~5.9 ± 0.2 km^2 and ~5 km (for main trunk), respectively. Silli Glacier shows a retreat of 153.8 ± 33.5 m in the past 42 years

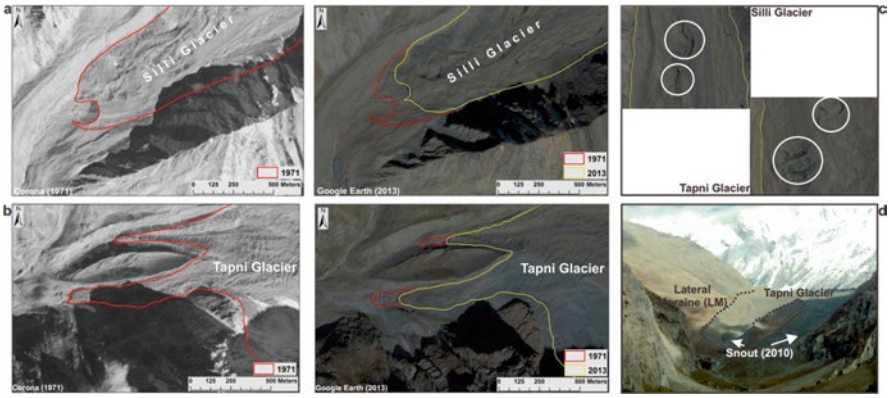

Fig. 9.3 Frontal area and terminus change for the debris-covered glaciers in the upper Ravi basin (Satellite data from USGS and Google Earth)

Table 9.2 Frontal area change for the glaciers with clean ice-covered, debris-covered and proglacial lake

Years			1971–1989	1989–2002	2002–2013	1971–2013
Silli	Total	(10^3 m^2)	46 (±3.1)	14.7 (±2.4)	29.3 (±3.1)	90 (±4.1)
	Annual	(10^3 m^2)	2.6 (±0.2)	1.1 (±0.2)	2.7 (±0.3)	2.1(±0.1)
Tapni	Total	(10^3 m^2)	12.5 (±1.1)		10.6 (±0.9)	23.1 (±1.3)
	Annual	(10^3 m^2)	0.4 (±0.03)		1 (±0.1)	0.5 (±0.03)
Nlkora Glacier	Total	(10^3 m^2)	211.1 (±8.3)	103 (±6.3)	123.2 (±5.3)	437.2 (±12.2)
	Annual	(10^3 m^2)	11.7 (±0.5)	7.9 (±0.5)	11.2 (±0.5)	10.4 (±0.3)
Thamsar	Total	(10^3 m^2)	63.3 (±3.6)	70.8 (±3.5)	22.7 (±2.5)	156.9 (±5.4)
	Annual	(10^3 m^2)	3.5 (±0.2)	5.4 (±0.3)	2.1 (±0.2)	3.7 (±0.1)
Glacier with lake	Total	(10^3 m^2)	5.8 (±2.6)	10.9 (±4.9)	20.7 (±5.6)	37.4 (±6.2)
	Annual	(10^3 m^2)	0.3 (±0.1)	0.8 (±0.4)	1.9 (±0.5)	0.9 (±0.1)

(1971–2013), with an average rate of 3.7 ± 0.8 m per year. The total frontal area vacated by the Silli Glacier during this time period was estimated to be 0.09 ± 0.004 km^2 (0.002 ± 0.0001 km^2 a^{-1}) which is approximately 1.5 % of the total loss. The recession rate during the last decades (2002–2013) was comparatively higher than the 1989–2002 decade (Fig. 9.3a, Tables 9.2 and 9.3). Remarkably, the rate of retreat (~24.4 m a^{-1}) significantly increases with the recent (~2013) snout location of Silli Glacier compared with the historical snout position of glacier mapped in SoI toposheets (1963). Tapni Glacier (5.6 ± 0.2 km^2) is another debris-covered glacier having ~66 % debris-covered area and length of ~8 km. However, it shows comparatively insignificant change in terms of terminus and frontal area change during the past four decades. The total area vacated by the Tapni Glacier for the period between 1971 and 2013 is 0.02 ± 0.001 km^2 (0.001 ± 0.00003 km^2 a^{-1}) which is approximately 0.4 % of the total loss, showing total retreat of 135.3 ± 33.5 m (3.2 ± 0.8 m a^{-1}) (Fig. 9.3b, Tables 9.2 and 9.3). Additionally, the same overestimate of glacier recession has been found for Tapni Glacier as its 1971 or recent (~2013)

Table 9.3 Terminus average change for the glaciers with clean ice-covered, debris-covered and proglacial lake

Year		1971–1989	1989–2002	2002–2013	1971–2013
Silli	Total retreat (m)	53.8 (±46.1)	39.4 (±46.5)	60.6 (±34)	153.8 (±33.5)
	Retreat rate (m/year)	3 (±2.6)	3 (±3.6)	5.5 (±3.1)	3.7 (±0.8)
Tapni	Total retreat (m)	77.6 (±29.4)		57.7 (±34)	135.3 (±33.5)
	Retreat rate (m/year)	2.5 (±1)		5.2 (±3.1)	3.2 (±0.8)
Nlkora Glacier	Total retreat (m)	74.7 (±46.1)	47.9 (±46.8)	50.9 (±34)	173.5 (±33.5)
	Retreat rate (m/year)	4.1 (±2.6)	3.7 (±3.6)	4.6 (±3.1)	4.1 (±0.8)
Thamsar	Total retreat (m)	83.2 (±46.1)	60.4 (±46.5	38.5 (±34)	182.1 (±33.5)
	Retreat rate (m/year)	4.6 (±2.6)	4.6 (±3.6)	3.5 (±3.1)	4.3 (±0.8)
Glacier with lake	Total retreat (m)	30.4 (±46.10)	54.4 (±46.5)	82 (±34)	166.8 (±33.5)
	Retreat rate (m/year)	1.7 (±2.6)	4.2 (±3.6)	7.5 (±3.1)	4 (±0.8)

glacier outlines compared with the 1963 SoI maps. A comparison of 1963 glacier outline as mapped from SoI toposheet and glacier outline of 1971 as mapped from Corona high-resolution datasets reveals that Tapni Glacier lost an area of 1 km^2 (0.13 km^2 a^{-1}) with an annual retreat rate of 144.2 m for 8 years – a rather unrealistic value. The study suggests that the glacier change using historical SoI maps overestimates the results and provides comparatively higher glacier recession rate in the basin.

9.4.2 Frontal Area and Terminus Change for the Clean Ice-Covered Glaciers

There are 75.1 % of ice-covered glaciers in the Ravi basin and most of them are small in size (Chand and Sharma 2015b). Accordingly, clean ice-covered Thamsar and Nlkora Glaciers were selected as representative glacier, according to their area, morphology and location in Dhaula-Dhar and Pir-Panjal ranges, respectively. Their terminus and frontal area change represents the response of clean ice-covered glacier to climate change during the last four decades (~1971–2013). Thamsar Glacier is one of the well-known clean ice-covered glaciers in the upper Ravi glaciered area of Dhaula-Dhar ranges. It is the source of Thamsar *nalla* which joins the Ravi river from its left side near Bara Bhangal village and the major water resources for the downstream villages. The average recession of the Thamsar Glacier between 1971 and 2013 was estimated to be 182.1 ± 33.5 m with an annual rate of 4.3 m ± 0.8, whereas the total area vacated by the glacier for the same period is 0.2 ± 0.005 km^2 with an annual rate of 0.004 ± 0.0001 km^2 which is approximately 19.4 % of the total loss which is significantly higher than the estimated total loss percentage for

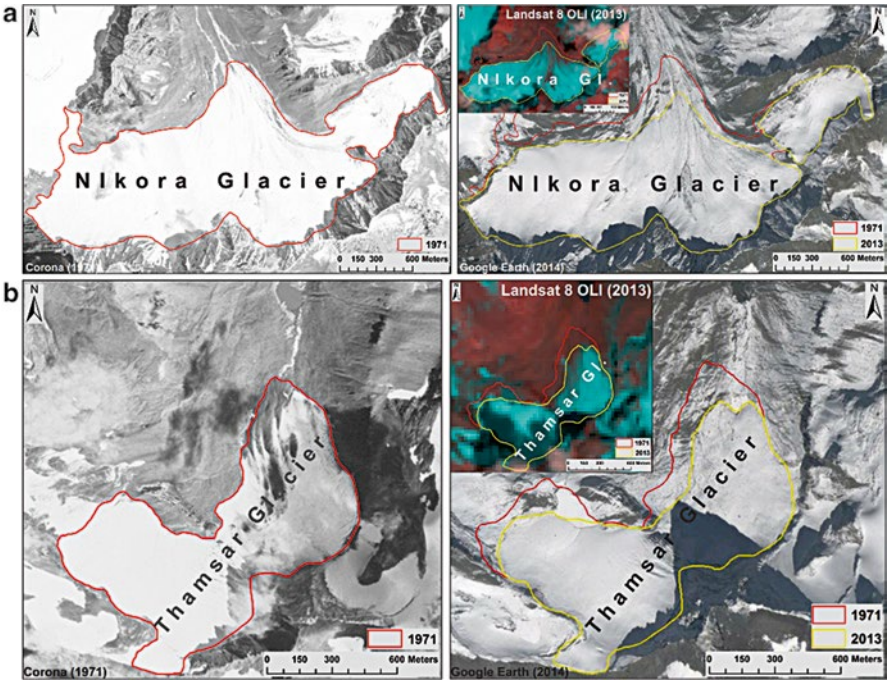

Fig. 9.4 Frontal area and terminus change for the clean ice-covered glacier in the upper Ravi basin (Satellite data from USGS and Google Earth)

the above debris-covered glaciers (Fig. 9.4b, Tables 9.2 and 9.3). Additionally, the same overestimate of glacier recession has been found for the clean ice-covered Thamsar Glacier with the glacier terminus mapped from SoI toposheet (~1963) with the high-resolution satellite data of Corona for 1971. Thamsar Glacier had receded 2.7 km for 8 years (1963–1971) which is impossible within such a short period of time (Table 9.4). Besides, the high-resolution dataset of Corona (1971) clearly shows the extent of proglacial lake in front of glacier which reveals the glacier mapping error in SoI toposheets and the same has been reported for the other glaciers across the Himalayan region (Raina and Srivastava 2008; Bhambri and Bolch 2009; Bhambri et al. 2012) (Fig. 9.7).

The Nlkora Glacier is a clean ice-covered glacier in the Budhil subbasin of Ravi and located in the Pir-Panjal ranges. It also shows a significant area loss during the last four decades. The average recession of the Nlkora Glacier between 1971 and 2013 was estimated to be 173.5 ± 33.5 m with an annual rate of 4.1 ± 0.8 m, whereas the total area vacated by the glacier was estimated to be 0.4 ± 0.01 km^2 with an annual rate of 0.01 ± 0.0003 km^2 which is approximately 15.4 % of the total loss (Fig. 9.4a, Tables 9.2 and 9.3). We found that the Nlkora Glacier fragments into two parts during the last four decades. Similar fragmentation trends have been reported in other glaciered areas of the Himachal region (Kulkarni et al. 2007; Bhambri et al. 2011). It is also significantly higher than the estimated total loss percentage for the debris-covered glaciers in the basin.

Table 9.4 Terminus change along central flow line for the glaciers with clean ice-covered, debris-covered and proglacial lake

Year		1971–1989	1989–2002	2002–2013	1971–2013
Silli	Total retreat (m)	7.1 (±46.1)	25.1 (±46.5)	88.2 (±26.7)	120.3 (±33.5)
	Retreat rate (m/year)	0.4 (±2.6)	1.9 (±3.6)	8 (±3.1)	2.9 (±0.8)
Tapni	Total retreat (m)	105.3 (±29.4)		50.3 (±34)	155.6 (±33.5)
	Retreat rate (m/year)	3.4 (±1)		4.6 (±3.1)	3.7 (±0.8)
Nlkora Glacier	Total retreat (m)	183.5 (±46.1)	43.5 (±46.8)	94.1 (±34)	321.1 (±33.5)
	Retreat rate (m/year)	10.2 (±2.6)	3.3 (±3.6)	8.6 (±3.1)	7.6 (±0.8)
Thamsar	Total retreat (m)	48.2 (±46.1)	45.2 (±46.5	86.8 (±34)	180.2 (±33.5)
	Retreat rate (m/year)	2.7 (±2.6)	3.5 (±3.6)	7.9 (±3.1)	4.3 (±0.8)
Glacier with lake	Total retreat (m)	32.4 (±46.10)	86.5 (±46.5)	94.5 (±34)	213 (±33.5)
	Retreat rate (m/year)	1.8 (±2.6)	6.7 (±3.6)	8.6 (±3.1)	5.1 (±0.8)

9.4.3 Frontal Area and Terminus Change for the Glacier with Lake

The glaciers with proglacial lakes in their front show a significant change in their area during the past few decades as reported across the Himalayan region, especially for the Nepal and Sikkim Himalaya (Basnett et al. 2013). Accordingly, the study selected a glacier with proglacial lake in its front to see how such type of glacier behaves in the Ravi basin of Himachal Himalaya. The average recession of the glacier between 1971 and 2013 was estimated to be 166.8 ± 33.5 m with an annual rate of 4 ± 0.8 m, whereas the total area vacated by the glacier is 0.04 ± 0.006 km^2 with an annual rate of 0.0009 ± 0.0001 km^2 which is approximately 9.4 % of the total loss which is significantly higher than debris-covered glaciers and comparatively lower than estimated total loss percentage for the clean ice-covered glaciers in the basin (Fig. 9.5, Tables 9.2 and 9.3).

9.4.4 Climate Trends

The trend of temperature and precipitation time series of NCEP/NCAR and MERRA (1950–2014 and 1979–2014, respectively) was analysed to examine its behavioural pattern over the time period. The results of Mann–Kendall and sequential Mann–Kendal trend test are presented in Table 9.5. The winter (DJF) average temperature at 600 hPa (NCEP/NCAR), 700 hPa (NCEP/NCAR) and 850 hPa (MEERA-2D) shows increasing trend at 5 % significance level, while the winter average temperature at 850 hPa (NCEP/NCAR) shows significant upward trend at 1 % significance level. Similarly, the annual time scale illustrates the increasing trend at 5 %

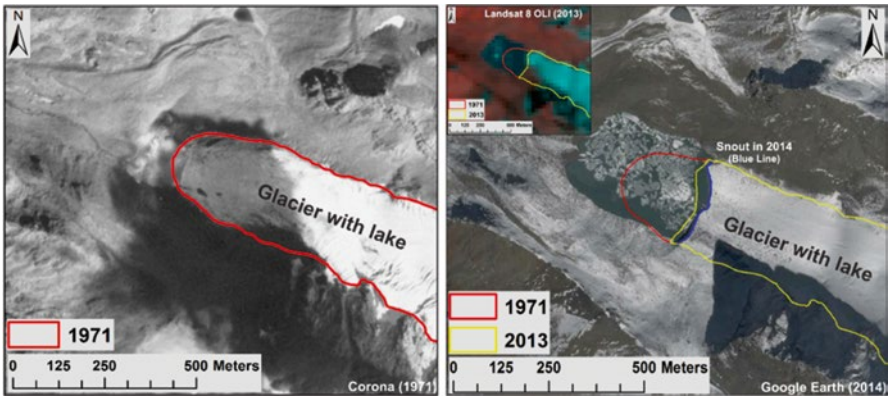

Fig. 9.5 Frontal area and terminus change for the glacier with lake in the upper Ravi basin (Satellite data from USGS and Google Earth)

Table 9.5 Temperature and precipitation trends for NCEP/NCAR (1950–2014) and MERRA-2D (1979–2014) based on the Mann–Kendall nonparametric test

Data	Parameters	Mann–Kendall results	Annual	Winter	Pre-monsoon	Monsoon	Post-monsoon
NCEP/NCAR (1950–2014)	Temperature (600 hPa)	Z	2.3608	1.9928	1.3135	1.1436	1.6305
		ΔT (°C a^{-1})	0.0094	0.0147	0.0091	0.0052	0.0134
	Temperature (700 hPa)	Z	2.0155	2.4344	0.5548	0.4756	1.6815
		ΔT (°C a^{-1})	0.0083	0.0176	0.0044	0.0021	0.0158
	Temperature (850 hPa)	Z	1.4607	2.6212	0.1529	−0.1076	1.3191
		ΔT (°C a^{-1})	0.0069	0.0191	0.0009	−0.0006	0.0146
	Precipitation (mm)	Z	−1.7220	−2.1230	−2.8930	−1.8740	−0.8440
		ΔP (°C a^{-1})	−0.0167	−0.0130	−0.0154	−0.0241	−0.0090
MERRA-2D (1979–2014)	Temperature (250 hPa)	Z	4.8000	2.3292	2.6288	4.8627	1.9205
		ΔT (°C a^{-1})	0.0507	0.0504	0.0576	0.0487	0.0425
	Temperature (500 hPa)	Z	1.2123	0.0136	0.8581	2.1657	0.3405
		ΔT (°C a^{-1})	0.0103	0.0013	0.0099	0.0207	0.0062
	Temperature (850 hPa)	Z	−0.5585	2.1657	1.2667	−2.7923	−0.0681
		ΔT (°C a^{-1})	−0.0059	0.0353	0.0260	−0.0523	−0.0009

significance level for 600 and 700 hPa (NCEP/NCAR). The maximum value of Sen's slope 0.035 °C/year and 0.019 °C/year was noticed during winter temperature at 850 hPa for MERRA and NCEP/NCAR, respectively. This demonstrates that the rate of increasing temperature in higher altitude is less in comparison to lower altitudes. Overall, the result demonstrates significant rise in temperature during winter season at 600, 700 and 850 hPa. The sequential Mann–Kendal trend test for annual and winter season temperature indicates significant increasing trend, with forward line in each case crossing the confidence line (1.96) (Fig. 9.6). This result supports

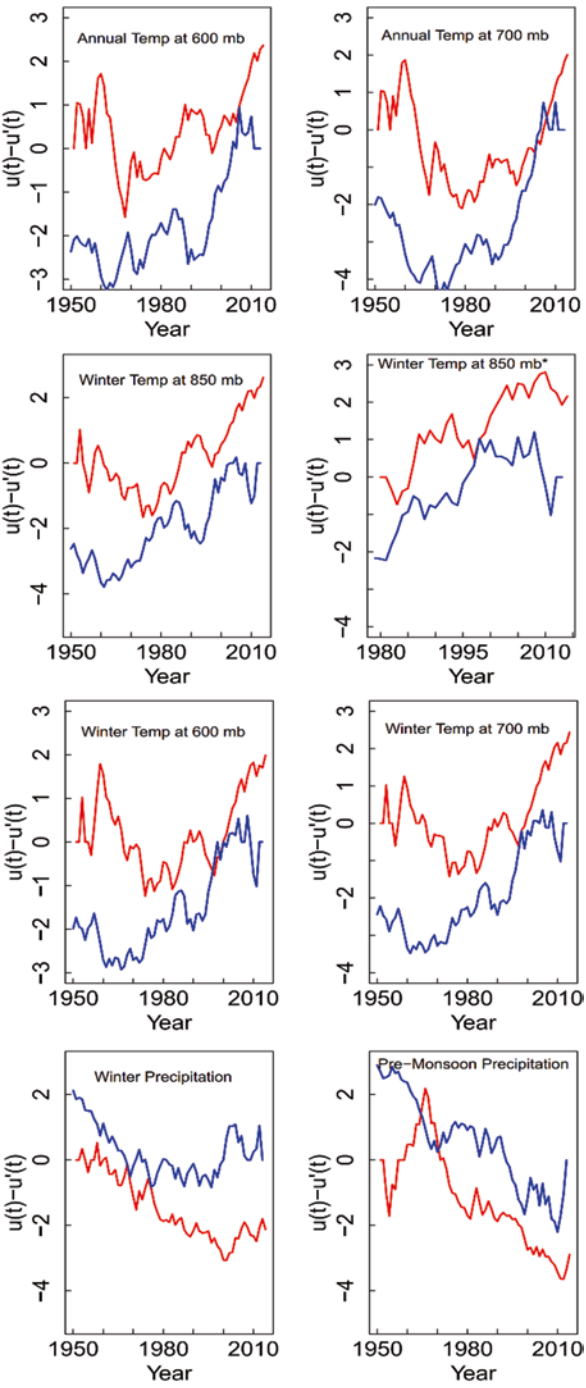

Fig. 9.6 Temperature and precipitation trends for grid (32.5° N, 76.5° E) of upper Ravi basin during the past half century for NCEP/NCAR (1950–2014) and from 1979 to 2014 for MERRA-2D (Note: *red* and *blue line* shows forward [u(t)] and backward [u' (t)]) (Satellite data from USGS and Google Earth)

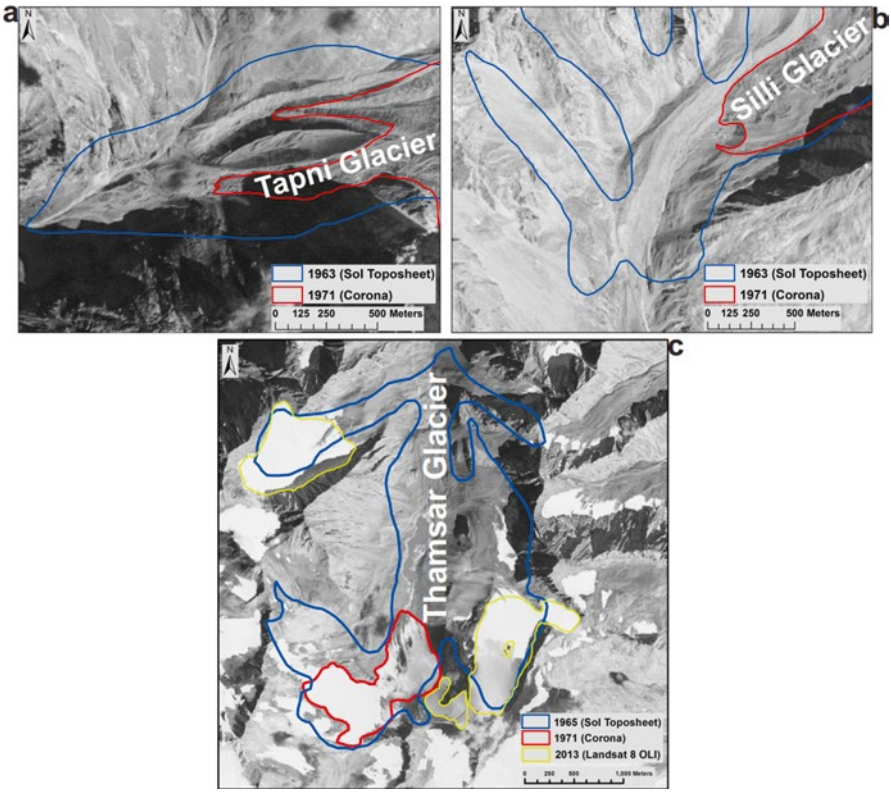

Fig. 9.7 Frontal area and terminus change comparison between SoI toposheets and high-resolution Corona datasets (1971) (Satellite data from USGS and Google Earth)

the earlier increasing trend of annual and winter season temperature at 5 % significance level (Table 9.5). The winter and pre-monsoon precipitation shows decreasing trend at 5 % and 1 % significance level at the rate of −0.012 and −0.015 mm/year, respectively, while the perceptible water shows decreasing trend in winter, pre-monsoon and monsoon season at 1 % significance level. The monsoon season has recorded significant decrease in perceptible water (−0.025 mm/year). The result shows significant decreasing trend in precipitation and perceptible water during all seasons except post-monsoon. The sequential Mann–Kendal trend test also reveals the same trend and supports the result derived from Mann–Kendall trend test (Fig. 9.6). Figure 9.6 illustrates the decreasing precipitation trend during winter and pre-monsoon season at 5 % and 10 % significance level where the beginning of decreasing trend has been observed after 1965.

9.5 Discussion

9.5.1 Heterogeneity in Fluctuation of Glaciers with Clean Ice-Covered, Debris-Covered and Proglacial Lake

The study reported that the clean ice-covered glaciers has a strong correlation with the total higher percent glacier area loss as compared to debris-covered glaciers which is consistent with the results in other glaciated regions across the Himalaya (Scherler et al. 2011; Bolch et al. 2008a; Nainwal et al. 2008; Racoviteanu et al. 2009; Bhambri et al. 2011; Bahuguna et al. 2014; Chand and Sharma 2015b). However, the glacier with extensive debris cover reported less recession rate and area loss which suggested that the thick debris cover on glaciers leads, in general, to less frontal retreat or even stable tongues, as it lowers the rate of surface melting (Benn and Owen 2002; Benn et al. 2012). Debris cover defines the differential rates of melting as near the terminus a thick debris cover retards melting, but at the upper reaches of the glacier tongue, the thinner debris cover causes higher rates of melting (Basnett et al. 2013). This causes a lessening, or even reversal, of the surface gradient (Bolch et al. 2011; Benn et al. 2012) and leads to the formation of supraglacial lakes (Bennett et al. 2010). Such supraglacial lakes are clearly visible on the debris-covered ablation part of the glaciers, e.g. Tapni and Silli. During the field, the supraglacial ponds with exposed ice in steep to near vertical sections have been found on the ablation zone of the debris-covered glaciers, and further number of supraglacial ponds was mapped from the Google Earth high-spatial-resolution image on the ablation zone of debris-covered glacier (Fig. 9.3c). Some of the ponds increased in size as observed from multi-temporal remote sensing datasets during the last 4 years which possibly shows down-wasting, trending of the glacier without any significant change in its terminus position. It needs further deeper study to know the response of debris covered on the glacier dynamics in response to climate warming. Furthermore, the glacier with proglacial lake or moraine-dammed lake in front of its terminus also shows comparatively significant area loss the same as observed in Jammu & Kashmir, Himachal, Nepal and Sikkim region of Himalaya (Kulkarni et al. 2006; Bolch et al. 2008b; Govindha Raj 2010; Raj et al. 2013; Basnett et al. 2013). The lakes at the terminus of glaciers modify the stress regime of the glacier ice in contact. The presence of the lakes increases the terminus disintegration by the process of calving and also transmits thermal energy to the ice front, accelerating melting which leads to a loss in glacier area (Sakai 2000; Gardelle et al. 2011). However, there are no such glaciers with lake found in basin except in one case which has been discussed. Additionally, studies have reported a much larger lake growth in front of glaciers in the eastern Himalaya than in the central and drier northwest regions (Gardelle et al. 2011).

The present analysis has taken average length from the intersection of the stripes and along the central flow line to yield the change rate during the last four decades (Table 9.4). Their comparison shows more and less similar tendencies, but measurement based on single point of the glacier only may result into either underestimation

Table 9.6 Comparison between SoI toposheets and Corona (1971)/recent data (2013) in terms of frontal area and terminus change for the glaciers with clean ice-covered, debris-covered and proglacial lake

Glaciers	Area loss	1963–1971	1963–2013
Tapni	Total area loss (km^2)	1.01	1.03
	Annual loss (km^2)	0.13	0.02
	Total average retreat (m)	1153.48	1178.31
	Rate of retreat (m/year)	144.18	23.57
Silli[a]	Total average retreat (m)	1100.52	1220.86
	Rate of retreat (m/year)	137.57	24.42
Thamsar[a, b]	Total average retreat (m)	2716.6	2896.82
	Rate of retreat (m/year)	452.8	60.4

[a]Terminus change calculated along the central flow line
[b]Change from 1965 (SoI toposheet of 1965)

or overestimation of recession and is more susceptible to outliers (Bhambri et al. 2012; Chand and Sharma 2015a). Averaging along the front is a more robust method and provides more reliable estimations, especially in the situation where the glaciers do not have well-defined snout or terminus. The rate of retreat of glacier length and the discrepancy in total area loss may possibly be due to frontal glacier-margin morphology, e.g. in the case of higher frontal width–length ratio (Chand and Sharma 2015a).

This study reveals that highly erroneous rate of recession and area vacated for most of the studied glaciers has been found as compared to the glacier outlines derived from SoI map (1968) with Corona data (1971), recent remote sensing data and field observations (for selected glaciers) (Fig. 9.7 and Table 9.6). The toposheets are being used as the authentic source of database/information in various public and private user need-based requirements like surveying, infrastructure, surface elevation data, forest area delineation, land use/land cover and glacier change studies for the past few decades (Raju and Ghosh 2003). Thus, SoI toposheets are an important source of database for historical information, but it should be cautiously used for the glacier change studies due to seasonal change in land cover characteristics. Moreover, the previous study by Bhambri and Bolch (2009) reported the aerial photographs used for glacier mapping in SoI toposheets (e.g. for Himachal Himalaya) that has been acquired during the early or late winter seasons when the deglaciated area covered with seasonal snow further hinders the accurate mapping or identification of glacier terminus. Thus, the comparison of historical glacier outlines for SoI maps with recent glacier outlines provides overestimated results in terms of glacier change as discussed above. Remarkably, Ahmad et al. (2004) estimated 10 km^2 vacation of the Gangotri glacier between 1985 and 2001, based on topographic map and satellite image which comes to overestimation of ~24 times as reported (~0.41 ± 0.03 km^2) by Bhambri et al. (2012) using high-resolution satellite datasets. This study suggests that the earlier estimation exclusively based on the SoI maps is highly erroneous and, therefore, needs reassessments and recalculations of all such areas where these were used in order to correct records for the glacier recession/area

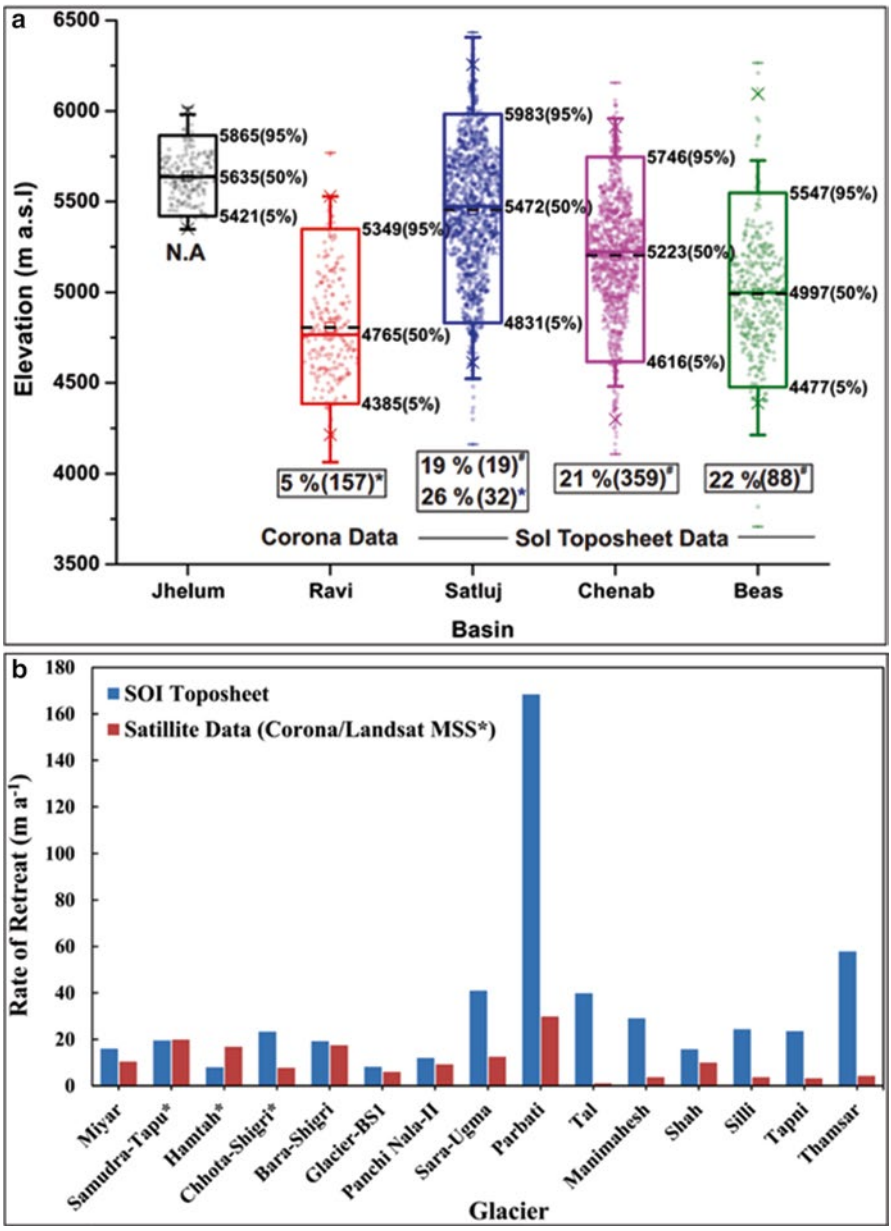

Fig. 9.8 Glacier change trends in Himachal Himalaya. (**a**) Glacier area loss corresponding to mean glacier elevation in the different basins of Himachal Himalaya, #Kulkarni et al. 2007; *Mir et al. 2013; *Chand and Sharma 2015b). (**b**) comparison of calculated glacier change using SoI toposheet and high-resolution Corona data and Landsat MSS (*Pandey and Venkataraman 2013; Chand and Sharma 2015a, b; Chand and Sharma 2016 In Printing)

changes for the Indian Himalaya (Figs. 9.7b and 9.8b). Therefore, the SoI maps of 1960s–1970s must be used with precaution for glacier frontal changes and in assessing overall glacier morphology changes. Besides, the declassified high-spatial-resolution imagery of Corona and Hexagon acquired during the same period provides great potential to derive the past/historic glacier outlines in comparison with contemporary glacier outlines derived from high-resolution satellite images (Bhambri and Bolch 2009; Bolch et al. 2010b; Chand and Sharma 2015a, b).

9.5.2 Comparison with Other Glaciers of the Himalayan Region

The areal changes of the glaciers in the Ravi basin confirm an expected and published trend of glacier retreat (Shukla and Dutta 2005; Chand and Sharma 2015a, b). However, the rate of retreat is less than previously estimated from SoI toposheet analysis, e.g. for Manimahesh glacier (29.1 m a^{-1}, clean ice-covered glacier) and Tal glacier (39.9 m a^{-1}, debris-covered glacier). Additionally, the recession rate for debris-covered glaciers in the Ravi basin is also comparatively lower than other debris-covered glaciers observed in Himachal Himalaya using the SoI toposheets, e.g. Samudra Tapu (20 m a^{-1}), Chhota Shigri (7 m a^{-1}), Parbati (168.4 m a^{-1}), Sara-Umga (41 m a^{-1}), Bara-Shigri (30 m a^{-1}) and Miyar (17 m a^{-1}) (Fig. 9.8). The main reason for the discrepancy is probably the interpretation of the glacier terminus on SoI topographic maps which is known to be a significant challenge in glacier terminus mapping (Bhambri and Bolch 2009; Chand and Sharma 2015a, b). Moreover, the long-term rate of retreat, for a period of past 40 years, is available for around 100 glaciers in the Himalaya (Bolch et al. 2012; Kulkarni and Karyakarte 2014). The mean loss of glacial length for four decades is approximately 621 ± 468 m with large variations in terms of retreat, advance and stable terminus position across the Himalayan region (Kulkarni and Karyakarte 2014). In the central Himalaya, changes in glacier terminus were reported for glaciers, e.g. Gangotri (19.9 m a^{-1}), Milam (25 m a^{-1}), Dokriani (15 m a^{-1}), Tipra (14 m a^{-1}), Chorabari (6.4 m a^{-1}), Pindari (6.4 m a^{-1}), Satopanth (22.9 m a^{-1}) and Bhagirath-Kharak (7.4 m a^{-1}) based on SoI toposheets and remote sensing data with limited field observations (Bhambri et al. 2012; Mehta et al. 2014; Nainwal et al. 2008; Raj 2011). Studies suggest that almost all glaciers are retreating although the rate of retreat varies from one glacier to another. In addition, glacier terminus and area change have been observed in other regions of the Himalaya, e.g. Drang-Drung (9 m a^{-1}) in the Greater Himalaya of Jammu and Kashmir region, Rekha-Samb (12 m a^{-1}) in Nepal Himalaya and Zemu (14 m a^{-1}), South Lhonak (42 m a^{-1}), and Rathong (18 m a^{-1}) in Sikkim (Kulkarni and Karyakarte 2014). Most of them are showing retreating trend during the past decades. However, some large glaciers have advanced or been stable recently in the northwestern Himalaya and in the Karakoram (Schmidt and Nüsser 2009; Iturrizaga 2011; Hewitt 2011).

In addition, area changes have been measured for several thousand glaciers in Hindu Kush-Himalaya (H-K). For instance, small high-altitude glaciers in the Trans-Himalaya of Ladakh had a shrinkage rate of ~0.4 % a^{-1} from 1969 to 2010 (Schmidt and Nüsser 2012). In the Indian Himalaya, shrinkage rates are regionally variable: ~0.2 to ~0.7 % a^{-1}, 1960s to 2001–2004 (11 Indian catchments, Kulkarni 2012; Kulkarni et al. 2007); 0.12 ± 0.07 %a^{-1}, 1968–2007 (Garhwal Himalaya, Bhambri et al. 2011); ~0.16 ± 0.1 % a^{-1}, 1990s to 2010 (Sikkim Himalaya, Basnett et al. 2013); ~0.78 ± 0.03 % a^{-1}, 1980–2010 (Bhutan, Bajracharya et al. 2014); and ~0.3–0.6 % a^{-1}, ~1970 to ~2005 (Tibet, Nie et al. 2010). Although recent studies indicate that many H-K glaciers have stable fronts since 2000 (Bhambri et al. 2013; Bahuguna et al. 2014), glaciers in the western, central and eastern Karakoram region show long-term irregular behaviour with frequent advances and possible slight mass gain (Bhambri et al. 2013; Bolch et al. 2012; Gardelle et al. 2013; Hewitt 2011; Kääb et al. 2012). In the eastern Hindu Kush, west of the Karakoram, 25 % of the glaciers were stable or advancing during 1976–2007 (Sarikaya et al. 2012). This irregular behaviour of Himalayan glaciers in general could be attributed to local/regional topography (Haeberli 1990), local/regional climatic system (Kargel et al. 2005), glacier hypsometry (Furbish and Andrews 1984), the characteristics and thickness of supraglacial debris cover on the glacier surface (Bolch et al. 2008a; Scherler et al. 2011), the glacier size and ratio of accumulation area to total area (Kulkarni et al. 2007), contributions from tributary glaciers (Nainwal et al. 2008) and their geometrical/morphological properties (Mehta et al. 2014).

9.5.3 Climate Considerations

The retreating behaviour of glaciers on regional scale is mainly attributed to climate change through their dependence on temperature and precipitation regimes and discussed here. The winter average temperature for the basin has slightly increased during the past half century (1950–2014) (Fig. 9.6). The rate of increased trend is significant, and thus it is important that slight change in temperature has an impact on the glacier fluctuation. Besides, the continuous increase in average temperature for the winter month is also more significant in terms of glacier fluctuation as it may be one of the causative reasons to simultaneous occurrence of ablation and accumulation during the winter month in the upper Ravi basin (Kulkarni et al. 2010; Chand and Sharma 2015b). A study of the temperature trends in the northwest Himalayan region (Bhutiyani et al. 2007) shows that a significant warming of 1.6 °C has occurred over the last century in winter, taking place at a faster rate, with the highest warming rates recorded in the period 1991–2002. This warming has been due to a rise in both maximum temperatures and minimum temperatures, though the maximum temperatures have gone up more rapidly. The study also shows that significant warming started in the late 1960s, with the highest rate of increase between 1990 and 2009. The results show a decreasing trend in annual and winter average precipitation during the last five decades (Fig. 9.6). Additionally, in the northwestern

Himalaya, a significant decreasing trend has been reported in the monsoon precipitation during the period 1866–2006 (Bhutiyani et al. 2009). Additionally, a recent study shows reduced snowfall over the western Himalaya in a warm climate (Dimri et al. 2008). Reduction of snowfall can be explained by the combined effect of climate change and mesoscale influences of the mountains. The snowfall shows a decreasing trend over all the mountain ranges. The snowfall decreased by 280 cm over the Pir-Panjal ranges (Shekhar et al. 2010). It suggests that the decrease trend in total precipitation may affect the accumulation regime of the glaciers and further change the cumulative mass balance of the glaciers into negative. However, the lack of long-term field-observed climate data within the basin along with the influence of topographical parameters as well as glacier morphology, thickness and distribution of debris-covered area makes it difficult to determine the significant effects of climate parameters on glacier variability for the Ravi basin. Therefore, the availability of long-term meteorological data and field-based direct mass–balance measurements within/nearby or adjoining basin and including geodetic estimates of glacier mass changes will provide a valuable database and further improve knowledge on the response of glaciers to climatic parameters in the Ravi basin of Himachal Himalaya.

9.6 Conclusion

This study provides a comprehensive multi-temporal glacier change for the glaciers with clean ice-covered, debris-covered and proglacial lake for the upper Ravi basins, Himachal Himalaya, from 1971 to 2013. The major findings and conclusion drawn from the present study are as follows:

- The study suggests that the clean ice-covered glaciers (~15.4 %, 19.4 %) have a strong correlation with the total higher percent glacier area loss as compared to debris-covered glaciers (0.4–1.5 %) as it is also consistent with the results in many other mountain regions in the Himalaya. Besides, the glacier with lake has been reported to have 9.4 % of glacier loss during the last four decades (~1971–2013) which is also significant but comparatively lower than clean ice-covered glacier and significantly higher than debris-covered glacier. It clearly shows that the nature of surface material defines the rates of melting as near the terminus a thick debris cover retards melting. However, it requires deeper studies in the near future to look into overall perspective of surface melting and down-wasting throughout the glacier surface.
- The study suggests that an apparent higher rate of glacier retreat in the Himachal Himalaya could be the result of overestimation of glacier cover in the old datasets due to the use of SoI topographic maps the same as observed for almost all the studied glaciers. High-spatial-resolution images of declassified Corona are efficient for mapping the historical glacier terminus and its morphology and conceivably provide more consistent results than SoI topographic maps and coarse-

resolution satellite datasets. It can be used as a valuable resource for monitoring the historic extent of the glacier with higher accuracy.

- The average winter temperature at every altitude increased significantly during 1950–2014, while precipitation during annual and in winter months also shows decreasing trend over the same period. However, the current availability of reanalysis climate data for the study area has to be validated before concluding the complex glacier–climate interactions, and thus further availability of field observed meteorological data and climatological investigations will help to disentangle the complex glacier–climate interactions.

Acknowledgements We are thankful to the University Grant Commission, New Delhi, for the financial support for this work. The authors are also grateful to Jawaharlal Nehru University, New Delhi, for providing the research facilities. We also thank USGS for providing Landsat TM/ETM+/OLI and Corona data. The first author is grateful to Mr. Bruce Raup, GLIMS (http://www.glims.org/), for providing ASTER data for this research at no cost. The first author acknowledges Dr. Rakesh Bhambri for his valuable suggestions during the preparation of this manuscript.

References

Agrawal A, Sharma AR, Tayal S (2014) Assessment of regional climatic changes in the Eastern Himalayan region: a study using multi-satellite remote sensing data set. Environ Monit Assess 186:6521–6536. doi:10.1007/s10661-014-3871-x

Ahmad S, Hasnain SI, Arha CD et al (2004) Analysis of satellite imageries for characterization of glacio-morphological features of the Gangotri Glacier, Ganga headwater, Garhwal Himalaya. Proc Work Gangotri Glacier Spec Publ Ser Surv India 80:61–67

Badarinath KVS, Sharma AV, Kaskaoutis DG et al (2010) Solar dimming over the tropical urban region of Hyderabad, India: effect of increased cloudiness and increased anthropogenic Aerosols. J Geophys Res 115:1–18

Bahuguna IM, Rathore BP, Brahmbhatt R et al (2014) Are the Himalayan glaciers retreating? Curr Sci 106:1008–1013

Bajracharya SR, Maharjan SB, Shrestha F (2014) The status and decadal change of glaciers in Bhutan from the 1980s to 2010 based on satellite data. Ann Glaciol 55:159–166. doi:10.3189/2014AoG66A125

Banerjee A, Shankar R (2013) On the response of Himalayan glaciers to climate change. J Glaciol 59:480–490. doi:10.3189/2013JoG12J130

Basnett S, Kulkarni AV, Bolch T (2013) The influence of debris cover and glacial lakes on the recession of glaciers in Sikkim Himalaya, India. J Glaciol 59:1035–1046. doi:10.3189/2013JoG12J184

Benn DI, Owen LA (2002) Himalayan glacial sedimentary environments: a framework for reconstructing and dating the former extent of glaciers in high mountains. Quat Int 97–98:3–25. doi:10.1016/S1040-6182(02)00048-4

Benn DI, Bolch T, Hands K et al (2012) Response of debris-covered glaciers in the Mount Everest region to recent warming, and implications for outburst flood hazards. Earth Sci Rev 114:156–174. doi:10.1016/j.earscirev.2012.03.008

Bennett G, Evans D, Carbonneau P, Twigg D (2010) Evolution of a debris-charged glacier landsystem, Kvíárjökull, Iceland. J Maps 6:40–67

Bhambri R, Bolch T (2009) Glacier mapping: a review with special reference to the Indian Himalayas. Prog Phys Geogr 33:672–704. doi:10.1177/0309133309348112

Bhambri R, Bolch T, Chaujar RK, Kulshreshtha SC (2011) Glacier changes in the Garhwal Himalaya, India, from 1968 to 2006 based on remote sensing. J Glaciol 57:543–556. doi:10.3189/002214311796905604

Bhambri R, Bolch T, Chaujar RK (2012) Frontal recession of Gangotri Glacier, Garhwal Himalayas, from 1965 to 2006, measured through high-resolution remote sensing data. Curr Sci 102:1462–1466

Bhambri R, Bolch T, Kawishwar P et al (2013) Heterogeneity in glacier response in the upper Shyok valley, northeast Karakoram. Cryosph 7:1385–1398. doi:10.5194/tc-7-1385-2013

Bhutiyani MR, Kale VS, Pawar NJ (2007) Long-term trends in maximum, minimum and mean annual air temperatures across the Northwestern Himalaya during the twentieth century. Clim Change 85:159–177. doi:10.1007/s10584-006-9196-1

Bhutiyani MR, Kale VS, Pawar NJ (2009) Climate change and the precipitation variations in the northwestern Himalaya: 1866–2006. Int J Climatol 30:535–548. doi:10.1002/joc.1920

Bolch T, Buchroithner M, Pieczonka T, Kunert A (2008a) Planimetric and volumetric glacier changes in the Khumbu Himal, Nepal, since 1962 using Corona, Landsat TM and ASTER data. J Glaciol 54:592–600. doi:10.3189/002214308786570782

Bolch T, Buchroithner MF, Peters J et al (2008b) Identification of glacier motion and potentially dangerous glacial lakes in the Mt. Everest region/Nepal using spaceborne imagery. Nat Hazards Earth Syst Sci 8:1329–1340. doi:10.5194/nhess-8-1329-2008

Bolch T, Menounos B, Wheate R (2010a) Landsat-based inventory of glaciers in western Canada, 1985–2005. Remote Sens Environ 114:127–137. doi:10.1016/j.rse.2009.08.015

Bolch T, Yao T, Kang S et al (2010b) A glacier inventory for the western Nyainqentanglha Range and the Nam Co Basin, Tibet, and glacier changes 1976–2009. Cryosphere 4:419–433. doi:10.5194/tc-4-419-2010

Bolch T, Pieczonka T, Benn DI (2011) Multi-decadal mass loss of glaciers in the Everest area (Nepal Himalaya) derived from stereo imagery. Cryosphere 5:349–358. doi:10.5194/tc-5-349-2011

Bolch T, Kulkarni A, Kääb A et al (2012) The state and fate of Himalayan glaciers. Science 336:310–314. doi:10.1126/science.1215828

Chand P, Sharma MC (2015a) Frontal changes in the Manimahesh and Tal Glaciers in the Ravi basin, Himachal Pradesh, northwestern Himalaya (India), between 1971 and 2013. Int J Remote Sens 36:4095–4113

Chand P, Sharma MC (2015b) Glacier changes in the Ravi basin, north-western Himalaya (India) during the last four decades (1971–2010/13). Glob Planet Change 135:133–147. doi:10.1016/j.gloplacha.2015.10.013

Chand P, Sharma MC (2016) Monitoring frontal changes of the Shah Glacier in the Ravi basin, Himachal Himalaya (India) from 1965 to 2013. Natl Acad Sci Lett 3935:109–114. doi:10.1007/s40009-016-0420-x. http://link.springer.com/article/10.1007%2Fs40009-016-0420-x

Dimri AP, Kumar A, Satyawali PK, Ganju A (2008) Climatic variability of weather parameters over the western Himalayas: a case study. Proc Natl Snow Sci Workshop 11–12

Duhan D, Pandey A, Gahalaut KPS, Pandey RP (2013) Spatial and temporal variability in maximum, minimum and mean air temperatures at Madhya Pradesh in central India. Compt Rendus Geosci 345:3–21. doi:10.1016/j.crte.2012.10.016

Furbish JD, Andrews JT (1984) The use of hypsometry to indicate long-term stability and response of valley glaciers to changes in mass transfer. J Glaciol 30:199–211

Gardelle J, Arnaud Y, Berthier E (2011) Contrasted evolution of glacial lakes along the Hindu Kush Himalaya mountain range between 1990 and 2009. Glob Planet Change 75:47–55. doi:10.1016/j.gloplacha.2010.10.003

Gardelle J, Berthier E, Arnaud Y, Kääb A (2013) Region-wide glacier mass balances over the Pamir-Karakoram-Himalaya during 1999–2011. Cryosphere 7:1263–1286. doi:10.5194/tc-7-1263-2013

Govindha Raj KB (2010) Remote sensing based hazard assessment of glacial lakes: a case study in Zanskar basin, Jammu and Kashmir, India. Geomatics Nat Hazards Risk 1:339–347. doi:10.1080/19475705.2010.532973

Granshaw FD, Fountain AG (2006) Glacier change (1958–1998) in the North Cascades National Park Complex, Washington, USA. J Glaciol 52:251–256
Haeberli W (1990) Glacier and permafrost signals of 20th-century warming. Ann Glaciol 4:99–101
Hall DK, Bayr KJ, Schöner W et al (2003) Consideration of the errors inherent in mapping historical glacier positions in Austria from the ground and space (1893–2001). Remote Sens Environ 86:566–577
Hamed KH, Ramachandra Rao A (1998) A modified Mann-Kendall trend test for autocorrelated data. J Hydrol 204:182–196. doi:10.1016/S0022-1694(97)00125-X
Hewitt K (2007) Tributary glacier surges: an exceptional concentration at Panmah Glacier, Karakoram Himalaya. J Glaciol 53:181–188. doi:10.3189/172756507782202829
Hewitt K (2011) Glacier change, concentration, and elevation effects in the Karakoram Himalaya, Upper Indus Basin. Mt Res Dev 31:188–200. doi:10.1659/MRD-JOURNAL-D-11-00020.1
Immerzeel WW, van Beek LPH, Bierkens MFP (2010) Climate change will affect the Asian water towers. Science 328:1382–1385. doi:10.1126/science.1183188
Immerzeel WW, Pellicciotti F, Bierkens MFP (2013) Rising river flows throughout the twenty-first Supplementary century in two Himalayan information glacierized watersheds. Nat Geosci 6:742–745. doi:10.1038/NGEO1896
Iturrizaga L (2011) Trends in 20th century and recent glacier fluctuations in the Karakoram Mountains. Zeitschrift für Geomorphol Suppl Issues 55:205–231. doi:10.1127/0372-8854/2011/0055S3-0059
Kääb A, Berthier E, Nuth C et al (2012) Contrasting patterns of early twenty-first-century glacier mass change in the Himalayas. Nature 488:495–498. doi:10.1038/nature11324
Kargel JS, Abrams MJ, Bishop MP et al (2005) Multispectral imaging contributions to global land ice measurements from space. Remote Sens Environ 99:187–219. doi:10.1016/j.rse.2005.07.004
Kendall MG (1970) Rank correlation methods, 4th edn. Charles Griffin, London
Kulkarni AV (2012) Monitoring Himalayan cryosphere using remote sensing techniques. J Indian Inst Sci 90:457–469
Kulkarni A, Karyakarte Y (2014) Observed changes in Himalayan glaciers. Curr Sci 106:237–244
Kulkarni AV, Rathore BP (2005) Alarming retreat of Parbati glacier, Beas basin, Himachal Pradesh. Curr Sci 88:1844–1850
Kulkarni AV, Dhar S, Rathore BP et al (2006) Recession of samudra tapu glacier, chandra river basin, Himachal Pradesh. J Indian Soc Remote Sens 34:39–46
Kulkarni AV, Bahuguna IM, Rathore BP et al (2007) Glacial retreat in Himalaya using Indian Remote Sensing satellite data. Curr Sci 92:69–74
Kulkarni AV, Rathore BP, Singh SK (2010) Distribution of seasonal snow cover in central and western Himalaya. Ann Glaciol 51:123–128. doi:10.3189/172756410791386445
Kumar R, Singh S, Singh Randhawa S et al (2014) Temperature trend analysis in the glacier region of Naradu Valley, Himachal Himalaya, India. Compt Rendus Geosci 346:213–222. doi:10.1016/j.crte.2014.09.001
Marh BS (1986) Geomorphology of the Ravi River. Inter-India Publications, Delhi, India
Mayewski PA, Jeschke PA (1979) Himalayan and Trans-Himalayan glacier fluctuations since AD 1812. Arct Alp Res 11:267–287
Mehta M, Dobhal DP, Bisht MPS (2011) Change of Tipra Glacier in the Garhwal Himalaya, India, between 1962 and 2008. Prog Phys Geogr 35:721–738. doi:10.1177/0309133311411760
Mehta M, Dobhal DP, Kesarwani K et al (2014) Monitoring of glacier changes and response time in Chorabari Glacier, Central Himalaya, Garhwal, India. Curr Sci 107:281–289
Mir RA, Jain SK, Saraf AK, Goswami A (2013) Glacier changes using satellite data and effect of climate in Tirungkhad basin located in western Himalaya. Geocarto Int 29:293–313. doi:10.1080/10106049.2012.760655
NASA Giovanni (2013) Ocean color radiometry online visualization and analysis. http://giovanni.gsfc.nasa.gov/giovanni/

Nainwal HC, Negi BDS, Chaudhary M et al (2008) Temporal changes in rate of recession: evidences from Satopanth and Bhagirath Kharak glaciers, Uttarakhand, using Total Station Survey. Curr Sci 94:653–660

Nie Y, Zhang Y, Liu L, Zhang J (2010) Glacial change in the vicinity of Mt. Qomolangma (Everest), central high Himalayas since 1976. J Geogr Sci 20:667–686. doi:10.1007/s11442-010-0803-8

Pandey P, Venkataraman G (2013) Changes in the glaciers of Chandra–Bhaga basin, Himachal Himalaya, India, between 1980 and 2010 measured using remote sensing. Int J Remote Sens 34:5584–5597. doi:10.1080/01431161.2013.793464

Pandey AC, Ghosh S, Nathawat MS (2011) Evaluating patterns of temporal glacier changes in Greater Himalayan Range, Jammu & Kashmir, India. Geocarto Int 26:321–338. doi:10.1080/10106049.2011.554611

Paul F, Svoboda F (2009) A new glacier inventory on southern Baffin Island, Canada, from ASTER data: II. Data analysis, glacier change and applications. Ann Glaciol 50:22–31

Paul F, Barry RG, Cogley JG et al (2009) Recommendations for the compilation of glacier inventory data from digital sources. Ann Glaciol 50:119–126

Paul F, Barrand NE, Baumann S et al (2013) On the accuracy of glacier outlines derived from remote-sensing data. Ann Glaciol 54:171–182. doi:10.3189/2013AoG63A296

Racoviteanu AE, Paul F, Raup B et al (2009) Challenges and recommendations in mapping of glacier parameters from space: results of the 2008 Global Land Ice Measurements from Space (GLIMS) workshop, Boulder, Colorado, USA. Ann Glaciol 50:53–69

Raina V, Srivastava D (2008) Glacier atlas of India. Geological Society of India, Bangalore

Raj KBG (2011) Recession and reconstruction of Milam Glacier, Kumaon Himalaya, observed with satellite imagery. Curr Sci 100:1420–1425

Raj KBG, Remya SN, Kumar KV (2013) Remote sensing-based hazard assessment of glacial lakes in Sikkim Himalaya. Curr Sci 104:359–364

Raju PVSPP, Ghosh S (2003) Role of remote sensing and digital cartography in sustainable development. India Cartogr 23:88–95

Rao AR, Hamed KH, Chen H-L (2003) Nonstationarities in hydrologic and environmental time series. Kluwer Academic Publishers, Dordrecht

Sakai A (2000) Role of supraglacial ponds in the ablation process of a debris-covered glacier in the Nepal Himalaya. Debris-Covered Glaciers. IAHS Publ. no. 265, pp 119–130

Sarikaya MA, Bishop MP, Shroder JF, Olsenholler J (2012) Space-based observations of Eastern Hindu Kush glaciers between 1976 and 2007, Afghanistan and Pakistan. Remote Sens Lett 3:77–84. doi:10.1080/01431161.2010.536181

Scherler D, Bookhagen B, Strecker MR (2011) Spatially variable response of Himalayan glaciers to climate change affected by debris cover. Nat Geosci 4:156–159. doi:10.1038/ngeo1068

Schmidt S, Nüsser M (2009) Fluctuations of Raikot Glacier during the past 70 years: a case study from the Nanga Parbat massif, northern Pakistan. J Glaciol 55:949–959. doi:10.3189/002214309790794878

Schmidt S, Nüsser M (2012) Changes of High Altitude Glaciers from 1969 to 2010 in the Trans-Himalayan Kang Yatze Massif, Ladakh, Northwest India. Arctic Antarct Alp Res 44:107–121. doi:10.1657/1938-4246-44.1.107

Sen PK (1968) Estimates of the regression coefficient based on Kendall's Tau. J Am Stat Assoc 63:1379–1389

Shekhar MS, Chand H, Kumar S et al (2010) Climate-change studies in the western Himalaya. Ann Glaciol 51:105–112. doi:10.3189/172756410791386508

Shukla S, Dutta S (2005) Generation of baseline data on secular movement of selected glaciers in Ravi Basin, Chamba District, Himachal Pradesh (Tal and Manimahesh Glaciers)

Sneyers S (1990) On the statistical analysis of series of observations Technical note no. 143, WMO No. 725 415

Spate OHK, Learmonth ATA (1967) India and Pakistan – a general and regional geography. Methuen and Co. Ltd, Delhi, India

Yue S, Hashino M (2003) Long term trends of annual and monthly precipitation in Japan. J Am Water Resour Assoc 39:587–596. doi:10.1111/j.1752-1688.2003.tb03677.x

Chapter 10
Current and Future Glacial Lake Outburst Flood Hazard: Application of GIS-Based Modeling in Himachal Pradesh, India

Simon K. Allen, Andreas Linsbauer, Christian Huggel, S.S. Randhawa, Yvonne Schaub, and Markus Stoffel

Abstract Most studies concerning the hazard from glacial lake outburst floods have focused on the threat from lakes that have formed over the past century, some of which have demonstrated significant growth in response to recent warming of the climate system. However, attention is shifting toward the anticipation of future hazard and risk associated with new lakes that will develop as glaciers continue to retreat and water accumulates within depressions in the exposed bed topography. Using the Indian Himalayan state of Himachal Pradesh as a case study, this chapter provides both a review and implementation of modern approaches to assess current and future glacier lake outburst flood hazard over large spatial scales. Across Himachal Pradesh, the formation of new lakes over the next decades will lead to a minimum two- to threefold increase in land area affected by potential lake outburst floods in several districts. Generally the potential increase in glacial lake outburst flood frequency is demonstrated to be even greater, owing to the heightened opportunity for ice or rock avalanches to impact into larger and more numerous glacial lakes. Methods described herein allow early anticipation of future threats, providing a scientific basis for sound adaptation and planning responses.

S.K. Allen (✉)
Department of Geography, University of Zurich, Zurich, Switzerland

Institute for Environmental Sciences, University of Geneva, Geneva, Switzerland
e-mail: simon.allen@geo.uzh.ch

A. Linsbauer
Department of Geography, University of Zurich, Zurich, Switzerland

Department of Geosciences, University of Fribourg, Fribourg, Switzerland

C. Huggel • Y. Schaub
Department of Geography, University of Zurich, Zurich, Switzerland

S.S. Randhawa
State Centre on Climate Change, Himachal Pradesh, India

M. Stoffel
Institute for Environmental Sciences, University of Geneva, Geneva, Switzerland

Dendrolab.ch, Institute of Geological Sciences, University of Berne, Berne, Switzerland

R.B. Singh et al. (eds.), *Climate Change, Glacier Response, and Vegetation Dynamics in the Himalaya*, DOI 10.1007/978-3-319-28977-9_10

Keywords GLOF • Hazard • Overdeepenings • Future lakes

10.1 Introduction

The disappearance of mountain glaciers and the expansion of large glacial lakes are among the most recognizable and dynamic impacts of climate warming in the alpine environment. In combination with altered stability of surrounding rock and ice walls, the potential threat from glacial lake outburst flooding is thus evolving over time (Clague and O'Connor 2014; Deline et al. 2014; Kääb et al. 2005b; Schaub et al. 2013). With residential, tourism, and particularly hydropower infrastructure expanding higher into alpine valleys, and human demand on limited hydrological resources intensifying, increasing conflicts with the natural environment are expected (Huggel et al. 2008).

Glacial-related outburst floods refer to the sudden discharge of a water reservoir that has formed either underneath, at the side, in front, within, or on the surface of a glacier, and related dam structures can be composed of ice, moraine or bedrock. In the Himalaya, as elsewhere in the world, considerable focus has been on flood hazard associated with the catastrophic failure of moraine-dammed lakes, for which the term glacial lake outburst flood (GLOF) is commonly applied in the literature (Liu et al. 2013; Quincey et al. 2007; Richardson and Reynolds 2000; Vuichard and Zimmermann 1987). In addition to posing a significant threat to lives and infrastructure in Central Asia, GLOFs are also widely documented in the Andes (Anacona et al. 2014; Lliboutry et al. 1977; Reynolds 1992), North America (Clague and Evans 2000; O'Connor et al. 2001), and Europe (Haeberli 1983; Haeberli et al. 2001). Failure of moraine-dammed lakes occurs when the material strength of the dam structure is exceeded by driving forces, including the weight of the impounded water mass, shear stresses from seepage, and overtopping or additional momentum from displacement waves (Korup and Tweed 2007) (Fig. 10.1). In the Himalaya, displacement waves from large impacts of ice or rock are thought to have contributed to over 50 % of catastrophic moraine dam failures (Richardson and Reynolds

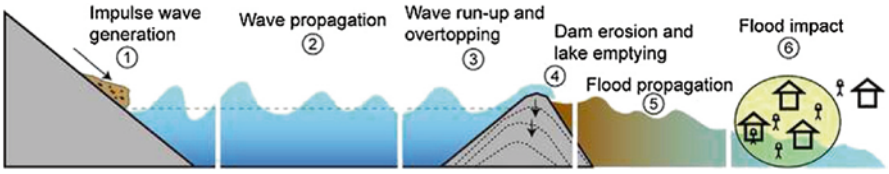

Fig. 10.1 Schematic sketch showing a typical glacial lake outburst chain resulting from an initial mass movement. *1* A mass movement (ice, rock, or debris) enters a lake, producing *2* a displacement wave that *3* overtops and *4* incises and erodes the dam area. *5* A flood then travels downstream where *6* populated areas and infrastructure are exposed. Note that displacement waves can be catastrophic with or without erosion of the dam area and, as such, can threaten also apparently stable bedrock-dammed lakes (Figure reproduced from Worni et al. (2014), with permission)

2000). GLOFs characteristically transform into hyper-concentrated or debris flows following the entrainment of loose, unconsolidated paraglacial debris (e.g., Worni et al. 2012), and some of the most devastating and far-reaching impacts have involved subsequent flow transformations or chain reactions, such as damming of valleys, secondary outbursts, and debris flows (e.g., Huggel et al. 2005; Lliboutry et al. 1977). As such, approaches to glacial lake outburst hazard assessment must consider large spatial scales, not restricted by administrative or political boundaries.

Typically, glacial flood disasters or apparent threats over recent decades have involved terminal or lateral moraine dams that formed during the Little Ice Age (between the years 1400 and 1900) and lakes that have filled during the subsequent thinning and retreat of glaciers during the twentieth century (Clague and O'Connor 2014). While in general the threat from such lakes may be diminishing over time, assuming that the most unstable lakes would already have failed, the Himalaya is noted as one area in particular where large proglacial lakes trapped behind Little Ice Age moraines are continuing to evolve (Clague and O'Connor 2014). For such lake reservoirs developing on or at the margins of glaciers, remote sensing-based methodologies and geographic information systems (GIS) have proven appropriate tools for monitoring hazardous developments across large spatial scales (e.g., Huggel et al. 2002; Wessels et al. 2002). In view of projected future warming and continued retreat of alpine glaciers (Church et al. 2013), attention has shifted beyond monitoring, toward the anticipation of where new lakes will form. Such lakes are unlikely to be impounded by large moraine dams, which requires the glacier to remain stationary for a sufficient length of time, but will form in bedrock depressions or overdeepenings in the exposed glacier bed (Frey et al. 2010). While such lakes may form attractive landscape features, and even offer potential for hydropower generation (Haeberli and Hohmann 2008), a primary concern is the potential threat from overtopping waves generated by mass movements of ice and rock (Fig. 10.1), particularly as warming may destabilize the surrounding steep slopes (Deline et al. 2014). Therefore, methods have been recently developed that enable not only the identification of where new lakes might form in the exposed bed topography but also to recognize source areas where steep rock and ice can detach and impact into glacial lakes under both current and future (ice-free) conditions (Linsbauer et al. 2012; Schaub et al. 2013). In combination with modeling of GLOF paths (Huggel et al. 2003) and recognition of affected land areas, a suite of methods is thereby available with which a first-order assessment of the changing GLOF hazard can be implemented across large spatial scales.

This chapter provides both a review and implementation of modern GIS-based approaches to assess change in glacier lake outburst hazard in the Indian Himalayan state of Himachal Pradesh. The purpose of this contribution is therefore twofold: to (1) familiarize the reader with the available methodological approaches at this scale and (2) demonstrate results and interpret their relevance for hazard and risk management in a large Himalayan state. Section 10.2 provides an overview of current understanding of GLOF hazard across the Himalaya based on available lake inventories and more specifically presents an updated inventory for the study area

of Himachal Pradesh. Sections 10.3, 10.4, and 10.5 then review and implement approaches to modeling future lake development, lake predisposition to mass movement impacts, and recognition of downstream affected areas. These approaches are then brought together in Sect. 10.6, to provide an illustrative synthesis of the changing glacial lake outburst hazard and risk across Himachal Pradesh.

The western Indian Himalayan state of Himachal Pradesh (pop ca. six million) has been selected as a specific focus area within a joint Swiss-Indo Indian Himalayas Climate Adaptation Programme (IHCAP; www.ihcap.in), and with a land area of ca 55,000 km^2, it is comparable in size to Switzerland. The elevation range within the state spans from 450 to 7000 m a.s.l, and the climate varies from tropical in the lower hills to temperate in the middle Himalayan region to cold and dry in the higher mountains. The state is characterized by a high dependency on agriculture, together with growing tourism and hydropower sectors, which together contribute toward a relatively high level of economic growth and employment but also create unique environmental challenges in the context of climate change.

10.2 Glacial Lake Inventories

Glacial lake inventories provide information on the distribution of mapped lakes, their size, type, dam characteristics and other factors that may be relevant for a hazard assessment. Where possible, this knowledge can be supplemented with information on past lake outburst disasters in a given region, to identify, for example, common triggering and outburst mechanisms, event timing and seasonal components, and discharge characteristics (Vilimek et al. 2013). One of the earliest glacial-related flood hazard inventories was completed for ice-dammed lakes in the Karakoram Himalaya (Hewitt 1982), recognizing some 30 glaciers that formed substantial dams on the Upper Indus and Yarkand river and cataloging related disasters over the previous 200 years. While such ice-dammed lakes can exhibit cyclic behavior and are thereby reoccurring threats, other glacial lake reservoirs are typically new emerging problems without historical precedence. The fact that these reservoirs generally form slowly, and can be identified at the surface, enables the application of optical remote sensing and digital terrain analyses for monitoring hazardous developments (Kääb et al. 2005a). In the Himalaya, lake expansion and volume calculations have been reported for the Bhutan Himalayas (Fujita et al. 2008; Komori 2008), and lake expansion and related glacier dynamics have been monitored in the Mt. Everest region of Nepal (Bolch et al. 2008; Wessels et al. 2002), and potentially dangerous lakes cataloged in the southeastern Tibetan Plateau (Wang et al. 2011) and Northern Tien Shan (Bolch et al. 2011) based on modern application of remote sensing and topographic analyses.

Larger-scale coordinated national or transnational efforts to map and assess the threat of Himalayan glacial lakes have primarily been led by the International Centre for Integrated Mountain Development (ICIMOD) (see Ives et al. 2010 for an overview). Many of these studies have employed semiautomated lake mapping

techniques based on the Normalized Difference Water Index (NDWI), typically applied using the blue and near-infrared channels of Landsat or equivalent imagery, which express maximum and minimum reflectance differences for glacial water and give good discrimination from ice and snow (Huggel et al. 2002). In total 8790 glacial lakes have been mapped across the Hindu-Kush Himalayan countries of Bhutan, China, Nepal, Pakistan, and India (excluding the states of Arunachal Pradesh and Jammu and Kashmir), of which around 200 have been classified as potentially dangerous based on semi-qualitative and subjective criteria (Ives et al. 2010). Employing a more objective and automated classification of GLOF hazard across the Himalaya region, Fujita et al. (2013) have demonstrated that potential glacial lake flood volumes are largest in Eastern Nepal and the Bhutan Himalayas, where glacier lakes are also bigger and expanding most rapidly (Gardelle et al. 2011). The first glacial lake inventory to cover the five glaciated Indian Himalayan states of Jammu and Kashmir, Himachal Pradesh, Uttarakhand, Sikkim, and Arunachal Pradesh was constructed from Landsat ETM+ 30 m resolution imagery from the years 2000 and 2002 (Worni et al. 2013). In their broad hazard assessment considering dam morphology and geometry, potential for lake impacts from mass movements of rock and ice, and potential downstream damage to life and property, more than 100 critical or potentially critical lakes were identified, particularly in the eastern state of Sikkim.

For the purposes of this chapter, glacial lakes across Himachal Pradesh have been remapped using latest Landsat 8 imagery from 2013 to 2014, providing an important baseline against which future changes in GLOF hazard can be assessed. Considering a minimum lake area of 0.01 km^2, and selecting only those lakes located above 3500 m and either dammed or fed by glacial processes, 120 lakes are now identified within the state watershed area, including lakes within the immediate upstream area of the Satluj basin in neighboring China (Fig. 10.2). This is a significant increase from the 45 lakes mapped previously for 2000/2002 (Worni et al. 2013) and demonstrates the limitations and subjectivity associated with glacial lake inventories, even when semiautomatic remote sensing procedures are used. The NDWI (used in both the 2000/2002 and 2013/2014 inventories) is sensitive to scene specific properties and selected lake/no-lake threshold, becomes ineffective when lakes are snow covered or frozen, and struggles to delineate some lakes from blue glacial ice. These factors undoubtedly limited the number of lakes identified in 2000/2002, in addition to the more restricted definition of glacial lakes employed by Worni et al. (2013), requiring that lakes be in very close proximity to glacial ice. Despite these limitations which suggest caution in comparing inventories from different studies, at least 5 new lakes have clearly emerged in the Himachal Pradesh watershed over the past decade, and 15 lakes have increased their surface area in the order of 10–200 %. This includes the rapidly expanding Gopang Garth lake, one of only two lakes in Himachal Pradesh that have been classified as critical, while potentially critical lakes have been identified across nearly all glaciated districts of Himachal Pradesh (Worni et al. 2013) (Fig. 10.2). Lake volumes (an important factor for GLOF hazard) cannot be established directly from optical remote sensing, although empirically derived equations based on measured mean lake depths and

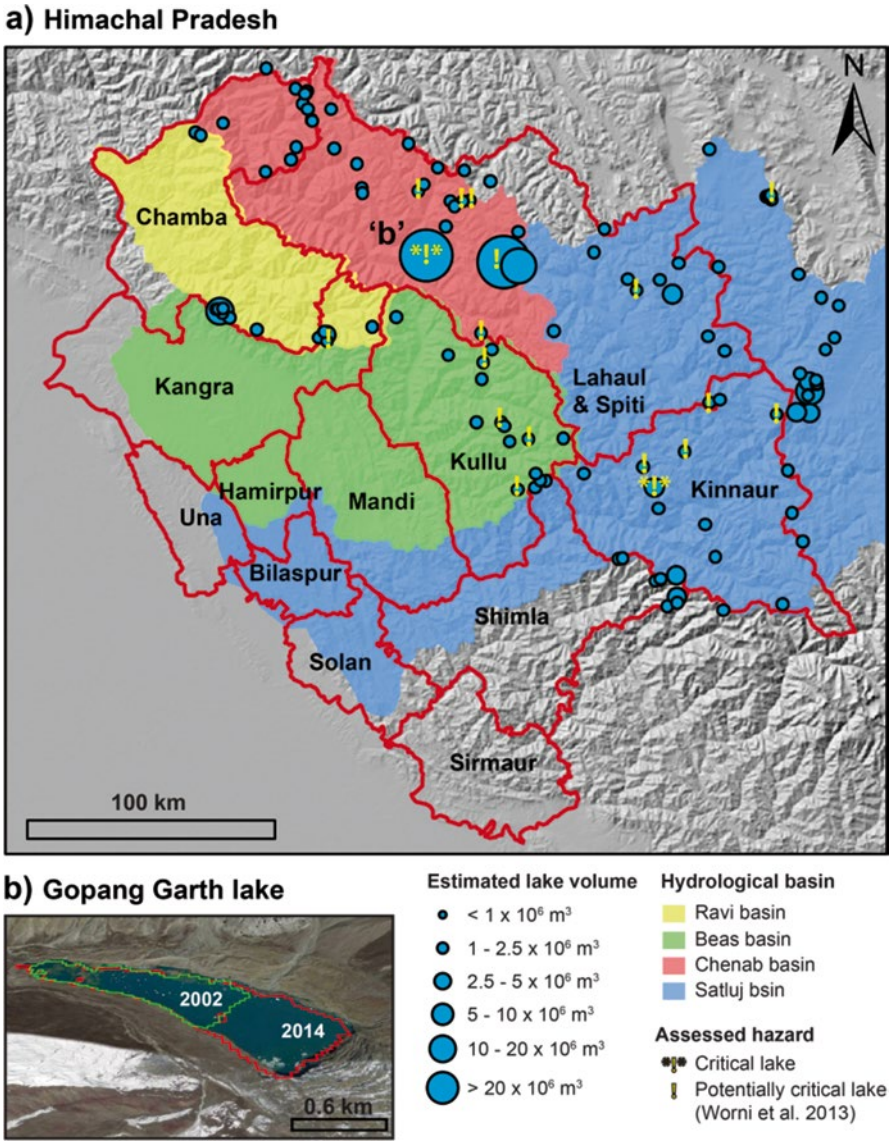

Fig. 10.2 (**a**) Glacial lake distribution across the Indian state of Himachal Pradesh for 2013/2014. Four main hydrological basins are indicated, and district administrative boundaries are in *red*. The volume estimate for the 120 lakes is after Huggel et al. (2002). Critical and potentially critical lakes classified by Worni et al. (2013) are also indicated, but this does not constitute a complete assessment for all lakes. (**b**) The Google Earth image compares the Landsat-derived extent of Gopang Garth lake in 2002 with 2014 (Source: Author)

areas can relate lake area to volume (Huggel et al. 2002; O'Connor et al. 2001). The relationship derived by Huggel et al. (2002):

$$V = 0.104 \cdot A^{1.42}$$

where area (A) is area in m^2 and volume (V) is in m^3 is based partially on the evidence from glacial lakes in the Himalaya, although it may underestimate the actual volumes of larger lakes by up to 80 %, owing to the large natural variability of lake depth in relation to area (Huggel et al. 2004a).

10.3 Future Lake Development

The erosive power of glaciers can form large depressions at the bed, and when such overdeepened parts are exposed due to glacier retreat and filled with water, rather than sediments, new lakes can form (Clague and Evans 1994). Hence, by detecting overdeepenings in the glacier bed, sites of potential future lake formation can be identified. As the glacier surface topography can be seen as a smoothed image of the underlying bed (Oerlemans 2001), surface slope is a key factor in determining ice thickness variability and detecting such overdeepenings. Frey et al. (2010) presented a multilevel strategy for the identification of overdeepened parts of glacier beds. On the first level, a simple slope threshold of <5° is applied to detect flat areas potentially suitable for lake formation. On the second level, the changes in surface slope, glacier width and crevasse patterns are evaluated (Fig. 10.3). On a third, more sophisticated level, the model GlabTop was applied to estimate ice thickness distribution and bed topography across a large region of the Swiss Alps.

GlabTop (Glacier bed Topography) computes ice thicknesses based on an ice dynamical approach, and the assumption of perfect plasticity of ice, which relates glacier thickness to its local surface slope via the basal shear stress. Basel shear stress is estimated for each glacier and based on an empirical relation between shear stress and elevation range (Haeberli and Hoelzle 1995), which implicitly includes mass turnover and hence a mass balance gradient (Linsbauer et al. 2012). While the glacier-wide estimated basal shear stress value determines the overall thickness of the glacier, the modeling of thickness variability for local glacier parts is established from the zonal mean of the surface slope within 50 m elevation bins (Linsbauer et al. 2012; Paul and Linsbauer 2012). The latest version of the model (GlabTop2), as applied and discussed in the Himalayan context by Frey et al. (2014), is fully automated and requires only a DEM and glacier outline mask as input. The resulting modeled ice thickness distribution is subtracted from the surface DEM to obtain the bed topography, i.e., a DEM without glaciers. The overdeepenings in the glacier beds are detected by filling them with the ArcGIS hydrology tool "fill" and a slope grid derived from the filled DEM. By selecting slope values <1° within the glacier outlines, the overdeepenings in the glacier beds are found. The difference grid

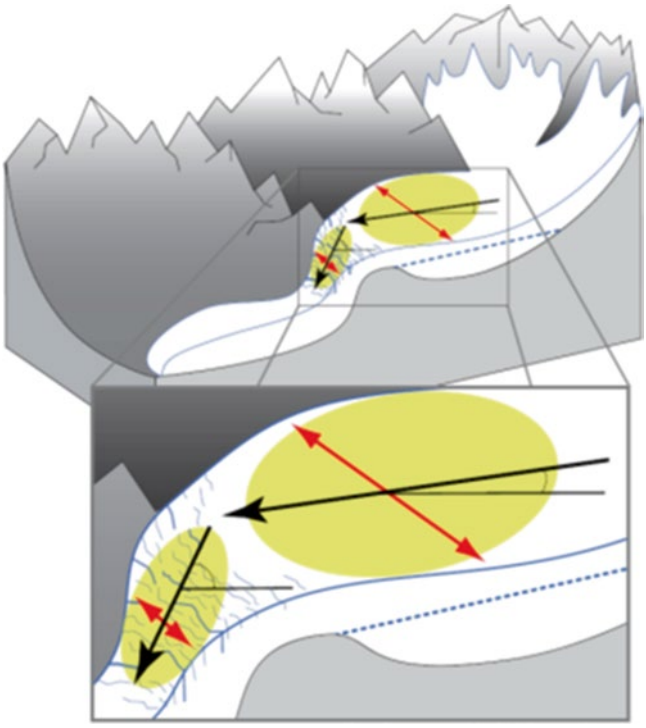

Fig. 10.3 Simplified schematic sketch showing three surface morphological criteria that can indicate potential overdeepenings in the bed topography (*blue dashed line*) where new lakes may develop. The *black arrows* indicate a sudden steepening of the slope, the *red arrows* show a narrowing of the glacier width, and the *yellow areas* indicate a flat and crevasse-free region above a heavily crevassed area (Figure reproduced from Frey et al. (2010) with permission)

between the filled DEM and the former DEM without glaciers is used to quantify the area and volume of the overdeepenings/potential lakes (Linsbauer et al. 2012).

Application of the GlabTop2 model for the state of Himachal Pradesh used the Global DEM (version 2) from the Advanced Spaceborne Thermal Emission and Reflection Radiometer (ASTER GDEM2) with a spatial resolution of ~30 m (Hayakawa et al. 2008) and glacier outlines from Frey et al. (2012). Maximum ice thicknesses exceeding 250–300 m are typically modeled for many larger valley glaciers in the districts of Lahaul and Spiti and Kullu, but generally thicknesses less than 100 m predominate for the smaller glaciers and in ablation areas (Fig. 10.4). In total, more than 4000 potential overdeepenings are modeled with surface areas >0.01 km^2 (Table 10.1). Whereas the locations of overdeepenings are generally rather robust (Linsbauer et al. 2012), overdeepenings located at glacier termini have to be interpreted with care. This is because they can be very shallow, input data (DEM and glacier outlines) may not align exactly causing modeling artifacts, or the 50 m elevation bin for slope averaging exceeds the glacier termini (slope is not completely averaged within the glacier boundaries). In order to refine the focus to

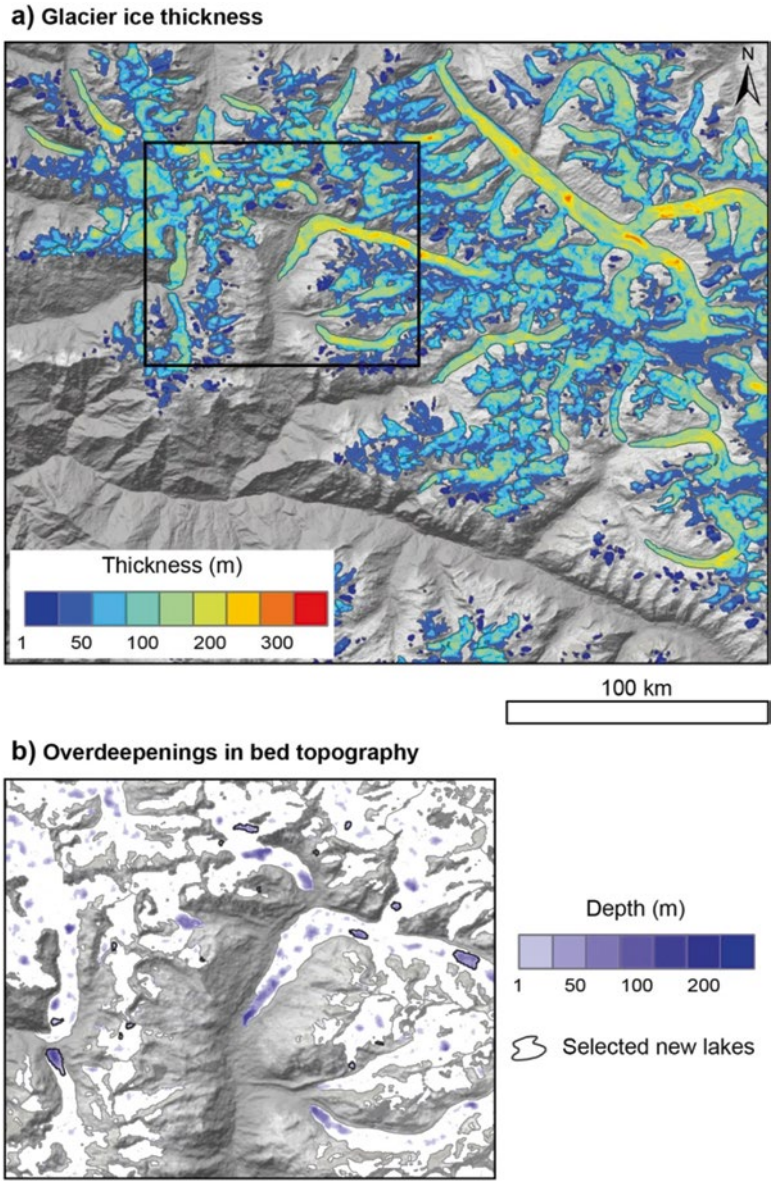

Fig. 10.4 GlabTop2 modeled (**a**) ice thicknesses and (**b**) overdeepenings in the glacier bed topography for a glaciated area above the Parvati valley, Kullu district, India. Final selected overdeepenings where new lakes are considered most likely to develop within the exposed bed topography are indicated (Source: Author)

Table 10.1 The selection of potential new lakes within modeled overdeepenings in the glacier bed, listed for four main hydrological basins (see Fig. 10.2) and for the entire state watershed area of Himachal Pradesh. The number of potential lakes remaining after each sequential selection step is indicated. The total and mean modeled volume of the final lake selection is given

	Selection steps to identify new lakes based on modeled overdeepenings (number of lakes)			
Hydrological basin	1. >0.01 km^2	2. Below mean elevation of the glacier	3. Above a topographic steepening	Total (mean) volume of selected potential new lakes ($m^3 \times 10^6$)
Ravi	163	125	15	18.7 (1.2)
Beas	601	453	63	112.5 (1.8)
Chenab	1866	1566	98	93.9 (1.0)
Satluj	1262	1120	76	52.7 (0.7)
State wide	4253	3572	279	313.9 (1.1)

those situations where potential lakes are considered most likely to develop in the coming decades (approximately 10–50 years), only those lakes below the current mean elevation of the glacier (approximating the glacier ablation area) were selected for further analyses. In a third and final selection step, a key topographic criterion established by Frey et al. (2010) was automated in a GIS environment to identify only those overdeepenings located above a sudden steepening in the topography of the glacier surface (as illustrated in Fig. 10.5). This steepening was approximated by mean slope values >25° within a zone 300 m immediately below the overdeepening and identifies situations where there is a higher likelihood of a thick overdeepened part of the glacier occurring, with thinner ice below (see overdeepening C in Fig. 10.5). Following the selection process, 279 potential new lakes are identified across the state of Himachal Pradesh (see Table 10.1 and examples shown in Figs. 10.4b and 10.5) and used for subsequent analyses presented in Sects. 10.4, 10.5, and 10.6. This represents less than 10 % of all modeled overdeepenings in the glacier bed topography and, thus, should be considered a conservative lower estimate for the actual number of glacial lakes that may develop in the future. Maximum lake depths exceed 100 m, with the modeled mean depth across all 279 lakes being 15 m. Although the greatest number of potential new lakes is identified in the Chenab and Satluj basins, the total volume of water stored in the potential lakes is largest in the Beas basin, owing to significantly larger mean lake volumes modeled and selected here (Table 10.1).

10.4 Lake Impact Predisposition

As indicated by Richardson and Reynolds (2000), mass movements of ice and rock are the most common reported trigger of GLOF events in the Himalaya. In the future, as lakes form in exposed depressions eroded at the glacier bed, this trigger mechanism is expected to increase in importance, given new lakes will be forming

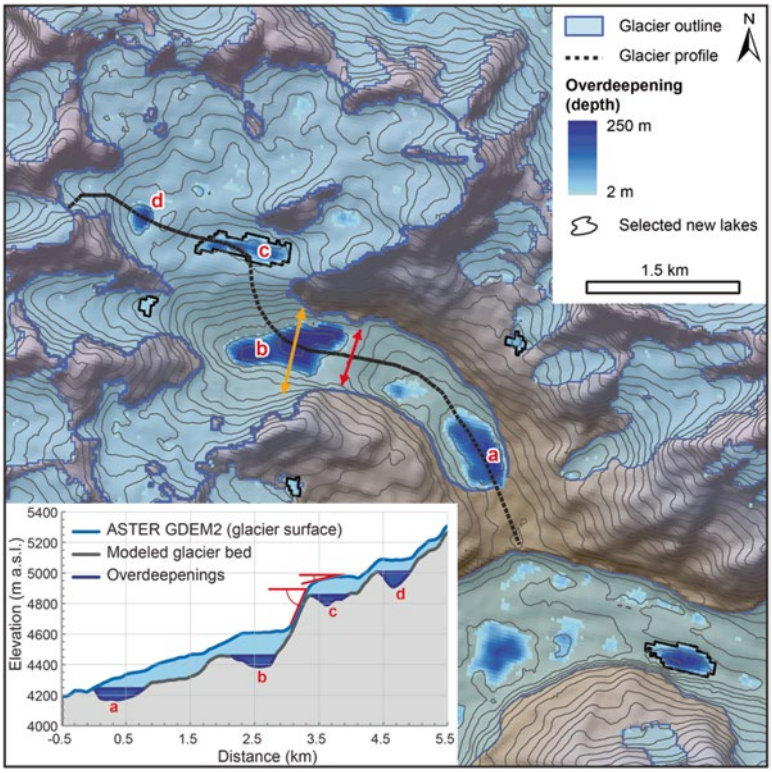

Fig. 10.5 Longitudinal profile through a glacier above the Parvati valley, Kullu district, India, showing four large overdeepenings modeled with GlabTop2 and demonstrating some of the morphological criteria introduced by Frey et al. (2010) (see Fig. 10.3). The *red lines* in the profile graph indicate a distinct break in slope (*c*); the *orange* and *red arrows* show a narrowing of the glacier width (*b*). Based on the criteria applied herein, overdeepening C is selected as a most likely location where a new lake will form (Source: Author)

at increasingly higher altitudes in closer proximity to steep, potentially destabilized high-mountain flanks. While these new lakes will primary be dammed by bedrock rather than loose moraine material, they will still be susceptible to overtopping from displacement waves generated by ice or rock avalanches. Ice avalanche starting zones are generally distinguished based on their slope morphology (Alean 1985). Cliff-type situations originate from the steep frontal section of a glacier and are typically low-volume, high-frequency events. In contrast, the more seldom ramp-type situation involves a failure at the glacier bed and release of a large volume of glacial ice (e.g., Huggel et al. 2005). The stability of such glaciers is intimately linked to topography and temperature (Haeberli et al. 1989); cold glaciers become unstable at much steeper (ca 45°) slope angles, relative to warmer glaciers (ca 25°), suggesting climate warming could directly alter the frequency and spatial distribution of ice avalanches (Stoffel and Huggel 2012). Climate influence on rock slope

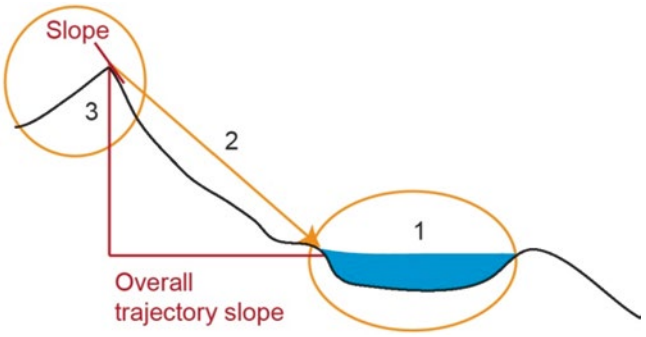

Fig. 10.6 Schematic sketch summarizing the concept of topographic potential used to determine the predisposition of a glacial lake to mass movement impacts of rock and ice. *1* A glacial lake has to be situated within *2* the attainable run-out distance (based on the overall trajectory slope or angle of reach) from *3* potentially unstable steep rock and ice slopes (based on slope angle) (Figure modified from Schaub (2014))

stability in glaciated mountain regions is more complex, with various processes operating on a range of spatial scales, some of which remain poorly understood (see McColl 2012 for a comprehensive review). Nonetheless, an apparent increase in rockfall activity has been observed in several regions of the European Alps over the past 100 years, especially in peri- and paraglacial environments, coincident with rising global temperatures, glacial recession, and thawing of permafrost (Huggel et al. 2012).

Local detailed mapping of potential source areas of unstable ice and rock is feasible for case studies and may be assessed qualitatively using high-resolution satellite imagery (Worni et al. 2013). However, in view of anticipating future GLOF hazard across large spatial scales, where potential new lakes may number hundreds or even thousands, automated approaches are warranted that can quantify the threat of ice and rock impacts. Procedures based on spectral band segmentation of remotely sensed imagery and slope classification have been widely used to map areas of steep ice, for example, and possible impacts into glacial lakes have been modeled (e.g., Allen et al. 2009; Huggel et al. 2004b). The GIS-based approach demonstrated here has been recently integrated within a comprehensive risk analyses of current and future (ice-free) conditions in the Swiss Alps (see Schaub 2014 for a full description) and is founded on the concept of topographic potential (Romstad et al. 2009). Topographic potential encompasses (a) the potential for rock or ice to detach (parameterized by slope angle) and (b) the potential for the resulting rock and/or ice avalanche to reach a glacial lake (parameterized by the overall trajectory slope or angle of reach) (see Fig. 10.6). For implementation within Himachal Pradesh, we do not distinguish whether the slope is bedrock or ice covered and assume an impact into a lake is possible from any slope >30° (cf. Allen et al. 2011; Fischer et al. 2012), where the overall slope trajectory is >25 % (cf. Bolch et al. 2011; Noetzli et al. 2003; Romstad et al. 2009). The combined area (given in km^2) within each lake watershed fulfilling these two criteria is referred to as the lake impact

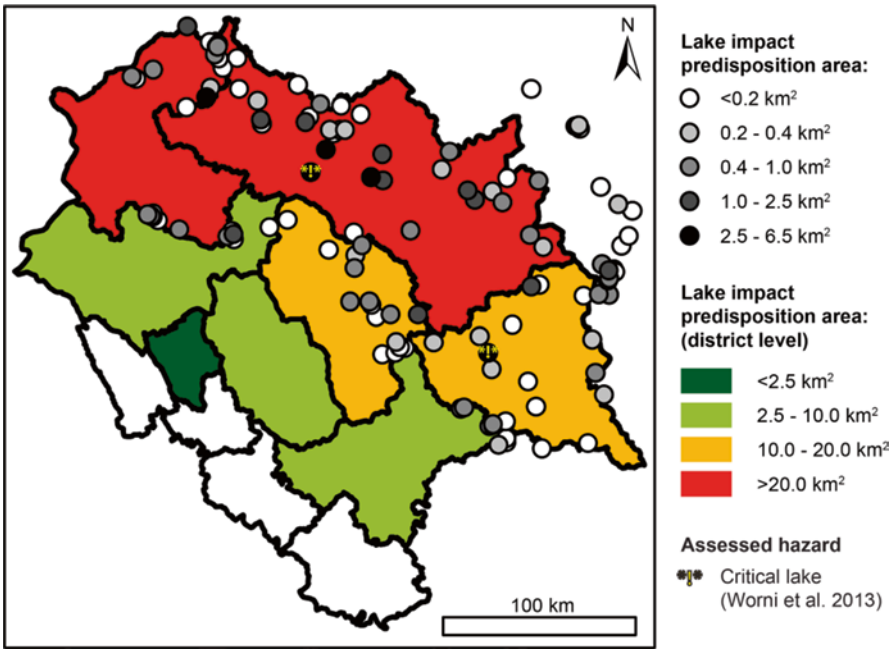

Fig. 10.7 GIS-based modeling of lake predisposition to mass movement impacts. Values are based on the area (km^2) within each lake watershed where slope values are >30° and the overall trajectory slope (angle of reach to the lake) is >25 %. Topographic data is from the Global Digital Elevation Model (GDEM) version 2 of the Advanced Spaceborne Thermal Emission and Reflection Radiometer (ASTER). Aggregated results show the lake impact predisposition area summed for each district watershed (Source: Author)

predisposition area. Although other regional-scale parameters such as slope lithology, glacial history, and permafrost conditions can be integrated to further refine the detection of unstable terrain (Schaub 2014), such data is generally lacking for many high-mountain regions.

In Himachal Pradesh, the catchment area of Lahaul and Spiti district contains not only the largest number of glacial lakes but also contains a high proportion of lakes where the impact predisposition area is large (Fig. 10.7). At this scale, in the absence of further information on triggering processes and dam characteristics, districts with the largest lake impact predisposition area may be expected to have the greatest likelihood (or probability of occurrence) of outburst flood events. Generally, the potential for mass movement triggering of GLOFs in Himachal Pradesh is seen to decrease with distance south from the main Himalayan range (Fig. 10.7). Although the districts of Mandi and Hamipur do not have any glacial lakes within their administrative borders, their upstream catchment areas extend north into higher elevation reaches of the Beas and Satluj basins, where lakes are threatened by potential ice and rock impacts. Both lakes previously assessed as "critical" (Worni et al. 2013) are also identified here as having a high predisposition to impacts from rock and ice.

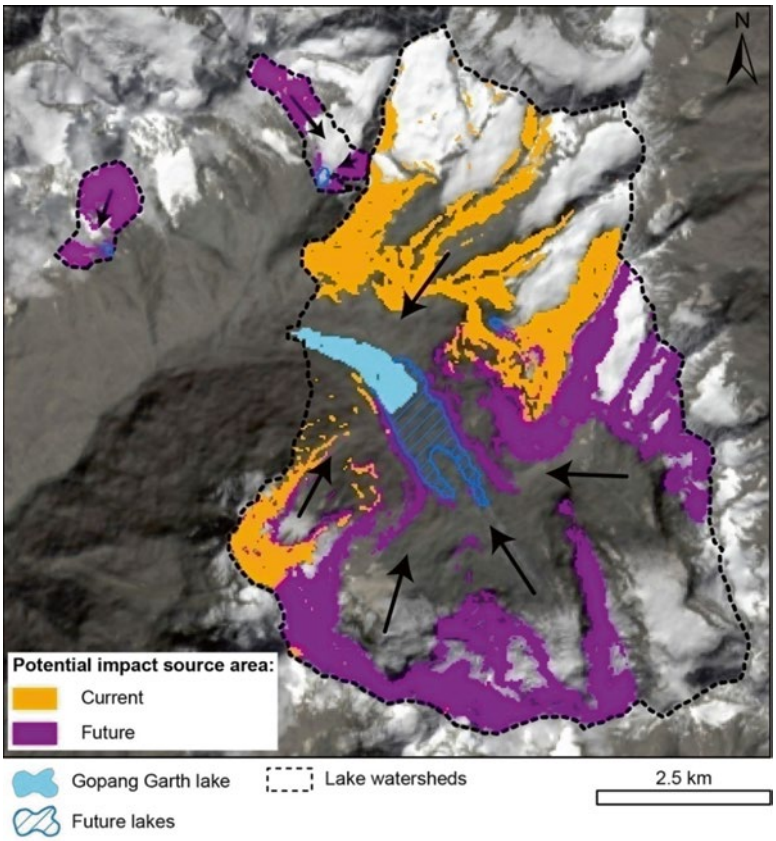

Fig. 10.8 Area around Gopang Garth proglacial lake in the district of Lahaul and Spiti, showing potential source areas of steep (>30°) ice and rock within an overall trajectory slope of >25 % of current and future glacial lakes. *Arrows* provide an approximate indication of the direction from which mass movements of ice or rock may impact the lakes (Source: Author)

The concept of topographic potential provides a simple yet robust indication of how GLOF frequency will increase in response to continued deglaciation. The potential area from which mass movements of ice and rock can detach from will increase over time, not only as existing lakes expand higher into the surrounding basins but also as new lakes develop (Fig. 10.8). As demonstrated for the Gopang Garth area, steep (>30°) ice or rock slopes within a 25 % overall slope trajectory to the current lake are mostly limited to the terrain immediately adjacent to the lake. However, as the lake expands in the future to fill the modeled overdeepened area, the potential source area for rock or ice avalanches that may reach the lake significantly increases to include much of the watershed. Whereas the current lake is mostly susceptible to impacts striking perpendicular to the lake orientation, future impacts may enter the lake from an angle which directs full-wave energy toward the lake outlet.

10.5 GLOF-Affected Land Area

As described for Himachal Pradesh, some district watersheds extend upstream into glaciated areas far beyond the local administrative boundaries. A key component and next step for any large-scale GLOF hazard assessment therefore requires that the maximum affected downstream area for any flood event is determined, based on the so-called "worst-case" scenario modeling. While a range of advanced 2-D and 3-D hydrodynamic models have been used to create detailed GLOF inundation maps (see Westoby et al. 2014 for a comprehensive review), high computational costs and the requirement for high-resolution topographic data limit their application for larger-scale GLOF hazard assessment. In contrast, GIS-based flow routing methods are computationally simple and have been used to simulate outburst events from a large number of glacial lakes in the Swiss Alps (Huggel et al. 2003) and Southern Alps of New Zealand (Allen et al. 2009).

The modified single-flow (MSF) model is a GIS-based hydrological flow routing algorithm that calculates the flow direction from one DEM pixel to another according to the steepest downward gradient between each pixel and its eight neighbors (after O'Callaghan 1984), modified to allow flow spreading of up to 45° from the main flow direction (see Huggel et al. 2003 for a full model description). In addition to determining the extent of area potentially affected by the flow path, the model can also establish for every pixel a qualitative probability of being affected by the event flow path, based on distance from the lake source and lateral deviation from the central flow path. The maximum downstream travel distance for each GLOF path is determined using an empirically derived worst-case scenario defined by the overall trajectory slope to the source lake, with values as low as 5 % (3° angle of reach) appropriate for highly mobile sediment-laden events (Huggel et al. 2004a). Beyond these worst-case run-out distances, no severe damages can be expected. It is important to note that approaches such as the MSF have no strict physical basis and do not account for geotechnical conditions within the flow channel. As such, there is no direct information on flow volumes or velocities, sediment eroded, or deposition volumes, and run-up or overtopping of obstructions in the flow path cannot be simulated. Nevertheless, at large spatial scales, the MSF-derived first-order assessment of downstream affected area provides a reasonable proxy for the magnitude of the GLOF hazard and provides a useful basis for identifying exposed infrastructure and communities under both current and future conditions.

MSF modeling of GLOF paths has been completed for both current and future glacial lakes within the watershed area of Himachal Pradesh (Fig. 10.9), revealing that even when maximum worst-case run-out distances are considered, the GLOF hazard is largely confined to the three mountainous districts of Lahaul and Spiti, Chamba, and Kullu, with some few paths affecting also Kangra, Mandi, and Shimla. The development of new lakes in the future does not alter the number of districts potentially affected by GLOFs, i.e., future GLOF paths remain confined to those districts currently affected by potential paths. In terms of total area affected (sum of all pixels affected by GLOF paths), Lahaul and Spiti will see the greatest increase

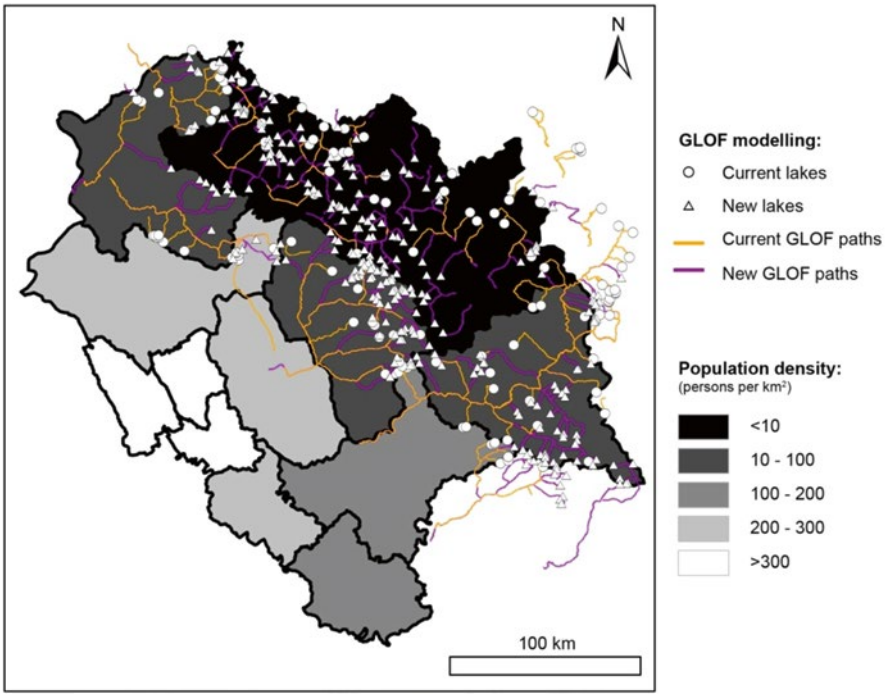

Fig. 10.9 GIS-based worst-case scenario modeling of potential GLOF path extent for current glacial lakes and for new lakes projected to develop as glacier recession exposes overdeepenings in the bed topography (see Sect. 10.3). Current paths overlay the new GLOF paths, to emphasize where new threats are emerging. The base image shows population density for the 12 districts of Himachal Pradesh (From Census India, 2011 – www.censusindia.gov.in)

resulting from the future formation of new lakes (235 % increase in area affected by GLOF paths). However, much of this mountainous district is inhabitable, and hence, population density is low, decreasing the likelihood that GLOFs will directly threaten exposed people or village infrastructure (see Sect. 10.6). Fortunately the most heavily populated districts in Himachal Pradesh are also the districts with zero or limited land area affected by potential GLOFs. It is noted that GLOFs originating beyond the Indian boarder can potentially affect districts within Himachal Pradesh, highlighting the large scales involved and transnational approaches required to manage GLOF hazard.

10.6 Synthesis of Changing GLOF Hazard and Risk

Based on the distribution of current and potential newly forming glacial lakes, the predisposition of these lakes to mass movements of ice and rock, and recognition of the maximum affected area from any potential lake outburst events, it is possible to

demonstrate some first-order understanding of changing GLOF hazard across large spatial scales.

Disaster risk is the consequence of a physical hazard, intersecting with vulnerable and exposed people, infrastructure, or services (IPCC 2012). Sections 10.4 and 10.5 addressed the hazard component of GLOFs for a large Indian Himalayan state, in terms of the probability of occurrence (based on modeled predisposition of the lake to mass impact triggered outburst flooding) and in terms of the potential magnitude (based on the modeled affected downstream land area). The overall hazard therefore for each district watershed is calculated here simply as a function of the probability of occurrence and potential magnitude, i.e.:

$$\begin{aligned}\text{GLOF hazard} = {} & \text{probability of occurrence(lake impact predisposition area)} \\ & \times \text{potential magnitude (affected land area)}\end{aligned}$$

Resulting values are considered unitless and in no way constitute an assigned hazard level in the engineering sense, but rather provide a comparative measure that can be used to explore changing patterns of hazard and risk between the different districts, establishing a basis for prioritization of resources toward hazard management and further studies. The term *risk* is likewise not applied in a strict nor quantitative sense here, because the vulnerability component (primarily a social, political, and economic construction) required for a complete disaster risk assessment is not provided. Here, the hazard component is combined with a simple measure of exposure (total district population), to better illustrate where GLOFs represent a risk to people living in Himachal Pradesh, i.e.:

$$\text{GLOF risk} = \text{GLOF hazard} \times \text{population}$$

The large potential for ice and rock avalanche impacts into glacial lakes, and large area affected by potential GLOF paths, results in a relatively high overall GLOF hazard in the heavily glaciated and mountainous district of Lahaul and Spiti (Fig. 10.10a). However, when district population is considered, the risk profile looks very different, and highest GLOF risk under current conditions is demonstrated for the smaller and more densely populated districts of Chamba and Kullu (Fig. 10.10b). This of course assumes that the populated villages within each district actually coincide with the land areas affected by the simulated GLOF paths – an assumption that may be robust in the case of Kullu where the simulated GLOF paths cross much of the district, but less so in Chamba. In Shimla, for example, the GLOF hazard appears localized to the extreme northern and eastern margins of the district, so the relatively high risk demonstrated for this district is most likely overstated. Further aggregation of the modeling results to reduced administrative scales (block or village level) would improve such an assessment. While risk to population is emphasized in this example, risk patterns might look very different if exposure of, e.g., hydropower or tourist infrastructure and agricultural or ecosystem services was assessed.

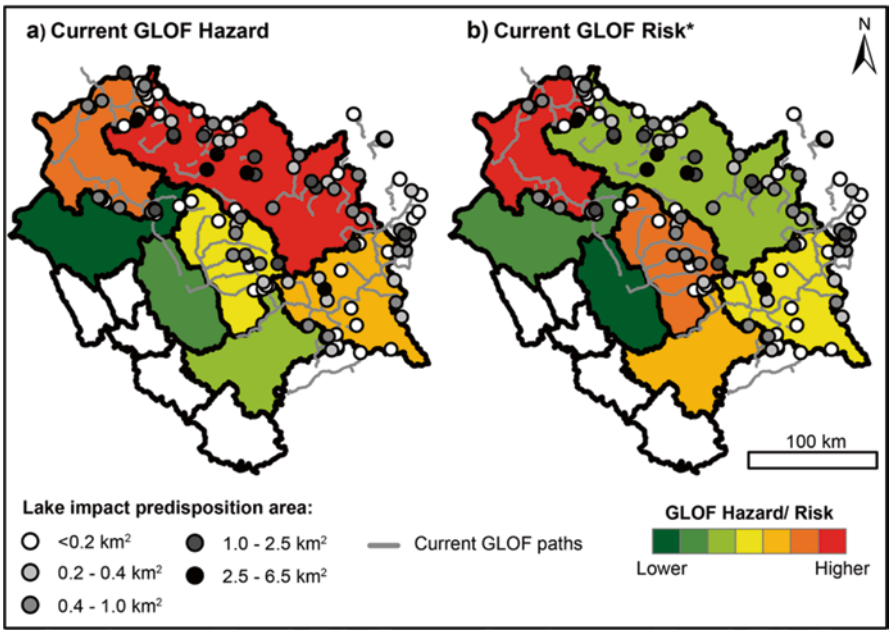

Fig. 10.10 (**a**) District-level aggregated results of lake impact predisposition modeling (Sect. 10.4) combined with MSF modeling of downstream affected areas (Sect. 10.5) to establish a relative GLOF hazard ranking for the districts of Himachal Pradesh. (**b**) Hazard ranking values are normalized by district population, to establish a relative GLOF risk level. Five districts are not affected by any potential GLOF hazard or risk. *Hazard/risk indication is intended to provide a comparative measure between districts and does not constitute a formal or quantified rating (Source: Author)

The relative distribution of GLOF hazard is not expected to change significantly in the future, as glaciers retreat, existing lakes expand, and new lakes form in overdeepenings in the exposed glacier bed. Future risk is not assessed and would require projected information on population trends, which in turn will be influenced by future socioeconomic conditions, employment opportunities, and migration patterns. The greatest hazard will remain in Lahaul and Spiti, where most new lakes will form, but notably, the hazard level in Kullu and Kinnaur will rise above that of Chamba, where comparatively few new lakes are simulated to form (Fig. 10.11a). Across all districts, the absolute hazard level (and corresponding risk) can be expected to increase significantly, as the overall potential for impacts of rock and ice into glacial lakes increases (Fig. 10.11b), and the affected downstream area within simulated GLOF paths increases (Fig. 10.11c). Generally across most districts, the simulated increase in lake impact predisposition area (and therefore potential future GLOF frequency) is of an order of magnitude larger than the simulated increase in GLOF-affected area. The district of Kullu is noteworthy in this regard, as large increases in both the potential frequency and land area affected by future GLOFs are modeled, relative to current conditions. Particular emphasis for

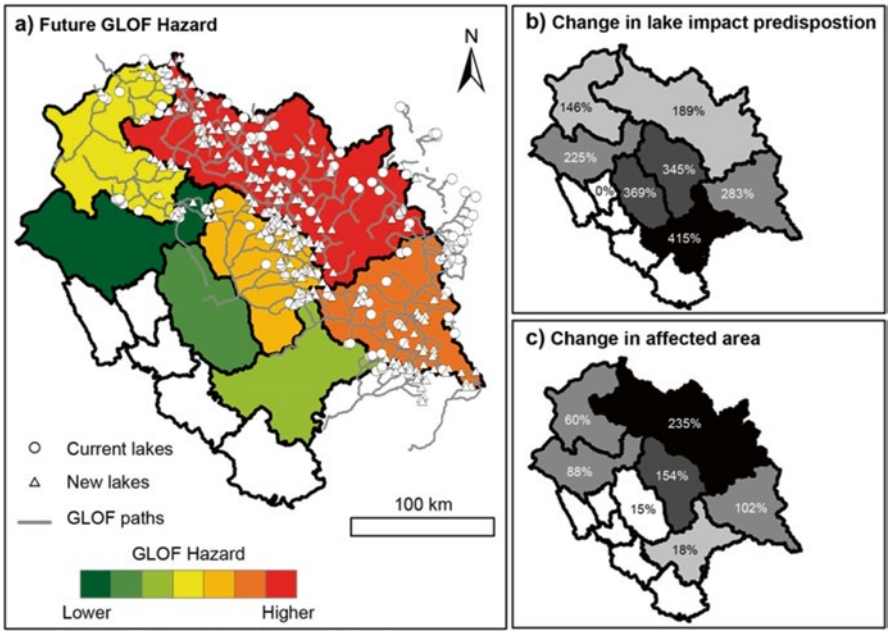

Fig. 10.11 (**a**) The same as Fig. 10.10a, but including future new lakes modeled in the overdeepenings within the glacier bed (Sect. 10.3). Due to the large number of lakes, the lake impact predisposition area for individual lakes is not indicated to preserve clarity. (**b**) Percentage increase in aggregated district-scale lake impact predisposition area (Sect. 10.4) and **c** GLOF-affected area (Sect. 10.5), resulting from the formation of new lakes. Percentage increases for each district are calculated relative to current values. *Dark shading* indicates larger increases. The assessment does not account for the possibility that some lakes may become filled with sediment, dry up, and disappear over time (Source: Author)

ongoing monitoring and further study could be given to those lakes with the highest likelihood for impacts of rock and ice, especially where closer inspection reveals that associated GLOF paths intercept with populated villages or infrastructure. In these instances, advanced numerical modeling approaches could provide a basis for comprehensive hazard zonation for the current GLOF threat if sufficiently high-resolution topographic data is available (e.g., Worni et al. 2013). For new lakes, modeled information regarding future lake depths and volumes (Sect. 10.3) could provide a basis for semiempirical estimates of maximum discharge (e.g., Huggel et al. 2002) and, thus, contribute toward a quantified hazard rating.

10.7 Conclusions

Most research concerning the hazard from glacial lake outburst floods has focused on the threat from lakes that have formed over the past century and which continue to expand rapidly in response to recent warming of the climate system. However,

attention is shifting toward the anticipation of future hazard and risk associated with new lakes that will develop as glaciers continue to retreat and dramatically different landscapes are uncovered. Nowhere will this threat be more pronounced than in the Himalaya, where the majority of the world's glaciers are found and where the dynamics of nature interact closely with livelihoods and anthropogenic resources.

Using the Indian Himalayan state of Himachal Pradesh as a case study, this chapter has introduced and demonstrated a suite of approaches that enable both current and future GLOF hazard to be assessed over large spatial scales. Emphasis has been given to the changing potential for GLOFs triggered by mass movements of ice or rock and recognition of downstream affected areas. Other climate-related factors, including thawing of ice-cored moraines, permafrost degradation, heavy precipitation, and rapid snowmelt, also influence GLOF activity and may also be assessed in view of future changes in the high-mountain climate system. With early anticipation of future threats, adaptation and planning responses can be optimized and the risk of disaster minimized.

Acknowledgments ArcGIS models used to assess lake impact predisposition were developed and kindly provided by Marco Serraino. The studies in Himachal Pradesh are conducted within the Indian Himalayas Climate Adaptation Programme (IHCAP) supported by the Swiss Agency for Development and Cooperation (SDC) in cooperation with the Department of Science & Technology, Government of India, and with support from the Government of Himachal Pradesh.

References

Alean J (1985) Ice avalanches: some empirical information about their formation and reach. J Glaciol 31:324–333

Allen SK, Schneider D, Owens IF (2009) First approaches towards modelling glacial hazards in the Mount Cook region of New Zealand's Southern Alps. Nat Hazards Earth Syst Sci 9:481–499

Allen SK, Cox SC, Owens IF (2011) Rock avalanches and other landslides in the central Southern Alps of New Zealand: a regional study considering potential climate change impacts. Landslides 8:33–48

Anacona PI, Mackintosh A, Norton KP (2014) Hazardous processes and events from glacier and permafrost areas: lessons from the Chilean and Argentinean Andes. Earth Surf Process Landf. doi:10.1002/esp.3524

Bolch T, Buchroithner MF, Peters J, Baessler M, Bajracharya S (2008) Identification of glacier motion and potentially dangerous glacial lakes in the Mt. Everest region/Nepal using spaceborne imagery. Nat Hazards Earth Syst Sci 8:1329–1340

Bolch T, Peters J, Yegorov A, Pradhan B, Buchroithner M, Blagoveshchensky V (2011) Identification of potentially dangerous glacial lakes in the northern Tien Shan. Nat Hazards 59:1691–1714. doi:10.1007/s11069-011-9860-2

Church JA et al (2013) Sea level change. In: Stocker TF et al (eds) Climate change 2013: the physical science basis. Contribution of Working Group I to the fifth assessment report of the Intergovernmental Panel on Climate Change. Cambridge University Press, Cambridge, pp 1137–1216. doi:10.1017/CBO9781107415324.026

Clague JJ, Evans SG (1994) Formation and failure of natural dams in the Canadian Cordillera. Geol Surv Can Bull 464:39

Clague JJ, Evans SG (2000) A review of catastrophic drainage of moraine-dammed lakes in British Columbia. Quat Sci Rev 19:1763–1783
Clague JJ, O'Connor JE (2014) Glacier-related outburst floods. In: Haeberli W, Whiteman C (eds) Snow and ice-related hazards, risks, and disasters. Elsevier, Netherlands
Deline P et al (2014) Ice loss and slope stability in high-mountain regions. In: Haeberli W, Whiteman C (eds) Snow and ice-related hazards, risks, and disasters. Elsevier, Netherlands
Fischer L, Purves RS, Huggel C, Noetzli J, Haeberli W (2012) On the influence of topographic, geological and cryospheric factors on rock avalanches and rockfalls in high-mountain areas. Nat Hazards Earth Syst Sci 12:241–254
Frey H, Haeberli W, Linsbauer A, Huggel C, Paul F (2010) A multi-level strategy for anticipating future glacier lake formation and associated hazard potentials. Nat Hazards Earth Syst Sci 10:339–352
Frey H, Paul F, Strozzi T (2012) Compilation of a glacier inventory for the western Himalayas from satellite data: methods, challenges, and results. Remote Sens Environ 124:832–843
Frey H et al (2014) Estimating the volume of glaciers in the Himalayan–Karakoram region using different methods. Cryosphere 8:2313–2333
Fujita K, Suzuki R, Nuimura T, Sakai A (2008) Performance of ASTER and SRTM DEMs, and their potential for assessing glacial lakes in the Lunana region, Bhutan Himalaya. J Glaciol 54:220–228
Fujita K, Sakai A, Takenaka S, Nuimura T, Surazakov AB, Sawagaki T, Yamanokuchi T (2013) Potential flood volume of Himalayan glacial lakes. Nat Hazards Earth Syst Sci 13:1827–1839
Gardelle J, Arnaud Y, Berthier E (2011) Contrasted evolution of glacial lakes along the Hindu Kush Himalaya mountain range between 1990 and 2009. Global Planet Change 75:47–55
Haeberli W (1983) Frequency and characteristics of glacier floods in the Swiss Alps. Ann Glaciol 4:85–90
Haeberli W, Hoelzle M (1995) Application of inventory data for estimating characteristics of and regional climate-change effects on mountain glaciers: a pilot study with the European Alps. Ann Glaciol 21:206–212
Haeberli W, Hohmann R (2008) Climate, glaciers and permafrost in the Swiss Alps 2050: scenarios, consequences and recommendations. In: Kane DL, Hinkel KM (eds) Ninth international conference on permafrost. Institute of Northern Engineering, University of Alaska, Fairbanks
Haeberli W, Alean JC, Müller P, Funk M (1989) Assessing risks from glacier hazards in high mountain regions: some experiences in the Swiss Alps. Ann Glaciol 13:96–102
Haeberli W, Kääb A, Vonder Mühll D, Teysseire P (2001) Prevention of outburst floods from periglacial lakes at the Gruben Glacier, Valais, Swiss Alps. J Glaciol 47
Hayakawa YS, Oguchi T, Lin Z (2008) Comparison of new and existing global digital elevation models: ASTER G-DEM and SRTM-3. Geophys Res Lett 35:17404. doi:10.1029/2008GL035036
Hewitt K (1982) Natural dams and outburst floods in the Karakorum Himalaya. IAHS Publ 138:259–269
Huggel C, Kääb A, Haeberli W, Teysseire P, Paul F (2002) Remote sensing based assessment of hazards from glacier lake outbursts: a case study in the Swiss Alps. Can Geotech J 39:316–330
Huggel C, Kääb A, Haeberli W, Krummenacher B (2003) Regional-scale GIS-models for assessments of hazards from glacier lake outbursts: evaluation and application in the Swiss Alps. Nat Hazards Earth Syst Sci 3:647–662
Huggel C, Haeberli W, Kääb A, Bieri D, Richardson S (2004a) An assessment procedure for glacial hazards in the Swiss Alps. Can Geotech J 41:1068–1083
Huggel C, Kääb A, Salzmann N (2004b) GIS-based modeling of glacial hazards and their interactions using Landsat-TM and IKONOS imagery. Nor J Geogr 58:61–73
Huggel C, Zgraggen-Oswald S, Haeberli W, Kääb A, Polkvoj A, Galushkin I, Evans SG (2005) The 2002 rock/ice avalanche at Kolka/Karmadon, Russian Caucasus: assessment of extraordi-

nary avalanche formation and mobility and application of QuickBird satellite imagery. Nat Hazards Earth Syst Sci 5:173–187
Huggel C, Haeberli W, Kääb A (2008) Glacial hazards: perceiving and responding to threats in four world regions. In: Orlove B, Luckman B, Wiegandt E (eds) The darkening peaks: glacial retreat in scientific and social context. University of California Press, Berkeley, pp 66–80
Huggel C, Allen S, Deline P, Fischer L, Noetzli J, Ravanel L (2012) Ice thawing, mountains falling—are alpine rock slope failures increasing? Geol Today 28:98–104
IPCC (2012) Managing the risks of extreme events and disasters to advance climate change adaptation. A special report of working groups I and II of the Intergovernmental Panel on Climate Change. In: Field CB et al (eds) Cambridge University Press, Cambridge, p 582
Ives JD, Shrestha RB, Mool PK (2010) Formation of glacial lakes in the Hindu Kush-Himalayas and GLOF risk assessment. ICIMOD, Kathmandu
Kääb A et al (2005a) Remote sensing of glacier- and permafrost-related hazards in high mountains: an overview. Nat Hazards Earth Syst Sci 5:527–554
Kääb A, Reynolds JM, Haeberli W (2005b) Glacier and permafrost hazards in high mountains. In: Huber UM, Bugmann HKM, Reasoner MA (eds) Global change and mountain regions. An overview of current knowledge. Springer, Dordrecht, pp 225–234
Komori J (2008) Recent expansions of glacial lakes in the Bhutan Himalayas. Quat Int 184:177–186
Korup O, Tweed F (2007) Ice, moraine, and landslide dams in mountainous terrain. Quat Sci Rev 26:3406–3422
Linsbauer A, Paul F, Haeberli W (2012) Modeling glacier thickness distribution and bed topography over entire mountain ranges with GlabTop: application of a fast and robust approach. J Geophys Res 117:3007. doi:10.1029/2011JF002313
Liu J-j, Tang C, Cheng Z-l (2013) The two main mechanisms of Glacier Lake Outburst Flood in Tibet, China. J Mt Sci 10:239–248
Lliboutry L, Morales AB, Pautre A, Schneider B (1977) Glaciological problems set by the control of dangerous lakes in Cordillera Blanca, Peru. I. Historic failure of morainic dams, their causes and prevention. J Glaciol 18:239–254
McColl S (2012) Paraglacial rock-slope stability. Geomorphology 153–154:1–16
Noetzli J, Hoelzle M, Haeberli W (2003) Mountain permafrost and recent Alpine rock-fall events: a GIS-based approach to determine critical factors. In: Phillips M, Springman SM, Arenson LU (eds) PERMAFROST, proceedings of the eighth international conference on permafrost, vol 2. Swets & Zeitlinger, Zurich, pp 827–832
O'Callaghan JF (1984) The extraction of drainage networks from digital elevation data. Comput Vis Graph Image Process 28:323–344
O'Connor JE, Hardison JH, Costa JE (2001) Debris flows from failures of Neoglacial-Age moraine dams in the Three Sisters and Mount Jefferson wilderness areas, Oregon. US Geological Survey Professional Paper 1606
Oerlemans J (2001) Glaciers and climate change. Balkema, Rotterdam
Paul F, Linsbauer A (2012) Modeling of glacier bed topography from glacier outlines, central branch lines, and a DEM. Int J Geogr Inf Sci 26:1173–1190
Quincey DJ, Richardson SD, Luckman A, Lucas RM, Reynolds JM, Hambrey MJ, Glasser NF (2007) Early recognition of glacial lake hazards in the Himalaya using remote sensing datasets. Global Planet Change 56:137–152
Reynolds JM (1992) The identification and mitigation of glacier-related hazards: examples from the Cordillera Blanca, Peru. In: McCall GJH, Laming DJC, Scott SC (eds) Geohazards natural and man-made. Chapman and Hall, London, pp 143–157
Richardson SD, Reynolds JM (2000) An overview of glacial hazards in the Himalayas. Quat Int 65(66):31–47
Romstad B, Harbitz C, Domaas U (2009) A GIS method for assessment of rock slide tsunami hazard in all Norwegian lakes and reservoirs. Nat Hazards Earth Syst Sci 9:353–364

Schaub Y (2014) Outburst floods from high-mountain lakes: risk analysis of cascading processes under Present and future conditions. PhD thesis, Department of Geography, University of Zurich, Switzerland

Schaub Y, Haeberli W, Huggel C, Künzler M, Bründl M (2013) Landslides and new lakes in deglaciating areas: a risk management framework. In: Margottini C, Canuti P, Sassa K (eds) Landslide science and practice. Springer, Berlin, pp 31–38

Stoffel M, Huggel C (2012) Effects of climate change on mass movements in mountain environments. Prog Phys Geogr 36:421–439

Vilimek V, Emmer A, Huggel C, Schaub Y, Würmli S (2013) Database of glacial lake outburst floods (GLOFs)–IPL project No. 179. Landslides 11:161–165

Vuichard D, Zimmermann M (1987) The 1985 catastrophic drainage of a moraine-dammed lake, Khumbu Himal, Nepal: causes and consequences. Mt Res Dev 7:91–110

Wang W, Yao T, Gao Y, Yang X, Kattel DB (2011) A first-order method to identify potentially dangerous glacial lakes in a region of the southeastern Tibetan Plateau. Mt Res Dev 31:122–130

Wessels R, Kargel JS, Kieffer HH (2002) ASTER measurement of supraglacial lakes in the Mount Everest region of the Himalaya. Ann Glaciol 34:399–408

Westoby MJ, Glasser NF, Brasington J, Hambrey MJ, Quincey DJ, Reynolds JM (2014) Modelling outburst floods from moraine-dammed glacial lakes. Earth Sci Rev 134:137–159. doi:http://dx.doi.org/10.1016/j.earscirev.2014.03.009

Worni R, Stoffel M, Huggel C, Volz C, Casteller A, Luckman B (2012) Analysis and dynamic modeling of a moraine failure and glacier lake outburst flood at Ventisquero Negro, Patagonian Andes (Argentina). J Hydrol 444–445:134–145

Worni R, Huggel C, Stoffel M (2013) Glacier lakes in the Indian Himalayas – from an area-wide glacial lake inventory to on-site and modeling based risk assessment of critical glacial lakes. Sci Total Environ 468–469:s71–s84

Worni R, Huggel C, Clague JJ, Schaub Y, Stoffel M (2014) Coupling glacial lake impact, dam breach, and flood processes: a modeling perspective. Geomorphology 224:161–176. doi:10.1016/j.geomorph.2014.06.031

Chapter 11
Estimating Recent Glacier Changes in Central Himalaya, India, Using Remote Sensing Data

Suraj Mal, R.B. Singh, and Udo Schickhoff

Abstract Changing glacier snout positions, surface area, and mass balance are considered as important indicators of climate change. Climatic warming and cooling are reflected through shrinkage and expansion of glaciers, often without significant time lags. Glaciers are important sources of water supply for lowlands and thus have significant influence on ecosystem services, agriculture, and socioeconomic conditions. The economy of the Indo-Gangetic Plain is particularly vulnerable in this respect. Therefore, the present study assesses recent changes (2001–2013) of glaciers in central Himalayan region using remote sensing data. A total of 31 glaciers were mapped on Landsat ETM+ (2001) and OLI (2013) and compared to estimate the changes in snout positions. The study reveals that there are significant variations in glacier retreat. The retreat rate varies between 5.6 m^{-1} (Lawan Glacier) and about 35.6 m^{-1} (Pachu Glacier). A total of 6 glaciers retreated with less than 10 m^{-1}, 16 between 10 and 20 m^{-1}, 6 between 20 and 30 m^{-1}, and 3 more than 30 m^{-1}. An attempt has also been made to assess underlying driving forces of the varying retreat rate of glaciers. The elevation of snouts, the area, and the length of glaciers have implications on snout retreat rate. There are, however, some other important factors, e.g., accumulation area ratio, slope angles of accumulation and ablation, amount of rainfall and snowfall, temperature conditions, and debris cover, that have significant bearings on glacier retreat.

Keywords Glacier retreat • Climate change • Central Himalaya • India

S. Mal (✉)
Department of Geography, Shaheed Bhagat Singh College,
University of Delhi, Delhi, India
e-mail: surajdse@gmail.com

R.B. Singh
Department of Geography, Delhi School of Economics,
University of Delhi, Delhi, India
e-mail: rbsgeo@hotmail.com

U. Schickhoff
CEN Center for Earth System Research and Sustainability,
Institute of Geography, University of Hamburg, Hamburg, Germany

R.B. Singh et al. (eds.), *Climate Change, Glacier Response, and Vegetation Dynamics in the Himalaya*, DOI 10.1007/978-3-319-28977-9_11

11.1 Introduction

The Himalayan glaciers are globally recognized to be sensitive to climate variability and important indicators of climate change (Khalsa et al. 2004; Jiawen et al. 2006; Bajracharya et al. 2007). They are observed to react in highly sensitive manner to climate changes due to their proximity to the melting point (Zemp et al. 2006; Bajracharya et al. 2015). Therefore, the study of spatio-temporal behaviors of glaciers over a period can significantly contribute to an improved understanding of climate change in remote mountain regions, e.g., in the Himalaya, where the network of meteorological observatories is poor and measurements are sparse (Bhambri et al. 2011a, b; Deota et al. 2011; Mehta et al. 2011). Besides, most of the meteorological observatories are biased to valley floors and certain aspects (Gerlitz et al. 2014); consequently, their observations are often representative of the climate of certain elevations and aspects.

Extensive studies on the glaciers of the Hindu Kush-Karakoram-Himalaya (HKH) region reveal their differential recessional behaviors (Bajracharya 2007; Kulkarni et al. 2007; Raina 2010; Bhambri et al. 2011a; Bolch et al. 2012; Kulkarni and Karyakarte 2014). The snout retreat rates significantly vary in different parts of the HKH mountains, owing to local physiography, status of debris cover (Scherler et al. 2011), accumulation area ratio, area of ablation zone, and equilibrium line altitude (Kulkarni et al. 2004; Deota et al. 2011; Venkatesh et al. 2013; Mal and Singh 2013). These local factors significantly modify the melting of glaciers. Dobhal et al. (2013) and Schmidt and Nüsser (2009) suggest that a thin debris cover can increase the melting of glacier and may lead to downwasting in the upper ablation zone, while a thick debris cover may reduce the melting and further the retreat rate of snout. According to Venkatesh et al. (2013), "the slope is a very important factor of snout retreat. Steep slopes cause increased down-slope advancement of glaciers that is balanced by the melting due to climate change. It leads to almost zero rate of advance/retreat or stationary snout positions (e.g. Zemu glacier). On the other hand, the lower slope angles restrict down-slope movements and climatic factors play more dominant role that make them more sensitive to local climate change leading to higher retreat of snout (e.g. Gangotri glacier)."

The glaciers are important sources of water supply particularly in the summer season for the large human population, agricultural activities, and industrial requirements in Himalayan Mountain and northern Indian plains (Mehta et al. 2011; Bolch et al. 2012; Mal and Singh 2013). Therefore, glaciers have indirect but significant influences on ecosystem services, river water discharge, agricultural crop production and food security, and socioeconomic conditions of northern Indian plains (Bolch et al. 2012). The glacier shrinkages can have serious consequences on economy and environment. Therefore, it is urgently required to understand and assess the recent behaviors of glaciers in Indian Himalaya. Thus, the present study aims to study recent changes (2001–2013) of glaciers in and around Nanda Devi region, central Himalaya, India.

11.2 Study Area

The present study was conducted in and around Nanda Devi National Park. Geographically, the study area lies in the Indian central Himalaya (upper watersheds of river Rishi Ganga, Dhauliganga, Pindar, and Gori Ganga). The study area is located in the districts of Chamoli (Garhwal Himalaya), Pithoragarh, and Bageshwar (Kumaon Himalaya) of Uttarakhand, extending from 79°40′ E to 80°25′ E longitude and from 30°35′ N to 30°10′ N latitude (Fig. 11.1). The study area is part of an important high-altitude Himalayan protected area, which is characterized by large number of ridges and peaks including Dunagiri (7066 m), Kalanka (6931 m), Nanda Devi East (7434 m), Nanda Khat (6611 m), Trishul (7120 m), Nanda Devi (7816 m), Trishuli (7074 m), and Hardeol (7151 m) (Bisht et al. 2011).

These peaks and high-altitude basins harbor a huge concentration of glaciers (Bisht et al. 2011), e.g., Uttari Nanda Devi, Dakkhni Nanda Devi, Dakkhni Rishi, Milam, Pindari, Kalabaland, Trishul, Pachu, Lawan, Ramni, Ghankhawi, etc. Some of the major tributaries (rivers) emerge from these glaciers including Pindar River from Pindari Glacier; Rishi Ganga River from Uttari Nanda Devi, Dakkhni Nanda Devi, and Dakkhni Rishi glaciers; Gori Ganga from Milam Glacier, etc. The main Rishi Ganga valley (NDNP) has been closed for mountaineering and other human

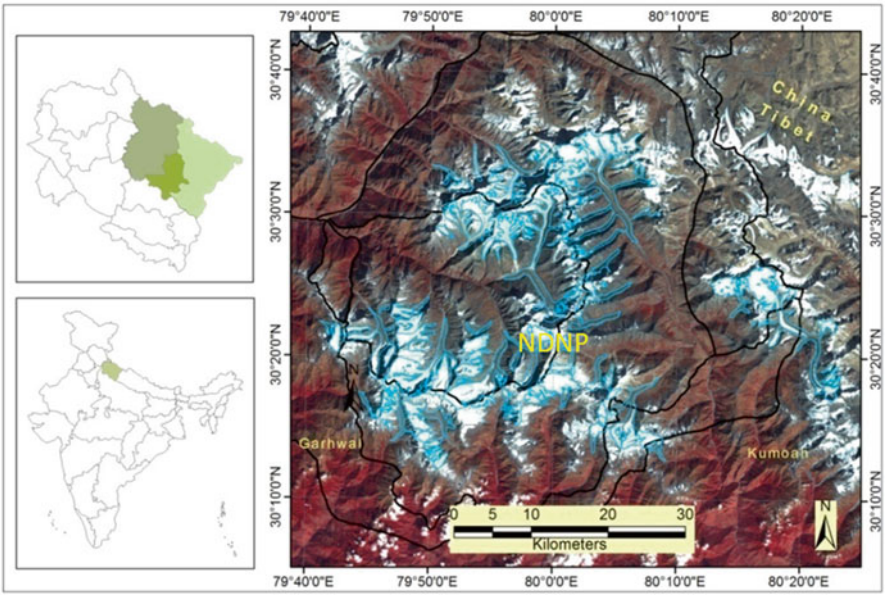

Fig. 11.1 Location of the study area in Central Himalaya, Uttarakhand (Source: Suraj Mal, RB Singh, U. Schickhoff)

activities since 1982 (Banerjee 2003). As a result, the glaciers of NDNP have been rarely studied at field. Bisht et al. (2011) have however conducted a few field-based investigations in the valley. Other glaciers such as Milam and Pindari are relatively better accessible and studied at field and also by using remote sensing methods (e.g. Raj 2011; Raj et al. 2014). Dunagiri is also a relatively well-researched glacier at field. Therefore, the study area provides new and complementary opportunities to study glacier responses to climate change.

11.3 Database and Methods

The study is primarily based on analysis and comparison of Landsat satellite data, which was also supported by field-based investigations of some glaciers. Landsat 7 Enhanced Thematic Mapper (ETM+) of 20 October 2001 and Landsat 8 Operational Land Imager (OLI) satellite images of 29 October 2013 were acquired from the website of US Geological Survey, i.e., www.earthexplorer.org. The ETM+ satellite image provides data in eight spectral bands. The spatial resolution is 30 m for one to seven bands, while the eighth band (panchromatic) is acquired at 15 m spatial resolution (Chander et al. 2009). The OLI satellite data consist of 11 spectral bands, wherein the spatial resolution for one to seven bands and the ninth band is 30 m, and the eighth (panchromatic) is acquired at 15 m and 10–11 bands at 100 m spatial resolution (http://landsat.usgs.gov/landsat8.php).

The standard false-color composites (FCC) of Landsat 7 ETM+ (432) and Landsat 8 OLI (543) were prepared and merged with their respective high-resolution panchromatic bands (eighth band, 15 m) using Brovey transform method following Bahuguna et al. (2007). It produced high-resolution images, thus helpful in efficiently identifying and mapping snout positions even in shadow and substantially debris-covered areas (Bahuguna et al. 2007). The snouts were identified based on shadow of ice wall of glacier and emergence of stream/river from glacial ice. The glacier outlines were derived based on manual digitization on both the images. It is, however, a time-consuming and labor-intensive work (Paul et al. 2004) but efficient method of glacier mapping. The accuracy of mapping is largely dependent on skills of experts or digitizer (Paul et al. 2013). There are other methods, e.g., band ratioing, morphometric glacier mapping (Kamp et al. 2011), supervised classification and Normalized Difference Snow Index (NDSI) (Bolch et al. 2008), object-based classification (Rastner et al. 2014), etc., available for glacier mapping, but they require manual corrections in debris-covered ice in lower ablation zone and in upper accumulation zone to estimate the boundary between two glaciers (Bolch et al. 2008; Kamp et al. 2011).

The glacier outlines were compared at the snout positions in order to estimate total retreat. The total retreat was then divided by number of years (12) to calculate the rate of snout retreat (Dobhal et al. 2004). The lengths of glaciers were estimated along the central flow line of glacier (Bhambri et al. 2012). The area of glaciers was calculated using ArcGIS. The elevation of snout position was estimated

based on ASTER Global Digital Elevation Model version 2 (GDEM2). In order to understand the influence of snout elevation, length, and area of glaciers on the rate of retreat, simple regression method was used. The orientation of glacier was estimated based on ASTER GDEM2, where glacier types were determined based on Sah et al. (2005).

11.4 Results and Discussion

11.4.1 Glacier Distribution and Characteristics

A total of 31 glacier snouts could be identified on both the satellite images of the study area based on shadows of snout and emergence of rivers. There are, however, more than ten glaciers, for which the snouts could not be identified due to (1) the snout positions were heavily debris covered; (2) there was no shadow of snouts, as the glacier and forefield had similar and regular slopes; and (3) the river was too shallow near the snout so that its emergence could not be clearly identified. Thus, they were not included in the present study. The marked slope changes in the snout area, as derived from the ASTER GDEM2, improved the accuracy of snout identification and glacier mapping in the ablation zone. Of the total 31 glaciers investigated, 12 were small glaciers (<5 km^2), 7 glaciers had areas between 5 and 10 km^2 and 5 between 10 and 15 km^2, and 7 were large glaciers (>15 km^2) (Fig. 11.2). Milam, Kalabaland, Trishul, Uttari Nanda Devi, Dakkhni Rishi, and Bagini are among the large glaciers, whereas Silasamudra, Dunagiri, Sakram, Lawan, etc. are among the small glaciers (Table 11.1).

A total of 5 glaciers were observed to have length less than 5 km, 18 glaciers between 5 and 10 km, and 7 glaciers more than 7 km (Fig. 11.3). Glacier types were also identified based on Sah et al. (2005). A total of 18 glaciers were identified to be of simple basin type, 5 of compound basins type (very large glaciers), and 8 of compound basin type (Fig. 11.4). Simple basin has only one area of accumulation,

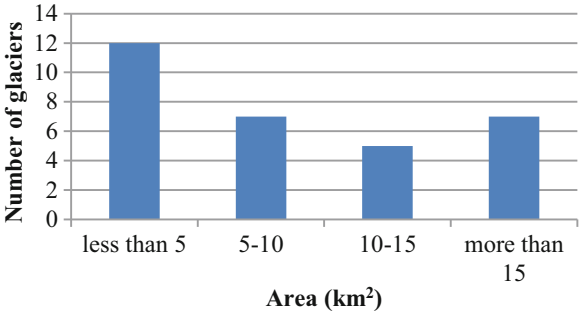

Fig. 11.2 Glacier distribution by area (Source: Suraj Mal, RB Singh, U. Schickhoff)

Table 11.1 Varying retreat rate of glaciers and relationships with local physiographic conditions (2001–2013), based on Landsat satellite images

Name	Type	Orientation	Area (km^2)	Elevation of snout	Length km (2013)	Retreat rate (m^{-1}) (2001–2013)
Bagini	Compound basins	North-west	20.08	4404	11.6	18.5
Barhaa	Compound basins	East-west	3.96	4049	3.3	18.7
Bethartoli	Compound basin	North-east	9.27	3965	6.8	20.0
Bidalgwar	Simple basin	Northeast-southeast	6.05	3728	8.4	9.4
Burphu	Simple basin	Northeast-southwest	9.35	3999	7.7	32.7
Dakkhni Nanda Devi	Compound basin	Southwest-northwest	12.25	4421	9.9	10.1
Dakkhni Rishi	Simple basin	Southwest-northeast	20.44	4558	12.2	11.8
Dunagiri	Simple basin	South-northwest	2.00	4340	4.8	11.4
Ghankhawi	Simple basin	Southwest-northwest	4.90	3930	6.1	8.3
Kafini	Simple basin	North-south	4.15	3951	6.2	19.1
Kalabaland	Compound basins	North-south	35.35	3840	15.3	21.5
Kimphu	Simple basin	West-east	6.09	4272	8.2	13.9
Lawan	Simple basin	Southwest-northeast	3.77	4213	5.8	11.8
Milam	Compound basins	Northwest-southeast	56.42	3626	16.4	28.4
Mrigthuni	Simple basin	Northwest-southeast	12.22	4282	8.2	33.8
Nanda Ghunti	Compound basin	South-northwest	12.61	4134	9.9	18.2
Pachu	Simple basin	West-northeast	4.00	4179	6.6	35.6
Pindari	Simple basin	North-south	11.00	3812	5.9	18.8
Poting	Simple basin	Northwest-southeast	5.21	3708	5.4	29.5
Ramni	Compound basin	Northeast-southwest	15.52	4814	9.2	12.5
Sakram	Simple basin	Southwest-northeast	2.92	4212	5.8	17.0
Shalang	Compound basin	Southwest-northeast	14.40	3933	11.7	11.3
Silasamudra	Simple basin	Southeast-northwest	1.89	3764	5.2	15.7
Trishul	Compound basin	South-northeast	34.19	4408	14.4	22.4

(continued)

Table 11.1 (continued)

Name	Type	Orientation	Area (km^2)	Elevation of snout	Length km (2013)	Retreat rate (m^{-1}) (2001–2013)
Unnamed Ronti	Simple basin	South-northwest	4.33	3976	5.7	22.1
Unnamed Utt[a] ND tri 1	Compound basin	North-southeast	8.01	4868	6.7	8.4
Unnamed Utt ND[b] tri 2	Simple basin	North-southwest	1.78	5105	3.4	17.1
Unnamed Utt ND tri[c] 3	Simple basin	North-south	0.45	5130	16.8	8.5
Unnamed_ inlawan	Compound basin	North	3.11	4400	4.6	5.6
Unnamed_north of Milam	Simple basin	Southwest-northeast	5.71	4963	4.7	18.1
Uttari Nanda Devi	Compound basins	North-south	30.21	4209	15.7	6.2

[a]Uttari
[b]Nanda Devi
[c]Tributary

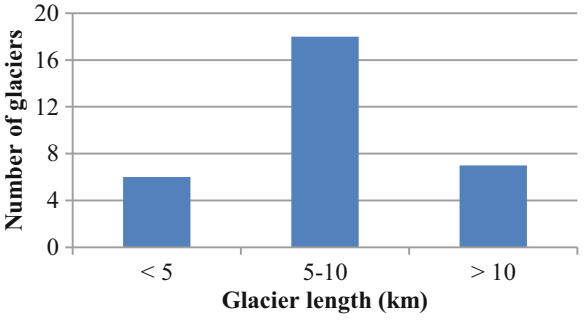

Fig. 11.3 Glacier distribution by length (Source: Suraj Mal, RB Singh, U. Schickhoff)

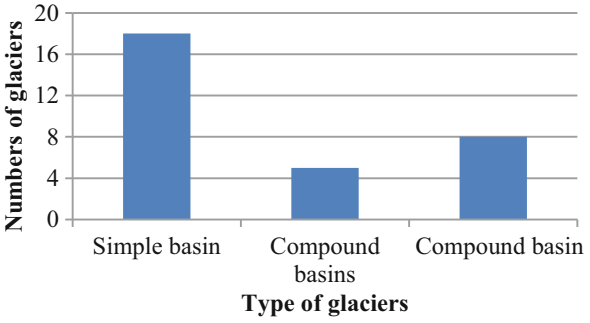

Fig. 11.4 Typology of glaciers, according to Sah et al. (2005) (Source: Suraj Mal, RB Singh, U. Schickhoff)

whereas compound basin has two or more accumulations. In the compound basins, many valley glaciers feed one glacier (Sah et al. 2005).

11.4.2 Glacier Retreat and Its Driving Forces

All the glaciers have been observed to retreat in the study area. There are, however, significant variations in glacier retreat. The retreat rate varies between 5.6 m^{-1} for Lawan Glacier and 35.6 m^{-1} for Pachu Glacier. Of the total 31 studied glaciers, 6 were observed to retreat at low rate (<10 m^{-1}), 7 between 10 and 15 m^{-1}, 9 between 15 and 20 m^{-1}, 4 between 20 and 25 m^{-1}, and 5 more than 25 m^{-1} (Fig. 11.5). Uttari Nanda Devi, Ghankhawi, Bidalgwar, etc. are some of the glaciers that have retreated with lower rates, while Poting, Burphu, Milam, Pachu, Mrigthuni, etc. have retreated at higher rates. The glacier retreat calculated for the recent decade in this study is relatively lower than estimated by Bisht et al. (2011) for a longer period of time.

The glacier recession across the mountains of the world (Oerlemans 2005; Zemp et al. 2006; Bajracharya et al. 2015) has been related to global warming and climate change in the last century (Bolch et al. 2012). However, their varying retreating rates in different parts of the globe remain largely unexplained in terms of different climate change conditions and variety of physiographic factors and due to the inaccessibility of glaciers, limiting the field-based measurements and investigations (Deota et al. 2011; Scherler et al. 2011). In fact, glaciers show differential recessional patterns across the Himalayan region (Bajracharya et al. 2015) owing to local topography; orientations; slope of bedrock; altitudes of snouts and altitudinal ranges of glacier (head to toe); area and length of glaciers; status of debris cover; area of accumulation and ablation zone; equilibrium line altitude (Kulkarni et al. 2004); trends of snowfall, rainfall, and temperature and climatic zone; etc. (Raina 2010; Scherler et al. 2011; Deota et al. 2011; Mal and Singh 2013; Venkatesh et al. 2013). It is difficult to estimate all of these factors purely based on remote sensing images, and therefore attempt has been made to analyze elevation of snout positions based on ASTER GDEM2, length of glaciers along the central flow line, and area of glaciers based on Landsat satellite images. Further, simple regression analysis was

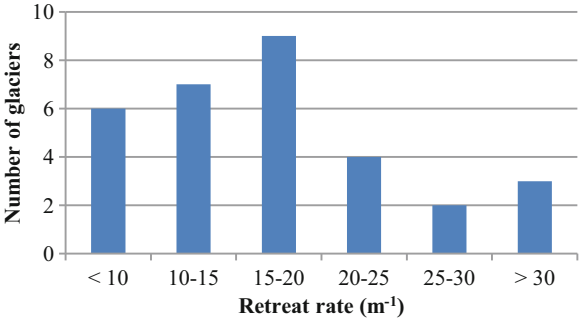

Fig. 11.5 Variation in glaciers retreat in the study area (Source: Suraj Mal, RB Singh, U. Schickhoff)

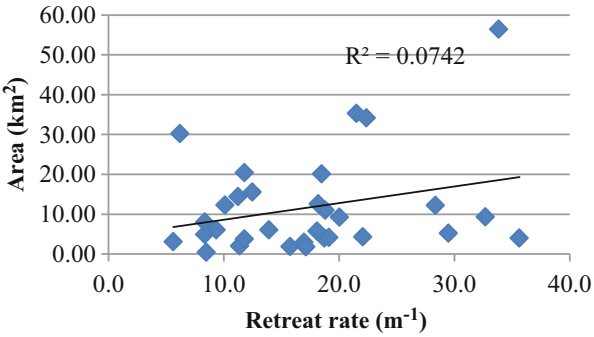

Fig. 11.6 Scatter plot showing relationship between retreat rate and glacier area (Source: Suraj Mal, RB Singh, U. Schickhoff)

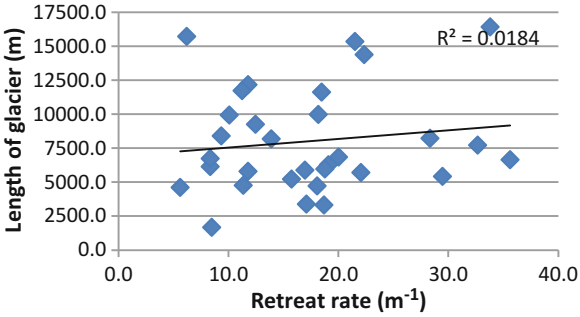

Fig. 11.7 Scatter plot showing relationship between retreat rate and glacier length (Source: Suraj Mal, RB Singh, U. Schickhoff)

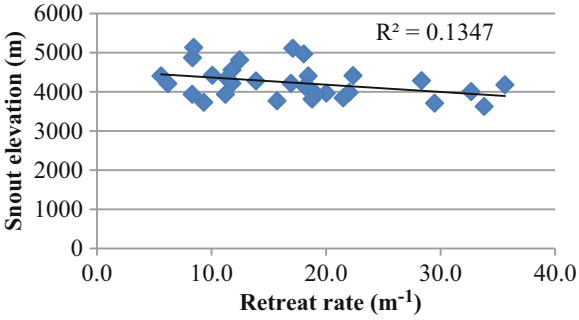

Fig. 11.8 Scatter plot showing relationship between retreat rate and snout elevation (Source: Suraj Mal, RB Singh, U. Schickhoff)

deployed to analyze the influence of these factors on the glacier retreat. The area and length of glacier did not reveal significant influence on glaciers retreat rate (Figs. 11.6 and 11.7). On the other hand, the elevation of snout positions was found to significantly influence the rate of glacier retreat (Fig. 11.8).

In our earlier studies, it was found that glaciers having higher snout elevations have retreated with relatively lower retreat rate and those with lower snout elevation retreated at higher retreat rates, as lower snout positions are in higher temperature zone and higher snout positions in lower temperature zones (Mal and Singh 2013). Similar effects were observed by Venkatesh et al. (2013). Snout elevations were recorded as high as 4500–5100 m above mean sea level (Dunagiri, Ramni, Dakkhini Rishi glaciers), and these glaciers retreated at lower rates (<15 m^{-1}). Some of the glaciers (Milam, Poting, Kalabaland glaciers) with lower elevation snout positions retreated at relatively higher rates.

In many studies, the rise of temperature has been regarded as the main and direct important factor of glacier retreat (Zemp et al. 2006; Bhambri et al. 2011b). Likewise, the negative trend of snowfall in winter season in Indian Himalayan region (Shekhar et al. 2010), as a result of rising temperature (Dimri and Kumar 2008), is also responsible for it, as snowfall feeds snow to upper glacier regions. Decline in snowfall may result in poor health of glaciers (Duan et al. 2006) and negative mass balance even in the accumulation zone. Therefore, status and trend of snowfall is very important to understand the health of glaciers (Bolch et al. 2012). The combined effects of reduced precipitation and warmer temperature conditions have led to glacier shrinkages (Jiawen et al. 2006; Bajracharya et al. 2014).

Many areas in recent decades are also experiencing transformation of precipitation from snowfall to rainfall (Bhutiyani et al. 2007, 2009; Dimri and Kumar 2008). Such changes have accelerated the rate of melting of glacier ice (Bolch et al. 2012), thus leading to increased retreat rates. The rainwater has higher temperature than that of ice. Consequently, when rainwater falls on glacier ice, the glacier ice melts quickly and higher retreat rates are observed (Mal and Singh 2013).

Similar effects have been observed at glaciers with many supraglacial lakes or glacial lakes in front of snouts, e.g., at Rolwaling Glacier and Tsho Rolpa Glacier Lake in Nepal (ICIMOD 2011). Direct and prolonged contact of glacial lakes with glacier ice and snouts accelerates the melting of glacial ice and further increases its retreat. The glacial lakes have also increased across the Himalayan region leading to increasing melting rates of glaciers (Nie et al. 2013; Dobhal et al. 2013). In some cases, streams emerging from the upper tributary glaciers terminate on main valley glaciers. It also increases the melting of glacial ice, and consequently higher retreat rates of glaciers are observed. Similar conditions are found in case of Milam Glacier (Mal and Singh 2013). There is a small stream terminating into the main valley glacier that emerges from one of the right tributary glaciers. It has led to higher melting rate of snout of Milam Glacier in its right side.

Debris cover also significantly influences the melting rate of Himalayan glaciers leading to changing dynamics of snout positions, modification of albedo and energy balance over glacier surface, and modification in response of glaciers to changing climatic conditions (Veettil et al. 2014; Dobhal et al. 2013). Ice melting is significantly determined by thickness and area of debris cover over the glaciers (Scherler et al. 2011; Schmidt and Nüsser 2009). Thin and patchy debris covers are found in the upper ablation zone, which enhances the melting of the ice in summer season

(Schmidt and Nüsser 2009). A thin debris cover leads to downwasting and surface lowering of glaciers (Schmidt and Nüsser 2009). Thicker debris cover, on the contrary, is confined to the lower ablation zone of glaciers and acts as a protector of glacier ice and reduces the melting rate (Dobhal et al. 2013; Hewitt 2005; Schmidt and Nüsser 2009). It also slows down the glacier's response to climatic warming (Scherler et al. 2011). According to Dobhal et al. (2013), a higher melting rate is recorded in case of thin (<5 cm) debris cover in the upper ablation zone, and melting is significantly lower in case of a thick (>5 cm) debris cover in lower ablation zone. Similarly, Scherler et al. (2011) suggest that most of the heavily debris-covered Himalayan glaciers have stable fronts and Tibetan glaciers retreat at higher rates, where debris cover is negligible. Therefore, observed retreat of snout positions may not directly represent changing climatic conditions and can lead to erroneous conclusions (Venkatesh et al. 2013; Schmidt and Nüsser 2009).

11.5 Conclusion

The glaciers in the study area have retreated in recent past. There are, however variations in the rate of retreat. Glaciers have shown different behavior even within the same basins and under similar climatic conditions. Such variations of glaciers may be linked to local physiographic conditions (slope, aspect, elevation of snout, elevation range between snout and head of the glacier, etc.), characteristics of glaciers (total area, accumulation area, ablation area, status of equilibrium line altitude, length-width-depth), status of debris cover, and trends of temperature and precipitation. Therefore, the snout behavior of individual glaciers may not be direct reflection of climatic warming; instead, it may be the adjustment of glaciers to local physiographic and atmospheric conditions. Consequently, the snout retreat has to be carefully interpreted in the light of multiple influencing factors. The mass balance of glaciers may be considered a more suitable proxy of changing climatic conditions.

Acknowledgment The study was supported by DAAD under short research stay program, which was conducted at CEN Center for Earth System Research and Sustainability, Institute of Geography, University of Hamburg, Germany. The authors are thankful to Dr Manish Mehta, Scientist, Wadia Institute of Himalayan Geology (WIHG), Dehradun, India, for valuable discussions and suggestions.

References

Bahuguna IM, Kulkarni AV, Nayak S, Rathore BP, Negi HS, Mathur P (2007) Himalayan glacier retreat using IRS 1C PAN stereo data. Int J Remote Sens 28(2):437–442. doi:10.1080/01431160500486674

Bajracharya SR, Mool PK, Shrestha BR (2007) Impact of climate change on Himalayan glaciers and glacial lakes : Case Studies on GLOF and Associated Hazards in Nepal and Bhutan.

International Center for Integrated Mountain Development (ICIMOD), Kathmandu, Nepal. http://lib.icimod.org/record/22442/files/attachment_169.pdf
Bajracharya SR, Maharjan SB, Shrestha F (2014) The status and decadal change of glaciers in Bhutan from the 1980s to 2010 based on satellite data. Ann Glaciol 55(66):159–166. doi:10.3189/2014AoG66A125
Bajracharya SR, Maharjan SB, Shrestha SB, Guo W, Liu S, Immerzeel W, Shrestha B (2015) The glaciers of the Hindu Kush Himalayas: current status and observed changes from the 1980s to 2010. Int J Water Resour Dev 31:1–13. doi:10.1080/07900627.2015.1005731
Banerjee AK (2003) Nanda Devi Biosphere Reserve: the landscape plan of management (Part-1). Ministry of Environment and Forests. Government of India, New Delhi
Bhambri R, Bolch T, Chaujar RK (2011a) Mapping of debris-covered glaciers in the Garhwal Himalayas using ASTER DEMs and thermal data. Int J Remote Sens 32(23):8095–8119
Bhambri R, Bolch T, Chaujar RK, Kulshreshtha SC (2011b) Glacier changes in the Garhwal Himalaya, India, from 1968 to 2006 based on remote sensing. J Glaciol 57(203):543–556
Bhambri R, Bolch T, Chaujar RK (2012) Frontal recession of Gangotri Glacier, Garhwal Himalayas, from 1965 to 2006, measured through high resolution remote sensing data. Curr Sci 102(10):489–494
Bhutiyani MR, Kale VS, Pawar NJ (2007) Long-term trends in maximum, minimum and mean annual air temperatures across the Northwestern Himalaya during the twentieth century. Clim Chang 85(1–2):159–177
Bhutiyani MR, Kale VS, Pawar NJ (2009) Climate change and the precipitation variations in the northwestern Himalaya: 1866–2006. Int J Climatol 30(4):535–548
Bisht MPS, Mehta M, Nautiyal SK (2011) Impact of depleting glaciers on the Himalayan biosphere reserve- a case study of Nanda Devi Biosphere Reserve, Uttarakhand Himalaya. In: Bisht MPS, Pal D (eds) Mountain resource management: application of remote sensing and GIS. Transmedia Publication, Srinagar, pp 17–31
Bolch T, Buchroithner M, Pieczonka T, Kunert A (2008) Planimetric and volumetric glacier changes in the Khumbu Himal, Nepal, since 1962 using Corona, Landsat TM and ASTER data. J Glaciol 54(187):592–600
Bolch T, Kulkarni AV, Kaab A, Huggel C, Paul F, Cogley JG, Frey H, Kargel JS, Fujita K, Scheel M, Bajracharya S, Stoffel M (2012) The state and fate of Himalayan glaciers. Science 336:310314. doi:10.1126/science.1215828
Chander G, Markham B, Helder D (2009) Summary of current radiometric calibration coefficients for Landsat MSS, TM, ETM+ and EO-1 ALI Sensors. Remote Sens Environ 113:893–903
Deota BS, Trivedi YN, Kulkarni AV, Bahuguna IM, Rathore BP (2011) RS and GIS in mapping of geomorphic records and understanding the local controls of glacial retreat from the Baspa Valley, Himachal Pradesh, India. Curr Sci 100(10):1555–1563
Dimri AP, Kumar A (2008) Climatic variability of weather parameters over the western Himalayas: a case study. In: Satyawali PK, Ganju A (eds) Proceedings of the national snow science workshop, 11–12 January 2008, Chandigarh, India. Snow and Avalanche Study Establishment (SASE), Chandigarh, pp 167–173
Dobhal DP, Gergan JT, Thayyen RJ (2004) Recession and morphogeometrical changes of Dokriani Glacier (1962–1995), Garhwal Himalaya, India. Curr Sci 86:692–696
Dobhal DP, Mehta M, Srivastava D (2013) Influence of debris cover on terminus retreat and mass changes of Chorabari Glacier, Garhwal region, central Himalaya, India. J Glaciol 59(217):961–971. doi:10.3189/2013JoG12J180
Duan K, Yao T, Thompson LG (2006) Response of monsoon precipitation in the Himalayas to global warming. J Geophys Res 111:D19110. doi:10.1029/2006JD007084
Gerlitz L, Conrad O, Thomas A, Böhner J (2014) Warming patterns over the Tibetan Plateau and adjacent lowlands derived from elevation- and bias-corrected ERA-Interim data. Clim Res 58:235–246. doi:10.3354/cr01193
Hewitt K (2005) The Karakoram anomaly? Glacier expansion and the 'elevation effect', Karakoram Himalaya. Mt Res Dev 25(4):332–340

ICIMOD (2011) Glacial lakes and glacial lake outburst floods in Nepal. International Centre for Integrated Mountain Development, Kathmandu

Jiawen R, Zhefan J, Jianchen PU, Xian Q (2006) Glacier variations and climate change in the central Himalaya over the past few decades. Ann Glaciol 43:218–222

Kamp U, Byrne M, Bolch T (2011) Glacier fluctuations between 1975 and 2008 in the greater Himalaya range of Zanskar, Southern Ladakh. J Mt Sci 8:374–389. doi:10.1007/s11629-011-2007-9

Khalsa SJS, Dyurgerov MB, Khromova T, Raup BH, Barry RG (2004) Space-based mapping of glacier changes using ASTER and GIS tools. IEEE Trans Geosci Remote Sens 42(10):2177–2183

Kulkarni AV, Karyakarte Y (2014) Observed changes in Himalayan glaciers. Curr Sci 106(2):237–244

Kulkarni AV, Rathor BP, Alex S (2004) Monitoring of glacial mass balance in the baspa basin using accumulation area ratio method. Curr Sci 86(1):185–190

Kulkarni AV, Bahuguna IM, Rathore BP, Singh SK, Randhawa SS, Sood RK, Dhar S (2007) Glacial retreat in Himalaya using Indian remote sensing satellite data. Curr Sci 92(1):69–74

Mal S, Singh RB (2013) Differential recession of glaciers in Nanda Devi Biosphere Reserve, Garhwal Himalaya, India. In: Cold and mountain region hydrological systems under climate change: towards improved projections. Proceedings of H02, IAHS-IAPSO-IASPEI Assembly, Gothenburg, Sweden. IAHS Publ 360. IAHS Press, Wallingford, pp 71–76

Mehta M, Dobhal DP, Bisht MPS (2011) Change of Tipra Glacier in the Garhwal Himalaya, India, between 1962 and 2008. Prog Phys Geogr 35(6):721–738. doi:10.1177/0309133311411760

Nie Y, Liu Q, Liu S (2013) Glacial lake expansion in the Central Himalayas by Landsat Images, 1990–2010. PLoS One 8(12):83973. doi:10.1371/journal.pone.0083973

Oerlemans J (2005) Extracting a climate signal from 169 glacier records. Science 308:675–677

Paul F, Huggel C, Kaab A (2004) Combining satellite multispectral image data and a digital elevation model for mapping debris-covered glaciers. Remote Sens Environ 89:510–518

Paul F, Barrand NE, Baumann S, Berthier E, Bolch T, Casey K, Frey H, Joshi SP, Konovalov V, Le Bris R, Mo¨ Lg N, Nosenko G, Nuth C, Pope A, Racoviteanu A, Rastner P, Raup B, Scharrer K, Steffen S, Winsvold S (2013) On the accuracy of glacier outlines derived from remote-sensing data. Ann Glaciol 54:171–182. doi:10.3189/2013AoG63A296

Raj KBG (2011) Recession and reconstruction of Milam glacier, Kumaon Himalaya, observed with satellite imagery. Curr Sci 100(9):1420–1425

Raj KBG, Kumar KV, Mishra R, Mukhtar MA (2014) Remote sensing based assessment of glacial lake growth on Milam glacier, Goriganga Basin, Kumaon Himalaya. J Geol Soc India 83:385–392

Raina VK (2010) MoEF discussion paper: Himalayan glaciers – a state-of-art review of glacial studies, glacial retreat and climate change. Ministry of Environment and Forests and GB Pant Institute of Himalayan Environment and Development, Almora

Rastner P, Bolch T, Totarnicola C, Paul F (2014) A comparison of pixel- and object-based glacier classification with optical satellite images. IEEE J Sel Top Appl Earth Obs Remote Sens 7(3):853–862. doi:10.1109/JSTARS.2013.2274668

Sah M, Philip G, Mool PK, Bajracharya SR, Shrestha B (2005) Uttaranchal Himalaya, India inventory of glaciers and glacial lakes and the identification of potential glacial lake outburst floods (GLOFs) affected by global warming in the mountains of Himalayan region. Wadia Institute of Himalayan Geology (WIHG), International Centre for Integrated Mountain Development (ICIMOD), Asia-Pacific Network for Global Change (APN), Global Change SysTem for Analysis, Research, and Training (START) and United Nation's Environmental Programme (UNEP)

Scherler D, Bookhagen B, Strecker MR (2011) Spatially variable response of Himalayan glaciers to climate change affected by debris cover. Nat Geosci Lett 4:156–159. doi:10.1038/NGEO1068

Schmidt S, Nüsser M (2009) Fluctuations of Raikot Glacier during the past 70 years: a case study from the Nanga Parbat massif, northern Pakistan. J Glaciol 55(194):949–959

Shekhar MS, Chand H, Kumar S, Srinivasan K, Ganju A (2010) Climate-change studies in the western Himalaya. Ann Glaciol 51(54):105–111

Veettil BK, Bremer UF, Grondona AFB, Souza SFD (2014) Recent changes occurred in the terminus of the debris-covered Bilafond Glacier in the Karakoram Himalayas using remotely sensed images and digital elevation models (1978–2011). J Mt Sci 11(2):398–406. doi:10.1007/s11629-013-2677-6

Venkatesh TN, Kulkarni AV, Srinivasan J (2013) Relative effect of slope and equilibrium line altitude on the retreat of Himalayan glaciers. Cryosphere 6:301–311. doi:10.5194/tc-6-301-2012

Zemp M, Haeberli W, Hoelzle M, Paul F (2006) Alpine glaciers to disappear within decades? Geophys Res Lett 33:1–4. doi:10.1029/2006GL026319

Chapter 12
Instability Processes Triggered by Heavy Rain in the Garhwal Region, Uttarakhand, India

Manish Mehta, D.P. Dobhal, Tanuj Shukla, and Anil K. Gupta

Abstract On 16 and 17 June 2013, high-intensity rainfall (>400 mm) in different parts of the state of Uttarakhand caused devastating flash floods and triggered widespread landslides incurring heavy losses to the infrastructure, agricultural fields, human and animal lives, roads and widespread destruction of natural resources. Such a magnitude of disaster was perhaps not witnessed by the region at least over the last 100 years. Thus, this disaster can be considered as an extreme climatic event of the century. The extent and intensity of the tragedy can easily be visualised by the fact that all the famous shrines of the Uttarakhand state, located in high mountainous, snow-bound areas such as Badrinath (3133 m asl on Alaknanda River), Kedarnath (3584 m asl on Mandakini River), Gangotri (3140 m asl on Bhagirathi River), Yamunotri (3291 m asl on Yamuna River) and Hemkund Sahib (4433 m asl on Alaknanda River), were badly affected by this extreme fury of the nature.

Keywords Rainfall • Disaster • Alaknanda River • Uttarakhand • Indian Himalaya

12.1 Introduction

The Himalaya, the youngest mountain chain in the world, is very fragile and vulnerable to the climate change. The lofty mountains of the Himalaya are home to the largest ice mass outside the polar regions, aptly termed as Third Pole. There are ~9575 glaciers with an estimated area of 37,466 Km^2 in the Indian administrative part of the Himalaya (Raina and Srivastava 2008). The distributions of the glaciers in the Indian Himalayan states are uneven. This variability may be due of the vast extension of the Himalaya along with rugged topography and varying climatic

M. Mehta (✉) • A.K. Gupta
Wadia Institute of Himalayan Geology, Dehradun, Uttarakhand, India
e-mail: msmehta75@gmail.com

D.P. Dobhal • T. Shukla
Centre for Glaciology, Wadia Institute of Himalayan Geology, Dehradun, Uttarakhand, India

R.B. Singh et al. (eds.), *Climate Change, Glacier Response, and Vegetation Dynamics in the Himalaya*, DOI 10.1007/978-3-319-28977-9_12

conditions. They are perennial source of water to the three great rivers of India – the Indus, the Ganga and the Brahmaputra – and lifeline of millions of people in the region.

Recent climate changes have a significant impact on high-mountain glacial environment. Due to continuously rising air temperature all over the world, the precipitation pattern at higher altitude is changing from solid (snow) to liquid (rain) (Immerzeel et al. 2010). This high-altitude rain causes rapid melting of snow/ice resulting in the formation and expansion of moraine-dammed, supraglacial and cirque lakes which will be potentially dangerous in downstream valley (Dobhal et al. 2013).

The recent flash flood which occurred on 16 and 17 June 2013 in different parts of Uttarakhand state resulted in heavy loss of infrastructure, agricultural fields, lives and roads and widespread devastation of natural resources. Such a cumulative large-scale disaster has not been recorded in the history of the region in at least last 100 years. Thus this disaster is to be considered as an extreme climatic event of the century. The extent and intensity of the tragedy can easily be visualised by the fact that all the famous shrines of the Uttarakhand state, located in high mountainous, snow-bound areas such as Badrinath (3133 m asl Alaknanda river), Kedarnath (3584 m asl, Mandakini river), Gangotri (3140 m asl Bhagirathi river), Yamunotri (3291 m asl Yamuna river) and Hemkund Sahib (4433 m asl, Alaknanda), were badly affected by this fury of nature. Mandakini river valley of Rudraprayag district is amongst the worst affected where maximum damage and casualties have been reported. Due to this flash flood event, the landscape of Uttarakhand has changed, making the whole region more fragile and vulnerable.

12.2 Physiographical Setting of the Area

The investigated area is situated between Devprayag and Badrinath (Fig. 12.1). Geologically, the area is composed of Palaeozoic-Mesozoic sedimentary succession resting upon the crystalline basement with fault/thrust contact. The area between Devprayag and Badrinath lies in meta-sedimentary Garhwal group rock and Vaikrita Group (Valdiya et al. 1999) of Central Crystalline (Heim and Gansser 1939). In general, rock types are sandstone, slate, phyllite, conglomerate, etc. in Garhwal group and mica schist, quartzites, mylonite, gneiss, pegmatite, granite, etc. in Vaikrita group. The sequence has been intruded by the Badrinath and Gangotri granite dated 465 ± 5 ma (Bhanot et al. 1978). Tectonically, the southern front of the mountain is divided into three lithotectonic units that are separated by southward younging thrusts. The southern and the youngest is Himalayan Frontal Thrust (HFT) that brings Siwaliks on to Ganga foreland, the Main Boundary Thrust (MBT) brings Lesser Himalayan metasedimentaries over Siwaliks and then the Main Central Thrust (MCT) thrusts Higher Himalayan Crystallines over the Lesser Himalaya. All these thrust zones are characterised by zones of weak and pulverised rocks that are prone to failures.

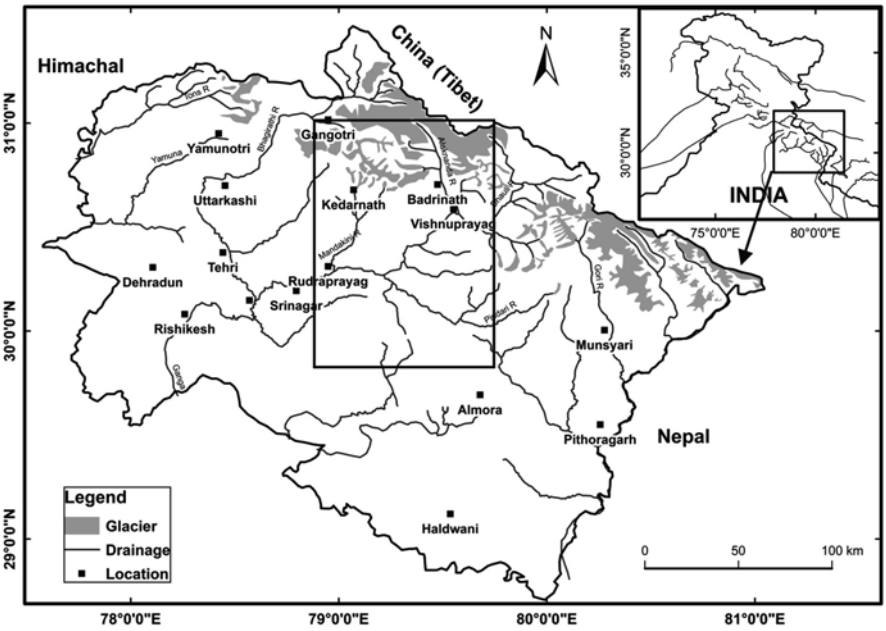

Fig. 12.1 Drainage and glacier map of Uttarakhand. The *rectangle box* shows the study area (Source: Author)

In the Himalaya, the precipitation and basin runoff generally decrease from the east to west due to gradual weakening of westward-moving Indian Summer Monsoon (ISM) trough (Immerzeel et al. 2010; Ali et al. 2013). In the east, ISM precipitation dominates, while in the west, westerly circulation and cyclonic storms contribute about two-third of the total annual precipitation. Westerlies contribute two-third of the total snowfall in high altitudes during winter; the remaining one-third results from summer precipitation during southwest monsoon circulation (Armstrong 2011). The Uttarakhand is located on the western fringe of the Central Himalaya, dominated by monsoon precipitation in summer and winter precipitation from western disturbances (Owen et al. 1996). The general climate of the Uttarakhand is temperate, marked by seasonal variations in temperature and is affected by tropical monsoons. January is the coldest month, with daily high temperatures averaging below freezing in the north and near 21 °C in the southeast. In the north, July is the hottest month, with temperatures typically rising from about 7 °C to about 20 °C daily. In the southeast, May is the warmest month, with daily temperatures normally ranging between 38 and 27 °C. Most of the state's roughly 1500 mm annual precipitation is brought by the southwest monsoon, which occurs from July through September. In the northern parts of the state, 3–5 m of snowfall is common between December and March. General pattern of rainfall distribution shows two belts of high precipitation that are controlled by orographic structure of the mountain range. The first high-precipitation belt lies in the south over Siwalik Hills where average rainfall is 1200 mm/a, and the second lies over the physio-

graphic transition of the Lesser and Higher Himalaya where around 2000 mm of rainfall occurs annually. The remaining part of the mountain is rather semi-arid. During 16–17 June 2013 places like Uttarkashi, Devprayag and Haridwar recorded more than 300 mm of rainfall within 2 days.

The climate of glaciated regions of the Himalaya, because of inaccessibility of the areas and poor meteorological and hydrological data, is rather not well documented. The Chorabari Glacier that lies at the head of Mandakini River has been monitored by Wadia Institute of Himalayan Geology, Dehradun, since 2003. This meteorological observatory (3820 m asl) installed monitors air temperature, wind speed and precipitation of glacier at an altitude of 3820 m asl. The data from this observatory as published recently by Mehta et al. (2014) suggests the average daily air temperature range from −13.5 to 11.6 °C, while the maximum and minimum air temperature range between −9.4 to 16.7 °C and −19.5 to 9.8 °C, respectively, between 2007 and 2012 (Mehta et al. 2014).

Summer precipitation in glaciated regions is highly influenced by the monsoon, and average rainfall recorded between 2007 and 2012 was 1309 mm (June–October). Winter precipitation generally occurs between December and March when the westerlies are dominant in the area as they move eastward over northern India and is the main source of snow accumulation. No instrumental data was available for winter snowfall; however, residual snow depth fluctuated between 25 and 50 cm in April and early May at 4000 m asl during the period from 2003 to 2010 (Dobhal et al. 2013); snow normally melts before the commencement of the monsoon in mid-June.

12.3 Result and Discussion

12.3.1 The Event of June 2013

Exceptional early monsoon rain between 15 and 17 June 2013 combined with melting snow caused horrific flood in the rivers of the Garhwal Himalaya (Bhagirathi, Alaknanda, Mandakini and Yamuna River) and subsequently triggered widespread landslides. Thousands of pilgrims got stranded at various pilgrim places and en route (Dobhal et al. 2013). Due to heavy downpour, the activation of landslide and flash flood in the region has caused huge damage to lives, infrastructure and property in Garhwal, Uttarakhand. In downstream of these rivers, places like Lambagar, Govindghat, Bhyundar and Pulna village in Alaknanda valley and Kedarnath, Rambara, Gaurikund and Sonprayag in Mandakini valley and Uttarkashi, Gangotri, Sangamchatti and Dharli in Bhagirathi basin were severely damaged or completely washed out. The catastrophic event of June 2013 took more than 6000 human lives with more than this number being untraceable, and >100,000 people have been affected. The quick survey by an agency of the World Bank estimated the financial loss incurred due the event was more than $250 million, and over US$500 million damage appeared in the media. Due to this flash flood event in the Uttarakhand, the

landscape of the area has changed making the whole region more fragile and vulnerable. Such a magnitude of disaster was perhaps not witnessed by the region at least over the last 100 years (Rautela 2013).

The extent and intensity of the tragedy can easily be visualised by the fact that all the famous shrines of the Uttarakhand state, located in high mountainous, snow-bound areas, such as Badrinath (3133 m asl on Alaknanda River), Kedarnath (3584 m asl on Mandakini River), Gangotri (3140 m asl on Bhagirathi River), Yamunotri (3291 m asl on Yamuna River) and Hemkund Sahib (4433 m asl on Alaknanda River) were badly affected by this extreme fury of the nature. In this report we cover the devastated area that lies within the Bhagirathi River basin, which forms the part of Uttarkashi, Tehri and Pauri district in the Lesser and Higher Garhwal Himalaya. The area is characterised by highly rugged topography and very high relief having sharp ridges with prominent dip slopes. Lithologically, the area constitutes medium- to high-grade metamorphic and sedimentary rocks classed as Garhwal formation and Central Crystalline.

12.3.2 Mandakini Valley

The Mandakini River is a tributary of Alaknanda River which originates from Chorabari Glacier and comprising of an area of 2250 Km^2. The elevation variations in the basin are ranging from 640 to 6940 m asl forming broad U-shaped valley in the upper reaches and V-shaped gorges in down valley while flowing through Higher and Lesser Himalayan terrains. The major tributaries of this river are Vasuki Ganga (Son Ganga), Kali Ganga, Madhyamaheshwar and Markanda Ganga, while other small tributaries are Laster Gad, Helaun Gad, Kakragad, Kyunja Gad, Kyar Gad and Ghasta Gad flowing on both sides of the valley and finally merging into the Alaknanda River at Rudraprayag (Fig. 12.2). The valley has complex topography having high mountain chains with glacierised basin in the north and fluvial terraces in the central and lower parts. The Chorabari and Companion are two largest glaciers besides a few other small glaciers including ice apron, hanging glaciers, glacierete and cirque glaciers (Mehta et al. 2012). The area has a couple of high-altitude lakes which are directly fed by snow/ice melt and rainwater. Geologically the area falls in the Lesser Himalaya and Higher Himalaya consisting of metabasics, phyllites, carbonates and quartzites in the lower valley and mainly Central Crystalline rocks in the higher reaches comprising of alternate band of deformed amphibolites, calc silicate lances, quartzites, mylonitic, biotite-rich fine grain gneisses, augen gneisses and phyllonites (Valdiya et al. 1999).

During the recent flash flood that occurred on 16 and 17 June 2013, the Mandakini river valley is amongst the worst affected area of the Uttarakhand where the maximum damage and casualties have been reported (Dobhal et al. 2013). Two hydropower projects which are under the conduction stage in the valley have also been affected by this flash flood event.

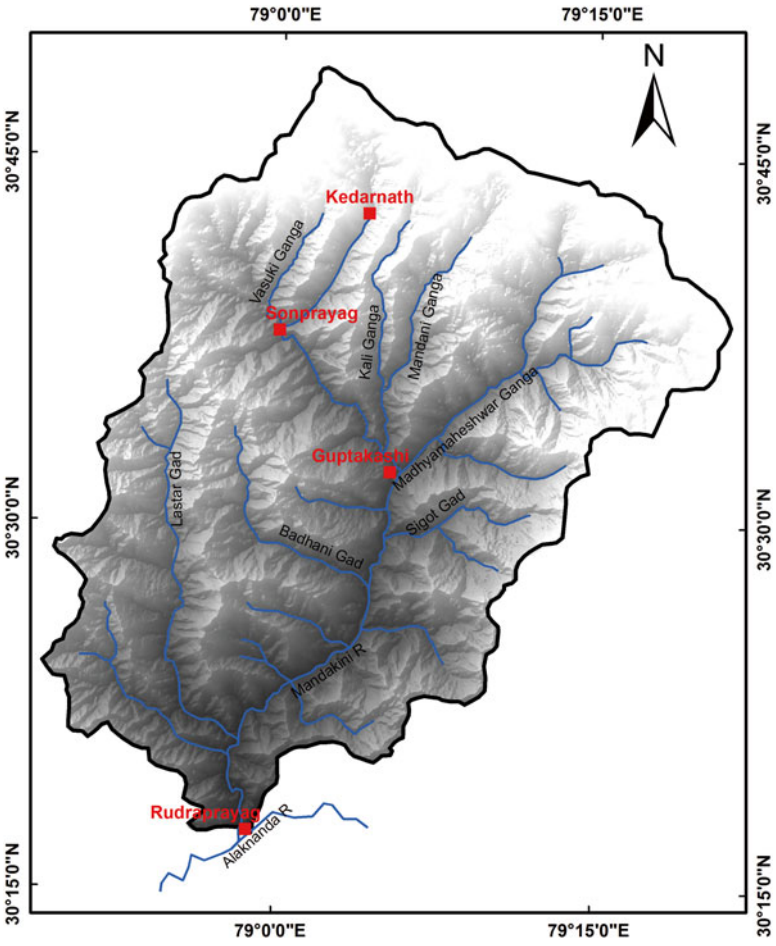

Fig. 12.2 Topography and drainage pattern of Mandakini valley (Source: Author)

12.3.2.1 Flood Event and Assessments

Between en route of Rudraprayag and Gaurikund, about 80 Km motor road (NH 112) is either badly damaged or washed out at different places. The large number of massive landslides has been activated on both sides of the valley (Fig. 12.3). Agastyamuni Tilwara towns and villages located on the right and left banks of the river are badly damaged or road completely washed out. The riverbed is refilled by the sediments, and the riverbed level is raised by 5–10 m. The powerhouse site of (L&T) is completely covered by debris (Fig. 12.3). Most of muck disposal sites (Total 14 No) in the upstream and downstream of the powerhouse have been rolled out during the swelling flow of Mandakini. It is also observed that the Mandakini has shifted its course in many places and now flowing on the left bank along with

Fig. 12.3 The number of massive landslides has been activated on both sides of the valley, and the powerhouse site of (L&T) is completely covered by debris (Source: Author)

the motor road, and sediments are deposited on the right bank. The sizes of the boulders vary from 1 to 5 m and are semi-angular in shape indicating that they have not been transported from long distance (Fig. 12.3). The maximum discharge recorded was 1378 m^3 on 16 June at 9 am (L&T official data, no data collected 16 onwards), and rainfall recorded at Kund site during the period was 104.8 and 117.4 mm on 16 and 17 June 2013, respectively (Figs. 12.4 and 12.5).

At Kund (near semi-village) 10 Km upstream from the powerhouse, where the barrage site is located (under construction), is badly damaged on the right side of the river. Here, huge amounts of sediments are deposited over the riverbed. Upslope in the north from the barrage site, evidences of subsidence are clearly visible in and around the semi-village and motor road (Fig. 12.3). On the way to Kalimath, the

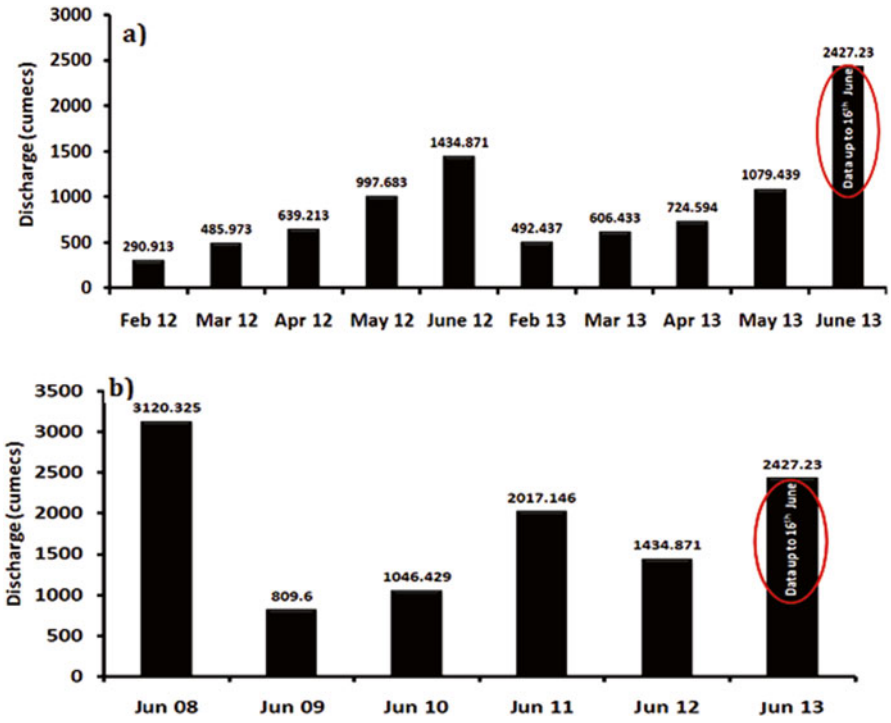

Fig. 12.4 Monthly discharge (**a**) and discharge in June (2008–2013, **b**) in Mandakini river at Singoli-Bhatwari Power House (Source: L&T office)

road is extensively damaged either by landslides or river toe cutting. A number of landslides (old and new) have occurred throughout the valley. A massive landslide (~400×60 m, Fig. 12.3) occurred on the left bank of Kali River just 200 m down from Kalimath and has completely ruined about 800 m of motor road, and a huge amount of sediment is deposited on the left bank of Kali River. There are signatures of damming and breaching of river at many places as huge amounts of sediments are deposited at both banks of the river. A lot of sediments have already been transported with river water during the flash flood. On the way to Kalimath, river Madmaheshwar joins to Kali Ganga near Guptkashi. It seems that Madmaheshwar was also caught by the flash flood as a huge amount of sediments is spread over at the termini of the river. The thickness of sediments deposited here is about 10–15 m as a house which is built near the river bank is completely overlaid by flood sediments. The hydropower site located in the valley is also washed away during the flood (Fig. 12.3).

Upstream from Kalimath towards Sitapur (Phata-Byung project, Lanco), the valley is deep and narrow and has not much damage except a few landsides observed all along either sides of river Mandakini. Upstream the valley (From Sitapur town) is again extensively affected by the flood; near Sitapur town, the barrage site of Phata-Byung project is completely smashed; however, the location of the barrage site is

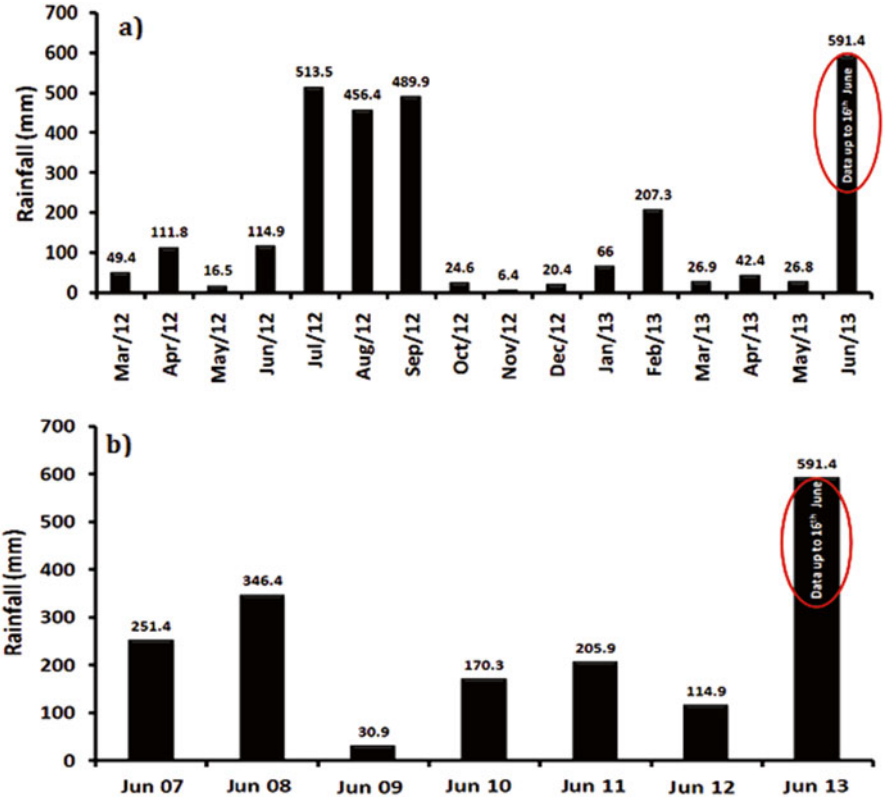

Fig. 12.5 Monthly average rainfall (**a**) and average rainfall for June (2007–2013, **b**) in lower Mandakini River basin at Singoli-Bhatwari (Source: L&T office)

narrow, and bounded by steep rock wall and upslope side, the area has become slightly wide (Fig. 12.6). As per the information received from project officers, the water level started rising from 16 June evening onwards. Due to the high river flow, huge amount of sediments including large boulders and chunks of trees filled the river and blocked the river at the barrage site. The amount of water was so huge that the river level rose by ~15–20 m. The main tunnel (~4 m dia) was also filled by the flood sediments. On 17 June at 9 am, the discharge suddenly increased, which may be due to breaching of the Chorabari lake at Kedarnath area washing out the barrage site as well as the settlements near Sitapur. This process continued up to late evening, because of continuous rain in the area. The river flows started to reduce on 18 June and returned to its normal flow on 19 June. The signature of river flood level and deposition of sediments (fine sand silt deposit) clearly indicates that there was impounding of water and breach of lake on 17 June as large volume of water came from the Chorabari. It is also observed that the sediments including boulders that came from higher area settled down between Gaurikund and Sitapur.

Fig. 12.6 Toe cutting by the river that destroyed the dam site (Source: Author)

12.3.3 Alaknanda Valley (8 and 9 December 2013)

Alaknanda River originates from Satopanth Glacier (3870 m asl), located just 10 Km upstream from Shri Badrinath shrine. The major tributaries (up to Vishnuprayag, confluence of Alaknanda and Dhauliganga) are Saraswati, Khir Ganga, Lakshman Ganga (Bhyundar Ganga) and Khanakul Ganga, which originated from Tara Glacier (5068 m asl), Khiro Glacier (3940 m asl), Tipra Glacier (3795 m asl) and Kagbhusandi Lake (4370 m asl), respectively (Fig. 12.7). The Alaknanda River merges into Dhauliganga at Vishnuprayag (1445 m asl), which

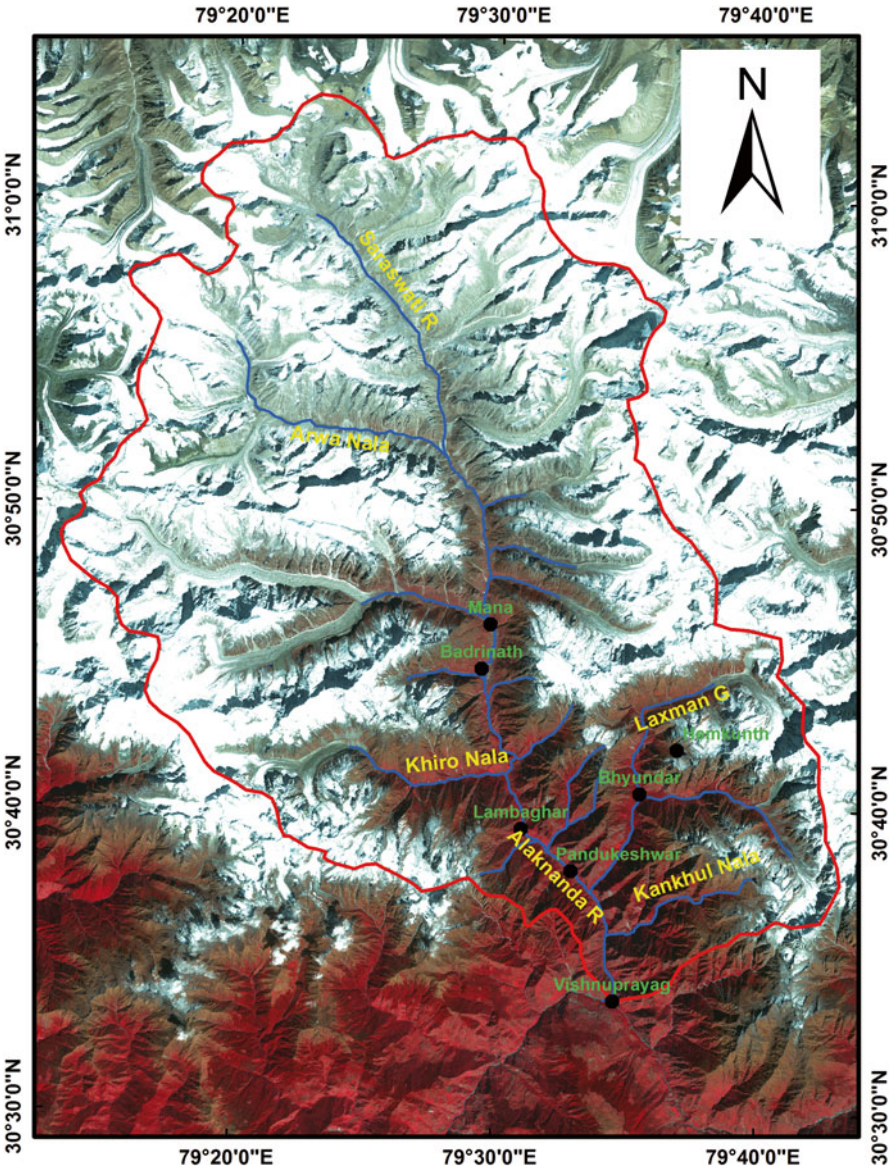

Fig. 12.7 Topography and drainage pattern of Alaknanda valley (Source: Author)

originated from Niti Glacier (4136 m asl). The valley has complex topography having high snow-clad mountain chains with glacierised and glaciated valleys in the north and fluvial terraces in the central and lower parts. A variety of drainage pattern show predominant control of structural elements combined with sub-aerial denudation processes.

Geomorphologically the area is rugged terrain with mountainous ridges, intervening deep gorges and steep to very steep slope valleys. Both valley side slopes at their base forms large number of convex features due to colluvial fan deposits. Gentle slopes are normally either along the valley floors or high-altitudinal zone in the form of meadow (bugyal, Alpine zone). Geologically, the area forms a part of the Central Crystalline of the Higher Garhwal Himalaya (Heim and Gansser 1939). The Central Crystalline is separated from the calc-zone of Chamoli formation by the Main Central Thrust (MCT) which passes through at Helang south of Vishnuprayag (1445 m asl). In the north, the northwest-southeast trending Tethyan Thrust separates Central Crystalline from the Tethyan sedimentary zone. At Vishnuprayag the rocks are primarily made of quartzites, folded biotite gneiss at the base overlaid by micashist. The Pandukeshwar quartzites form the steep-sloped high-relief zone in the upper Alaknanda valley.

12.3.3.1 Flood Event and Assessments

Along the valley from Satopanth Glacier (head of the river) to Vishnuprayag (termination of river into Dhauliganga), the worst affected area is observed between Lambagar and Govindghat. It has been observed that in the higher areas like Badrinath (heavily populated in June) and upstream, the effect of torrential rain that occurred on 15–17 June 2013 was less as compared to down valley from Badrinath. Prolonged heavy downpouring on 16 and 17 June 2013 resembled a 'cloud burst' type of event in the Khiro and Bhyundar river valley that badly hit for 10 Km area between Lambagar and Govindghat. The Khiro river emerges from Khero Glacier, flows northwest-southeast for about 8 Km and terminates into Alaknanda near Hanuman Chatti just a few hundred metres upstream from Lambagar (plate 4). The nature of flood appearing in the valley may be due to the cloudburst (rainfall data not available) or temporary blockade (damming) in the Khiro river by landslide/rock fall/avalanche that might have occurred in the valley due to extensive rain and rapid snow glacier melting. Sudden breaching of blockade made the river more furious and eroded the valley wall and brought down a huge amount of sediment trees and boulders and spread over all around its termini and down valley of Alaknanda River. The valley is filled by debris and river level has raised by >20 m (Fig. 12.8). The river is arrested by Vishnuprayag hydro project (400 MW) barrage, but due to the scrolling and swelling of the river, a large amount of sediments chocked the barrage bays and also washed out a bay on the left side of the river (Fig. 12.8). Morphologically, the valley is narrow bounded by steep rock slope in the right flank, and in left of the valley, the remnants of glacier deposit indicate the past extension of the glacier. Due to accumulation of huge water in the barrage, the hydrological pressure builds towards the week zone (left flank of the valley) and rapidly moves down valley with removing barrage bay number 4 and scoops out the valley floor, motor road and valley wall deposit. At such situations, there are no ways to validate the official report (M/s J.P.) On the status of the barrage, gates were being opened on 15 June and powerhouse shut down on 16 June.

Fig. 12.8 Photograph showing the fury of nature in Alaknanda valley (Source: Author)

Downstream from the Lambagar (barrage site), the valley is narrow with high gradient. Sudden release of a large volume of water carrying a huge amount of sediments and flowing on the steep gradient directly hit Pandukeshwar village and completely washed away the lower part of the village. In between areas, the Lambagar village, motor road and footpath are extensively damaged (plate 4). At Pandukeshwar the river has shifted its path towards the right side of the valley which is much closer to the village (Fig. 12.8). The size (5–10 m long), shape and concentration of boulders are self-explanatory of the furry of the river Alaknanda on that day. There are a number of large and small landslides activated on both sides of the valley and also damaged roads and footpaths. The Bhyundar Ganga originates from Tipra Glacier and Hemkund Sahib (4000 m asl) and flows for about 18 Km before merging to Alaknanda, and Govindghat was also trapped by similar weather event. During the event, the Bhyundar and Pulna villages were completely washed out, and footpath, agricultural land and infrastructure were badly damaged. The sediments brought by the river directly hit the Govindghat town and smashed the lower part of the town and roads. Between Govindghat and Vishnuprayag, the river drained in a narrow and deep gorge, and the impact of the flood event appears to be minimised.

12.4 Conclusion

The study implied that there are two zones in the Himalaya that are most vulnerable during such extreme events. Zone I lies above the Main Central Thrust (MCT) where the rocks are thrusted and tectonically deformed and hill slopes are steeper and where the mountains receive the highest rainfall. Such geologic and physiographic conditions make this region most reactive to heavy rainfall events. For example, this survey has shown that the area above Badrinath route had most number of landslides and where the bridges and culverts were also damaged. Zone II lies in the lower reaches where the hill slopes are rather gentler and rains are lesser intense, but the higher population density and anthropogenic interference combined with week rocks like phyllites made the few zones that failed during the event, and therefore the survey witnessed another cluster of damaged roads and high density of landslides in the Lesser Himalaya. Another important information that this exercise brought out was the collapse of the fill terrace. The fill types of terraces that were within the reach of the flood or were densely populated with poor drainage and sewer network collapsed due to undercutting by the bulging river.

12.5 Recommendations

1. In a dense network of river discharge measurement, automatic weather stations should be deployed. This network should be connected via satellite. This will help in understanding the changing pattern of rainfall and river response time.

2. In riverbeds, the lowest level of fill terraces should not be allowed for any civil construction. However, these areas can be used for agricultural activities.
3. Complete ban on the construction of buildings or any forms of shelters over the highly unstable and active debris slopes like screen fans which are susceptible to change in angle of repose due to any alteration. The zones of river confluences should also be avoided.
4. It is a well-known fact that thick forests and vegetal cover minimise soil erosion and gulley formation due to the protection of slope by leaves and branches and binding of the soil by root systems. Therefore a massive and well-adapted afforestation programme coupled with its protection leading to survival of plants should be taken up.
5. Roads should be aligned along the rivers but at higher elevation. There should be service roads linking villages and fields from the trunk roads.
6. In Alaknanda valley there are two zones that are prone to landslides. Zone I lies above the MCT and the second in the periphery of the Tehri reservoir. Zone I which has the lowest vegetation and steeper slopes is highly sensitive to such extreme events and therefore should be avoided for permanent settlements. Since all shrines are located in these areas, we recommend buffer community zones should be created in the lower elevations and only controlled passage to pilgrims should be allowed. Several helipads and mobile hospitals with all emergency facilities should be developed during the Yatra season.

Acknowledgement Authors are grateful to the Director of Wadia Institute of Himalayan Geology, Dehradun, Uttarakhand for providing the necessary facility. Thanks are also given to the scientific staff of Centre for Glaciology for their help and support during field work. We are also thankful to the Department of Science and Technology, Ministry of Science, Government of India, for financial supports to carry out this work.

References

Ali SN, Biswas RH, Shukla AD, Juyal N (2013) Chronology and climatic implications of late quaternary glaciations in the Goriganga valley, central Himalaya, India. Quat Sci Rev 73:59–76

Armstrong RL (2011) The glaciers of the Hindu Kush-Himalayan region – a summary of the science regarding glacier melt/retreat in the Himalayan, Hindu Kush, Karakoram, Pamir, and Tien Shan mountain ranges. ICIMOD, Kathmandu, p 17

Bhanot VK, Kwartra SK, Kansal AK, Pandey BK (1978) Rb-Sr whole rock age for Chail Series of northwestern Himalaya. J Geol Soc India 19:224–225

Dobhal DP, Gupta AK, Mehta M, Khandelwal DD (2013) Kedarnath disaster: facts and plausible causes. Curr Sci 105(2):171–174

Heim A, Gansser A (1939) "Central Himalaya" geological observations of Swiss expedition 1936. Hindustan Pub. Corp, New Delhi, p 243

Immerzeel WW, Beek LPHV, Bierkens MFP (2010) Climate change will affected the Asian water tower. Science 324:1382–1385

Mehta M, Majeed Z, Dobhal DP, Srivastava P (2012) Geomorphological evidences of post LGM glacial advancements in the Himalaya: study from Chorabari Glacier, Garhwal Himalaya, India. J Earth Syst Sci 121(1):149–163

Mehta M, Dobhal DP, Kesarwani K, Pratap B, Kumar A, Verma A (2014) Monitoring of glacier changes and response time in Chorabari Glacier, Central Himalaya, Garhwal, India. Curr Sci 107(2):281–289

Owen LA, Benn DI, Derbyshire E, Evans DJA, Mitchell WA, Richardson S (1996) Quaternary glacial history of the Lahul Himalaya, Northern India. J Quat Sci 11:25–42

Raina VK, Srivastava D (2008) Glacier atlas of India. Geological Society of India, Bangalore, p 316

Rautela P (2013) Lessons learnt from the Deluge of Kedarnath, Uttarakhand, India. Asian J Environ Disaster Manag 5(2):43–51

Valdiya KS, Paul SK, Tara C, Bhakuni SS, Upadhyay RC (1999) Tectonic and lithological characterization of Himadri (Great Himalaya) between Kali and Yamuna rivers, Central Himalaya. Himal Geol 20:1–17

Chapter 13
The Need for Community Involvement in Glacial Lake Field Research: The Case of Imja Glacial Lake, Khumbu, Nepal Himalaya

Teiji Watanabe, Alton C. Byers, Marcelo A. Somos-Valenzuela, and Daene C. McKinney

Abstract This chapter explores the relationship between research on glacial lake outburst floods (GLOFs), a lack of communication of results, and resultant confusion among local inhabitants. First, this chapter reviews the progress of research on Imja Glacial Lake (Imja Tsho) in the Mt. Everest region of Nepal, one of the most extensively studied lakes in the Himalaya and which is considered by some to be among the most dangerous lake. Secondly, the lack of community involvement in Imja Glacial Lake research since studies began in the late 1980s is covered, followed by a discussion of the confusion that communities have felt as a result of conflicting opinions regarding the lake's actual risk of flooding. Thirdly, we argue for the need of a "science-based, community-driven" approach to glacial lake and other climate change research in the interests of finding meaningful and effective solutions to contemporary problems. Developing a new framework of research, community involvement, and action will be important not only for local communities but also for scientists in GLOF-prone areas of the Himalaya as well as elsewhere in the world.

Keywords Imja Glacial Lake • Glacial lake outburst flood (GLOF) • Community involvement • Research for action • Nepal

T. Watanabe (✉)
Faculty of Environmental Earth Science, Hokkaido University,
N10, W5, Sapporo 060-0810, Hokkaido, Japan
e-mail: twata@ees.hokudai.ac.jp

A.C. Byers
Institute of Arctic and Alpine Research, University of Colorado at Boulder,
Boulder, CO 80309, USA

M.A. Somos-Valenzuela • D.C. McKinney
Department of Civil, Architectural & Environmental Engineering, University of Texas at Austin, Austin, TX 78712, USA

R.B. Singh et al. (eds.), *Climate Change, Glacier Response, and Vegetation Dynamics in the Himalaya*, DOI 10.1007/978-3-319-28977-9_13

13.1 Introduction

Studies on GLOF in the Himalaya commenced rather recently when compared with the longer history of research elsewhere in the world, such as Iceland (e.g., Thorarinsson 1939) and Peru (e.g., Kinzl 1940, see Carey et al. 2012). Some of the first descriptions of glacial lakes in the Himalaya were made by Hagen (1963) of Imja Glacial Lake (Imja Glacier Lake or Imja Tsho) in the eastern Khumbu region, Nepal, and by Gansser (1966) in the Bhutan Himalaya. Buchroithner et al. (1982), Fushimi et al. (1985), and Ives (2013:168) examined the 1977 GLOF that occurred in the Nare Drangka (drangka = Sherpa for river) on the west-facing slopes of Ama Dablam (6812 m) of central Khumbu. In 1985, another GLOF (Dig Tsho) occurred from the Langmoche Glacier, western Khumbu, where members of the United Nations University Mountain Hazards Mapping Project were sent for field-based observation (Vuichard and Zimmermann 1986, 1987). Their descriptions of the 1985 Dig Tsho outburst led to the first assessment of GLOFs by the International Centre for Integrated Mountain Development (ICIMOD) (Ives 1986), in which Imja Glacial Lake was identified as a rapidly expanding supraglacial lake (Ives 2015).

Hammond (1988) conducted the first GLOF-related study on Imja Glacial Lake. Since then, the number of GLOF-related publications has increased greatly, with Imja now being one of the most studied glacial lakes in the Himalaya. Local residents, however, particularly those living in the village of Dingboche, voiced displeasure to the authors in 2009 and 2011 over the growing number of foreign and Nepali scientists studying the lake, citing their lack of communication and reluctance to share results as the main culprits. What information they did receive about the lake was mixed, with some scientists warning that a catastrophic flood was imminent while others downplayed the risk. As a result, uncertainty and confusion surrounded Imja Glacial Lake in the eyes of local communities, which the authors decided to attempt to resolve if at all possible. The following sections review the history of research at Imja Glacial Lake; the attempts to, for the first time, engage local people in the research and discussions; and finally lessons learned and recommendations regarding next steps necessary to promote a better blending of science and local communities.

13.2 Study Area

Imja Glacial Lake is located about 9 km south of Mount Everest (Fig. 13.1). Its altitude is about 5010 m and area is 1.257 km^2 as of 2012 (Somos-Valenzuela et al. 2014). The water volume is 75.2 million m^3, and the maximum depth is 149.8 m as of 2014 (Kargel et al. 2015). The lake is bordered by lateral moraines to the north and south, the Lhotse Shar Glacier to the east, and debris-covered "dead ice" surrounded by the terminal and lateral moraines to the west. Salerno et al. (2012) consider the lake as a proglacial lake rather than a supraglacial lake because the eastern (upper) shoreline consists of the terminus of the glacier.

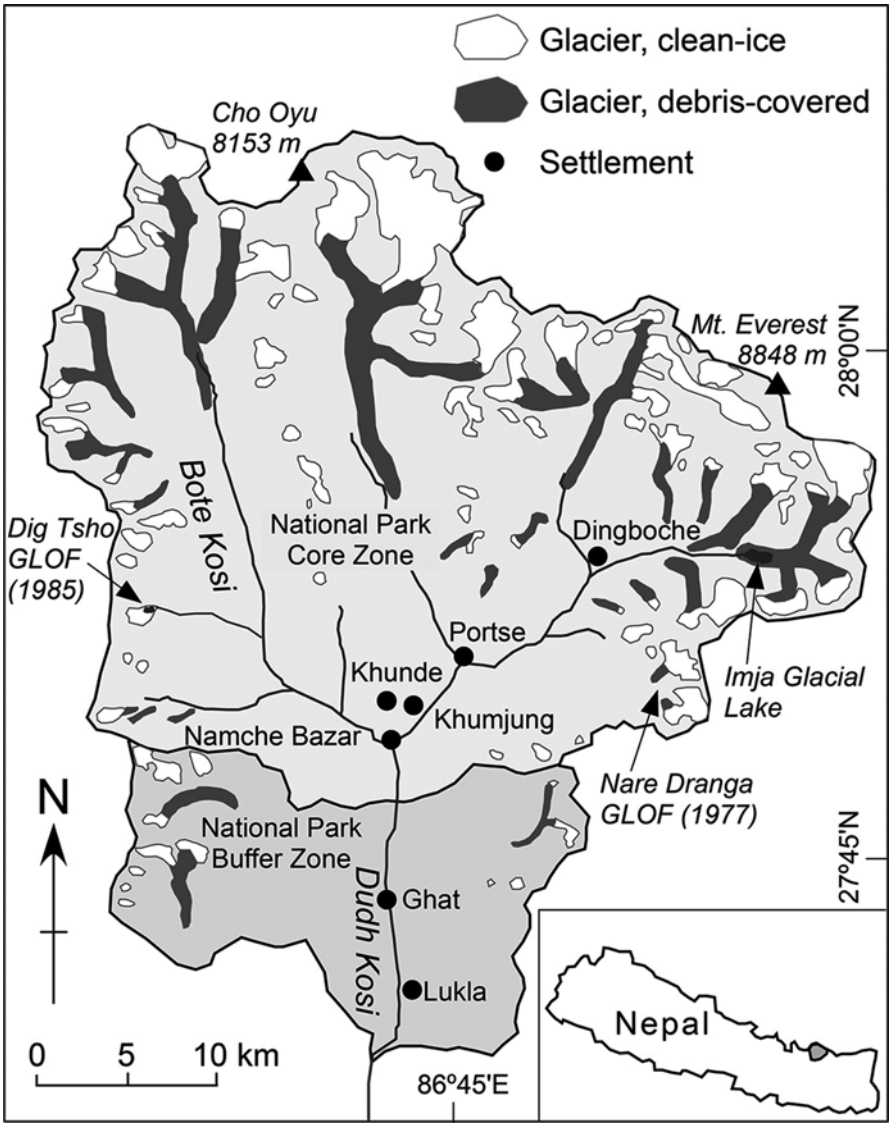

Fig. 13.1 Study area and the close view of Imja Glacial Lake (Source: Author)

Since the late 1990s, the lake has received a large amount of attention from scientists and the media because of its status as one of the most dangerous glacial lakes in the Himalaya (e.g., Mool et al. 2001; ICIMOD 2011). Other reports have exaggerated the lake's GLOF potential and damage to downstream populations, infrastructure, and agricultural land (Ives 2004, 2013), causing a considerable amount of confusion for the scientific, donor, and local communities alike.

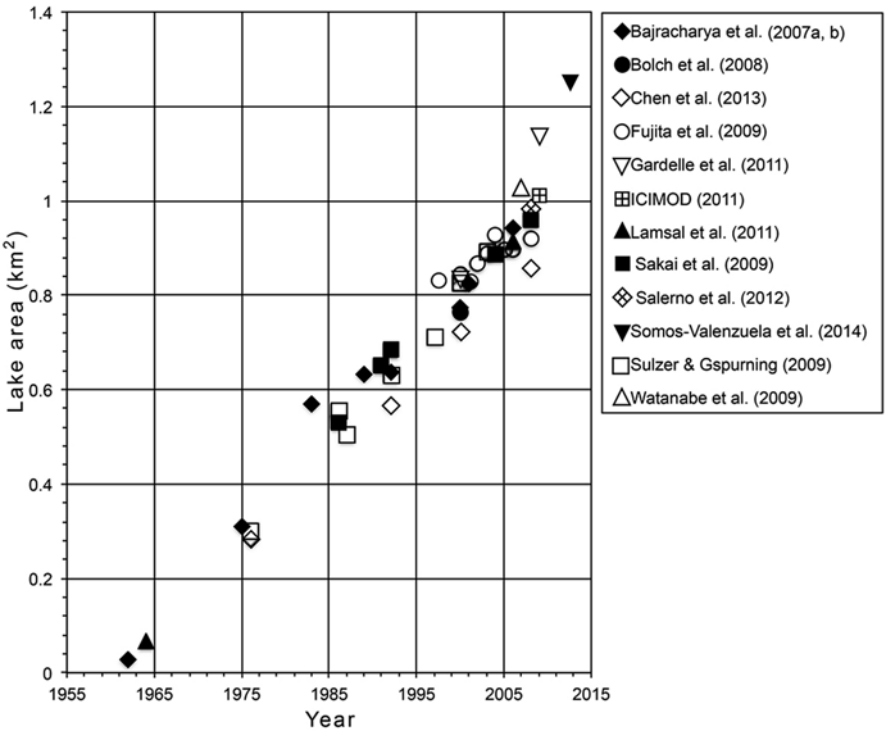

Fig. 13.2 Imja's lake area expansion from 1962 to 2012. There are no other Himalayan glacial lakes that have been studied by so many scientists (Source: Author)

13.3 GLOF-Related Studies on Imja Glacial Lake

13.3.1 History of Research

Hagen (1963) first described the surface condition of the debris-covered Imja Glacier, noting that there were five small ponds on the surface. As mentioned previously, Hammond (1988) conducted the first GLOF-related study of Imja Glacial Lake for her Master's thesis. Hammond was followed by Watanabe (1992) and Watanabe et al. (1994, 1995) who demonstrated the rapid melt of the dead ice near the terminal moraine. A number of studies since then have discussed the growth of the lake (Yamada 1998; Gspurning et al. 2004; Bajracharya et al. 2007a, b; Quincey et al. 2007; Watanabe et al. 2009; Ives et al. 2010; Lamsal et al. 2011; Chen et al. 2013, 2014; Racoviteanu et al. 2014). Somos-Valenzuela (2014) and Somos-Valenzuela et al. (2014) summarized lake area expansion as estimated by previous and ongoing studies as shown in Fig. 13.2. This figure shows both the large number of studies that have been conducted as well as the general trend of the increasing area. However, Fujita et al. (2009) questioned the continuation of the lake's rapid expansion, stating that lake expansion rate from 2000 to 2011 was 0.011 km^2/year

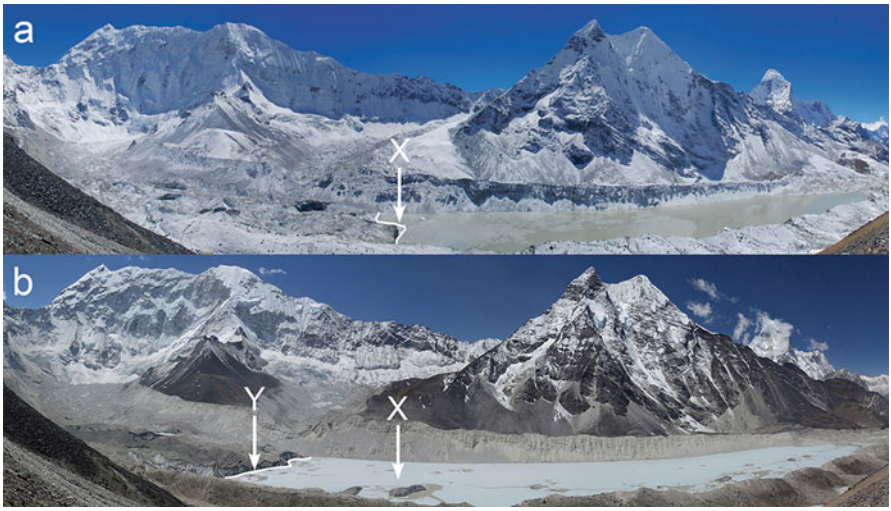

Fig. 13.3 Imja Glacial Lake in 2007 (**a**) and in 2014 (**b**). The glacier terminus in 2007 (*X*) experienced calving processes that resulted in significant lake expansion by May of 2014 (*Y*) (Photographs by Alton C. Byers)

while that until 2000 was 0.022 km^2/year. The lake area in 2008 by Fujita et al. (2009) was 0.92 km^2 and that by Salerno et al. (2012) was 0.98 km^2. The lake area in 2009 by Gardelle et al. (2011) was 1.138 km^2 and in 2012 was 1.257 km^2 (Somos-Valenzuela et al. 2014). Somos-Valenzuela et al. (2014) obtained an expansion rate of 0.039 km^2/year for the period from 2002 to 2012. Collectively, there is considerable discrepancy in lake expansion results.

Recent expansion of the lake has been occurring on the proximal (eastern) shoreline (upwards), which is mainly due to ice calving (Sakai et al. 2003; Hambrey et al. 2008; Fujita et al. 2009; Watanabe et al. 2009). Somos-Valenzuela et al. (2014) showed that the glacier terminus at the eastern lakeshore has been retreating at a rate of 52.6 m/year between 2002 and 2012, while a rate of 31.6 m/year was recorded for the period between 1992 and 2002. Further, Bajracharya et al. (2007a) showed that the lake expanded 74 m/year from 2001 to 2006, while it was 42 m/year from 1962 to 2001.

Another method that visually illustrates Imja Lake's growth is repeat photography (Byers 2005, 2007; Byers et al. 2012, 2013a), which clearly illustrates the dramatic changes in Imja Glacier since photographed by the Austrian climber cartographer Erwin Schneider in 1955 (Byers 2010; see Plates 4 in Byers 2007). The accelerated recent upward lake expansion in the 2010s was also successfully demonstrated (Fig. 13.3).

Yamada and Sharma (1993) conducted the first bathymetric survey of Imja Glacial Lake in 1992 and found the average and maximum depth of the lake attained 47.0 m and 98.5 m, respectively. Sakai et al. (2003, 2005) and Fujita et al. (2009) updated the lake bathymetry in 2002 and compared the changes between 1992 and 2002. They found the average and maximum lake depth became 41.6 m and 90.5 m,

respectively. This means that the lake had not deepened, but the lake area and volume had been enlarged from 0.60×10^6 to 0.86×10^6 m^2 and from 28.0 to 35.8 million m^3, respectively. Somos-Valenzuela et al. (2014) conducted a sonar bathymetric survey and water volume estimate in 2012: the maximum lake depth obtained was 116.3 ± 5.2 m and the volume was 61.7 ± 3.7 million m^3. Further, Kargel et al. (2015) reported the most recent bathymetry results in October 2014 where the maximum depth was found to be 149.8 m and the water volume was 75.2 million m^3, both of which are much larger than those reported for 2012. This result also suggests the acceleration of the lake growth during the 2010s.

The dead ice in Imja Glacier is melting with concurrent changes in its surface morphology (Watanabe et al. 1994, 1995; Benn et al. 2012). Sakai et al. (2007) measured surface topography of the dead-ice area in 2001 and 2002 and compared the spillway morphology measured by Watanabe et al. (1995) in 1994. Results indicated that dead ice melting along the spillway (outlet channel) has lowered the lake level by some 37 m over the last four decades (Watanabe et al. 2009; Lamsal et al. 2011).

There has been a tendency for lake level to decline since the 1960s (Fig. 13.4). The most recent observations, however, suggest that the lowering rate may have slowed down since 2007. Fujita et al. (2009) suggested that no significant change in the lake level had occurred between 2001 and 2007 (i.e., 5009 m a.s.l., F in Fig. 13.4), although the in situ measurement and ALOS-DEM datum both in 2006 provided altitudes of 5004 m a.s.l. (H in Fig. 13.4) and 5006 m a.s.l. (I in Fig. 13.4), respectively. Since the late 2000s, the lake level decline is likely to have slowed down or even to have stopped (G–J in Fig. 13.4). The recent accelerated rate of the upward lake expansion, i.e., the accelerated glacier retreat (Byers et al. 2013a), might have contributed to the slowed decline of the lake level. On the other hand, if the decline of the lake level continues, it can potentially affect the outlet (spillway) channel incision, i.e., the outlet could evolve into a new arm of the lake when the width of the outlet is enlarged (Benn et al. 2012).

Seepage also affects the enlargement of the outlet complex and can also be a GLOF trigger. The potential seepage area around the terminal moraine and its nearby lateral moraines changes due to the changes of both the dead-ice surface morphology and the lake level (Watanabe et al. 2009). Watanabe et al. (2009) had not observed any seepage during the field survey; however, Somos-Valenzuela (2014: 18) found seepage at two sites of the terminal moraine on three separate occasions in 2011–2012.

The enlargement rates of the outlet complex and seepage are strongly related to the spatial distribution and thickness of the ice covered by debris in the "dead-ice" area. A few scientific teams have attempted geophysical surveys on the "dead-ice" area, but no clear results have been obtained so far (Somos-Valenzuela 2014).

Lamsal et al. (2011) showed that the lowering of the glacier surface in the east of the lake was as large as 47.4 m from 1964 to 2006, which was much larger than that in the "dead-ice" area (16.9 m). Nuimura et al. (2012) also found the surface lowering of the Imja Glacier at a rate of -0.81 ± 0.22 m/year for the period from 1992 to 2008.

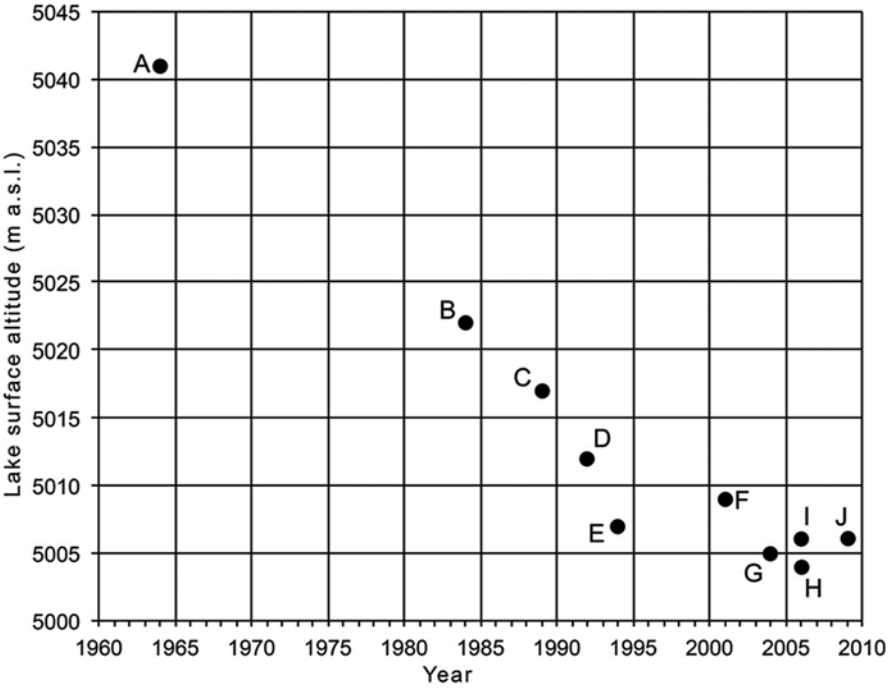

Fig. 13.4 Imja Lake level decline from 1964 to 2009. (**a**) Corona image and the altitude from the 1:2500 map produced by air photographs; (**b**) 1:50,000 map; (**c**, **e**, **h**, **j**) in situ measurement (Watanabe et al. 2009); (**d**) 1:2500 map produced by air photographs; (**f**) Sakai et al. (2007); (**g**) in situ measurement by Dr. Katsuhiko Asahi; (**I**) ALOS image (Lamsal et al. 2011). Note that each measurement was done in different seasons. There are no measurements on seasonal fluctuations, and Chikita et al. (2000) showed about 0.6 m of the lake level fluctuation in 5 days in July 1997 (Source: Authors)

Studies of flood estimates from Imja Glacial Lake are still limited (Bajracharya et al. 2007b; ICIMOD 2011). Braun and Fiener (1995) attempted to produce sketch maps of the land surface that would be flooded down valley from the lake site to Ghat (Fig. 13.1), referencing the damaged area caused by the 1985 Dig Tsho GLOF. Bajracharya et al. (2007a) estimated the flood arrival time from Imja Glacial Lake to Dingboche to be 13.9 min and to Ghat at 46.4 min. Somos-Valenzuela et al. (2015) suggested that Imja Lake be lowered by at least 10 m, and preferably 20-m reduction, to significantly reduce its risk of flooding.

Kattelmann and Watanabe (1998) discussed general approaches to reducing the GLOF hazard from Imja Glacial Lake. Kattelmann and Watanabe (1998) and Bajracharya et al. (2007b), among others, also suggest the importance of introducing an early warning system. A Japanese team with the help from ICIMOD installed a system for a near real-time monitoring of a part of Imja Glacial Lake and

emphasized the advantage of such a system (Fukui et al. 2008). Unfortunately, the video camera and other system equipment had fallen into disrepair within 2 years.

Khanal et al. (2015) discussed a risk assessment methodology and estimated the monetary loss due to a GLOF from Imja Glacial Lake, conducting 23-group discussions with local inhabitants along the Imja Valley/Dudh Kosi Basin. Their estimates include the loss of cultivated land of 314 ha, number of directly affected persons at 5784 and indirectly affected at 96,767 persons, and loss of 445 houses, 25 bridges, and 3 schools, among other infrastructure. The monetary losses include $US 8.917 million of real estate, $US0.932 million of agricultural land, and $US 2.037 million of public infrastructure.

13.3.2 History of Research

There are more than 20 studies that have examined Imja Glacial Lake and many more studies that have discussed or referenced it. Detailed analyses of Imja in terms of the lake's development history, morphological transformation, bathymetry, and geophysical structure of the moraines have been conducted since the 1980s. Although Imja Glacial Lake has been classified as dangerous (e.g., Mool et al. 2001; Kattelmann 2003), there are different views on the trend of the lake's areal expansion. Further, perceptions on the dangers of a GLOF from Imja have recently changed, from highly dangerous to medium or low danger (Bolch et al. 2008; Hambrey et al. 2008; Watanabe 2008; Fujita et al. 2009; Watanabe et al. 2009), although considerable disagreement remains (Somos-Valenzuela 2014: 48). Hambrey et al. (2008), for example, concluded that the lake is stable. Budhathoki et al. (2010) stated that Imja has a moderate risk of a GLOF, although they might have overestimated this by using the entire water volume as opposed to the potential flood volume (PFV; see Somos-Valenzuela et al. 2014). Watanabe (2008), Fujita et al. (2009), Watanabe et al. (2009), and ICIMOD (2011) also stated that the lake is relatively stable. This shift from "dangerous" to "stable" was likely derived from combinations of longer-term, diversified, and more accurate study approaches. The most recent studies, on the other hand, suggest that a rapid upward expansion of the lake is occurring (Fig. 13.3), and seepage is now regularly observed at the terminal moraine (Somos-Valenzuela 2014). This second shift from "stable view" to "less stable view" suggests that the changes of the lake conditions may have recently accelerated, and the rate might be further accelerated from this point onward. It is not entirely clear what communities would be affected by a GLOF from Imja, with the exception of a few villages such as Dingboche and Phunki (Somos-Valenzuela 2014: 199). As will be seen, local people living in Chaurikharka, Khumjung, and Namche VDCs nevertheless ranked the potential GLOF hazard from Imja Glacial Lake as their number one priority during a recent series of local adaptation plan of action (LAPA) community consultations (Byers and Thakali 2015).

13.4 Community Involvement in the GLOF Research of Imja Glacial Lake

13.4.1 The Importance of Regular Communications

The authors conducted a number of consultations with local communities in the Dingboche region between 2009 and 2011. During the Andean-Asian Mountains Global Knowledge Exchange expedition to Imja Glacial Lake in 2011 (Byers et al. 2013a), local inhabitants voiced strong objections to the numerous international and national researchers who had been studying Imja Glacial Lake for over 30 years (Byers 2012). A few local representatives clearly stated that Japanese scientists in particular had been the source of much tension, as they rarely shared the results of their research. They accused a group of Japanese climbers of frightening local communities by exaggerating the dangers of a GLOF during interviews. Sherpa (2014) also described such local attitudes toward scientists. As mentioned previously, an international team attempted to establish an early warning system by using a wireless LAN setup with geo-ICT tools and technologies with a local community (Fukui et al. 2008). However, the locals had a different view of the project as well as the community's involvement, saying that they would not use mobile phones as a tool to receive a warning message because they only used their phones for day-to-day communications. This response was most likely due to the lack of attention paid by the international team in explaining the effectiveness of using mobile phones for early warning purposes to the local communities, as mobile phones have since proven to be quite effective (e.g., as demonstrated in May 2012 during the Seti Khola flood in central Nepal (Regmi 2015, pers. comm.).

Ives (2005) emphasizes the need of involving local inhabitants before any action connected to glacial lake research or mitigation is undertaken. During the September, 2011, Andean-Asian Mountains Global Knowledge Exchange expedition to Imja Glacial Lake, local people were invited to participate in discussions at the lake concerning its history, growth, potential triggers, and level of risk (Fig. 13.5). In March of 2012, the High Mountains Adaptation Partnership (HiMAP; www.highmountains.org) was established by the Mountain Institute and University of Texas at Austin, with support from the US Agency for International development (Byers 2012; Byers et al. 2013b). HiMAP is based on a "science-based, community-driven" approach where the results of glacial lake and other climate change research are routinely shared with local communities, thereby facilitating the development of the most accurate, knowledge-based local adaptation plans of action (LAPA) possible (Byers et al. 2013b). Although there was a high level of uncertainty surrounding Imja Glacial Lake during the September 2011 visit, the availability of reliable information led to its ranking as the number one threat and vulnerability in the final LAPA plan (Byers and Thakali 2015). HiMAP has also collaborated with the United Nations Development Programme (UNDP), which launched the Community Based Flood and Glacial Lake Outburst Risk Reduction Project (CFGORRP) for the period from 2013 to 2017, as well as with the Department of Hydrology and

Fig. 13.5 International and national scientists discussing the rapid lake expansion and future mitigation measures of GLOF from Imja Glacial Lake on the lateral moraine of the Imja Glacier (Photograph by Teiji Watanabe, September 14, 2011)

Meteorology (DHM) of the Nepal Government and GEF (UNDP 2013a). The promotion of local involvement, collaboration, and sharing of information with a wide range of stakeholders is quite timely considering the acceleration of Imja Glacial Lake's expansion.

13.4.2 An Integrated Approach

For decades, research and action projects, such as development and nature conservation initiatives, have been independently designed, funded, and conducted with little involvement by scientists or local communities. There have been occasional opportunities for scientists to provide the results of their data during the project design phase, but the goals of the donor-driven projects were often different and the scientific findings ignored (Fig. 13.6a). Likewise, the active involvement of local people in a project became secondary to the goals and objectives of the city-bound donor or government agency. Unfortunately, this represents the current status of most projects in the high mountain world.

As mentioned previously, the number of studies conducted about Imja Glacial Lake as well as other glacial lakes is increasing. The use of different field methods with different thresholds of accuracy has resulted in different opinions regarding the actual danger of a GLOF at Imja Glacial Lake. It is our opinion that the current United Nations Development Programme to mitigate the GLOF danger from Imja Glacial Lake remains in need of a careful review of existing studies, including the

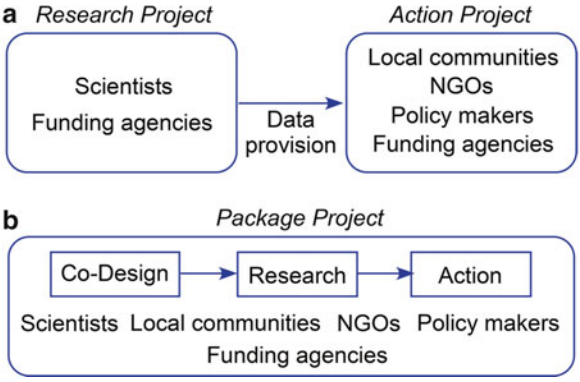

Fig. 13.6 Relationship between a research project and an action project. (**a**) Typical current relationship (research project and action project are independent from the design stage. Scientists may provide some data to the action project), (**b**) Future framework of all-in-one package (This project is co-designed by all stakeholders with the common funds towards the same final goal as the Future Earth suggests; see www.futureearth.org)

launch of additional studies where indicated, if the project hopes to achieve success. The overall purpose of UNDP's CFGORRP is to reduce human and material losses from GLOF events in the area. For this purpose, the project plans to reduce the level of the lake at least 3 m over a period of 1 year and to install and operate a community-based low-tech early warning system. These two approaches to mitigate GLOF risk from Imja Glacial Lake are not new. The Nepal Government has implemented two similar approaches in Tsho Rolpa (ICIMOD 2011). However, the siphon system to reduce the lake level met with limited success, largely related to the project running out of funds, and the early warning system did not function properly. Clearly, Nepal needs a success story related to the effective lowering and risk reduction of a potentially dangerous glacial lake, and there exists no better opportunity at present than Imja.

Although UNDP suggests a 3-m reduction of the lake level based on the UNDP Government of Nepal Country Programme Action Plan (CPAP) Output 7.3.2 (UNDP 2013b: 50), Somos-Valenzuela et al. (2015) argued that at least a 10-m reduction of the lake level (preferably 20-m reduction) would be necessary to realistically reduce risk. We suggest that the UNDP project should be open to additional inputs from different stakeholders and research results, as well as incorporating the knowledge derived from existing studies.

UNDP (2013a: 46) writes that the project has been designed to avoid duplication and instead will work in partnership with several key institutions and ongoing or proposed initiatives that will support the achievement of the project's planned outcomes. Even if the project uses the information from existing studies, however, the exclusion of even small but critical parts of the research results would not produce the best solutions available and could lead to costly mistakes, such as the failure to construct a lake lowering system capable of further lowering in the future. Moreover,

the outcome of the project (e.g., 3-m reduction of the lake level) should be reconsidered when additional research results recommend further lowering.

When a project requests the assistance of scientists, several obstacles are often encountered. One is that research teams often need a longer period of time to complete their work than the donor prefers, leaving the researchers to provide whatever they can within the allotted time frame. This could lead to a delivery of misleading and false conclusions by the scientists. Additionally, an action project may ignore current research views if different from those upon which the project was based. As an alternative, the current High Mountains Adaptation Partnership led by TMI has the advantage of directly translating its research results into action, because it can set a time frame of the project to meet the research requirement.

We suggest that a better framework would consist of an integrated project with both research and action components (Fig. 13.6b). In the integrated project, all stakeholders participate in the project's design, from the very beginning and with the same final goal in mind. The relative importance of the research component and action component can vary, depending on the final goal and the duration. It can share all scientific uncertainties and discrepancies among the stakeholders, including those from different scholarly communities, by which the shared issues can be discussed from a new point of view. Further, the involvement of local communities needs to be strengthened within any framework. If a wider range of locals are involved in a project at the co-designing stage, the gaps between the communities and the outside stakeholders will be minimized. This could result in a more effective cooperation and lead to a better chance of success of the project. Unnecessary threats to the local inhabitants could be also mitigated by more regular communication between the scientists and locals. The integrated framework approach shows promise of being effective not only for local communities but also for scientists, donors, governments, and other stakeholders as well.

13.5 Conclusions

This chapter discussed the following three points, which were drawn from the GLOF-related studies and activities from Imja Glacial Lake.

1. GLOF studies are relatively new in the Himalaya. There has been rapid and growing progress in recent research, which has been characterized by an application of diversified methodologies. These research activities, however, resulted in the discrepancy of some results: for example, several recent studies have concluded that Imja Glacial Lake contains no immediate danger of flooding, and others show accelerated upward lake expansion. The situations of the lake are always changing, meaning that continuous monitoring is important even if the lake poses little danger at present; it could become quite dangerous within 20 or more years. In addition, the discrepancies within the accumulated GLOF-related

studies could lead to more confusion among the local inhabitants if not explained and discussed on a regular basis.

2. Most previous research activities on GLOF have been conducted under a basic research design, with little attention paid to involving local communities and/or to the applied nature and use of the results. This has often resulted in misunderstandings about the danger of GLOFs among local communities, resentment against outside scientists, and loss of credibility among donors and research groups. New models that blend science, local participation, communication, and integrated approaches to problem solving are needed if the best solutions to contemporary climate change problems are to be found.
3. GLOF and climate change research projects for action as well as action projects with research assistance have been initiated in the Imja Valley/Dudh Kosi Basin. A new framework of integrated projects that contain both research and action components is advocated here, for the Himalaya and beyond, which would also allow stakeholders to use the same funds for both research and action. By involving the widest range of stakeholders possible, such an integrated approach would benefit both scientists and local communities alike.

References

Bajracharya SR, Mool PK, Shrestha BR (2007a) Impact of climate change on Himalayan glaciers and glacial lakes: case studies on GLOF and associated hazards in Nepal and Bhutan. International Centre for Integrated Mountain Development (ICIMOD), Kathmandu

Bajracharya B, Shrestha AB, Rajbhandari L (2007b) Glacial lake outburst floods in the Sagarmatha region: hazard assessment using GIS and hydrodynamic modeling. Mt Res Dev 27:336–344. doi:10.1659/mrd.0783

Benn DI, Bolch T, Hands K, Gulley J, Luckman A, Nicholson LI, Quincey D, Thompson S, Toumi R, Wiseman S (2012) Response of debris-covered glaciers in the Mount Everest region to recent warming, and implications for outburst flood hazards. Earth Sci Rev 114:156–174. doi:10.1016/j.earscirev.2012.03.008

Bolch T, Buchroithner MF, Peters J, Baessler M, Bajracharya S (2008) Identification of glacier motion and potentially dangerous glacial lakes in the Mt. Everest region/Nepal using spaceborne imagery. Nat Hazards Earth Syst Sci 8:1329–1340. doi:10.5194/nhess-8-1329-2008

Braun M, Fiener P (1995) Report on the GLOF Hazard Mapping Project in the Imja Khola/Dudh Kosi Valley, Nepal. Department of Hydrology and Meteorology and German Agency for Technical Cooperation, Kathmandu

Buchroithner MF, Jentsch G, Wanivenhaus B (1982) Monitoring of recent geological events in the Khumbu Area (Himalaya, Nepal) by digital processing of Landsat MSS data. Rock Mech 15:181–197

Budhathoki KP, Bajracharya OR, Pokharel BK (2010) Assessment of Imja Glacier Lake outburst flood (GLOF) risk in Dudh Koshi River Basin using remote sensing techniques. J Hydrol Meteorol 7(1):75–91

Byers AC (2005) Contemporary human impacts on alpine ecosystems in the Sagarmatha (Mt. Everest) National Park, Khumbu, Nepal. Ann Assoc Am Geogr 95:112–140

Byers AC (2007) An assessment of contemporary glacier fluctuations in Nepal's Khumbu Himal using repeat photography. Himal J Sci 4:21–26

Byers AC (2010) Fifty years of climate, culture, and landscape change in the Sagarmatha (Mt. Everest) National Park, Nepal. Educ About Asia 15:3, Winter 2010

Byers AC (2012) An introduction: enhancing the control and management of dangerous glacial lakes through Himalayan-Andean exchange and collaboration. Andean-Asian Mountains Global Knowledge Exchange on Glaciers, Glacial lakes, Water & Hazard Management and Adaptation Partnership Workshop, pp 12–15

Byers AC, Thakali S (2015) Khumbu local adaptation plan of action. Sagarmatha (Everest) National Park, Khumbu, Nepal. The Mountain Institute/High Mountains Adaptation Partnership, Kathmandu

Byers AC, McKinney DC, Somos-Valenzuela MA, Watanabe T (2012) Glacial lakes of the Hinku and Hongu valleys, Makalu-Barun National Park and Buffer Zone, Nepal. Proceedings, Andean-Asian Mountains Global Knowledge Exchange on Glaciers, Glacial lakes, Water & Hazard Management and Adaptation Partnership Workshop, pp 16–32

Byers AC, McKinney DC, Somos-Valenzuela MA, Watanabe T, Lamsal D (2013a) Glacial lakes of the Hinku and Hongu valleys, Makalu-Barun National Park and Buffer Zone, Nepal. Nat Hazards. doi:10.1007/s11069-013-0689-8

Byers AC, McKinney DC, Thakari S, Somos-Valenzuela MA (2013b) Promoting science-based, community-driven approaches to climate change adaptation in glacierized mountain ranges. Geography 99(3):143–152

Carey M, Huggel C, Bury J, Portocarrero C, Haeberli W (2012) An integrated socio-environmental framework for glacier hazard management and climate change adaptation: lessons from Lake 513, Cordillera Blanca, Peru. Climate Change 112:733–767

Chen W, Doko T, Fukui H, Yan W (2013) Changes in Imja Lake and Karda Lake in the Everest region of Himalaya. Nat Resour 4:449–455

Chen W, Doko T, Liu C, Ihcinose T, Fukui H, Feng Q, Gou P (2014) Changes in Rongbuk Lake and Imja Lake in the Everest region of Himalaya. Int Arch Photogramm Remote Sens Spat Inf Sci XL-2:259–266

Chikita K, Joshi SP, Jha J, Hasegawa H (2000) Hydrological and thermal regimes in a supraglacial lake: Imja, Khumbu, Nepal Himalaya. Hydrol Sci J 45(4):507–521

Fujita K, Sakai A, Nuimura T, Yamaguchi S, Sharma RR (2009) Recent changes in Imja glacial lake and its damming moraine in the Nepal Himalaya revealed by in situ surveys and multi-temporal ASTER imagery. Environ Res Lett 4:045205. doi:10.1088/1748-9326/4/4/045205

Fukui H, Limlahapun P, Kameoka T (2008) Real time monitoring for Imja glacial lake in Himalaya – global warming front monitoring system. SICE Annu Conf 2008:2578–2581

Fushimi H, Ikegami K, Higuchi K, Shankar K (1985) Nepal case study: catastrophic floods. IAHS Publ 149:125–130

Gansser A (1966) Geological research in the Bhutan Himalaya. Mountain World 1964/65. Swiss Foundation for Mountain Research, Zurich, pp 87–97

Gardelle J, Arnauda Y, Berthier E (2011) Contrasted evolution of glacial lakes along the Hindu Kush Himalaya mountain range between 1990 and 2009. Glob Planet Chang 75:47–55

Gspurning J, Kosta R, Sulzer W (2004) Application of available geodata in high mountain environmental research – examples from the Khumbu Himal Area (Nepal). Proceedings of the 19th European and Scandinavian Conference for ESRI Users, 8–10 November 2004. Copenhagen

Hagen T (1963) The evaluation of the highest mountain in the world. In: Hagen T, Dyrenfurth GO, von Fürer-Haimendorf C, Schneider E (eds) Mount Everest. Oxford University Press, London, pp 1–96

Hambrey MI, Quincey DJ, Glasser NF, Reynolds JM, Richardson SJ, Clemmens S (2008) Sedimentological, geomorphological and dynamic context of debris-mantled glaciers, Mount Everest (Sagarmatha) region, Nepal. Quat Sci Rev 27:2361–2389

Hammond JE (1988) Glacial lakes in the Khumbu region, Nepal: an assessment of the hazards. Master's thesis, University of Colorado at Boulder

ICIMOD-International Centre for Integrated Mountain Development (2011) Glacial lakes and glacial lake outburst floods in Nepal. International Centre for Integrated Mountain Development (ICIMOD), Kathmandu

Ives JD (1986) Glacial lake outburst floods and risk engineering in the Himalaya, Occasional Paper no. 5. ICIMOD, Kathmandu
Ives JD (2004) Himalayan perceptions: environmental change and the well-being of mountain peoples. Routledge, London
Ives JD (2005) Global warming–a threat to Mountain Everest? Mt Res Dev 25(4):391–394
Ives JD (2013) Sustainable mountain development: getting the facts right. Jagadamba Press, Lalitpur
Ives JD (2015) Prelude: mountains in an uncertain world. In: Grover VI, Borsdorf A, Breuste JH, Tiwara PC, Frangetto FW (eds) Impact of global changes on mountains: responses and adaptation. CRC Press, Boca Raton, pp 3–14
Ives JD, Shrestha RB, Mool PK (2010) Formation of glacial lakes in the Hindu Kush-Himalayas and GLOF risk assessment. ICIMOD, Kathmandu
Kargel J, Leonard G, Regmi D, Haritashya U, Chand M, Pradhan S, Sapkota N, Byers A, Joshi S, McKinney D, Mool P, Somos-Valenzuela M, Huggel C (2015) Glacier dynamics and outburst flood potential from the Imja and Thulagi Glacier-Lake systems (Nepal). Geophysical Research Abstracts 17, EGU2015-15554-1
Kattelmann R (2003) Glacial lake outburst floods in the Nepal Himalaya: a manageable hazard? Nat Hazards 28:145–154
Kattelmann R, Watanabe T (1998) Approaches to reducing the hazard of an outburst flood of Imja Glacier Lake, Khumbu Himal. In: Chalise SR, Khanal NR (eds) Ecohydrology of high mountain areas. ICIMOD, Kathmandu, pp 359–366
Khanal NR, Mool PK, Shrestha AB, Rasul G, Ghimire PK, Shrestha RB, Joshi SP (2015) A comprehensive approach and methods for glacial lake outburst flood rick assessment, with examples from Nepal and the transboundary area. Int J Water Resour Dev. doi: http://dx.doi.org/10.1080/07900627.2014.994116
Kinzl H (1940) Los glaciares de la Cordillera Blanca. Rev Cien (Organo Fac Cien Biol Físicas Matemáticas Univ Mayor San Marcos) 42:417–440
Lamsal D, Sawagaki T, Watanabe T (2011) Digital terrain modelling using Corona and ALOS PRISM data to investigate the distal part of Imja Glacier, Khumbu Himal, Nepal. J Mt Sci 8:390–402
Mool PK, Bajracharya SR, Joshi SP (2001) Inventory of glaciers, glacial lakes and glacial lakes outburst floods, Nepal. ICIMOD, Kathmandu
Nuimura T, Fujita K, Yamaguchi S, Sharma RR (2012) Elevation changes if glaciers revealed by multitemporal digital elevation models calibrated by GPS survey in the Khumbu region, Nepal Himalaya, 1992–2008. J Glaciol 58:648–656
Quincey DJ, Richardson SD, Luckman A, Lucas RM, Reynolds JM, Hambrey MJ, Glasser NF (2007) Early recognition of glacial lake hazards in the Himalaya using remote sensing datasets. Glob Planet Chang 56:137–152
Racoviteanu AE, Arnaud Y, Baghuna IM, Bajracharya SR, Berthier E, Bhanbri R, Bolch T, Byrne M, Chaujar RK, Frauenfelder R, Kääb A, Kamp U, Kargel JS, Kulkarni AV, Leonard GJ, Mool PK, Sossna I (2014) Himalayan glaciers (India, Bhutan, Nepal): satellite observations of thinning and retreat. In: Kargel JS, Leonard GJ, Bishop MP, Kääb A, Raup BH (eds) Global land Ice measurements from space. Springer, Berlin, pp 549–582
Sakai A, Yamada T, Fujita K (2003) Volume change of Imja Glacier Lake in the Nepal Himalayas. International symposium on disaster mitigation and basin wide water management. pp. 556–561
Sakai A, Fujita K, Yamada T (2005) Expansion of the Imja glacier lake in the east Nepal Himalaya. In: Mavlyudov BR (ed) Glacier caves and glacial karst in high mountains and polar regions. Institute of Geography RAS, Moscow, pp 74–79
Sakai A, Saito M, Nishimura K, Yamada T, Iizuka Y, Harada K, Kobayashi S, Fujita K, Gurung CB (2007) Topographical survey of end moraine and dead ice area at Imja Glacier Lake in 2001 and 2002. Bull Glaciol Res 24:29–36
Sakai A, Nishimura K, Kadota T, Takeuchi N (2009) Onset of calving at supraglacial lakes on debris-covered glaciers of the Nepal Himalaya. J Glaciol 55(193):909–917

Salerno F, Thakuri S, D'Agata C, Smiraglia C, Chiara E, Viviano G, Tartari G (2012) Glacial lake distribution in the Mount Everest region: uncertainty of measurement and conditions of formation. Glob Planet Chang 92–93:30–39

Sherpa PY (2014) Climate change, perceptions, and social heterogeneity in Pharak, Mount Everest region of Nepal. Hum Organ 73(2):153–161

Somos-Valenzuela MA (2014) Vulnerability and decision risk analysis in Glacier Lake Outburst Floods (GLOF). Case Studies: Quillcay Sub Basin in the Cordillera Blanca in Peru and Dudh Koshi Sub Basin in the Everest Region in Nepal. PhD thesis, Univ. of Texas at Austin

Somos-Valenzuela MA, McKinney DC, Rounce DR, Byers AC (2014) Changes in Imja Tsho in the Mount Everest region of Nepal. Cryosphere 8:1661–1671. doi:10.5194/tc-8-1661-2014

Somos-Valenzuela MA, McKinney DC, Byers AC, Rounce DR, Portocarrero C, Lansal D (2015) Assessing downstream flood impacts due to a potential GLOF from Imja Tsho in Nepal. Hydrol Earth Syst Sci 19:1401–1412. doi:10.5194/hess-19-1401-2015

Sulzer W, Gspurning J (2009) High mountain geodata as a crucial criterion of research: Case studies from Khumbu Himala (Nepal) and Mount Aconcagua (Argentina). Int J Remote Sens 30:1719–1736

Thorarinsson S (1939) Ice-dammed lakes of Iceland, with particular reference to their value as indicators of glacier oscillations. Geogr Ann 21(3-4):216–242

UNDP – United Nations Development Programme (2013b) Country Programme Action Plan (CPAP) between The Government of Nepal and The United Nations Development Programme 2013–2017. Government of Nepal and UNDP, Kathmandu

UNDP – United Nations Development Programme (2013a) Community based glacier lake outburst and flood risk reduction in Nepal, project document. UNDP Environmental Finance Services, Kathmandu

Vuichard D, Zimmermann M (1986) The Langmoche flashflood, Khumbu Himal, Nepal. Mt Res Dev 6(1):90–94

Vuichard D, Zimmermann M (1987) The 1985 catastrophic drainage of a moraine dammed lake, Khumbu Himal, Nepal: cause and consequences. Mt Res Dev 7:91–110

Watanabe T (1992) Human impact and landscape changes in the Nepal High Himalaya. PhD thesis, University of California at Davis

Watanabe T (2008) Global warming and crisis of the world natural heritage sites: a case study in Sagarmatha (Mt. Everest) National Park. Glob Environ Res 13(2):113–122 [In Japanese]

Watanabe T, Ives JD, Hammond JE (1994) Rapid growth of a glacial lake in Khumbu Himal, Nepal: prospects for a catastrophic flood. Mt Res Dev 14:329–340

Watanabe T, Kameyama S, Sato T (1995) Imja Glacier dead-ice melt rates and changes in a supraglacial lake, 1989–1994, Khumbu Himal, Nepal: danger of lake drainage. Mt Res Dev 15:293–300

Watanabe T, Lamsal D, Ives JD (2009) Evaluating the growth characteristics of a glacial lake and its degree of danger of outburst flooding: Imja Glacier, Khumbu Himal, Nepal. Nor Geogr Tidsskr (Nor J Geogr) 63:255–26

Yamada T (1998) Glacier lakes and its outburst flood in the Nepal Himalaya. Monograph no. 1, Data Center for Glacier Research. Japanese Society of Snow and Ice, Tokyo

Yamada T, Sharma CK (1993) Glacier lakes and outburst floods in the Nepal Himalaya. IAHS Publ 218:319–330

Chapter 14
Understanding Factors Influencing Hydro-climatic Risk and Human Vulnerability: Application of Systems Thinking in the Himalayan Region

Gourav Misra, Harekrishna Misra, and Christopher A. Scott

Abstract The Uttarakhand flash floods of 2013 have been dubbed as the "Himalayan Tsunami". The region has been subjected to severe changes in its high-mountain glacial environment. The risk of disasters striking this region has therefore considerably increased in recent times because of the increased human activities and unplanned urbanization, which along with changing climate affects the fragile social-ecological system (SES) in the region. This chapter deals with the study of the SES wellbeing in the Himalayas in light of the 2013 Uttarakhand disaster with focus on the drivers and the interrelationships among them. Systems thinking (ST) is the foundation of the proposed framework for this case study. Application of ST principles provides insights to the way environment has been responding to the stimuli. ST approaches provided the scope to confirm that drivers and dimensions like population, anthropogenic induced disturbances (deforestation and hydel projects) and education (disaster preparedness) need to be given priorities for addressing the challenges. The case of Uttarakhand in India indicates that the systemic behaviour for measuring SES wellbeing can be measured through standard dimensions. However, systematic behaviour analysed through events and pattern analyses, causal-loop diagrams and circular referencing loops provided deeper insights that have differently influenced this systemic behaviour.

Keywords Social-ecological system (SES) wellbeing • Disaster • Systems thinking • Vulnerability

G. Misra
International Water Management Institute, Anand 388001, Gujarat, India
e-mail: gouravmisra@gmail.com

H. Misra
Institute of Rural Management Anand, Anand 388001, Gujarat, India
e-mail: hkmishra@irma.ac.in

C.A. Scott (✉)
Udall Center for Studies in Public Policy/School of Geography & Development, University of Arizona, Tucson, AZ, USA
e-mail: cascott@email.arizona.edu

R.B. Singh et al. (eds.), *Climate Change, Glacier Response, and Vegetation Dynamics in the Himalaya*, DOI 10.1007/978-3-319-28977-9_14

14.1 Introduction

The Indian state of Uttarakhand is situated in the world's highest and youngest mountain range. The geology of the area is deformed, degraded and dissected by structural deformities and drainages. It is seismically very active and is plagued by frequent earthquakes and landslides. This region is therefore highly unstable and this is further compounded by variable climatic conditions and rapidly expanding anthropogenic interferences in the form of unplanned urbanization, deforestation, mining, and hydropower projects.

The Uttarakhand flash floods of 2013 have been dubbed as the "Himalayan Tsunami". On 16th and 17th June 2013, heavy and prolonged rainfall compounded with high-volume glacial melt caused overflowing of the Chorabari Lake and the tributaries Madhu Ganga and Dudh Ganga that eventually led to the Mandakini River bursting its banks and devastating communities and ecosystems. During this period, the state received heavy to extremely heavy rainfall (about 65–245 mm, IMD 2013) because of the fusion of westerlies and the monsoonal cloud system (Prakash 2013; IMD 2013). Apart from the heavy rains, the high glacial melt in the months of May and June due to rising temperatures also led to the increase in lake water volume and the overflowing of the lakes. As a result, the town of Kedarnath suffered great devastation that caused thousands of deaths, severe damage to buildings, leaving large numbers of pilgrims stranded in the valley (Prakash 2013; DMMC 2013).

The region has been subjected to severe changes in its high-mountain glacial environment. The risk of disasters striking this region has therefore considerably increased in recent times because of the increased human activities and unplanned urbanization to cater to the ever-increasing influx of tourists and pilgrims in to the state. Reclamation of rivers coupled with deforestation for large-scale and unplanned urbanization has led to change in river courses, increased surface flow with high sediment load, and rise of river bed due to deposition of debris. Such impediment to normal river flow courses leads to ecological imbalances with catastrophic consequences. These changes in the course of river flow were also seen during the cloudburst on 16th and 17th June when the Alaknanda River and its tributary Mandakini were flooded and started flowing in their old courses where human settlements had come up (Dobhal et al. 2013, The Third Pole 2013). Such natural and human coupled hazards are therefore imminent to cause large-scale destruction in the absence of effective disaster preparedness, risk assessment, and longer-term programs and policy measures.

Therefore, in view of the above, this chapter aims to apply a systems thinking conceptual framework to:

1. Social-ecological assessment of risk and framing of guidelines for planned human activities in the form of land use change, i.e. urbanization, deforestation, etc.
2. Contribute to the development of an action plan for ensuring preparedness in case of reoccurrence of similar disasters

This chapter discusses the environmental change and human vulnerability in the context of ecosystem resilience and its interaction with various drivers. The factors affecting the resilience of SESs need to be studied for understanding the effects on human wellbeing and also the anthropogenic effects on loss of resilience.

The ability of any SES to absorb shocks or disturbances defines its resilience. Regime shifts (i.e. the shift of the ecosystem from one stable state to another) as well as management tools and policy alternatives are therefore an active area of study (Rocha et al. 2014; Scott and Buechler 2013). Regime shifts can occur due to abrupt or continuous change in the drivers. Regime shift is succeeded by loss of resilience and hence the study of a dynamic SES such as the Mandakini watershed in Uttarakhand would help in unravelling the factors or drivers responsible for such shifts. Analysis of long-term data can help predict the mean state and the natural variability of the ecosystem and the points where the shifts/changes occur. Several studies (Prakash 2013; DMMC 2013; DeYoung 2004) indicate the role of climate and hydrology but provide limited insights into the effects of coupled anthropogenic activities and policies on ecosystem resilience (i.e. natural-human interaction).

This chapter is organized as follows. In Sect. 14.2, a conceptual framework is presented with the aim to understand the factors leading up to events such as the June 2013 floods in Uttarakhand. In the following Sect. 14.3, understanding derived from application of the framework is mapped to the calamity in Uttarakhand. In Sect. 14.4, limitations of this work are discussed along with scope for further research.

14.2 Conceptual Framework

It is believed that calamities and disasters are mostly man-made. They occur due to inaccurate assessment of cause and effect relationships among various contributors, complex and dynamic behaviour of the contributors, and restrictive pressure on livelihood opportunities that humans face in the society. These contributors are also likely to be affected by political, social, and economic considerations that societies adopt for development. However, for attaining resilient outcomes, it is essential that holistic approaches are taken. The conceptual framework presented in Fig. 14.1 is based on this understanding, which is further explained below. The framework recognizes that disasters/calamities are outcomes of the processes that aim to support SESs in place. Any interventions around this system have been influenced by ecological, social, and economic dimensions. While doing so, it is thus imperative to take a holistic approach through systems thinking (ST) principles and create a measurement system so that impacts of interventions are measured holistically. This measurement is also considered to be helpful in supporting design and analyses of policies created for governance and use of resources for development.

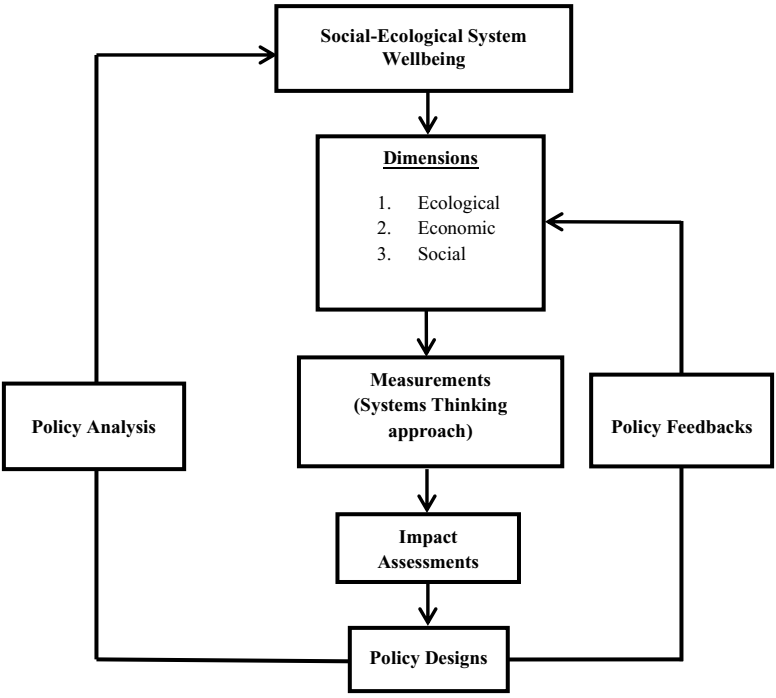

Fig. 14.1 The framework for the study (Source: Authors)

14.2.1 Systems Thinking (ST)

ST (Edson 2008; Misra 2013) is the foundation of the proposed framework. ST is a discipline that enforces measures for capturing holistic views of challenges, including solutions proposed through stakeholder participation. ST is opposed to traditional thinking in many ways. First, ST does not believe in "top-down" approach to address problems. Second, it argues in favour of "economies of flow" and is opposed to "economies of scale". This means external influences are to be accounted for during assessment of problems and finding solutions. Third, it tries to examine patterns of events.

> Rather than thinking of the world in "parts" that form "wholes", we start by recognizing that we live in a world of "wholes" within "wholes". Rather than trying to put the pieces together to make the whole, we recognize that the world is already whole.

In this chapter paper, some of the critical dimensions of systems thinking are taken up for evaluating the events in Uttarakhand. They are as presented below:

I. Examine ST through "systemic" and "systematic" behaviour of the events.
II. Find out whether events recur and display a pattern.

III. Cause and effects may not be generally linearly posited. There are likely to be multiple causal pathways, feedbacks, and other constraints.
IV. Attempt to see the "whole" picture of the issue at hand (do not miss the forest for the trees).

This case study deals with the resilience of the SES wellbeing in the Himalayas in light of the 2013 Uttarakhand disaster with focus on the drivers and the interrelationships among them. The resilience of a SES can be classified into social, ecological, and economic dimensions, which constitute various drivers whose interaction determines the joint outcome behaviour of the SES. These dimensions as per systems thinking approach need to undergo systemic and systematic behavioural measurements.

14.2.1.1 Systemic Behavioural Measurements

Systemic behaviour measurements in ST approach include overarching problem areas rather than focusing on individual problems. However, measurements with systemic views provide the scope to adopt "reductionist approach" to guide the planners in a systematic manner. In this chapter, the following arguments are considered important to measure ecosystem wellbeing of a region based on the attributes presented in Fig. 14.1.

$$Ecosystem\,wellbeing = f\,\text{Dimension}_{(\text{ecological},\text{economic},\text{social})} \tag{14.1}$$

$$Dimension_{Ecological} = f\begin{pmatrix}\text{Hydrology},\text{Forest cover},\text{Net Sown area},\text{Cropping intensity},\\ \text{Biodiversity},\text{Invasive species},\text{Soil degradation},\ldots\end{pmatrix} \tag{14.2}$$

$$Dimension_{Economic} = f\begin{pmatrix}\text{Income},\text{taxes},\\ \text{land productivity},\text{GDP per unit of energy use},\ldots.\end{pmatrix} \tag{14.3}$$

$$Dimension_{Social} = f(\text{Literacy},\text{awareness},\text{health},\text{unemployment},\ldots\ldots) \tag{14.4}$$

14.2.1.2 Systematic Behavioural Measurements

Under this measurement, all the dimensions discussed above are systematically analysed through "cause and effect relationship" studies. Indicative relationships are presented in Fig. 14.2.

In Fig. 14.2, a schematic representation is made to explain the circular referencing of cause and effects for ecosystem wellbeing in a region. It is argued that the ecosystem is affected by the social, ecological, and economic behaviour of human agents. Unless these behaviours are regulated with a balanced approach to sustain livelihood systems in the region, it is quite likely that disasters would recur.

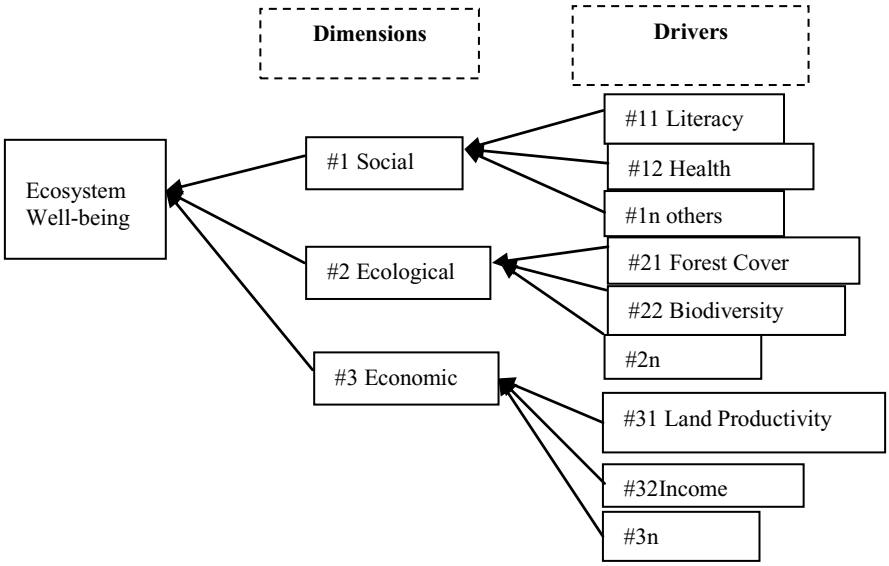

Fig. 14.2 Cause and effect relationships (Source: Authors)

Having made an impact assessment of these drivers on the river basin, policy recommendations need to be made in accordance with gap between positive (what is) and normative (what should be) outcomes. These policy changes are expected to feedback into the existing dimensions of the river basin ecosystem, convert into drivers, thereby setting in motion a causal loop, determining subsequent SES outcomes and so on.

14.2.1.3 Recurrence of Events and Pattern

The state of Uttarakhand is vulnerable to multiple disasters like floods, earthquakes, landslides, fires, etc. It ranks in the top five in the list of natural disaster-prone states of India (DMMC 2015). Some of the major flash floods and cloudbursts in Uttarakhand are listed in Table 14.1 below (table adapted from Planning Commission-GOI 2006; NIDM 2015):

It may be noted that recurrence of events (flash floods and cloudbursts) is high over a period time. Flash floods with high recurrence over the years during 1989 and 2013 have displayed a pattern as well. This pattern is for a period during the months of May and September in a particular year. Recurrence of cloudbursts is also an annual affair during 2002 and 2012 with a low frequency, and the pattern is not understandable. However, data as presented in Table 14.1 above are conclusive in establishing a strong recurrence.

Table 14.1 Some of the major flash floods and cloudbursts in Uttarakhand

Flash floods	Cloudbursts
Date; location	*Date; location*
05-09-1989; Karanprayag, Chamoli	2002; Khetgaon
26-12-1991; Uttarkashi, Uttarkashi	2004; Ranikhet
30-07-1994; Chaukhutia, Almora	2007; Pithoragarh and Chamoli
02-08-1997; Near Neelkanth, Haridwar	2008; Pithoragarh
17-07-2001; Near Meykunda, Rudraprayag	2009; Munsiyari Tehsil, Pithoragarh
20-07-2003; Didihat, Pithoragarh	21 July 2010; Almora
21-05-2004; Kapkot, Bageshwar	18 August 2010; Kapkot, Bageshwar
09-06-2004; Kapkot, Bageshwar	13 September 2012; Chwanni, Mangoli, and Kimana villages of Okhimath block in Rudraprayag
21-07-2005; Vijaynagar, Rudraprayag	
13-08-2007; Didihat, Pithoragarh	
25-07-2009; Joshimath, Chamoli	
2009; Munsiyari, Pithoragarh	
19-07-2010; Kot, Pauri	
20-07-2010; Khatima, Rudrapur, Udham Singh Nagar	
31-07-2010; Dehradun	
18-08-2010; Dhari, Nainital	
24-08-2010; Jaspur, Udham Singh Nagar	
08-09-2010; Karanprayag, Chamoli	
11-09-2010; Nyalgarh, Pauri	
18-09-2010; Belbandgoth, Champawat	
18-09-2010; Jwalapur Kasim, Haridwar	
20-09-2010; Dhari, Nainital	
22-09-2010; Kot, Pauri	
06-05-2011; Raipur, Dehradun	
15-08-2011; Tuneda, Bageshwar	
03-08-2012; Asi Ganga Valley, Uttarkashi District	
June, 2013; Mandakini, Uttarakhand	

14.2.1.4 The "Whole" Picture

Systems thinking (ST) (Misra 2013) considers it important to paint a whole picture for any recurring problem. It is argued that any recurring problem is the result of poor articulation of ST-based action plans. It is also often difficult to capture the cause and effects of any problem holistically in the beginning of analyses. However, ideally, citizens, planners, and interventionists need to cocreate strategies for sustainable society, ecology, and especially overall development.

It is often under discourse that an "individual household" could be treated as a unit of development whereas society is its superset. However, under ST principles, it tends to examine whether there is a scope to have analogous treatment like a tree in the forest. With ST principles, it may be worth considering the challenge of managing wellbeing of a tree by ignoring the forest or vice versa. Like a tree in a larger forest, a household similarly is influenced by its context – society, environment, and policies formulated for use of infrastructure, commons, and resources for livelihoods. It means a household is not only a unit of economic activities (production and consumption) but also is part of ecology, society, and political environment that influence its quality of life and livelihoods. Just as trees aggregate to form forests with other related entities like river, water bodies, birds, animals, and humans, the "whole" around the "individual household" tends to include many coexisting entities in the ecosystem. Thus, it is important to examine the "whole" and needs to be examined for suitable ecosystem. Disasters, with ST principles, are termed as man-made, and therefore, it may be worth examining the patterns and cause-effects of such events.

14.3 Case of Uttarakhand

The Himalayan regions experience numerous disasters annually, and earthquakes, landslides, and flooding contribute to almost half of the incidents (Shaw and Nabanapudi 2015). The state of Uttarakhand, India, situated in the Himalayan mountain range is no different and plagued by natural disasters. Landslides, floods, and heavy rainfall have frequently created havoc in the lives of the people in the region. It is seismically active and therefore highly unstable, and this is further compounded by unfavourable climatic conditions and uncontrolled anthropogenic interferences in the form of unplanned urbanization, deforestation, mining, and hydropower projects.

The region has been subjected to severe changes in its high-mountain glacial environment. The risk of disasters striking this region has therefore considerably increased in recent times because of the increased human activities and unplanned urbanization to cater to the ever-increasing influx of tourists and pilgrims in to the state. Reclamation of rivers coupled with deforestation for large-scale and unplanned urbanization has led to change in river courses. Such impediment to normal river flow courses leads to ecological imbalances with catastrophic consequences.

The 2013 flash floods in Uttarakhand can therefore be evaluated in the systems thinking context. Prolonged heavy rainfall and glacial melt caused by increased temperatures were responsible for bursting of the rivers and also indicate the role of extreme weather events causing disasters. Another theory put forward is that the reclamation of rivers coupled with deforestation for large-scale and unplanned urbanization led to change in river courses, increasing surface flow with high sediment load, and rise of river bed due to deposition of debris (Prakash 2013; Dobhal 2013; The Third Pole 2013; Singh 2013). With the effect of climate change being

felt increasingly in the form of increasing temperatures in the Indian subcontinent – about 0.3–0.6 °C in the last 100 years (IPCC 2007) and predicted to increase further in the coming decades – the frequency of disasters is expected to rise. The increase in climate-related disaster events and human casualties has been reported to be increasing at the rate of 6 % and 9 %, respectively (Shaw and Nabanapudi 2015; DMMC 2015; Sharma and Dobriyal 2014). Several studies (Bajracharya 2009; SAARC 2008) and the 2013 Uttarakhand disaster (Chopra 2014) also show a rapid melting of the Himalayan glaciers in recent times and present indications of impending disasters in times to come. Figure 14.5 shows the precipitation and air temperatures trends for the last 40 years in this context (data is based on Indian Meteorological Department (IMD) and Tropical Rainfall Measurement Mission). The average temperatures have been on a greater increasing slope, whereas the average rainfall trend is less steep in comparison. The year of Uttarakhand disaster, 2013, which also shows a big spike in rainfall, is on an increasing trend which along with the rising trend in average temperatures provides a grim picture of the future if precautions and corrective measures in the form of disaster preparedness and prompt rescue measures are not taken.

14.3.1 Systems Thinking Perspectives

Application of ST principles provides insights to the way environment has been responding to the stimuli. In the case of Uttarakhand, rainfall is one of the major contributors to the disasters. Therefore, three steps of ST principles have been applied in this Uttarakhand case: (a) nonlinearity between temperature and rainfall leading to disasters, (b) pattern of relationship between temperature and rainfall, and (c) causal loop analyses for the disaster.

14.3.1.1 Events and Patterns

As explained earlier, disasters are expected to be the "surprises" for Uttarakhand, and they should not continuously recur. In this case, floods, flash floods, landslides, incidence of poverty, etc. can be categorized as "events". Although the role of environment in such disasters has been debated and discussed a lot, there is a clear relationship between natural disasters and anthropogenic factors. Unabated constructions, reclamation of land from rivers, hydropower projects, and road laying to accommodate the ever-increasing tourist influx in the state has impacted the already environmentally fragile ecosystem of the state.

An Article by Singh (2013) goes on further to prove this by citing data from the Uttarakhand state transport department. The department reports a 1.5 times increase in the number of registered vehicles (83,000–183,000) over the period of 2005–2013. And a vast majority of these vehicles are for transporting pilgrims and tourists. Such vehicle figures jumped from 4000 in 2005 to 40,000 in 2013, an almost

ten time increase. The proportion of new tourist vehicles to total registered vehicles jumped from a mere 5 % in 2005 to 22 % in 2013. These figures provide further strength to the established correlation between landslides and tourism increase in mountains (Singh 2013a, b; Seethapati 2015).

Additionally there are 98 existing Hydro-Electric Projects (HEPs) in Uttarakhand with plans to increase this number to 336 in the future, out of which the largest number (122) are commissioned in the disaster-prone Alaknanda valley (SANDRP 2013). Most of these hydropower HEPs involve deforestation, which increases the threat of soil erosion due to runoff, landslides, and floods. An extensive and conclusive study (Chopra 2014) also discusses the role of HEPs in disturbing the ecology of the Uttarakhand and eventually contributing to the disaster of the 2013. It is argued that HEPs alter the course of river flow due to submergence, drying of rivers downstream in non-monsoon due to diversions into tunnels, and fragmentation of rivers due to multiple HEPs on a stream. This leads to irreversible impacts on the ecosystem and biodiversity in the mountainous region. The role of extreme climate events like unprecedented heavy rainfall and climate change impacts has also been discussed. One of the causes of the bursting of the lake is reported to be warm rainfall on snow that led to overflowing of the Chorabari Lake. Also the dams were not equipped to contain huge amounts of flood water and prevent flooding downstream. A combination of natural climatic and anthropogenic factors therefore led to the 2013 disaster.

Systemic Behaviour Measurements

In the case of Uttarakhand, it may be worthy considering the events contributing adversely to the SES wellbeing. Thus, the systemic behaviour can be represented as Eqs. 14.5, 14.6, 14.7, 14.8, 14.9, and 14.10 below:

$$SES\ wellbeing = f\,\mathrm{Dimension}_{(\mathrm{Events})} \tag{14.5}$$

$$Dimension_{Events} = f(\mathrm{Social}, \mathrm{Economic}, \mathrm{Ecological}) \tag{14.6}$$

$$Dimension_{Event-Flood} = f(\mathrm{Social}, \mathrm{Economic}, \mathrm{Ecological}) \tag{14.7}$$

$$Dimension_{Event-Flood-Social} = f(\mathrm{Tourism}, \mathrm{unplanned\ urbanization}, ..) \tag{14.8}$$

$$Dimension_{Event-Flood-Economic} = f(\mathrm{Hydro\ \ Electric\ Projects}, \mathrm{low\ income}, \mathrm{weak\ housing\ structures} * \ldots.) \text{ resulting in low resilience} \tag{14.9}$$

$$Dimension_{Event-Flood-Ecological} = f(\mathrm{Heavy\ rainfall}, \mathrm{deforestation}, \mathrm{glacier\ melt}, \mathrm{temperatures} \ldots..) \tag{14.10}$$

*As per the Vulnerability Atlas of India, in Uttarakhand approximately 56 % of houses are made of mud, unburnt brick, and stonewall. This is a sign of very high vulnerability, considering probability of earthquakes, landslides, flash floods, cloudbursts, etc. (DMMC 2015).

Systematic Behaviour Measurements

As explained earlier, systematic measurements are based on measurable and identifiable cause and effect relationships that are presented through ST approaches. In the case of Uttarakhand, SES wellbeing are severely influenced by the flash flood and landslides leading to loss of human lives, property, and livelihoods of people due to ecological imbalances. These events are recurring and pattern oriented. Thus, there is scope to evaluate the cause and effects of such events and their contributions to the environment and society.

It is important to examine under systematic measurements whether pattern of the behaviour could be of linear or nonlinear in nature. ST principles acknowledge that causal relationships to be nonlinear at metalevel though systematic analyses for micro measurements may seem to be linear. Therefore, it may be worth discussing linear and nonlinear behaviour in this section with some clarity. The behaviour between two variables, for example, is said to be linear if the magnitude across two different time periods remains same. In Fig. 14.3, this linear behaviour is presented. In the timelines t1 and t2, slope m_1 and slope m_2 remain the same for the variables. This prediction, however, may have the complexities of the equation $Y = mX + C$ where C becomes a constant influencer in the system.

Nonlinearity is understood to be a phenomenon that presents different correlations that datasets provide during a time period. This is explained in Fig. 14.4 where a generic case of linearity is presented.

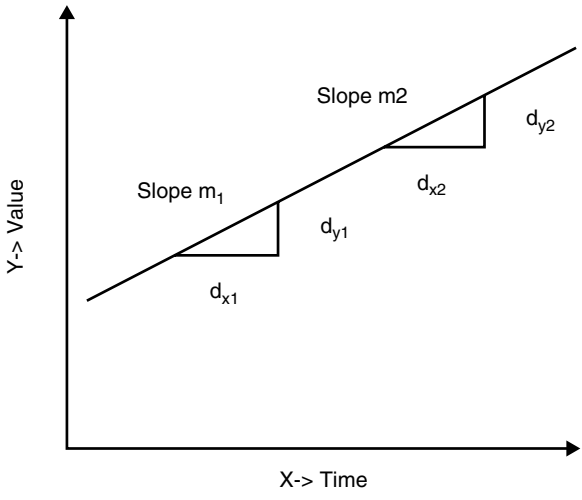

Fig. 14.3 Linear pattern in causal relationships (Source: Authors)

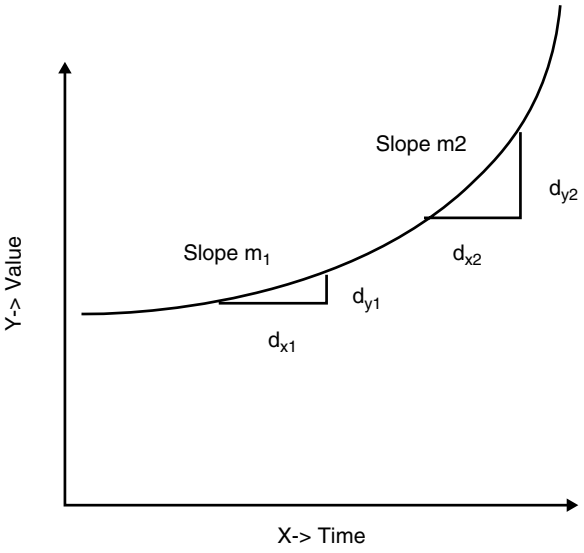

Fig. 14.4 Nonlinear pattern in causal relationships (Source: Authors)

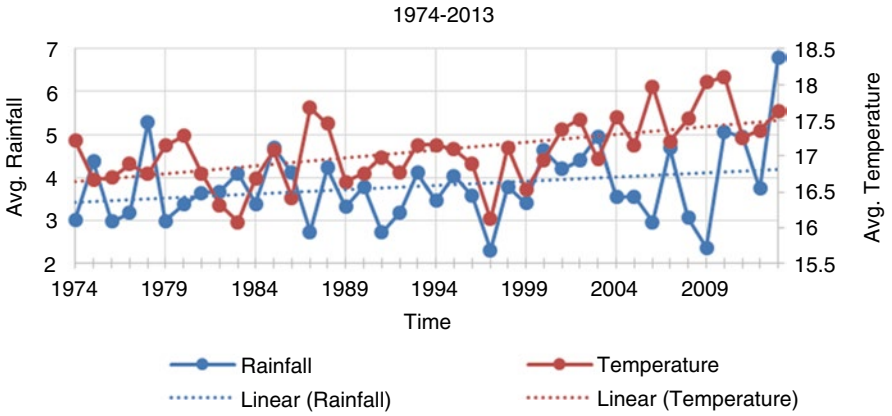

Fig. 14.5 Averaged annual temperature (deg. Celsius) and rainfall (mm) data for the state of Uttarakhand (1974–2013) (Source: Authors)

In this case study of Uttarakhand, two influencers, i.e. temperature rise and rainfall, are taken up for analyses. In Figs. 14.4 and 14.5, relationships between these two influencers are presented. It may be noted that pattern of this relationship is "nonlinear" which is a major qualifier for validating ST principles.

It may be noted that in Fig. 14.5, the average temperature and rainfall during the period 1974–2013, though provides a pattern, do not have same slopes.

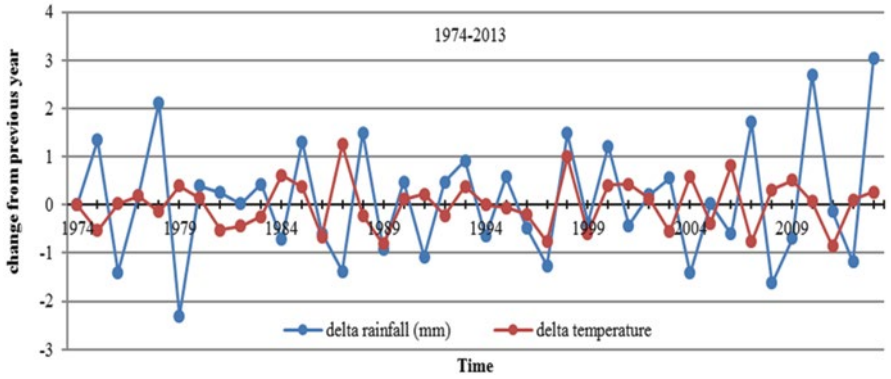

Fig. 14.6 Annual incremental or delta rainfall and temperature values showing nonlinearity (Source: Authors)

This behaviour is supported in Fig. 14.6 where the $d_{temperature}$ (delta temperature) and $d_{rainfall}$ (delta rain fall) present different values at a particular timeline. Therefore, slopes in those timelines are concluded to be of different magnitudes. Note: In this analysis under systems thinking baseline has not been considered as "static" because of continuous occurrence of events. Under circular referencing, the t_0 (initiation time) itself is dynamic. Therefore, the baseline in this analysis is an annual affair, which means every preceding year that is the base year for the current year. The delta values (−ve or +ve) will showcase the linearity pattern. So the graphs presented in Fig. 14.6 are nonlinear in nature.

In Fig. 14.8, a generic causal loop diagram for Uttarakhand scenario is presented. Inspiration to present this scenario is derived from Fig. 14.2. This diagram, though is not holistic, provides an indicative results with circular referencing of multidimensional contributions encompassing social, ecological, and economic issues prevalent in Uttarakhand.

Figure 14.7 presents a holistic approach discussing various dimensions and drivers of SES wellbeing. As shown in Fig. 14.8, SES wellbeing is dependent of social, economic, and ecological factors. Whereas social issues are predominantly influenced by population density in the region, ecological dimension is influenced by large-scale construction of hydel projects and deforestation. Population density is because of tourist influx and birth rate that India faces in general. Economic activities have generated pressure on land and forest in the region leading to rise in temperature as well as recurrence of flash floods. It may be worth noting that this cause-effect relationship has circular effects, which mean that all the dimensions contribute to each other in the timeline for Uttarakhand.

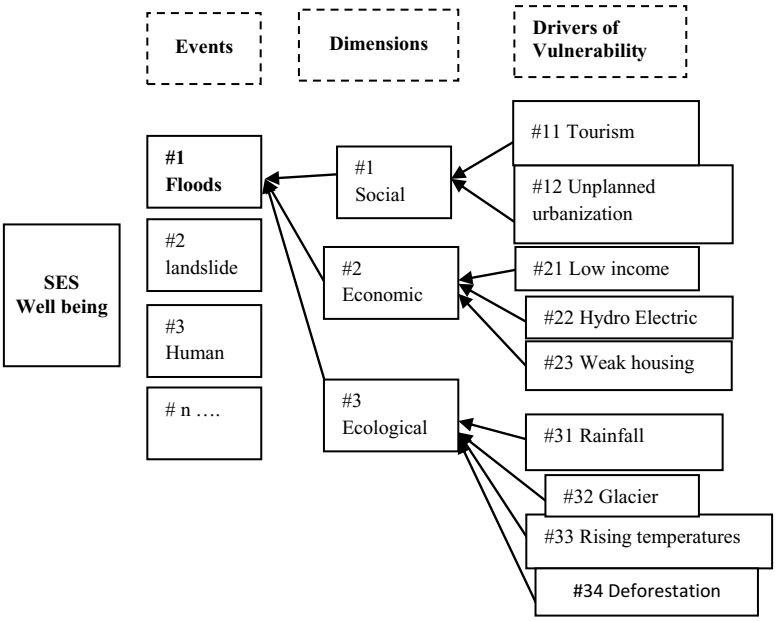

Fig. 14.7 Cause and effect relationships (Source: Authors)

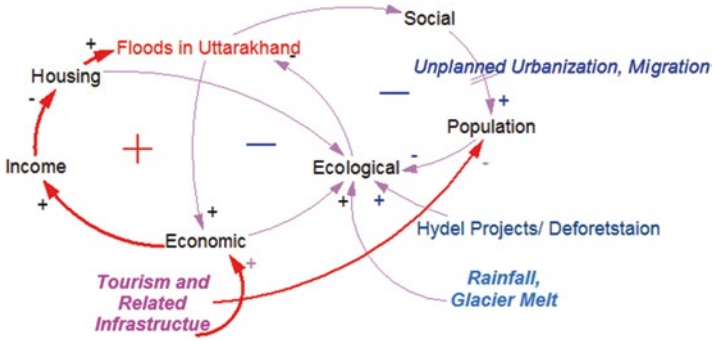

Fig. 14.8 Causal loop diagram for Uttarakhand scenario (Note: + effects denote direct influence whereas −signs denote indirect influences) (Source: Authors)

14.4 Conclusion

In this chapter, the case of Uttarakhand, India, from the Himalayan region is presented to examine appropriateness of applying ST principles to explore causes and likely effects of the events that occur in disaster management paradigm. Another objective was to ascertain whether systemic behaviour could be translated into

specific systematic measurements so that certain clarity would emerge to address the complex challenge that society faces like disasters. Through this case study, it could be ascertained that measuring social, economic, and ecological dimensions could assess systemic behaviour. Besides, it could be verified from secondary sources that systemic measurements provide insights to complex phenomena, and these complexities could be measured by analysing each dimension through systematic analyses of dimensions, identifying drivers for each of these dimensions. It is also evident from the analyses that systematic measurements have the scope to analyse the cause and effects through circular referencing and reinforcing contributions of the drivers. It was also observed that each case provided different situations through which social, economic, and ecological dimensions contributed to the disasters and in turn to the SES wellbeing. Despite contributions specific to the cases, ST approaches provided the scope to confirm that drivers and dimensions like population, deforestation, and education (disaster preparedness) need to be given priorities for addressing the challenges.

The case of Uttarakhand in India indicates that the systemic behaviour for measuring SES wellbeing can be measured through standard dimensions. However, systematic behaviour analysed through events and pattern analyses, causal-loop diagrams, and circular referencing loops provided deeper insights that have differently contributed/ influenced this systemic behaviour. Uttarakhand is situated in the high mountainous environment with large-scale unplanned urbanization, glacial melt, and reclamation of land from rivers acting as main contributors to flooding events. The various contributors and influencers are discussed in Eqs. 14.5–14.10 as functional dependencies and Figs. 14.2 and 14.7 as cause-effect relationships. Here flood is a common phenomenon and is a recurring event. Outcomes of such events have been loss of human life and income generation opportunities, stress on livelihood options, and degradation of the environment with loss of ecosystem services. In addition, ecological vulnerability has also increased. This case-based study provides the scope for policymakers to take cognizance of systemic issues while addressing the systematic influencers in the local context.

There are two limitations of this work. The first one relates to use of data. Data for analyses and formation of the case is drawn from secondary sources. ST approaches require supporting primary sources of data and validation processes through case studies and other related quantitative methods. The second limitation is analysing patterns for the relationship between temperature and rainfall. The datasets used are large, and thus analyses based on their mean may mask the results at the ground level. Future works therefore are planned for taking up these measures and come up with insightful analyses.

Acknowledgment This research is partially supported by the project entitled “The irrigation-hydropower nexus in the Ganges headwaters” with the support from the International Water Management Institute under the Water, Land, and Ecosystems Program of the Consultative Group for International Agricultural Research. Special thanks are extended to Prof. Suraj Mal for the invitation to contribute this chapter.

References

Bajracharya SR, Mool P (2009) Glaciers, glacial lakes and glacial outburst floods in the Mount Everest region, Nepal. Ann Glaciol 50(53):81–86

Chopra R, Das BP, Dhyani H, Verma A, Venkatesh HS, Vasistha HB, Dobhal DP, Juyal N, Sathyakumar S, Pathak S, Chauhan TKS (2014) Assessment of environmental degradation and impact of hydroelectric projects during the June 2013 Disaster in Uttarakhand. Part I-Main Report. Submitted to The Ministry of Environment and Forests Government of India, April, 2014. Retrieved March 04, 2015 from http://www.indiaenvironmentportal.org.in/files/file/environmental%20degradation%20&%20hydroelectric%20projects.pdf

DeYoung B, Harris R, Alheit J, Beaugrand G, Mantua N, Shannon L (2004) Detecting regime shifts in the ocean: data considerations. Prog Oceanogr 60:143–164

Disaster Mitigation & Management Centre Uttarakhand Secretariat (DMMC) Government of Uttarakhand (2013) Uttarakhand Disaster Recovery Project (P146653) World Bank Assisted. Retrieved March 04, 2015 from http://dmmc.uk.gov.in/files/pdf/Final_ESMF_2.pdf

Disaster Mitigation & Management Centre Uttarakhand Secretariat (DMMC) State Disaster Management Action Plan for the State of Uttarakhand. Retrieved March 16, 2015 from http://dmmc.uk.gov.in/files/pdf/complete_sdmap.pdf. Last modified 16-03-2015

Dobhal DP, Gupta AK, Mehta M, Khandelwal DD (2013) Kedarnath disaster: facts and plausible causes. Curr Sci 105(2):171–174

Edson R (2008) Systems thinking applied, a primer. Applied Systems Thinking Institute, Virginia. Version 1.1 Copyright 2008 Analytic Services Inc. Retrieved December 01, 2015 from http://www.anser.org/docs/systems_thinking_applied.pdf

India Meteorological Department (IMD), Ministry of Earth Sciences, Government of India (2013) A preliminary report on heavy rainfall over Uttarakhand during 16–18 June 2013. Retrieved March 16, 2015 from http://imd.gov.in/doc/uttrakhand_report_04_09_2013.pdf

IPCC (2007) Climate change 2007. In: Solomon S, Qin D, Manning M, Chen Z, Marquis M, Averyt KB, Tignor M, Miller HL (eds) The physical science basis, contribution of Working group I to the 4th assessment report of the intergovernmental panel on climate change. Cambridge University Press, Cambridge. ISBN: 978-0-521-88009-1 (pb: 978-0-521-70596-7)

Misra HK (2013) Emerging role of systems thinking oriented E-governance for supporting MDGs: learning in Indian context, The 7th International Conference on Theory and Practice of Electronic Governance (ICEGOV2013), Seoul, South Korea, 22–25 October. Published in the Proceedings of ACM

Misra HK (2013b) Information systems management in business and development organizations: text and cases. PHI Learning Private Limited, New Delhi. ISBN ISBN 978-81-203-4796-0

NIDM, Uttarakhand. Last modified 16-03-2015. National Disaster Risk Reduction Portal. Retrieved March 16, 2015 from http://nidm.gov.in/pdf/dp/Uttara.pdf

Parkash S (2013) Brief report on visit to Alaknanda Valley, Uttarakhand Himalaya during 22–24 June 2013. National Institute of Disaster Management, New Delhi. Retrieved June 24, 2014 from http://www.indiaenvironmentportal.org.in/files/file/Uttarakhand%20Disaster.pdf

Planning Commission, Government of India (2006) Report of the task force on The Mountain Ecosystems (Environment and Forest Sector) for eleventh five year plan. Retrieved February 23, 2015 from http://www.planningcommission.nic.in/aboutus/committee/wrkgrp11/tf11_ecosys.pdf

Rocha JC, Biggs R, Peterson G (2014) Regime shifts: what are they and why do they matter? Regime Shifts Database. Retrieved February 22, 2015 from www.regimeshifts.org

SAARC (2008) SAARC workshop on the climate change and disasters: emerging trends and future strategies. SAARC Disaster Management Center. 21–22 August 2008, Kathmandu, Nepal. Retrieved April 05, 2015 from http://saarc-sdmc.nic.in/pdf/publications/climate/cover.pdf

Scott CA, Buechler SJ (2013) Iterative driver-response dynamics of human-environment interactions in the Arizona-Sonora borderlands. Ecosphere 4(1): Article 2, doi:10.1890/ES12-00273.1

Seethapati PV Identification of landslide-prone areas using remote sensing techniques. Retrieved January 25, 2015 from http://www.moef.nic.in/downloads/public-information/Hazard-Summaries.pdf

Sharma P, Dobriyal P (2014) Climate change and agricultural sector in Uttarakhand. J Stud Dyn Chang (JSDC) 1(1):6–14. ISSN: 2348-7038

Shaw R, Nabanapudi HK, editors (2015) Disaster risk reduction methods, approaches and practices. Chapter 8 mitigating climatic and human induced disaster risks through ecosystem resilience: harmonizing built and natural environments in the HKH region. e-ISBN: 978-4-431-55242-0. doi10.1007/978-4-431-55242-0

Singh J (2013) Man-made reasons for Uttarakhand disaster | Down To Earth. Web article: 18 June 2013. Retrieved January 25, 2015 from http://www.downtoearth.org.in/content/man-made-reasons-uttarakhand-disaster

Singh J (2013) What really happened in Uttarakhand | Down To Earth. Web article: 3 July 2013. Retrieved December 09, 2014 from http://www.downtoearth.org.in/content/what-really-happened-uttarakhand

South Asian Network on Dams, Rivers & People. SANDRP (2013) Dams, rivers and people Vol. 11. Issue5-6. June-July 2013. Retrieved March 16, 2015 from http://sandrp.in/DRP_June_July2013.pdf

The Third Pole. thethirdpole.net (2013) Building in old river courses magnified Uttarakhand disaster. Web article: 15-07-2013. Retrieved February 22, 2015 from http://www.thethirdpole.net/building-in-old-river-courses-magnified-uttarakhand-disaster-2/

Part III
Climate Change and Vegetation Dynamics

Chapter 15
Climate Change and Treeline Dynamics in the Himalaya

Udo Schickhoff, Maria Bobrowski, Jürgen Böhner, Birgit Bürzle, Ram Prasad Chaudhary, Lars Gerlitz, Jelena Lange, Michael Müller, Thomas Scholten, and Niels Schwab

Abstract Treelines are sensitive to changing climatic conditions, in particular to temperature increases, and the majority of global alpine treelines has shown a response to recent climate change. High temperature trends in the Himalaya suggest a treeline advance to higher elevations; it is largely unknown, however, how broader-scale climate inputs interact with local-scale factors and processes to govern treeline response patterns. This paper reviews and synthesizes the current state of knowledge regarding sensitivity and response of Himalayan treelines to climate warming, based on extensive field observations, published results in the widely scattered literature and novel data from ongoing research of the present authors.

Palaeoecological studies indicate that the position of Himalayan treeline ecotones has been sensitive to Holocene climate change. After the Pleistocene-Holocene transition, treelines advanced in elevation to a position several hundred metres higher than today under warm-humid conditions and reached uppermost limits in the early Holocene. Decreasing temperatures below early and mid-Holocene levels induced a downward shift of treelines after c. 5.0 kyr BP. The decline of subalpine forests and treeline elevation in the more recent millennia was coincident with weakening monsoonal influence and increasing anthropogenic interferences.

U. Schickhoff (✉) • M. Bobrowski • J. Böhner • B. Bürzle • N. Schwab
CEN Center for Earth System Research and Sustainability,
Institute of Geography, University of Hamburg, Hamburg, Germany
e-mail: udo.schickhoff@uni-hamburg.de

R.P. Chaudhary
RECAST Research Centre for Applied Science and Technology, Tribhuvan University, Kathmandu, Nepal

L. Gerlitz
Section Hydrology, GFZ German Research Centre for Geosciences, Potsdam, Germany

J. Lange
Institute of Botany and Landscape Ecology, University of Greifswald, Greifswald, Germany

M. Müller • T. Scholten
Department of Geosciences, Chair of Soil Science and Geomorphology, University of Tübingen, Tübingen, Germany

R.B. Singh et al. (eds.), *Climate Change, Glacier Response, and Vegetation Dynamics in the Himalaya*, DOI 10.1007/978-3-319-28977-9_15

To assess current treeline dynamics, treeline type, treeline form, seed-based regeneration and growth patterns are evaluated as sensitivity indicators. Anthropogenic treelines are predominant in the Himalaya; upslope movement of these treelines is related to the effects of land-use change. Near-natural treelines, rare nowadays, are usually developed as krummholz treelines which are relatively unresponsive. Strong competition within the krummholz belt and dense dwarf scrub heaths further upslope largely prevents the upward migration of tree species and retards treeline advance to higher elevation. However, intense recruitment of treeline trees within the treeline ecotone and beyond indicates beneficial preconditions for future treeline ascent. Growth patterns of treeline trees are particularly sensitive to higher winter and pre-monsoon temperatures, suggesting that moisture supply in the pre-monsoon season might be an effective control of future treeline dynamics. Modelled upslope range expansions of treeline trees point to potentially favourable bioclimatic conditions for an upward shift of treelines.

Keywords Holocene • Monsoon • Niche modelling • Recruitment • Seedling • Soil moisture • Soil temperature • Tree radial growth • Treeline advance • Treeline form • Treeline type

15.1 Introduction

Impacts of climate change have affected natural and human systems on all continents and across the oceans in recent decades, with emerging evidence of strong and comprehensive impacts on mountain regions of the world (Huber et al. 2005; Körner et al. 2005; Schickhoff 2011; Grover et al. 2015). Subjected to above-average warming, mountain and glacier environments are highly vulnerable and especially sensitive to changes in climate. Cascading, more or less globally consistent effects on physical systems include mountain permafrost degradation, shrinking glaciers, changing snowpacks, and changing water discharge and availability in rivers and streams (IPCC 2014). With regard to mountain biota, substantial evidence has accumulated reinforcing the conclusion that observed changes in plant and animal phenology and growth have occurred in response to higher temperatures (Cook et al. 2012; Peñuelas et al. 2013), and that the distribution of many plant and animal species has shifted upwards in elevation (Lenoir et al. 2008; Gonzalez et al. 2010; Chen et al. 2011; Gottfried et al. 2012; Pauli et al. 2012).

Thus, it is generally assumed that impacts of contemporary climate change also modify patterns and processes in alpine treeline ecotones and ultimately affect the altitudinal position of treelines in mountains of the world (Holtmeier and Broll 2005, 2007; Wieser et al. 2014). This assumption is based on strong general links between thermal deficiency and treeline position that have resulted in a consensus that treeline positions at continental and global scales are thermally limited, with variations induced by specific local site conditions. In the course of a long history

of treeline research, correlations between treeline formation and air and soil temperatures have been repeatedly established (e.g. Däniker 1923; Wieser and Tausz 2007; Holtmeier 2009; Richardson and Friedland 2009; Körner 2012; Paulsen and Körner 2014; Weiss et al. 2015). At a global scale, treeline formation and maintenance appear to coincide with a growing season mean air temperature ranging from 5.5 to 7.0 °C and a growing season mean soil temperature of 6.4 ± 0.7 °C (Körner 1998, 2007, 2012; Körner and Paulsen 2004). However, considerable deviations from a global treeline isotherm occur at local scales, suggesting a rather broad error term with regard to a global soil temperature threshold. For instance, we assessed a growing season mean soil temperature of 7.5 ± 0.5 °C at a near-natural treeline in Rolwaling/Nepal (Müller et al. 2016). Mean temperatures which do not exist in nature are obviously rather rough indicators of thermal deficiency at treeline elevations.

Given the repeated climatically caused treeline fluctuations during the Holocene (MacDonald et al. 2000; Reasoner and Tinner 2009; Schwörer et al. 2014) and the general dependency of the upper limit of tree life on heat balance, it seems apparent that climate warming will improve growth conditions of treeline forest stands, generate higher stand densities and induce treelines to advance to higher elevations (Grace et al. 2002; Dullinger et al. 2004; Smith et al. 2009). However, treeline movement to greater elevations is a complex process which is extremely difficult to predict since the sensitivity of global treelines to recent climate change is highly diverse. Observed responses at treelines are quite inconsistent and sometimes contradictory, spanning the entire gradient from static treelines with rather insignificant responses to dynamic treelines substantially migrating upslope (e.g. Camarero and Gutiérrez 2004; Daniels and Veblen 2004; Danby and Hik 2007; Kullman and Öberg 2009; Moiseev et al. 2010; Liang et al. 2011; Kullman 2014; Mathisen et al. 2014; Schickhoff et al. 2015). The variability in the response of treelines to changes in climate is reflected in a recent meta-analysis based on a global dataset of 166 sites for which treeline dynamics had been reported since AD 1900. Fifty-two percent of the sites showed advancing treelines, while 47 % did not reveal any elevational shifts; 1 % experienced treeline recession (Harsch et al. 2009). In old-settled mountain regions, e.g. in the European Alps where pastoral use, logging, mining and other land-use impacts had lowered the treeline during the Holocene, land abandonment and the general decline of human impact are usually the dominant driver for treeline movement to higher elevations (Gehrig-Fasel et al. 2007; Vittoz et al. 2008). However, when substantial treeline advances during the twentieth century are reported, effects of land use and climate change are often hard to disentangle (e.g. Baker and Moseley 2007).

To explain the gradient from complete treeline inertia to rapid upslope migration, the local-scale complexity of abiotic and biotic site factors and their interrelationships have to be considered that collectively result in nonlinear responses to climate. Response variability must be attributed to the interaction of broad-scale climate inputs and fine-scale modulators of treeline patterns (Holtmeier and Broll 2005, 2007, 2009; Batllori and Gutiérrez 2008; Elliott 2011; Malanson et al. 2007, 2011). It is still largely unknown, however, how local-scale site conditions such as abiotic

site factors, plant interactions associated with facilitation, competition and feedback systems modify treeline response patterns to region-wide climate controls. The mechanisms of seedling establishment and growth to maturity across the treeline ecotone are of particular interest in this respect (Smith et al. 2003, 2009; Wieser et al. 2014). Different treeline forms (diffuse, abrupt, island, krummholz) obviously show varied responsiveness and may allow inferences on the general mechanisms controlling response patterns (Harsch and Bader 2011), but it is still an open question to what extent treeline form can be used to predict treeline dynamics. In order to analyze how local-scale factors and processes mediate the broader-scale climate inputs and interact and govern sensitivity and response of treelines, complex research approaches at local and landscape scales and in different treeline environments are needed (Holtmeier 2009; Malanson et al. 2011; Wieser et al. 2014).

Recently, the scientific interest in treelines increased considerably since treeline ecotones are potentially promising research objects for detecting and monitoring climate change effects. While European and North American mountains have been a major focus in treeline research programmes, comparatively very few studies have been conducted in the Himalayan mountain system. Information on altitudinal position, physiognomy and treeline-forming tree species is more or less sufficiently documented in the widely scattered literature (Schweinfurth 1957; Champion and Seth 1968; Stainton 1972; Troll 1972; Gupta 1983; Puri et al. 1989; Singh and Singh 1992; Schickhoff 2005; Miehe et al. 2015). However, recent reviews illustrated the deficient state of knowledge of Himalayan treelines, only very scanty information has been published with regard to sensitivity and response to climate change (cf. Schickhoff 2005; Dutta et al. 2014; Schickhoff et al. 2015).

Large warming trends (up to 1.2 °C per decade at higher altitudes) have been observed in the Himalaya in the past 30–40 years (Shrestha and Aryal 2011; Gerlitz et al. 2014; Hasson et al. 2016, Chap. 2 in this volume). Considering the sensitivity of mountain biota and ecosystems in the Himalaya to climate change (Xu et al. 2009; Shrestha et al. 2012; Telwala et al. 2013; Aryal et al. 2014; Anup and Ghimire 2015), substantial effects on Himalayan treeline ecotones are to be expected. Since treeline ecotones in the Himalaya are strongly modified by human impact (Miehe and Miehe 2000; Schickhoff 2005), it is often a challenge to detect a clear climate change signal and to exclude land-use change as a driver of treeline dynamics. Respective research has to concentrate on the few remaining near-natural treeline sites (Fig. 15.1). This paper summarizes the most current knowledge about sensitivity and response patterns of Himalayan treelines to climate change, updating a previous review (Schickhoff et al. 2015) and complementing it by inferring insights from palaeoecological studies.

15.2 Holocene Climatic Changes and Treeline Fluctuations

In view of the direct relationship between thermal conditions and the elevational position of treelines, it is obvious that treeline ecotones have been sensitive to changing climatic conditions in the course of the Holocene and have reflected

Fig. 15.1 Altitudinal zonation of a near-natural north-facing treeline in the central Himalaya: upper subalpine forests of *Abies spectabilis* and *Betula utilis* (leaves still unfolded) give way to *Rhododendron campanulatum* krummholz at c. 4000 m, Rolwaling, Nepal (Schickhoff, 2013-04-15) (Source: Udo Schickhoff)

general long-term climatic trends. It has been documented for many mountain regions of the world, in particular for the European Alps, the Scandes and the Rocky Mountains, that treelines have been fluctuating throughout postglacial times in response to climatic oscillations (Lang 1994; Tinner and Theurillat 2003; Reasoner and Tinner 2009; Körner 2012). Respective information on the Himalaya, however, is still comparatively poor and mainly based on fossil pollen in high-elevation mires and lakes. Complementary plant macrofossil and charcoal studies, missing to date even in the wider region with a few exceptions (e.g. Kaiser et al. 2009; Kramer et al. 2010a), will be valuable in determining the local occurrence of tree taxa at treeline elevations. On the other hand, numerous palaeoclimatic studies have generated insights into changing climatic conditions in South Asia during the Holocene, especially with regard to monsoon variability (e.g. Overpeck et al. 1996; Prasad and Enzel 2006; Clift and Plumb 2008; Cai et al. 2012). Thus, available proxy data allow the inference of a fairly clear pattern of Holocene treeline fluctuations. In the following we review the current knowledge about Holocene climate and subalpine/alpine vegetation changes in order to detect treeline shifts across the Himalayan mountain system in spatial and temporal differentiation.

In general, the reaction of Himalayan treelines to changes in climatic conditions during the Holocene roughly follows the well-established temperate zone response pattern with upslope movement during warmer periods and recession during cooler phases. However, the emerging picture of Holocene treeline fluctuations reveals considerable regional variations throughout the Himalaya which show that factors

other than temperature play a significant role. Moisture balance is a crucial control in this respect, largely depending on the monsoon intensity that has changed with spatial and temporal variability on a regional scale (Staubwasser 2006). Other critical factors include soil physical and chemical properties, disturbance regimes (fire, avalanches, other extreme events), individual tolerances and ecological demands of tree species, regeneration, migrational lags and competition from established vegetation (Holtmeier 2009). Despite regional variations, the general course of Himalayan treeline fluctuations during the Holocene is in agreement with studies from other extratropical mountain regions. After the Pleistocene-Holocene transition (c. 11.7 kyr BP), Asian monsoon precipitation increased dramatically (Morrill et al. 2003), resulting in warm and moist climatic conditions. Treelines advanced in elevation to a position several hundred metres higher than today, thus reaching uppermost limits in the early Holocene (Fig. 15.2). Decreasing temperatures below early and mid-Holocene levels induced a general and widespread downward shift of treelines after c. 5.0 kyr BP. The decline of subalpine forests and treeline elevation in the more recent millennia was coincident with weakening monsoonal influence and increasing anthropogenic interferences. However, Holocene treeline history was by no means uniform throughout the entire Himalayan mountain system. Substantial spatial and temporal differences become apparent at regional to local scales.

15.2.1 Hindukush-Karakorum-Himalaya in N Pakistan, W Tibet

Comparatively scanty information is available for the far NW of the mountain system (Hindukush-Karakorum-Himalaya in N Pakistan, adjacent W Tibet). After the transition to warmer conditions and reforestation in the postglacial period (Singh 1963; Agrawal et al. 1989), enhanced precipitation and maximum moist and warm conditions prevailed between 10.7 and c. 7.0 kyr BP (Gasse et al. 1996; Brown et al. 2003). Increased humidity influx into the arid/semiarid mountain region north of the main Himalayan range had been sufficient for the development of closed coniferous forests in the upper montane and subalpine belt as far as the upper Ishkoman Valley, location of the present-day northernmost pine forest (*Pinus wallichiana*) (Schickhoff 2000a). Schlütz (1999) documented a dense *Pinus wallichiana* forest thriving at high elevation in the Rakhiot Valley (Nanga Parbat) at least since 7.9 kyr BP. Reinforced monsoonal rains at 7.2 kyr BP and increasing winter and spring precipitation from the westerlies after 6.3 kyr BP enhanced total precipitation effectiveness (Prasad and Enzel 2006), resulting in the dominance of *Picea*, *Betula* and *Salix* at treeline elevations in the Nanga Parbat area (Schlütz 1999). Miehe et al. (2009a) provided evidence of the local existence of a forest habitat (*Pinus wallichiana*) in the Yasin Valley (E Hindukush) until around 5.7 kyr BP. Climate history and vegetation reconstruction suggest a treeline ascent to higher elevation than

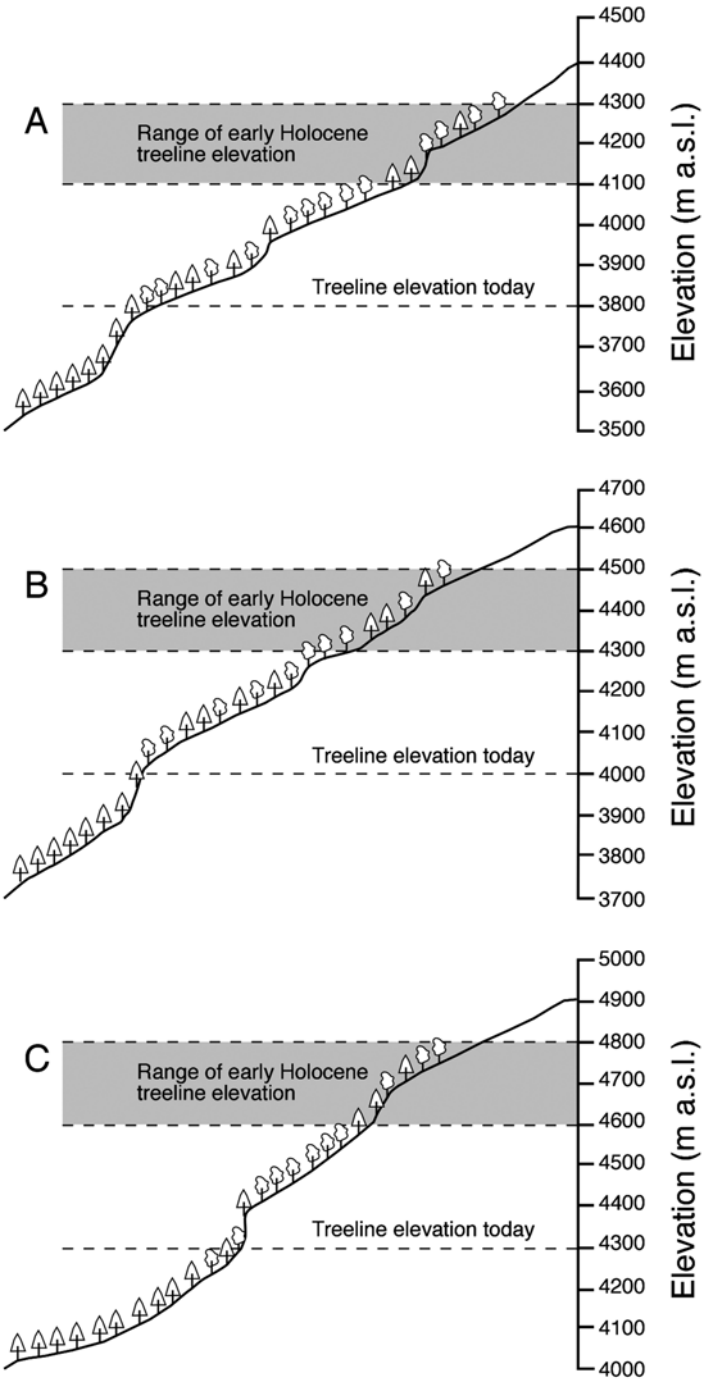

Fig. 15.2 Himalayan treeline elevation today and in the early Holocene, based on temperatures 1.5–2.5 K higher than today and using a lapse rate of 0.5 K per 100 m (cf. Böhner 2006; Reasoner and Tinner 2009; Kramer et al. 2010a; treeline elevations after Schickhoff 2005). (**a**) W Himalaya; (**b**) central Himalaya; (**c**) E Himalaya (Source: Udo Schickhoff)

today during early to mid-Holocene. Decreasing monsoonal precipitation and increasing aridity after c. 5.0 kyr BP are documented for the wider region (Overpeck et al. 1996; Morrill et al. 2003) including the Ganga Plain (Sharma et al. 2004) and were also inferred from pollen analyses in Yasin Valley (Schlütz 1999). Drier conditions resulted in the dwindling of more hygrophilous species (*Pinus* in Yasin; *Betula*, *Salix*, *Picea* at Nanga Parbat) (Schlütz 1999). The general climate deterioration after 5.0 kyr BP, in particular decreasing temperatures, suggests a decline of subalpine forests and a treeline depression close to current elevations. Substantial human activities at treelines in the far NW can be anticipated at least for the past five millennia but most probably go back to the mid-Holocene. Miehe et al. (2009a) attribute the decline of high-altitude conifer forests in the E Hindukush around 5.7 kyr BP to the influence of mobile livestock keepers. Increased grazing intensity since 2.7 kyr BP and significant land-use intensification in the past centuries are evident from the reinforced occurrence of grazing weeds and other cultural indicators in pollen profiles from Yasin and Nanga Parbat (Jacobsen and Schickhoff 1995; Schlütz 1999). Available data are not sufficient to assess whether the medieval warm period (MWP), which is reflected in tree ring growth in the Karakorum (Esper et al. 2007), and/or the following 'Little Ice Age' (LIA) caused significant treeline dynamics. However, the cold-wet LIA period (fifteenth to eighteenth centuries) in the wider region with widespread glacial advances (Yang et al. 2009) might have caused dieback and recruitment gaps at treeline elevations and suggests a slight downward shift of treelines.

15.2.2 West and Central Himalaya in India

Available information on Holocene climate history and vegetation dynamics in the West and Central Himalaya in India is much more comprehensive due to a larger set of pollen analyses and other proxy data. In agreement with climate reconstructions for the far NW, the postglacial climate amelioration that had proceeded with several setbacks culminated after the Pleistocene-Holocene transition. Rawat et al. (2015) ascertained increased monsoon intensity with a warm and wet climate for Lahaul between 11.6 and 8.8 kyr BP. Likewise, maximum monsoonal activity and a change to warmer and most humid conditions were inferred for Ladakh between c. 11.0 and 9.2 kyr BP (Bhattacharyya 1988; Demske et al. 2009; Leipe et al. 2014). A palynological analysis of a sediment profile from the Garhwal Himalaya adjoining to the SE corroborated the early Holocene climatic amelioration (Bhattacharyya et al. 2011), which continued until mid-Holocene throughout the West and Central Himalaya in India (Bhattacharyya 1989; Sharma 1992; Sharma and Gupta 1997; Phadtare 2000; Ranhotra et al. 2001; Anoop et al. 2013; Rawat et al. 2015). An enhancement of the winter westerly flow, assessed for Ladakh between 9.2 and 4.8 kyr BP (Demske et al. 2009), contributed to maximum humidity levels. However, the early Holocene climatic amelioration was interrupted by several cooler and/or drier spells, e.g. between 8.8 and 8.1 kyr BP in Lahaul (Rawat et al. 2015) and

between 7.2 and 6.6 kyr BP in Garhwal (Phadtare 2000). Nevertheless, in response to favourable climatic conditions, species composition and distribution of forest types changed remarkably during the early Holocene. In Ladakh, a significant expansion of open juniper forests (Bhattacharyya 1989) indicates the increase in temperature and humidity. On the more monsoon-influenced Himalayan south slope (Jammu and Kashmir, Himachal Pradesh, Uttarakhand), thermophilous trees of the genera *Quercus*, *Pinus*, *Alnus*, *Juglans*, etc. became established reflecting a general increase of later successional broadleaved trees and forests at the expense of conifers (Singh and Agrawal 1976; Dodia et al. 1985; Bhattacharyya et al. 2011; Rawat et al. 2015). At higher altitudes, the replacement of alpine meadows by subalpine birch (*Betula utilis*) forests, as inferred for Himachal Pradesh and Garhwal (Bhattacharyya 1988; Bhattacharyya et al. 2011), indicates a widespread treeline advance by several 100 m during the early Holocene (cf. Fig. 15.2). The upward shift of treelines was most likely interrupted during cooler and drier phases as suggested by a treeline descent below Gangotri Glacier between 8.3 and 7.3 kyr BP (Bhattacharyya et al. 2011). Here, climate reverted to warm-moist conditions between 7.3 and 6.0 kyr BP, causing the re-expansion of birch forests and the decline in steppe elements which had become prominent during the period of decreasing humidity (Bhattacharyya et al. 2011).

The mid-Holocene thermal optimum with a stronger-than-present summer monsoon was followed by slightly cooler and distinctly drier conditions, albeit not synchronously throughout the West and Central Himalaya in India. Bhattacharyya et al. (2011) assessed a trend towards drier climatic conditions for the Gangotri Valley (Garhwal) already after 6.0 kyr BP. At lower elevations and further south in Garhwal, Kotlia and Joshi (2013) inferred a cold and dry phase between 5.1 and 3.5 kyr BP. A significant shift towards aridity was described for Ladakh and Lahaul after 4.8 kyr BP (Demske et al. 2009; Leipe et al. 2014; Rawat et al. 2015). The majority of palynological case studies from Jammu and Kashmir to Kumaon reconstructed the weakest monsoon phase with decreasing rainfall and cooler climatic conditions for the time period between 5.0 and 3.0 kyr BP (Dodia et al. 1985; Sharma and Chauhan 1988; Sharma and Gupta 1997; Phadtare 2000; Trivedi and Chauhan 2008). These findings are in line with a significant decline of the Asian monsoon between 5.0 and 4.3 kyr BP identified by Morrill et al. (2003), which triggered severe drought events on the Tibetan Plateau (Herzschuh 2006) and most likely even the collapse of the Indus Valley Civilization (Staubwasser et al. 2003; Gupta et al. 2006). The change to cooler and drier climatic conditions provoked a decline in oak and other broadleaved tree species, while conifers regained dominance (Dodia et al. 1985; Sharma and Gupta 1997), and the treeline presumably shifted downwards (cf. Kramer et al. 2010a). From 4.0 kyr BP onwards, it is increasingly difficult to disentangle climatic and human impacts on treeline dynamics. The first appearance of Cerealia and cultural pollen indicates the introduction of farming and the proliferation of cultivation between 4.0 and 3.0 kyr BP in the West and Central Himalaya in India (Vishnu-Mittre 1984; Dodia et al. 1985; Sharma and Gupta 1997; Trivedi and Chauhan 2008). The development of mixed mountain agriculture with pastoralism on alpine meadows marks the beginning of human-induced treeline decline in the late

Holocene which was most likely several orders of magnitude higher than climate-driven subalpine forest retreat and treeline depression, in particular on south-facing slopes (cf. Schickhoff 2005; Schickhoff et al. 2015).

The more recent millennia saw the consecutiveness of climatic oscillations between cold-dry and warm-humid phases. In most of the subregions relatively dry and cold conditions prevailed between c. 2.5 kyr BP and 500 AD (Kar et al. 2002; Chauhan and Sharma 2000; Chauhan et al. 2000; Chakraborty et al. 2006; Phadtare and Pant 2006; Demske et al. 2009), followed by the MWP and the transition to the LIA. The latter phases become apparent in all palynological analyses, albeit not exactly synchronous in terms of age dating. Morrill et al. (2003) date the transition between MWP and LIA to 1300 AD in the Asian monsoon realm. These more recent climatic oscillations are associated with moderate treeline shifts. Chauhan et al. (2000) and Chauhan (2006) inferred from their pollen profiles a treeline advance in response to the MWP and a subsequent treeline descent during LIA in upper Spiti and in Kullu District, Himachal Pradesh (see also Yadav et al. 2011). Likewise, palynological data for the post-LIA phase suggest a treeline advance to higher elevations in the Gangotri Valley (Kar et al. 2002). An upward shift of the treeline in the range of 750 m since 1730 AD as postulated by Phadtare and Pant (2006) for the Pinder Valley (Kumaon) seems, however, to be unrealistic in the light of reference data from other mountain regions. Körner (2012) even considers the LIA too small an event to trigger a significant treeline shift. Massive deforestation and dramatically increased anthropogenic activities during the past centuries which can be reconstructed from palynological analyses (Sharma and Chauhan 1988; Sharma 1992; Sharma and Gupta 1995; Gupta and Nautiyal 1998; Trivedi and Chauhan 2008) as well as from historical documents (Schickhoff 1995, 2005, 2012) complicate the attribution of treeline dynamics to climatic forcing.

15.2.3 Nepal Himalaya

As in the regions adjoining to the west, the climatic amelioration after the Pleistocene-Holocene transition is associated with an upward shift in treeline position. Yonebayashi and Minaki (1997) inferred a treeline advance and an expansion of *Pinus* and *Quercus* trees under warmer climatic conditions in the Arun Valley, E Nepal, after c. 11.0 kyr BP. The change to warmer and more humid conditions in W Nepal in the further course of the early Holocene is indicated by an increase of *Quercus* and temperate genera at the expense of conifers and birch (Yasuda and Tabata 1988). Stronger summer monsoons with increased rainfall were also assessed for the Kali Gandaki Valley, Central Nepal (Saijo and Tanaka 2002), where inner-Himalayan *Pinus wallichiana* forests had established in the early to mid-Holocene (Miehe et al. 2009a). The end of the Holocene climatic optimum around 5.5 kyr BP as determined by Schlütz and Zech (2004) for Gorkha roughly parallels the climate history of the West Himalaya. Drier climatic conditions were assessed in the Muktinath Valley (Kali Gandaki) after 5.4 kyr BP (Miehe et al. 2002) and in W

Nepal after 4.5 kyr BP (Yasuda and Tabata 1988). The general climatic decline in the Subboreal is characterized by a downward shifting of altitudinal vegetation zones and a treeline depression (Schlütz and Zech 2004). As in other Himalayan regions, late Holocene treeline decline was most likely not triggered by climatic forcing alone. Miehe et al. (2002) dated the onset of pastoral land use and barley cultivation in Muktinath to 5.4 kyr BP and 4.5 kyr BP, respectively. Miehe et al. (2009a) argue that the sudden decline of *Pinus* forests in Muktinath around 5.4 kyr BP was related to the use of fire and other activities of early nomads and settlers. First significant human impact and deforestation in Gorkha as well as increasing human impact in Muktinath was detected for the time period between 3.0 and 2.0 kyr BP (Schlütz and Zech 2004; Miehe et al. 2002). Likewise, effects of climatic forcing and human impact on treeline dynamics during recent centuries are hardly to disentangle. The LIA shrinking of *Abies* and *Tsuga* in Gorkha is accompanied by increased grazing pressure and fire frequency (Schlütz and Zech 2004); a similar interference of effects can be presumed for the Langtang Valley after its colonization in the fifteenth century (cf. Beug and Miehe 1999).

15.2.4 East Himalaya

The transition to warmer and more humid conditions in the early Holocene parallels the climate development in other Himalayan regions and has been documented in several studies (e.g. Sun et al. 1986; Walker 1986; Jarvis 1993; Shen et al. 2006; Kramer et al. 2010a, b; Song et al. 2012; Xiao et al. 2014). Investigations of the corresponding vegetation dynamics point to distinct expansions of high-altitude forest cover and a significant treeline advance. In the Hengduan Mountains (Yunnan, Sichuan), alpine vegetation was replaced by early successional *Betula* forests, *Picea-Abies* forests and *Rhododendron* shrublands after 11.7 kyr BP (Kramer et al. 2010a; Xiao et al. 2014). In the further course of climate warming, a temperature increase of 3–4 K from pre-Holocene conditions triggered an enhanced upward shift of treelines to a position around 400–600 m higher than today after 10.7 kyr BP (Kramer et al. 2010a) (cf. Fig. 15.2). Higher temperatures and the intensification of the summer monsoon resulted in a substantial expansion of forest cover also in other parts of Yunnan and in Arunachal Pradesh after 10.2 kyr BP (Sun et al. 1986; Walker 1986; Ghosh et al. 2014). Recent palaeoecological studies with higher temporal resolution (Kramer et al. 2010a) detected a climate deterioration in the Hengduan Mountains between 8.1 and 7.2 kyr BP which is related to the 8.2 kyr BP event observed in most records from the northern hemisphere (Alley et al. 1997; Dixit et al. 2014). The return to colder and drier conditions involved a downward shift of treelines indicated by a sharp decrease of *Betula* and other tree pollen (Kramer et al. 2010a; Yang J et al. 2010). After this cold spell, treelines shifted upwards again under warm and wet climatic conditions. The Holocene climatic optimum between c. 6.9 and 4.4 kyr BP (Kramer et al. 2010a; Xiao et al. 2014) is characterized by advancing treelines, e.g. in E Tibet to an elevation 500 m higher

than today (Yu et al. 2000). Dense moist evergreen forest cover was prevalent at lower elevations (Ghosh et al. 2015), while broadleaved trees, *Tsuga*, *Picea* and *Abies*, were dominant in the upper montane and subalpine belt (Kramer et al. 2010a; Song et al. 2012; Xiao et al. 2014).

After 4.4 kyr BP, colder and drier climatic conditions prevailed in the Hengduan Mountains. Mean July temperatures decreased to about 2–3 K below the mid-Holocene level, and treelines shifted downwards, probably attaining a magnitude of 400–600 m (Kramer et al. 2010a). A rising trend of dryness was assessed for Arunachal Pradesh after 3.8 kyr BP (Ghosh et al. 2014), a weakening of the summer monsoon for Assam after 4.2 kyr BP (Bera and Basumatary 2013). Thus, palaeoclimatic data indicate a later onset of temperature and humidity decline after the mid-Holocene climate optimum compared to the West Himalaya. Relatively cold and dry conditions prevailed in NE India until 2.2 kyr BP (Mehrotra et al. 2014). As in other Himalayan regions, climate-driven forest retreat and treeline depression during late Holocene were reinforced by human influence. Earliest records of human activity and grazing indicators in pollen profiles in Yunnan and Sichuan were traced back to c. 3.4 kyr BP (Kramer et al. 2010a; Yang J et al. 2010), but anthropogenic interferences might have played a major role much earlier as it has been ascertained for other parts of the Tibetan Plateau (Frenzel 1994; Miehe et al. 2008, 2009b). Thus, treeline oscillations during the past three millennia seem to be rather related to human impact than to climatic forcing. In spite of increased anthropogenic disturbance in the past centuries (Jarvis 1993; Chauhan and Sharma 1996), palynological data suggest a treeline advance during the MWP, a decline in arboreal pollen and treeline descent during LIA, an increase of *Quercus*, *Betula*, *Alnus* and Rosaceae pollen at higher altitudes and a renewed treeline shift towards higher elevation after LIA (Sharma and Chauhan 2001; Bhattacharyya et al. 2007). However, given the alternating regional temperature history during the past centuries (Yang B et al. 2010), it is still unclear whether significant climate-driven treeline shifts before, during and after the LIA actually occurred.

15.3 Treeline Sensitivity and Response

15.3.1 Treeline Types and Treeline Forms

It is evident from past treeline fluctuations that treeline elevation has always been tracking changing temperatures in the course of the Holocene, albeit with varied time lags which are hard to quantify given the available data. Since the future thermal level at treeline elevations will most likely be distinctly higher compared to present conditions and to conditions during the mid-Holocene climate optimum (IPCC 2013), an upslope movement of subalpine forests and a treeline advance to higher elevations can be anticipated, given that no other factors adversely affect tree growth and regeneration (Holtmeier 2009).

Fig. 15.3 Climatic treeline at c. 4050 m with *Abies densa* and several *Rhododendron* spp., Kangchendzonga National Park, Sikkim (Schickhoff, 2015-03-26) (Source: Udo Schickhoff)

The susceptibility of treelines to respond to changing climatic conditions varies considerably among different treeline types and treeline forms (Schickhoff et al. 2015). Climatic treelines (Fig. 15.3) show comparatively high susceptibility and are more likely to reflect climate tracking since increases in temperature sums and growing season length will affect growth patterns, regeneration and treeline position, at least in the long term (Holtmeier and Broll 2007; Körner 2012). However, the direct influence of climate warming is variegated in complex ways by local-scale abiotic and biotic site factors and their manifold interactions acting as thermal modifiers. For instance, the varying microtopography in treeline ecotones exerts a modified influence on soil temperatures, soil moisture or the distribution of trees (Holtmeier and Broll 2005, 2012; Case and Duncan 2014). Notwithstanding the basically high susceptibility of climatic treelines, their sensitivity is controlled by these thermal modifiers with a notable scope of fluctuation in the medium term (several years to a few decades), while the long-term response in terms of treeline shifts might be more homogeneous.

By contrast, orographic and edaphic treelines are largely resistant to the effects of climate warming. The establishment of trees in orographic treeline ecotones remains primarily under the control of orographic factors such as debris slides, rockfalls, snow avalanches, etc., regardless of higher temperatures. Likewise, edaphic treelines are hardly affected in the medium term, unless pedogenetic processes accelerate and favour the establishment of tree seedlings and tree invasion. Anthropogenic treelines are comparable to climatic treelines in terms of sensitivity

Fig. 15.4 Anthropogenic treeline in Manang, Nepal, showing an abrupt transition to alpine grazing lands (Schickhoff, 2013-09-24) (Source: Udo Schickhoff)

to climate warming. In many mountain regions, cessation of pastoral use and other human impact in recent decades has generated prolific regeneration, increased tree establishment within the treeline ecotone and invasion into treeless areas above the anthropogenic forest limit. These directional changes are readily attributed to effects of global warming; they result, however, in most cases from decreasing land use (Gehrig-Fasel et al. 2007; Vittoz et al. 2008; Holtmeier 2009; Schickhoff 2011).

In the Himalayan mountain system, we consider the vast majority of treelines to be anthropogenic (Fig. 15.4) and a relatively low percentage to be orographically/edaphically and climatically determined (Schickhoff et al. 2015). Animal husbandry, timber logging, fuelwood collection and the like are integral parts of village economies for millennia (see above), and have transformed treeline ecotones, in particular on south-facing slopes, to such an extent that treeline depressions of up to 500–1000 m occur (Miehe 1997; Miehe and Miehe 2000; Schickhoff 2005; Miehe et al. 2015). On north-facing slopes, which have a much lower utilization potential, the extension of alpine grazing grounds and the overuse of subalpine forests (Schmidt-Vogt 1990; Schickhoff 2002) have resulted in substantial treeline depressions as well. For instance, a difference between current and potential treeline of up to 300 m was assessed in Kaghan Valley, West Himalaya (Schickhoff 1995). Thus, present-day landscape patterns at treeline elevations are cultural landscape patterns. Treelines on south slopes are almost exclusively anthropogenic. Only very few near-natural treeline ecotones, more or less undisturbed by human impact, persist in remote, sparsely populated valleys which are not connected to the road network

and/or where plants and animals are protected for religious reasons (Miehe et al. 2015; Schickhoff et al. 2015). A substantial medium-term treeline response to climate warming is to be expected from the tiny fraction of climatic treelines only and from those anthropogenic treelines which are no longer exposed to important human disturbance. However, the vast majority of anthropogenic treelines will be subjected to continued intensive land use in the foreseeable future. Thus, the proportional distribution of treeline types in the Himalaya suggests a rather low responsiveness to climate warming, at least in terms of treeline shifts (Schickhoff et al. 2015).

To explain the variability of treeline response to climate warming, treeline spatial patterns have to be taken into consideration. A general link between treeline form and dynamics (Lloyd 2005; Harsch et al. 2009) was recently substantiated by Harsch and Bader (2011), who distinguished in their global study four treeline forms with wide geographic distribution (diffuse, abrupt, island, krummholz). They found diffuse treelines, formed and maintained primarily by growth limitation, to exhibit a strong response signal, while abrupt, island and krummholz treelines, controlled by seedling mortality and dieback, are comparatively unresponsive. Since treeline forms in the Himalaya are predominantly controlled by anthropogenic disturbances, they cannot easily be classified into discrete classes. Diffuse treelines are largely limited to less disturbed or near-natural sites in southern aspects which have become very rare. The occurrence of abrupt and island treelines under natural conditions can be virtually excluded. When abrupt treelines occur (Fig. 15.4), e.g. *Betula* treelines in Manang Valley, Nepal, they are caused by land use (cf. Shrestha et al. 2007). The far majority of less disturbed or near-natural Himalayan treelines, mainly confined to north-facing slopes, has to be categorized as krummholz treelines (cf. Fig. 15.1; Schickhoff et al. 2015). Since krummholz treelines usually show a rather low responsiveness to climate warming, substantial treeline shifts at these near-natural Himalayan treelines are to be expected in the long term only. However, a substantial short- to medium-term response can be anticipated in terms of increased vertical stem growth and enhanced recruitment of seedlings (Schickhoff et al. 2015).

15.3.2 Seed-Based Regeneration

The establishment of seedlings and a successful performance during early life stages is the prior condition for any treeline advance to higher elevations (Holtmeier 2009; Smith et al. 2009; Zurbriggen et al. 2013). In the Himalaya, tree recruitment in treeline ecotones is not well understood. Nevertheless, some conclusions on effective regeneration with regard to treeline response to climate warming can be drawn. The number of respective seedling studies is limited, and available studies are reviewed in Schickhoff et al. (2015). High levels of recruitment in recent decades become apparent from these studies, as long as the respective treeline ecotones are not too heavily disturbed by grazing and other human impact. Little information on treeline seed-produced regeneration is available from the northwestern,

western and central Himalayan mountain regions in Pakistan and India. Generally low regeneration rates were assessed in subalpine forest stands in the Karakoram, in line with retarded growth processes and slow stand development cycles under semiarid-subhumid climatic conditions (Schickhoff 2000b). By contrast, intense recruitment patterns were reported from the humid Himalayan south slope. Treeline elevations in Himachal Pradesh and Uttarakhand showed high levels of recruitment, with increasing establishment of pine (*Pinus wallichiana*) and birch (*Betula utilis*) seedlings even above the treeline zone (Dubey et al. 2003; Gairola et al. 2008, 2014; Rai et al. 2013). An increasing number of studies on seed-based regeneration are available from Nepal. Sufficiently regenerating treeline forests with high densities of seedlings and saplings and seedlings occurring above the treeline are consistently reported from Manang Valley, Annapurna Conservation Area (Shrestha et al. 2007; Ghimire and Lekhak 2007; Ghimire et al. 2010; Kharal et al. 2015). Similar results were achieved at different treeline sites in Langtang National Park (Gaire et al. 2011; Shrestha et al. 2015a), in Manaslu Conservation Area (Gaire et al. 2014) and in Mt. Everest Nature Reserve (S Tibet) (Lv and Zhang 2012). High levels of recruitment of *Abies spectabilis* in recent decades with seedlings and saplings at much higher elevations than uppermost cone-bearing tree individuals were a consistent result of these studies. By contrast, a relatively low number of *Abies* seedlings and saplings above treeline was assessed in Makalu Barun National Park (Chhetri and Cairns 2015). Seedling abundance is often positively correlated with soil moisture (Ghimire and Lekhak 2007; Zhang et al. 2010) and temperature parameters (Lv and Zhang 2012; Gaire et al. 2014). Concordant results were obtained in the East Himalaya, including intense recruitment of *Abies densa* in subalpine forests of Bhutan (Gratzer et al. 2002; Gratzer and Rai 2004), considerably increased Smith fir (*Abies georgei* var. *smithii*) recruitment in recent decades in the Sygera Mountains (SE Tibet) (Ren et al. 2007; Liang et al. 2011; Wang et al. 2012) and high rates of Smith fir regeneration with the percentage of seedlings/saplings increasing upslope across the treeline ecotone in the Hengduan Mountains (NW Yunnan) (Wong et al. 2010).

The emerging pattern of a generally intense regeneration at Himalayan treeline sites which are less or not disturbed by pastoral use is corroborated by new results from ongoing research projects of the present authors in two study areas in Nepal (Rolwaling Valley, Gaurishankar Conservation Area; Langtang Valley, Langtang National Park) (cf. Schickhoff et al. 2015; Schwab et al. 2016). At a newly established treeline study site in Rolwaling Valley, east-central Nepal, we assessed largely prolific regeneration (Table 15.1) with seedling establishment of *Betula utilis*, *Abies spectabilis*, *Rhododendron campanulatum* and *Sorbus microphylla* and thriving of saplings to some extent far above the upper limit of adult trees (Fig. 15.5). Some individuals of more than 2 m height even grow vigorously above the *Rhododendron campanulatum* krummholz belt, i.e. 100–150 m above the treeline which is located at 3900 m (NW-exp.)/4000 m (NE-exp.). In spite of this recruitment, we found the dense krummholz belt to be an effective barrier for upslope migration of other tree species, expressed by a negative correlation between abundance and density of *R. campanulatum* and recruitment of other tree species (Schwab et al. 2016).

Table 15.1 Number of seedlings/saplings (<7 cm breast height diameter; N ha^{-1}) of *Betula utilis*, *Abies spectabilis*, *Rhododendron campanulatum* and *Sorbus microphylla* in the treeline ecotone in Rolwaling Valley according to slope exposure and altitudinal zone

Altitudinal zone		Altitude (m)	*Betula utilis*	*Abies spectabilis*	*Rhododendron campanulatum*	*Sorbus microphylla*	Total
NE slope	A	3780–3880	754	453	1209	1450	3866
	B	3920–3980	179	872	5388	975	7414
	C	4020–4080	104	53	6103	2257	8517
	D	4120–4220	0	0	819	191	1010
	Total	–	1013	1378	13,519	4873	20,807
NW slope	A	3760–3780	3517	1996	612	2058	8183
	B	3820–3880	1288	819	8338	825	11,270
	C	3920–3980	69	81	4125	269	4544
	D	4020–4240	12	25	1712	238	1987
	Total	–	4886	2921	14,787	3390	25,984

Updated from Schickhoff et al. (2015)

Fig. 15.5 *Abies spectabilis* sapling at 4200 m in *Rhododendron anthopogon* dwarf scrub heath, Rolwaling, Nepal, c. 200 m above treeline (Schickhoff, 2013-08-20) (Source: Udo Schickhoff)

Permanently dense foliation of evergreen *Rhododendron* and potential allelopathic effects that have been shown for other species of this genus (Chou et al. 2010) obviously prevent the establishment of seedlings of competing tree species to a large extent. Maximum seedling/sapling density of more than 11,000 N/ha occurs in uppermost subalpine forests immediately below the transition to the krummholz belt (elevational zone B; NW slope). *R. campanulatum* has its most intense

Table 15.2 Cumulative numbers of seedlings/saplings (N ha^{-1}) of *Betula utilis*, *Abies spectabilis*, *Rhododendron campanulatum* and *Sorbus microphylla* in the treeline ecotone in Langtang Valley according to altitude and size classes

Size class (cm)										
Altitude (m)	0–19	20–49	50–99	100–149	150–199	200–299	300–399	400–499	500–7 cm dbh	Total
3850	5441	1134	522	631	603	131	69	69	78	8678
3900	6269	1834	909	628	719	172	59	41	34	10,665
3950	6778	1225	566	500	434	122	75	169	206	10,075
4000	4741	772	513	459	425	63	34	84	159	7250
4050	3694	403	231	213	253	97	75	78	75	5119
4100	3631	497	253	269	259	113	69	34	25	5150
4150	397	184	69	47	75	31	22	16	19	860
4200	19	28	16	13	9	3	0	0	0	88
Total	30,970	6077	3079	2760	2777	732	403	491	596	47,885

dbh diameter at breast height

recruitment at treeline elevations (zones B and C; cf. Table 15.1; Schwab et al. 2016). We assessed significantly positive correlations of seedling/sapling abundance with soil moisture for *Abies*, *Betula* and *Rhododendron* and with soil temperature for *Abies*, *Betula* and *Sorbus*, in each case over almost all size classes. Thus, higher soil moisture and higher soil temperatures indicate higher recruitment density of the majority of treeline tree species. *R. campanulatum* saplings (up to a height of 2 m) were found to be negatively correlated with soil temperature; germinants and large shrubs of this species, however, showed a positive correlation (Schickhoff et al. 2015).

In accordance with the observations in Rolwaling, we found the production of viable seeds and the supply of treeline ecotones with fertile seeds in Langtang Valley to be sufficient to generate relatively high rates of seedling establishment, even beyond the actual upper limit of contiguous forests between 4000 and 4100 m. We assessed maximum seedling/sapling density at 3900 and 3950 m with 10,665 N/ha and 10,075 N/ha, respectively, before the recruit abundance sharply decreases above 4100 m, slightly above the transition from cloud forests to dwarf scrub heaths (Table 15.2). In contrast to countless seedlings/saplings of *Sorbus microphylla* and *R. campanulatum*, recruitment of *Abies spectabilis* is relatively sparse and obviously related to grazing impact and the removal of adult trees as seed sources (Fig. 15.6). Regeneration of *Betula utilis* is also less intense; birch seedlings, however, are far more homogeneously distributed across size classes compared to the other species, with numerous saplings of greater size classes established at the treeline and above the upper limit of contiguous forests (cf. Schickhoff et al. 2015; see also Sujakhu et al. 2014). We conclude from these high levels of recruitment within and beyond treeline ecotones in both near-natural study sites (Rolwaling, Langtang) that seed-based regeneration will not restrict future treeline advance to higher elevations.

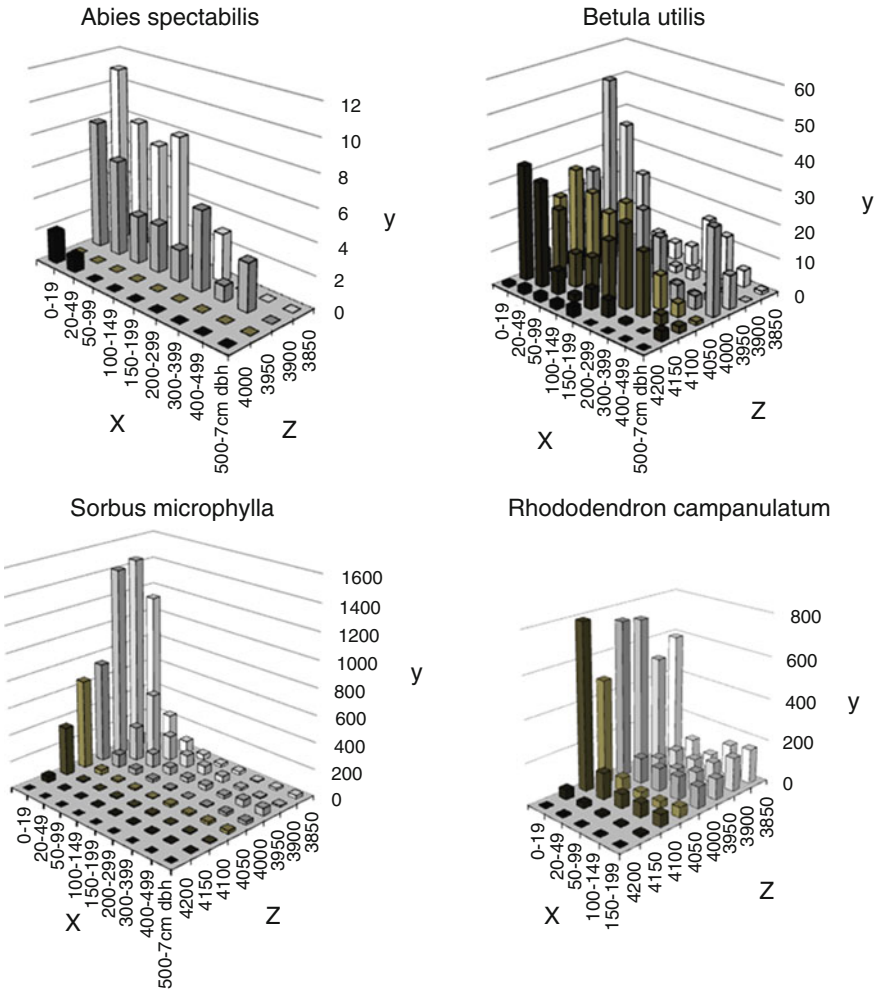

Fig. 15.6 Seedling/sapling density in the treeline ecotone in Langtang Valley according to altitude and size classes (*x* axis = size class; *y* axis = quantity; *z* axis = altitude) (Modified from Schickhoff et al. 2015) (Source: Udo Schickhoff)

15.3.3 Tree Growth-Climate Relationships

As evident from climatically shaped growth forms at treeline elevations, tree growth is sensitive to decreasing temperatures and related harsh climatic and climatically induced ecological conditions. Thus, tree physiognomy usually reflects changing environmental conditions related to climatic alteration. Accelerated, climate warming-induced height growth of previously low-growing tree individuals has been reported from different treeline ecotones for recent decades (e.g.

Lescop-Sinclair and Payette 1995; Kullman 2000; Kullman and Öberg 2009). As for the Himalaya, the recent expansion of treeline ecotones, subalpine forests and alpine scrub detected, for instance, by Rai et al. (2013) in Himachal Pradesh and Uttarakhand during 1980–2010, has most likely been accompanied by enhanced height growth of individual trees as well. Regeneration analyses at the Langtang and Rolwaling study sites provide evidence of successful regeneration even under the harsh climatic conditions above the krummholz belt, with saplings partially projecting above the snow cover (Fig. 15.7; Schwab et al. 2016). Height growth of these recruits might have accelerated recently. Further analyses and data evaluations will provide more detailed information on physiognomic changes in response to climate warming from Rolwaling and other Himalayan treelines.

In contrast to height growth, radial growth is less affected by decreasing temperatures when approaching the upper treeline but shows more pronounced response to climate warming (Körner 2012). In humid mountain regions, climate warming usually results in enhancements of tree radial growth, but under arid or semiarid conditions or in regions with seasonal drought periods, climate warming is often associated with a decline in tree radial growth (Schickhoff et al. 2015 and further references therein). In the Himalaya, dendroclimatological results available to date are inconsistent with studies showing evidence of climate warming-related increase in tree-ring widths and others that detected decreasing tree radial growth (see below). In general, radial growth response to changing climatic conditions is spatially differentiated and species-specific (Schickhoff et al. 2015; Schwab et al. 2015). Himalayan treeline conifers seem to be more responsive to temperature than precipitation change, with W and central Himalayan conifers being more responsive to winter and pre-monsoon temperatures and E Himalayan conifers being more responsive to summer temperatures in most case studies. Tree-ring growth in E Himalaya is obviously less sensitive to climate variation compared to W Himalayan sites and trees (Bhattacharyya and Shah 2009).

Tree growth-climate relationships in the NW and W Himalaya are not consistent. Growth of high-elevation junipers has been shown to be more responsive to temperature variation in the Karakorum (Esper et al. 2002, 2007), while in Lahaul it is more influenced by precipitation (Yadav et al. 2006; Bräuning et al. 2016). Some studies, based on tree-ring width chronologies of *Pinus wallichiana*, *Cedrus deodara* and *Picea smithiana* from high-altitude forests and treeline sites, point to distinctly positive responses of tree growth to recent climate warming, reflected by accelerated growth in the past decades and significantly positive correlations with mean annual and winter (DJF) temperatures (Singh and Yadav 2000; Borgaonkar et al. 2009, 2011). However, another pattern of tree growth-climate relationships is currently emerging from an increasing number of studies: ring-width chronologies from treeline sites and other high-elevation sites in Himachal Pradesh and Uttarakhand reveal a strong sensitivity of tree growth to pre-monsoon temperature and humidity conditions. Bhattacharyya and Yadav (1990), Yadav and Singh (2002) and Yadav et al. (2004) detected significantly negative correlations with long-term pre-monsoon temperature series using *Abies spectabilis*, *Taxus wallichiana* and *Cedrus deodara* tree-ring sequences. A negative correlation of pre-monsoon

Fig. 15.7 Tall saplings of *Betula utilis* (c. 2 m) growing 100–150 m above the current treeline in Langtang Valley, Nepal (Schickhoff, 2010-07-21) (Source: Udo Schickhoff)

temperature with total ring width and a positive correlation of pre-monsoon precipitation with ring width are apparently widespread dendroecological patterns in the West and Central Himalaya in India (cf. Borgaonkar et al. 1999; Pant et al. 2000; Bhattacharyya et al. 2006; Ram and Borgaonkar 2013, 2014). Increased evapotranspiration and soil moisture deficits induced by higher temperatures during the relatively dry spring months obviously impede tree growth in particular on sites which are prone to drought stress.

Recent dendroecological studies in Nepal corroborate these results. Significantly negative correlations with long-term pre-monsoon temperature series were detected in *Abies spectabilis* tree-ring data from near-treeline sampling locations in Humla District (Sano et al. 2005) and in Langtang National Park (Gaire et al. 2011; Shrestha et al. 2015b). The pre-monsoon period has been shown to be also critical for broad-leaved treeline trees. Dawadi et al. (2013) assessed for the growth of birch trees at treeline sampling sites in Langtang Valley a positive correlation with March-May precipitation and an inverse relationship with pre-monsoon temperatures. Liang et al. (2014) confirmed for study sites in Sagarmatha National Park, Langtang National Park and Manaslu Conservation Area that reduced pre-monsoon moisture availability is a primary growth-limiting factor for *Betula utilis* at treeline and that years with high percentage of missing rings or narrow rings coincide with dry and warm pre-monsoon seasons (see also Gaire et al. 2014). These findings are in accordance with results from current research of the present authors based on a ring-width chronology of *Betula utilis* from treeline sites in Langtang Valley dating back

to AD 1657, showing a negative correlation of tree-ring width with pre-monsoon temperature and a positive correlation with pre-monsoon precipitation (unpubl. data). A significant negative correlation with May temperature has also been detected for *Juniperus tibetica* on the semiarid southern Tibetan Plateau (He et al. 2013; Liu et al. 2013). Other studies from Nepal highlight a strong positive relationship of *Abies spectabilis* ring width with higher winter temperatures prior to growing season (Bräuning 2004; Gaire et al. 2014).

In the E Himalaya, the ring width of several treeline conifers was also found to be sensitive to winter season temperature, while their maximum latewood density was positively correlated with summer temperature (Bräuning and Mantwill 2004; Bräuning 2006; Bräuning and Grießinger 2006; Fan et al. 2009). Positive relationships with winter temperatures for *Abies densa* and with May temperature for *Larix griffithiana* were assessed near treelines in Sikkim and Arunachal Pradesh, while tree growth was inversely related to summer temperatures (Chaudhary and Bhattacharyya 2000; Bhattacharyya and Chaudhary 2003). Ring-width chronologies of *Abies georgei* var. *smithii* growing at treeline in the Sygera Mountains (SE Tibet) revealed accelerated growth in the past decades and significantly positive correlations with monthly mean and minimum temperatures of most months, particularly in summer (Liang et al. 2009, 2010). Zhu et al. (2011) reported a similar response to summer temperatures for *Picea likiangensis* var. *balfouriana* at treelines in the Bomi-Linzhi region (SE Tibet).

Summing up, studies on tree growth-climate relationships in the Himalaya show non-uniform, species-specific and spatially differentiated results. However, most case studies concordantly indicate a positive relationship of ring width with higher winter temperatures. Warmer conditions during winter season facilitate the storage of higher levels of hydro-carbonates and are beneficial to root system activity and carbon absorption and transportation (He et al. 2013). At W and central Himalayan treelines, growth patterns are particularly responsive to pre-monsoon temperature and humidity conditions. Here, treeline trees may be increasingly subjected to drought stress during the dry pre-monsoon season for which high temperature trends were determined for the entire Himalayan Arc (Gerlitz et al. 2014; Schickhoff et al. 2015). Thus, tree growth in the more humid E Himalaya will most likely be positively influenced by climate warming during the coming decades. Pre-monsoon temperature and humidity conditions will control tree growth in the W and central Himalaya to a considerable extent, in spite of facilitation by higher winter temperatures.

15.4 Treeline Shifts

Under natural conditions, treeline advance to higher elevation in response to a warming climate is normally a medium- to long-term process in the order of several decades to hundred or more years. It is assumed that treeline positions are always lagging behind climatic fluctuations and that global treelines we observe today are

each in a specific state of climate tracking. Since the responsiveness of treelines to changing climatic conditions is varied, it is understandable that current observations on treeline shifts in response to recent climate change are globally heterogeneous. The varying degree of human impact on treelines adds to this heterogeneity in response. Response patterns include advancing as well as stagnating or rather unresponsive treelines. The comparability of global observations is limited since they are not based on a uniform treeline concept. The mere presence of seedlings is not synonymous with an actual treeline advance. Only the sustainable transition into subsequent sapling size classes and the establishment of trees beyond the current tree limit is indicative of a treeline shift (cf. Graumlich et al. 2005).

Hitherto documented Himalayan treeline shifts mirror the global pattern, in terms of both response heterogeneity and comparability of observations. Only very few studies addressed this topic to date; they can be grouped into studies based on dendroecological and forest ecological field data and those based on remote sensing and repeat photography (cf. Schickhoff et al. 2015). Most of the studies reported higher population density of trees and considerably increased number of seedlings in the treeline ecotone, but more or less stationary treeline positions or insignificant treeline shifts over recent decades. This applies in particular to field data-based studies (Gaire et al. 2011; Liang et al. 2011; Shrestha et al. 2015a; Chhetri and Cairns 2015; Schickhoff et al. 2015). When migration rates are calculated on the basis of uppermost seedling position, higher rates of upslope movement are found (Gaire et al. 2014). However, seedling establishment is not equivalent to effective regeneration and not to treeline advance. Seedlings have a generally low survival rate during the first years after germination and have to survive critical later life stages after projecting above the winter snow cover. Only when uppermost individuals survive, become established as trees and mature, an ecotone expansion should be termed treeline shift.

Remote sensing studies largely confirm the results of field studies. Landsat-based change detection of treeline ecotones in Himachal Pradesh and Uttarakhand indicated a general increase in green biomass and an expansion of fir and birch forests in recent decades, but no treeline shifts (Bharti et al. 2012; Rai et al. 2013). Bold statements of recent exceptional treeline advances in other remote sensing studies (Panigrahy et al. 2010; Singh et al. 2012) have turned out to be implausible (cf. Bharti et al. 2011; Negi 2012; Rawat 2012). A repeat photography study actually documented a treeline shift of almost 70 m in elevation at a slope in the Hengduan Mountains (NW Yunnan) since AD 1923 (Baker and Moseley 2007). Such great altitudinal shifts can be expected from anthropogenic treelines where treeline advance is rather a result of the cessation of pastoral use and other human disturbances than a clear climate change signal.

Modelling approaches are increasingly used to gain a better understanding of treeline dynamics in response to climate and land-use change and of underlying process-pattern relationships and to explore potential range shifts of treeline tree species (e.g. Dullinger et al. 2004; Wallentin et al. 2008; Paulsen and Körner 2014). In the Himalaya, modelling studies to project future geographic distribution of tree species have hardly been conducted so far. Recently, initial modelling studies with

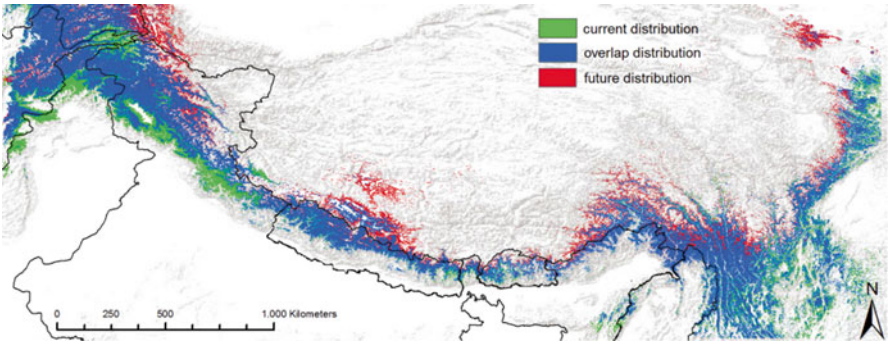

Fig. 15.8 Potential range shift of *Betula utilis* under novel climate conditions in AD 2070 (Modified from Schickhoff et al. 2015) (Source: Udo Schickhoff)

regard to environmental niches of the genus *Rhododendron* in Sikkim and of *Betula utilis* in Uttarakhand were published (Kumar 2012; Singh et al. 2013). In a preliminary study, we used ecological niche modelling to forecast the range shift of *Betula utilis* under novel climate conditions in AD 2070 (Schickhoff et al. 2015). The potential habitat of *Betula utilis* was predicted to shift to higher elevations and to expand into new habitats north of the Himalayan range (Fig. 15.8). Significant upslope expansions are modelled for Trans-Himalayan ranges in S Tibet. Range contractions are forecasted for the Indian W Himalaya, the S Hindukush and the Wakhan Corridor. Further modelling studies are badly needed in order to predict more accurately patterns and rates of treeline dynamics driven by climate change.

15.5 Conclusions

In view of the heterogeneity of treeline environments in the vast Himalayan mountain system, it is difficult to infer generally acceptable statements on treeline sensitivity and response to changing climatic conditions. However, several conclusions can be drawn from the present review that might be of relevance for treeline dynamics in other mountain regions beyond the Himalayan system. The Holocene Himalayan treeline history substantiates the conception that treeline elevation has been tracking temperatures over the postglacial millennia. The basic pattern of treeline fluctuations during the Holocene resembles those of other extratropical mountain regions but is accentuated by spatial and temporal differences at regional to local scales. Himalayan treelines reached uppermost limits during the Holocene thermal optimum, before a general and widespread downward shift of treelines was induced by deteriorating climatic conditions after c. 5.0 kyr BP. The palaeo-data suggest that treelines are currently in a dynamic process of climate tracking in response to recent climate warming and that a future advance of treelines is plausible at continued warming.

At near-natural Himalayan treelines, a significant move in elevation seems to be possible only in the long term. Near-natural or less disturbed treelines on north-facing slopes are usually developed as krummholz treelines which show a low responsiveness. Strong competition within the krummholz belt and dense dwarf scrub heaths further upslope adversely affects upward migration of tree species and retards treeline shifts. Nevertheless, high levels of recruitment with huge amounts of seedlings/saplings present within the treeline ecotone and to some extent beyond suggest that favourable preconditions for a future treeline advance exist. Species-specific competitive abilities during the recruitment phase or rather the effectiveness of recruitment suppression in the krummholz and dwarf scrub belts will control this advance. By contrast, anthropogenic treelines, predominant in the Himalaya, will show substantial short- and medium-term effects once pastoral use and other human disturbances will have ceased. Dendroecological studies point to a high sensitivity of mature Himalayan treeline trees to temperature. Tree radial growth is positively influenced by higher winter temperatures, and negatively influenced by higher pre-monsoon temperatures and increased drought stress in the pre-monsoon season, in particular in the W and central Himalaya. These findings suggest that moisture supply might be an effective control of future treeline dynamics. In general, the bioclimatic preconditions for a future treeline advance will be existent as indicated by predicted shifts to higher elevations of treeline tree species based on ecological niche modelling. Treeline shifts into treeless ecosystems will have large-scale consequences in terms of biodiversity, ecosystem function and ecosystem services, including reductions in alpine diversity and alterations of ecosystem productivity and carbon storage. A widespread upward encroachment of subalpine forests would also affect land-use potentials and tourism economies.

Acknowledgements We would like to thank several local people in Beding and Langtang who provided lodging and support in field data collection. Our thanks also go to the Deutsche Forschungsgemeinschaft (DFG SCHI 436/14-1, SCHO 739/14-1, BO 1333/4-1), the DAAD, the University of Hamburg and several foundations for financial support.

References

Agrawal DP, Kotlia BS, Kusumgar S, Gupta SK (1989) Quaternary palaeoenvironmental changes in Northwest India. In: Sahni A, Gaur R (eds) Perspectives in human evolution. Renaissance, Delhi, pp 223–260

Alley RB, Mayewski PA, Sowers T, Stuiver M, Taylor KC, Clark PU (1997) Holocene climatic instability: a prominent, widespread event 8200 yr ago. Geology 25:483–486

Anoop A, Prasad S, Krishnan R, Naumann R, Dulski P (2013) Intensified monsoon and spatiotemporal changes in precipitation patterns in the NW Himalaya during the early-mid Holocene. Quat Int 313:74–84

Anup KC, Ghimire A (2015) High-altitude plants in era of climate change: a case of Nepal Himalayas. In: Öztürk M, Hakeem KR, Faridah-Hanum F, Efe R (eds) Climate change impacts on high-altitude ecosystems. Springer, Cham, pp 177–187

Aryal A, Brunton D, Raubenheimer D (2014) Impact of climate change on human-wildlife-ecosystem interactions in the Trans-Himalaya region of Nepal. Theor Appl Climatol 115:517–529

Baker BB, Moseley RK (2007) Advancing treeline and retreating glaciers: implications for conservation in Yunnan, P.R. China. Arct Antarct Alp Res 39:200–209

Batllori E, Gutiérrez E (2008) Regional tree line dynamics in response to global change in the Pyrenees. J Ecol 96:1275–1288

Bera SK, Basumatary SK (2013) Vegetation history and monsoonal fluctuations during the last 12,500 years BP inferred from pollen record at Lower Subansiri Basin, Assam, Northeast India. Palaeobotanist 62:1–10

Beug HJ, Miehe G (1999) Vegetation history and human impact in the Eastern Central Himalaya (Langtang and Helambu, Nepal). Diss Bot 318, Cramer, Berlin

Bharti RR, Rai ID, Adhikari BS, Rawat GS (2011) Timberline change detection using topographic map and satellite imagery: a critique. Trop Ecol 52:133–137

Bharti RR, Adhikari BS, Rawat GS (2012) Assessing vegetation changes in timberline ecotone of Nanda Devi National Park, Uttarakhand. Int J Appl Earth Obs Geoinform 18:472–479

Bhattacharyya A (1988) Vegetation and climate during post glacial period in the vicinity of Rohtang Pass, Great Himalayan range. Pollen et Spores 30:417–427

Bhattacharyya A (1989) Vegetation and climate during the last 30,000 years in Ladakh. Palaeogeogr Palaeoclimatol Palaeoecol 73:25–38

Bhattacharyya A, Chaudhary V (2003) Late-summer temperature reconstruction of the eastern Himalayan region based on tree-ring data of *Abies densa*. Arct Antarct Alp Res 35:196–202

Bhattacharyya A, Shah SK (2009) Tree-ring studies in India, past appraisal, present status and future prospect. IAWA J 30:361–370

Bhattacharyya A, Yadav RR (1990) Growth and climate relationship in *Cedrus deodara* from Joshimath, Uttar Pradesh. Palaeobotanist 38:411–414

Bhattacharyya A, Shah SK, Chaudhary V (2006) Would tree-ring data of *Betula utilis* have potential for the analysis of Himalayan glacial fluctuations? Curr Sci 91:754–761

Bhattacharyya A, Sharma J, Shah SK, Chaudhury V (2007) Climatic changes during last 1800 yrs BP from Paradise Lake, Sela Pass, Arunachal Pradesh, Northeast Himalaya. Curr Sci 93:983–987

Bhattacharyya A, Ranhotra P, Shah SK (2011) Spatio-temporal variation of alpine vegetation vis-à-vis climate during Holocene in the Himalaya. Mem Geol Soc India 77:309–319

Böhner J (2006) General climatic controls and topoclimatic variations in Central and High Asia. Boreas 35:279–295

Borgaonkar HP, Pant GB, Rupa Kumar K (1999) Tree-ring chronologies from western Himalaya and their dendroclimatic potential. Int Assoc Wood Anat J 20:295–309

Borgaonkar HP, Ram S, Sikder AB (2009) Assessment of tree-ring analysis of high-elevation *Cedrus deodara* D. Don from western Himalaya (India) in relation to climate and glacier fluctuations. Dendrochronologia 27:59–69

Borgaonkar HP, Sikder AB, Ram S (2011) High altitude forest sensitivity to the recent warming: a tree-ring analysis of conifers from western Himalaya, India. Quat Int 236:158–166

Bräuning A (2004) Tree-ring studies in the Dolpo-Himalaya (western Nepal). TRACE – Tree Rings Archaeol Climatol Ecol 2:8–12

Bräuning A (2006) Tree-ring evidence of "Little Ice Age" glacier advances in southern Tibet. The Holocene 16:1–12

Bräuning A, Grießinger J (2006) Late Holocene variations in monsoon intensity in the Tibetan-Himalayan region – evidence from tree rings. J Geol Soc India 68:485–493

Bräuning A, Mantwill B (2004) Summer temperature and summer monsoon history on the Tibetan plateau during the last 400 years recorded by tree rings. Geophys Res Lett 31:L24205. doi:10.1029/2004GL020793

Bräuning A, Grießinger J, Hochreuther P, Wernicke J (2016) Dendroecological perspectives on climate change on the southern Tibetan plateau. In: Singh RB, Schickhoff U, Mal S (eds)

Climate change, glacier response, and vegetation dynamics in the Himalaya. Springer, Cham, Switzerland
Brown ET, Bendick R, Bourles DL, Gaur V, Molnar P, Raisbeck GM, Yiou F (2003) Early Holocene climate recorded in geomorphological features in Western Tibet. Palaeogeogr Palaeoclimatol Palaeoecol 199:141–151
Cai Y, Zhang H, Cheng H, An Z, Edwards RL, Wang X, Tan L, Liang F, Wang J, Kelly M (2012) The Holocene Indian monsoon variability over the southern Tibetan Plateau and its teleconnections. Earth Planet Sci Lett 335:135–144
Camarero JJ, Gutiérrez E (2004) Pace and pattern of recent treeline dynamics: response of ecotones to climatic variability in the Spanish Pyrenees. Clim Change 63:181–200
Case BS, Duncan RP (2014) A novel framework for disentangling the scale-dependent influences of abiotic factors on alpine treeline position. Ecography 37:838–851
Chakraborty S, Bhattacharya SK, Ranhotra PS, Bhattacharyya A, Bhushan R (2006) Palaeoclimatic scenario during Holocene around Sangla valley, Kinnaur northwest Himalaya based on multi proxy records. Curr Sci 91:777–782
Champion HG, Seth SK (1968) A revised survey of the forest types of India. Govt. of India, Delhi
Chaudhary V, Bhattacharyya A (2000) Tree ring analysis of *Larix griffithiana* from the Eastern Himalayas in the reconstruction of past temperature. Curr Sci 79:1712–1715
Chauhan MS (2006) Late Holocene vegetation and climate change in the alpine belt of Himachal Pradesh. Curr Sci 91:1562–1567
Chauhan MS, Sharma C (1996) Late-Holocene vegetation of Darjeeling (Jore-Pokhari), Eastern Himalaya. Palaeobotanist 45:125–129
Chauhan MS, Sharma C (2000) Late Holocene vegetation and climate in Dewar Tal area, Inner Lesser Garhwal Himalaya. Palaeobotanist 49:509–514
Chauhan MS, Mazari RK, Rajagopalan G (2000) Vegetation and climate in upper Spiti region, Himachal Pradesh during late Holocene. Curr Sci 79:373–376
Chen IC, Hill JK, Ohlemüller R, Roy DB, Thomas CD (2011) Rapid range shifts of species associated with high levels of climate warming. Science 333:1024–1026
Chhetri PK, Cairns DM (2015) Contemporary and historic population structure of *Abies spectabilis* at treeline in Barun valley, eastern Nepal Himalaya. J Mt Sci 12:558–570
Chou SC, Huang CH, Hsu TW, Wu CC, Chou CH (2010) Allelopathic potential of *Rhododendron formosanum* Hemsl in Taiwan. Allelopathy J 25:73–92
Clift PD, Plumb RA (2008) The asian monsoon: causes, history and effects. Cambridge Univ Press, Cambridge
Cook BI, Wolkovich EM, Davies TJ, Ault TR, Betancourt JL, Allen JM, Bolmgren K, Cleland EE, Crimmins TM, Kraft NJB, Lancaster LT, Mazer SJ, McCabe GJ, McGill BJ, Parmesan C, Pau S, Regetz J, Salamin N, Schwartz MD, Travers SE (2012) Sensitivity of spring phenology to warming across temporal and spatial climate gradients in two independent databases. Ecosystems 15:1283–1294
Danby RK, Hik DS (2007) Variability, contingency and rapid change in recent subarctic alpine treeline dynamics. J Ecol 95:352–363
Daniels LD, Veblen TT (2004) Spatiotemporal influences of climate on altitudinal treeline in northern Patagonia. Ecology 85:1284–1296
Däniker A (1923) Biologische Studien über Wald- und Baumgrenzen, insbesondere über die klimatischen Ursachen und deren Zusammenhänge. Vierteljahresschr Naturforsch Ges Zürich 68:1–102
Dawadi B, Liang E, Tian L, Devkota LP, Yao T (2013) Pre-monsoon precipitation signal in tree rings of timberline *Betula utilis* in the central Himalayas. Quat Int 283:72–77
Demske D, Tarasov PE, Wünnemann B, Riedel F (2009) Late glacial and Holocene vegetation, Indian monsoon and westerly circulation in the Trans-Himalaya recorded in the lacustrine pollen sequence from Tso Kar, Ladakh, NW India. Palaeogeogr Palaeoclimatol Palaeoecol 279:172–185
Dixit Y, Hodell DA, Sinha R, Petrie CA (2014) Abrupt weakening of the Indian summer monsoon at 8.2 kyr BP. Earth Planet Sci Lett 391:16–23

Dodia R, Agrawal DP, Vora AB (1985) New pollen data from Kashmir bogs: a summary. In: Agrawal DP, Kusumgar S, Krishnamurthy RV (eds) Climate and geology of Kashmir and Central Asia. TT Printers & Publ, New Delhi, pp 101–108

Dubey B, Yadav RR, Singh J, Chaturvedi R (2003) Upward shift of Himalayan pine in western Himalaya, India. Curr Sci 85:1135–1136

Dullinger S, Dirnböck T, Grabherr G (2004) Modelling climate-change driven treeline shifts: relative effects of temperature increase, dispersal and invisibility. J Ecol 92:241–252

Dutta PK, Dutta BK, Das AK, Sundriyal RC (2014) Alpine timberline research gap in Himalaya: a literature review. Indian For 140:419–427

Elliott GP (2011) Influences of 20th century warming at the upper tree line contingent on local-scale interactions: evidence from a latitudinal gradient in the Rocky Mountains, USA. Glob Ecol Biogeogr 20:46–57

Esper J, Schweingruber FH, Winiger M (2002) 1,300 years of climate history for western central Asia inferred from tree-rings. The Holocene 12:267–277

Esper J, Frank DC, Wilson RJ, Büntgen U, Treydte K (2007) Uniform growth trends among central Asian low-and high-elevation juniper tree sites. Trees 21:141–150

Fan ZX, Bräuning A, Yang B, Cao KF (2009) Tree ring density-based summer temperature reconstruction for the central Hengduan Mountains in southern China. Global Planet Change 65:1–11

Frenzel B (1994) Über Probleme der holozänen Vegetationsgeschichte Osttibets. Göttinger Geogr Abh 95:143–166

Gaire NP, Dhakal YR, Lekhak HC, Bhuju DR, Shah SK (2011) Dynamics of *Abies spectabilis* in relation to climate change at the treeline ecotone in Langtang National Park. Nepal J Sci Technol 12:220–229

Gaire NP, Koirala M, Bhuju DR, Borgaonkar HP (2014) Treeline dynamics with climate change at the central Nepal Himalaya. Clim Past 10:1277–1290

Gairola S, Rawal RS, Todaria NP (2008) Forest vegetation patterns along an altitudinal gradient in sub-alpine zone of west Himalaya, India. Afr J Plant Sci 2:42–48

Gairola S, Rawal RS, Todaria NP, Bhatt A (2014) Population structure and regeneration patterns of tree species in climate-sensitive subalpine forests of Indian western Himalaya. J For Res 25:343–349

Gasse F, Fontes JC, Van Campo E, Wei K (1996) Holocene environmental changes in Bangong Co basin (Western Tibet). Part 4: discussion and conclusions. Palaeogeogr Palaeoclimatol Palaeoecol 120:79–92

Gehrig-Fasel J, Guisan A, Zimmermann NE (2007) Tree line shifts in the Swiss Alps: climate change or land abandonment? J Veg Sci 18:571–582

Gerlitz L, Conrad O, Thomas A, Böhner J (2014) Warming patterns over the Tibetan Plateau and adjacent lowlands derived from elevation- and bias-corrected ERA-Interim data. Clim Res 58:235–246

Ghimire BK, Lekhak HD (2007) Regeneration of *Abies spectabilis* (D. Don) Mirb. in subalpine forest of upper Manang, north-central Nepal. In: Chaudhary RP, Aase TH, Vetaas O, Subedi BP (eds) Local effects of global changes in the Himalayas: Manang Nepal. Kathmandu, Bergen, pp 139–149

Ghimire BK, Mainali KP, Lekhak HD, Chaudhary RP, Ghimeray A (2010) Regeneration of *Pinus wallichiana* A.B. Jackson in a trans-Himalayan dry valley of north-central Nepal. Himal J Sci 6:19–26

Ghosh R, Paruya DK, Khan MA, Chakraborty S, Sarkar A, Bera S (2014) Late quaternary climate variability and vegetation response in Ziro Lake Basin, Eastern Himalaya: a multiproxy approach. Quat Int 325:13–29

Ghosh R, Bera S, Sarkar A, Paruya DK, Yao YF, Li CS (2015) A ~50 ka record of monsoonal variability in the Darjeeling foothill region, eastern Himalayas. Quat Sci Rev 114:100–115

Gonzalez P, Neilson RP, Lenihan JM, Drapek RJ (2010) Global patterns in the vulnerability of ecosystems to vegetation shifts due to climate change. Glob Ecol Biogeogr 19:755–768

Gottfried M, Pauli H, Futschik A, Akhalkatsi M, Barančok P, Benito Alonso JL, Coldea G, Dick J, Erschbamer B, Kazakis G, Krajči J, Larsson P, Mallaun M, Michelsen O, Moiseev D, Moiseev P, Molau U, Merzouki A, Nagy L, Nakhutsrishvili G, Pedersen B, Pelino G, Puscas M, Rossi G, Stanisci A, Theurillat JP, Tomaselli M, Villar L, Vittoz P, Vogiatzakis I, Grabherr G (2012) Continent-wide response of mountain vegetation to climate change. Nat Clim Chang 2:111–115

Grace J, Berninger F, Nagy L (2002) Impacts of climate change on the tree line. Ann Bot 90:537–544

Gratzer G, Rai PB (2004) Density dependent mortality versus spatial segregation in early life stages of *Abies densa* and *Rhododendron hodgsonii* in central Bhutan. For Ecol Manag 192:143–159

Gratzer G, Rai PB, Schieler K (2002) Structure and regeneration dynamics of *Abies densa* forests in central Bhutan. Centralbl Ges Forstwes 119:279–287

Graumlich LJ, Waggoner LA, Bunn AG (2005) Detecting global change at alpine treeline: coupling palaeoecology with contemporary studies. In: Huber UM, Bugmann HKM, Reasoner MA (eds) Global change and mountain regions. An overview of current knowledge. Springer, Dordrecht, pp 501–508

Grover VI, Borsdorf A, Breuste JH, Tiwari PC, Frangetto FW (2015) Impact of global changes on mountains. Responses and adaptations. CRC Press, Boca Raton

Gupta RK (1983) The living Himalayas, vol 1, Aspects of Environment and Resource Ecology of Garhwal. Today and Tomorrow's, New Delhi

Gupta C, Nautiyal DD (1998) Studies on Mansar Lake deposit, Jammu. Pollen analysis and palaeoclimatic changes. Geophytology 27:67–75

Gupta AK, Anderson DM, Pandey DN, Singhvi AK (2006) Adaptation and human migration, and evidence of agriculture coincident with changes in the Indian summer monsoon during the Holocene. Curr Sci 90:1082–1090

Harsch MA, Bader MY (2011) Treeline form – a potential key to understanding treeline dynamics. Glob Ecol Biogeogr 20:582–596

Harsch MA, Hulme PE, McGlone MS, Duncan RP (2009) Are treelines advancing? A global meta-analysis of treeline response to climate warming. Ecol Lett 12:1040–1049

Hasson S, Gerlitz L, Schickhoff U, Scholten T, Böhner J (2016) Recent climate change in High Asia. In: Singh RB, Schickhoff U, Mal S (eds) Climate change, glacier response, and vegetation dynamics in the Himalaya. Springer, Cham, Switzerland

He M, Yang B, Bräuning A (2013) Tree growth–climate relationships of *Juniperus tibetica* along an altitudinal gradient on the southern Tibetan Plateau. Trees 27:429–439

Herzschuh U (2006) Palaeo-moisture evolution at the margins of the Asian monsoon during the last 50 ka. Quat Sci Rev 25:163–178

Holtmeier FK (2009) Mountain timberlines. Ecology, patchiness, and dynamics. Springer, Dordrecht

Holtmeier FK, Broll G (2005) Sensitivity and response of northern hemisphere altitudinal and polar treelines to environmental change at landscape and local scales. Glob Ecol Biogeogr 14:395–410

Holtmeier FK, Broll G (2007) Treeline advance – driving processes and adverse factors. Landsc Online 1:1–21

Holtmeier FK, Broll G (2009) Altitudinal and polar treelines in the northern hemisphere – causes and response to climate change. Polarforschung 79:139–153

Holtmeier FK, Broll G (2012) Landform influences on treeline patchiness and dynamics in a changing climate. Phys Geogr 33:403-437

Huber UM, Bugmann HKM, Reasoner MA (eds) (2005) Global change and mountain regions. An overview of current knowledge. Springer, Dordrecht

IPCC (2013) Climate change 2013: the physical science basis. Contribution of the working group I to the fifth assessment report of the Intergovernmental Panel on Climate Change. Cambridge University Press, Cambridge

IPCC (2014) Climate change 2014: impacts, adaptation, and vulnerability. Part a: global and sectoral aspects. Contribution of the working group II to the fifth assessment report of the Intergovernmental Panel on Climate Change. Cambridge University Press, Cambridge

Jacobsen JP, Schickhoff U (1995) Untersuchungen zur Besiedlung und gegenwärtigen Waldnutzung im Hindukusch/Karakorum. Erdkunde 49:49–59

Jarvis DI (1993) Pollen evidence of changing Holocene monsoon climate in Sichuan Province, China. Quat Res 39:325–337

Kaiser K, Opgenoorth L, Schoch WH, Miehe G (2009) Charcoal and fossil wood from palaeosols, sediments and artificial structures indicating Late Holocene woodland decline in southern Tibet (China). Quat Sci Rev 28:1539–1554

Kar R, Ranhotra PS, Bhattacharyya A, Sekar B (2002) Vegetation vis-à-vis climate and glacial fluctuations of the Gangotri Glacier since the last 2000 years. Curr Sci 82:347–351

Kharal DK, Bhuju DR, Gaire NP, Rayamajhi S, Meilby H, Chaudhary A (2015) Population structure and distribution of *Abies spectabilis* (D. Don) in Central Nepal Himalaya: a comparison with the total woody vegetation of the forests at the three different elevation ranges in Manang District. Banko Janakari 25:3–14

Körner C (1998) A re-assessment of high elevation treeline positions and their explanation. Oecologia 115:445–459

Körner C (2007) Climatic treelines: conventions, global patterns, causes. Erdkunde 61:316–324

Körner C (2012) Alpine treelines. Functional ecology of the high elevation tree limits. Springer, Basel

Körner C, Paulsen J (2004) A world-wide study of high altitude treeline temperatures. J Biogeogr 31:713–732

Körner C, Ohsawa M, Spehn E, Berge E, Bugmann H, Groombridge B, Hamilton L, Hofer T, Ives J, Jodha N, Messerli B, Pratt J, Price M, Reasoner M, Rodgers A, Thonell J, Yoshino M (2005) Mountain systems. In: Hassan R, Scholes R, Ash N (eds) Ecosystems and human well-being: current state and trends, vol 1. Island Press, Washington, pp 681–716

Kotlia BS, Joshi LM (2013) Late Holocene climatic changes in Garhwal Himalaya. Curr Sci 104:911–919

Kramer A, Herzschuh U, Mischke S, Zhang C (2010a) Holocene treeline shifts and monsoon variability in the Hengduan Mountains (southeastern Tibetan Plateau), implications from palynological investigations. Palaeogeogr Palaeoclimatol Palaeoecol 286:23–41

Kramer A, Herzschuh U, Mischke S, Zhang C (2010b) Late glacial vegetation and climate oscillations on the southeastern Tibetan Plateau inferred from the Lake Naleng pollen profile. Quat Res 73:324–335

Kullman L (2000) Tree-limit rise and recent warming: a geoecological case study from the Swedish Scandes. Nors Geogr Tidsskr 54:49–59

Kullman L (2014) Treeline (*Pinus sylvestris*) landscape evolution in the Swedish Scandes – a 40-year demographic effort viewed in a broader temporal context. Nors Geogr Tidsskr 68:155–167

Kullman L, Öberg L (2009) Post-Little Ice Age tree line rise and climate warming in the Swedish Scandes: a landscape ecological perspective. J Ecol 97:415–429

Kumar P (2012) Assessment of impact of climate change on Rhododendrons in Sikkim Himalayas using Maxent modelling: limitations and challenges. Biodivers Conserv 21:1251–1266

Lang G (1994) Quartäre Vegetationsgeschichte Europas. Fischer, Jena

Leipe C, Demske D, Tarasov PE, Members HP (2014) A Holocene pollen record from the northwestern Himalayan lake Tso Moriri: implications for palaeoclimatic and archaeological research. Quat Int 348:93–112

Lenoir J, Gégout JC, Marquet PA, de Ruffray P, Brisse H (2008) A significant upward shift in plant species optimum elevation during the 20th century. Science 320:1768–1771

Lescop-Sinclair K, Payette S (1995) Recent advance of the arctic treeline along the eastern coast of Hudson Bay. J Ecol 83:929–936

Liang E, Shao XM, Xu Y (2009) Tree-ring evidence of recent abnormal warming on the southeast Tibetan Plateau. Theor Appl Climatol 98:9–18

Liang E, Wang Y, Xu Y, Liu B, Shao X (2010) Growth variations of *Abies georgei* var. *smithii* along altitudinal gradients in the Sygera Mts., southeastern Tibetan Plateau. Trees 24:363–373
Liang E, Wang Y, Eckstein D, Luo T (2011) Little change in the fir tree-line position on the southeastern Tibetan Plateau after 200 years of warming. New Phytol 190:760–769
Liang E, Dawadi B, Pederson N, Eckstein D (2014) Is the growth of birch at the upper timberline in the Himalayas limited by moisture or by temperature? Ecology 95:2453–2465
Liu J, Qin C, Kang S (2013) Growth response of *Sabina tibetica* to climate factors along an elevation gradient in South Tibet. Dendrochronologia 31:255–265
Lloyd AH (2005) Ecological histories from Alaskan tree lines provide insight into future change. Ecology 86:1687–1695
Lv LX, Zhang QB (2012) Asynchronous recruitment history of *Abies spectabilis* along an altitudinal gradient in the Mt. Everest region. J Plant Ecol 5:147–156
MacDonald GM, Velichko AA, Gattaulin VN (2000) Holocene treeline history and climate change across northern Eurasia. Quat Res 53:302–311
Malanson GP, Butler DR, Fagre DB, Walsh SJ, Tomback DF, Daniels LD, Resler LM, Smith WK, Weiss DJ, Peterson DL, Bunn AG, Hiemstra CA, Liptzin D, Bourgeron PS, Shen Z, Millar CI (2007) Alpine treeline of western North America: linking organism-to-landscape dynamics. Phys Geogr 28:378–396
Malanson GP, Resler LM, Bader MY, Holtmeier FK, Butler DR, Weiss DJ, Daniels LD, Fagre DB (2011) Mountain treelines: a roadmap for research orientation. Arct Antarct Alp Res 43:167–177
Mathisen IE, Mikheeva A, Tutubalina OV, Aune S, Hofgaard A (2014) Fifty years of tree line change in the Khibiny Mountains, Russia: advantages of combined remote sensing and dendroecological approaches. Appl Veg Sci 17:6–16
Mehrotra N, Shah SK, Bhattacharyya A (2014) Review of palaeoclimate records from Northeast India based on pollen proxy data of Late Pleistocene–Holocene. Quat Int 325:41–54
Miehe G (1997) Alpine vegetation types of the central Himalaya. In: Wielgolaski FE (ed) Polar and Alpine Tundra. Ecosystems of the World 3. Elsevier, Amsterdam, pp 161–184
Miehe G (2004) Himalaya. In: Burga CA, Klötzli F, Grabherr G (eds) Gebirge der Erde. Landschaft, Klima, Pflanzenwelt. Ulmer, Stuttgart, pp 325–359
Miehe G, Miehe S (2000) Comparative high mountain research on the treeline ecotone under human impact. Erdkunde 54:34–50
Miehe G, Miehe S, Schlütz F (2002) Vegetationskundliche und palynologische Befunde aus dem Muktinath-Tal (Tibetischer Himalaya, Nepal): Ein Beitrag zur Landschaftsgeschichte altweltlicher Hochgebirgshalbwüsten. Erdkunde 56:268–285
Miehe G, Kaiser K, Co S, Xinquan Z, Jianquan L (2008) Geo-ecological transect studies in northeast Tibet (Qinghai, China) reveal human-made mid-Holocene environmental changes in the upper Yellow River catchment changing forest to grassland. Erdkunde 62:187–199
Miehe G, Miehe S, Schlütz F (2009a) Early human impact in the forest ecotone of southern High Asia (Hindu Kush, Himalaya). Quat Res 71:255–265
Miehe G, Miehe S, Kaiser K, Reudenbach C, Behrendes L, Duo L, Schlütz F (2009b) How old is pastoralism in Tibet? An ecological approach to the making of a Tibetan landscape. Palaeogeogr Palaeoclimatol Palaeoecol 276:130–147
Miehe G, Miehe S, Böhner J, Bäumler R, Ghimire SK, Bhattarai K, Chaudhary RP, Subedi M, Jha PK, Pendry C (2015) Vegetation ecology. In: Miehe G, Pendry C, Chaudhary RP (eds) Nepal: An introduction to the natural history, ecology and human environment of the Himalayas. Royal Botanic Garden Edinburgh, pp 385-472
Moiseev PA, Bartysh AA, Nagimov ZY (2010) Climate changes and tree stand dynamics at the upper limit of their growth in the North Ural Mountains. Russ J Ecol 41:486–497
Morrill C, Overpeck JT, Cole JE (2003) A synthesis of abrupt changes in the Asian summer monsoon since the last deglaciation. The Holocene 13:465–476

Müller M, Schickhoff U, Scholten T, Drollinger S, Böhner J, Chaudhary RP (2016) How do soil properties affect alpine treelines? General principles in a global perspective and novel findings from Rolwaling Himal, Nepal. Prog Phys Geogr 40:135–160

Negi PS (2012) Climate change, alpine treeline dynamics and associated terminology: focus on northwestern Indian Himalaya. Trop Ecol 53:371–374

Overpeck J, Anderson D, Trumbore S, Prell W (1996) The southwest Indian Monsoon over the last 18 000 years. Clim Dyn 12:213–225

Panigrahy S, Anitha D, Kimothi MM, Singh SP (2010) Timberline change detection using topographic map and satellite imagery. Trop Ecol 51:87–91

Pant GB, Rupa Kumar K, Yamashita K (2000) Climatic response of *Cedrus deodara* tree-ring parameters from two sites in the western Himalaya. Can J For Res 30:1127–1135

Pauli H, Gottfried M, Dullinger S, Abdaladze O, Akhalkatsi M, Alonso JLB, Coldea G, Dick J, Erschbamer B, Calzado RF, Ghosn D, Holten JI, Kanka R, Kazakis G, Kollar J, Larsson P, Moiseev P, Moiseev D, Molau U, Mesa JM, Nagy L, Pelino G, Puscas M, Rossi G, Stanisci A, Syverhuset AO, Theurillat JP, Tomaselli M, Unterluggauer P, Villar L, Vittoz P, Grabherr G (2012) Recent plant diversity changes on Europe's mountain summits. Science 336:353–355

Paulsen J, Körner C (2014) A climate-based model to predict potential treeline position around the globe. Alp Bot 124:1–12

Peñuelas J, Sardans J, Estiarte M, Ogaya R, Carnicer J, Coll M, Barbeta A, Rivas-Ubach A, Llusia J, Garbulsky M, Filella I, Jump AS (2013) Evidence of current impact of climate change on life: a walk from genes to the biosphere. Glob Chang Biol 19:2303–2338

Phadtare NR (2000) Sharp decrease in summer monsoon strength 4000–3500 cal yr B.P. in the central higher Himalaya of India based on pollen evidence from alpine peat. Quat Res 53:122–129

Phadtare NR, Pant RK (2006) A century-scale pollen record of vegetation and climate history during the past 3500 years in the Pinder Valley, Kumaon Higher Himalaya, India. Geol Soc India 68:495–506

Prasad S, Enzel Y (2006) Holocene palaeoclimates of India. Quat Res 66:442–453

Puri GS, Gupta RK, Meher-Homji VM, Puri S (1989) Forest ecology, vol 2, Plant Form, Diversity, Communities and Succession. Oxford & IBH, New Delhi

Rai ID, Bharti R, Adhikari BS, Rawat GS (2013) Structure and functioning of timberline vegetation in the western Himalaya: a case study. In: Wu N, Rawat GS, Joshi S, Ismail M, Sharma E (eds) High-altitude rangelands and their interfaces in the Hindu Kush Himalayas. ICIMOD, Kathmandu, pp 91–107

Ram S, Borgaonkar HP (2013) Growth response of conifer trees from high altitude region of western Himalaya. Curr Sci 105:225–231

Ram S, Borgaonkar HP (2014) Tree-ring analysis over western Himalaya and its long-term association with vapor pressure and potential evapotranspiration. Dendrochronologia 32:32–38

Ranhotra PS, Bhattacharyya A, Kar R, Sekar B (2001) Vegetation and climatic changes around Gangotri glacier during Holocene. Geol Surv India Spec Publ 65:67–71

Rawat DS (2012) Monitoring ecosystem boundaries in the Himalaya through an 'eye in the sky'. Curr Sci 102:1352–1354

Rawat S, Gupta AK, Sangode SJ, Srivastava P, Nainwal HC (2015) Late Pleistocene–Holocene vegetation and Indian summer monsoon record from the Lahaul, Northwest Himalaya, India. Quat Sci Rev 114:167–181

Reasoner MA, Tinner W (2009) Holocene treeline fluctuations. In: Gornitz V (ed) Encyclopedia of palaeoclimatology and ancient environments. Springer, Dordrecht, pp 442–446

Ren QS, Yang XL, Cui GF, Wang JS, Huang Y, Wei XH, Li QL (2007) Smith fir population structure and dynamics in the timberline ecotone of the Sejila Mountain, Tibet, China. Acta Ecol Sin 27:2669–2677

Richardson AD, Friedland AJ (2009) A review of the theories to explain arctic and alpine treelines around the world. J Sustain For 28:218–242

Saijo K, Tanaka S (2002) Palaeosols of Middle Holocene age in the Thakkola Basin, Central Nepal, and their paleoclimatic significance. J Asian Earth Sci 21:323–329

Sano M, Furuta F, Kobayashi O, Sweda T (2005) Temperature variations since the mid-18th century for western Nepal, as reconstructed from tree-ring width and density of *Abies spectabilis*. Dendrochronologia 23:83–92

Schickhoff U (1995) Himalayan forest-cover changes in historical perspective. A case study in the Kaghan Valley, northern Pakistan. Mt Res Dev 15:3–18

Schickhoff U (2000a) The impact of Asian summer monsoon on forest distribution patterns, ecology, and regeneration north of the main Himalayan range (E-Hindukush, Karakorum). Phytocoenologia 30:633–654

Schickhoff U (2000b) Persistence and dynamics of long-lived forest stands in the Karakorum under the influence of climate and man. In: Miehe G, Zhang Y (eds) Environmental changes in High Asia. Proceedings of an international symposium at the University of Marburg. Marburger Geogr Schr 135. pp 250–264

Schickhoff U (2002) Die Degradierung der Gebirgswälder Nordpakistans. Faktoren, Prozesse und Wirkungszusammenhänge in einem regionalen Mensch-Umwelt-System. Erdwiss Forsch 41, Steiner, Stuttgart

Schickhoff U (2005) The upper timberline in the Himalayas, Hindu Kush and Karakorum: a review of geographical and ecological aspects. In: Broll G, Keplin B (eds) Mountain ecosystems. Studies in treeline ecology. Springer, Berlin, pp 275–354

Schickhoff U (2011) Dynamics of mountain ecosystems. In: Millington A, Blumler M, Schickhoff U (eds) Handbook of biogeography. Sage Publ, London, pp 313–337

Schickhoff U (2012) Der Himalaya: Wandel eines Gebirgssystems unter dem Einfluss von Klima und Mensch. In: Rintelner Symposium X. Berichte der Reinhold-Tüxen-Gesellschaft 24. pp 103–121

Schickhoff U, Bobrowski M, Böhner J, Bürzle B, Chaudhary RP, Gerlitz L, Heyken H, Lange J, Müller M, Scholten T, Schwab N, Wedegärtner R (2015) Do Himalayan treelines respond to recent climate change? An evaluation of sensitivity indicators. Earth Syst Dyn 6:245–265

Schlütz F (1999) Palynologische Untersuchungen über die holozäne Vegetations-, Klima- und Siedlungsgeschichte in Hochasien (Nanga Parbat, Karakorum, Nianbaoyeze, Lhasa) und das Pleistozän in China (Qinling-Gebirge, Gaxun Nur). Diss Bot 315, Cramer, Berlin

Schlütz F, Zech W (2004) Palynological investigations on vegetation and climate change in the Late Quaternary of Lake Rukche area, Gorkha Himal, Central Nepal. Veg Hist Archaeobot 13:81–90

Schmidt-Vogt D (1990) High altitude forests in the Jugal Himal (Eastern Central Nepal). Forest Types and Human Impact. Geoecol Res 6, Steiner, Stuttgart

Schwab N, Schickhoff U, Bürzle B, Hellmold J, Stellmach M (2015) Dendroecological studies in the Nepal Himalaya – review and outlook in the context of a new research initiative (TREELINE). In: Wilson R, Helle G, Gärtner H (eds) TRACE – tree rings in archaeology, climatology and ecology, vol 13. GFZ, Potsdam, pp 86–95

Schwab N, Schickhoff U, Müller M, Gerlitz L, Bürzle B, Böhner J, Chaudhary RP, Scholten T (2016) Treeline responsiveness to climate warming: insights from a krummholz treeline in Rolwaling Himal, Nepal. In: Singh RB, Schickhoff U, Mal S (eds) Climate change, glacier response, and vegetation dynamics in the Himalaya. Springer, Cham, Switzerland

Schweinfurth U (1957) Die horizontale und vertikale Verbreitung der Vegetation im Himalaya. Bonner Geogr Abh 20, Dümmlers Verlag, Bonn

Schwörer C, Kaltenrieder P, Glur L, Berlinger M, Elbert J, Frei S, Gilli A, Hafner A, Anselmetti FS, Grosjean M, Tinner W (2014) Holocene climate, fire and vegetation dynamics at the treeline in the Northwestern Swiss Alps. Veg Hist Archaeobot 23:479–496

Sharma C (1992) Palaeoclimatic oscillations since last deglaciation in western Himalaya: a palynological assay. Palaeobotanist 40:374–382

Sharma C, Chauhan MS (1988) Studies in the late Quaternary vegetational history in Himachal Pradesh. 4. Rewalsar Lake II. Pollen Spores 30:395–408

Sharma C, Chauhan MS (2001) Late Holocene vegetation and climate of Kupup (Sikkim), Eastern Himalaya, India. J Palaeontol Soc India 46:51–58
Sharma C, Gupta A (1995) Vegetational history of Nachiketa Tal, Garhwal Himalaya, India. J Nepal Geol Soc 10:29–34
Sharma C, Gupta A (1997) Vegetation and climate in Garhwal Himalaya during early Holocene: Deoria Tal. Palaeobotanist 46:111–116
Sharma S, Joachimski M, Sharma M, Tobschall HJ, Singh IB, Sharma C, Chauhan MS, Morgenroth G (2004) Lateglacial and Holocene environmental changes in Ganga plain, Northern India. Quat Sci Rev 23:145–159
Shen J, Jones RT, Yang X, Dearing JA, Wang S (2006) The Holocene vegetation history of Lake Erhai, Yunnan province, southwestern China: the role of climate and human forcings. The Holocene 16:265–276
Shrestha AB, Aryal R (2011) Climate change in Nepal and its impact on Himalayan glaciers. Reg Environ Chang 11(Suppl 1):S65–S77
Shrestha BB, Ghimire B, Lekhak HD, Jha PK (2007) Regeneration of tree line birch (*Betula utilis* D.Don) forest in trans-Himalayan dry valley in central Nepal. Mt Res Dev 27:259–267
Shrestha UB, Gautam S, Bawa KS (2012) Widespread climate change in the Himalayas and associated changes in local ecosystems. PLoS One 7:e36741. doi:10.1371/journal.pone.0036741
Shrestha KB, Hofgaard A, Vandvik V (2015a) Recent treeline dynamics are similar between dry and mesic areas of Nepal, central Himalaya. J Plant Ecol 8:347–358
Shrestha KB, Hofgaard A, Vandvik V (2015b) Tree-growth response to climatic variability in two climatically contrasting treeline ecotone areas, central Himalaya, Nepal. Can J For Res 45:1643–1653
Singh G (1963) A preliminary survey of the postglacial vegetational history of Kashmir Valley. Palaeobotanist 12:73–108
Singh G, Agrawal DP (1976) Radiocarbon evidence for deglaciation in north-western Himalaya, India. Nature 260:232
Singh JS, Singh SP (1992) Forests of Himalaya. Gyanodaya Prakashan, Nainital
Singh J, Yadav RR (2000) Tree-ring indications of recent glacier fluctuations in Gangotri, western Himalaya, India. Curr Sci 79:1598–1601
Singh CP, Panigrahy S, Thapliyal A, Kimothi MM, Soni P, Parihar JS (2012) Monitoring the alpine treeline shift in parts of the Indian Himalayas using remote sensing. Curr Sci 102:559–562
Singh CP, Panigrahy S, Parihar JS, Dharaiya N (2013) Modeling environmental niche of Himalayan birch and remote sensing based vicarious validation. Trop Ecol 54:321–329
Smith WK, Germino MJ, Hancock TE, Johnson DM (2003) Another perspective on altitudinal limits of Alpine timberlines. Tree Physiol 23:1101–1112
Smith WK, Germino MJ, Johnson DM, Reinhardt K (2009) The altitude of alpine treeline: a bellwether of climate change effects. Bot Rev 75:163–190
Song XY, Yao YF, Wortley AH, Paudayal KN, Yang SH, Li CS, Blackmore S (2012) Holocene vegetation and climate history at Haligu on the Jade Dragon snow mountain, Yunnan, SW China. Clim Change 113:841–866
Stainton JDA (1972) Forests of Nepal. Hafner, New York
Staubwasser M (2006) An overview of Holocene South Asian monsoon records- monsoon domains and regional contrasts. J Geol Soc India 68:433–446
Staubwasser M, Sirocko F, Grootes PM, Segl M (2003) Climate change at the 4.2 ka BP termination of the Indus valley civilization and Holocene south Asian monsoon variability. Geophys Res Lett 30(8):1425. doi:10.1029/2002GL016822
Sujakhu H, Gosai KR, Karmacharya SB (2014) Forest structure and regeneration pattern of *Betula utilis* D. Don in Manaslu conservation area, Nepal. Ecoprint 20:107–113
Sun X, Wu Y, Qiao Y, Walker D (1986) Late Pleistocene and Holocene vegetation history at Kunming, Yunnan Province, Southwest China. J Biogeogr 13:441–476

Telwala Y, Brook BW, Manish K, Pandit MK (2013) Climate-induced elevational range shifts and increase in plant species richness in a Himalayan biodiversity epicentre. PLoS One 8:e57103. doi:10.1371/journal.pone.0057103

Tinner W, Theurillat JP (2003) Uppermost limit, extent, and fluctuations of the timberline and treeline ecocline in the Swiss Central Alps during the past 11,500 years. Arct Antarct Alp Res 35:158–169

Trivedi A, Chauhan MS (2008) Pollen proxy records of Holocene vegetation and climate change from Mansar Lake, Jammu region, India. Curr Sci 95:1347–1354

Troll C (1972) The three-dimensional zonation of the Himalayan system. In: Troll C (ed) Geoecology of the high-mountain regions of Eurasia. Steiner, Wiesbaden, pp 264–275

Vishnu-Mittre (1984) Quaternary palaeobotany and palynology in the Himalaya: an overview. Palaeobotanist 32:158–187

Vittoz P, Rulence B, Largey T, Freléchoux F (2008) Effects of climate and land-use change on the establishment and growth of Cembran Pine (*Pinus cembra* L.) over the altitudinal treeline ecotone in the central Swiss Alps. Arct Antarct Alp Res 40:225–232

Walker D (1986) Late Pleistocene-early Holocene vegetational and climatic changes in Yunnan Province, southwest China. J Biogeogr 13:477–486

Wallentin G, Tappeiner U, Strobl J, Tasser E (2008) Understanding alpine tree line dynamics: an individual-based model. Ecol Model 218:235–246

Wang Y, Camarero JJ, Luo T, Liang E (2012) Spatial patterns of Smith fir alpine treelines on the south-eastern Tibetan Plateau support that contingent local conditions drive recent treeline patterns. Plant Ecol Div 5:311–321

Weiss DJ, Malanson GP, Walsh SJ (2015) Multiscale relationships between alpine treeline elevation and hypothesized environmental controls in the western United States. Ann Assoc Am Geogr 105:437–453

Wieser G, Tausz M (eds) (2007) Trees at their upper limit. Treelife limitation at the Alpine timberline. Springer, Dordrecht, pp 79–129

Wieser G, Holtmeier FK, Smith WK (2014) Treelines in a changing globalenvironment. In: Tausz M, Grulke N (eds) Trees in a changing environment. Springer, Dordrecht, pp 221–263

Wong MH, Duan C, Long Y, Luo Y, Xie G (2010) How will the distribution and size of subalpine *Abies georgei* forest respond to climate change? A study in Northwest Yunnan, China. Phys Geogr 31:319–335

Xiao X, Haberle SG, Shen J, Yang X, Han Y, Zhang E, Wang S (2014) Latest Pleistocene and Holocene vegetation and climate history inferred from an alpine lacustrine record, northwestern Yunnan Province, southwestern China. Quat Sci Rev 86:35–48

Xu J, Grumbine RE, Shrestha A, Eriksson M, Yang X, Wang Y, Wilkes A (2009) The melting Himalayas: cascading effects of climate change on water, biodiversity, and livelihoods. Conserv Biol 23:520–530

Yadav RR, Singh J (2002) Tree-ring analysis of *Taxus baccata* from the western Himalaya, India, and its dendroclimatic potential. Tree-Ring Res 58:23–29

Yadav RR, Singh J, Dubey B, Chaturvedi R (2004) Varying strength of relationship between temperature and growth of high level fir at marginal ecosystems in western Himalaya, India. Curr Sci 86:1152–1156

Yadav RR, Singh J, Dubey B, Misra KG (2006) A 1584-year ring width chronology of juniper from Lahul, Himachal Pradesh: prospects of developing millennia-long climate records. Curr Sci 90:1122–1126

Yadav RR, Bräuning A, Singh J (2011) Tree ring inferred summer temperature variations over the last millennium in western Himalaya, India. Clim Dyn 36:1545–1554

Yang B, Wang J, Bräuning A, Dong Z, Esper J (2009) Late Holocene climatic and environmental changes in arid central Asia. Quat Int 194:68–78

Yang B, Kang X, Bräuning A, Liu J, Qin C, Liu J (2010) A 622-year regional temperature history of southeast Tibet derived from tree rings. The Holocene 20:181–190

Yang J, Zhang W, Cui Z, Yi C, Chen Y, Xu X (2010) Climate change since 11.5 ka on the Diancang Massif on the southeastern margin of the Tibetan Plateau. Quat Res 73:304–312

Yasuda Y, Tabata H (1988) Vegetation and climatic changes in Nepal Himalayas II. A preliminary study of the Holocene vegetational history in the Lake Rara National Park area, West Nepal. Proc Indian Natl Sci Acad 54A:538–549

Yonebayashi C, Minaki M (1997) Late quaternary vegetation and climatic history of eastern Nepal. J Biogeogr 24:837–843

Yu G, Chen X, Ni J, Cheddadi R, Guiot J, Han H, Harrison SP, Huang C, Ke M, Kong Z, Li S, Li W, Liew P, Liu G, Liu J, Liu Q, Liu KB, Prentice IC, Qui W, Ren G, Song C, Sugita S, Sun X, Tang L, Van Campo E, Xia Y, Xu Q, Yan S, Yang X, Zhao J, Zheng Z (2000) Palaeovegetation of China: a pollen data-based synthesis for the mid-Holocene and last glacial maximum. J Biogeogr 27:635–664

Zhang L, Luo T, Liu X, Kong G (2010) Altitudinal variations in seedling and sapling density and age structure of timberline tree species in the Sergyemla Mountains, southeast Tibet. Acta Ecol Sin 30:76–80

Zhu HF, Shao XM, Yin ZY, Xu P, Xu Y, Tian H (2011) August temperature variability in the southeastern Tibetan Plateau since AD 1385 inferred from tree rings. Palaeogeogr Palaeoclimatol Palaeoecol 305:84–92

Zurbriggen N, Hättenschwiler S, Frei ES, Hagedorn F, Bebi P (2013) Performance of germinating tree seedlings below and above treeline in the Swiss Alps. Plant Ecol 214:385–396

Chapter 16
Treeline Responsiveness to Climate Warming: Insights from a Krummholz Treeline in Rolwaling Himal, Nepal

Niels Schwab, Udo Schickhoff, Michael Müller, Lars Gerlitz, Birgit Bürzle, Jürgen Böhner, Ram Prasad Chaudhary, and Thomas Scholten

Abstract At a global scale, the elevational position of natural upper treelines is determined by low temperatures during growing season. Thus, climate warming is expected to induce treelines to advance to higher elevations. Empirical studies in diverse mountain ranges, however, give evidence of both advancing alpine treelines as well as rather insignificant responses. Himalayan treeline ecotones show considerable differences in altitudinal position as well as in physiognomy and species composition. To assess the sensitivity of a near-natural treeline to climate warming at local scale, we analysed the relations between changes of growth parameters and temperature gradients along the elevational gradient in the treeline ecotone in Rolwaling valley, Nepal, by a multispecies approach. We observed species-specific transition patterns (diameter at breast height, height, tree and recruit densities) and varying degrees of abruptness of these transitions across the treeline ecotone resulting in a complex stand structure. Soil temperatures are associated with physiognomic transitions, treeline position and spatial regeneration patterns. In conclusion, treeline tree species have the potential to migrate upslope in future. Upslope migration, however, is controlled by a dense krummholz belt of *Rhododendron campanulatum*. Currently, the treeline is rather stable; however we found a prolific regeneration as well as signs of stand densification. Given the spatial heterogeneity

N. Schwab (✉) • U. Schickhoff • B. Bürzle • J. Böhner
CEN Center for Earth System Research and Sustainability,
Institute of Geography, University of Hamburg, Hamburg, Germany
e-mail: niels.schwab@uni-hamburg.de

M. Müller • T. Scholten
Department of Geosciences, Chair of Soil Science and Geomorphology, University of Tübingen, Tübingen, Germany

L. Gerlitz
Section Hydrology, GFZ German Research Centre for Geosciences,
Potsdam, Germany

R.P. Chaudhary
RECAST Research Centre for Applied Science and Technology, Tribhuvan University,
Kathmandu, Nepal

R.B. Singh et al. (eds.), *Climate Change, Glacier Response, and Vegetation Dynamics in the Himalaya*, DOI 10.1007/978-3-319-28977-9_16

of Himalayan treeline ecotones, further studies are needed to fully understand the complex conditions for the establishment and development of tree seedlings and the responsiveness of Himalayan treeline ecotones to climate change.

Keywords Density–diameter curve • Regeneration • Soil temperature • Species composition • Treeline dynamics • *Abies spectabilis* • *Betula utilis* • *Rhododendron campanulatum* • *Sorbus microphylla*

16.1 Introduction

At a global scale, the position of natural upper treelines is determined by low air and soil temperatures during growing season (e.g. Troll 1973; Stevens and Fox 1991; Holtmeier 2009; Körner 2012). Climate warming is expected to induce treelines to advance to higher elevations. Empirical studies in diverse mountain ranges, however, give evidence of both advancing alpine treelines as well as rather insignificant responses (Baker and Moseley 2007; Hofgaard et al. 2009; Wieser et al. 2009; Grigor'ev et al. 2013; Shrestha et al. 2014; Chhetri and Cairns 2015), pointing to an evident research deficit. Harsch et al. (2009) analysed data from 166 globally distributed treelines which dynamics were monitored since AD 1900. 47 % of the treelines did not show any elevational shift, while 52 % of the treelines advanced to higher altitudes and only 1 % showed recession. Apart from climate change, land use changes influence high-altitude vegetation patterns and treeline positions (e.g. Dirnböck et al. 2003; Bolli et al. 2007; Gehrig-Fasel et al. 2007; Pauchard et al. 2009; Schickhoff 2011; Penniston and Lundberg 2014; Piermattei et al. 2014; Durak et al. 2015). Thus there is the need to disentangle these effects to draw correct conclusions concerning the sensitivity of treelines to climate change.

Many studies detected above-average current warming trends between 0.6 and 1 °C per decade for the Himalayan region. Maximum values were found for the high elevations and during winter and pre-monsoon seasons (Shrestha et al. 1999; Liu and Chen 2000). For the Rolwaling valley, the target area of the present study, monthly temperature trends in the order of 0.7 °C per decade were assessed in winter and pre-monsoon seasons (Gerlitz et al. 2014). During monsoon, no statistically significant trends were identified. Trend analyses of precipitation amounts in the Himalayas do not show a consistent pattern. Some studies, however, detected negative trends of winter and pre-monsoon precipitation over the western and central Himalaya (Duan et al. 2006; Bhutiyani et al. 2010; Jain et al. 2013). An enhanced frequency of winter and pre-monsoon drought events was reported for western Nepal by Wang et al. (2013). Recent climatic changes will inevitably affect growth patterns and seedling performance at Himalayan treelines, albeit to a regionally differentiated extent (Schickhoff et al. 2015, 2016).

It is widely accepted that climate exerts a top-down control on local ecological processes at the treeline (e.g. Batllori and Gutiérrez 2008; Elliott 2011). However, it is not well understood how landscape-scale and local-scale abiotic and biotic fac-

tors and processes interact and influence the treeline and its response to climate change. Moreover, effects of climate warming often mix up with impacts of land use (Malanson et al. 2007; Batllori et al. 2009). In consequence, complex research approaches at local and landscape scales at natural treelines are needed (e.g. Malanson et al. 2011). Recent studies based on a global treeline data set suggest a close link between treeline form (spatial pattern) and dynamics. Harsch and Bader (2011) consider treeline form (diffuse, abrupt, island, krummholz) to be an indicator of controlling mechanisms (at the levels of direct tree performance, causative stresses and modifying neighbour interactions) and response to climate change. They confirmed the link between treeline form and dynamics established earlier (Lloyd 2005; Harsch et al. 2009) and supported the general suitability of treeline form for explaining the variability of response to climate warming. Apart from treeline form, tree species composition, tree density, diameter and height distributions can be indicators for treeline sensitivity to climate change. In addition, these parameters provide information on the establishment of recruits and their performance which are among the most significant indicators of treeline sensitivity (Germino et al. 2002; Holtmeier 2009; Körner 2012; Zurbriggen et al. 2013; Schickhoff et al. 2015, 2016).

In the Himalaya, only very few studies on treeline seedlings have been conducted so far, and tree recruitment in treeline ecotones is not well understood (Schickhoff 2005; Shi and Wu 2013; Dutta et al. 2014; Schickhoff et al. 2015, 2016). Hitherto available studies refer to treeline ecotones with deviating species compositions and population structures and generally to ecotones which have been disturbed by land use effects (e.g. Shrestha et al. 2007, 2014; Ghimire et al. 2010; Gaire et al. 2011; Sujakhu et al. 2013; Chhetri and Cairns 2015). Thus, their generalisability and informative value for near-natural treeline ecotones are limited. The present study was conducted in the framework of the research scheme TREELINE which focuses on spatially differentiated patterns and processes by correlating varied treeline responses to landscape- and local-scale site conditions and mechanisms (geomorphic controls, soil physical and chemical conditions, plant interactions associated with facilitation, competition and feedback systems). We present population structures from a near-natural treeline ecotone in Rolwaling Himal, Nepal, focussing on species compositions and growth parameters with an emphasis on the ratio of recruits to adult trees. Unlike most other treeline studies in Nepal (e.g. Shrestha et al. 2007; Lv and Zhang 2012; Sujakhu et al. 2013; Gaire et al. 2014), we assessed the treeline-forming tree species of our study area in its entirety. Near-natural treeline ecotones can contain codominant tree species which respond differently to climate change (Trant and Hermanutz 2014). In consequence, multispecies approaches to treeline dynamics, which survey all ecotone tree species, can capture the sensitivity of the ecotone to climate change sufficiently. We aim at (1) analysing species-specific patterns and abruptness of transitions of tree and recruit densities and growth parameters along the elevational gradient, (2) detecting altitudinal boundaries of tree species distributions and (3) assessing the relation between abrupt changes of growth parameters and temperature gradients along the altitudinal zoning of the ecotone and relating the results to the sensitivity to climate warming. We hypothesise that changes in tree

physiognomy (diameter at breast height (dbh), tree height, growth forms) and density occur species specific with varying abruptness intensities along the treeline ecotone, indicating complex spatial structures and resulting in several tree species limits inside the ecotone, each potentially susceptible to climate change. Air and soil temperatures are supposed to be crucial variables explaining species-specific responses.

16.2 Materials and Methods

16.2.1 The Study Area

The Rolwaling valley (27°52′ N; 86°25′ E) is located in Dolakha District, east-central Nepal, adjacent to the border of Tibet Autonomous Region. It is embedded in the Gaurishankar Conservation Area (2035 km^2), which has been a protected area since 2010 (Shrestha et al. 2010; Bhusal 2012). Our study site is located at a north-facing slope ranging from the closed subalpine forest via timberline and treeline to

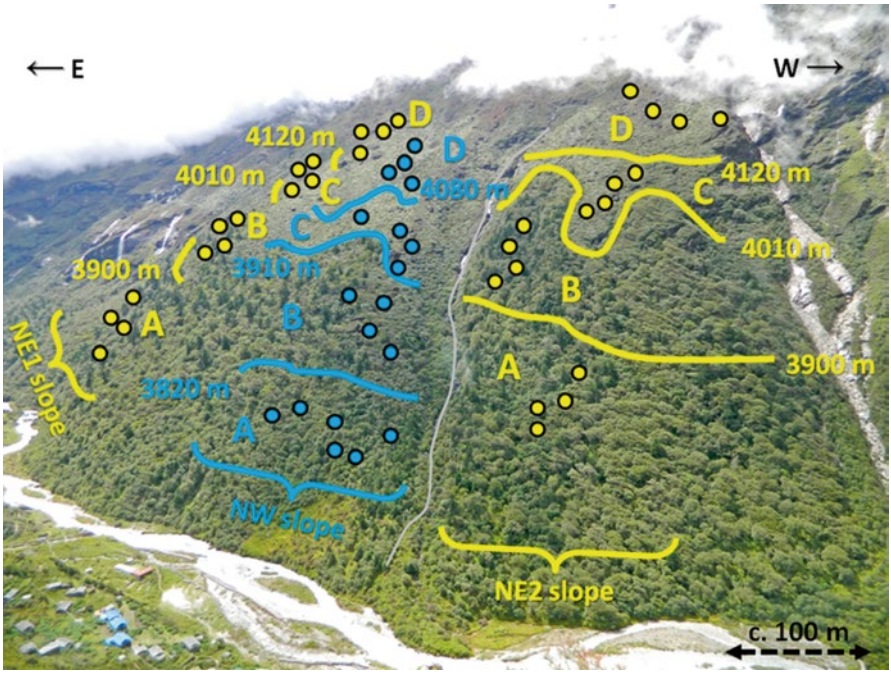

Fig. 16.1 Stratification of the study area by altitude (zones *A*, *B*, *C*, *D*) and aspect (NE, NW) and approximate location of plots (*blue* and *yellow points*) (Schwab, 18 September 2014) (Source: Niels Schwab)

the lower alpine vegetation zone (3740 m to 4250 m a.s.l.). We subdivided the study site into three slope sectors according to their deviating exposure (Fig. 16.1).

Due to the remote location without connection to the road network (3-day walking distance), the small human population and the fact that plants and animals in Rolwaling are protected to a certain extent by the recurring Buddhist theme of a sacred hidden valley (Sacherer 1979; Baumgartner 2015), the Rolwaling treeline exhibits a near-natural state (cf. Sect. 16.3.6) and represents a climatic treeline. The study slopes show no signs of fire or of grazing by cattle; wood cutting is negligible. The Rolwaling River separates the uninhabited north-facing study slope from the very sparsely populated south-facing slope where human impact is likewise low. Thus, in view of the fact that most Himalayan treeline sites are disturbed by land use effects (Schickhoff et al. 2015, 2016), the study slopes provide a unique research opportunity for detecting a climate change signal when assessing treeline dynamics.

The study sites cover the entire treeline ecotone. The lower reaches contain mixed forest stands with the upper limits of tall, upright-growing individuals of *Acer caudatum*, *Abies spectabilis* and *Betula utilis*. A krummholz belt with dense and largely impenetrable *Rhododendron campanulatum* thickets represents the transition to alpine dwarf scrub heaths with only small (dbh <7 cm) and stunted tree species individuals (Fig. 16.2).

16.2.2 Data Collection

We stratified the treeline ecotone according to the altitudinal zoning of tree species composition and stand structure into four altitudinal zones, reaching from closed forests (zone A) to alpine dwarf scrub heaths (zone D; Table 16.1). We established a total of 50 plots, each with a size of 20×20 m^2 (projected on a horizontal plain), comprising four randomly selected plots in each of the zones A–D at three slopes (two slopes NE-exposed, one slope NW-exposed; Table 16.1). Nomenclature of identified tree species follows Press et al. (2000). We measured dbh with a diameter measuring tape at 1.3 m above ground level (Van Laar and Akça 2007) and height of all trees with dbh ≥7 cm with a laser dendrometer (Laser Technology Criterion RD 1000, distance measurement: MDL LaserAce 300). Individuals of tree species with dbh <7 cm (recruits) were identified, counted and assigned to height classes (Table 16.2). We counted all stumps ≥7 cm diameter and measured diameters 10 cm above ground or, if stump height was less than 10 cm, at highest point above ground. We identified the species and cause of death (natural, anthropogenic, unidentified) in each plot. We classified the degree of decomposition of tree stumps into four classes (undecomposed, slight, medium, intense decomposition) to roughly estimate the dieback period (Schickhoff 2002). We assumed the intensely decomposed stumps to not influence the current stand structure. Vegetation surveys took place in April, May, July and August 2013 and September 2014.

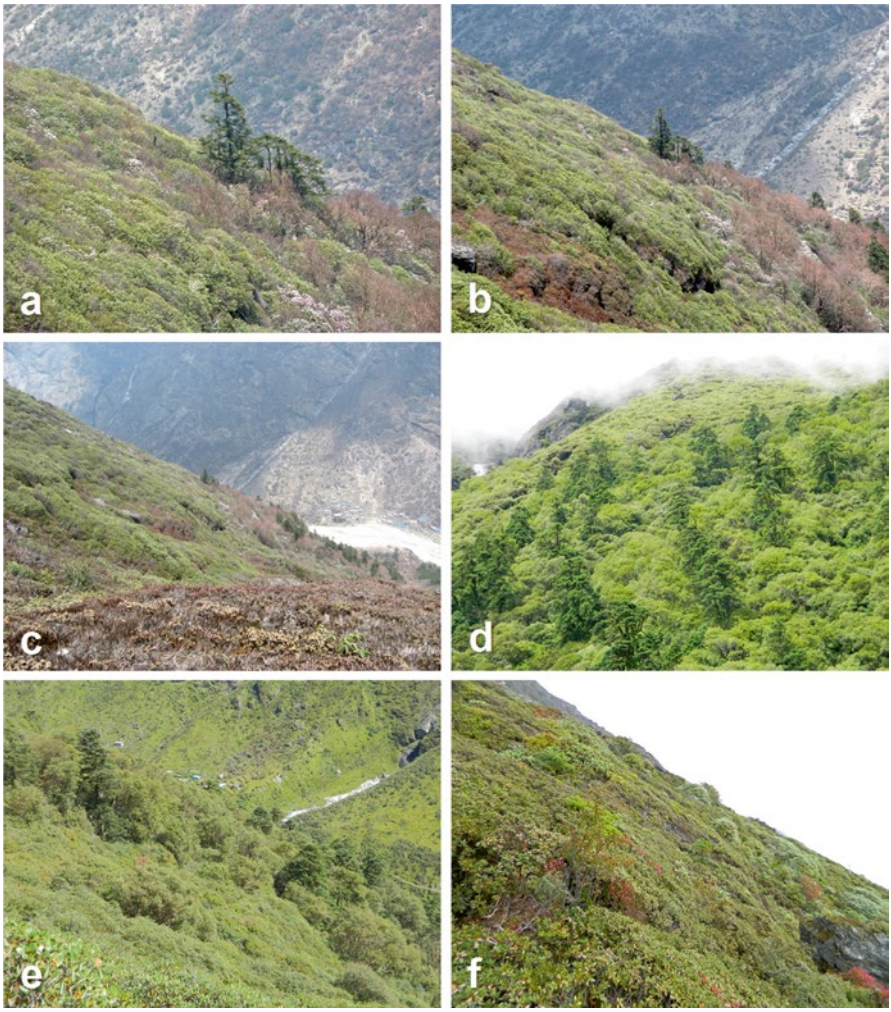

Fig. 16.2 Transition from closed forest to alpine dwarf scrub heath. (**a**) Uppermost stand of *A. spectabilis* at NE-slope (c. 4000 m a.sl.); (**b**) *Rh. campanulatum* krummholz (in *white-pink* bloom) and transition to *Abies-Betula* forest (zone B); (**c**) Elevational range from zone A to D with transition from B to C in focus; (**d**) Mixed forest stand of zone B and abrupt transition to *Rh. campanulatum* krummholz belt; (**e**) *Rh. campanulatum* krummholz (front) and abrupt transition to mixed *Abies-Betula* forest of zone B; (**f**) Alpine dwarf scrub heath with *Rh. campanulatum* and *Rhododendron* dwarf shrub species and single *S. microphylla* individuals (**a**–**c**: 5 May 2013; **d**: 23 July 2013; **e**–**f**: 17 September 2014; Schwab) (Source: Niels Schwab)

To relate soil temperature to growth parameters, we installed 34 modified Wi-Fi Plant sensors (Koubachi AG), which have monitored soil temperature in 10 cm depth in a 1 h interval since May 2013. For this paper we use data from June 2013 to May 2014. Thirty-two sensors were placed on the NW-exposed and on one of the NE-exposed slopes (2 transects × 4 altitudinal zones × 4 plots). Mobile climate sta-

Table 16.1 Study site properties

	Aspect	Zones			
		A	B	C	D
Slope 1	NE				
Altitude [m a.s.l.]		3830–3895	3920–3990	4015–4080	4180–4245
No. of plots		4	4	4	4
Slope 2	NE				
Altitude [m a.s.l.]		3795–3875	3925–3990	4040–4090	4130–4225
No. of plots		4	4	4	4
Slope 3	NW				
Altitude [m a.s.l.]		3770–3795	3845–3890	3925–4020	4140–4200
No. of plots		6	4	4	4
Total no. of plots		14	12	12	12
NE transition altitudes [m a.s.l.]		3900 (AB)	4010 (BC, TL)	4120 (CD)	
NW transition altitudes [m a.s.l.]		3820 (AB)	3910 (BC, TL)	4080 (CD)	
Vegetation		Mixed forest	Mixed forest	Krummholz	Alpine scrubs

Aspects: *NE* north-east, *NW* north-west, *TL* treeline

Table 16.2 Size classifications of tree species individuals and abruptness parameters

dbh [cm]	Height [cm]	Recruit class	Terms		Indication of abruptness for
<7	0–10	1	Seedlings	Recruits	Height, density
<7	11–50	2			
<7	51–130	3	Saplings		
<7	131–200	4			
<7	201–∞	5			
≥7	ns	–		Trees	dbh, height, density

dbh diameter at breast height, *ns* not specified

tions installed in the lower and upper part of the ecotone have recorded air temperatures since April 2013 (data evaluated until June 2014). Soil bulk density of field-moist soils was sampled using soil core cutters (100 cm^3) and analysed following DIN EN ISO 11272:2014. Additionally, atmospheric nitrogen deposition (NO_2, NH_3) was measured using passive devices (Passam AG) requiring no power for their operation. The samplers were placed in a special shelter 2 m above ground to protect them from rain and minimise wind influence. Exposition time was 2 weeks.

16.2.3 Data Analyses

We computed stem numbers and stand densities per hectare (ha) and visualised population structures and species compositions by plotting barplots and histograms of all samples and subsamples. Comparisons of our density–diameter distributions

Table 16.3 Definitions and interpretation of abruptness values

Abruptness	Definition/interpretation
−1,…,1	Maximum range
Positive	Decreasing parameter with elevation
Negative	Increasing parameter with elevation
−1	Transition from maximum to zero
−1	Transition from zero to maximum
0	No change
1/3 resp. −1/3	Linear transition in case of 4 zones
−0.33 ≤ abruptness ≤0.33	Gradual/smooth transition
−0.5 ≥ abruptness ≥0.5	Abrupt transition, change by half or more of the parameters range
0.33,…,0.5 resp. −0.33,…,−0.5	Intermediate transition

to other studies should be understood as only rough estimates due to the differing study-specific definitions of size classes and classification intervals. In order to analyse regeneration patterns, we calculated values for the mean height of recruits as mean of the class configurations. We calculated a regeneration index (*RI*) according to Schickhoff (2002):

$$RI = \sum_{i=1}^{5} \bar{x}_{\mathrm{med}(i)} n_i$$

where n_i is the number of recruits in the 5 recruit height classes (Table 16.2) and $\bar{x}_{\mathrm{med}(i)}$ is the median of the height class limits. In contrast to mean height values of recruits, the *RI* includes information of abundance and combines it with the recruits' height. Thus the *RI* provides information on growth performance and success of establishment beyond the seedling stage.

In order to describe and analyse variation in stand structures and to characterise abrupt or smooth/gradual transition patterns along the ecotone, we calculated the abruptness of transitions between subsequent zones ($\mathrm{abruptness}_{\mathrm{AB}}$, $\mathrm{abruptness}_{\mathrm{BC}}$, $\mathrm{abruptness}_{\mathrm{CD}}$). We computed the abruptness for various parameters (Table 16.2) using a modified approach by Wiegand et al. (2006) and Batllori and Gutiérrez (2008). The abruptness of the transitions was the difference of the scaled values of successive zones (lower zone minus upper zone; scaled range [0,1]):

$$\mathrm{abruptness}_{lh} = \frac{\bar{x}_{\mathrm{arith}(l)} - \min_l}{\max_l - \min_l} - \frac{\bar{x}_{\mathrm{arith}(h)} - \min_h}{\max_h - \min_h}$$

where l and h are the altitudinal zones (*A*, *B*, *C*, *D*). The lower zone (e.g. A) is denoted l and the successive higher zone (e.g. B) is denoted [h]. A positive abruptness indicates a transition of decreasing values with elevation as it is generally expected in a treeline ecotone while a negative abruptness points to an increasing value of a stand parameter with elevation (see Table 16.3 for further differentiation

of abruptness values). Total abruptness was gained as the arithmetic mean abruptness of all parameters under consideration at a specific transition. We calculated both the abruptness for all individuals of the stands and the species-wise abruptness.

Seasonal means for discrete time steps (0, 6, 12, 18 h local time) were calculated for air temperature for each climate station. Topographically induced 6 hourly temperature lapse rates ($\Delta T/\Delta Z*100$) were derived for the NW and NE transects to assign site-specific air temperatures (Gerlitz et al. 2016). We calculated growing season mean soil temperature at treeline and number of growing degree days according to Körner and Paulsen (2004). For soil temperatures we calculated abruptness values according to the above described procedure for mean annual and mean seasons' temperatures (MAM, JJAS, ON, DJF). All computations and figure plottings were carried out using 'base' and 'graphic' R functions (version 3.1.2; R Core Team 2014) and the packages 'plyr' (Wickham 2011) and 'vegan' (Oksanen et al. 2014).

16.3 Results

16.3.1 General Vegetation Patterns and Species Limits

In general, upper subalpine forests are primarily composed of *Betula utilis* and *Abies spectabilis*, with *Rhododendron campanulatum* and *Sorbus microphylla* forming a second tree layer. Closed forests give way to an extensive krummholz belt of *Rh. campanulatum* at c. 3910 m a.s.l. (NW)/4010 m a.s.l. (NE), which turns into alpine *Rhododendron* sp. dwarf scrub heaths at c. 4080/4120 m a.s.l (Fig. 16.2). Total plant species richness decreases from the closed forests in the subalpine zone across the treeline ecotone and increases again in the uppermost dwarf scrub heath plots of zone D at the transition to alpine grassland. Minimum species numbers are found in the krummholz belt zone C with a mean species number of 12 and in the lower dwarf scrub heath plots with 11 species. Zone A contains the maximum of 25 plant species (unpublished data by B. Bürzle).

We identified different tree species-specific altitudinal limits (i.e. 'the uppermost occurrence regardless of size', Körner 2012) throughout an altitudinal gradient from zone A to zone D (Fig. 16.3): We found the uppermost individuals of *Prunus rufa* at 3925 m a.s.l. (NE) resp. 3890 m a.s.l. (NW) in zone B, of *Acer caudatum* at 3950 m a.s.l. (NE) resp. 3890 m a.s.l. (NW) in zone B and of *Juniperus recurva* at 4080 m a.s.l. (NE, no *J. recurva* at NW) in zone C. All other species still occurred in zone D. We found *B. utilis* recruits at 4140 m a.s.l. in the lowest plot in zone D at the NW slope but in none of the higher plots. Thus the species limit of *B. utilis* appears to be at the lower part of zone D. In contrast, we found *A. spectabilis* individuals even at 4185 m a.s.l. Similarly, *S. microphylla* and *Rh. campanulatum* occur at nearly all plots in zone D (both maximum altitude 4245 m a.s.l.). Vegetation analyses above zone D point to a position of their tree species lines at the upper border of zone D (c. 4260 m, unpublished data by B. Bürzle, Fig. 16.3).

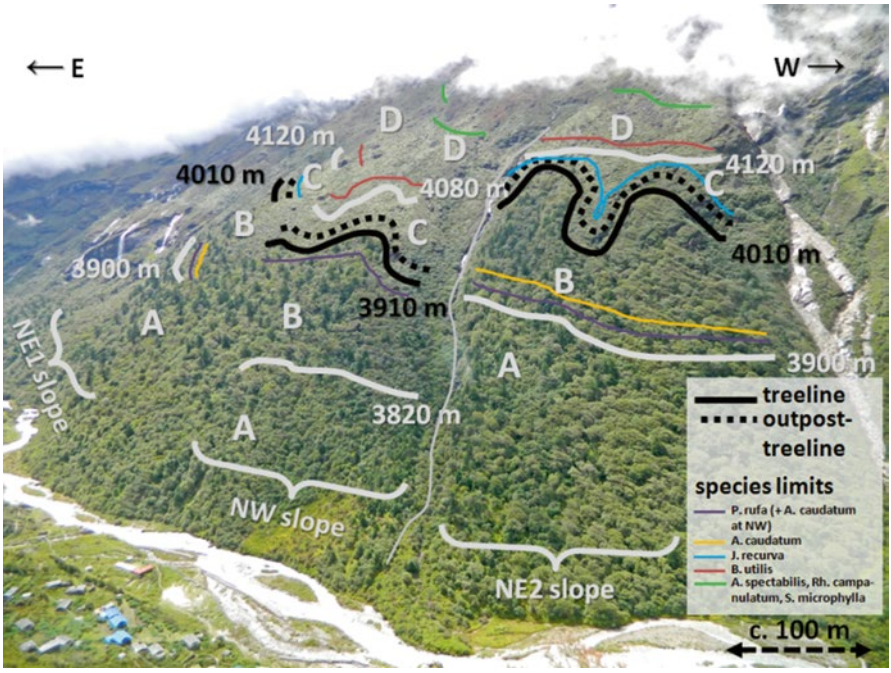

Fig. 16.3 Approximate locations of treeline, outpost-treeline and species limits (Schwab, 18 September 2014) (Source: Niels Schwab)

16.3.2 Tree Species Composition

The lowest zones A and B contain mixed forest stands where tall, upright-growing, adult individuals of most tree species reach their upper limits (*Acer caudatum* in A; *Abies spectabilis*, *Betula utilis* and *Prunus rufa* in B). Zone C represent the krummholz belt with dense and largely impenetrable *Rhododendron campanulatum* thickets and upper limits of stunted *A. spectabilis* and *B. utilis* tree individuals with dbh ≥7 cm. Zone D is occupied by alpine vegetation (mainly dwarf scrub heaths), interspersed with only low-growing individuals or young growth (dbh <7 cm) of *A. spectabilis*, *B. utilis* and *Rh. campanulatum* (Fig. 16.2). We found very few *Sorbus microphylla* individuals with dbh ≥7 cm in zone D (Figs. 16.4 and 16.5). The recruit density pattern (Fig. 16.6) mostly resembled the one of individuals with dbh ≥7 cm. The occurrence of *Juniperus recurva*, a species that can grow to tree size, remarkably differed between recruits and adults. We found no individual with dbh ≥ 7 cm; *J. recurva* recruits were existent in zones A, B and C. *Rh. campanulatum* and *S. microphylla* seedlings occurred in rather high abundance in zone D; however no tree-sized individual of these species was detected. We found the highest number of individuals of both trees and recruits in zone B. Zone C exhibited nearly the same

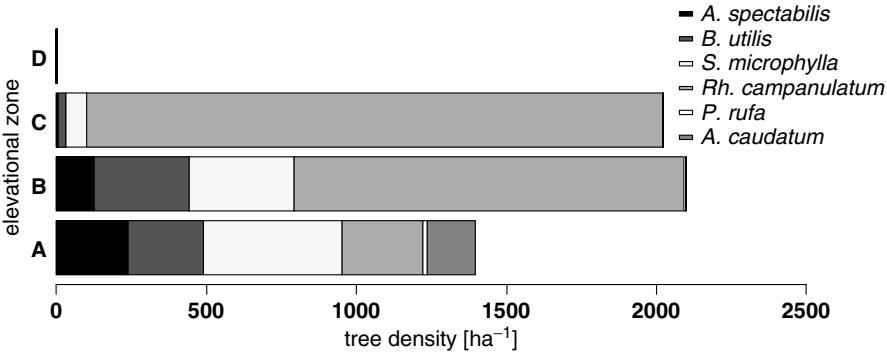

Fig. 16.4 Tree species density of individuals ≥7 cm dbh (trees) (Source: Niels Schwab)

number of trees per ha as zone B. Zones A and C resembled each other in terms of recruit numbers, whereas recruit density indicated distinct differences between both zones and zone B. However, altitudinal zones differed in the percentages of the individual species. *P. rufa* and *J. recurva* individuals occurred in very low abundance and are thus not analysed in detail.

All tree species occurring in zone A except the rare *P. rufa* exhibited evenly distributed numbers of individuals. *Rh. campanulatum* becomes more frequent with elevation. In zone C, *Rh. campanulatum* dominates the tree species composition and is accompanied by few *Sorbus* individuals. Although *Rh. campanulatum* accounts for more than 50 % of tree individuals and more than 75 % of recruits in zone B, the transition from zone B to C shows the most abrupt change in tree species composition along the altitudinal gradient. This abrupt change in species composition coincides with the most abrupt changes in annual and seasonal mean soil temperature at transition BC (cf. Sect. 16.3.7). *S. microphylla* occurred with high constancy and its density–diameter distribution points to an established population in zone C, which coexists aside the *Rh. campanulatum* population. Established recruit populations in zone D indicate the potential of *Rh. campanulatum* and *S. microphylla* to sprout and survive at least the early life stages at this high altitude (see discussion Sect. 16.4.3).

16.3.3 Stand Densities

Stand densities showed similar patterns in zones A, B and C: We found 7473 (zone A, standard deviation SD = 4432), 8748 (zone B, SD = 6718) and 7280 (zone C, SD = 3948) individuals per ha belonging to the recruit class (dbh <7 cm) (Figs. 16.6

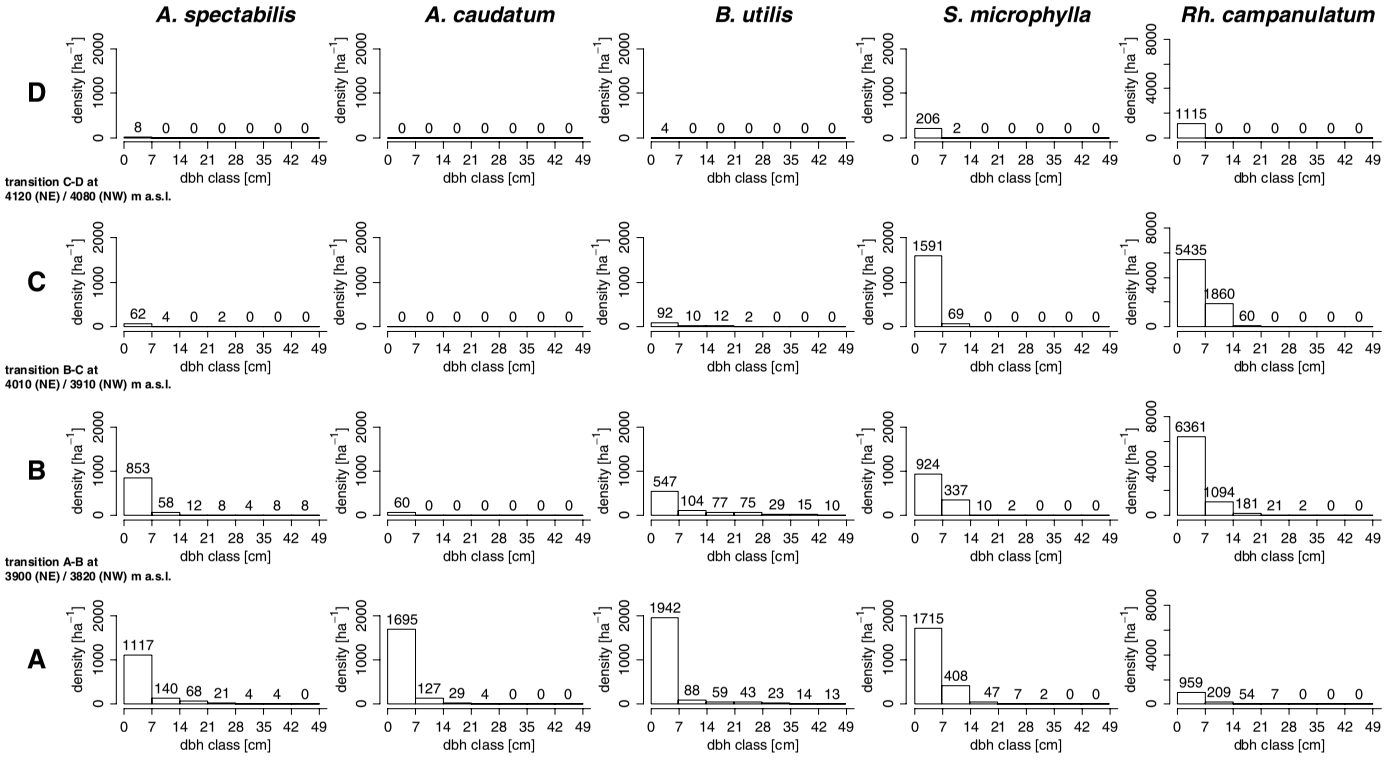

Fig. 16.5 Species-wise density–diameter distribution of the most abundant tree species in the altitudinal zones *A*, *B*, *C* and *D*. Only classes <49 cm dbh are printed. Note difference in scaling of *Rhododendron campanulatum* y-axis (Source: Niels Schwab)

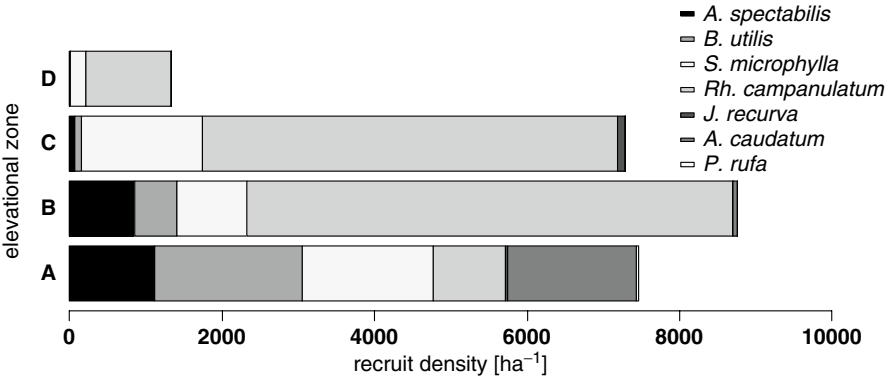

Fig. 16.6 Tree species density of individuals <7 cm dbh (recruits) (Source: Niels Schwab)

and 16.7). The number was significantly smaller in zone D. Here, 1333 individuals per ha (SD = 1197) represent more than one tree species recruit individual per 10 m^2 in the alpine dwarf scrub heath. However, zone D exhibited only two tree individuals per ha in the 7–14 cm dbh class and not a single individual of higher dbh classes. The number of trees in the dbh class 7–14 cm increased continuously with elevation from 984 trees per ha (SD = 386) in zone A to 1597 (SD = 869) in zone B and to 1943 (SD = 1246) in zone C. The following class (14–21 cm dbh) showed most individuals in zone A and B (258 resp. 283 trees per ha, SD = 157 resp. SD = 177) and only 73 trees per ha (SD = 104) in zone C. In the latter we sampled four trees per ha (SD = 9) in the 21–28 cm class; trees did not exceed 28 cm dbh. The number of individuals per class decreased with increasing dbh in zones A and B. All dbh classes in zone B revealed higher numbers of trees and recruits compared to zone A. Old trees exceeding 49 cm dbh doubled in number in zone B (31) compared to zone A (14, not shown in Fig. 16.7). The largest dbh were 114 cm in zone A and 113 cm in zone B.

16.3.4 Tree Species Population Structures and Regeneration

16.3.4.1 Density–Diameter Distributions

The different tree species *Abies spectabilis*, *Acer caudatum*, *Betula utilis*, *Sorbus microphylla* and *Rhododendron campanulatum* showed species-specific deviations from a basically similar density–diameter distribution (Fig. 16.5). A common characteristic is the reverse J-shape of the density–diameter distributions with significantly higher numbers of recruits in comparison to numbers of all other dbh classes. We found recruits only but no trees in nearly all uppermost reaches of each species' occurrences.

A. spectabilis: *A. spectabilis* exhibited high numbers of recruits <7 cm dbh in relation to the larger dbh classes in zones A and B. In general, this holds also for

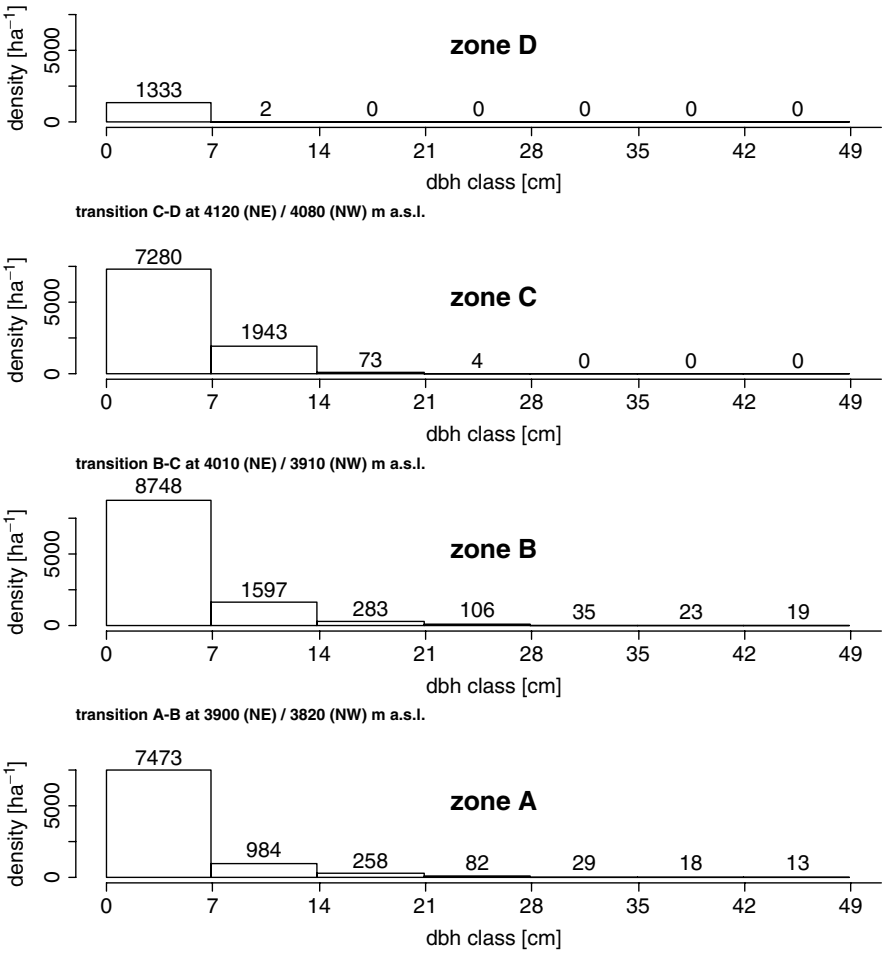

Fig. 16.7 Density–diameter distribution of all tree species in the altitudinal zones *A*, *B*, *C* and *D*. Only classes <49 cm dbh are printed (Source: Niels Schwab)

zone C; however recruit (62 per ha, SD = 120) and tree (6 per ha, SD = 12) abundances were very low and we did not find trees exceeding 22.8 cm dbh. In zone D only eight *A. spectabilis* recruits per ha (SD = 22) occurred and no individuals with dbh >7 cm. The number of trees exceeding 49 cm dbh differed in zones A and B: We found only four trees per ha in A and 27 per ha in B.

A. caudatum: *A. caudatum* occurred in zones A and B only and showed a high abundance of recruits (1695 per ha, SD = 1641) and tree individuals up to the dbh class 21–28 cm. No *A. caudatum* trees >7 cm dbh were detected in zone B, but 60 recruit individuals per ha (SD = 85).

B. utilis: Similar to *A. spectabilis*, the population structure of *B. utilis* differed with altitude. We found a high number of recruits in zone A (1942 per ha, SD = 1627)

and decreasing abundances in larger dbh classes. In contrast to *A. spectabilis*, *B. utilis* exhibits a higher number of trees in all classes from 7 to 42 cm dbh in zone B. Further, the number of *B. utilis* exceeding 42 cm dbh is higher in zone A (24 per ha) compared to B (14 per ha). The absolute number of *B. utilis* recruits in zone B (547 per ha, SD = 611) is smaller compared to *A. spectabilis* recruits, and the ratio of recruits to trees is smaller due to the higher number of individuals in the tree classes > 7 cm dbh. In zone C, *B. utilis* showed 92 recruits per ha (SD = 219) and tree individuals in higher number and larger dbh's than *A. spectabilis*. We found merely four *B. utilis* recruits per ha (SD = 14) in zone D.

S. microphylla: *S. microphylla* recruits are of high abundance in zones A (1715 per ha, SD = 1248), B (924 per ha, SD = 798) and C (1591 per ha, SD = 2064). In zone A, *S. microphylla* tree individuals occurred only up to the dbh class 28–35 cm. *S. microphylla* is the only species with a substantial number of individuals in zone C, apart from *Rh. campanulatum* (see below). Even 206 recruits per ha (SD = 297) were present in zone D.

Rh. campanulatum: The population structure of *Rh. campanulatum* differed significantly from other species. In zone A, the number of recruits (959 per ha, SD = 1180) and trees per ha were in the same range as other species. *Rh. campanulatum* recruits exhibited significantly higher abundances of recruits in zones B (6361 per ha, SD = 5893), C (5435 per ha, SD = 2395) and D (1115 per ha, SD = 963). This prolific regeneration was followed by correspondingly high abundances in the subsequent dbh classes. However, *Rh. campanulatum* populations were poor concerning maximum dbh, which was 22.5 cm in zone A, 29.8 cm in zone B and 18.7 cm in zone C. In zone D, we found only recruits <7 cm dbh. Zone C exhibited a much more homogeneous all-species configuration of the 7–14 cm dbh class due to the high percentage of *Rh. campanulatum* individuals and less recruits per ha compared to zone B. Altitudinal transitions in *Rh. campanulatum* populations did not follow the trend of other species in terms of decreasing dbh and abundance with elevation (cf. Fig. 16.5). The smaller SD values of *Rh. campanulatum* recruit densities in zones B, C and D indicate that *Rh. campanulatum* population is spatially more homogenous intra-zone than recruit populations of other species. In contrast to zone A, *Rh. campanulatum* accounts for the significantly higher all-species tree densities in zones B and C (Fig. 16.4).

Total all-species recruit densities of zones A, B and C did not differ as much as the tree densities. All species show L-shaped or reverse J-shaped density–diameter distributions (Fig. 16.5). At some altitudinal zones, several species exhibit a very pronounced L-shape indicating an overproportional number of recruits compared to the classes above 7 cm dbh, e.g. *A. caudatum* and *B. utilis* in zone A and *S. microphylla* in C. Zone A contains more recruits of *A. spectabilis*, *B. utilis* and *S. microphylla* compared to zone B, where their recruit numbers are distinctly lower compared to tree densities (Figs. 16.4, 16.5 and 16.6).

In summary, we assessed largely prolific regeneration of all tree species. Seedling establishment of *B. utilis*, *A. spectabilis* and *S. microphylla* occurred to some extent

far above the upper limit of adult trees. Some individuals of more than 2 m height even grew vigorously above the krummholz belt, where a small birch tree of 1.7 m in height was found in 4140 m a.s.l. Maximum recruit density occurred between 3920 and 3990 m a.s.l. (NE) resp. 3845–3890 m a.s.l. (NW) in zone B (more than 8700 N ha^{-1}), where *Rh. campanulatum* showed most intense recruitment (more than 6300 N ha^{-1}). Seedling/sapling density sharply decreased towards the alpine tundra (zone D), where only *Rh. campanulatum* and to some extent *S. microphylla* recruits occurred with considerable numbers of individuals.

16.3.4.2 Recruit Heights

The height class distributions of recruits showed clear variations between species and between altitudinal zones (Fig. 16.8). *Abies spectabilis* exhibited reverse J-shaped distributions in zones A and B, whereas the small numbers of recruits in zones C and D were rather homogenously distributed among classes. For *Acer caudatum*, we found a high percentage of tall recruits exceeding 2 m height and a slight increase in individual numbers from the 10 to 200 cm height classes in zone A. An evenly distributed small number of *A. caudatum* recruits occurred in zone B but was absent in zones C and D. *Betula utilis* recruits showed a heterogeneous distribution between height classes with a relative small number of seedlings smaller than 10 cm in height in zone A. In zone B, the taller height classes exceeding 50 cm had higher recruit densities. The same holds for zone C, however with distinctly smaller recruit numbers. In zone D, we found four *B. utilis* recruits per ha exclusively in the height class of 131–200 cm. *Sorbus microphylla* showed increasing class sizes with increasing recruit heights in zones A, B and C, except for the 10 cm class in zone B which contained c. three times more recruits than the subsequent 50 cm class. The distribution of *S. microphylla* recruits in zone D corresponds to a bell shape with no individuals smaller than 10 cm. *Rhododendron campanulatum* exhibited a reverse J-shape in zone A and a reverse L-shape with the overall highest number of recruits in any class in zone B with c. 4400 per ha in the ≤10 cm class. The height class distribution in zone C was rather homogenous, while it resembled the bell shape in zone D.

The average recruit height of all tree species was tallest in zone C followed closely by mean height in zone A (Fig. 16.9, black dotted line). Likewise, the recruits of most single species reached their maximum height in zone C. In general, recruits of *Prunus rufa*, *B. utilis*, *S. microphylla* and *A. caudatum* showed a mean height of more than 130 cm, which is taller than the recruit mean height of *Juniperus recurva*, *Rh. campanulatum* and *A. spectabilis* in all altitudinal zones. Recruits of all species in zone D showed a lower height growth compared to zone C, except for *B. utilis*, whose recruit height increased slightly. *B. utilis* was the only species with a continuous, however gentle, increase in mean recruit height with elevation. The average height of *B. utilis* and *S. microphylla* recruits were distinctly taller than *A. spectabilis* and *Rh. campanulatum* recruits in zone D (cf. Fig. 16.9). *S. microphylla* recruits' height did not change distinctly along the altitudinal gradient. The height of *Rh. campanulatum* recruits exhibited highest values in zone C and smallest in

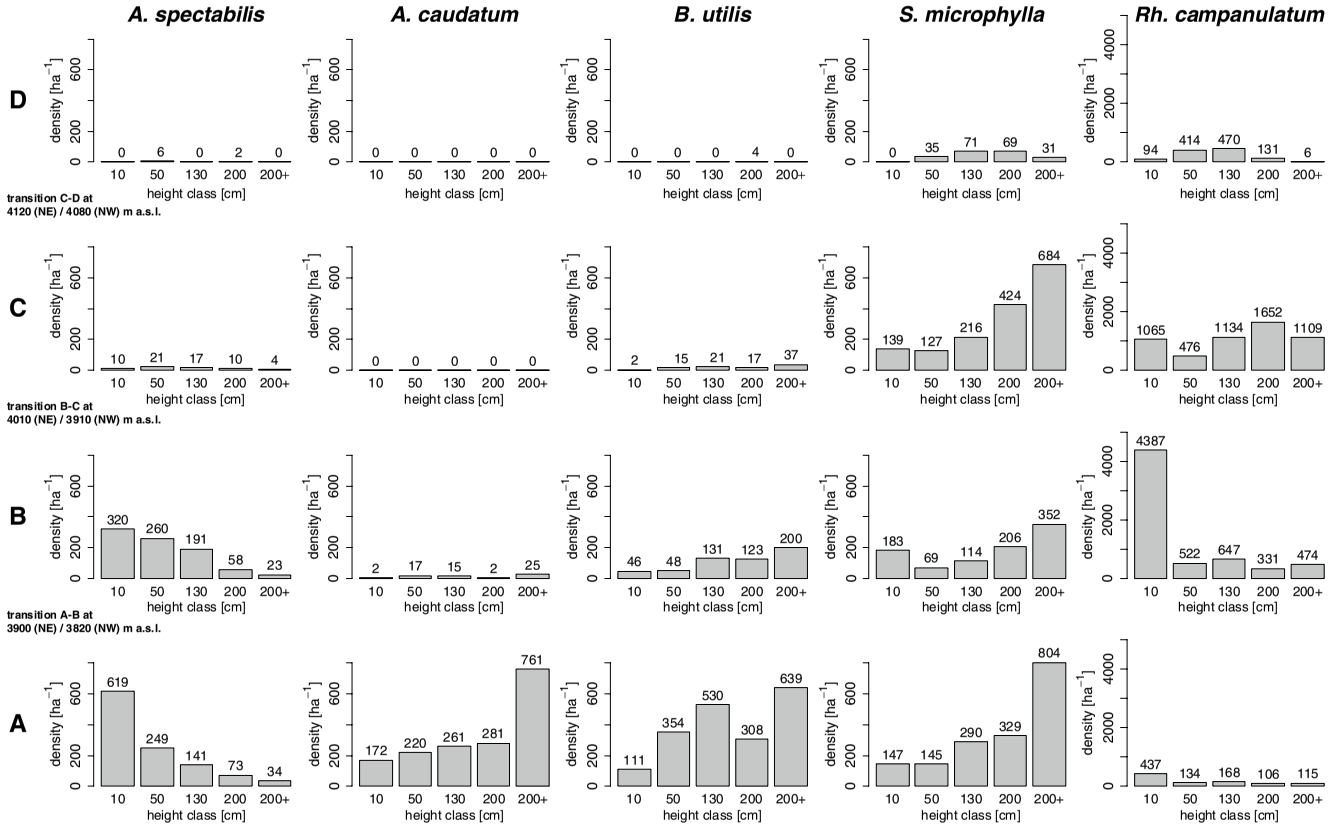

Fig. 16.8 Species-wise recruit (<7 cm dbh) height class distribution of the most abundant tree species in the altitudinal zones *A*, *B*, *C* and *D*. Height class intervals: 10: ≤10 cm, 50: ≤50 cm, 130: ≤130 cm, 200: ≤200 cm, 200+: >200 cm. Note difference in scaling of *Rhododendron campanulatum* y-axis (Source: Niels Schwab)

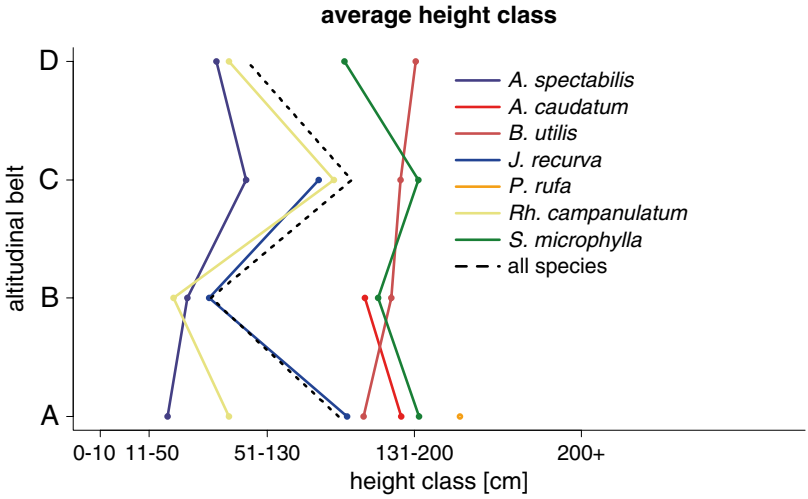

Fig. 16.9 Recruit height class distribution along the altitudinal gradient for all species and species wise (Source: Niels Schwab)

zone B (in average < 50 cm). *A. spectabilis* recruits showed compared to other species smallest heights in all zones except in zone B where *Rh. campanulatum* recruits did not reach the height level of *A. spectabilis*. Nevertheless, the mean height of *A. spectabilis* recruits increased constantly with elevation up to zone C (cf. Fig. 16.9).

16.3.4.3 Regeneration Index (*RI*)

The regeneration index (*RI*) of the recruits of all species showed the highest value in zone A, followed by C, B and D (Fig. 16.10, black dotted line). The single species showed different *RI* patterns: *Rhododendron campanulatum* exhibited the most conspicuous values along the altitudinal gradient with a rather low *RI* in zone A and an *RI* higher than any of the other species in zones B, C and D (Fig. 16.10). Like *Rh. campanulatum Sorbus microphylla* shows a non-uniform *RI* trend along the gradient with the second highest *RI* level of all species in zones B, C and D (Fig. 16.10). The *RI* reached nearly 130,000 in zone C, while the maximum of all other species except *Rhododendron* was only 7000 (*Betula utilis*). In contrast to *S. microphylla*, the *RI* value of *Acer caudatum* was very low in zone B. The *RI*s of *B. utilis* and *Abies spectabilis* constantly decreased towards zone D (Fig. 16.10). For instance, *A. spectabilis* showed a value of 25,000 in zone A, 20,000 in B and only 2400 and 260 in zones C and D. *Juniperus recurva* and *Prunus rufa* showed the overall smallest *RI* values in zones A and B (Fig. 16.10).

Depending on the regeneration indicator in focus, different species seem to perform better at different altitudinal positions. While the mean height (Fig. 16.9) shows whether the population of a species is able to reach a specific mean sprout height, the *RI* (Fig. 16.10) provides information on the actual performance of the recruits of a species by incorporating their abundance. Comparing values of both

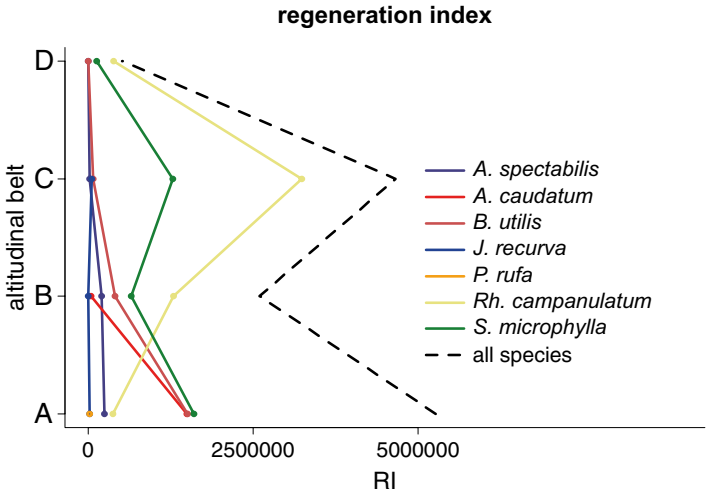

Fig. 16.10 Regeneration index *RI* species wise and sum of all species (Source: Niels Schwab)

indicators, it becomes obvious that the height–abundance patterns of the different species are complex and non-uniform. The small *RI* values of *B. utilis* in zones C and D contrast with their high mean heights. Obviously *B. utilis* recruits are able to grow at these altitudes but they do not grow in considerable abundance. On the other hand, *A. spectabilis* recruits with similarly low *RI* values in C and D grow up to a considerably lower height only, the lowest of all species in zones C and D. These relations indicate a comparatively better performance of *B. utilis* at these high-elevation environments. Both height and *RI* of *S. microphylla* exhibited high and even highest values and we even found rare tree individuals ≥7 cm dbh in zone D. The dbh classes above 14 cm dbh include only small numbers of *S. microphylla* in the lower zones (Fig. 16.5). *Rh. campanulatum* exhibited an enormously high *RI* and highest *Rhododendron*-specific mean height together with the absolute dominance in zone C (Figs. 16.4 and 16.6). In zone D, *Rh. campanulatum*'s heights are lower, and we did not find any individuals ≥7 cm dbh among the number of 1115 recruits per ha, which is more than five times the abundance of *S. microphylla* recruits.

16.3.5 Abruptness Patterns of Trees and Recruits at Elevational Transitions

In general, values of stand parameters such as dbh, tree height and tree density decreased with elevation. Along this gradient, the degree of abruptness of these parameters increased at the transitions between single zones (Fig. 16.11 and Tables 16.4 and 16.5). The abruptness of recruit density exhibited the same trend, while the abruptness in terms of recruit height classes was highest at the transition A to B, lowest at B to C and intermediate at the transition from zone C to D (Fig. 16.11 and Tables 16.4 and 16.5).

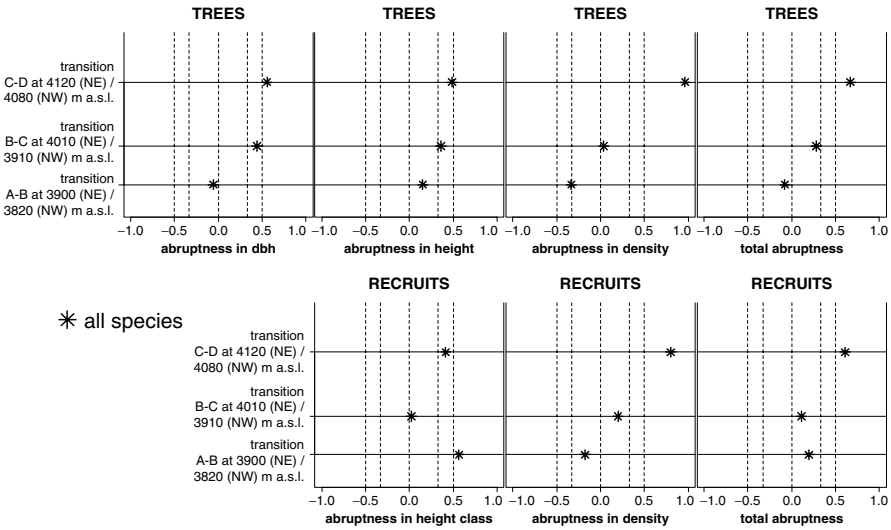

Fig. 16.11 Abruptness in dbh, height, density and sum of abruptness values for trees and recruits from zone *A* to *B*, *B* to *C* and *C* to *D* (Source: Niels Schwab)

The total all-species tree density (Table 16.4, Fig. 16.11) decreased most abruptly (abruptness = 0.96) at the transition CD, while the decrease was less but nearly equally abrupt for dbh and tree height at BC and CD (dbh: abruptness = 0.48 resp. 0.52; height: abruptness = 0.39 resp. 0.45). This pattern differed between single species: Density of *Betula utilis*, *Sorbus microphylla* and to a certain extent *Abies spectabilis* trees decreased abruptly at the transition from B to C (abruptness = 0.92 resp. 0.62 resp. 0.5), while *Rhododendron campanulatum*'s density increased intermediately from B to C (abruptness= −0.32) and dropped abruptly from maximum to the smallest density at the transition from C to D (abruptness = 1). Abruptness of the transitions with regard to dbh and tree height did not resemble density abruptness, neither for all species nor species-wise (Table 16.4).

For instance, *B. utilis*, *Rh. campanulatum* and *A. spectabilis* showed the most abrupt transitions in tree height at CD and this applied also for dbh of *B. utilis* and *Rh. campanulatum*. The majority of transitions of all species' trees showed positive abruptness values, indicating the decrease of dbh, height and stand density with elevation. Negative values mainly occurred at the transition from zone A to B, e.g. for all species density (intermediate, abruptness = −0.34), densities of *B. utilis* (smooth, abruptness = −0.21) and *Rh. campanulatum* (abrupt, abruptness = −0.54) and dbh of *A. spectabilis* (abrupt, abruptness = −0.53). While we found uniform numbers of abrupt and smooth transitions for trees of *A. spectabilis*, *B. utilis* and *Rh. campanulatum*, the smooth transitions nearly doubled the number of abrupt ones in case of *S. microphylla*.

The total all-species recruit density (Table 16.5 and Fig. 16.11) decreased most abruptly (abruptness = 0.8) at the transition from zone C to D, while there were distinct decreases in terms of recruit height at the transitions from zone A to B (abrupt, abruptness = 0.57) and from C to D (intermediate, abruptness = 0.41). As

Table 16.4 Abruptness of transitions of tree (dbh ≥7 cm) densities, dbh and height for all species and species–wise

	All species			*Abies spectabilis*			*Acer caudatum*			*Betula utilis*			*Prunus rufa*			*Rhododendron campanulatum*			*Sorbus microphylla*		
	Density	dbh	Height	Density	dbh	Height	Density	dbh	Height	Density	dbh	Height	Density	dbh	Height	Density	dbh	Height	Density	dbh	Height
CD	0.96	0.52	0.45	0.03	0.44	0.65	0.00	0.00	0.00	0.08	0.70	0.76	0.00	0.00	0.00	1.00	0.78	0.60	0.14	0.38	0.18
BC	0.04	0.48	0.39	0.50	0.56	0.35	0.00	0.00	0.00	0.92	0.26	0.22	0.44	1.00	0.90	–0.32	0.18	0.33	0.61	0.30	0.65
AB	–0.34	–0.06	0.16	0.47	–0.53	–0.28	1.00	1.00	1.00	–0.21	0.04	0.02	0.56	–0.14	0.10	–0.54	0.05	0.07	0.24	0.32	0.17

Table 16.5 Abruptness of transitions of recruit (dbh <7 cm) density and height for all species and species–wise

	All species		*Abies spectabilis*		*Acer caudatum*		*Betula utilis*		*Juniperus recurva*		*Prunus rufa*		*Rhododendron campanulatum*		*Sorbus microphylla*	
	Density	Height cl.	Density	Height cl.	Density	Height cl.	Density	Height cl.	Density	Height cl.	Density	Height cl.	Density	Height cl.	Density	Height cl.
CD	0.80	0.41	0.05	0.16	0.00	0.00	0.05	−0.43	1.00	0.96	0.00	0.00	0.80	0.43	0.92	1.00
BC	0.20	0.02	0.72	−0.68	0.04	0.94	0.24	−0.20	−0.96	−0.23	0.00	0.00	0.17	−1.00	−0.44	−0.88
AB	−0.18	0.57	0.24	−0.32	0.96	0.06	0.72	−0.37	0.17	0.27	1.00	1.00	−1.00	0.37	0.52	0.88

for trees this all-species pattern was not resembled by every single species: Density of *Rh. campanulatum* and *S. microphylla* recruits decreased abruptly at the transition from zone C to D (abruptness = 0.8 resp. abruptness = 0.92), while the most abrupt decreases of *A. spectabilis* and *B. utilis* recruits occurred at the transition BC (abruptness = 0.72) and AB (abruptness = 0.72), respectively. Again, abruptness of the transitions with regard to recruits' height did not resemble density abruptness neither for all species nor species-wise (Table 16.5). In general, we found many negative values, indicating increasing recruit heights with elevation. *Rh. campanulatum*, *S. microphylla* and *A. spectabilis* recruits' mean height increased abruptly at the transition from zone B to C (abruptness = −1.0 resp. abruptness = −0.88 resp. abruptness = −0.68). Except *B. utilis*, which showed increasing recruit height at all transitions, decreasing recruit heights at the transition from zone C to D were found. These were smooth for *A. spectabilis* (abruptness = 0.16), intermediate for *Rh. campanulatum* (abruptness = 0.43) and abrupt for *S. microphylla* (abruptness = 1.0).

16.3.6 Near-Natural State of Treeline Ecotone

All assessed density–diameter distributions resembled a reverse J- or L-shape, thus indicating a near-natural state of the Rolwaling treeline. The total number of tree stumps decreased considerably with elevation (Table 16.6). In zone B, the basal area of stumps (medium and less decomposition) amounted only to 3 % of the total basal area (living trees and stumps), while it was less than 0.5 % in zone C. Thus, wood cutting and its influence on stand structures is negligible. In zone A, the stump basal area was higher (21 %), but potential modifications of stand structure here do not affect timberline and treeline transitions at higher altitudes. The species composition of stumps of all decomposition classes exhibited *Sorbus microphylla* (c. 17 stumps per plot in average), *Acer caudatum* (c. 11) and *Betula utilis* (c. 9) as most affected in zone A. *S. microphylla* (c. 7), *Rhododendron campanulatum* (c. 7) and *B. utilis* (c. 6) accounted for most stumps in zone B (Table 16.6).

According to our field observations, influences of herbivores and domesticated animals can be ruled out. We found minimal evidence for deer, like faeces and bark stripping. We observed pika (*Ochotona* sp.), weasel (*Mustela* sp.) and snowcock (*Tetraogallus* sp.) more often, but no influence on treeline stand structures could be identified. Since the study slopes are separated by the river from settlements and thus very difficult to access, we did not observe any grazing impact. Further evidence for a negligible anthropogenic impact in the Rolwaling treeline ecotone is given by soil and atmospheric data. Investigations of bulk densities in the prevailing podzol soils revealed low mean values from 0.01 g cm^{-3} (decomposition layer) to a maximum of 1.14 g cm^{-3} (Ae horizons), indicating obviously undisturbed soils. Monitoring of atmospheric nitrogen deposition (nitrogen dioxide (NO_2), ammonia (NH_3)) below detection limit indicate no effect in the study area.

Table 16.6 Mean basal area of tree stumps (≥7 cm diameter) in proportion to stump + living trees (≥7 cm dbh) mean basal area in altitudinal zones *A, B, C* and *D* (in total and differentiated in causes of death) and species composition of stumps

Condition		***A***	***B***	***C***	***D***
Living trees	Basal area trees [m^2/ha]	28.77	47.93	13.29	0.01
Undecomposed + slight decomposition	**Stumps basal area (total basal area of living trees + stumps = 100 %) [%]**	**7.1**	**0.04**	**0.08**	**0.00**
	Natural cause [%]	0.00	43.36	0.00	–
	Anthropogenic cause [%]	93.71	56.64	0.00	–
	Unidentified cause [%]	6.29	0.00	100.00	–
Undecomposed + slight + medium decomposition	**Stumps basal area (total basal area of living trees + stumps = 100 %) [%]**	**19.04**	**2.89**	**0.49**	**0.00**
	Natural cause [%]	0.00	0.56	0.00	–
	Anthropogenic cause [%]	96.13	90.94	20.20	–
	Unidentified cause [%]	3.87	8.50	79.80	–
Undecomposed + slight + medium + intense decomposition	**Stumps basal area (total basal area of living trees + stumps = 100 %) [%]**	**64.65**	**20.81**	**5.15**	**0.00**
	Natural cause [%]	0.17	28.56	35.63	–
	Anthropogenic cause [%]	51.29	31.57	32.68	–
	Unidentified cause [%]	48.54	39.87	31.69	–
Species composition of stumps					
	Mean number of stumps per plot	***A***	***B***	***C***	***D***
All decomposition classes	*Abies spectabilis*	6.00	1.86	0.00	0.00
	Acer caudatum	11.00	0.00	0.00	0.00
	Betula utilis	9.00	5.67	2.50	0.00
	Prunus rufa	1.67	0.00	0.00	0.00
	Rhododendron campanulatum	3.00	6.67	4.00	0.00
	Sorbus microphylla	16.62	6.60	3.00	0.00
	Unidentified	9.00	5.00	0.00	0.00
	Sum	**56.28**	**25.79**	**9.50**	**0.00**

16.3.7 Soil and Air Temperatures

In general, mean soil and mean air temperatures show similarly decreasing trends with elevation (Fig. 16.12). In winter (DJF) and autumn (ON) seasons of 2013, the mean soil temperatures of zones B and D exceeded soil temperatures of the respective subjacent zones, most likely due to cold air drainage (A) and less irradiation and/or less snow cover insulation (evergreen *Rhododendron campanulatum* cover in zone C). We measured a growing season mean soil temperature of 7.5 ± 0.5 °C at the transition from zone B to C. Growing degree days differed between the two lower

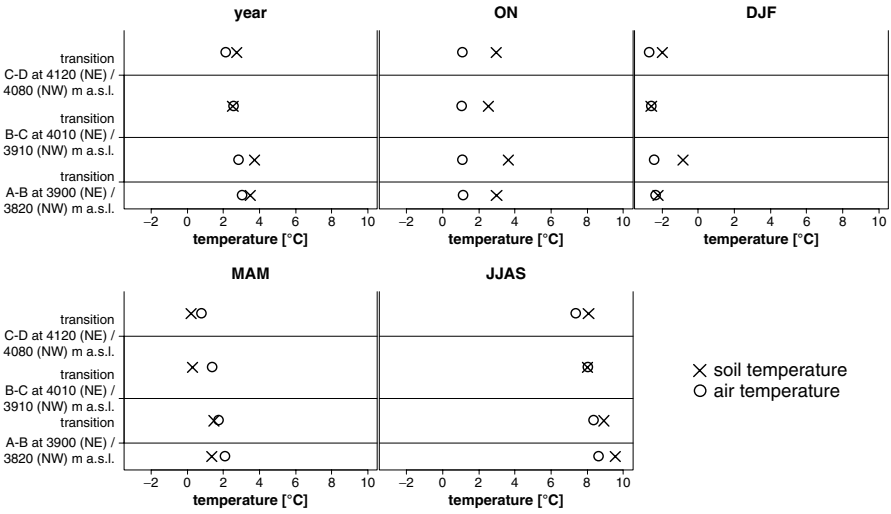

Fig. 16.12 Yearly and seasons' mean soil and air temperatures of the four altitudinal zones *A*, *B*, *C*, *D*. *ON* October/November, *DJF* December–February, *MAM* March–May, *JJAS* June–September (Source: Niels Schwab)

zones (A: 175 days, B: 177 days) and the upper zones (C: 158 days, D: 154 days) showing a shortening of the growing season in the uppermost zones by c. 3 weeks.

Yearly mean soil and air temperatures differed most in altitudinal zone B (soil: 3.7 °C; air: 2.8 °C) and nearly equalled in zone C (soil: 2.5 °C; air: 2.6 °C). At BC, the transitions of soil temperature (zone B → zone C; year: −1.2 °C; ON: −1.1 °C; DJF: −1.8 °C; MAM: −1.2 °C; JJAS: −0.9 °C) exceeded the differences of air temperatures (zone B → zone C; year: −0.3 °C; ON: −0.1 °C; DJF: −0.1 °C; MAM: −0.4 °C; JJAS: −0.3 °C). Soil temperatures exhibited abrupt transitions along the elevational gradient (Fig. 16.13). The annual mean soil temperature and mean soil temperatures of autumn, winter (all abruptness = 1) and spring (abruptness = 0.94) dropped very abruptly at the transition BC. This decrease was less pronounced in summer (abruptness = 0.59). We found rather unexpected increases of soil temperatures with increasing elevation at the AB and CD transitions in autumn (abruptness = −0.59 resp. abruptness = −0.39), winter (abruptness = −0.78 resp. abruptness = −0.34) and for the annual mean soil temperatures (abruptness = −0.22 resp. abruptness = −0.18). In spring, the soil temperatures of the transitions AB (abruptness = −0.08) and CD (abruptness = 0.06) were similar to each other. In summer, soil temperatures decreased nearly abruptly from zone A to B (abruptness = 0.41), while they differed only slightly at the transition from zone C to D (abruptness = −0.03).

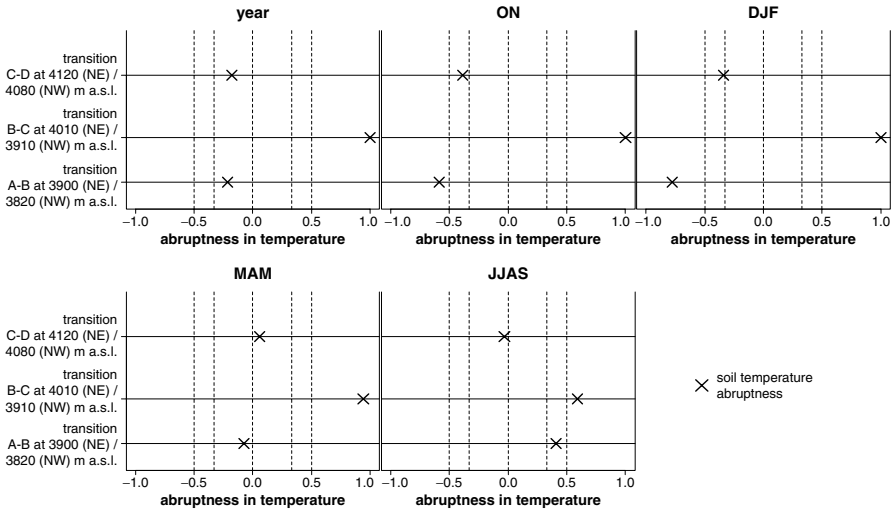

Fig. 16.13 Yearly and seasons' mean soil temperature abruptness along the altitudinal gradient at transitions from zone *A* to *B*, *B* to *C* and *C* to *D*. *ON* October/November, *DJF* December–February, *MAM* March–May, *JJAS* June–September (Source: Niels Schwab)

16.4 Discussion

16.4.1 Treeline Structure and Treeline Responsiveness to Climate Warming

In general, the tree species composition and altitudinal position of the Rolwaling treeline ecotone coincides with previous findings for north-facing slopes in central and E Nepal, where *Abies spectabilis*, *Betula utilis*, *Sorbus microphylla* and *Rhododendron campanulatum* dominate the ecotones between 3900 and 4400 m (Schickhoff 2005; Miehe et al. 2015). Considering the altitudinal zonation of vegetation within the treeline ecotone, in particular the dense *Rh. campanulatum* thicket in zone C, it is evident that the Rolwaling treeline has to be assigned physiognomically to treelines with a krummholz belt (cf. Holtmeier 2009). The contorted and gnarled growth form of *Rh. campanulatum* is, however, not necessarily genetically predetermined (cf. Miehe 1990), since there are some upright-growing individuals at lower altitudes in zones A and B (Fig. 16.14). *Rh. campanulatum* thickets in the lower C zone reach a considerable height of more than 3–4 m and stems may attain large diameters. Thus, these thickets can also be termed dwarf forests (cf. Masuzawa 1985). Towards their upper altitudinal limit at the transition CD, these thickets or dwarf forests are gradually reduced in height and become climatically stunted. Within the krummholz thicket in lower zone C, the uppermost tree individuals (>3 m height) of *A. spectabilis* and *B. utilis* mark the outpost-treeline sensu Körner (2012, Fig. 16.3), which is located slightly upslope (30–50 m altitude difference) from the treeline. The latter connects the uppermost patches of forest composed of

Fig. 16.14 *Rhododendron campanulatum* growing upright in zones *A* and *B* (**a** Schwab, 30 July 2013) and as krummholz in zone *C* (**b** Schwab, 29 September 2014) (Source: Niels Schwab)

trees with true tree habitus and coincides with the transition BC (4010 m NE; 3910 m NW) in our slope stratification scheme (cf. Figs. 16.1 and 16.2). Within the subalpine forest, *Abies* and *Betula* trees reach timber size up to the treeline, thus the difference in altitude between timberline and treeline is negligible (terminology sensu Körner 2012).

Variations in uppermost distribution limits of treeline species basically reflect species-specific physiological capacities to survive environmental stresses. Limits on upslope expansion can be imposed by potentially limiting resources (carbon, water, nutrients) and by physical factors, e.g. growing season length, frost intensity, wind exposure, abrasion, etc. (Crawford 2008). Obviously, physiological tolerances of treeline species in Rolwaling are sufficient to establish recruits far above the uppermost adult trees. The wide krummholz belt (up to 200 m altitude difference) with absolute dominance of *Rh. campanulatum* does not constitute an insurmountable barrier for other treeline species. Uppermost individuals of *A. spectabilis* (4185 m), *B. utilis* (4140 m) and *S. microphylla* (4245 m) occur above the krummholz belt in zone D. The tree species lines give evidence of successful regeneration even under the harsh climatic conditions of treeless terrain, at least to a sapling stage of 1–2 m height. Although these recruits are few in number, mostly stunted, mostly growing in the 'chamaephyte environment' (Wieser et al. 2014), and far away from reaching any tree size definition, they partially project above the snow cover and indicate the potential for treeline advance under more favourable environmental conditions. Even above the krummholz belt, tree species might be hindered by the dense alpine dwarf scrub heath vegetation (mainly composed of *Rhododendron anthopogon*, *Rhododendron lepidotum*, *Rhododendron setosum*) because shrub community competitive abilities might affect tree establishment (Körner 2012; Schickhoff et al. 2016; Chhetri and Cairns 2015). The recruit density of *A. spectabilis* decreases abruptly from B to C. The abrupt decrease indicates a lower potential for upward migration in comparison to *B. utilis* recruits which showed a smooth transition in density and height from B to C. *S. microphylla* has the best premise to advance to higher elevations given the negative abruptness values of *Sorbus* recruits at the transition from zone B to C and absolute density and mean height values.

How is the structure of the Rolwaling treeline related to the responsiveness to climate warming? Our data suggests that the extensive *Rh. campanulatum* krummholz belt plays a crucial role for any treeline shift to higher altitudes. High competitiveness and absolute dominance of *Rh. campanulatum* prohibits to a large extent upslope migration of other treeline tree species from the closed forests in zones A and B. Supposed allelopathic effects of *Rh. campanulatum* might contribute to the low establishment rates of other tree species in the krummholz thickets (Schickhoff et al. 2015, 2016). Thus, the treeline position is rather stable, and a considerable treeline advance is not to be expected in the medium term (several years to a few decades). Our results are in line with Harsch and Bader (2011), who concluded from a global treeline dataset a comparatively low responsiveness of krummholz treelines compared to diffuse treelines. They found the majority of diffuse treelines and only one third of krummholz treelines to be advancing, while abrupt and island treelines were found to be rather stable. The disjunction of mechanisms and environmental conditions primarily associated with these different treeline forms seem to explain this pattern (cf. Harsch and Bader 2011). Krummholz treelines in the Himalaya (cf. Miehe 1990, 1991; Schmidt-Vogt 1990; Miehe and Miehe 2000) have not been analysed so far with regard to their responsiveness to climate warming. Schickhoff et al. (2015) provide a first overview of the sensitivity of krummholz treelines in Rolwaling and Langtang. In the latter, seedling establishment beyond the actual upper limit of contiguous forests was detected which is a sign for a potential treeline shift. Chhetri and Cairns (2015) found a slight upward shift of an undisturbed diffuse treeline in Nepal's Makalu Barun National Park. However, they state that the treeline has advanced only until the early twentieth century. Other studies on treelines in Nepal Himalaya report tree and/or recruit densities of all occurring or selected species (Ghimire and Lekhak 2007; Shrestha et al. 2007, 2014; Gaire et al. 2010, 2011, 2014; Ghimire et al. 2010; Lv and Zhang 2012; Sujakhu et al. 2013). None of the cited studies refers to a treeline ecotone which is regarding dominance and spatial extent similar to zone C of our study area. In general, most treeline ecotones in Nepal are disturbed by human impact which has changed population structures since long.

Our data suggest that high abruptness values along the altitudinal gradient are associated with major changes in site factors. At the transition BC, i.e. the transition from upright-growing tree individuals to krummholz, we found the most abrupt change in soil temperatures. The distinct decrease in soil temperatures is obviously related to the dense foliage and canopy of the evergreen *Rh. campanulatum* thickets which provide a more efficient isolation of the soil surface from solar radiation and subsequent heat transformation compared to the upper subalpine *Abies-Betula* forest. Abrupt microenvironmental changes are commonly associated with abrupt treelines (cf. Harsch and Bader 2011; Cieraad and McGlone 2014), corresponding in the Rolwaling case to an abrupt transition from forest to krummholz. Although krummholz treelines represent a definite treeline form, they can obviously feature abrupt treeline characteristics (cf. Fig. 16.2).

In contrast to diffuse treelines, advances of both abrupt and krummholz treelines are connected rather to winter warming and reduced winter stress factors than to

growing season temperature (Harsch et al. 2009). Tree growth is assumed being rather limited by dieback (short-term stressors) than by limited biomass gain (long-term mild stress, Harsch and Bader 2011). In consequence, it is likely that the Rolwaling treeline is rather influenced by winter condition stress factors. These lead to plant damage and limit survival. Vertical growth in krummholz depends on the degree of structural microsite facilitation, e.g. reduced wind and sun exposure, and beyond treeline tall seedling growth is likely limited by the same factors (Smith et al. 2003). Thus, recruitment beyond treeline is restricted as long as vertical growth-limiting conditions prevail (Harsch et al. 2009). In Rolwaling, growing season temperature and length is likely to increase while duration of winter conditions (frost days) decreases (Gerlitz et al. 2014). Nevertheless, we assume that the consequences of winter conditions for plant growth will not change substantially because processes like wind abrasion, snow and ice damage occur regardless of the length of the frost period. Most likely heavy snowpack provokes mechanical stress and dieback in the krummholz belt. A short-term treeline shift in response to climate warming is not to be expected.

Obviously, *Rh. campanulatum* wood has mechanical properties which enable the described growth form, similar to the flexibility of, for example, *Alnus* sp., *Betula* sp., *Salix* sp. and *Nothofagus* sp. at various treelines on earth (Jalkanen and Konocpka 1998; Gallenmüller et al. 1999; Körner 2012). Most likely, this property facilitates the establishment of *Rh. campanulatum* under harsh climatic conditions.

B. utilis, and to a lesser extent *A. spectabilis* and *S. microphylla*, shows maximum abruptness values over different transitions (Tables 16.4 and 16.5). This distribution indicates that these species still perform well in growth parameters like dbh and tree height in zone C, while density decreases abruptly at lower altitude. Single individuals of *A. spectabilis*, *B. utilis* and *S. microphylla* appear to profit from variations in *Rh. campanulatum* density (canopy openings) and/or variations in environmental factors like exposition and soil parameters (microsite facilitation). The abruptness values of the Rolwaling treeline ecotone show a heterogeneous pattern across slopes and development stages (Tables 16.4 and 16.5 and Fig. 16.15) confirming the need for a differentiated categorization and species-specific analyses of treelines at local and landscape scales (Trant and Hermanutz 2014; Schickhoff et al. 2015, 2016).

16.4.2 Soil Temperature and Regeneration

In general, tree and recruit species compositions of altitudinal zones correspond to each other with distinct higher number of recruits than trees (Figs. 16.4, 16.5 and 16.6), indicating sustainable regeneration and stable populations. However, no tree individual of any species occurred in zone D (except *Sorbus microphylla*), while recruits of *Abies spectabilis*, *Betula utilis*, *S. microphylla* and *Rhododendron campanulatum* exist. These recruits are potential indicators for an upward shift of tree species distributions triggered by recent climate warming (see above), and a recent

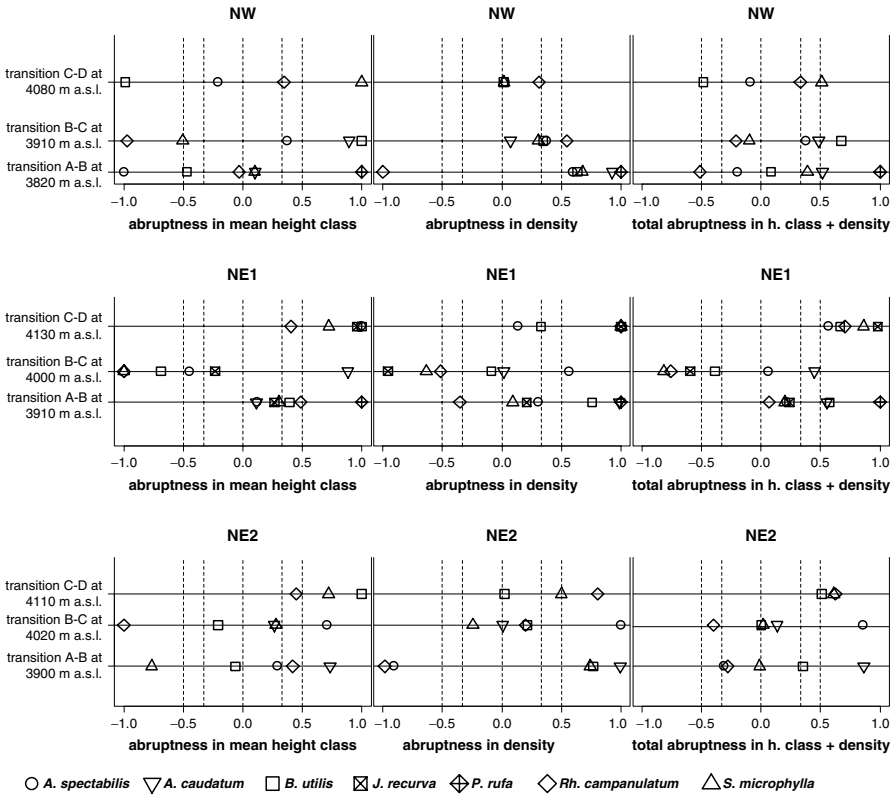

Fig. 16.15 Species- and slope-wise height, density and total recruit abruptness of transitions from zone *A* to *B*, *B* to *C* and *C* to *D* (Source: Niels Schwab)

increase in recruit density could increase the numbers of trees in the near future. The occurrence of recruits in zone D indicates the potential of tree species to become established above the krummholz belt.

Recruit densities of *A. spectabilis*, *B. utilis* and *S. microphylla* correlate positively in nearly all height classes with soil temperature. *Rh. campanulatum* densities correlate both, positively (height classes <3 cm and >200 cm) and negatively (height ≥3 cm and ≤200 cm; cf. Schickhoff et al. 2015). Thus, increasing soil temperatures potentially support the process of tree species establishment above the current treeline. Interestingly, soil temperatures at the Rolwaling treeline are higher compared to the global mean at treeline elevations. We measured a growing season mean soil temperature of 7.5 ± 0.5 °C under uppermost forest stands of *A. spectabilis* and *B. utilis* at the transition BC (Müller et al. 2015), a similar value as the warm temperate bioclimatic region seasonal mean temperature of 7.4 ± 0.4 °C, but distinctly higher than the global growing season mean soil temperature of 6.4 ± 0.7 °C (Körner 2012). This significant deviation from the global mean adds to the rather broad range of soil temperatures (5–9 °C) measured at treeline elevations (e.g.

Walter and Medina 1969; Winiger 1981; Bernoulli and Körner 1999; Körner and Paulsen 2004; Gehrig-Fasel et al. 2008; Shi et al. 2008; Hoch and Körner 2009; Kessler et al. 2014) and suggests a broadening rather than a narrowing of the error term of ±0.7 °C postulated by Körner (2012). In terms of soil temperatures, the Rolwaling treeline appears to be decoupled from rapid climate warming, i.e. the above-average soil temperatures might imply a retarded tracking of climate warming and a decelerated shift of treeline position (cf. Müller et al. 2015).

The more linear trend of air temperatures and in comparison to soil temperatures less pronounced differences between zone B and C can be attributed to the statistical method used to obtain these values (Gerlitz et al. 2016), while the soil temperatures were measured directly on site. However, heat deficiency above the subalpine forests is caused by a combination of low soil and air temperatures.

Above-average soil temperatures as well as an increasing number of growing degree days (representative for the Himalayan south slope; cf. Shrestha et al. 2012; Gerlitz et al. 2014) set the stage for an upward migration of tree species. We assume the current treeline to be located below its potential climatic limit. Since the ecotone is not affected by land use, the treeline is obviously suppressed by the given constellation of environmental factors (e.g. soil nutrient availability, krummholz barrier, allelopathic effects) and of facilitative (positive) resp. competitive (negative) interactions of recruits with neighbouring vegetation. The high numbers of *S. microphylla* recruits above the treeline (= in zones C and D) might result from a recent upward migration resp. stand densification and, if so, support the view of a species-specific response to climate change. Rather *S. microphylla* recruits than those of other tree species are capable to overcome the permanently densely foliated and potentially allelopathic krummholz belt.

16.4.3 Species-Specific Regeneration

In general, the results of our regeneration studies which show reverse J-shaped density–diameter distributions, and indicate intense and sustainable regeneration and thus the potential for upward migrations, are in line with other studies from treelines in Nepal (e.g. Ghimire and Lekhak 2007; Shrestha et al. 2007; Gaire et al. 2010, 2011, 2014; Ghimire et al. 2010; Sujakhu et al. 2013). In some of the J-shapes of these studies, the smallest dbh class is not included (Ghimire and Lekhak 2007; Shrestha et al. 2007) or shows smaller numbers than the subsequent class (Gaire et al. 2010, 2011, 2014; Sujakhu et al. 2013) putting their statements regarding intense and sustainable regeneration into a different perspective. Low numbers in the small dbh class indicate grazing impact by domesticated or wild animals which exacerbate the interpretation of the results regarding migration potentials. The species-specific low numbers in the tallest diameter classes or absence of classes above 50 cm dbh in some studies (Ghimire and Lekhak 2007, Gaire et al. 2010, 2011, 2014; Sujakhu et al. 2013) are signs indicating anthropogenic impacts. Some studies (Lv and Zhang 2012; Gaire et al. 2014) detected rather bell-shaped

density–diameter distributions or reverse J-shaped distributions (Gaire et al. 2010, 2011, 2014; Sujakhu et al. 2013) that do not correspond to the reverse J- or L-shaped ones we found in Rolwaling being to a much higher degree dominated by recruits. However, Gaire et al. (2014) assessed a significant upward shift, densification and high recruitment intensity of *Abies spectabilis* at their study site in Manaslu Conservation Area. Even in this study, the low dbh classes show only small numbers of recruits, especially in case of *Betula utilis*. In our study area, zone A provides a much better basis for regeneration of *A. spectabilis*, *B. utilis* and *Sorbus microphylla* compared to zone B, where their recruit numbers are distinctly lower compared to tree densities (Figs. 16.4, 16.5 and 16.6). The reason might be competitive advantages of *Rhododendron campanulatum* in zone B. However, the competitive strength of *Rh. campanulatum* seems to be strongest in zone C. This applies especially for the taller individuals (≥7 cm dbh).

Few studies from Nepal provide data on recruit densities. In Langtang valley, Gaire et al. (2010, 2011) found significantly less *B. utilis* recruits per ha, about the same number of *A. spectabilis* and significantly less *Rh. campanulatum* and *S. microphylla* recruits compared to the ecotone in Rolwaling. In comparison to our results, Schickhoff et al. (2015) found a comparable distribution of seedling and sapling species and slightly higher total numbers of recruits in Langtang. *Pinus wallichiana* recruit density was very high (c. 4500 N/ha at lower altitude; c. 1000 N/ha at higher altitude) in Manang (Ghimire et al. 2010); however the investigated forest was obviously dominated by this single species and thus showed a different species composition than the Rolwaling ecotone. In another study from Manang, *A. spectabilis* exhibited very high recruit numbers (c. 3200 N/ha). In the Manang study of Shrestha et al. (2007), *B. utilis* recruit numbers were comparable to the present study. In contrast, they found a very high number of *A. spectabilis* recruits at lower altitude (3500–3900 m a.s.l.; c. 5600 N/ha), while the number was distinctly smaller than ours at higher altitude (3900–4200 m a.s.l.; c. 160 N/ha). *Pinus wallichiana* showed a similar pattern with high numbers at lower and smaller numbers at higher altitude. Recruit densities of *A. spectabilis* and *B. utilis* in Manaslu Conservation Area resembled roughly the corresponding densities in Rolwaling. In contrast, *Rh. campanulatum* recruits occurred only rarely (c. 200 N/ha, Sujakhu et al. 2013). *A. spectabilis* recruit numbers were smaller in Barun valley (c. 200 N/ha; Chhetri and Cairns 2015) compared to Rolwaling. In summary, several studies from Nepal report continuous regeneration and potentials for treeline shifts, consistent with our findings.

In our study, the recruit height class distribution of *A. spectabilis* differs from *B. utilis*, *Acer caudatum* and *S. microphylla*. Obviously, the latter species grow faster and aggregate more individuals in taller height classes. The height class patterns reflect inter alia varying reproduction strategies: We found vegetative propagation (coppices) for *B. utilis* and *S. microphylla*, while *A. spectabilis* recruits grow separately from other individuals and sprout from seeds. As low temperatures restrict rather germination than layering (Holtmeier 2009; Wieser et al. 2014), temperatures obviously do not restrict seed-based regeneration of *A. spectabilis* given the recruit height class and dbh distributions. The results of recruit mean height and *RI* show

that *A. spectabilis* and *B. utilis* have the potential to develop above the transition BC beyond the seedling stage. The rare occurrence of trees indicates the potential to develop even further and become established. There are less *A. spectabilis* and *B. utilis* recruits in upper altitudinal zones, but the percentage of survivors that grow successfully to taller height classes is distinctly higher compared to lower elevation. Asynchronous shortages in seedling establishment in each zone at different time periods might be one reason for differing species- and altitudinal-specific patterns. Another reason could be that competitive stress is higher in the lower zones and thus a smaller percentage of recruits survive. More favourable light conditions appear to favour the growth of *B. utilis* in zone D and in openings in zone C. *S. microphylla* can be considered established in zones C and D given height class distribution and *RI*. Some species show no distinct signs of treeline shift but more obvious an intensified regeneration, indicating ongoing stand densification below treeline. This applies species specific especially for *A. spectabilis* in zones A and B, *B. utilis* in zone A, *S. microphylla* in zone A and C and *Rh. campanulatum* in zones B to D where we found evidences for stand densification. Climate warming impact may influence regeneration below treeline and treeline shift in different intensities (e.g. Camarero and Gutiérrez 2004; Wang et al. 2006; Kirdyanov et al. 2012; Gaire et al. 2014; Shrestha et al. 2014) which seems to apply for our study area.

Rh. campanulatum's population structure in zones C and D is a sign for its potential to spread out further (cf. Figs. 16.4, 16.5, 16.6 and 16.8). In comparison to zones C and D, *Rh. campanulatum* seems to grow under more intense competitive stress in zone B. While the high *RI* and the very high number of recruits smaller than 10 cm height point to a viable regeneration, the very low mean height and relative small numbers of recruits in classes above 10 cm height imply competitive pressure by other species and a distinct self-thinning process. Obviously, *Rh. campanulatum* keeps its regeneration capacity in the zones above, while the competitive strength of other species except *S. microphylla* seems to be reduced. As especially the *RI* of *S. microphylla* and also its average recruit height are relatively low in zone B, this species becomes more competitive in zones C and D. The shift in the ratio of recruits to trees at the specific tree species lines, recruit height and *RI* distributions indicate the potential for sustainable recruitment and tree growth. Positive correlations of recruit density with soil temperatures and soil moisture give evidence of the relevance of these site factors (cf. Schickhoff et al. 2015). However, other site factors, e.g. nutrient availability, microclimatic variations and germination conditions like surface structure and light conditions, might in addition hinder or facilitate intensified recruitment (e.g. Holtmeier and Broll 2005, 2010; Malanson et al. 2007; Hofgaard et al. 2009; Batllori et al. 2010; Renaud et al. 2011; Elliott 2012; Wang et al. 2012; Durak et al. 2015; Treml and Chuman 2015).

The high standard deviations of the mean densities which we present in the results reveal the heterogeneous patterns of the populations even within same altitudinal zones. Analyses of subsets of our sample, e.g. single slopes, confirm this finding. This applies also for general and species-specific abruptness patterns (e.g. recruits, species and slope-wise, Fig. 16.15 and Tables 16.4 and 16.5). This variability suggests differences in site conditions apart from altitude and thus a varied

potential for recruitment at local scales. No distinct differences in soil temperatures between zone C and D were detected during growing season (Figs. 16.12 and 16.13). If dissemination depended on temperature, only species which once was established in zone C could migrate easily to zone D as there is no temperature threshold to pass.

In summary we assessed a prolific regeneration in the Rolwaling treeline ecotone which indicates a considerable potential to respond to climate warming with a treeline shift. Any treeline advance, however, will be controlled to a large extent by the dense krummholz belt which acts as an effective barrier for upslope migration of treeline-forming tree species. Most likely the treeline in Rolwaling confirms the low responsiveness of near-natural Himalayan treelines and upward shifts only in the long term, despite the currently existing potential (Shrestha et al. 2014; Schickhoff et al. 2015, 2016; Chhetri and Cairns 2015).

16.5 Conclusions

Changes in tree dbh and tree and recruit height and density are species specific and occur with varying degrees of abruptness along the treeline ecotone. We identified several tree species lines inside the ecotone. The stand structure is complex; high standard deviations from mean values indicate heterogeneous patterns, differing between different slopes, species and altitudinal zones. Soil temperatures rather than lapse rate air temperatures are associated with physiognomic transitions, treeline position and spatial regeneration patterns. Thus, the Rolwaling treeline is potentially susceptible to climate change, and treeline tree species have the potential to migrate upslope in future with *Sorbus microphylla* showing particularly high dynamics. Upslope migration, however, is effectively controlled by the dense krummholz belt. Currently, the treeline is rather stable; however we found a prolific regeneration as well as signs of stand densification. Further investigations including dendroecological analyses will clarify the complex conditions for establishment and development from recruits to trees. Moreover, investigations at additional Rolwaling study sites and in other valleys are needed to better understand the spatial heterogeneity of Himalayan treeline ecotones and their responsiveness to climate change.

Acknowledgements We are grateful to Ram Bahadur, Bijay Raj Subedi, Simon Drollinger, Helge Heyken, Nina Kiese, Madan K. Suwal, Hanna Wanli and Ronja Wedegärtner who helped us during field work and to Julika Hellmold for suggestions on an earlier draft. We acknowledge Chandra Subedi for great support in logistics and administrative issues. B. Bürzle was funded by Studienstiftung des deutschen Volkes. We are indebted to the German Research Foundation

(DFG SCHI 436/14-1, SCHO 739/14-1, BO 1333/4-1), to Nepalese authorities for research permits and to the community in Rolwaling for the assistance in fieldwork, willingness to cooperate and hospitality.

References

Baker BB, Moseley RK (2007) Advancing treeline and retreating glaciers: implications for conservation in Yunnan, P.R. China. Arct Antarct Alp Res 39:200–209. doi:10.1657/1523-0430(2007)39[200:ATARGI]2.0.CO;2

Batllori E, Gutiérrez E (2008) Regional tree line dynamics in response to global change in the Pyrenees. J Ecol 96:1275–1288. doi:10.1111/j.1365-2745.2008.01429.x

Batllori E, Camarero JJ, Ninot JM, Gutiérrez E (2009) Seedling recruitment, survival and facilitation in alpine *Pinus uncinata* tree line ecotones. Implications and potential responses to climate warming. Glob Ecol Biogeogr 18:460–472. doi:10.1111/j.1466-8238.2009.00464.x

Batllori E, Camarero JJ, Gutiérrez E (2010) Current regeneration patterns at the tree line in the Pyrenees indicate similar recruitment processes irrespective of the past disturbance regime. J Biogeogr 37:1938–1950. doi:10.1111/j.1365-2699.2010.02348.x

Baumgartner R (2015) Farewell to yak and yeti? The Rolwaling Sherpas facing a globalised world. Vajra Books, Kathmandu

Bernoulli M, Körner C (1999) Dry matter allocation in treeline trees. Phyton (Austria) 39:7–12

Bhusal NP (2012) Buffer zone management system in protected areas of Nepal. Third Pole J Geogr Educ 11–12:34–44. doi:10.3126/ttp.v11i0.11558

Bhutiyani MR, Kale VS, Pawar NJ (2010) Climate change and the precipitation variations in the northwestern Himalaya: 1866–2006. Int J Climatol 30:535–548. doi:10.1002/joc.1920

Bolli JC, Rigling A, Bugmann H (2007) The influence of changes in climate and land-use on regeneration dynamics of Norway spruce at the treeline in the Swiss Alps. Silva Fenn 41:55–70

Camarero JJ, Gutiérrez E (2004) Pace and pattern of recent treeline dynamics: response of ecotones to climatic variability in the Spanish Pyrenees. Clim Chang 63:181–200. doi:10.1023/B:CLIM.0000018507.71343.46

Chhetri PK, Cairns DM (2015) Contemporary and historic population structure of *Abies spectabilis* at treeline in Barun valley, eastern Nepal Himalaya. J Mt Sci 12:558–570. doi:10.1007/s11629-015-3454-5

Cieraad E, McGlone MS (2014) Thermal environment of New Zealand's gradual and abrupt treeline ecotones. N Z J Ecol 38:12–25

Crawford RMM (2008) Plants at the margin: ecological limits and climate change. Cambridge University Press, Cambridge

Dirnböck T, Dullinger S, Grabherr G (2003) A regional impact assessment of climate and land-use change on alpine vegetation. J Biogeogr 30:401–417. doi:10.1046/j.1365-2699.2003.00839.x

Duan K, Yao T, Thompson LG (2006) Response of monsoon precipitation in the Himalayas to global warming. J Geophys Res Atmos 111:D19110. doi:10.1029/2006JD007084

Durak T, Żywiec M, Kapusta P, Holeksa J (2015) Impact of land use and climate changes on expansion of woody species on subalpine meadows in the eastern Carpathians. For Ecol Manag 339:127–135. doi:10.1016/j.foreco.2014.12.014

Dutta PK, Dutta BK, Das AK, Sundriyal RC (2014) Alpine timberline research gap in Himalaya: a literature review. Indian For 140:419–427

Elliott GP (2011) Influences of 20th-century warming at the upper tree line contingent on local-scale interactions: evidence from a latitudinal gradient in the Rocky Mountains, USA. Glob Ecol Biogeogr 20:46–57. doi:10.1111/j.1466-8238.2010.00588.x

Elliott G (2012) The role of thresholds and fine-scale processes in driving upper treeline dynamics in the Bighorn Mountains, Wyoming. Phys Geogr 33:129–145. doi:10.2747/0272-3646.33.2.129

Gaire N, Dhakal Y, Lekhak H, Bhuju D, Shah S (2010) Vegetation dynamics in treeline ecotone of Langtang National Park, Central Nepal. Nepal J Sci Technol 11:107–114. doi:10.3126/njst.v11i0.4132

Gaire NP, Dhakal YR, Lekhak HC, Bhuju DR, Shah SK (2011) Dynamics of *Abies spectabilis* in relation to climate change at the treeline ecotone in Langtang National Park. Nepal J Sci Technol 12:220–229. doi:10.3126/njst.v12i0.6506

Gaire NP, Koirala M, Bhuju DR, Borgaonkar HP (2014) Treeline dynamics with climate change at the central Nepal Himalaya. Clim Past 10:1277–1290. doi:10.5194/cp-10-1277-2014

Gallenmüller F, Bogenrieder A, Speck T (1999) Biomechanische und ökologische Untersuchungen an *Alnus viridis* (Chaix) DC. in verschiedenen Höhenlagen der Schweizer Alpen. Ber. Eidgenöss. Forsch.anst. Wald Schnee Landsch. 347. Publikationen WSL, Birmensdorf

Gehrig-Fasel J, Guisan A, Zimmermann NE (2007) Tree line shifts in the Swiss Alps: climate change or land abandonment? J Veg Sci 18:571–582. doi:10.1111/j.1654-1103.2007.tb02571.x

Gehrig-Fasel J, Guisan A, Zimmermann NE (2008) Evaluating thermal treeline indicators based on air and soil temperature using an air-to-soil temperature transfer model. Ecol Model 213:345–355. doi:10.1016/j.ecolmodel.2008.01.003

Gerlitz L, Bechtel B, Böhner J, Bobrowski B, Bürzle B, Müller M, Scholten T, Schickhoff U, Schwab N, Weidinger J (2016) Analytic comparison of temperature lapse rates and precipitation gradients in a Himalayan treeline environment – Implications for statistical downscaling. In: Singh RB, Schickhoff U, Mal S (eds) Climate change, glacier response, and vegetation dynamics in the Himalaya. Springer, Cham, pp 49–64

Gerlitz L, Conrad O, Thomas A, Böhner J (2014) Warming patterns over the Tibetan Plateau and adjacent lowlands derived from elevation- and bias-corrected ERA-Interim data. Clim Res 58:235–246. doi:10.3354/cr01193

Germino MJ, Smith WK, Resor AC (2002) Conifer seedling distribution and survival in an alpine-treeline ecotone. Plant Ecol 162:157–168. doi:10.1023/A:1020385320738

Ghimire B, Lekhak HD (2007) Regeneration of *Abies spectabilis* (D. Don) Mirb. in subalpine forest of Upper Manang, north-central Nepal. In: Chaudhary RP, Aase TH, Vetaas OR, Subedi BP (eds) Local effects of global changes in the Himalayas: Manang, Nepal. Tribhuvan University/ Nepal and University of Bergen, Norway, Kathmandu, pp 139–149

Ghimire B, Mainali KP, Lekhak HD, Chaudhary RP, Ghimeray AK (2010) Regeneration of *Pinus wallichiana* AB Jackson in a trans-Himalayan dry valley of north-central Nepal. Himal J Sci 6:19–26. doi:10.3126/hjs.v6i8.1798

Grigor'ev AA, Moiseev PA, Nagimov ZY (2013) Dynamics of the timberline in high mountain areas of the nether-polar Urals under the influence of current climate change. Russ J Ecol 44:312–323. doi:10.1134/S1067413613040061

Harsch MA, Bader MY (2011) Treeline form – a potential key to understanding treeline dynamics. Glob Ecol Biogeogr 20:582–596. doi:10.1111/j.1466-8238.2010.00622.x

Harsch MA, Hulme PE, McGlone MS, Duncan RP (2009) Are treelines advancing? A global meta-analysis of treeline response to climate warming. Ecol Lett 12:1040–1049. doi:10.1111/j.1461-0248.2009.01355.x

Hoch G, Körner C (2009) Growth and carbon relations of tree line forming conifers at constant vs. variable low temperatures. J Ecol 97:57–66. doi:10.1111/j.1365-2745.2008.01447.x

Hofgaard A, Dalen L, Hytteborn H (2009) Tree recruitment above the treeline and potential for climate-driven treeline change. J Veg Sci 20:1133–1144. doi:10.1111/j.1654-1103.2009.01114.x

Holtmeier F-K (2009) Mountain timberlines. Ecology, patchiness, and dynamics. Springer, New York

Holtmeier F-K, Broll G (2005) Sensitivity and response of northern hemisphere altitudinal and polar treelines to environmental change at landscape and local scales. Glob Ecol Biogeogr 14:395–410. doi:10.1111/j.1466-822X.2005.00168.x

Holtmeier F-K, Broll G (2010) Wind as an ecological agent at treelines in North America, the Alps, and the European Subarctic. Phys Geogr 31:203–233. doi:10.2747/0272-3646.31.3.203

Jain SK, Kumar V, Saharia M (2013) Analysis of rainfall and temperature trends in northeast India. Int J Climatol 33:968–978. doi:10.1002/joc.3483

Jalkanen R, Konocpka B (1998) Snow-packing as a potential harmful factor on *Picea abies*, *Pinus sylvestris* and *Betula pubescens* at high altitude in northern Finland. Eur J For Pathol 28:373–382. doi:10.1111/j.1439-0329.1998.tb01191.x

Kessler M, Toivonen JM, Sylvester SP, Kluge J, Hertel D (2014) Elevational patterns of *Polylepis* tree height (Rosaceae) in the high Andes of Peru: role of human impact and climatic conditions. Front Plant Sci 5:194. doi:10.3389/fpls.2014.00194

Kirdyanov AV, Hagedorn F, Knorre AA, Fedotova EV, Vaganov EA, Naurzbaev MM, Moiseev PA, Rigling A (2012) 20th century tree-line advance and vegetation changes along an altitudinal transect in the Putorana Mountains, northern Siberia. Boreas 41:56–67. doi:10.1111/j.1502-3885.2011.00214.x

Körner C (2012) Alpine treelines: functional ecology of the global high elevation tree limits. Springer, Basel

Körner C, Paulsen J (2004) A world-wide study of high altitude treeline temperatures. J Biogeogr 31:713–732. doi:10.1111/j.1365-2699.2003.01043.x

Liu X, Chen B (2000) Climatic warming in the Tibetan Plateau during recent decades. Int J Climatol 20:1729–1742. doi:10.1002/1097-0088(20001130)20:14<1729::AID-JOC556>3.0.CO;2-Y

Lloyd AH (2005) Ecological histories from Alaskan tree lines provide insight into future change. Ecology 86:1687–1695

Lv L-X, Zhang Q-B (2012) Asynchronous recruitment history of *Abies spectabilis* along an altitudinal gradient in the Mt. Everest region. J Plant Ecol 5:147–156. doi:10.1093/jpe/rtr016

Malanson G, Butler D, Fagre D, Walsh S, Tomback D, Daniels L, Resler L, Smith W, Weiss D, Peterson D, Bunn A, Hiemstra C, Liptzin D, Bourgeron P, Shen Z, Millar C (2007) Alpine treeline of Western North America: linking organism-to-landscape dynamics. Phys Geogr 28:378–396. doi:10.2747/0272-3646.28.5.378

Malanson GP, Resler LM, Bader MY, Holtmeier F-K, Butler DR, Weiss DJ, Daniels LD, Fagre DB (2011) Mountain treelines: a roadmap for research orientation. Arct Antarct Alp Res 43:167–177. doi:10.1657/1938-4246-43.2.167

Masuzawa T (1985) Ecological studies on the timberline of Mt. Fuji I. Structure of plant community and soil development on the timberline. Bot Mag Tokyo 98:15–28

Miehe G (1990) Langtang Himal: Flora und Vegetation als Klimazeiger und -zeugen im Himalaya. Dissertationes Botanicae 158. Cramer, Berlin

Miehe G (1991) Die Vegetationskarte des Khumbu Himal (Mt. Everest-Südabdachung) 1: 50 000: Gefügemuster der Vegetation und Probleme der Kartierung (The vegetation map of the Khumbu Himal (Mt. Everest South Slope) 1: 50,000. Vegetation patterns and problems of mapping). Erdkunde 45:81–94. doi:10.3112/erdkunde.1991.02.01

Miehe G, Miehe S (2000) Comparative high mountain research on the treeline ecotone under human impact. Carl Troll's "Asymmetrical zonation of the humid vegetation types of the world" of 1948 reconsidered. Erdkunde 54:34–50. doi:10.3112/erdkunde.2000.01.03

Miehe G, Miehe S, Böhner J, Bäumler R, Ghimire SK, Bhattarai K, Chaudhary RP, Subedi M, Jha PK, Pendry C (2015) Vegetation ecology. In: Miehe G, Pendry C, Chaudhary RP (eds) Nepal: An introduction to the natural history, ecology and human environment of the Himalayas. Royal Botanic Garden Edinburgh, pp 385–472

Müller M, Schickhoff U, Scholten T, Drollinger S, Böhner J, Chaudhary RP (2016) How do soil properties affect alpine treelines? General principles in a global perspective and novel findings from Rolwaling Himal, Nepal. Progr Phys Geogr 40:135–160. doi:10.1177/0309133315615802

Oksanen J, Blanchet FG, Kindt R, Legendre P, Minchin PR, O'Hara RB, Simpson GL, Solymos P, Stevens MHH, Wagner H (2014) Vegan: community ecology package. R package version 2.2-0. http://CRAN.R-project.org/package=vegan

Pauchard A, Kueffer C, Dietz H, Daehler CC, Alexander J, Edwards PJ, Arévalo JR, Cavieres LA, Guisan A, Haider S, Jakobs G, McDougall K, Millar CI, Naylor BJ, Parks CG, Rew LJ, Seipel T (2009) Ain't no mountain high enough: plant invasions reaching new elevations. Front Ecol Environ 7:479–486. doi:10.1890/080072

Penniston R, Lundberg A (2014) Forest expansion as explained by climate change and changes in land use: a study from Bergen, western Norway. Geogr Ann Ser Phys Geogr 96:579–589. doi:10.1111/geoa.12056

Piermattei A, Garbarino M, Urbinati C (2014) Structural attributes, tree-ring growth and climate sensitivity of *Pinus nigra* Arn. at high altitude: common patterns of a possible treeline shift in the central Apennines (Italy). Dendrochronologia 32:210–219. doi:10.1016/j.dendro.2014.05.002

Press JR, Shrestha KK, Sutton DA (2000) Annotated checklist of the flowering plants of Nepal. The Natural History Museum, London. http://www.efloras.org/flora_page.aspx?flora_id=110, updated online version accessed 21 Apr 2015

R Core Team (2014) R: a language and environment for statistical computing. R Foundation for Statistical Computing, Vienna

Renaud V, Innes JL, Dobbertin M, Rebetez M (2011) Comparison between open-site and below-canopy climatic conditions in Switzerland for different types of forests over 10 years (1998–2007). Theor Appl Climatol 105:119–127. doi:10.1007/s00704-010-0361-0

Sacherer J (1979) The high altitude ethnobotany of the Rolwaling Sherpas. Contrib Nepal Stud 6:45–64

Schickhoff U (2002) Die Degradierung der Gebirgswälder Nordpakistans: Faktoren, Prozesse und Wirkungszusammenhänge in einem regionalen Mensch-Umwelt-System. Steiner, Stuttgart

Schickhoff U (2005) The upper timberline in the Himalayas, Hindu Kush and Karakorum: a review of geographical and ecological aspects. In: Broll G, Keplin B (eds) Mountain ecosystems. Studies in treeline ecology. Springer, Berlin, pp 275–354

Schickhoff U (2011) Dynamics of mountain ecosystems. In: Millington AC, Blumler MA, Schickhoff U (eds) The SAGE handbook of biogeography. Sage, London, pp 313–337

Schickhoff U, Bobrowski M, Böhner J, Bürzle B, Chaudhary RP, Gerlitz L, Heyken H, Lange J, Müller M, Scholten T, Schwab N, Wedegärtner R (2015) Do Himalayan treelines respond to recent climate change? An evaluation of sensitivity indicators. Earth Syst Dyn 6:245–265. doi:10.5194/esd-6-245-2015

Schickhoff U, Bobrowski M, Böhner J, Bürzle B, Chaudhary RP, Gerlitz L, Lange J, Müller M, Scholten T, Schwab N (2016) Climate change and treeline dynamics in the Himalaya. In: Singh RB, Schickhoff U, Mal S (eds) Climate change, glacier response, and vegetation dynamics in the Himalaya. Springer, Cham, pp 271–306

Schmidt-Vogt D (1990) High altitude forests in the Jugal Himal (eastern central Nepal): forest types and human impact. Steiner, Stuttgart

Shi P, Wu N (2013) The timberline ecotone in the Himalayan region: an ecological review. In: Wu N, Rawat GS, Joshi S, Ismail M, Sharma E (eds) High-altitude rangelands and their interfaces in the Hindu Kush Himalayas. ICIMOD, Kathmandu, pp 108–116

Shi P, Körner C, Hoch G (2008) A test of the growth-limitation theory for alpine tree line formation in evergreen and deciduous taxa of the eastern Himalayas. Funct Ecol 22:213–220. doi:10.1111/j.1365-2435.2007.01370.x

Shrestha AB, Wake CP, Mayewski PA, Dibb JE (1999) Maximum temperature trends in the Himalaya and its vicinity: an analysis based on temperature records from Nepal for the period 1971–94. J Clim 12:2775–2786. doi:10.1175/1520-0442(1999)012<2775:MTTITH>2.0.CO;2

Shrestha BB, Ghimire B, Lekhak HD, Jha PK (2007) Regeneration of treeline Birch (*Betula utilis* D. Don) forest in a trans-Himalayan dry valley in central Nepal. Mt Res Dev 27:259–267. doi:10.1659/mrdd.0784

Shrestha UB, Shrestha S, Chaudhary P, Chaudhary RP (2010) How representative is the protected areas system of Nepal? Mt Res Dev 30:282–294. doi:10.1659/MRD-JOURNAL-D-10-00019.1

Shrestha UB, Gautam S, Bawa KS (2012) Widespread climate change in the Himalayas and associated changes in local ecosystems. PLoS ONE 7:e36741. doi:10.1371/journal.pone.0036741
Shrestha KB, Hofgaard A, Vandvik V (2014) Recent treeline dynamics are similar between dry and mesic areas of Nepal, central Himalaya. J Plant Ecol 8:347–358. doi:10.1093/jpe/rtu035
Smith WK, Germino MJ, Hancock TE, Johnson DM (2003) Another perspective on altitudinal limits of alpine timberlines. Tree Physiol 23:1101–1112
Stevens GC, Fox JF (1991) The causes of treeline. Annu Rev Ecol Syst 22:177–191. doi:10.1146/annurev.es.22.110191.001141
Sujakhu H, Gosai KR, Karmacharya SB (2013) Forest structure and regeneration pattern of *Betula utilis* D. Don in Manaslu Conservation Area, Nepal. Ecoprint Int J Ecol 20:107–113. doi:10.3126/eco.v20i0.11472
Trant AJ, Hermanutz L (2014) Advancing towards novel tree lines? A multispecies approach to recent tree line dynamics in subarctic alpine Labrador, northern Canada. J Biogeogr 41:1115–1125. doi:10.1111/jbi.12287
Treml V, Chuman T (2015) Ecotonal dynamics of the altitudinal forest limit are affected by terrain and vegetation structure variables: an example from the Sudetes mountains in central Europe. Arct Antarct Alp Res 47:133–146. doi:10.1657/AAAR0013-108
Troll C (1973) The upper timberlines in different climatic zones. Arct Alp Res 5:A3–A18. doi:10.2307/1550148
Van Laar A, Akça A (2007) Forest mensuration. Springer, Dordrecht
Walter H, Medina E (1969) Die Bodentemperatur als ausschlaggebender Faktor für die Gliederung der subalpinen und alpinen Stufe in den Anden Venezuelas (Vorläufige Mitteilung). Ber Dtsch Bot Ges 82:275–281. doi:10.1111/j.1438-8677.1969.tb02269.x
Wang T, Zhang Q-B, Ma K (2006) Treeline dynamics in relation to climatic variability in the central Tianshan mountains, northwestern China. Glob Ecol Biogeogr 15:406–415. doi:10.1111/j.1466-822X.2006.00233.x
Wang Y, Camarero JJ, Luo T, Liang E (2012) Spatial patterns of Smith fir alpine treelines on the south-eastern Tibetan Plateau support that contingent local conditions drive recent treeline patterns. Plant Ecol Divers 5:311–321. doi:10.1080/17550874.2012.704647
Wang S-Y, Yoon J-H, Gillies RR, Cho C (2013) What caused the winter drought in western Nepal during recent years? J Clim 26:8241–8256. doi:10.1175/JCLI-D-12-00800.1
Wickham H (2011) The split-apply-combine strategy for data analysis. J Stat Softw 40:1–29
Wiegand T, Camarero JJ, Rüger N, Gutiérrez E (2006) Abrupt population changes in treeline ecotones along smooth gradients. J Ecol 94:880–892. doi:10.1111/j.1365-2745.2006.01135.x
Wieser G, Matyssek R, Luzian R, Zwerger P, Pindur P, Oberhuber W, Gruber A (2009) Effects of atmospheric and climate change at the timberline of the central European Alps. Ann For Sci 66:402–402. doi:10.1051/forest/2009023
Wieser G, Holtmeier F-K, Smith WK (2014) Treelines in a changing global environment. In: Tausz M, Grulke N (eds) Trees in a changing environment. Springer, Dordrecht, pp 221–263
Winiger M (1981) Zur thermisch-hygrischen Gliederung des Mount Kenya (Causes and effects of the thermo-hygric differentiation of Mt. Kenya). Erdkunde 35:248–263. doi:10.3112/erdkunde.1981.04.02
Zurbriggen N, Hättenschwiler S, Frei ES, Hagedorn F, Bebi P (2013) Performance of germinating tree seedlings below and above treeline in the Swiss Alps. Plant Ecol 214:385–396. doi:10.1007/s11258-013-0176-z

Chapter 17
Dendroecological Perspectives on Climate Change on the Southern Tibetan Plateau

Achim Bräuning, Jussi Grießinger, Philipp Hochreuther, and Jakob Wernicke

Abstract Tree rings are indicators of historic environmental changes and plant response to past and current climate change. Summer temperature reconstructions from maximum latewood density on the southeastern Tibetan plateau (TP) for the past 600 years revealed cool summer temperatures between ca. 1580 and 1790 A.D., corresponding to the "Little Ice Age (LIA)." This period was characterized by several glacier advance periods, with a maximum glacier extent ending around 1740–1780 A.D. and smaller readvance phases during the early nineteenth to late nineteenth century. Stable carbon isotope analyses of tree-ring cellulose indicate species-specific ecophysiological response patterns of trees to environmental conditions related to enhanced atmospheric CO_2 levels and drier site conditions which might affect future forest composition. Spatial patterns of altitudinal changes of climate-growth relationships indicate the dominance of different growth-limiting factors in different regions of the TP. In semiarid regions along the western distribution limit of forests, moisture availability during the growing season is most relevant for growth of juniper tree species even in high altitudes. In contrast, warmer temperatures have a stimulating effect on radial growth close to the upper tree limit on the humid eastern TP. These findings are corroborated by first studies of cambial phenology, indicating a stimulating influence of early growing season temperatures on cell formation. In the dry northeastern TP, wet conditions during the main growing season in June are favorable for radial growth. Due to the low number of studies and a long history of human impact on forests, a climate-driven upward shift of the upper tree limit cannot yet clearly be stated. Tree-ring analyses on long-living dwarf shrubs may increase the potential for dendrochronological climate reconstructions beyond the upper limit of tree growth on the TP.

Keywords Tibetan plateau • Climate reconstruction • Tree rings • Stable isotopes • Dendroecology • Glacier history

A. Bräuning (✉) • J. Grießinger • P. Hochreuther • J. Wernicke
Institute of Geography, Friedrich-Alexander-University Erlangen-Nürnberg, Wetterkreuz 15, 91058 Erlangen, Germany
e-mail: achim.braeuning@fau.de

R.B. Singh et al. (eds.), *Climate Change, Glacier Response, and Vegetation Dynamics in the Himalaya*, DOI 10.1007/978-3-319-28977-9_17

17.1 Introduction

The Tibetan plateau (TP) and its southern declivity are strongly influenced by the Asian summer monsoon system, which consists of the overlapping Indian (ISM) and East Asian summer monsoon (EASM) branches, reaching the TP from south-western and eastern directions, respectively. During May to September, pressure gradients between the TP and surrounding oceans trigger the transport of warm-humid air masses from (i) the Bay of Bengal (ISM) and (ii) the Pacific Ocean (EASM) towards the Himalayas and the eastern TP, whereas during other seasons, westerly winds may strongly affect the TP (Bothe et al. 2011). As a result, instable air masses are forced to rise, leading to orographic rain along the marginal mountain ranges of the TP and hence to a pronounced moisture gradient leewards (Fig. 17.1). For the regional ecosystems, the monsoonal summer rainfall is the major source of precipitation during the vegetation period. Solid precipitation during the summer monsoon season is also crucial for the mass balance of monsoonal glaciers that are important long-term freshwater storages and form the major river sources for South and Southeast Asia (Immerzeel et al. 2010).

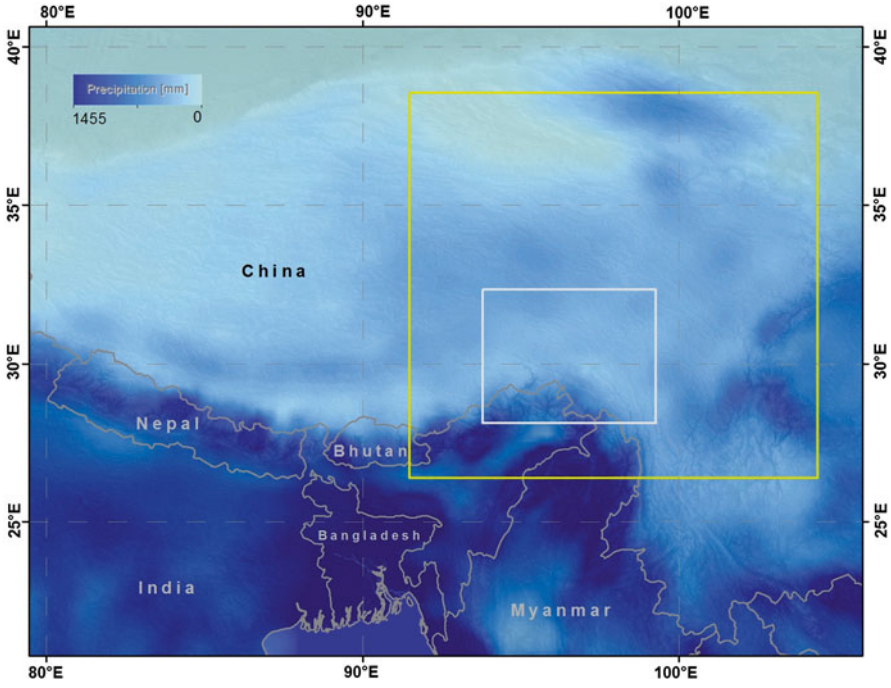

Fig. 17.1 Average July precipitation in High Asia calculated for the period 2000–2011 (Data are taken from the High Asia Refined analysis data (HAR) using a spatial resolution of 30 km (Maussion et al. 2014)). *White* and *yellow rectangles* show areas of Figs. 17.2 and 17.5, respectively

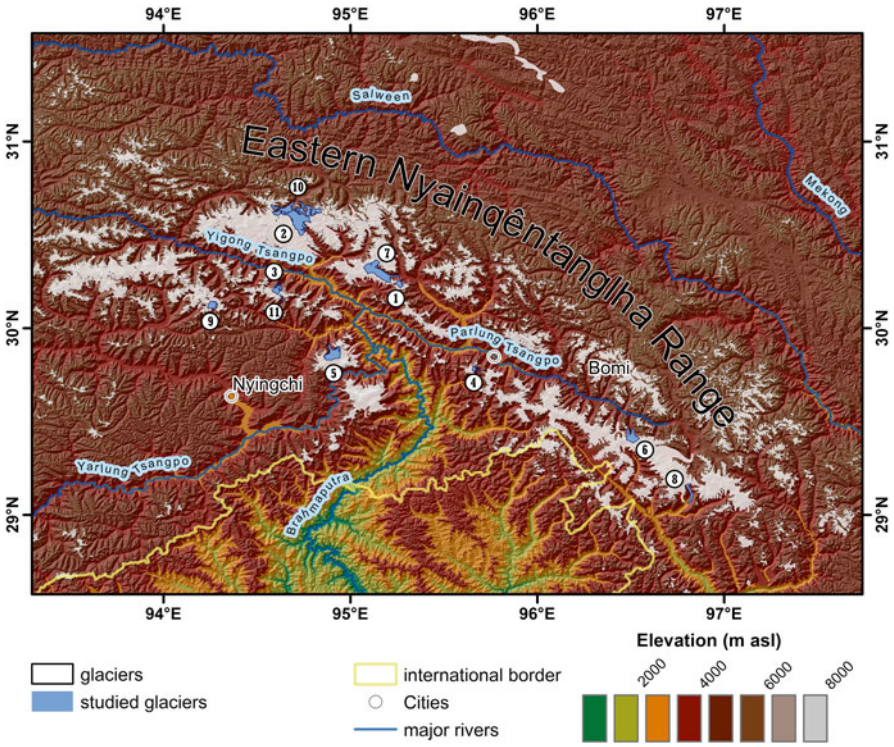

Fig. 17.2 Topography of the study area. Numbers indicate glaciers with dated LIA moraines: (*1*) Baitong, (*2*) Ruoguo, (*3*) Xinpu, (*4*) Gawalong, (*5*) Gyala Peri, (*6*) Midui, (*7*) Zepu, (*8*) Arza, (*9*) Xincuo, (*10*) Xuequ, (*11*) Gongpu (undated), ordered by minimum LIA moraine age (c.f. Fig. 17.3)

The recent decades have witnessed significant trends of decreasing precipitation coupled with increasing temperatures across the Himalaya-Tibet region (Wei and Fang 2013; Shrestha et al. 2012). Especially in the southeastern part of the TP, these trends are supposed to exceed natural climate variability (Wang et al. 2008; You et al. 2010). Due to the lack of meteorological data before the 1950s and the scarcity of existing climate stations, a final assessment of these observed changes is still challenging. As a consequence, there is a strong demand for regional paleoclimate data which can help to better understand the apparent changes in climate and landscape (e.g., glacier variability, climate-induced landscape dynamics) in a long-term perspective.

Trees are valuable biological archives recording environmental and ecological changes. In the formation of annual growth rings that can be precisely dated, tree-ring data are suitable to reconstruct past ecological and/or climate variability (e.g., Schweingruber 1996; Briffa et al. 1998a). Using different tree-ring parameters, like ring width, maximum latewood density, or variations of stable isotopes in wood cellulose, can provide proxies sensitive to different climate elements and seasons.

From an ecological perspective, the investigation of stable isotopic variations in tree rings ($\delta^{13}C$, $\delta^{18}O$, $\delta^{2}H$, $\delta^{15}N$) can help to disentangle climate-driven changes on the tree level (e.g., Saurer et al. 2003, 2004; McCarroll et al. 2009; Gagen et al. 2011). An increasing number of studies from the TP-Himalayan region have shown the tremendous potential of tree-ring based climate reconstructions to quantify regional climate and ecological variations (e.g., Bräuning and Mantwill 2004; Yadav et al. 2011; Grießinger et al. 2011; Sano et al. 2012; He et al. 2013a, b; Yang et al. 2014; Wernicke et al. 2015). In this chapter, we do not attempt to provide a complete review on tree-ring based climate reconstructions from the TP. We rather highlight recent findings on hydroclimatic changes on the very humid and sensitive southeastern TP. In addition, we compare regional climate reconstructions with changes in the cryosphere to unravel the interplay between climate change and glacier fluctuations (Hochreuther et al. 2015; Loibl et al. 2014, 2015). Finally, we discuss evidence for ecological changes in tree response to environment and vegetation dynamics in sensitive vegetation zones.

17.2 Trees as Archives of Past Climate and Landscape Changes

Landscapes on the TP are currently undergoing considerable changes as a response to climate warming. Monsoonal glaciers have suffered from substantial mass loss during the last decades (Bolch et al. 2012; Yao et al. 2012; Zhang et al. 2013). For the past centuries, glacier moraines can be used as witnesses of former ice extents. For that purpose, various dating techniques like cosmogenic nuclides (esp. ^{10}Be) and radiocarbon dating of organic compounds (^{14}C) have been widely applied (see Yang et al. 2008; Xu and Yi 2014 for comprehensive overviews). Even though these techniques were applied widely for moraine dating, they lack in dating precision on various time scales (Geyh 2005). Dendrochronology provides very precise dating control of climatic variations and landscape dynamics and is a very helpful method for glacier extent reconstruction if a former glacier advance reached below the upper tree line. Trees are tilted or destroyed by advancing ice mark periods of glacier advances, while trees growing on moraine crests may be used to provide minimum dates for glacier retreat (Bräuning 2006). The limited number of existing dendroglaciological studies that have yet been carried out on the southeastern TP indicate a strong spatial difference between study regions.

Besides climatic conditions, glacier dynamics depend on relief parameters, especially size and steepness of the ablation area and the surrounding slopes, as well as on size and shape of the accumulation area (Scherler et al. 2011). Hence, occurrence of moraine stages may vary according to glacier aspect, size, and topography. Beside the complex topographic conditions, climatic gradients play a modifying role for glacier mass balances. For example, the amount of precipitation (Fig. 17.1), the ratio of liquid to solid precipitation, and the dates of monsoon onset and cessation lead to changes in glacier surface albedo. The interference of these factors

increases potential errors when comparing local glacier fluctuations over large distances. Thus, attempts to reconstruct regional glacier chronologies should be based on climatically homogenous settings.

By using remote-sensing techniques, Loibl et al. (2014) analyzed 1964 glaciers on the southeastern TP regarding past- to present-day equilibrium-line altitude (ELA) changes. They found that local variations of ELA positions are mainly depending on the size of the accumulation area and on glacier size in a nonlinear way. The majority of glaciers on the southeast TP are north oriented, and their terminal positions descent considerably lower down than those of glaciers of any other direction, underlining the importance of exposition by reducing direct solar insolation. The cases of Xinpu and Gongpu glaciers provide excellent examples: both descent from Mt. Pulongu (6,300 m a.s.l.) in opposite directions (S/N) and have only slightly differing accumulation area sizes. However, the recent glacier termini are located in significantly different elevations of 3,300 m and 3,900 m, respectively (Hochreuther et al. 2015).

Glacier studies on the southeastern TP covering the last millennium and thus including the so-called Little Ice Age (LIA, ca. 1450–1800 A.D.; Bradley and Jones 1993; Wanner et al. 2008) are rare. ^{14}C ages of tilted or killed trees embodied in terminal moraines have been used to date glacier advances. In contrast, dendrochronological techniques mostly focus on glacier retreat dates using the maximum age of in situ living trees covering the respective landforms (for methods see Yang et al. 2008 for an overview of studies). The majority of LIA maximum advance moraines date to 1760 A.D. ± 20 years (Fig. 17.3a), likely marking the end of the LIA on the southeastern TP. Moraines of former advance phases are rarely preserved, as they were often impacted during younger readvance phases. Older LIA stages can best be observed by multilobate glacier settings (e.g., Xinpu or Zepu, see Loibl et al. 2015 for details). In equally rare cases, single trees have been found able to survive minor glacier readvances, offering the chance to date these via formation of reaction wood by tilting or by the occurrence of frost rings (e.g., Bräuning 2006). Conclusively, three major glacier retreat phases can be distinguished since the beginning of the LIA: (i) prior to 1540, (ii) predating 1630, and (iii) are treat prior to 1740 which marked the major LIA advance phase. Interestingly, the dated moraines at the western and eastern margins of the Nyainqêntanglha Range (Xuequ, Xincuo, Arza, see Fig. 17.2) exhibit considerably younger ages (1885, 1876, and 1833, respectively).

Summer precipitation serves as the major mass gain for the monsoonal temperate glaciers on the southeastern TP and has been found to be the most influential climatic variable for local glacier mass balance (e.g., Zhang et al. 2013). Hence, variations in annual or summer precipitation significantly contribute to glacier fluctuations. However, only very few precipitation reconstructions are currently available for this very humid region. A reconstruction of August precipitation anomalies from the southern TP (Grießinger et al. 2011, Fig. 17.3b) exhibits continuously high-precipitation levels throughout the LIA, covering periods of glacier advance and glacier meltdown. Thus, summer precipitation alone seems not the only controlling factor for variations of glacier length of monsoonal temperate glaciers.

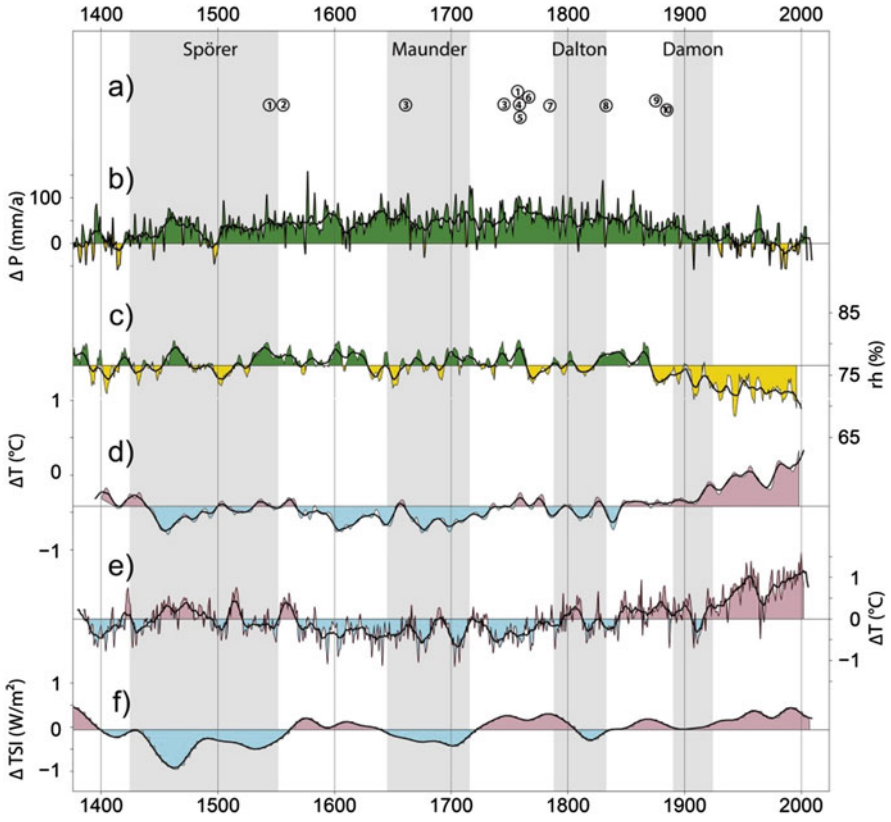

Fig. 17.3 Glacier fluctuations on the southeastern Tibetan plateau (TP) compared to regional and global climate reconstructions. (**a**) Minimum moraine ages of glacier advance phases during the Little Ice Age. Numbers refer to local glaciers mapped in Fig. 17.2, glaciers 1 and 3 exhibit multiple stages/lobes. (**b**) summer precipitation anomalies for the southern TP (Grießinger et al. 2011). (**c**) summer relative humidity on the eastern TP (Wernicke et al. 2015). (**d**) northern hemispheric temperature anomalies (Shi et al. 2013) (**e**) August temperature on the southeastern TP (Zhu et al. 2011). (**f**) global total solar irradiance (TSI, Steinhilber et al. 2009). *Gray vertical bars* indicate periods of reduced solar activity

A comparison of the moraine ages to reconstructions of relative humidity (Wernicke et al. 2015, Fig. 17.3c) reveals no direct relationship between glacier retreat and humidity. Regardless of glacier size and aspect, all minimum ages of glacier retreats from major advance stages during the last centuries coincide with episodes of above-average northern hemispheric annual temperatures (Shi et al. 2013, Fig. 17.3d). The dependency of glacier length to annual temperature has been reported on a global scale (e.g., Oerlemans 2005). Since the relationship between climate and glacier fluctuations is complex, annual temperature proves to have an integral function; though colder temperatures in single years do not necessarily cause a mass gain for glaciers due to the possibility of reduced precipitation or

moisture input, a series of consecutive cold years will generally result in a positive mass balance.

Reconstructions of August temperature based on maximum latewood density reflect variations of climate during the summer monsoon period (Fig. 17.3e). However, summer climate does not have the integral character of annual temperature since it does not capture the considerable variance of spring and early summer climate (Bolch et al. 2010). Depending on other factors, like monsoon onset or total precipitation amount, the impact of August temperatures on glacier mass balance varies considerably (Mölg 2012). A direct relationship, not considering other relevant factors, is therefore statistically improbable. Total solar irradiance (TSI, Fig. 17.3f) plays a key role in determining north hemispheric temperature. Nonetheless it cannot fully explain glacier fluctuations on the TP during the LIA. Other factors, like, e.g., volcanic activity (Briffa et al. 1998b; Loibl et al. 2015), may be masking the relationship between TSI and surface climatic elements at a local site. Thus, the relationship of TSI and glacier fluctuations is characterized by feedback mechanisms. The period of increased solar irradiance in the early eighteenth century induced a global temperature rise and initiated the termination of the last major phase of the LIA. This is documented by a clustering of dating results of major moraine stages in the late eighteenth century (Fig. 17.3a).

A parallel increase/decrease of temperature and precipitation would lead to a negative mass balance of monsoonal glaciers and hence to a faster back wasting of glaciers on the southeastern TP. Negative temperature excursions lasting over decades, however, set the frame for glacier advances, due to a lowering of the ELA and consequently a surplus of solid precipitation (Bolch et al. 2010). This relationship is also valid in the reverse case, and the recent ELA rise is widely regarded as the main reason for the recent glacier retreat. It was shown that these processes cease at elevations above 5,000 m a.s.l. (Qin et al. 2009). The majority of the monsoonal temperate glaciers currently have lower ELA positions, with lowest ELA altitudes in the southeastern TP (Loibl et al. 2014). As a consequence, the monsoonal temperate glaciers are highly sensitive to changes in temperature and moisture. They are advancing during cool and summer moist periods that very likely have prevailed during most parts of the LIA.

17.3 Tree Responses to Long-Term Environmental Trends

In the former section we discussed tree-ring evidence for reconstructing historic climate changes. However, also other ecological trends may have an impact on tree growth and ecological reactions of physiological processes as they may be recorded by stable isotope variations in annually formed tree rings. From a dendroecological perspective, variations in tree-ring $\delta^{13}C$ are potential indicators of changes of the environmental and ecophysiological conditions during tree growth. The plant physiological background underlying stable carbon isotope variations in tree rings has been thoroughly investigated during the recent decades and is well understood (e.g., Seibt et al. 2008; Leavitt 2010; Gessler et al. 2014). Since the major carbon source for terrestrial plants is atmospheric CO_2, the "storage" of environmental

information in tree-ring $\delta^{13}C$ is mainly controlled by processes on leaf-level (Gessler et al. 2014). Therefore, any superposed change of the $^{13}C/^{12}C$ relationship of atmospheric CO_2 will lead to substantial changes of tree-ring $\delta^{13}C$. Since the late 1950s high-precision measurements reported a strong increase in atmospheric CO_2 from 316 ppm in 1959 to 350 ppm in 2014 due to fossil fuel combustion (Keeling et al. 2005; www.esrl.noaa.gov/gmd/ccgg/trends, Fig. 17.4). Parallel with this increase in $CO_{2\,ATM}$ is the depletion in atmospheric $\delta^{13}C$, leading to a shift in the $^{13}C/^{12}C$ relationship in atmospheric CO_2 and hence a change of $\delta^{13}C$ during carbon fixation (Friedli et al. 1986; Gessler et al. 2014).

Stable carbon isotope ratios ($\delta^{13}C$) in tree rings from trees growing at high-elevation sites in the subhumid eastern TP show substantial linkages to local climate, albeit species-specific changes in their long-term trends are obvious (Grießinger 2008). Figure 17.4 shows a comparison of spruce (*Picea balfouriana*) and juniper (*Juniperus tibetica*) $\delta^{13}C_{ATMcorr}$-variations from a site located in 4,400 m elevation near Qamdo. During the preindustrial period prior to 1850, both time series show a high variability and a slightly decreasing long-term trend in $\delta^{13}C$ until the mid-nineteenth century, which is stronger for juniper (−0.2‰) than for spruce (−0.06‰). After 1850, a distinctive but tree-species strengthening in this negative $\delta^{13}C_{tree\text{-}ring}$ trend can be observed. The obvious tipping point for the onset of the maximum decrease rate can be dated to the beginning of the twentieth century, which is consistent to findings of studies from other regions (Marshall and Monserud 1996; McCarroll and Loader 2004; Treydte et al. 2006; Knorre et al. 2010). Surprisingly, this decrease in $\delta^{13}C_{tree\text{-}ring}$ is much stronger in spruce (−2‰) than in juniper trees (−0.5‰). Similar absolute values of a 1–2‰ decrease in $\delta^{13}C_{tree\text{-}ring}$ since 1800 were also found in the mentioned studies, although none of them compared two tree species at one site simultaneously. Our findings clearly indicate a species-dependent response towards changes of environmental conditions. Although this apparent trend cannot be related to a change in climate or rising atmospheric CO_2 content solely (Cernusak et al. 2013; Gessler et al. 2014), it is obvious that tree species on the TP are facing fundamental ecophysiological responses through climate change. In fact, rising CO_2 will, e.g., lead to an increase in leaf-level discrimination through stomatal conductance, changes in the photosynthetic rate, or of intrinsic water-use efficiency (iWUE).

17.4 Dendroecological Evidence for Recent Environmental Changes

In the sections above, we used dendrochronological data to evaluate former environmental changes. However, trees are also recorders of recent changes of environmental processes. In the final section, we want to have a closer look on applied fields of dendroecological studies on the landscape level as well as to recent trends in tree-ring research in areas beyond the tree limit. At first, however, we want to reflect how

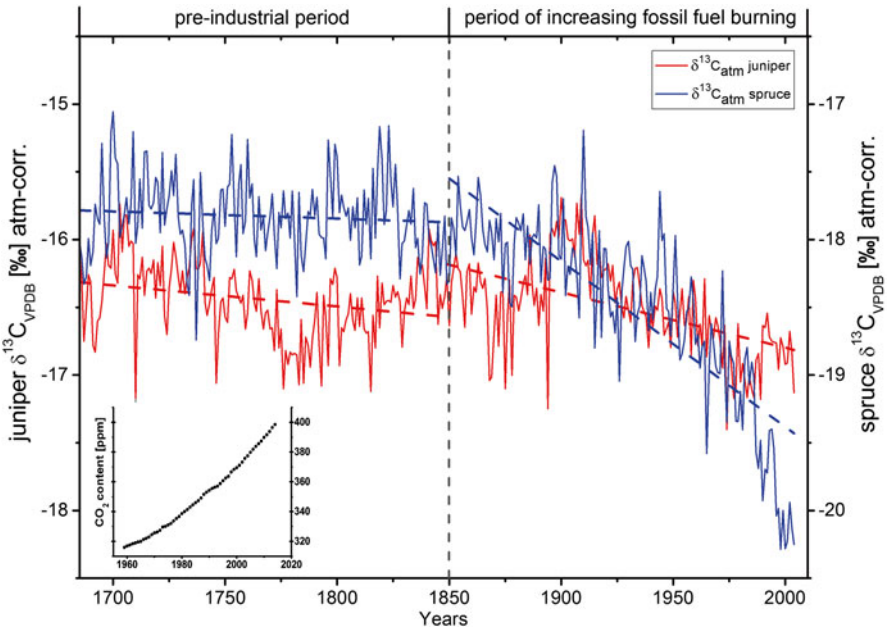

Fig. 17.4 $\delta^{13}C_{tree\text{-}ring}$ time series of juniper (*red line*) and spruce (*blue line*) tree rings from Qamdo/SE-Tibet. Both time series are corrected for an increasing atmospheric CO_2 content. *Dashed lines* indicate trends for the preindustrial period and since the beginning of industrialization around 1850, respectively. Inlay shows the annual atmospheric CO_2 content at Mauna Loa/Hawaii (Data from Tans & Keeling NOAA/ESRL; www.esrl.noaa.gov/gmd/ccgg/trends/)

short-term climatic signals are transferred into annual growth layers of wood, and how altitudinal gradients affect spatial patterns of tree response to regional climate.

17.4.1 Cambial Phenology of High-Elevation Conifer Species

On the humid southeastern Tibetan plateau where annual precipitation sums of more than 600 mm occur, species-rich subtropical mountain conifer forests are found, where the upper tree line (4,400 m a.s.l.) is formed by Smith fir (*Abies georgei* var. *smithii*) and blackseed juniper (*Juniperus saltuaria*) (Liang et al. 2011a). While ring-width variations at such sites are in general good recorders of temperature fluctuations, it is not known how interannual differences in climate and short-term climatic extreme events influence wood formation at such sensitive sites. High-resolution studies on cambial dynamics combining wood anatomical and cambial modeling approaches are able to shed more light on these important ecological questions. For example, a comparison of the cambial phenology of ca. 40 and 160-year-old Smith fir trees growing in 3,850 m elevation revealed that in 2008

cambial activity started around May 10 in young trees and was delayed to May 31 in old trees. The phase of cell enlargement of newly formed xylem cells ended around August 23, whereas thickening of secondary cell walls terminated end of September, so that the total period of wood formation varied from 5 months in young trees to 4 months in old trees, respectively (Liu et al. 2013, for location see Fig. 17.5). Cell formation rates were positively correlated to minimum air temperatures occurring around 1 week before cell formation, indicating that in cool and humid environments temperature is the dominant controlling factor for tree radial growth. Studying wood formation of Qilian juniper (*Sabina przewalskii*) along an altitudinal gradient in the semiarid northern Tibetan plateau, Wang et al. (2015) found that the initiation of the growing season in May was triggered by warmer spring (April) temperatures, whereas growth rates during the main growing season in June correlated with precipitation. The duration of the growing season at the upper tree line lasted between 41 and 51 days in 2011 and 2012, respectively. These findings indicate that tree-growth rates at high-elevation sites may be controlled by different climatic factors in different climate zones of the TP, and that response of forest ecosystems to climate change may be spatially very heterogeneous and complex.

17.4.2 Growth-Climate Relationships Along Climatic Gradients

To reconstruct past climate variations from tree-ring width, statistical calibration functions are established between available climate station data and tree-ring chronologies. After validation, these relationships are used in a transfer function to reconstruct paleoclimate (Fritts 1976), assuming that the current dependencies of growth on climate were also working during former periods. In mountain regions, topography has a strong impact in modifying the regional climatic regime (Thomas and Herzfeld 2004), so that tree-growth relationships to climate may vary with elevation. However, the degree to which elevation-dependent climatic gradients impact climate-growth relations seems to be controlled by the overall climate regime. Figure 17.5 illustrates examples of juniper chronologies from four study areas experiencing different moisture conditions. At each study site, two well-replicated ring-width chronologies of juniper trees were developed. Climate data from the next climate stations were used to establish correlation functions between ring width and precipitation and temperature during a 15-month time window considering a period from July of the previous growing period until September of the current growing season.

In the semiarid steppe forests at Dulan on the northern TP, mean annual precipitation is 212 mm, showing a high interannual variability. The regional forests are dominated by Qilian juniper (*Sabina przewalskii*) and are located close to the western distribution limit of forests. At Dulan, both established chronologies show a strong positive influence of precipitation during the growing season (Fig. 17.5), whereas temperature shows a negative correlation to tree growth, indicating that hot

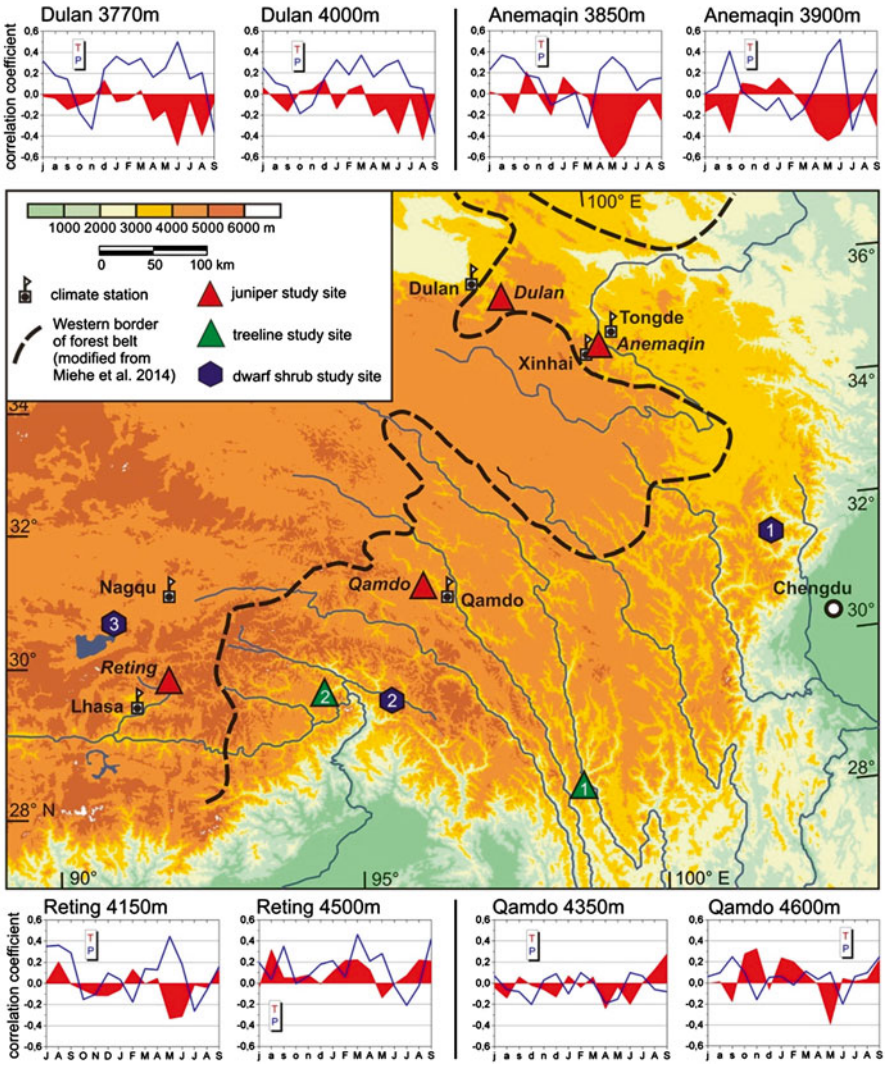

Fig. 17.5 Correlation coefficients between ring-width chronologies of junipers and temperature (*red*) and precipitation (*blue*) of nearby climate stations from July of the previous growing season to September of the current growing season. Symbols for previous year's month are written in lowercase letters. At Reting and in Anemaqin, regional means of two climate stations were used. At each study site (*red triangles*), juniper chronologies from different elevations were developed (site elevation indicated in correlation diagram). Tree-line studies (*green triangles*): (*1*) Baker and Moseley (2007); (*2*) Liang et al. (2011b); Shrub studies (hexagons): (*1*) Liang and Eckstein (2009); (*2*) Liang et al. (2015); (*3*) Liang et al. (2012)

and dry conditions during the growing period are causing stress to the trees. This climate-growth relationship is slightly weaker at the higher site, probably indicating that the degree of drought stress becomes less with increasing elevation. Nevertheless,

the general dependency of growth rates on available moisture is persistent, thus Qilian juniper has successfully been used to reconstruct regional precipitation variation over the last millennia (e.g., Zhang et al. 2003; Gou et al. 2010; Shao et al. 2010; Yang et al. 2014). In the less arid Anemaqin Mountains further southeast, mean annual precipitation is above 520 mm. The negative influence of summer temperature and the positive influence of summer precipitation on tree growth still remain (Gou et al. 2010; Wischnewski et al. 2013), although the signal is restricted to a smaller seasonal window during the early growing season in May and June.

In the humid eastern and southern margins of the TP, altitudinal forest belts become more species-rich and complex, and hence temperature topography plays a more differentiating role in modifying growth-climate relationships (Bräuning 1994; Fan et al. 2009). Juniper (*Juniperus tibetica*) trees at site Qamdo growing at the upper tree line in 4,600 m altitude with about 540 mm mean annual precipitation show a higher temperature signal than trees growing at lower elevations. On the southern Tibetan plateau near Reting with a mean annual precipitation sum of around 400 mm, moisture availability during the pre-monsoon season from March to May has a positive impact on tree growth. At the lower study site, moisture availability throughout the year is of great importance (He et al. 2013b). Besides, high summer temperatures are negatively correlated with ring width at the lower site, whereas close to the upper tree line; this adverse effect reverses to a positive influence of temperature on tree growth, probably due to reduced evapotranspiration rates under cooler climatic conditions. Nevertheless, the major dependency of tree growth remains relatively weakly altered by altitudinal gradients (Liang et al. 2010; Li et al. 2012; He et al. 2013a), and thus well-replicated tree-ring width chronologies are able to preserve a species-specific regional climatic signal useful for climate reconstruction.

17.4.3 Tree Line Changes and Use of Dwarf Shrubs in Dendroclimatology

From the recessional trends of glaciers, ELAs as well as increasing trends of temperature and decreasing moisture (Fig. 17.3), one might expect a positive response of temperature-limited vegetation boundaries and an upward shift of tree-line position. On the Tibetan plateau, however, the position of the natural upper tree limit has been lowered considerably due to the impacts of fire and millennia-long grazing of sheep, goats, and yak by Tibetan herdsmen (Baker and Moseley 2007; Miehe et al. 2014). Thus, it is difficult to find upper tree limits with a natural transition between high-elevation forest and alpine vegetation. Hence, the number of tree-line dynamics studies is rather limited.

A recent advance of the upper tree limit was observed by comparison with historical photographs near Baima Xue Snow Mountain at the southeastern edge of the Tibetan plateau (Baker and Moseley 2007). However, it was difficult to ascertain whether the observed advancement of *Larix potaninii* var. *macrocarpa* trees into

alpine shrubland was primarily triggered by climate warming or regional land use change practices. In the humid southeastern TP, Liang et al. (2011b) analyzed seedling recruitment and dynamics of the local tree line formed by Smith fir (*Abies georgei* var. *smithii*). Although tree recruitment strongly accelerated after 1950 parallel to an increase in winter temperature, the position of the uppermost trees remained almost constant during the past ca. 200 years. However, given the lag response of tree line to climatic changes, an uplift of the upper tree limit might be expected if the climate warming trend continues.

Recent studies have revealed the potential of alpine dwarf shrub species for dendroclimatological analyses (for a recent summary, see Myer-Smith et al. 2015). In the humid southern Tibetan plateau, various species of *Rhododendron* form the understory of mountain forests, but numerous species are also found above the upper tree limit. Ring-width variations of the ca. 40–80 cm tall snowy rhododendron (*R. nivale*) were positively correlated with temperatures in July of the growing season and November before the growth year (Fig. 17.5). Warmer temperatures, snow protection, and less cold conditions in autumn seem to be favorable for dwarf shrub growth (Liang and Eckstein 2009). Another dwarf shrub widely distributed on the TP and the Himalayas, *Cassiope fastigiata*, shows distinct growth rings that can be synchronized among individuals in order to establish site temperature-sensitive ring-width chronologies, which are similar to neighboring ring-width chronologies from high-elevation sites (Liang et al. 2015; Fig. 17.5). More than 300-year-old individuals of Wilson juniper (*Juniperus pingii* var. *wilsonii*) growing in almost 4,800 m a.s.l. elevation near lake Nam Co in a continental climate respond positively to May and June precipitation and negatively to temperature, indicating that the local moisture conditions during the early growing season are of great importance at radiation-rich and windy sites on the TP (Liang et al. 2012; Fig. 17.5).

17.5 Conclusions

Tree rings offer widely distributed and precisely dated paleoclimate proxies across the Tibetan plateau and the surrounding high mountain regions, including the west Chinese mountain ranges along the eastern and southern margin of TP, the Himalayas, Karakoram, Hindu Kush, and Tian Shan. They provide centennial to multimillennial chronologies showing a species-specific response to climate that is determined by the climatic regime and the tree-ring parameter under consideration. Despite the long-lasting and intense human impact, the potential of dendrochronology to reconstruct long-term environmental trends as well as frequency and distribution of extreme climatic events is by far not exhausted. Trees are recorders of environmental change, providing unique opportunities to monitor climate changes and related ecosystem responses in vulnerable high mountain regions. Considering the high potential age of a so far still unknown number of dwarf shrub species, there seems to be good chance to extend existing dendroclimatological studies and

climate reconstructions into regions beyond the tree limit which characterize wide areas on the TP and the semiarid steppes of High Asia.

Acknowledgments We acknowledge the financial support by the German research foundation (DFG) priority program 1372 through the project "Monsoonal variations and climate change during the late Holocene derived from tree rings and glacier fluctuations" (BR 1895/21-1) and the German Federal Ministry of Education and Research (BMBF) through the project "Climate variability and landscape dynamics in southeast Tibet and the Eastern Himalaya during the Late Holocene: reconstructed from tree rings, soils, and climate modeling" (CLASH) within the joint project Central Asia – Monsoon dynamics and Geo-ecosystems (CAME). We furthermore acknowledge the collaboration and support of Liang Eryuan and Zhu Haifeng (Tibetan Plateau Institute, CAS, Beijing), Lily Wang (Institute of Geographical Sciences, CAS, Beijing), Yang Bao and He Minhui (Cold and Arid Regions Environmental and Engineering Research Institute, CAS, Lanzou), and Fan Zexin (Xishuangbanna Tropical Botanical Garden, CAS, Kunming).

References

Baker BB, Moseley RK (2007) Advancing tree line and retreating glaciers: implications for conservation in Yunnan, P.R. China. Arc Antarc Alp Res 39:200–209

Bolch T, Yao T, Kang S, Buchroithner MF, Scherer D, Maussion F et al (2010) A glacier inventory for the western Nyainqentanglha range and the Nam Co Basin, Tibet, and glacier changes 1976–2009. Cryosphere 4(3):419–433

Bolch T, Kulkarni A, Kääb A, Huggel C, Paul F, Cogley JG, Frey H, Kargel JS, Fujita K, Scheel M, Bajracharya S, Stoffel M (2012) The state and fate of Himalayan glaciers. Science 336(6079):310–314

Bothe O, Fraedrich K, Zhu X (2011) Large-scale circulations and Tibetan Plateau summer drought and wetness in a high-resolution climate model. Int J Climatol 31:832–846

Bradley RS, Jones PD (1993) 'Little Ice Age' summer temperature variations: their nature and relevance to recent global warming trends. The Holocene 3(4):367–376

Bräuning A (1994) Dendrochronology for the last 1400 years in eastern Tibet. GeoJournal 34(1):75–95

Bräuning A (2006) Tree-ring evidence of 'Little Ice Age' glacier advances in Southern Tibet. The Holocene 16(3):369–380

Bräuning A, Mantwill B (2004) Increase of Indian summer monsoon rainfall on the Tibetan plateau recorded by tree rings. Geophys Res Lett 31:L24205. doi:10.1029/2004GL020793

Briffa KR, Schweingruber FH, Jones PD, Osborn TJ, Harris IC, Shiyatov SG, Vaganov EA, Grudd H (1998a) Trees tell of past climates: but are they speaking less clearly today? Philos Trans R Soc Lond Biol Sci 353:65–73

Briffa KR, Jones PD, Schweingruber FH, Osborn TJ (1998b) Influence of volcanic eruptions on Northern Hemisphere summer temperature over the past 600 years. Nature 393(6684):450–455

Cernusak LA, Ubierna N, Winter K, Holtum JAM, Marshall JD, Farquhar GD (2013) Environmental and physiological determinants of carbon isotope discrimination in terrestrial plants. New Phytol 200:950–965

Fan Z, Bräuning A, Cao K, Zhu S (2009) Growth-climate responses of high-elevation conifers in the central Hengduan Mountains, southwestern China. For Ecol Manag 258:306–313. doi:10.1016/j.foreco.2009.04.017

Friedli H, Löscher H, Oeschger H, Siegenthaler U, Stauffer B (1986) Ice core record of the C/ C ratio of atmospheric CO in the two past centuries. Nature 324:237–238

Fritts HC (1976) Tree rings and climate. Academic, London

Gagen M, Finsinger W, Wagner-Cremer F, Mccarroll D, Loader NJ, Robertson I, Jalkanen R, Young G, Kirchhefer A (2011) Evidence of changing intrinsic water-use efficiency under rising atmospheric CO concentrations in Boreal Fennoscandia from subfossil leaves and tree ring δ C ratios. Glob Change Biol 17(2):1064–1072

Gessler A, Ferrio JP, Hommel R, Treydte K, Werner RA, Monson RK (2014) Stable isotopes in tree rings: towards a mechanistic understanding of isotope fractionation and mixing processes from the leaves to the wood. Tree Physiol 34(8):796–818

Geyh MA (2005) Handbuch der physikalischen und chemischen Altersbestimmung. WissenschaftlicheBuchgesellschaft, Darmstadt

Gou X, Deng Y, Chen F, Yang M, Fang K, Gao L, Yang T, Zhang F (2010) Tree ring based stream flow reconstruction for the Upper Yellow River over the past 1234 years. Chin Sci Bull 55:4179–4186

Grießinger J (2008) Untersuchungen zur Klimavariabilität auf dem Tibetischen Plateau – Ein Beitrag auf der Basis stabiler Kohlenstoff- und Sauerstoffisotopen in Jahrringen von Bäumen waldgrenznaher Standorte. Dissertation Universität Stuttgart, Schriften des Forschungszentrums Jülich. Reihe Energie & Umwelt/Energy& Environment 19

Grießinger J, Bräuning A, Helle G, Thomas A, Schleser G (2011) Late Holocene Asian summer monsoon variability reflected by δ18 O in tree-rings from Tibetan junipers. Geophys Res Lett 38(3):L03701

He M, Yang B, Bräuning A (2013a) Tree growth – climate relationships of *Juniperus tibetica* along an altitudinal gradient on the southern Tibetan Plateau. Trees 27:429–439

He M, Yang B, Bräuning A, Wang J, Wang Z (2013b) Tree-ring-derived millennial precipitation record for the southern Tibetan Plateau and its possible driving mechanism. The Holocene 23(1):36–45

Hochreuther P, Loibl D, Wernicke J, Zhu H, Grießinger J, Bräuning A (2015) Ages of major Little Ice Age glacier fluctuations on the southeast Tibetan Plateau derived from tree-ring-based moraine dating. Palaeogeogr Palaeoclimatol Palaeoecol 422:1–10

Immerzeel WW, Van Beek LPH, Bierkens MFP (2010) Climate change will affect the Asian water towers. Science 328(5984):1382–1385

Keeling CD, Piper SC, Bacastow RB, Wahlen M, Whorf TP, Heimann M, Meijer HA (2005) Atmospheric CO and CO exchange with the terrestrial biosphere and oceans from 1978 to 2000: observations and carbon cycle implications. In: Ehleringer JR, Cerling TE, Dearing MD (eds) A history of atmospheric CO2 and its effects on plants, animals and ecosystems. Springer, New York, pp 83–113

Knorre A, Siegwolf R, Saurer M, Sidorova OV, Vaganov EA, Kirdyanov AV (2010) Twentieth century trends in tree ring stable isotopes ($\delta^{13}C$ and $\delta^{18}O$) of *Larix sibirica* under dry conditions in the forest steppe in Siberia. J Geophys Res 115:G03002

Leavitt SW (2010) Tree-ring C–H–O isotope variability and sampling. Sci Total Environ 408:5244–5253

Li Z, Liu G, Fu B, Hu C, Luo S, Liu X, He F (2012) Anomalous temperature–growth response of *Abies faxoniana* to sustained freezing stress along elevational gradients in China's western Sichuan Province. Trees 26:1373–1388

Liang E, Eckstein D (2009) Dendrochronological potential of the alpine shrub Rhododendron nivale on the south-eastern Tibetan Plateau. Ann Bot 104:665–670

Liang E, Wang Y, Xu Y, Liu B, Shao X (2010) Growth variation in *Abies georgei* var. *smithii* along altitudinal gradients in the Sygera Mountains, southeastern Tibetan Plateau. Trees 24:363–373

Liang E, Liu B, Zhu L, Yin Z (2011a) A short note on linkage of climatic records between a river valley and the upper timberline in the Sygera Mountains, southeastern Tibetan Plateau. Glob Planet Chang 77:97–102

Liang E, Wang Y, Eckstein D, Luo T (2011b) Little change in the fir tree-line position on the south-eastern Tibetan Plateau after 200 years of warming. New Phytol 190:760–769

Liang E, Lu X, Ren P, Li X, Zhu L, Eckstein D (2012) Annual increments of juniper dwarf shrubs above the tree line on the central Tibetan Plateau: a useful climatic proxy. Ann Bot 109:721–728

Liang E, Liu W, Ren P, Dawadi B, Eckstein D (2015) The alpine dwarf shrub *Cassiope fastigiata* in the Himalayas: does it reflect site-specific climatic signals in its annual growth rings? Trees 29:79–86

Liu B, Li Y, Eckstein D, Zhu L, Dawadi B, Liang E (2013) Has an extending growing season any effect on the radial growth of Smith fir at the timberline on the southeastern Tibetan Plateau? Trees 27:441–446

Loibl D, Lehmkuhl F, Grießinger J (2014) Reconstructing glacier retreat since the Little Ice Age in SE Tibet by glacier mapping and equilibrium line altitude calculation. Geomorphology 214:22–39

Loibl D, Hochreuther P, Schulte P, Hülle D, Zhu H, Bräuning A, Lehmkuhl F (2015) Toward a late Holocene glacial chronology for the eastern Nyainqêntanglha Range, southeastern Tibet. Quat Sci Rev 107:243–259

Marshall J, Monserud R (1996) Homeostatic gas-exchange parameters inferred from 13C/12C in tree rings of conifers. Oecologia 105:13–21

Maussion F, Scherer D, Mölg T, Collier E, Curio J, Finkelnburg R (2014) Precipitation seasonality and variability over the Tibetan Plateau as resolved by the High Asia Reanalysis. J Clim 27:1910–1927

McCarroll D, Loader NJ (2004) Stable isotopes in tree rings. Quat Sci Rev 23:771–801

McCarroll D, Gagen MH, Loader NJ, Robertson I, Anchukaitis KJ, Los S, Young GHF, Jalkanen R, Kirchhefer A, Waterhouse JS (2009) Correction of tree ring stable carbon isotope chronologies for changes in the carbon dioxide content of the atmosphere. Geochim Cosmochim Acta 73(6):1539–1547

Miehe G, Miehe S, Böhner J, Kaiser K, Hensen I, Madsen D, Liu J, Opgenoorth L (2014) How old is the human footprint in the world's largest alpine ecosystem? A review of multiproxy records from the Tibetan Plateau from the ecologists' viewpoint. Quat Sci Rev 86:190–209

Mölg T, Maussion F, Yang W, Scherer D (2012) The footprint of Asian monsoon dynamics in the mass and energy balance of a Tibetan glacier. Cryosphere 6:1445–1461

Myers-Smith IH, Hallinger M, Blok D, Sass-Klaassen U, Rayback SA, Weijers SJ, Trant A, Tape KD, Naito AT, Wipf S, Rixen C, Dawes MAA, Wheeler J, Buchwal A, Baittinger C, Macias-Fauria M, Forbes BC, Lévesque E, Boulanger-Lapointe N, Beil I, Ravolainen V, Wilmking M (2015) Methods for measuring arctic and alpine shrub growth: a review. Earth Sci Rev 140:1–13

Oerlemans J (2005) Extracting a climate signal from 169 glacier records. Science 308(5722):675–677

Qin J, Yang K, Liang S, Guo X (2009) The altitudinal dependence of recent rapid warming over the Tibetan Plateau. Clim Chang 97(1–2):321–327

Sano M, Ramesh R, Sheshshayee MS, Sukumar R (2012) Increasing aridity over the past 223 years in the Nepal Himalaya inferred from a tree-ring $\delta^{18}O$ chronology. The Holocene 22(7):809–817

Saurer M, Cherubini P, Bonani G, Siegwolf R (2003) Tracing carbon uptake from a natural CO_2 spring into tree rings: an isotope approach. Tree Physiol 23:997–1004

Saurer M, Siegwolf RTW, Schweingruber FH (2004) Carbon isotope discrimination indicates improving water-use efficiency of trees in northern Eurasia over the last 100 years. Glob Chang Biol 10:2109–2120

Scherler D, Bookhagen B, Strecker MR (2011) Hillslope-glacier coupling: the interplay of topography and glacial dynamics in High Asia. J Geophys Res F: Earth Surface 116(2):1–21

Schweingruber FH (1996) Tree rings and environment. Dendroecology. Birmensdorf, Swiss Federal Institute for Forest, Snow and Landscape Research. Berne, Stuttgart, Vienna, Haupt. 609 pp

Seibt U, Rajabi A, Griffiths H, Berry JA (2008) Carbon isotopes and water use efficiency: sense and sensitivity. Oecologia 155:441–454

Shao X, Xu Y, Yin Z, Liang E, Zhu H, Wang S (2010) Climatic implications of a 3585-year tree-ring width chronology from the northeastern Qinghai-Tibetan Plateau. Quat Sci Rev 29:2111–2122

Shi F, Yang B, Mairesse A, von Gunten L, Li J, Bräuning A, Yang F, Xiao X (2013) Northern Hemisphere temperature reconstruction during the last millennium using multiple annual proxies. Clim Res 56(3):231–244

Shrestha UB, Gautam S, Bawa KS (2012) Widespread climate change in the Himalayas and associated changes in local ecosystems. PLoS ONE 7(5):e36741. doi:10.1371/journal.pone.0036741

Steinhilber F, Beer J, Fröhlich C (2009) Total solar irradiance during the Holocene. Geophys Res Lett 36(19):1–5

Tans P, Keeling R (2015) NOAA/ESRL www.esrl.noaa.gov/gmd/ccgg/trends/ and www.scrippsco2.ucsd.edu/

Thomas A, Herzfeld U (2004) Regeotop: new climatic data fields for east Asia based on localized relief information and geostatistical methods. Int J Climatol 24:1283–1306

Treydte KS, Schleser GH, Helle G, Frank DC, Winiger M, Haug GH, Esper J (2006) The twentieth century was the wettest period in northern Pakistan over the past millennium. Nature 440(7088):1179–1182

Wang B, Bao Q, Hoskins B, Wu G, Liu Y (2008) Tibetan Plateau warming and precipitation changes in East Asia. Geophys Res Lett 35(14):L14702

Wang Z, Yang B, Deslauriers A, Bräuning A (2015) Intra-annual stem radial increment response of Qilian juniper to temperature and precipitation along an altitudinal gradient in northwestern China. Trees Struct Funct 29:25–34

Wanner H, Beer J, Bütikofer J, Crowley TJ, Cubasch U, Flückiger J, Goosse H, Grosjean M, Joos F, Kaplan JO, Küttel M, Müller SA, Prentice IC, Solomina O, Stocker TF, Tarasov P, Wagner M, Widmann M (2008) Mid- to Late Holocene climate change: an overview. Quat Sci Rev 27(19–20):1791–1828

Wei Y, Fang Y (2013) Spatio-temporal characteristics of global warming in the Tibetan Plateau during the last 50 years based on a generalised temperature zone – elevation model. PLoS ONE 8(4):e60044. doi:10.1371/journal.pone.0060044

Wernicke J, Grießinger J, Hochreuther P, Bräuning A (2015) Variability of summer humidity during the past 800 years on the eastern Tibetan Plateau inferred from δ O of tree-ring cellulose. Clim Past 11:327–337

Wischnewski J, Herzschuh U, Rühland K, Bräuning A, Mischke S, Smol JP, Wang L (2013) Recent ecological responses to climate variability and human impacts in the Nianbaoyeze Mountains (eastern Tibetan Plateau) inferred from pollen, diatom and tree ring data. J Paleolimnol. doi:10.1007/s10933-013-9747-1

Xu X, Yi C (2014) Little Ice Age on the Tibetan Plateau and its bordering mountains: evidence from moraine chronologies. Glob Planet Chang 116:41–53

Yadav RR, Bräuning A, Singh J (2011) Tree-ring inferred summer temperature variations over the last millennium in western Himalaya, India. Clim Dyn 36:1545–1554. doi:10.1007/s00382-009-0719-0

Yang B, Bräuning A, Zhibao D, Ziyin Z, Jiao K (2008) Late Holocene monsoonal temperate glacier fluctuations on the Tibetan Plateau. Glob Planet Chang 60(1–2):126–140

Yang B, Qin C, Wang J, He M, Melvin TM, Osborn TJ, Briffa KR (2014) A 3,500-year tree-ring record of annual precipitation on the northeastern Tibetan Plateau. Proc Natl Acad Sci 111:2903–2908

You Q, Kang S, Pepin N, Flüge WA, Sanchez-Lorenzo A, Yan Y, Zhang Y (2010) Climate warming and associated changes in atmospheric circulation in the eastern and central Tibetan Plateau from a homogenized dataset. Glob Planet Chang 72(1–2):11–24

Yao T, Thompson LG, Yang W, Yu W, Gao Y, Guo X, Yang X, Duan K, Zhao H, Xu B, Pu J, Lu A, Xiang Y, Kattel DB, Joswiak D (2012) Different glacier status with atmospheric circulations in Tibetan Plateau and surroundings. Nat Clim Chang 2:663–667

Zhang Q, Cheng G, Yao T, Kang X, Huang J (2003) A 2,326-year tree-ring record of climate variability on the northeastern Qinghai-Tibetan Plateau. Geophys Res Lett 30(14):1739. doi:10.1029/2003GL017425

Zhang G, Kang S, Fujita K, Huintjes E, Xu J, Yamazaki T, Haginoya S, Wei Y, Scherer D, Schneider C (2013) Energy and mass balance of Zhadang glacier surface, central Tibetan Plateau. J Glaciol 59(213):137–148

Zhu H, Shao X, Yin Z, Xu P, Xu Y, Tian H (2011) August temperature variability in the southeastern Tibetan Plateau since AD 1385 inferred from tree rings. Palaeogeogr Palaeoclimatol Palaeoecol 305(1–4):84–92

Chapter 18
Spatially Variable Vegetation Greenness Trends in Uttarakhand Himalayas in Response to Environmental Drivers

Niti B. Mishra and Gargi Chaudhuri

Abstract Over the last few decades, Western Himalayas experienced high population growth and increase in exploitative land use practices. This trend coupled with influence of climatic variability has resulted in significant negative effects on vegetation cover and productivity. This study aims to understand the spatial patterns and severity of these impacts in Uttarakhand Himalayas. Specifically, the objectives of this study are twofold: first, to quantify interannual trends in vegetation greenness by conducting nonparametric Mann-Kendall trend analysis on MODIS-NDVI time series (2000–2014) and, second, to assess distribution of this trend with respect to land use land cover properties and elevation zones. The results show that out of the total vegetated area in Uttarakhand, 2,686.95 km^2 (5.69 %) showed changes in the vegetation greenness and 73.64 % of this change was significant negative trend (browning). While areas with <800 m elevation showed dominant browning, those between 800 and 1600 m showed significant positive trend (greening), and majority of areas >1600 m were characterized by browning trend. Majority of intensively cultivated irrigated croplands in the Himalayan foothills and areas around growing urban centers showed widespread browning, whereas areas of rainfed cultivation showed dominant greening. Browning was also dominant in closed needle leaf forests and alpine shrublands, except areas where human impacts has led to more mixed patterns. These results highlight previously unreported fine-scale spatial variations in vegetation productivity trend with respect to both elevation and LULC properties.

Keywords Vegetation trend • Uttarakhand Himalaya • MODIS-NDVI • Land cover • Land use • Elevation • Greening • Browning

N.B. Mishra (✉) • G. Chaudhuri
Department of Geography and Earth Science, University of Wisconsin-La Crosse, La Crosse, WI 54601, USA
e-mail: nmishra@uwlax.edu; nitibhushan.mishra@gmail.com

R.B. Singh et al. (eds.), *Climate Change, Glacier Response, and Vegetation Dynamics in the Himalaya*, DOI 10.1007/978-3-319-28977-9_18

18.1 Introduction

Mountain ecosystems in subtropical latitudes of Asia, such as the Himalayas, are important repository of biodiversity, water, and several other ecological resources (Singh and Singh 1987; Ives 2004). This region with its abundance of natural resource provides ecosystem services to millions of people living locally and in the Indo-Gangetic plains (Singh 2006). The Himalayan region is characterized by high relief, strongly structured climatic gradients and contains ecosystems that are understudied, ecologically sensitive, and vulnerable (Xu et al. 2009). Several recent climate studies in Himalayas have shown spatially variable but significant increase in temperature trend over the last three decades (Immerzeel et al. 2010; Shrestha et al. 1999). Increasing population, particularly in the Western Himalayas (e.g., Uttarakhand), has led to unprecedented resource exploitation unhindered by lack of sustainable environmental policies (Tiwari 2008; Pandit and Grumbine 2012; Semwal et al. 2004). Like other subtropical mountain systems, environmental changes in the Himalayas are generally linked with vegetation-related changes such as declining forest cover and biodiversity (Pandit et al. 2007; Xu et al. 2009; Tiwari 2008). Furthermore, in tropical mountain ecosystems, vegetation communities have been found to show higher sensitivity to climatic changes compared to their temperate counterparts (Gottfried et al. 2012; Walther et al. 2005). Thus, characterization of long-term vegetation trends for the Himalayan region can provide important understanding of vegetation responses to both environmental and anthropogenic drivers of change (Shrestha et al. 2012; Mishra and Chaudhuri 2015).

Field-based assessments of vegetation productivity and dynamics in mountain ecosystems are generally limited in scope and scale mainly due to the inaccessibility and logistical issues (Gottfried et al. 2012). Remote sensing-based vegetation monitoring overcomes these challenges and cannot only complement field data but also provide large spatial coverage (Lillesand and Kiefer 1994). For remote sensing of vegetation dynamics, satellite-derived vegetation indices such as the Normalized Difference Vegetation Index (NDVI) have been widely used because of its correlation with chlorophyll abundance and gross primary productivity (Goetz and Prince 1999; Myneni et al. 1995). Furthermore, several previous studies have utilized NDVI time series data such as from NOAA-AVHRR and MODIS in various ecosystems to describe temporal trends in vegetation productivity at regional scale by quantifying interannual and seasonal vegetation dynamics (Barichivich et al. 2014; Myneni et al. 1997). These studies have confirmed that NDVI trends were influenced by changes in climate and/or land cover properties (Mishra and Chaudhuri 2015; Shrestha et al. 2012).

Changes in vegetation productivity and/or cover can be influenced by climatic fluctuation (e.g., rainfall, temperature), disturbance (e.g., fire regime), and anthropogenic activities (e.g., urbanization, agricultural expansion). Characterization of long-term vegetation greenness trends is vital for detecting early warning signals of degradation or improvement in vegetation conditions, as well as its specific locations (Menzel 2002). This study focuses on the state of Uttarakhand in northern

India and aims to characterize the spatial distribution of interannual vegetation greenness trends using 14-year MODIS-NDVI time series data. Furthermore, the spatial association of detected trend is examined with elevation gradient and LULC properties. Finally, the causation behind the detected distribution of vegetation greenness trend has been examined using existing literature and ancillary information.

18.2 Study Area

Uttarakhand has a total area of 53,484 km^2 and shows great variation in elevation, climate, and vegetation properties (Fig. 18.1). Majority of the study area is mountainous (93 %) of which 65 % is covered by forests (Negi 2009). Uttarakhand receives a mean annual rainfall of 1546 mm, of which more than two-thirds is during monsoon season (June–September). The spatial distribution of rainfall shows marked variation due to steep altitudinal gradient from south to north. The vegetation type changes with altitude, for example, the region above 4800 m is non-vegetated, the region between elevations of 3000 and 4800 m is occupied by

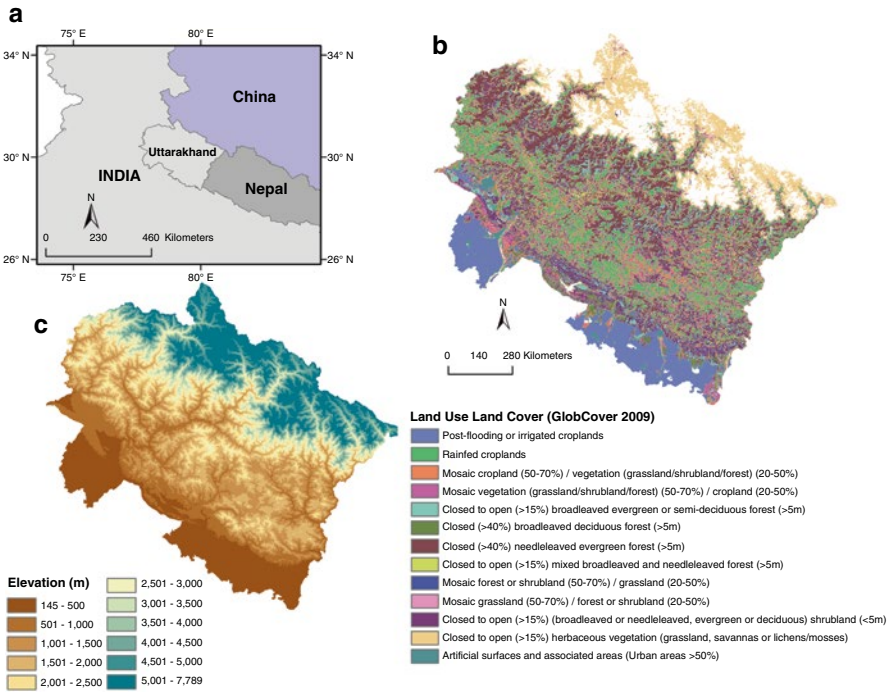

Fig. 18.1 (**a**) Location of Uttarakhand in India; (**b**) land use land cover map of Uttarakhand (Source: GlobCover 2009); and (**c**) elevation distribution in Uttarakhand derived from ASTER DEM

Western Himalayan alpine shrubs and meadows, and the region below tree line is dominated by the temperate Western Himalayan subalpine conifer forest. At 3000–2600 m elevation, they transition to temperate Western Himalayan broadleaf forest which lie between 2600 and 1500 m. The Himalayan subtropical pine forests dominate the region below 1500 m of elevation (Singh and Singh 1987). The lowland areas of Uttarakhand are dominated by the Upper Gangetic Plain moist forests and Terai-Duar savannas, and majority of these vegetation types have been cleared for agriculture with few remaining patches (Tiwari 2000). The highly biodiverse forested area in Uttarakhand is protected and conserved by the state and national government in forms of six national parks, six wildlife sanctuaries, and two conservation reserves. This state is also one of the major contributors of the tourism sector in India, attracting significant numbers of domestic and international tourists (Phukan et al. 2012).

18.3 Data and Methods

The study used MODIS MO13Q1 16-day composite 250 m NDVI product (Collection 5) acquired from NASA (www.reverb.echo.nasa.gov). The product is developed from atmospherically corrected bidirectional surface reflectance and has been masked for water, clouds, heavy aerosols, and cloud shadows (Huete et al. 2002). Fourteen years of NDVI data is utilized from scenes of day 81, year 2000, to day 65, year 2014. The study area is located at the intersection of four MODIS tiles (h24v05, h24v06, h25v05, and h25v06) that are mosaicked and reprojected to UTM projection (Zone 44N), the pixel spatial resolution is resampled to 300 m, and the images are cropped along the political boundary of Uttarakhand. Elevation is derived from ASTER GDEM2 elevation product that provides 30 m spatial resolution and includes substantial improvements from its predecessor GDEM1 (Tachikawa et al. 2011). Land use land cover information for Uttarakhand is derived from GlobCover 2009 product (Bontemps et al. 2011).

As a preprocessing step, the NDVI time series is de-noised using the Savitzky-Golay procedure to remove the impacts of contamination such as clouds. The MOD13 pixel reliability layer is used to weight data in the temporal filtering. The de-noised NDVI time series is used to calculate mean annual NDVI for each pixel by averaging the 23 composite images for each year. This procedure resulted in 14 mean annual NDVI images. For detecting interannual vegetation trends, Mann-Kendall trend analysis is utilized (Mann 1945; Kendall 1938) which has been increasingly employed for characterizing trends as it is especially suitable for small sample sizes and is less affected by outliers (Yue and Wang 2004). Mann-Kendall tau (τ) coefficient is a nonparametric hypothesis to test for statistical dependence of observations from two random variables X and Y. For a time series, assume that x_i and x_j are the observations at times i and j, respectively, and then any pair of observations $((i, x_i)$ and $(j, x_j))$ are said to be concordant if both $i > j$ and $x_i > x_j$ or if both $i < j$ and $x_i < x_j$. They are said to be discordant if $i < j$ and $x_i > x_j$ or if $i > j$ and $x_i < x_j$.

If $i \neq j$ and $x_i = x_j$, the pair is neither concordant nor discordant, and then Mann-Kendall tau (τ) is then simply the relative frequency of concordant minus the relative frequency of discordances and can be calculated as

$$\tau = \frac{\sum_{i=1}^{n-1} \sum_{j=i+1}^{n} \sin(xi - xj)}{C_2^n} \tag{18.1}$$

and

$$\sin(xi - xj) = \begin{cases} 1 \, if \;\; xi - xj < 0 \\ 0 \, if \;\; xi - xj = 0 \\ 1 \, if \;\; xi - xj > 0 \end{cases} \tag{18.2}$$

where C_2^n is the total number of pairwise combinations of n observations.

Ranging from −1 to 1, $\tau = 1$ means consistently increasing trend and $\tau = -1$ consistently decreasing trend; τ coefficient is expected to be zero if no trend exists. The significance level of the trend can be evaluated by using p value (Kaspersen et al. 2011). To understand the elevation and land use land cover-specific trends in vegetation productivity, the statistically significant Mann-Kendall trend values are further spatially analyzed with respect to 6 altitudinal zones and 13 vegetated land use land cover classes (Fig. 18.1b) for Uttarakhand.

18.4 Result and Discussion

18.4.1 Distribution of Trend Considering Altitudinal Gradient

Spatial distribution of statistically significant trend (p values <0.01) in vegetation greenness over the 14-year study period is visualized in Fig. 18.2. Out of the total vegetated area in Uttarakhand (47,177.92 km^2), 2,686.95 km^2 (5.69 %) showed statistically significant trend. Out of this, the proportions of areas with negative and positive trend were 73.64 % and 26.36 %, respectively (Table 18.1). Figure 18.3 shows distribution of these trends in overall greenness with respect to six altitudinal zones. More than 90 % of the area with observed significant trend is located below 3200 m elevation, and a very small fraction of total area showed significant trend in greenness above 3200 m (Fig. 18.3). Table 18.1 shows proportion of positive and negative overall greenness within each altitudinal zones. Vegetation greenness trend shows spatially contrasting patterns among the six altitudinal zones. For example, the region below the elevation of 800 m has dominant negative trend, whereas the region between elevations of 800–1600 m shows dominant positive trend. The region above 1600 m shows dominant negative trend in interannual greenness. The overall results also suggest that with increasing elevation, high statistical significance decreases considerably (Fig. 18.3).

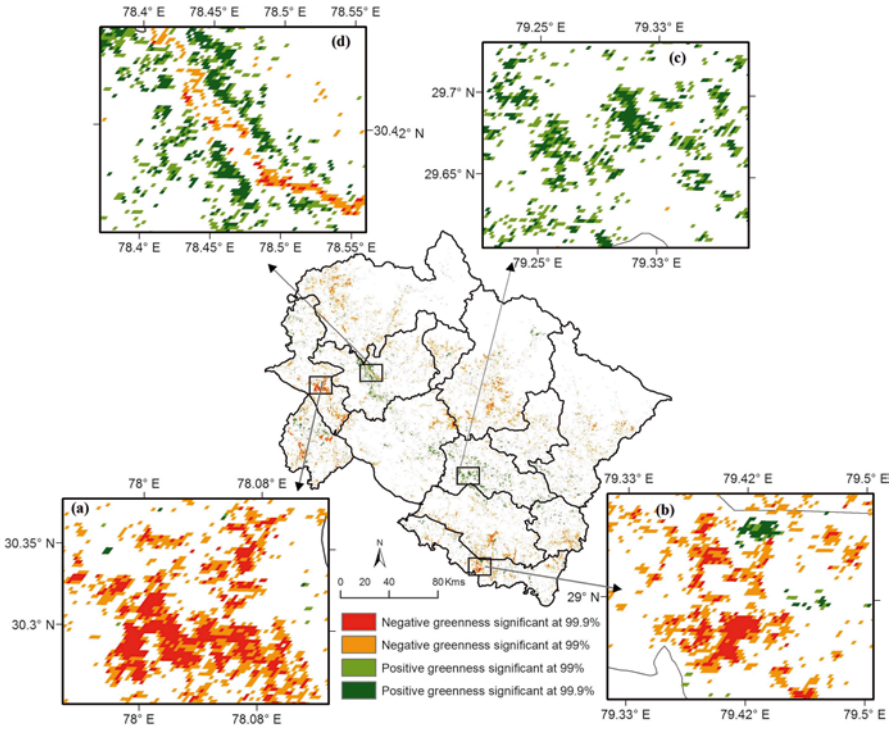

Fig. 18.2 (**a**) Map of Uttarakhand illustrating Mann-Kendall trend of overall greenness from 2000 to 2014 for pixels with high statistical significance. *Inset* maps highlight selected portions of the main map displaying different trends in overall greenness

18.4.2 Distribution of Trend Considering LULC Properties

Results show high spatial variation in land use land cover class-specific vegetation greenness trend (Fig. 18.2). The areal distribution of land use land cover-specific interannual greenness trend (either positive or negative) for Uttarakhand Himalayas using the GlobCover 2009 product is shown in Table 18.1. Majority of large urban centers in Uttarakhand (e.g., Dehradun, Haldwani, Roorkee, Haridwar) are located in the plains and Himalayan foothills due to ease of transport and accessibility. The areas in and around these urban centers (examples shown in Fig. 18.2a, b) show dominant negative trend (i.e., browning) for the study period (Table 18.1). During the last few decades, Uttarakhand Himalayas has experienced rapid urbanization, especially since 2000 when Uttarakhand gained statehood, which triggered multiple lands clearing for civil construction and infrastructural development projects. The total population of the state increased by 15.83 % between 2001 and 2011, and urban population increased from 25.67 % in 2001 to 30.23 % in 2011 (India 2011). Recent estimates suggest that 5.85 % of the natural forested area was lost due to urban growth in the state between 1981 and 2011 (Tiwari and Joshi 2012). Therefore,

Table 18.1 Trend distribution considering different LULC classes in Uttarakhand

Land use land cover class	Total area (km^2)	Areas with significant trend (km^2)		
		Total	Negative	Positive
Post-flooding or irrigated croplands (or aquatic)	5,506.56	489.96	378.45	111.51
Rainfed croplands	8,161.20	396.99	131.22	265.77
Mosaic cropland (50–70 %)/vegetation (grassland/shrubland/forest) (20–50 %)	3,741.75	237.60	109.8	127.8
Mosaic vegetation (grassland/shrubland/forest) (50–70 %)/cropland (20–50 %)	3,850.92	157.41	78.84	78.57
Closed to open (>15 %) broadleaved evergreen or semi-deciduous forest (>5 m)	1,950.48	117.72	114.84	2.88
Closed (>40 %) broadleaved deciduous forest (>5 m)	2,094.12	96.84	80.19	16.65
Closed (>40 %) needleleaved evergreen forest (>5 m)	7,327.08	631.17	595.44	35.73
Closed to open (>15 %) mixed broadleaved and needleleaved forest (>5 m)	2,881.17	161.46	137.25	24.21
Mosaic forest or shrubland (50–70 %)/grassland (20–50 %)	311.85	14.94	11.34	3.6
Mosaic grassland (50–70 %)/forest or shrubland (20–50 %)	474.12	30.15	27.9	2.25
Closed to open (>15 %) (broadleaved or needleleaved, evergreen or deciduous) shrubland (<5 m)	5,584.77	257.49	232.47	25.02
Closed to open (>15 %) herbaceous vegetation (grassland, savannas, or lichens/mosses)	5,097.24	27.90	16.56	11.34
Artificial surfaces and associated areas (urban areas >50 %)	197.01	67.32	64.62	2.7
Total	47,178.27	2,686.95	1,978.92	708.03

the browning trend can be directly attributed to conversion of forest or agricultural land to urban cover.

Outside the urban centers, agriculture is the most significant economic activity with rainfed agriculture being practiced in terraced fields (Mittal et al. 2008). Majority of these rainfed agricultural areas show positive greenness trend (Table 18.1 and Fig. 18.2c). On the contrary, the plain and Terai areas of Uttarakhand (below 800 m elevation) are intensively irrigated (produce two crops per year) and show significant browning trend (Table 18.1). To understand the causation behind these greening and browning will require further analysis of spatiotemporal pattern of rainfall distribution and trend of agricultural production in the irrigated and rainfed cropped areas.

Over the last few decades, infrastructure development in the form of dam construction has been an important driver of land use land cover change in Uttarakhand

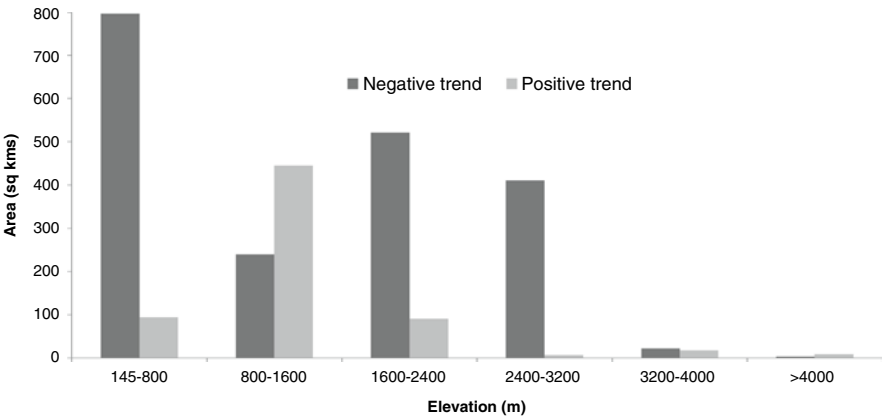

Fig. 18.3 Overall greenness trend distribution at different elevation gradients

Himalayas, and this trend is expected to continue as several major hydel power projects are to be constructed within next decade (Pandit and Grumbine 2012). Besides land use land cover change, the construction of dams in seismically active Himalayas has been much debated, though with some support due to the advantages of increased irrigation and hydel power generation (Rana et al. 2007). The result of this study reveals highly contrasting and spatially complex patterns in seasonal greening and browning trends in and around areas where dams are constructed. An example of spatially contrasting trend is shown in Fig. 18.2d which highlights the changing interannual vegetation greenness trend around the Tehri dam in the Tehri Garhwal district. A large low-lying part of the area shows negative trend due to the submergence of pre-2005 agricultural and forested land due to the filling of the Tehri dam reservoir. Studies have reported that more than 50 km^2 area was submerged due to the reservoir filling. On the contrary, the area upslope of this submerged zone depicted positive trend. This could be attributed to the indirect impact of the resulting reservoir that could have potential impacts on the microclimate (e.g., increased moisture availability) and vegetation productivity.

Among different forest types, majority of the area covered by closed needleleaved evergreen forest shows dominant negative trend (browning) for the study period (Fig. 18.4 and Table 18.1). Interestingly, majority of these brownings in closed needleleaved evergreen forest are located inside protected areas (Binsar Wildlife Sanctuary, Govind Pashu Vihar Wildlife Sanctuary) that are far from existing human settlements/roads. Thus, the negative trend can be attributed to the changing precipitation and/or temperature pattern in the region. Previous studies have reported increase in average temperature in subtropical mountain systems including the Himalayan system over the last few decades following the average global warming trend (Immerzeel et al. 2010; Rangwala and Miller 2012). Existing literature on the relationship between climate and vegetation in mountain ecosystems suggests that increasing temperature combined with no gain in precipitation has negative impact on vegetation productivity in subtropical mountains, a

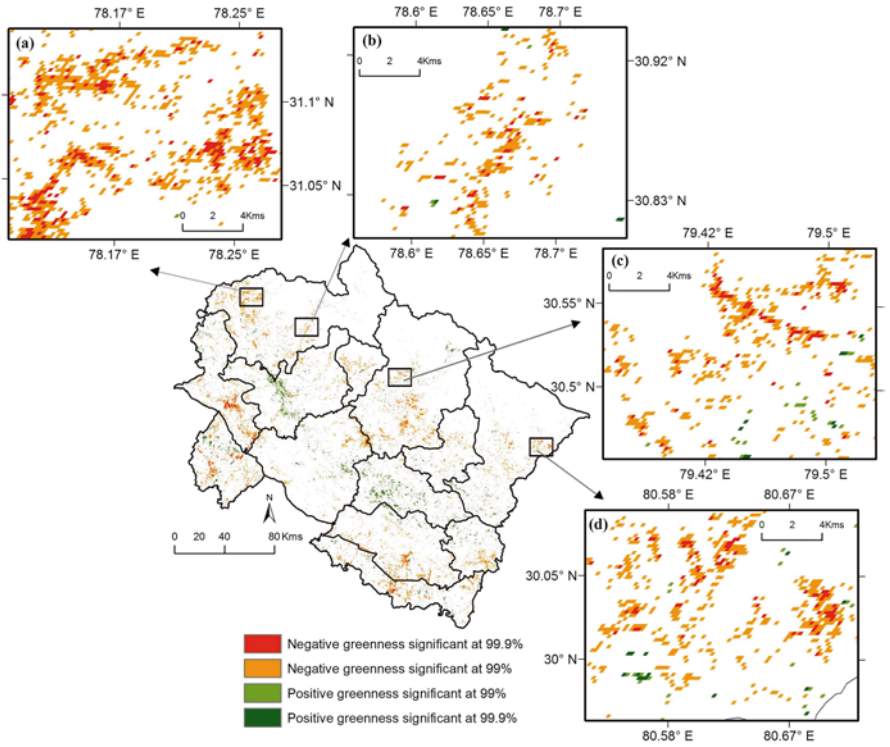

Fig. 18.4 Map of Uttarakhand illustrating Mann-Kendall trend of overall greenness from 2000 to 2014 for pixels with high statistical significance. Inset maps highlight selected portions of the main map displaying different trends in overall greenness dominantly the result of climatic factors

phenomenon widely known as *temperature induced moisture stress* (D'Arrigo et al. 2004) which could be the cause behind observed vegetation browning in high altitude environments, including the Uttarakhand Himalayas (Krishnaswamy et al. 2014; Pounds et al. 1999; de Jong et al. 2013). Besides forested area, significant percent of area showing significant trend in greenness also falls under closed to open shrubland, and majority of it is browning trend (Table 18.1).

18.5 Conclusion and Future Perspectives

The present study utilized satellite-derived time series data on vegetation greenness to characterize seasonal trends in vegetation over the Uttarakhand Himalayas and examine trend distribution across the elevation gradients and LULC types. We detected very interesting elevation and LULC-specific spatiotemporal patterns in seasonal trend distribution, which is the manifestation of LULC changes and/or changing climatic drivers (e.g., precipitation/temperature regime). Large parts of

Himalayan ecosystem remains understudied in terms of the impacts of ongoing climatic variability and human activities on fragile vegetation communities. This study attempts to fill this knowledge gap by analyzing freely available earth observation data to characterize interannual trends in vegetation greenness and trend distribution with respect to different elevation gradients and land use land cover classes. Our results represent considerable improvements over the previous studies in the Himalayas that are based on coarser spatial resolution (e.g., NOAA-AVHRR) time series and are only able to detect very broad vegetation trends. MODIS-NDVI images with relatively high spatial resolution enabled us to stratify and relate greenness/brownness trends to various land use land cover classes and expand our understanding on how different vegetation types may respond differently to changing environmental drivers. The 250 m MODIS-NDVI time series product is the highest spatial resolution time series data currently available that also provides regional scale coverage. However, considering the spatial heterogeneity in land use patterns that is often observed in lower elevation area (i.e., Siwalik) in Western Himalayas, higher spatial resolution images (e.g., Landsat, SPOT) will provide more detailed vegetation trends which may be more accurate depending on the spatial heterogeneity of cover types. Results obtained using such higher spatial resolution products could also be used to validate trend magnitude and direction obtained from coarser resolution products. Furthermore, lack of environmental data at comparable spatio-temporal scales hinders analysis on exact causation of the changing vegetation productivity in a functionally diverse and spatially heterogeneous area such as Uttarakhand Himalayas. More recent availability of multi-temporal high spatial resolution imagery (<5 m) makes it possible to infer the drivers of changing vegetation trend in and around anthropogenically altered areas. It is however much more challenging to interpret drivers of detected trend in protected areas (e.g., national parks) due to either scarcity of in situ time series climate data (e.g., temperature, rainfall) or the very coarse spatial resolution (>5 km) of satellite-derived estimates. Due to rapidly increasing population, growing connectivity between urban growth centers, and implementation of various socioeconomic developmental projects (e.g., dam construction) in ecologically sensitive areas, the negative impacts of anthropogenic activities are expected to accelerate in the near future and could contribute to increasing environmental vulnerability in Uttarakhand Himalayas. To address these challenges, in future more local scale case studies that integrate and relate in situ data on changes in vegetation structural/functional properties with relevant satellite derived matrices at multiple scales would be required.

References

Barichivich J, Briffa KR, Myneni R, Schrier GVD, Dorigo W, Tucker CJ, Osborn TJ, Melvin TM (2014) Temperature and snow-mediated moisture controls of summer photosynthetic activity in northern terrestrial ecosystems between 1982 and 2011. Remote Sens 6(2):1390–1431

Bontemps S, Defourny P, Bogaert EV, Arino O, Kalogirou V, Perez JR (2011) GLOBCOVER 2009-products description and validation report

D'Arrigo RD, Kaufmann RK, Davi N, Jacoby GC, Laskowski C, Myneni RB, Cherubini P (2004) Thresholds for warming-induced growth decline at elevational tree line in the Yukon Territory, Canada. Glob Biogeochem Cycles 18(3):7. doi:10.1029/2004gb002249

de Jong R, Verbesselt J, Zeileis A, Schaepman ME (2013) Shifts in global vegetation activity trends. Remote Sens 5(3):1117–1133. doi:10.3390/rs5031117

Goetz SJ, Prince SD (1999) Modelling terrestrial carbon exchange and storage: evidence and implications of functional convergence in light-use efficiency. Adv Ecol Res 28(28):57–92. doi:10.1016/s0065-2504(08)60029-x

Gottfried M, Pauli H, Futschik A, Akhalkatsi M, Barančok P, Alonso JLB, Coldea G, Dick J, Erschbamer B, Kazakis G (2012) Continent-wide response of mountain vegetation to climate change. Nat Clim Chang 2(2):111–115

Huete A, Didan K, Miura T, Rodriguez EP, Gao X, Ferreira LG (2002) Overview of the radiometric and biophysical performance of the MODIS vegetation indices. Remote Sens Environ 83(1–2):195–213. doi:10.1016/s0034-4257(02)00096-2

Immerzeel WW, van Beek LPH, Bierkens MFP (2010) Climate change will affect the Asian water towers. Science 328(5984):1382–1385. doi:10.1126/science.1183188

India Co (2011) Uttarakhand final population totals 2011

Ives J (2004) Himalayan perceptions: environmental change and the well-being of mountain peoples. Routledge, London

Kaspersen PS, Fensholt R, Huber S (2011) A spatiotemporal analysis of climatic drivers for observed changes in Sahelian vegetation productivity (1982–2007). Int J Geophys 2011:1–15

Kendall MG (1938) A new measure of rank correlation. Biometrika 30:81–93

Krishnaswamy J, John R, Joseph S (2014) Consistent response of vegetation dynamics to recent climate change in tropical mountain regions. Glob Chang Biol 20(1):203–215. doi:10.1111/gcb.12362

Lillesand TM, Kiefer RW (1994) Remote sensing and image interpretation. Wiley, New York

Mann HB (1945) Nonparametric tests against trend. Econometrica: J Econ Soc 13:245–259

Menzel A (2002) Phenology: its importance to the global change community. Clim Chang 54(4):379–385

Mishra NB, Chaudhuri G (2015) Spatio-temporal analysis of trends in seasonal vegetation productivity across Uttarakhand, Indian Himalayas, 2000–2014. Appl Geogr 56:29–41

Mittal S, Tripathi G, Sethi D (2008) Development strategy for the hill districts of Uttarakhand. Indian Council for Research on International Economic Relations. New Delhi, India

Myneni RB, Hall FG, Sellers PJ, Marshak AL (1995) The interpretation of spectral vegetation indexes. IEEE Trans Geosci Remote Sens 33(2):481–486. doi:10.1109/36.377948

Myneni RB, Keeling C, Tucker C, Asrar G, Nemani R (1997) Increased plant growth in the northern high latitudes from 1981 to 1991. Nature 386(6626):698–702

Negi SP (2009) Forest cover in Indian Himalayan states-an overview. Indian J For 32(1):1–5

Pandit MK, Grumbine RE (2012) Potential effects of ongoing and proposed hydropower development on terrestrial biological diversity in the Indian Himalaya. Conserv Biol 26(6):1061–1071. doi:10.1111/j.1523-1739.2012.01918.x

Pandit MK, Sodhi NS, Koh LP, Bhaskar A, Brook BW (2007) Unreported yet massive deforestation driving loss of endemic biodiversity in Indian Himalaya. Biodivers Conserv 16(1):153–163. doi:10.1007/s10531-006-9038-5

Phukan H, Rahman Z, Devdutt P (2012) Effect of spiritual tourism on financial health of the Uttarakhand state of India. Int J Res Commer IT Manag 2(2):1–7

Pounds JA, Fogden MPL, Campbell JH (1999) Biological response to climate change on a tropical mountain. Nature 398(6728):611–615. doi:10.1038/19297

Rana N, Sati S, Sundriyal Y, Doval MM, Juyal N (2007) Socio-economic and environmental implications of the hydroelectric projects in Uttarakhand Himalaya, India. J Mt Sci 4(4):344–353

Rangwala I, Miller JR (2012) Climate change in mountains: a review of elevation-dependent warming and its possible causes. Clim Chang 114(3–4):527–547. doi:10.1007/s10584-012-0419-3

Semwal RL, Nautiyal S, Sen K, Rana U, Maikhuri R, Rao K, Saxena K (2004) Patterns and ecological implications of agricultural land-use changes: a case study from central Himalaya, India. Agric Ecosyst Environ 102(1):81–92

Shrestha AB, Wake CP, Mayewski PA, Dibb JE (1999) Maximum temperature trends in the Himalaya and its vicinity: an analysis based on temperature records from Nepal for the period 1971–94. J Clim 12(9):2775–2786. doi:10.1175/1520-0442(1999)012<2775:mttith>2.0.co;2

Shrestha UB, Gautam S, Bawa KS (2012) Widespread climate change in the Himalayas and associated changes in local ecosystems. PloS One 7(5). doi:10.1371/journal.pone.0036741

Singh J (2006) Sustainable development of the Indian Himalayan region: linking ecological and economic concerns. Curr Sci 90(6):784–788

Singh J, Singh S (1987) Forest vegetation of the Himalaya. Bot Rev 53(1):80–192

Tachikawa T, Kaku M, Iwasaki A, Gesch D, Oimoen M, Zhang Z, Danielson J, Krieger T, Curtis B, Haase J (2011) ASTER global digital elevation model version 2–summary of validation results. ASTER GDEM Validation Team (http://www.jspacesystemsorjp/ersdac/GDEM/ver-2Validation/Summary_GDEM2_v alidation_report_final pdf)

Tiwari PC (2000) Land-use changes in Himalaya and their impact on the plains ecosystem: need for sustainable land use. Land Use Policy 17(2):101–111. doi:10.1016/s0264-8377(00)00002-8

Tiwari P (2008) Land use changes in Himalaya and their impacts on environment, society and economy: a study of the Lake Region in Kumaon Himalaya, India. Adv Atmos Sci 25(6):1029–1042. doi:10.1007/s00376-008-1029-x

Tiwari PC, Joshi B (2012) Urban growth in Himalaya. MRI NEWS 7

Walther GR, Beißner S, Pott R (2005) Climate change and high mountain vegetation shifts. In: Mountain ecosystems. Springer, Berlin, pp 77–96

Xu J, Grumbine RE, Shrestha A, Eriksson M, Yang X, Wang Y, Wilkes A (2009) The melting Himalayas: cascading effects of climate change on water, biodiversity, and livelihoods. Conserv Biol 23(3):520–530. doi:10.1111/j.1523-1739.2009.01237.x

Yue S, Wang C (2004) The Mann-Kendall test modified by effective sample size to detect trend in serially correlated hydrological series. Water Resour Manag 18(3):201–218

Chapter 19
Impact of Glacial Recession on the Vegetational Cover of Valley of Flowers National Park (a World Heritage Site), Central Himalaya, India

M.P.S. Bisht, Virendra Rana, and Suman Singh

Abstract With the growing threat of global warming, it has been projected that the Himalayan ecosystem will be severely affected. However, the nature and the magnitude of this ecosystem response are still elusive. Although the entire Himalayan region is prone to climatic perturbation, the high-altitude terrain is considered to be most fragile because of the presence of the microclimatic domain sustained by glaciers and snow line fluctuation (both long term and short term). Our recent observations in one of the most sensitive valleys of the Himalaya, the Valley of Flowers National Park, have shown that during the past 46 years the main Tipra valley glacier has receded 535 m. As a consequence, vegetation has appeared to occupy the vacated area. For the first time, three montane warm-loving species, *Pinus wallichiana* A.B. Jackson [at 3865 m above sea level (a.s.l.)], *Picea smithiana* (at 3700 m asl) (Wall.) Boiss., and *Populus ciliata* Wall. ex Royle (at 3712 m asl), have shown upward migration from the established altitudes of 2500 to 3800 m asl, from 2700 to 3700 m asl, and from 3000 to 3700 m, respectively. These observations are the very first suggesting that the alpine ecosystem has begun to respond to changes in temperature and precipitation during the past 50 years.

Keywords Upward shift • Glacier recession • Climate • Central Himalaya

19.1 Introduction

The rising temperatures and loss of ice and snow in the Himalayan region have cascading effects on water availability (amount, seasonality), biodiversity (endemic species distribution and habitats), ecosystem boundary shifts (tree line movements, high-elevation ecosystem changes), and global feedback (monsoonal

M.P.S. Bisht (✉) • V. Rana • S. Singh
Department of Geology, HNB Garhwal University, Srinagar (Garhwal), Uttarakhand, India
e-mail: mpbisht@gmail.com

R.B. Singh et al. (eds.), *Climate Change, Glacier Response, and Vegetation Dynamics in the Himalaya*, DOI 10.1007/978-3-319-28977-9_19

shifts, loss of soil carbon) (Xu et al. 2009). Recently, there has been increasing evidence of species range shifts resulting from changes in climate. Most of these shifts relate ground truth biogeographic data to a general warming trend at regional or global levels (Lenoir et al. 2008). The Indian Himalaya occupies a special place in the mountain ecosystems of the world. This young and active orogen is not only important from the climatic point of view and as a storehouse of freshwater (Mehta et al. 2011; Körner 1995) but also harbors a rich diversity of flora and fauna (Rawat 2003).

Alpine habitats in the Himalaya are relatively young, extremely heterogeneous, fragile, and dynamic. Summer and winter precipitation, topography, soil and soil composition, and food chain aspects as well as glacial recession strongly influence the distribution of species (Körner 2007; Bliss 1971; Sarkar 2007). The glaciofluvial and fluvial zones are areas that could show the upward shift of vegetation (Bisht 2012). In addition to its effects on the current functioning of ecosystems, species diversity influences the resilience and resistance of ecosystems to environmental changes (Chapin et al. 2000; Sarkar 2007). The diversity of life forms, plant community composition, adaptation to extreme climatic conditions and global warming, and microclimatic variation in the alpine region are attracting current investigation. With the background of these factors, the present investigation was undertaken in the Valley of Flowers National Park to understand the impact of glacial recession on the upward shift of plants in the vicinity of Tipra Glacier (Fig. 19.1).

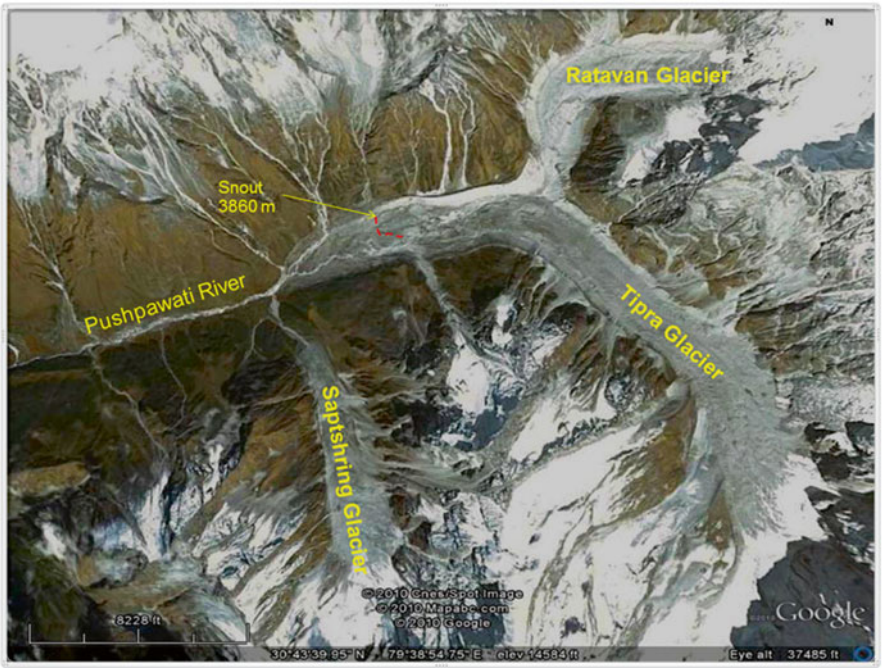

Fig. 19.1 Synoptic view of study area (Pushpawati Valley, the very famous Valley of Flowers) with Tipra Glacier and its tributary glaciers (Source: Author)

Several studies predict that climate warming will cause significant decline in biodiversity across a wide variety of alpine habitats (Lenoir et al. 2008). Plant communities will likely increase in species cover but decrease in diversity and evenness in a nonlinear response to global warming (Mehta et al. 2011; Gaur 1999). The ability of species to respond to climate change depends on being able to "track" shifting climatic zones and colonize new territory or to adapt their physiology and seasonal behavior to changing conditions (Naithani 1985, 1986; Hajra and Balodi 1995). Existing species appear, however, to shift their geographic distribution as though tracking the changing climate, rather than remaining stationary and evolving new forms (Gaur 1999). Along elevational gradients, niches for shifting species may decrease in size (Rana 2007). In montane ecosystems, it has been projected that a 1 °C increase in mean annual temperature will result in a shift in isotherms of about 160 m in elevation or 150 km^2 in area. The alpine tree line ecotone is useful for monitoring climate change, although such studies are complicated by biogeography, species ecology, site history, and anthropogenic influences (Gaur 1999). The climatic, orographic, and geologic barriers of the Himalaya may also prevent migration of species along latitudinal gradients.

19.2 Shrinking of Glacial Mass

The Tipra Bank Glacier (identification no. 5013206-092) (Kaul 1999) is one of the medium-size, north- to northwest-facing valley glaciers in the present study area that originates from the northern slope of Gauri Parbat (6601 m) and flows toward north to northwest for about 7 km, covering an area of 7.5 km^2 with an estimated ice volume of 13.11 (Mehta et al. 2011). The geomorphic setup of the proglacial area is evidenced by a typical U-shaped trough filled with glacial deposits, cirques, and hanging glaciers in addition to the outwash plain. Relicts of nine successive recessional moraines well preserved in the valley, starting from 3560 to 3840 m above sea level (a.s.l.) in height (Figs. 19.2 and 19.3), are clear-cut evidence of glacier recession during the recent past. Considering the 1962 Survey of India (SOI) topographic maps with 2008 data (beginning of the present study), the total shift on snout position was measured as 763 m, which gives an average backward shift of snout position in the past 45 years of about 16.95 m/year. The vertical component, as evidenced by the vertical scarp face of lateral moraines exposed along the valley sides, varies from 50 to 110 m in height to the present glacier surface, which clearly indicates the high recession of the overall glacial mass in both the horizontal and vertical components during the past five decades.

Tipra Glacier is the largest ice mass (7.5 km in length and 0.5 km average width) of the 12 glacierized bodies referred to as V1 to V12 (Table 19.1, Fig. 19.4) in the Pushpawati River catchment (Valley of Flowers: 30°42′ to 30°7′ N and 79°33′29″ to 79°42′13″ E). It covers approximately 19.37 % of the total 87.50 km^2 catchment area. The study reveals that in the past 26 years, that is, from 1984 to

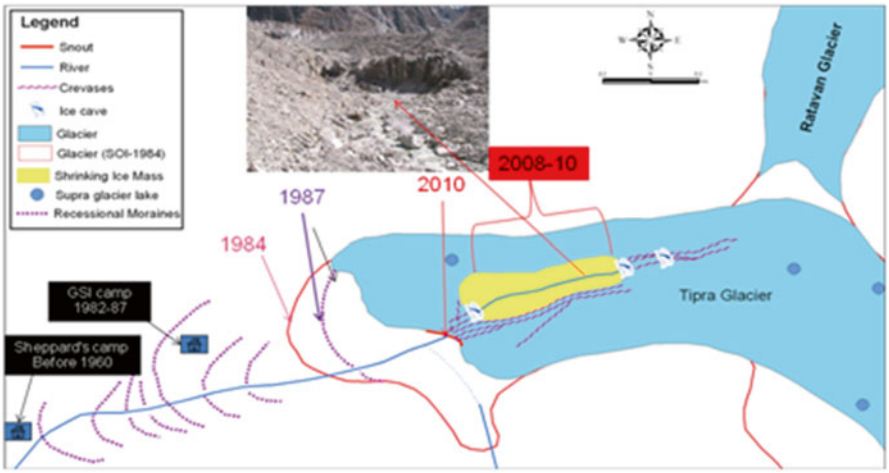

Fig. 19.2 Retreat of Tipra Glacier (1984–2010) and shrinking of ice mass to bed level (*inset*). Based on Survey of India topographic maps (1962 and 1984), Reports of Geological Survey of India (1984–1987), and regular monitoring by the present authors (2008–2011) (Source: Author)

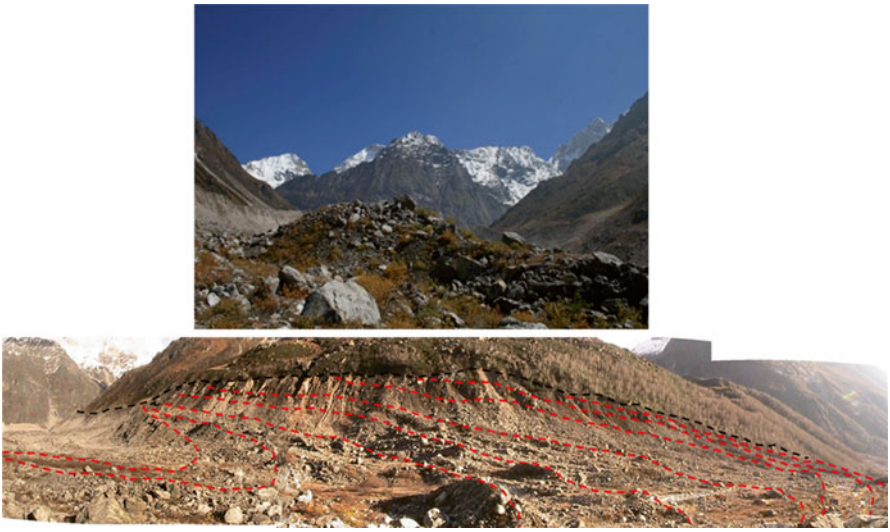

Fig. 19.3 Relicts of recessional moraines in Tipra Glacier. Cross-sectional (*above*) and longitudinal (*below*) views extrapolated by *dashed lines* (Source: Author)

2010, approximately 2.5 km^2 of the 23 km^2 covered by the glacier has been vacated. During this period two comparatively smaller ice bodies (V_4 and V_{10}) have completely vanished, and two others (V_9 and V_{11}) are at the verge of complete melting: this gives an average recessional rate of 14.15 m/year during 1984–2010 (Bisht 2012) (Table 19.2).

Table 19.1 Glacierized area in the Valley of Flowers National Park

Glacier number	Area covered, 1984 (km^2)[a]	Vacated area, 2010 (km^2)[c]	Area covered, 2010 (km^2)[d]
V1	0.7038	0.161	0.5428
V2	1.0282	0.2401	0.7881
V3	0.0894	0.024	0.0654
V4	0.2479	0.2479	0
V5	0.4538	0.1968	0.257
V6	0.6442	0.2008	0.4434
V7	7.7469	0.1237	7.6232
V8[b]	8.8805	0.6191	8.2614
V9	0.368	0.1777	0.1903
V10	0.0474	0.0474	0
V11	0.2252	0.1225	0.1027
V12	2.5814	0.3471	2.2343
Total	23.0167	2.5081	20.5086

[a]Survey of India (SOI)
[b]Tipra Glacier
[c]DGPS Survey by author
[d]IRS P6 LISS III data

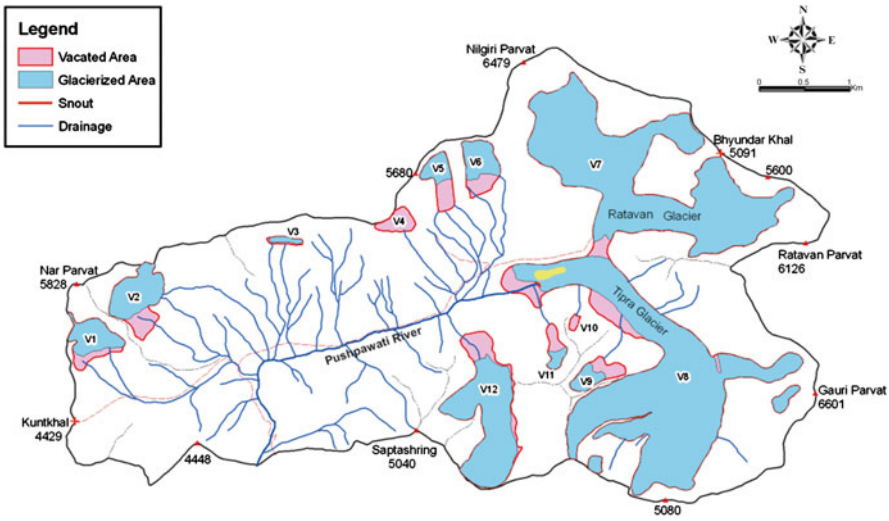

Fig. 19.4 Map showing glacierized zone in the Valley of Flowers National Park and total area vacated during 1984–2010 (Source: Author)

19.3 Geomorphic Units and Vegetational Succession

On the basis of landform characteristics and the geomorphic processes involved, plus vegetational succession, the valley floor has been divided into three basic broad geomorphic units (Table 19.3): (1) the glacial zone (above 3800 m asl), (2) the

Table 19.2 Average rate of recession in Tipra Glacier as calculated by various authors for different periods

Authors	Period	Rate of recession
Vohra (1981)	1960–1986	12.50 m/year
Mehta et al. (2011)	1962–2002	13.00 m/year
Bisht (2012)	1984–2010	14.15 m/year

Table 19.3 Geomorphic zoning of Valley of Flowers and the landforms

Geomorphic units	Topographic zone	Altitudinal range (m)	Landforms present
Glacial zone	Upper zone	>3800	Horn, arête, cirque, col, hanging valleys, U-shape valleys, ice table, ice cave, serac, supraglacial lake, crevasse, mullion, moraines, ogives, tills, tillites, etc.
Periglacial zone	Middle zone	3200–3800	Meadows, scree and talus cone, patterned ground, tors, pro-glacial lake, stair-wedge, soil creep, terracettes, etc.
Fluvial zone	Lower zone	<3200	Waterfall, cascades, gorges, alluvial fans, terraces, floodplain deposits, etc.

glaciofluvial zone (3200–3800 m asl), and (3) the fluvial zone (below 3200 m asl). The Tipra Glacier is flanked by three levels of lateral moraines, indicating past extension of the glaciers. Tipra Glacier initially flowed northward to a distance of about 4 km, then turned left toward the northwest, making a confluence with its tributaries, the Ratavan and Saptshring glaciers downstream, and supplying their ice melt to the Pushpawati River (Fig. 19.1). The details of these geomorphic units and the landforms available are given in Table 19.3, followed by detailed descriptions.

In the upper zone, the predominance of glacial landforms such as cirque, bringschuld, icefall, crevasses, mullions, ogives, and ice tables are some of the features indicating a definite movement of ice bodies in this zone and hence are a sign of rapid melting of the ice mass. Wherever rocks or a thin veneer of soil is exposed in the valley slopes, pioneer species such as mosses, lichens, sedges, and grasses have grown up (Rana et al. 2010). It was also observed that the areas that were fully or partially covered with snow and ice during the first field visit in 2008 were completely vacated in 2011 and occupied by pioneer species such as *Arenaria* (Rana et al. 2010).

The second geomorphic zone ranges between 3200 and 3800 m asl in the study area. It covers the peripheral zone of perpetual snow line, that is, the equilibrium line altitude (ELA), to the present snout of Tipra Glacier. This is a permafrost zone, and a zone of ablation, where glaciers start moving with some melting. The zone includes a huge amount of weathered rock material with varying thickness of till and tillites, commonly known as a supraglacier moraine. The moraines are loose unconsolidated rock material that sometimes provides a suitable place for plants to grow, but a series of successive deposits of these recessional moraines indicates there is a continuous shift in the position of the snout with the passage of time. This zone is significant from the aspect of vegetational succession. It is observed that despite movement in the underlying ice mass along with supraglacial moraines

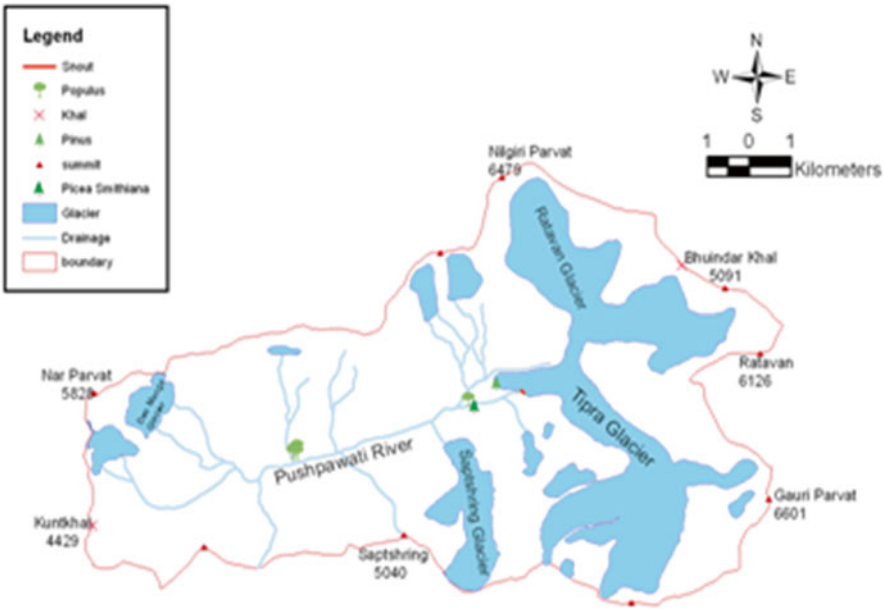

Fig. 19.5 Location of woody plants in the Tipra Glacier of the Valley of Flowers National Park: *Populus ciliata* (3712 m asl) (**a**); *Pinus wallichiana* (3865 m asl) (**b**); *Picea smithiana* (3700 m asl) (**c**) (Source: Author)

(approximately 50–75 m thick), the plants survive in minus temperatures for a sufficient time until the mass collapses or the plants are uprooted by expansion of crevasses in the ice body. It was also observed during the study that in addition to common woody species such as *Rhododendron campanulatum*, *R. lepidotum*, and *Juniper*, some unusual compositions of plant species such as *Pinus wallichiana*, *Picea smithiana*, *Rhododendron barbatum*, *Populus ciliata*, and *Rosa macrophylla*, comparatively low altitudinal woody plants, are gradually occupying this zone (Figs. 19.5 and 19.6). It was also observed that throughout the year these plants not only survived have well but have increased in number and spread over the entire zone of ablation. Some of the significant geomorphic features such as supraglacial lakes, seracs, ice caves, mullions (Fig. 19.7), both extensional and longitudinal, as well as crisscross crevasses followed by the collapse of huge supraglacial materials and exposure of a long englacial channel, followed by upward shifting of snout location, are indications of rapid glacial recession in the valley (Fig. 19.8).

The zone where the maximum fluvial process is operative in the study area is categorized under the third category, the fluvial zone (below 3200 m asl). This zone is marked by being filled with valley fill sediments such as large talus cones, relicts of moraines, terraces including floodplain deposits, huge areas covered with landslide debris, and wide meadows with green turf; these valley fill sediments are covered with all types of vegetation, that is, herbs, shrubs, and trees. Ice melting through valley side channels originating from hanging glaciers, ice walls, and even main

Fig. 19.6 Saplings of the woody plants recorded above the snout (3865 m asl) of the Tipra Glacier: *Pinus wallichiana* (3865 m asl) (**a**); *Populus ciliata* (3712 m asl) (**b**); *Picea smithiana* (3700 m asl) (**c**) (Source: Author)

Fig. 19.7 Ice cave (*above*) and mullion (*below*) are typical examples of poor glacial health of Tipra Glacier in the Valley of Flowers National Park: ice cave full of supraglacial overburden mass (**a**) and mullion following a transverse crevasse in Tipra Glacier (**b**) (Source: Author)

valley glaciers are the chief source of water for plant and animal life. Temperature fluctuates between −10 and 25°°C annually. Because of the rich diversity of the flora in this zone, the valley was identified as the "Valley of Flowers National Park," one of the core zones of the Nanda Devi Biosphere Reserve, and later was declared a "World Heritage Site" in 2005 by the World Heritage Committee. With the enchanting beauty of the overall landscape and its floral diversity, this particular zone of the valley was declared an ecotourism zone, where thousands of tourist, researchers, nature lovers, and environmentalists visit each year. However, it has been observed during the course of this study that the floristic pattern and density have been gradually changed and reduced (as the common people say, "Phoolon Ki Ghati," that is, the "valley of flowers is becoming flowerless"). The percentages of

herbaceous plants are decreasing with the increase of shrubs (e.g., *Salix* and *Rosa* sp.) and trees (e.g., birch trees, *Populus* sp.), which clearly indicates that the present temperature is not that preferred by the herbs reported in the preceding 30–35 years. Most of the year the valley side slopes seem barren, without snow cover, so the alpine herbs, grasses, and woody creepers such as *Rhododendron*, *Cotoneaster*, and *Juniper* are rapidly occupying the vacated areas, including morainic dumps, large scree fans, and even exposed bedrock (Fig. 19.8).

The overall land use/land cover pattern shows that of a total 87.50 km^2 area of the catchment, nearly 19.37 % is covered with perpetual snow; forest cover occupies

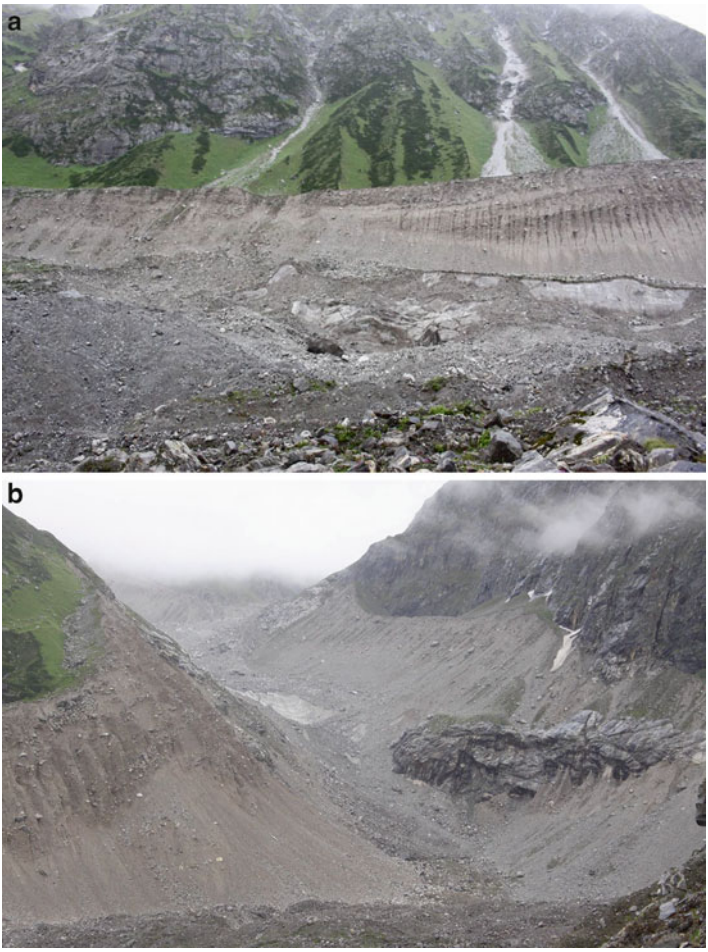

Fig. 19.8 Shrinking of glacier vertically (**a**), evidenced by the exposure of 110 m of free face of left lateral moraine and collapse of huge ice mass in the center of Tipra Glacier; and horizontally (**b**), by the separation of Ratavan, a tributary glacier from Tipra Glacier. The alpine herbs, grasses, and woody creepers, such as species of *Rhododendron*, *Cotoneaster*, and *Juniper*, are rapidly occupying the vacated areas such as the valley side slopes and huge scree fans (Source: Author)

3.00 %, meadow/grassland 13.18 %, and barren/rocky terrain approximately 38.73 %. The alpine meadows that appear constitute one of the most fascinating biomes in India. The lower boundary of the alpine zone is demarcated by a distinct tree line, which typically terminates at around 3300 ± 200 m in comparison to 3800 ± 200 m in the Eastern Himalaya (Körner 2004). The area immediately above the tree line is occupied by *krummholz* (stunted forest) formation (Billings 1974; Bliss 1971), and above this zone the vegetation comprises closely woven and dwarf shrubs (Chapin et al. 2000; Walker et al. 2006).

19.4 Methodology

The study was carried out by regular field visits from 2008 to 2011 during the months of April to November. The three zones that were identified were based on earth surface processes as well as vegetational succession, as already discussed. Regular monitoring of snout position as well as average percentage of the populations of plant species in each zone, and evaluation of the shifting behavior of the vegetation, were carried out by observation on a 10 × 10 m sample quadrant area marked in each zone. Finally, vacated area/change detection on the glacierized zone, using IRS P6 LISS III data of the past two decades supported by various field surveys, was calculated. The plant species have been identified by consulting the Herbarium of Garhwal University, Srinagar, Garhwal (GUH), Botanical Survey of India, Dehradun (BSD), and Forest Research Institute, Dehradun (DD). Current available literature has been used for proper nomenclature, and specimens properly labeled with all the relevant information and necessary remarks have been submitted to the Herbarium of HNB Garhwal University Srinagar, Garhwal (GUH).

19.5 Results and Discussion

The Tipra Glacier is a medium-size valley glacier within a World Heritage Site, the Valley of Flowers National Park, and is marked on the Survey of India Toposheet No. 53 N/10. This glacier has been retreating rapidly in recent years; the present recession rate of the glacier is 14.15 m per year (Bisht 2012). It has three distinct levels of lateral moraines, and the relicts of nine terminal moraines well preserved in the valley indicate the glacier mass shrank very fast both horizontally and vertically after LGM (Last Glacial Maxima) and the evacuated area was occupied by vegetational succession. Pioneer plant species such as *Arenaria* reached above the zone of accumulation near the ELA, that is, around 4500 m asl (Rana et al. 2010), and woody plants such as *Populus ciliata* (3712 m asl), *Picea smithiana* (at 3700 m asl), and *Pinus wallichiana* (3865 m asl) are some of the most alarming occurrences of high alpine vegetation. It is hoped that the present data would have some use in future references whenever any study is conducted to assess the present state of this

glacier. Glaciers and small ice caps in the temperate environment are sensitive indicators and react to even the slightest change in temperature; thus, they provide reliable information on historical temperature changes. Mountain glaciers provide a valuable tool for the reconstruction of Holocene climatic changes. They give valuable information about different reactions of the glaciers to fluctuations in the climate, as these can be expected during any future climate changes.

As has been observed, there is a gradual upward migration of the vegetation as well as changes in its diversity with the changes in some of the common natural processes, such as shrinking of the ice mass, increase in the summer period as compared to the winter, and increase in the rainfall pattern. Further, we have found that the glaciofluvial zone has rich diversity compared to the glacial zone: it provides a consistent supply of germplasm for acropetal succession and migration of vegetation in the glaciofluvial zone. Alpine plants are well adapted for such changing environments (Rawat 2003; Körner 2007; Billings 1974). Ice melt supplies the required water for irrigation that is routed through Pushpawati River. Currently, the mass, volume, area, and length of glacier and water supply are decreased, and the ground is developing for migration of plants. Studies suggest that between 1962 and 2002 about 535 m of recession occurred in the Tipra valley glacier, at an average rate of 13.4 m/year. During 2002–2006 and 2006–2008, the recession was 83 m and 45 m, respectively. If we compute the recession rate for 1962 and 2010, it comes to 14.15 m/year. Presently, because of the recession, the vacated area has debris, fine soil particles, rich soil moisture, and nutrition sources, which aid vegetation adaptation, colonization, and possibly upward migration. One of the most interesting findings of the present study is the occurrence of *Populus ciliata* (3712 m asl) and *Picea smithiana* (at 3700 m asl), and the most alarming is the occurrence of *Pinus wallichiana* (3865 m asl) in the glaciofluvial zone (Fig. 19.6). These species are growing in bushy form, a form that is common in the alpine habitat (Bliss 1971). The conventional habitats of these species are 2600 to 3000 m asl, respectively. In the Valley of Flowers National Park, their actual habitat is generally in a lower altitude of the valley at elevation ranges of 3600 m, 2700 m, and 2600 m, respectively. Although few studies have been conducted in the valley (Table 19.4), there is no other earlier record of the presence of these species at this elevation (Dubey et al. 2003).

Table 19.4 Synoptic view of conventional elevation and range of present saplings in study area

Tree saplings	Duthie (1906)	Polunin and Stainton (1984)	Naithani (1985)	Hajra and Balodi (1995)	Gaur (1999)	Bisht et al. (2010)
Populus ciliata	6000–11,000 ft	2100–3600 m	2000–3000 m	2200–2600 m	2500 m	3600 m
Picea smithiana	6000–11,000 ft	2100–3600 m	2500 m	2200–3000 m	2100 m	3700 m
Pinus wallichiana	6000–10,000 ft	1800–4300 m	2900–3000 m	2000–3500 m	2000–3200 m	3800 m

Although preliminary in nature, these observations based on the occurrence of warm-loving species in the alpine zone can be interpreted as an ecological response to global warming and microclimatic fluctuation in the Valley of Flowers National Park. If the trend persists, it may lead to proliferation of hardy species over the ecologically sensitive shrubs and bushes that constituted the primordial vegetation of the Valley of Flowers.

Acknowledgments The authors are grateful to the Chief Wild Life Warden and Director, Nanda Devi Biosphere Reserve, Uttarakhand, for their kind permission to visit inside the core zone, and also thankful to the Ministry of Environment and Forest, Government of India, New Delhi, for financial assistance.

References

Billings WD (1974) Adaptation and origins of alpine plants. Arct Antarct Alp Res 6:129–142

Bisht MPS (2012) Impact of glacier recession on the vegetative cover of the Valley of Flowers, Uttaranchal Himalaya. Ministry of Environment and Forests, Government of India

Bisht MPS, Mehta M, Nautiyal SK (2010) Impact of depleting glaciers on the Himalayan Biosphere Reserve: a case study of Nanda Devi Biosphere Reserve, Uttarakhand Himalaya. In: Bisht MPS, Devendra Pal (eds) Mountain resources management (Application of remote sensing and GIS). Transmedia Publications, Srinagar (Garhwal), pp 17–33

Bliss LC (1971) Arctic and alpine plant life cycles. Annu Rev Ecol Evol Syst 2:405–438

Chapin FS III, Zavaleta S, Eviner VT, Naylor RL, Vitousek PM, Reynolds HL, Hooper DU, Lavorel S, Sala OE, Hobbie SE, Mack MC, Diaz S (2000) Consequences of changing biodiversity. Nature (Lond) 405:234–242

Dubey BR, Yadav JS, Chaturvedi R (2003) Upward shift of Himalayan pine in Western Himalaya, India. Curr Sci 85:1135–1136

Duthie JF (1906) Catalogue of the plants of Kumaon and of the adjacent portions of Garhwal and Tibet based on the collections made by Strachey and Winterbottom during the years 1846–1849. London, Rep. Bishen Singh Mahendra Pal Singh, Dehradun, 1994

Gaur RD (1999) Flora of the District Garhwal: North West Himalaya (with ethnobotanical notes). Transmedia, Srinagar

Hajra PK, Balodi BS (1995) Plant wealth of Nanda Devi Biosphere Reserve. Botanical Survey of India, Howrah

Kaul MK (1999) Inventory of Himalayan glaciers. A contribution to the International Hydrological Program. Special Publication. Geological Survey of India, pp 34–165

Körner C (1995) Alpine plant diversity: a global survey and functional interpretation. In: Chapin FS, Korner C (eds) Arctic and alpine biodiversity: patterns, causes and ecosystem consequences. Springer, New York, pp 45–62

Körner C (2004) Mountain biodiversity, its causes and function. AMBIO 13:11–17

Körner C (2007) The use of 'altitude' in ecological research. Trends Ecol Evol 22:570–574

Lenoir J, Gegout JC, Marquet PA, Ruffray P, Brisse H (2008) A significant upward shift in plant species optimum elevation during the 20th century. Science 320:1768–1771

Mehta M, Dobhal DP, Bisht MPS (2011) Change of Tipra Glacier in the Garhwal Himalaya, India, between 1962 and 2008. Prog Phys Geogr 35:721–738. doi:10.1177/0309133311411760

Naithani BD (1984–1985) Flora of Chamoli, 2 vols. Botanical Survey of India, Howarah

Naithani, BD (1986) Ethnobotanical studies of the flora of Garhwal. Ph.D. Thesis (Unpublished). HNB Garhwal University Srinagar, Garhwal

Polunin O, Stainton A (1984) Flowers of the Himalaya. Oxford Press, New Delhi

Rana CS (2007) Ethnobotanical studies on the medicinal plants of Nanda Devi Biosphere Reserve, Uttaranchal. Garhwal University Srinagar, Garhwal

Rana CS, Rana V, Bisht MPS (2010) An unusual composition of the plant species in the zone of ablation (Tipra glacier), Garhwal Himalaya. Curr Sci 99(5):574–576

Rawat DS (2003) An investigation on the habitat and adaptive feature of alpine plants in Garhwal Himalaya. Garhwal University Srinagar, Garhwal

Sarkar S (2007) An open access data base for Himalayan environmental management. Himalayan J Sci 4:7–8

Vohra CP (1981) Himalayan glaciers. In: Lall JS, Maddie AD (eds) Himalayan aspects of change. Oxford University Press, Delhi, pp 138–151

Walker MD, Wahren CH, Hollister RD, Henry GHR, Ahlquist LE, Alatalo JM, Bret-Harte MS, Calef MP, Callaghan TV, Carroll AB, Epstein HE, Jonsdottir IS, Klein JA, Magnusson B, Molau U, Oberbauer SF, Rewa SP, Robinson CH, Shaverp GR, Suding KN, Thompson CC, Tolvanen A, Totland Ø, Turner PL, Tweedie CE, Webber PJ, Wookey PA (2006) Plant community response to experimental warming across the Tundra biome. Proc Natl Acad Sci USA 103(5):1342–1346

Xu J, Edward GR, Shrestha A, Eriksson M, Yang X, Wang Y, Wilkes A (2009) The melting Himalayas: cascading effects of climate change on water, biodiversity and livelihoods. Conserv Biol 3:520–530

Chapter 20
Snow Cover Dynamics and Timberline Change Detection of Yamunotri Watershed Using Multi-temporal Satellite Imagery

Manish Kumar and Pankaj Kumar

Abstract This paper is an attempt to examine the impact of climate change over snow cover and timberline dynamics in the alpine zone of Yamunotri watershed in the Garhwal Himalaya. The study extracts dynamics of snowline and timberline using Landsat TM data of two different time periods, i.e. 1990 and 2010. Temporal images of study area were processed in the GIS environment using Normalized Difference Snow Index (NDSI) and Normalized Difference Vegetation Index (NDVI) algorithm on ERDAS Imagine and ArcGIS 9.3. To determine the height of the snow and timberline, Shuttle Radar Topographic Mission (SRTM) data was used. The result reveals that the snow cover in 1990 was estimated at 707 km^2 which decreased to 552 km^2 in 2010. The average height of timberline in Yamunotri watershed was 3580 m in the year 1990 and 3660 m in 2010, while the average height of snowline was 4480 m in 1990 and 4660 m in 2010. These data suggest that due to global warming the timberline in the alpine zone has been shifted towards higher elevation at an average rate of 4 m/year during the last 20 years (i.e. 1990–2010). The snowline has also shifted towards higher elevation at an average rate of 9 m/year. During this period, about 68.58 km^2 non-timber areas of the alpine zone were converted into timber area at an average rate of 3.42 km^2/year, while during the same period, about 155 km^2 snow cover areas were converted into non-snow cover area at an average rate of 7.75 km^2/year.

Keywords Snow cover • Climate change • Treeline • Indian Himalaya

M. Kumar
Department of Geography, Kalindi College, University of Delhi, Delhi, India

P. Kumar (✉)
Department of Geography, Delhi School of Economics, University of Delhi, Delhi, India
e-mail: Pankajdsedu@gmail.com

R.B. Singh et al. (eds.), *Climate Change, Glacier Response, and Vegetation Dynamics in the Himalaya*, DOI 10.1007/978-3-319-28977-9_20

20.1 Introduction

Geographically alpine areas are the areas situated between timberline and snowline. Most of the plant species have set their upper altitudinal limits by various climatic parameters and by limitation of resources, and alpine ecosystems are known for reacting sensitively to climate change. Several studies show that climate change has impact on vegetation line ingression at higher altitudes of alpines (Noble 1993). Comprehensive analyses on vegetation ingression in alpine regions of Europe are being carried out under the Global Observation Research Initiatives in Alpine Environments (GLORIA) project (Pauli et al. 2006). Panigrahy et al. (2010) have used the term "timberline" to denote the ecological identity of upper altitudinal limit of tree growth in mountain ecosystem. Satellite remote sensing data provides synoptic view and historical records for a wide area to study alpine treeline and changes in the recent past (Singh et al. 2012). In the last few decades, timberline has got more attention from ecologists due to its high sensitivity to changing climate than other ecosystems (Crawford 1997; Lloyd and Graumlich 1997; Peterson 1998; Cullen et al. 2001; Camarero and Gutiérrez 2004). Past studies from the timberline zones show that the vegetation has fluctuated in the past in response to long-term climatic changes. Studies on the impact of ongoing warming under the background influence of greenhouse gases also show that during the past few decades plant species have shifted to higher elevations and the shifting rate varies with species and largely depends on their sensitivity to climate. Strong evidence of climate-induced upward migration of alpine plants has been reported from the Alps in Europe (Grabherr et al. 1994).

Snow cover also plays an important role in the climate system by changing the energy and mass transfer between the atmosphere and the surface. In recent years, a great deal of attention has been paid to monitoring and mapping of snow cover and snowline especially in Himalayan region. The Himalayas has one of the largest concentrations of glaciers and permanent snowfields outside the polar region and accounts for about 70 % of the non-polar glaciers (Kaur et al. 2009). Satellite remote sensing offers the opportunity to monitor and evaluate various snow parameters and processes at regional and global scale (Hall and Martinec 1985; Hall et al. 2005), and the remote sensing technique has been used extensively for snow cover monitoring in the Himalayan region with the help of numerous satellite sensors (Kulkarni and Rathore 2003). Geographical information system (GIS) and remote sensing technology facilitate fast and efficient ways to analyse, visualise and report the seasonal snow cover changes. Investigation of snow cover and snowline variation in Baspa basin was carried out using remote sensing and GIS techniques. The major difficulty in snow cover monitoring, using an automated technique in the Himalayan region, is the mountain shadow and confusing signature of snow and cloud in the visible and near infrared region. Normalized Difference Snow Index (NDSI) method effectively addresses this issue and has advantages when compared to the supervised and hybrid techniques, as it can detect snow even under mountain shadow and is not influenced by topographic conditions (Kulkarni et al. 2006). This is an

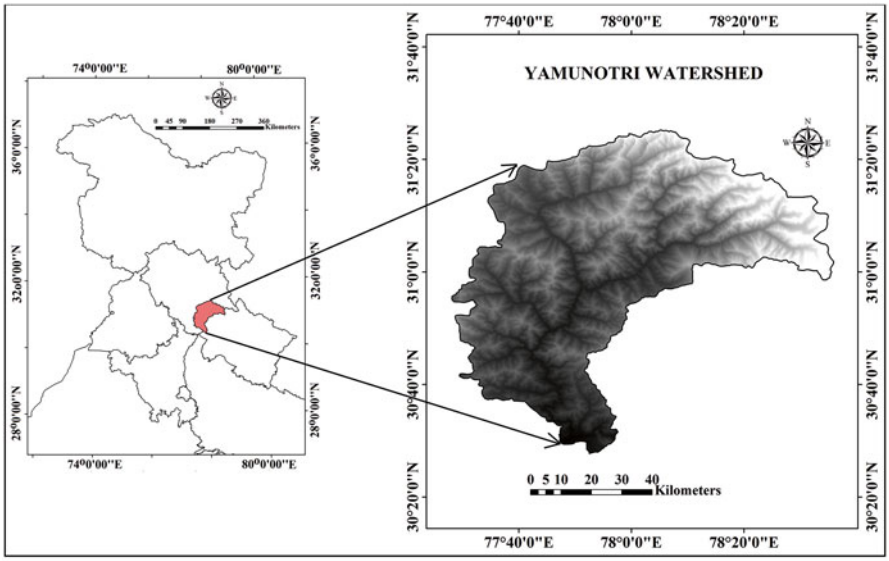

Fig. 20.1 Location map of the study area (Source: Author)

effective index for mapping snow cover in rugged terrain (Hall et al. 1995). The fundamental objective of the present study is to apply NDSI and NDVI technique for understanding impact of climate change on snow cover and timberline dynamics in the alpine zone of Yamunotri watershed in the Garhwal Himalaya.

20.2 Study Area

The study area, viz. the Yamunotri watershed (Fig. 20.1) which extends between 30°28′27″N to 31°24′42″N latitude and 77°35′41″E to 78°34′42″E longitudes, encompasses an area of 5023.38 km^2. Yamuna flows north-west to south-east flowing river situated in the western part of the Uttarakhand state in the central Himalaya. The altitude of the watershed varies between 445 and 6307 m.

20.3 Materials and Methods

20.3.1 Database

Data and software used in this study are: (i) Landsat Thematic Mapper (TM) multispectral image of the year 1990 and 2010 of 30 m spatial resolution, (ii) Shuttle Radar Topography Mission (SRTM) digital elevation dataset for elevation data, (iii)

Survey of India topographic map at 1:50,000 scale and (iv) ArcGIS 9.3 (ESRI) and ERDAS Imagine 9.3 (Leica Geosystems, Atlanta, USA) software packages.

20.3.2 Methodology

The base map of study area was prepared in the ArcGIS 9.3 software by using the survey of India toposheet at the scale of 1:50,000, and then watershed boundary was checked and corrected by superimposing the digital elevation model (DEM) data derived from the SRTM digital elevation dataset with 90 m spatial resolution and ± 15 m vertical accuracy. A rectification has been done in Landsat TM images using base map coordinates (i.e. UTM projection and 44 N zone) for the purpose to identify the study area. To interpret shadowed area in the hilly terrain, false colour composite image was created by using 2, 3 and 4 bands. The Landsat dataset provided by Global Land Cover Network were radiometrically and geometrically (ortho-rectified with UTM/WGS 84 projection) corrected. To separate the snow cover from non-snow cover area and vegetative to non-vegetative area, NDSI and NDVI were estimated for both TM images of the year 1990 and 2010 using the following equation (Hall et al. 2002):

$$\mathbf{NDSI} = \left(\mathbf{TM\ Band\ 2} - \mathbf{TM\ Band\ 5}\right) / \left(\mathbf{TM\ Band\ 2} + \mathbf{TM\ Band\ 5}\right)$$

where TM Band 2 and TM Band 5 are the reflectance of the green and shortwave infrared bands, respectively.

$$\mathbf{NDVI} = \left(\mathbf{TM\ Band\ 4} - \mathbf{TM\ Band\ 3}\right) / \left(\mathbf{TM\ Band\ 4} + \mathbf{TM\ Band\ 3}\right)$$

where TM Band 4 and TM Band 3 are the reflectance of the near infrared and red bands, respectively.

The NDSI raster data of the years 1990 and 2010 were then reclassified into two classes, i.e. snow cover and non-snow cover area. To segregate the snow-covered area from non-snow-covered area, Hall et al. (1998) suggested a NDSI threshold of >0.40 be used to map snow cover.

The upper limit of timberline was delineated using NDVI values ranging from >0.40 to be used to map timberline (http://www.earthobservatory.nasa.gov).

After displaying the NDSI and NDVI imagery on the screen of Arc map, the snowline and timberline in the watershed area were digitised for both years (i.e. 1990 and 2010). These lines were overlaid on the DEM data for estimating the average elevation, and then a point shape file has been created in Arc catalogue, keeping the snapping mode on; the digitization was done, over 1 year, i.e. 1990, and then the digitised points were masked by the mask function from DEM data, so that each point bear some heights, and then those points were exported into the Microsoft Excel sheet, and the average height has been estimated. The same process is being repeated for the year 2010.

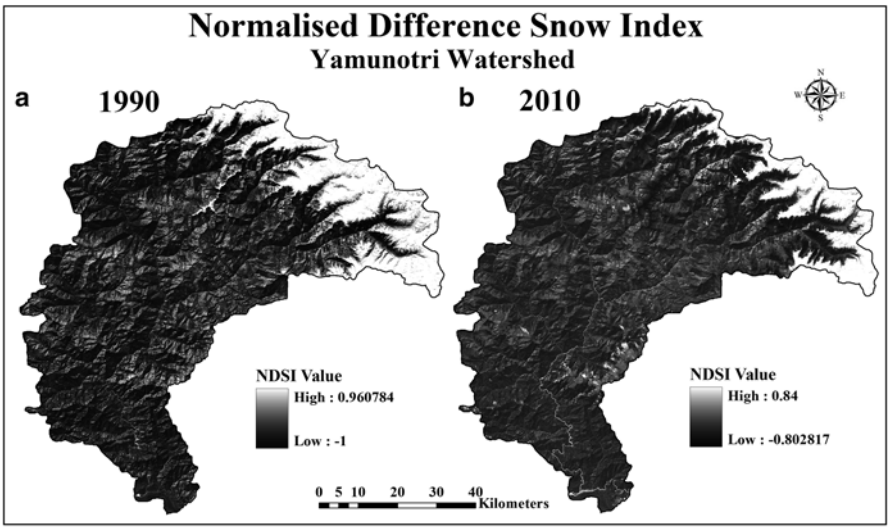

Fig. 20.2 Normalized Difference Snow Index (NDSI) of Yamunotri watershed during (**a**) 1990 and (**b**) 2010 (Source: Author)

20.4 Results and Discussion

The results obtained through the analysis of NDSI and NDVI imagery are diagrammatically illustrated in Figs. 20.2, 20.3, 20.4 and 20.5, and data are registered in Tables 20.1, 20.2, 20.3 and 20.4. A brief account of these results is discussed in the following paragraphs.

20.4.1 Status and Dynamics of Snow Cover

From Fig. 20.3 which is based on NDSI values of Fig. 20.2, area under snow cover during different years was worked out which is presented in Tables 20.1, 20.2, 20.3 and 20.4. The area under snow cover during the years 1990 and 2010 were worked out and presented in Table 20.1. The result reveals that the snow cover in 1990 was estimated at 707 km^2, while it was decreased to 552 km^2 in 2010 (Table 20.1). The snow cover area in the Yamunotri watershed has depleted considerably during the study period (1990–2010). For the period about 155 km^2 snow cover of the Yamunotri watershed has been converted into non-snow cover area at an average rate of 7.75 km^2/year (Table 20.4). The average height of snowline in 1990 was 4480 m, and in 2010 it was 4660 m (Table 20.2). These data reveal that the snowline has shifted towards higher elevation in the watershed about 180 m during the last 20 years (i.e. 1990–2010) at the rate of 9 m/year (Table 20.3).

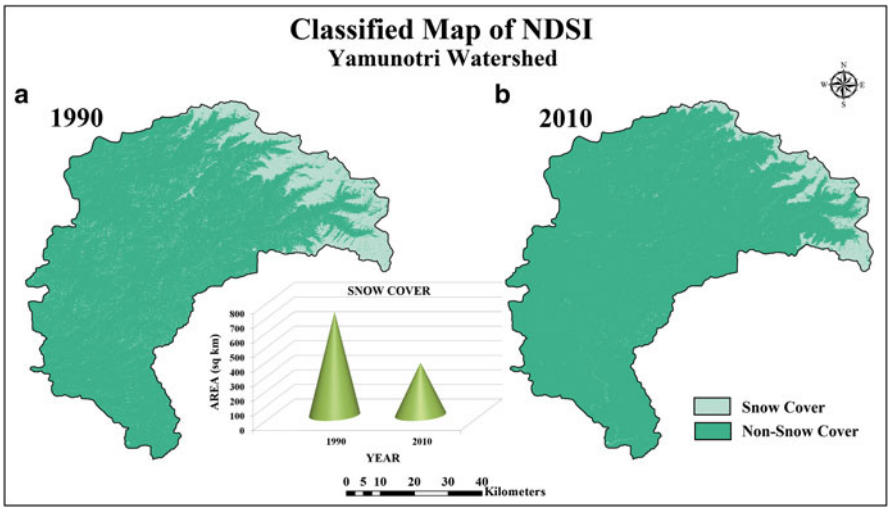

Source: Landsat TM Imagery

Fig. 20.3 Distribution of snow cover area based on NDSI values (>0.4) in different years in the Yamunotri watershed: (**a**) 1990 and (**b**) 2010 (Source: Author)

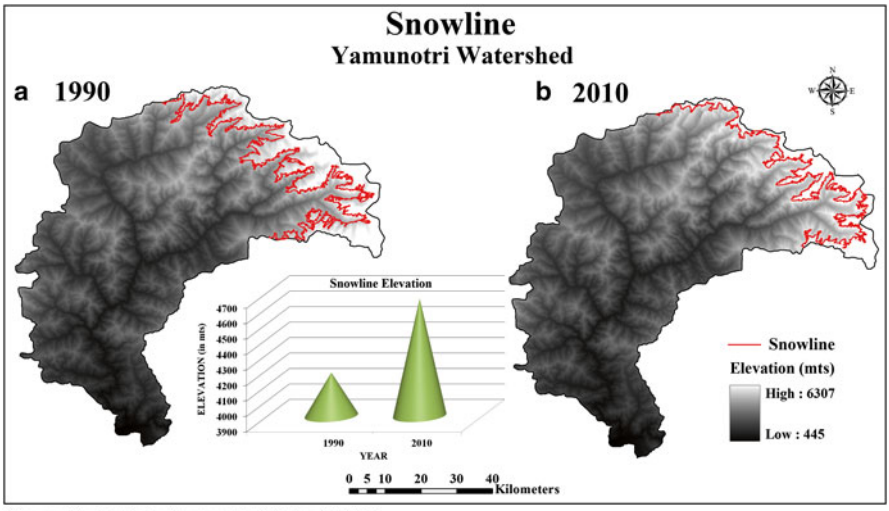

Source: Shuttle Radar Topographic Mission (SRTM)

Fig. 20.4 Distribution of snowline based on NDSI values (>0.4) in different years in the Yamunotri watershed: (**a**) 1990 and (**b**) 2010 (Source: Author)

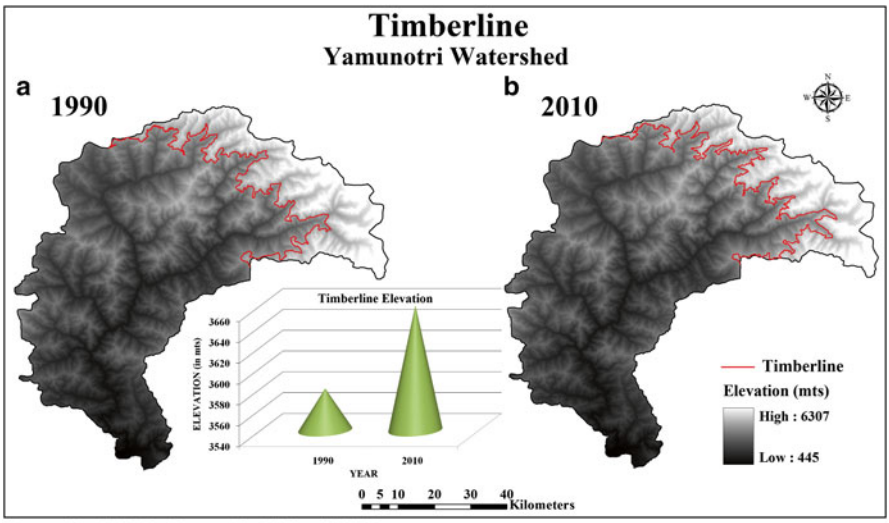

Source: Shuttle Radar Topographic Mission (SRTM)

Fig. 20.5 Distribution of timberline based on NDVI values (>0.4) in different years in the Yamunotri watershed: (**a**) 1990 and (**b**) 2010 (Source: Author)

Table 20.1 Area under snow cover during 1990 and 2010 in the Yamunotri watershed

Snow area (km^2)		Change in snow area (km^2)
1990	2010	1990–2010
707	552	−155

Table 20.2 Average height of timber and snowline during 1990 and 2010 in the Yamunotri watershed

Year	Timberline average height (m)	Snowline average height (m)
1990	3580	4480
2010	3660	4660

20.4.2 Status and Dynamics of Timberline

Figure 20.4 depicts the geographical location of timberline of the Yamunotri watershed in 1990 which is based on the NDVI values, i.e. >0.4. The DEM overlay on this timberline suggests that the average height of timberline in the watershed was about 3580 m in 1990 and 3660 m in 2010. The result suggests that the timberline might have shifted towards higher elevations during the last 20 years (Table 20.4). The timberline does not coincide with a contour line because elevation is not the only factor by which the timberline is controlled. Other parameters such as aspect (Kank et al. 2005), slope steepness and rockiness also influence the timber growth

Table 20.3 Amount and rate of timberline and snowline shift during 1990 and 2010 in the Yamunotri watershed, Garhwal Himalaya, India

Year	Period	Shift of snowline		Change from snow to non-snow area	
		Amount (m)	Amount (m/year)	Amount (km^2)	Rate of change (km^2/year)
1990–2010	20	180	9	155	7.75

Table 20.4 Amount and rate of change in timber during 1990 and 2010 in the Yamunotri watershed, Garhwal Himalaya, India

Year	Period	Shift of timberline		Change from non-timber to timber area	
		Amount (m)	Amount (m/year)	Amount (km^2)	Rate of change (km^2/year)
1990–2010	20	80	4	68.58	3.42

and development. Due to timber shifting during 1990–2010, about 68.58 km^2 non-timber area of the watershed in between 3580 and 3660 m elevation has been converted into timber area at an average rate of 3.42 km^2/year (Table 20.4).

20.5 Conclusion

A temporal monitoring of snow cover and timberline through satellite remote sensing of different years may play a pivotal role in ecological planning and watershed management. It is evident from this study that the snow cover is depleting steadily in the Yamunotri watershed. The present study carried out in a Garhwal Himalayan watershed, viz. the Yamunotri, reveals that during the last two decades (i.e. 1990–2010) about 155 km^2 area of the Yamunotri watershed has been converted into non-snow cover area from snow cover area. With the help of these data, it is found that the snow cover area in Yamunotri watershed is depleting at the average rate of 7.75 km^2/year. The average height of snowline in 1990 was 4480 m, and it has shifted towards higher elevation in 2010 at 4660 m elevation. The result also reveals that the timberline has shifted towards higher elevation in the watershed. It is evident from this study that the snow cover area is depleting steadily in the Garhwal Himalaya. If the trend of snow cover depletion continues, the hydrological balance of the region will be disturbed which may result in severe environmental degradation, socio-economic disruption and ecological damages in the Garhwal Himalayan region.

References

Camarero JJ, Gutiérrez E (2004) Pace and pattern of recent treeline dynamics: response of ecotones to climatic variability in the Spanish Pyrenees. Climate Change 63:181–200

Crawford RMM (1997) Consequences of climatic warming for plants of the northern and polar regions of Europe. Flora Colon 5(6):65–78

Cullen LE, Stewart GH, Duncan RP, Palmer JG (2001) Disturbance and climate warming influences in New Zealand Nothofagus tree-line population dynamics. J Ecol 8:1061–1071

Grabherr G, Gottfried M, Pauli H (1994) Climate effects on mountain plants. Nature 369:448

Hall DK, Martinec J (1985) Remote sensing of ice and snow. Chapman and Hall, New York

Hall DK, Foster JL, Chien JYL, Riggs GA (1995) Determination of actual snow covered area using Landsat TM and digital elevation model data in Glacier National Park. Mont Polar Rec 31:191–198

Hall DK, Kelly REJ, Foster JL, Chang ATC (2005) Hydrological applications of remote sensing: surface states: snow. In: Anderson MG (ed) Encyclopedia of hydrological sciences. Wiley, Chichester, p 3456

Kank RJ, Barancok P (2005) Monitoring of climatic change impacts on alpine vegetation – first approach. Ekologia (Bratislava) 24:411–418

Kaur R, Saikumar D, Kulkarni AV (2009) Variations in snow cover and snowline altitude in Baspa basin. Curr Sci 96(9):1255–1258

Kulkarni AV, Rathore BP (2003) Snow cover monitoring in Baspa basin using IRS WiFS data. Mausam 54:335–340

Kulkarni AV, Singh SK, Mathur P, Mishra VD (2006) Algorithm to monitor snow cover using AWiFS data of RESOURCESAT-1 for the Himalayan region. Int J Remote Sens 27:2449–2457

Lloyd AH, Graumlich LJ (1997) Holocene dynamics of treeline forests in the Sierra Nevada. Ecology 78(4):1199–1210

Noble KE (1993) A model to the responses of isotones to climate change. Ecol Appl 3:396–403

Panigrahy S, Anitha D, Kimothi MM, Singh SP (2010) Timberline change detection using topographic map and satellite imagery. Trop Ecol 51(1):87–91

Pauli H, Gottfried M, Reiter K, Klettner C, Grabherr G (2006) Signals of range expansions and contractions of vascular plants in the high Alps, observations (1994–2004) at the GLORIA master site Schrankogel, Tyrol, Austria. Glob Chang Biol 12:1–10

Peterson DL (1998) Climate limiting factors and environmental change in highaltitude forests of Western North America. In: Beniston M, Innes JL (eds) The impact of climate variability in forests. Springer, Heidelberg, pp 198–208

Singh CP, Panigrahy S, Thapliyal A, Kimothi MM, Soni P, Parihar JS (2012) Monitoring the alpine treeline shift in parts of the Indian Himalayas using remote sensing. Curr Sci 102(4):559–562